

Talanta

The International Journal of Pure and Applied Analytical Chemistry

Editors-in-Chief

Professor G.D. Christian, University of Washington, Department of Chemistry, 36 Bagely Hall, P.O. Box 351700, Seattle, WA 98195-1700, U.S.A.

Professor J.-M. Kauffmann, Université Libre de Bruxelles, Institut de Pharmacie, Campus de la Plaine, C.P. 205/6, Boulevard du Triomphe, B-1050 Bruxelles, Belgium

Associate Editors

Professor J.-H. Wang, Research Center for Analytical Sciences, Northeastern University, Box 332, Shenyang 110004, China

Professor J.L. Burguera, Los Andes University, IVAQUIM, Faculty of Sciences, P.O. Box 542, 5101-A Mérida, Venezuela.

Assistant Editors

Dr R.E. Synovec, Department of Chemistry, University of Washington, Box 351700, Seattle, WA 98195-1700, U.S.A.

Professor J.-C. Vire, Université Libre de Bruxelles, Institut de Pharmacie, Campus de la Plaine, C.P. 205/6, Boulevard du Triomphe, B-1050 Bruxelles, Belgium

Talanta

R. Apak (Istanbul, Turkey)
L.G. Bachas (Lexington, KY, U.S.A.)
E. Bakker (Auburn, AL, U.S.A.)
D. Barceló (Barcelona, Spain)
K. S. Booksh (Tempe, AZ, U.S.A.)
C.M.A. Brett (Coimbra, Portugal)
Yi. Chen (Beijing, China)
R. G. Compton (Oxford, U.K.)
S. Cosnier (Grenoble, France)
D. Diamond (Dublin, Ireland)
M.-R. Fuh (Taipei, Taiwan)
A.G. González (Seville, Spain)
V.K. Gupta (Roorkee, India)
I. Gutz (Sao Paulo, Brazil)

E.H. Hansen (Lyngby, Denmark)
P. de B. Harrington (OH, U.S.A.)
Y. van der Heyden (Belgium)
W.L. Hinze (Winston-Salem, NC, U.S.A.)
B. Karlberg (Stockholm, Sweden)
U. Karst (Enschede, The Netherlands)
Y. Lin (Richland, WA, U.S.A.)
R. Lobinski (Pau, France)
C.A. Lucy (Edmonton, AB, Canada)
M.D. Luque de Castro (Cordoba, Spain)
I.D. McKelvie (Victoria, Australia)
S. Montomizu (Okayama, Japan)
E. Morosonova (Moscow, Russia)
D. Nacapricha (Bangkok, Thailand)

J.-M. Pingarron (Madrid, Spain)
E. Pretsch (Zürich, Switzerland)
W. Schuhmann (Bochum, Germany)
M. Shamsipur (Kermanshah, Iran)
P. Solich (Hradec Králové, Czech Republic)
K. Suzuki (Yokohama, Japan)
D.L. Tsalev (Sofia, Bulgaria)
B. Walczak (Katowice, Poland)
R. von Wandruszka (Moscow, U.S.A.)
J. Wang (Tempe, AZ, U.S.A.)
J.D. Winefordner (Gainesville, U.S.A.)
Xiu-Ping Yan (Tianjin, China)
E.A.G. Zagatto (Piracicaba, SP, Brazil)

Copyright © 2007 Elsevier B.V. All rights reserved

Publication information: *Talanta* (ISSN 0039-9140). For 2007, volumes 71–73 are scheduled for publication. Subscription prices are available upon request from the Publisher or from the Regional Sales Office nearest you or from this journal's website (<http://www.elsevier.com/locate/talanta>). Further information is available on this journal and other Elsevier products through Elsevier's website: (<http://www.elsevier.com>). Subscriptions are accepted on a prepaid basis only and are entered on a calendar year basis. Issues are sent by standard mail (surface within Europe, air delivery outside Europe). Priority rates are available upon request. Claims for missing issues should be made within six months of the date of dispatch.

Orders, claims, and journal enquiries: please contact the Customer Service Department at the Regional Sales Office nearest you:

Orlando: Elsevier, Customer Service Department, 6277 Sea Harbor Drive, Orlando, FL 32887-4800, USA; phone: (+1) (877) 8397126 [toll free number for US customers], or (+1) (407) 3454020 [customers outside US]; fax: (+1) (407) 3631354; e-mail: usjcs@elsevier.com

Amsterdam: Elsevier, Customer Service Department, PO Box 211, 1000 AE Amsterdam, The Netherlands; phone: (+31) (20) 4853757; fax: (+31) (20) 4853432; e-mail: nlinfo-f@elsevier.com

Tokyo: Elsevier, Customer Service Department, 4F Higashi-Azabu, 1-Chome Bldg, 1-9-15 Higashi-Azabu, Minato-ku, Tokyo 106-0044, Japan; phone: (+81) (3) 5561 5037; fax: (+81) (3) 5561 5047; e-mail: jp.info@elsevier.com

Singapore: Elsevier, Customer Service Department, 3 Killiney Road, #08-01 Winsland House I, Singapore 239519; phone: (+65) 63490222; fax: (+65) 67331510; e-mail: asiainfo@elsevier.com

USA mailing notice: *Talanta* (ISSN 0039-9140) is published monthly by Elsevier B.V. (P.O. Box 211, 1000 AE Amsterdam, The Netherlands). Annual subscription price in the USA US\$ 3,818 (valid in North, Central and South America), including air speed delivery. Application to mail at periodical postage rate is paid at Rathway, NJ and additional mailing offices.

USA POSTMASTER: Send address changes to *Talanta*, Publications Expediting Inc., 200 Meacham Avenue, Elmont, NY 11003.

AIRFREIGHT AND MAILING in the USA by Publications Expediting Inc., 200 Meacham Avenue, Elmont, NY 11003.

Review

Chemometrics based on fuzzy logic principles in environmental studies

Aleksander Astel*

*Environmental Chemistry Research Unit, Biology and Environmental Protection Institute, Pomeranian Pedagogical Academy,
22a Arciszewskiego Str., 76-200 Słupsk, Poland*

Received 12 April 2006; received in revised form 14 September 2006; accepted 27 September 2006

Available online 30 October 2006

Abstract

Nowadays, environmetrics based on the principles of fuzzy logic has become an important and sophisticated statistical instrument in modern science, being an adequate tool to investigation the principles of interaction of elements/variables and their integration into a system. This paper is intended mainly for a wide community of ecologist, which are interested in principles of using fuzzy logic in environmental researchers. Properties of environmetrics based on fuzzy logic principles as a useful tool of investigation in environmental studies, are considered and discussed both in the terms of objectives and the examples of using techniques under interest concerning air, water and land ecological systems.

© 2006 Elsevier B.V. All rights reserved.

Keywords: Environmetrics; Fuzzy logic; Air; Water; Land; Forecasting; Modeling; Classification

Contents

1. Environmetrics based on fuzzy logic principles—common tendencies	2
1.1. Forecasting	2
1.2. Classification	2
1.3. Modeling	2
2. Air	3
2.1. Air pollution	3
2.2. Precipitation	4
2.3. Rainfall forecasting	4
2.4. Ozone layer	5
2.5. Aerosols	5
3. Water	6
3.1. Sea water	6
3.2. Rivers and streams	6
3.3. Flood forecasting	7
3.4. Ground water	8
3.5. Spring water	8
3.6. Drinking water	8
3.7. Wastewater	9
4. Land	9
4.1. Soil	9
5. Conclusions	11
References	11

* Tel.: +48 59 8405 423; fax: +48 59 8405 475.

E-mail address: astel@pap.edu.pl.

1. Environmetrics based on fuzzy logic principles—common tendencies

Chemometrics has been evolving as a subdiscipline in chemistry for over 30 years as the need for advanced statistical and mathematical methods has increased with sophistication of chemical instrumentation and processes [1]. As defined by Massart et al. [2], “chemometrics is a chemical discipline that uses mathematics, statistics, and formal logic to design or select optimal experimental procedures, to provide maximum relevant chemical information by analyzing chemical data and to obtain knowledge about chemical systems”. Nowadays, the chemometrics is not only limited to formal logic. Named as environmetrics and often based on fuzzy logic principles is concerned with the application and development of statistical methodologies in environmental sciences.

Fuzzy logic was introduced in the 60s [3]. It simplifies the process of taking decisions by simulating the way of reasoning of a human expert in environments characterized by uncertainty and imprecision. The idea behind fuzzy logic is that an element can belong partially to several subsets, unlike classical logic (Boolean) where belonging or not to a set are mutually exclusive. The degree of belonging to a set is a value between 0 and 1, usually determined by to what extent an element belongs to a fuzzy subset or a category of a variable. The concept of a fuzzy set is illustrated schematically by a simple example connected with environmental research in Fig. 1. The horizontal axis represents an environmental quality, such as a pollutant concentration which is always positive, and the vertical dashed line is the environmental standard, or objective. In this co-ordinate system three fuzzy sets are defined representing good, medium and poor environmental quality. The vertical axis shows the membership degree (membership function), which can have various equations of each fuzzy set. Scientific details on the methodology of various chemometrical techniques with implemented fuzzy logic rules can be found elsewhere [4–9] and are not presented in details in this review due to the difficulty of making it representative as the list of available techniques and possible variations is huge. Despite this we decided to present briefly the possible major objectives which can be accomplished successfully using chemometrics based on fuzzy logic principles: forecasting, modeling and classification.

1.1. Forecasting

Time series (TS) are sequences of independent random variables (observations) describing a phenomenon at successive

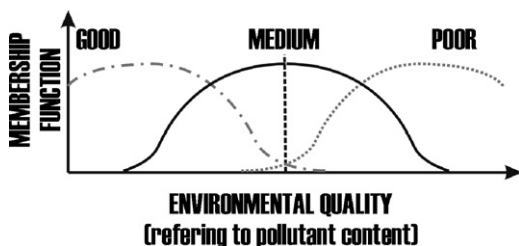


Fig. 1. Schematic explanation of fuzzy sets.

points in time. The main purpose of TS analysis is: (i) to make a statistical analysis of relations between successive observations; (ii) to predict (forecast) future values of the TS; (iii) to detect mechanisms that govern changes in the observed phenomenon in time, in other words, to determine the nature of the phenomenon represented by the sequence of observations. Nowadays, the time series analysis is commonly connected with neural network approach. Artificial neural networks (ANNs) are mathematical models consisting of a network of computation nodes called neurons and the connections between them. Adaptation of a neural network to solving a particular task takes place through a training process using typical stimulations and required responses corresponding to them, and not through defining an algorithm and writing it down in the form of a program, as would be the case in traditional modeling methods [10].

1.2. Classification

A basic problem that arises in a wide variety of fields, including analytical chemistry is the so-called clustering problem. Classification is useful, since it allows meaningful generalizations to be made about large quantities of data by recognizing among them a few basic patterns. It plays a key role in searching for structures in data. Each of these structures is called cluster or class. A class is a group of individuals (e.g., soil samples or pixels of a image) which resemble each other more strongly, in terms of particular properties, than they resemble members of other classes. There are various ways in which classification may be carried out. Generally, two types of algorithm are distinguished, these being hierarchical and non-hierarchical or relocation clustering. Both methods require the calculation of a (dis)similarity matrix. This (dis)similarity which is really a measure of the proximity of the pair of objects (points) in the p-dimensional characteristic space, defined by the p properties measured for each individual, is usually expressed in terms of either the Euclidean or the Mahalanobis distance between the two points.

1.3. Modeling

Fuzzy systems, including fuzzy logic and fuzzy set theory, provide a rich and meaningful addition to standard logic. The mathematics generated by these theories is consistent, and fuzzy logic may be a generalization of classic logic. The applications which may be generated from or adapted to fuzzy logic are wide-ranging, and provide the opportunity for modeling of conditions which are inherently imprecisely defined, despite the concerns of classical logicians. Many systems may be modeled, simulated, and even replicated with the help of fuzzy systems, not the least of which is human reasoning itself. Fuzzy logic is the way the human brain works, and we can mimic this in machines so they will perform somewhat like humans [11].

Uncertainty analysis, common in environmental studies can be dealt with fuzzy methods where uncertainty is due to vagueness or “fuzziness” rather than only to randomness. Therefore, environmental data or classes of ecological objects can be defined as fuzzy sets with not sharply defined boundaries

that reflects better the continuous character of nature [12]. The application of fuzzy theory is extended to various applications, for example, in assessing an environmental impact on product's life cycle [13,14], estimating aggregative risk of various environmental activities, pollution sources and routes in a given process [15], evaluating ecosystem sustainability [16–21], quantifying the ecological impacts of human activities [22], facilitating decision analysis of polluted environmental components which might menace to human health [23,24]. Developing decision support for environmental application is an intricate, challenging task. Fuzzy logic could be fruitful in development of a decision support systems for water and raw materials resource management [25] or to the simplification of decision-making in environments characterized by uncertainty and imprecision. It is based on the idea of building a model capable to simulate the way an expert reasons. The main breakthrough of fuzzy interference with respect to traditional mathematics models lies in the fact that relationship between inputs and outputs is not determined by complex equations, but by a set of logical rules, reflecting an expert's knowledge [14].

The major advantages connected with an application of environmetrics based on the principles of fuzzy logic can be described as follows:

- enables the synthesis of quantitative information into qualitative output which is more readable to decision makers and regulators,
- explicitly considers and propagate uncertainties,
- scalable modular form, enabling easy accommodation to new hazard and exposure parameters,
- programmable for computer applications and it can become a risk analysis tool for air, water and soil quality monitoring.

It should be emphasized that fuzzy logic is not a new chemometric technique but kind of modification of techniques already being of great use in environmental studies. Fuzzy logic enables

chemometric techniques to work more efficiently and cover wider spectrum of possible applications (Fig. 2).

This paper reviews major areas of environmetrics based on the application of fuzzy logic principles related to various environmental components (air, water and land) and then highlights some of new directions that environmetric techniques are taking. Moreover, the goal of this paper is to assess the usability of fuzzy logic approach not only in terms of environmental components investigation but also in a term of major objectives (modeling, forecasting, classification, etc.).

2. Air

In this section, papers dealing with an application of environmetrics based on the principles of fuzzy logic to chemical characteristics of air pollution (by direct analysis of air or indirect by analysis of precipitation), ozone layer consumption and aerosols conditions are reviewed.

2.1. Air pollution

Air pollution monitoring programs aim monitoring pollutants and their probable adverse effects at various locations over concerned area. An assessment of urban air quality using fuzzy synthetic evaluation was described by Onkal-Engin et al. [26]. Air pollution data such as SO₂, CO, NO₂, O₃ and total suspended particulate matter collected at six quality-monitoring stations located in western part of Istanbul was compared to air quality index (AQI). The results obtained from simple fuzzy classification and fuzzy comprehensive assessment brought almost identical results and even more optimistic than AQI. Successful classification was possible due to high frequency of temporal data recording (daily through the period of 20 months) and high spatial area of research. Moreover, authors established that the usage of membership function and predetermined weights increases the sensitivity of fuzzy synthetic evaluation.

Similar approach with using fuzzy synthetic evaluation technique to risk-based prioritization of air pollution monitoring was described by Khan and Sadiq [27]. The existing methods of monitoring location prioritization do not consider both factors, hazard and exposure, at a time. Towards this, risk-based approach has been proposed which combines exposure frequency (probability of occurrence/exposure) and potential hazard (consequence). Authors used a common air pollutants like CO, NO_x, PM₁₀ and SO as a hazard parameters to establish a fuzzy evaluation matrices for hazard parameters in air quality monitoring network designed around a refinery in Canada. Fuzzy evaluation matrices for exposure parameters: population density, location and population sensitivity were also developed. Subsequently, fuzzy risk was determined at geographical locations using fuzzy compositional rules. Finally, authors prioritized locations based on defuzzified risk (crisp value of risk, defined as a risk value) and identified the most important monitoring locations.

Pokrovsky et al. [28] presented an alternative approach to the conventional dynamics and photochemical models to forecast urban air pollutants. A fuzzy logic-based model was developed

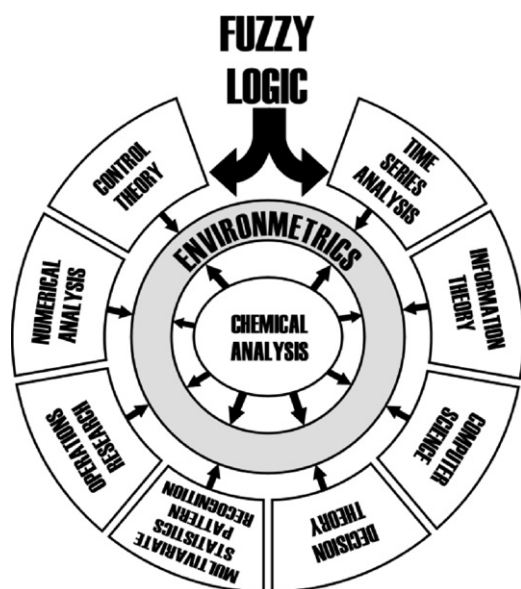


Fig. 2. Possible applications of fuzzy logic in environmetrics.

to study the impact of meteorological factors on the evolution of air pollutant levels and to describe them quantitatively. The developed model was based on simulation of diurnal cycles of principal meteorological variables (wind speed and direction, solar irradiance and air temperature) and the corresponding patterns of various air pollutants (O_3 , NO_2 , NO , NO_x). In addition, the spatial patterns of these parameters were also studied. Both temporal and spatial parameter distribution were considered in order to investigate impacts of meteorological factors and were incorporated into the models as state vectors in the multidimensional space. The study established that the most of the weather and air pollution phenomena could be simulated by sequences of its conservative inside some fuzzy sets and the transition from one fuzzy set to another.

Predicting atmospheric pollutant concentration in both urban and industrial areas is of great significance for decision-making. Nunnari et al. [29] used neural techniques based on fuzzy logic principles to the modeling of time-series of atmospheric pollution data in the province of Syracuse (Sicily). Basing on pre-processed data they predicted in a short and medium scale the concentration of O_3 , NMHC, NO_2 and NO_x which are typical of the photolytic cycle of nitrogen. Pre-processing phase was required to identify non-valid data due to malfunctions of the recording equipment. In case of forecasting using neural networks it is fundamental to extract non-valid data from the learning patterns and use temporal data recorded continuously at high frequency. To handle the lack of some samples in time series several strategies can be used. In some cases, mainly when the amount of missing data is low, it can be replaced by prediction value with a simple model, or even by interpolation value (between two closest samples). However, it is always a risk to replace data, because this will affect the final model. For this reason they decided to avoid forming patterns for model identification when there was data missing and because of this they observed less accuracy of neuro fuzzy networks than of multilayer one, and additionally, limited capacity of extracting knowledge, which represents a transparent form of modeling from which user can obtain useful indications regarding phenomena being investigated or which he can integrate with his own personal knowledge. In this section another study should, the one presented by Nunnari et al. [30], in which the authors inter-compared several statistical techniques for modeling SO_2 concentration a point such as neural networks, fuzzy logic and generalized additive techniques based on validated temporal data recorded at high frequency. The inter-compared techniques were ranked in terms of their capability to predict critical episodes.

Characterization of the uncertainty associated with air emission estimates is often of critical importance especially in the compilation of air emission inventories. Romano et al. [31] proposed the methodology of fuzzy logic implementation to estimate uncertainty of sulfur dioxide (SO_2), nitrogen oxides (NO_x), carbon monoxide (CO) and particulate matter (PM) emission in two Italian electric power plants. The fuzzy logic estimation (FLE) was performed basing on temporal, precise data recorded through 1 year as a daily average emission in one plant and as a hourly average data in the other. These authors were successful due to FLE compared to Monte Carlo algorithm and bootstrap

procedure which provided non significantly differing results. The study established that fuzzy logic can be useful if considering environmental data as vague, logic, indefinite and ambiguous and especially in all the situations when distribution of emission data is not precisely known and only a few measurement results are available, and also in case of only qualitative information.

2.2. Precipitation

To maintain healthy ecosystems, it is increasingly imperative that decision makers or land managers should be prepared to monitor and assess levels of atmospheric pollutants and ecological effects in national parks, wildlife refuges and wilderness areas. Atmospheric deposition of various chemical substances (e.g., sulphur and/or nitrogen) has the potential to damage sensitive terrestrial and aquatic ecosystems [32].

Various classification procedures, hierarchical and non-hierarchical crisp and fuzzy clustering, cross-classification fuzzy clustering and principal components analysis (PCA) (varimax rotation)—combined with receptor modeling were applied to a data set consisting of wet deposition loads of major ions from five sampling sites in Central Austria collected in a period of 10 years (1984–1993). The data classification with respect to the sampling sites as objects showed that a distinct separation between the northern Alpine rim and in the inner Alpine region is achieved. This indicates the role of geographical disposition of the sampling sites [33].

2.3. Rainfall forecasting

The application of fuzzy logic systems seems to be an effective tool both for investigation of chemical composition of precipitation and for rainfall events forecasting [34,35]. Ramírez et al. used an artificial neural network (AAN) to construct a nonlinear mapping between output data from two institutes in Brazil. The main objective was to generate site-specific quantitative forecast of daily rainfall performed for six locations in São Paulo State. The analysis was made using a feed forward neural network and resilient propagation-learning algorithm. Meteorological variables such as: potential temperature, vertical component of the wind, specific humidity, air temperature, precipitable water, relative vorticity and moisture divergence flux were used as input data to the trained networks, which generated rainfall forecast for the next step. Additionally, predictions with a multiple linear regression model were compared to those of ANN. The results showed that ANN forecasts superior to the ones obtained by the linear regression model and revealed a great potential for an operational suite. A watershed management program is usually based on the results of watershed modeling. Accurate modeling results are decided by the appropriate parameters and input data. It is crucial to use temporal, continuous and precise data in a stage of model rules creation. Rainfall is the most important for watershed modeling. Precipitation characteristics, such as rainfall intensity and duration, usually exhibit significant spatial variation, even within small watersheds. Therefore, properly describing the spatial variation of rainfall is essential for predicting the water movement in a

watershed. Chang et al. [35] tested a modified method, combining the inverse distance and fuzzy theory to precipitation interpolation. In the study the genetic algorithm (GA) based on the daily rainfall records generated at six stations in 2002 was used to determine the parameters of fuzzy membership functions, which represented the relationships between the location without rainfall and its surrounding rainfall gauges. The objective in the optimization process was to minimize the estimated error of precipitation. Due to high spatial area and temporal data recorded with daily intervals Chang et al. were successful because the estimated error was usually reduced by implemented method, particularly when there were large and irregular elevation differences between the interpolated area and its vicinal rainfall gauging stations.

2.4. Ozone layer

Due to the complex relationships and the necessity for forecast in atmospheric studies, air pollution modeling is a task for which fuzzy logic methods are amicably suited. The destruction of ozone takes place through a number of pathways. A various relationships between meteorological conditions, ozone consumption pathways and ozone concentration have been examined in several studies which used a combination of statistical regression, graphical analysis, fuzzy logic-based methods and cluster analysis [36–39]. The study showed the feasibility of the identification of a model allowing to predict the future ozone concentration from past and present information (pollution, meteorological information). Authors presented a fuzzy logic-based method to identify the forecasting models. Moreover, they emphasized the advantages of these prediction models consisting on expressing the models obtained in the form of fuzzy rules. Basing on post-days instantaneous measurements recorded continuously every 5 min up to 3 a.m. researchers tried to predict the concentration of ozone as a value representative for a midday on current day and a medium value for a whole day. Another trials were carried out and showed that forecasting based on fuzzy logic give the best results, not only in terms of correlation, but also in terms of explanation and prediction.

A new method of ozone forecasting using fuzzy expert and neural network systems were developed recently by Heo and Kim [40]. The fuzzy expert system was tested in forecasting the possibility of high ozone levels (equal to or above 80 ppb) for the following day in Seoul (Korea). The authors succeeded due to the structure of input data (precise, hourly data for air pollutants and meteorological variables) and including a correction function to the forecast model (can be updated whenever a new ozone episode appears). Even if the input variables were affected by photochemical formation, atmospheric accumulation or transport of ozone, the equipment of the system with correction functions results in self-correction ability.

Mintz et al. [41] presented the implementation of an automated fuzzy logic method termed modified learning method from examples (MLFE) in predicting surface ozone levels. Hourly ozone concentrations during summer months in the Edmonton (Canada) were predicted with MLFE models and the results were compared to models used by Environment

Canada (CHRONOS, CANFIS). Analogically to the work of Heo and Kim [40], continuous (hourly) and precise input data were used in a creation of model rules. To compare MLFE model ability with other models the root mean square error, mean absolute error and scatter plots were used. The best MLFE models were found to consist of few inputs: past 6 h ozone concentration, temperature and humidity. The coefficient of determination and slope results ranged from 0.70 to 0.85 and from 0.53 to 0.78, respectively. The statistical comparison of MLFE to the CHRONOS and CANFIS models showed the new model had better results and good agreement with the actual data, particularly for the daylight hour forecast. Authors emphasized the simplicity of MLFE method and a fact that MLFE does not require extensive computing power, and could serve as a useful tool for air quality monitoring.

2.5. Aerosols

Hierarchical, nonhierarchical, and fuzzy clustering techniques appeared helpful in identification of various heavy metal-containing particle types [42,43]. Van Malderen collected aerosol samples over the southern bight of the North Sea from an aircraft. This way, during 16 flights, 96 samples were collected for single-particle analysis. Almost 45 000 individual particles were analyzed with electron probe X-ray microanalysis. More than 5000 of these were found to contain significant concentrations of one or more of the heavy metals Cr, Pb, and Zn. Significant differences in abundances were detected in the North Sea heavy metal aerosol, depending on the origin of the air masses. In samples being under terrestrial impact 50 times more Zn- and Pb-containing particles were found than in samples with a marine history. The Cr abundances in the marine sector were found in the magnitude of one-third of the values for continental sectors. This might indicate a rather undefined marine source, for example the recycling of previously deposited material by reinjection into the atmosphere by sea spray. The highest values for Cr-, Pb-, and Zn-containing particles were always detected under southeastern wind directions. Jambers established that fuzzy hierarchical clustering technique results in different particle grouping which can be apportioned to their possible sources [43].

Ambient atmospheric particles were studied by Held et al. [44] at an ecosystem research site in the Fichtelgebirge mountains in Central Europe by single particle analysis and bulk impactor measurements. Fuzzy clustering analysis of mass spectra of individual aerosol particles allowed chemical classification of the atmospheric aerosol. During the campaign, inorganic salts, mineral particles, and carbonaceous particles, with varying degrees of secondary components, were identified. These chemical classes exhibited preferential size ranges leading to a characteristic pattern of relative abundances with respect to particle size. A more detailed analysis revealed that 65–80% of all particles were assigned almost exclusively to one chemical class. These particle populations are assumed to be externally mixed with respect to the identified chemical classes. The temporal variations of the nitrate to ammonium ratio (ranging from 0.37 to 0.81) determined by both impactor measurements and single particle analyses were in good agreement.

The study on composition of atmospheric aerosols applying combined hierarchical, non-hierarchical and fuzzy clustering was described in details by Treiger et al. [45]. The authors determined Na, Mg, Al, Si, P, S, Cl, K, CA, Ti, Mn, Zn, Ba and Pb using electron probe X-ray microanalysis technique and investigated the combined application of clustering techniques to find reasonable choice for the number of clusters and to demonstrate new visualization means for the representation of clustering results based on analysis of individual aerosol particles.

Basing on three previous examples it has to be emphasized that fuzzy clustering techniques in contrary to modeling and forecasting do not require data sets characterized by thousands of values recording in the long time period, high frequency or high precision. Efficient cluster analysis is possible for relatively small number of determination characterized by uncertainty common in environmental studies.

3. Water

This section is dedicated to an application of environmetrics based on the principles of fuzzy logic to major aspects concerning water on Earth, including lakes, rivers and oceans, ground- and sewage water, and also problems of water pollution and purification. The fuzzy logic algorithm has been successfully employed also in the studies of watershed management [46,47], hydro-ecological modeling over watersheds of mesoscale size [48], rainfall-runoff processes [49–51], flood forecasting [52–54], water quality problems [55] and solute transport in saturated/unsaturated zones [56–58].

3.1. Sea water

The problems associated with water quality in coastal areas are of growing concern since the increase of pollution in these areas may have serious environmental consequences. Numerical models are being extensively used to predict the water quality, and to provide reliable tools for water quality management in estuarine and coastal areas. Mpimpas et al. [59] applied a fuzzy set theory for the definition of the imprecise parameters, which are used in a water pollution model. Authors expressed physico-chemical coefficients and the loads of pollution sources in the form of triangular fuzzy numbers and then successfully combined a two-dimensional finite algorithm with fuzzy logic analysis for solution of the advection-dispersion equation for ten different water quality variables (chlorophyll-a, coliforms, organic nitrogen, ammonia nitrogen, nitrite nitrogen, nitrate nitrogen, organic phosphorus, inorganic phosphorus, biochemical oxygen demand and dissolved oxygen shortage) in the Gulf of Thermaikos (Northern Greece). Application of fuzzy modeling enabled representation of imprecise data and production of imprecise output in the form of fuzzy numbers, with minimal input data requirements and without the need of a large number of computations. The technique yielded the most confident value of each quality variable, and was very efficient for the determination of the extreme values of these quantities.

Kuncheva et al. [60] implemented a fuzzy model of 10 heavy metal (Hg, C, Cr, Cu, Ni, Pb, Zn, As, Mn and Fe) loadings in

Liverpool bay. Each metal concentration was associated with a fuzzy set “polluted”, defined over the set of 70 sampling sites. The higher concentration was associated with higher degree of membership of the site and moreover six different fuzzy aggregation techniques were used. The results visualization (geographical scatterplots of metal loadings) showed that product aggregation was most indicative for the locations of the disposal grounds, mean aggregation reflected sediment movement in the bay well and maximum aggregation indicated all highly polluted sites. Without fuzzy modeling based on 20 km² sampling grid the visualization and interpretation of the results could be more complicated.

The application of fuzzy systems in case of sea water is not only limited to chemical analysis. Wave prediction is one of the most important issues in coastal and ocean engineering studies. Kazeminezhad et al. [61] investigated the adaptive-network-based fuzzy inference system (ANFIS) and coastal engineering manual (CEM) methods for predicting wave parameters. The data set comprises of fetch-limited wave data and over water wind data gathered from deep-water location in Lake Ontario (Canada). As was previously mentioned, the crucial point in case of modeling and forecasting is the ability of complete time series data sets evaluation during model rules creation. The researchers used two independent time series data sets: one to develop the ANFIS models as wave predictor models (wave data was collected for 20 min at 1 h intervals at a sampling frequency of 2.56 Hz while wind data for 8 min at 1 h intervals, at a frequency of 1.88 Hz—both variables were determined through 8 months) and the other to test the developed ANFIS model and also the CEM method. Results indicated that ANFIS outperforms the CEM method in terms of prediction capability as the scatter index of predictions of ANFIS is less than that of CEM method. In particular, the CEM method overestimates the significant wave height and underestimates the peak spectral period, while ANFIS results in more accurate predictions.

3.2. Rivers and streams

Various fuzzy approaches such as fuzzy cluster analysis, principal components analysis or fuzzy recognition are being used to assess the environmental waters quality by testing the mathematical models and computer programs. Fuzzy cluster analysis and fuzzy recognition were successfully used by Chen [62] to model a large set of data from the Min River (China). The efficiency of the robust fuzzy principal components analysis (FPCA) algorithm on a data set concerning the water quality of the Danube River for a period of 11 consecutive years were described by Sârbu and Pop [63]. In contrary to requirements for forecasting or modeling the authors successfully performed chemometric analyses basing on monthly average values of 19 water parameters only (pH, chemical oxygen, demand-COD, equivalent oxygen, Ca²⁺, Mg²⁺, Fe²⁺, Cl⁻, SO₄²⁻, HCO₃⁻, NO₂⁻, NO₃⁻, PO₄³⁻, NH₃, NH₄⁺, alkalinity, hardness, dry residue, and suspension). In case of classical PCA two component model explained only 39.8% of the total variance while the two major components extracted by FPCA (“factor of alkalinity-hardness” and “factor of ammonium salts”) explained 91.7% of

the total variance. FPCA method brings better results mainly because it is more compressible than classical PCA.

In many cases proper identification of water quality conditions in a river system based on limited observations is an essential task for meeting the goals of environmental management. Chang et al. [64] undertook the challenge of identification river water quality using three fuzzy synthetic evaluation techniques to classification of water quality conditions in comparison to the outputs generated by conventional procedure such as the Water Quality Index. Basing on discrete data set (pH, dissolved oxygen, biochemical oxygen, suspended solids and $\text{NH}_3\text{-N}$) collected at seven mid- and down-stream sampling stations they demonstrated the technique's application potential for Tseng-Wen River system in Taiwan. Chang et al. concluded that without proper consideration of the fuzziness embedded in the input and output data, the classification could become pessimistic due to the inherent uncertainties. However, in this case, more accurate information was obtained by using fuzzy information intensity and defuzzification. The study proved a highly usefulness of developed fuzzy synthetic evaluation approach described in verification of water quality conditions for the Total Maximum Daily Load (TMDL) program for constructing an effective water quality management strategy.

Lee et al. [65] examined the applicability of the fuzzy interference mechanism to develop a fuzzy expert system (ES) for proper determination of water quality classification system (WQCS) from uncertain and imprecise ecological information. Lee et al. were successful because they generated 30 fuzzy rules for WQCS precisely. The comparison of performance of the fuzzy expert system and the conventional expert system for the determination of class, toxicity, and rarity shared that the smoothly varying curves of WQCS determination by the fuzzy expert system represented real-world experience more realistically than stepwise curves from the conventional ES.

The proper definition of fuzzy rules was crucial for the description of elements of the hydrological cycle such as infiltration, surface runoff and unsaturated flow in research presented by Bárdossy [66]. Hierarchical fuzzy rule systems were derived under consideration of space-time inhomogenities. The authors considered with the help of fuzzy rules the movement of soil moisture in a heterogeneous soil column and the surface runoff. The study established a few advantages of fuzzy rule-based models application, one of which was the ease of model coupling, for examples, a model of a flow in porous media may be coupled with a bacteriological growth model. Another advantage is that fewer parameters are required in this approach than in the classical models, and these models run much faster giving good results.

An interactive fuzzy approach was applied by Lee and Chang [67] to develop a water quality management plan in a river basin for solving multi-objective optimization problems (involving vague and imprecise information related to data, model formulation and the decision maker's preferences). Incorporating economic and environmental factors (river water quality, assimilative capacity and wastewater treatment cost) authors demonstrated the capability of the fuzzy interactive multi-objective optimization approach. Basing on discrete data collected at a

sampling frequency of four times a year they established that allowable pollution loading presented as BOD_5/day (biochemical oxygen demand) [kg] may be identified according to the interactive fuzzy approach.

3.3. Flood forecasting

The fuzzy approach is often used to flood forecasting. The fuzzy set theory assisted by genetic algorithm as a methodology for the treatment of precipitation uncertainty in rainfall-runoff-routing modeling was presented by Maskey et al. [52] and Nayak et al. [53]. Basing on continuous (cumulative for every 3 h) precipitation data collected at one sampling point Maskey showed the great potential of the fuzzy extension principle combined with a genetic algorithm for the propagation of uncertainty. He used the random disaggregation of precipitation into sub-periods to take into account uncertainty due to the unknown temporal distribution of the precipitation. He suggested that using space- and time-averaged precipitation over the catchment may lead to erroneous forecasts. In the contrary, enlargement of spatial sampling area connected with shorten time interval of precipitation cumulation should lead to more precise forecasting. Nayak determined the most appropriate set of input variables and on this basis it was established that the river flow of Narmada behaves more like an autoregressive process. As the precipitation is weighted only a little by the model, the last time-steps of measured runoff were dominating the forecast. Thus, a forecast based on expected rainfall became very inaccurate. Although good results for one-step-ahead forecasts were received, the accuracy deteriorates as the lead time increases. Using the one-step-ahead forecast model recursively to predict flows at higher lead time, however, produces better results as opposed to different independent fuzzy models to forecast flows at various lead times.

An artificial neural network was successfully applied as a prediction tool to forecast water level at Dhaka (Bangladesh), for up to seven lead days in advance, with a high accuracy level by Liong et al. [68]. In addition, high accuracy degree was accompanied with a very short computational time, that made NN a desirable advance warning forecasting tool. A sensitivity analysis was also performed to retain only the most sensitive gauging stations for the Dhaka station. The resulting reduction of gauging stations negligibly affected the prediction accuracy level. Moreover, the work concerning the possibility of measurement failure in any of the gauging stations during the critical flow level at Dhaka required prediction tools which can interpret linguistic assessment of flow levels. A fuzzy logic approach was introduced with a few membership functions, depending on necessity, for the input stations with five membership functions for the output station. Membership functions for each station were derived from their respective water level frequency distributions, after the Kohonen neural network was used to group the data into clusters. The proposed approach in deriving membership function showed a number of advances over another commonly used approach. As the major important advantage it should be emphasized that comparing prediction results with measured data, the obtained prediction accuracy level was comparable with that of the data driven neural network approach.

Many types of ecological data are qualitative, characterized by discrete categories and, hence, are difficult to incorporate into classification schemes or forecasting models designed to produce a numerical results. Mahabir et al. [69] used fuzzy variables in order to organize knowledge that is expressed linguistically into a formal analysis to forecast seasonal runoff. For example, high snow pack, average snow pack and low snow pack became variables. Applying fuzzy logic, a water supply forecast was created aiming the classification of potential runoff into three forecast zones: low, average and high. Spring runoff forecasts from the fuzzy expert systems were found to be considerably more reliable than the regression models in forecasting the appropriate runoff zone, especially in terms of identifying low or average runoff years. Based on the modeling results in these two basins, it was concluded that fuzzy logic has a promising potential for providing reliable water supply forecasts.

3.4. Ground water

A fuzzy knowledge-based decision support system for ground water pollution risk evaluation was presented by Uricchio et al. [70]. The combined value was used consisting of both intrinsic vulnerability of a specific local aquifer, obtained by implementing a parametric managerial model (SINTACS), and a degree of hazard value based on specific human activities. To overcome incomplete information an algorithmic and a qualitative approach was applied, basing on expert judgment incorporated into the system's knowledge base. The decision support system was based on the uncertainty of the environmental domain using fuzzy logic and evaluating the reliability of the results due to information availability.

The framework for evaluation of nitrate control strategies that use spatially variable nitrogen input in the presence of imprecise information was presented by Wold et al. [71]. In this study three different farming practices were examined to predict their effects on nitrate leaching reduction: first - conventional application in which fertilizer is applied at a uniform rate over the field, second - variable rate application (VRA) in which fertilizer is applied in a spatially variable pattern according to demand over the entire model area and third - a well headprotection area (WHPA) in which fertilizer is applied in a spatially variable pattern according to demand in the vicinity of the water supply well. To consider uncertainty stemming from the unsaturated zone model output, in addition to aquifer parameters, a new groundwater modeling technique was developed in which fuzzy set theory was combined with finite-difference modeling methods. The ground water model incorporated imprecise parameters such as transmissivity into the modeling process through the use of fuzzy set theory. Imprecision was encoded directly into the finite-difference equations using fuzzy numbers as input, and level-set operations combined with non-linear optimization were used to solve the system equation. The study established that transient fuzzy groundwater flow model with pumpage indicates that the imprecision in hydraulic heads increases with time, but decreases with the distance from the well. VRA over large areas was the most effective method to reduce groundwater pollution, while WHPA could also reduce the non-point source pollution

of groundwater to a great extent with less cost. The authors concluded that fuzzy modeling techniques provide a realistic methods to handle the imprecise data in groundwater flow and transport simulation processes.

Many environmental concerns direct the attention of hydrologists to the problem of infiltration and water movement in the unsaturated zones. Bárdossy et al. [56] used a fuzzy approach for multidimensional modeling of water movement in the soil matrix. The study emphasize low sensitivity of the models to parameters change, high stability and no mass balance errors what is particularly important for hydrological situations with very dry soil and large sudden changes in soil moisture, such as thunderstorms (i.e., on a dry soil). The study established that fuzzy models can be extended with additional components of the water dynamics in the subsurface such as water extraction by plant roots, or bypass-flow in a macroporous soils.

In the paper of Khadam and Kaluarachchi [72] the multi-criteria decision analysis with probabilistic risk assessment for the management of polluted ground water is presented. The authors explored three potential approaches for alternative ranking: a structured explicit decision analysis, a heuristic approach of the order of criteria importance and a fuzzy logic approach based on fuzzy dominance and similarity analysis.

However, not every fuzzy logic approach using trials is successful. Sahoo et al. [73] implemented an adaptive neural network-based fuzzy interference system to pesticide prediction in ground water in domestic wells. In this case the authors did not obtain satisfactory results and probable reason for the failure of ANFIS could be attributed to fuzzy interference system, which was unable to make proper fuzzy rules from the training data sets. The reason of such failure may lie in a wrong selection of training data set. The reliable training data set is of great importance in case of supervised chemometric techniques.

3.5. Spring water

Various fuzzy clustering algorithms were successfully applied in the study of several German and Romanian natural spring waters using discrete data obtained from samples collected from spatial dispersed sampling sites covering, for example, a large percentage of the Romanian natural spring waters. The characteristic clustering technique produced fuzzy partitions of the spring water properties involved and thus proved to be a useful tool for studying (dis)similarities between different ions (i.e., speciation). Using cross-classification algorithm the authors obtained only a fuzzy partition of the mineral waters, but also a fuzzy partition of their chemical characteristics. This way it was possible to identify which ions and other physico-chemical features are responsible for the similarities or differences observed between various groups of mineral waters [74].

3.6. Drinking water

Interpreting water quality data routinely generated for control and monitoring purposes (classification) in water distribution system is a complex task for utility managers. In most cases

data for diverse water quality indicators (physico-chemical and microbiological) are generated at diversified times and locations in the distribution system. To simplify and improve the understanding and the interpretation of drinking water quality in the distribution system Sadiq et al. [75–77] proposed efficient risk-based fuzzy synthetic evaluation technique for aggregating effects of disinfection by-products found in drinking water. Initially, membership function for cancer and non-cancer risk associated with trihalomethanes and haloacetic acids were used to establish the fuzzy evaluation matrices. Subsequently, weighted evaluation matrices for both types of risks were established by performing cross products on the weighted vectors (founded on the analytic hierarchy process) and the fuzzy evaluation matrices. In the final stage, the weighted evaluation matrices of cancer and non-cancer risk were aggregated to determine the final risk rating. Proposed procedure can successfully be applied by water managers (for selecting water treatment procedures according to disinfection by-products (DBPs) risk reduction), government managers responsible for regulations and environmental epidemiologists (to estimate human exposure to DBPs in drinking water for cancer and non-cancer epidemiological studies).

3.7. Wastewater

The process of wastewater biological or chemical treatment is subjected to wide fluctuations, both in flows and organic loadings, which often result in performance degradation or even plant's failure. The successful management of this critical situations involves forecast and solution of a complex control design, assuming that on-line information concerning the quality of the plant influent is available and that the plant is equipped with flow control devices to alter the flow patterns. There is a necessity of implementation of an efficient control techniques. Examples of fuzzy control of disturbances in a wastewater treatment process implementation are known [78–86]. A fast predicting neural fuzzy model for high-rate anaerobic wastewater treatment systems was presented in work of Tay and Zhang [79]. The Tay's group obtained good results because the model was able to predict the response (volumetric methane production, effluent total organic carbon and volatile fatty acids) of the system in the presence of organic loading, hydraulic and alkalinity loading rates.

Other expert system for monitoring and diagnosis of anaerobic hybrid pilot wastewater treatment plants was also successfully implemented by Puñal et al. [80,81]. A wide set of operational conditions were applied, working at different chemical oxygen demand, organic loading rates and hydraulic residence time. The expert system successfully identified two frequent anomalous situations, hydraulic and organic overloads. In both cases, the ES delivered valuable recommendations and, after following them, the anaerobic wastewater treatment recovered its normal state in a short period of time.

The state and control of overloads in the anaerobic wastewater treatment plant (AWTP) using fuzzy logic was under interest of Murnleitner et al. [82]. System based on fuzzy logic principles was designed to handle very strong fluctuations in the concentration of the substrate and the volumetric loading rate. Hydrogen concentration together with methane concentration,

gas production rate, pH and the filling level of the acidification buffer tank were used as input variables for the fuzzy logic system. The manipulated variables were the flow rate from the acidification buffer tank into the methane reactor, the temperature and pH of both reactors, the circulation rate of the fixed bed reactor, back flow from the methane reactor into the acidification, and the control of the feed into the acidification buffer tank. The authors performed the research in the two-stage laboratory scale AWTP and concluded that treatment plant overload state could be recognized by the measurement of hydrogen, methane, pH, and the gas rate, whereof economical sensors are available. Very strong fluctuations in the loading were handled automatically, even a restart of the feeding with a very high chemical oxygen demand concentration (>100 g/L) after several days of stand-by was possible.

An intelligent control system for wastewater treatment processes has been developed and successfully applied to full-scale, high-rate, activated sludge process control by Ohtsuki et al. [83]. Other authors [84–86] designed, simulated and evaluated a fuzzy control system in an activated sludge wastewater treatment plant. The study presented by Kalker et al. established that the developed high-level fuzzy controller of aeration performs better than two conventional controllers in terms of energy consumption and, at the same time, results in a slightly better effluent quality.

In process control, fuzzy controllers can be applied to almost all kinds of processes but their nature makes these systems suitable for application in controlling time-varying, ill-defined and non-linear systems. One of these systems is aeration in biological wastewater treatment process. The advantages of aeration fuzzy logic-based control system (AFLBS) in comparison to two ordinary aeration process controllers have been presented by Ferrer et al. [87]. Three controllers were compared taking into account economic saving and stability in the dissolved oxygen concentration around the set point. Stability was compared considering two parameters: average deviation and instantaneous average dissolved oxygen concentration. The authors proved that significant economic savings can be obtained while using AFLBS controllers. In fact, 40% saving of energy was obtained over the conventional on/off aeration control system. Stability was greatly improved analogically with the use of a fuzzy controller.

4. Land

One of the major interests in soil analysis is the integrated evaluation of soil properties, which might be indicators of soil quality (classification). In this section, researches dealing with application of environmetrics based on the principles of fuzzy logic for chemical characteristics of the soil pollution are reviewed.

4.1. Soil

Soil information is essential to any terrestrial ecological modeling and management activity. Polygon soil maps produced from surveys are in the most cases the major source of information on the spatial distribution of soil properties for a

variety of land analysis and management activity. However, there are some problems (limited coverage at a fixed scale, locational errors, attribute errors, insufficient information in the mapping units) regarding the use of current soil maps in geographic analysis and especially in geographic information system (GIS). The methodology of combination of fuzzy logic with GIS and expert system development techniques to infer soil series from environmental condition was presented by Zhu et al. [88]. The study presents preliminary results from the methodology using a limited set of environmental variables for an experimental watershed in Montana. The methodology for every point in the area produced a soil similarity vector (SSV) showing the similarity of the soil at the point to a prescribed set of soil series. The major founding of the study was that the SSV produced from methodology can be used to infer local soil properties at values intermediate to the typical or central values assigned to each possible series. Another approaches to soil classification were presented by others [89–94]. Fuzzy classification of JERS-1 radar satellite image was developed for soil salinity mapping by Metternicht [89]. The study shows that fuzzy classification of FERS-1 SAR data provides reliable detection with overall accuracy equal to 81% of areas degraded by salinity-alkalinity processes. Fuzzy logic application covers many examples of analytical assessment of soil degradation and pollution. The impact of a phosphatic fertilizer plant on the adjacent environment was examined by Szczepaniak et al. [90]. Selected rare earth elements, heavy metals and metalloids (Na, Mg, Al, K, Sc, Ca, Cr, Ti, V, Mn, Ni, Fe, Co, Zn, Se, As, Br, Sr, Rb, Mo, Ag, Sb, I, Ba, Cs, La, Ce, Eu, Sm, Tb, Dy, Yb, Hf, Ta, W, Th and U) were determined in substrates and products, waste by-product, and grass and soil samples. Two fuzzy principal components analysis methods for robust estimation of principal components were applied and compared with classical PCA. The study established the degree of pollution from elements in the environment extending for 1 km along southerly and easterly directions from fertilizer plant. Analysis of soil samples proved to be more useful than grass samples for investigation of pollution, due to soil ability to accumulate elements through years of exposure, while grass assimilates elements during a 1-year period only. The obtained results confirmed that classical PCA is sensitive to outliers and fuzzy PCA is not that sensitive, which is extremely important in case of analyzing diversified environmental data. Important founding was that fuzziness does not change the natural relation of domestic data, and moreover Co and Zn which occur naturally in living organisms such as grass, were less distanced from one to another in two- or three-dimensional space in case of fuzzy robust principal analysis.

Sârbu et al. [91] used fuzzy hierarchical characteristics clustering (FHiCC) and fuzzy horizontal characteristics clustering (FHoCC) of the 35 grass and soil samples based on the 37 chemical element concentrations to observe similarities and dissimilarities between grass and soil samples. He was successful due to implementation of a new approach named fuzzy cross-classification algorithm (FHCsC) allowed the qualitative and quantitative identification of the characteristics (element concentrations) responsible for the observed similarities and dissimilarities between the grass and soil samples. Fuzzy clustering

and its influence on ranking using the technique of Hasse diagrams was evaluated by Pudenz et al. [92]. The authors compared 59 ecosystems in Germany, Baden Württemberg with respect to their pollution with Pb, Zn, Cd and S. The possible relationships between geochemistry of basal till and chemistry of surface soil at forested sites in Finland were evaluated by Lahdenperä et al. [93]. On the basis of concentrations of several elements in the organic and mineral soil layer analyzed with use of fuzzy clustering the authors proved that the correlation between element concentrations in basal till and the two uppermost layers of mineral soil was better within areas of distinct till geochemistry. Surface soil chemical variables were clearly better in discriminating fertility classes of forest sites than element concentrations in basal till.

Markus and McBratney [94] investigated the occurrence of Pb, Zn, Cu, and Cd in the topsoil of an inner-city suburb of Sydney, Australia. The total heavy metal concentrations in the topsoil of Glebe were determined along with their spatial distribution. They were successful due to sampling procedure. Stratified random sampling was conducted within 1-ha square areas taking a samples at 1 m separation from each stratum as a means to investigating spatial variation. In the next step, using fuzzy clustering five groups of large high-risk areas characterized by increasing contamination were divided. Soil disturbance and distance from road explained 24% of the variation in total Pb concentration, 15% in total Zn and Cu concentrations, and 13% in total Cd concentration.

The unsuitability of formal risk analysis methods and various sources of incompleteness, uncertainty and vagueness of the whole research field motivate the use of fuzzy methods, and in particular the use of fuzzy classification providing a rough ranking method. Many authors implemented fuzzy classification of sites suspected of being polluted [95]. The status of combined heavy metal (Cd, Cr, Cu, Pb, Zn, Hg, As) and organo-chlorine pesticides (HCH, DDT) pollution in soil was investigated using fuzzy comprehensive assessment by Shen et al. [96]. The soil pollutants were selected as assessment parameters to form an assessment factor set based on soil monitoring data in the Taihu Lake region. An assessment criteria set was established according to National Soil Environmental Quality Standard. Fuzzy comprehensive assessment showed that the overall soil quality could be categorized as class I (all values in mg/kg: $Cd \leq 0.20$, $Cr \leq 90$, $Cu \leq 35$, $Pb \leq 35$, $Zn \leq 100$, $Hg \leq 0.15$, $As \leq 15$, $DDT \leq 0.05$, $HCH \leq 0.05$), nevertheless, the high coefficients of variation for levels of DDT, Cd and Hg indicated the existence of some point-source pollution. The obtained results confirmed that on account of the imprecision of soil environmental measurements, the fuzzy comprehensive assessment method provides a scientific basis for analyzing and evaluating the environmental quality of soil.

Fuzzy logic algorithm for runoff-induced sediment transport from bare soil surfaces was applied by Tayfur et al. [97]. The objective of the study was to develop a fuzzy logic algorithm to predict runoff-driven seducements loads from bare soil surfaces, and compare the performance of the fuzzy model with that of artificial neural networks and physics-based models. The

sediment load predicted by the fuzzy model was in satisfactory agreement with the measured sediment load data.

5. Conclusions

Basing on reviewed papers concerning environmental components (air/water/soil aspects) it is clear that chemometrics based on the principles of fuzzy logic is being introduced successfully in various fields of chemistry and environmental studies. Moreover, three major objectives could be indicated: modeling, forecasting and classification. All of them can be accomplished using techniques mentioned above. Some of discussed techniques have been developed strictly for environmental applications and characterized by useful requirements given below. For modeling and forecasting (using neural networks or time series analysis) a fundamental task is to extract non-valid data from the learning pattern (forecasting) or from the data set used in a stage of the model rules creation. Temporal data recorded continuously at high frequency are recommended for this purposes. Classification performed by factorial techniques (i.e., FPCA) or cluster analysis based on fuzzy logic principles brings satisfactory results even while using district, non-temporal data sets.

Methods based on fuzzy sets usually rely on a judgment as to the degree of uncertainty or fuzziness associated with the output of an environmental system or model. However, they can reduce significantly the computation involved with complex environmental systems. These methods may be also used to treat concepts not defined numerically or find applications to many decision-making processes which involve seemingly incompatible variables from the social and economic science [98]. It seems obvious that the field of chemometric approaches presented in this paper continues to evolve. New tools will be developed and deployed as new data analysis challenges and posed to the environmetrics community.

References

- [1] P.K. Hopke, *Anal. Chim. Acta* 500 (2003) 365.
- [2] D.L. Massart, B. Vandeginste, L. Buydens, S. De Jong, *Handbook of Chemometrics and Qualimetrics*, vol. 20 A, Elsevier, 1998.
- [3] L. Zadeh, *Info. Ctl.* 8 (1965) 338.
- [4] G.J. Klir, B. Yuan, *Fuzzy Sets and Fuzzy Logic: Theory and Applications*, Prentice Hall, New York, USA, 1995.
- [5] P. Hájek, *Metamathematics of Fuzzy Logic*, Kluwer Academic Publishers, Boston, USA, 1998.
- [6] J.F. Baldwin, *Fuzzy Logic and Fuzzy Reasoning*, Wiley, Chichester, UK, 1994.
- [7] T.J. Ross, *Fuzzy Logic with Engineering Applications*, Wiley, New York, USA, 2004.
- [8] J.J. Buckley, E. Eslami, *An Introduction to Fuzzy Logic and Fuzzy Sets*, Physica Verlag, Heidelberg, Germany, 2002.
- [9] L.A. Zadeh, *Info. Ctl.* 12 (1968) 94.
- [10] A. Astel, J. Mazerski, Ż. Polkowska, J. Namieśnik, *Adv. Env. Res.* 8 (2004) 337.
- [11] <http://www.fuzzy-logic.com/Ch1.htm>.
- [12] A. Salski, *Ecol. Inform.* 1 (2002) 3.
- [13] H.M.G. Van der Werf, Ch. Zimmer, *Chemosphere* 36 (1998) 2225.
- [14] B. González, B. Adenso-Díaz, P.L. González-Torre, *Resour. Conserv. Recycl.* 37 (2002) 61.
- [15] R. Sadiq, T. Husain, *Environ. Model. Soft.* 20 (2005) 33.
- [16] L.A. Andriantiatsaholiniaina, V.S. Kouikoglu, Y.A. Phillis, *Ecol. Econ.* 48 (2004) 149.
- [17] T. Prato, *Ecol. Model.* 187 (2005) 361.
- [18] M. Enea, G. Salemi, *Ecol. Model.* 135 (2001) 131.
- [19] Y.A. Phillis, L.A. Andriantiatsaholiniaina, *Ecol. Econ.* 37 (2001) 435.
- [20] A. Parashar, R. Palwal, P. Rambabu, *Environ. Impact. Assess. Rev.* 17 (1997) 427.
- [21] G.A. Mendoza, R. Prabhu, *Ecol. Indic.* 3 (2003) 227.
- [22] W. Silvert, *Ecol. Model.* 96 (1997) 1.
- [23] A.M.O. Mohamed, K. Côté, *Waste Manag.* 19 (1999) 519.
- [24] M. Poch, J. Comas, I. Rodrigueaz-Roda, M. Sánchez-Marré, U. Cortés, *Environ. Model. Soft.* 19 (2004) 857.
- [25] J. Mysiak, C. Giupponi, P. Rosato, *Environ. Model. Soft.* 20 (2005) 203.
- [26] G. Onkal-Engin, I. Demir, H. Hiz, *Atmos. Environ.* 38 (2004) 3809.
- [27] F.I. Khan, R. Sadiq, *Environ. Monit. Assess.* 105 (2005) 261.
- [28] O.M. Pokrovsky, R.H.F. Kwok, C.N. Ng, *Comput. Geosci.* 28 (2002) 119.
- [29] G. Nunnari, A.F.M. Nucifora, C. Randieri, *Ecol. Model.* 111 (1998) 187.
- [30] G. Nunnari, S. Dorling, U. Schlink, G. Cawley, R. Foxall, T. Chatterton, *Environ. Model. Soft.* 19 (2004) 887.
- [31] D. Romano, A. Bernetti, R. De Lauretis, *Environ. Inter.* 30 (2004) 1099.
- [32] T.J. Sullivan, M.C. Saunders, K.A. Tonnessen, B.L. Nash, B.J. Miller, *Knowl. Based Syst.* 18 (2005) 55.
- [33] V. Simeonov, H. Puxbaum, S. Tsakovski, C. Sârbu, M. Kalina, *Environmetrics* 10 (1999) 37.
- [34] M.C.V. Ramirez, H.F. de Campos Velho, N.J. Ferreira, *J. Hydrolog.* 301 (2005) 146.
- [35] C.L. Chang, S.L. Lo, S.L. Yu, *J. Hydrolog.* 314 (2005) 92.
- [36] N. Peton, G. Dray, D. Pearson, M. Mesbah, B. Vuillot, *Environ. Model. Soft.* 15 (2000) 647.
- [37] S.A. Abdul-Wahab, Ch. S. Bakheit, S.M. Al-Alawi, *Environ. Model. Soft.* 20 (2005) 1263.
- [38] S.A. Abdul-Wahab, S.M. Al-Alawi, *Environ. Model. Soft.* 17 (2002) 219.
- [39] S.A. Abdul-Wahab, W. Bouhama, H. Ettouney, B. Sowrby, B.D. Crittenden, *Environ. Sci. Pollut. Res.* 3 (1996) 195.
- [40] J.S. Heo, D.S. Kim, *Sci. Total Environ.* 325 (2004) 221.
- [41] R. Mintz, B.R. Young, W.Y. Svrcek, *Comput. Chem. Eng.* 29 (2005) 2049.
- [42] H. Van Malderen, S. Hoornaert, R. Van Grieken, *Environ. Sci. Technol.* 30 (1996) 489.
- [43] W. Jambers, A. Smekens, R. Van Grieken, V. Shevchenko, V. Gordeev, *Colloids Surf. A: Physicochem. Eng. Aspects* 120 (1997) 61.
- [44] A. Held, K.P. Hinz, A. Trimborn, B. Spengler, O. Klemm, *Aerosol Sci.* 33 (2002) 581.
- [45] B. Treiger, I. Bondarenko, H. Van Malderen, R. Van Grieken, *Anal. Chim. Acta* 317 (1995) 33.
- [46] N.B. Chang, G.G. Weu, Y.L. Chen, *Eur. J. Oper. Res.* 99 (1997) 289.
- [47] A.P. Raj, D.N. Kumar, *Fuzzy Sets Syst.* 100 (1998) 89.
- [48] A.X. Zhu, D.S. Mackay, *J. Hydrol.* 248 (2001) 54.
- [49] E.C. Ozekan, L. Duckstein, *J. Hydrol.* 253 (2001) 41–68.
- [50] P.S. Yu, T.C. Yang, *J. Hydrol.* 238 (2000) 1–14.
- [51] T. Wagener, H.S. Wheater, *J. Hydrol.* 320 (2006) 132.
- [52] S. Maskey, V. Guinot, R.K. Price, *Adv. Water Res.* 27 (2004) 889.
- [53] P.C. Nayak, K.P. Sudheer, K.S. Ramasastri, *Hydrol. Proc.* 19 (2005) 955.
- [54] L. Xiong, Y. Asaad, Y. Shamseldin, K.M. O'Connor, *J. Hydrol.* 245 (2001) 196.
- [55] R.S. Lu, S.L. Lo, *Water Res.* 36 (2002) 2264.
- [56] A. Bárdossy, A. Bronstert, B. Merz, *Adv. Water Resour.* 18 (1995) 237.
- [57] C. Dou, W. Woldt, I. Bogardi, M. Dahab, *J. Contam. Hydrol.* 27 (1997) 107.
- [58] C. Dou, W. Woldt, I. Bogardi, *J. Hydrol.* 220 (1999) 74.
- [59] H. Mpimpas, P. Anagnostopoulos, J. Ganoulis, *Ecol. Model.* 142 (2001) 91.
- [60] L.I. Kuncheva, J. Wrench, L.C. Jain, A.S. Al-Zaidan, *Environ. Model. Soft.* 15 (2000) 161.
- [61] M.H. Kazeminezhad, A. Etemad-Shahidi, S.J. Mousavi, *Ocean Eng.* 32 (2005) 1709.
- [62] G.N. Chen, *Chim. Acta* 271 (1993) 115.
- [63] C. Sârbu, H.P. Pop, *Talanta* 65 (2005) 1215.
- [64] N.B. Chang, H.W. Chen, S.K. Ning, *J. Environ. Manag.* 63 (2001) 293.

- [65] H.K. Lee, K.D. Oh, D.H. Park, J.H. Jung, S.J. Yoon, *Water Sci. Tech.* 36 (1997) 199.
- [66] A. Bárdossy, *Ecol. Model.* 85 (1996) 59.
- [67] C.S. Lee, S.P. Chang, *Water Res.* 39 (2005) 21.
- [68] S.Y. Liong, W.H. Lim, T. Kojiri, T. Hori, *Hydrol. Proc.* 14 (2000) 431.
- [69] C. Mahabir, F.E. Hicks, R. Fayek, *Hydrol. Proc.* 17 (2003) 3749.
- [70] V.F. Uricchio, R. Giordano, N. Lopez, *J. Environ. Manag.* 73 (2004) 189.
- [71] W. Wold, M. Dahab, I. Bogardi, C. Dou, *Water Sci. Tech.* 33 (1996) 249.
- [72] I.M. Khadam, J.J. Kaluarachchi, *Impact Assess. Rev.* 23 (2003) 683.
- [73] G.B. Sahoo, C. Ray, H.F. Wade, *Ecol. Model.* 183 (2005) 29.
- [74] C. Sârbu, H.W. Zwanziger, *Anal. Lett.* 34 (2001) 1541.
- [75] R. Sadiq, M.J. Rodriguez, *J. Environ. Manag.* 73 (2004) 1.
- [76] R. Sadiq, M.J. Rodriguez, *Sci. Total Environ.* 321 (2004) 21.
- [77] R. Sadiq, M.J. Rodriguez, *Chemosphere* 59 (2005) 177.
- [78] A. Müller, S. Marsili-Libelli, A. Aivasidis, T. Lloyd, S. Kroner, C. Wandrey, *Water Res.* 31 (1997) 3157.
- [79] J.H. Tay, X. Zhang, *Water Res.* 34 (2000) 2849.
- [80] A. Puñal, A. Lorenzo, E. Roca, C. Hernández, J.M. Lema, *Water Sci. Tech.* 40 (1999) 237.
- [81] A. Puñal, E. Roca, J.M. Lema, *Water Res.* 36 (2002) 2656.
- [82] E. Murnleitner, T.M. Becker, A. Deglado, *Water Res.* 36 (2002) 201.
- [83] T. Ohtsuki, T. Kawazoe, T. Masui, *Water Sci. Tech.* 37 (1998) 77.
- [84] T.J.J. Kalker, C.P. Van Goor, P.J. Roeleveld, M.F. Ruland, R. Babuška, *Water Sci. Tech.* 39 (1999) 71.
- [85] P. Teppola, S.P. Mujunen, P. Minkkinen, *Chem. Intel. Lab. Syst.* 41 (1998) 95.
- [86] P. Teppola, P. Minkkinen, *J. Chemom.* 13 (1999) 445.
- [87] J. Ferrer, M.A. Rodrigo, A. Seco, J.M. Peña-roja, *Water Sci. Tech.* 38 (1998) 209.
- [88] A.X. Zhu, L.E. Band, B. Dutto, T.J. Nimlos, *Ecol. Model.* 90 (1996) 123.
- [89] G.I. Metternicht, *Ecol. Model.* 111 (1998) 61.
- [90] K. Szczepaniak, C. Sârbu, A. Astel, E. Raińska, M. Biziuk, O. Culicov, M.V. Frontasyeva, *CEJCh* 4 (2006) 29.
- [91] C. Sârbu, K. Szczepaniak, A. Astel, M. Biziuk, *Chem. Ecol. Eng.* 5–6 (2004) 587.
- [92] S. Pudenz, R. Brüggemann, B. Luther, A. Kaune, K. Kreimes, *Chemosphere* 40 (2000) 1373.
- [93] A.M. Lahdenperä, P. Tamminen, T. Tarvainen, *Appl. Geochem.* 16 (2001) 123.
- [94] J.A. Markus, A.B. McBratney, *Aust. J. Soil Res.* 34 (1996) 453.
- [95] K. Lehn, K.H. Temme, *Ecol. Model.* 85 (1996) 51.
- [96] G. Shen, Y. Lu, M. Wang, Y. Sun, *J. Environ. Manag.* 76 (2005) 355.
- [97] G. Tayfur, S. Ozdemir, V.P. Singh, *Adv. Water Resour.* 26 (2003) 1249.
- [98] B. Fisher, *Atmos. Environ.* 37 (2003) 1865.

Solid phase extraction and preconcentration of uranium(VI) and thorium(IV) on Duolite XAD761 prior to their inductively coupled plasma mass spectrometric determination[☆]

Funda Armagan Aydin^{a,b}, Mustafa Soylak^{a,*}

^a *Erciyes University, Faculty of Art and Science, Department of Chemistry, 38039 Kayseri, Turkey*

^b *General Directorate of State Hydraulic Works, Technical Research and Quality, Control Department, 06100 Ankara, Turkey*

Received 9 July 2006; received in revised form 3 October 2006; accepted 5 October 2006

Available online 28 November 2006

Abstract

A simple and effective method is presented for the separation and preconcentration of thorium(IV) and uranium(VI) by solid phase extraction on Duolite XAD761 adsorption resin. Thorium(IV) and uranium(VI) 9-phenyl-3-fluorone chelates are formed and adsorbed onto the Duolite XAD761. Thorium(IV) and uranium(VI) are quantitatively eluted with 2 mol L⁻¹ HCl and determined by inductively coupled plasma-mass spectrometry (ICP-MS). The influences of analytical parameters including pH, amount of reagents, amount of Duolite XAD761 and sample volume, etc. were investigated on the recovery of analyte ions. The interference of a large number of anions and cations has been studied and the optimized conditions developed have been utilized for the trace determination of uranium and thorium. A preconcentration factor of 30 for uranium and thorium was achieved. The relative standard deviation ($N=10$) was 2.3% for uranium and 4.5% for thorium ions for 10 replicate determinations in the solution containing 0.5 µg of uranium and thorium. The three sigma detection limits ($N=15$) for thorium(IV) and uranium(VI) ions were found to be 4.5 and 6.3 ng L⁻¹, respectively. The developed solid phase extraction method was successively utilized for the determination of traces thorium(IV) and uranium(VI) in environmental samples by ICP-MS.

© 2006 Elsevier B.V. All rights reserved.

Keywords: Thorium(IV); Uranium(VI); Duolite XAD761; Solid phase extraction; Environmental samples; ICP-MS

1. Introduction

Uranium and thorium find extensive application as nuclear fuel in power plants and their main sources are soil, rocks, plants, sand and water [1]. Uranium and thorium are known to cause acute toxicological effects for human and their compounds are potential occupational carcinogens [1]. These elements and compounds are highly toxic which cause progressive or irreversible renal injury. Nuclear spent fuels generally contain actinides like uranium, thorium and various fission products [2]. Due to these importances of uranium and thorium, the determination of uranium and thorium in environmental and biological samples has considerable potential as a tool for assessment of human exposure [3]. The direct determination of

uranium and thorium by the instrumental techniques including inductively coupled plasma atomic emission spectrometry and inductively coupled plasma-mass spectrometry is still difficult because of insufficient sensitivity, lack of selectivity, presence of complex matrix, poor precision and accuracy [4–6]. To solve these problems, enrichment and separation techniques including solvent extraction, coprecipitation, ion-exchange, electrodeposition, etc. [7–11] have been used in the analytical chemistry laboratories for uranium and thorium. Solid phase extraction is one of the important preconcentration-separation procedures for trace heavy metals ions, due to its simplicity and limited usage of the organic solvents [12–17]. Solid phase extraction of uranium and thorium is also a popular subject in the analytical chemistry [18–20]. Shamsipur et al. [21] have proposed a solid phase extraction procedure for ultratrace uranium(VI) in natural waters using octadecyl silica membrane disks modified by tri-*n*-octylphosphine oxide. A chelating resin has been synthesised by Gladis and Rao [22] by the reaction with Amberlite XAD-4 and 5-aminoquinoline-8-ol for the uranyl ion uptake. The determina-

[☆] This study is a part of PhD thesis of Funda Armagan Aydin.

* Corresponding author. Fax: +90 352 4374933.

E-mail address: soylak@erciyes.edu.tr (M. Soylak).

tion of uranium and thorium in natural waters with a high matrix concentration using solid phase extraction inductively coupled plasma-mass spectrometry has been performed by Unsworth et al. [23]. Metilda et al. [24] have prepared catechol functionalized aminopropyl silica gel for the separation and preconcentration of uranium(VI) from thorium(IV) in soil and sediment samples. Ghasvand and Mottaabed [25] have proposed a solid phase extraction procedure of ultratrace uranium by mixtures of dicyclohexyl-18-crown-6 and tri-*n*-octylphosphine oxide. The selective enrichment and separation of U(VI) and Th(IV) in trace and macroscopic levels using malonamide grafted polymer from acidic matrices has been performed by Raju and Subramanian [26].

In the presented work, a solid phase extraction procedure for the separation-preconcentration of ultratrace U(VI) and Th(IV) as 9-phenyl-3-fluorone chelates on Duolite XAD761 resin has been presented prior to their ICP-MS determination. The effects of analytical parameters including pH of the solution, amounts of 9-phenyl-3-fluorone and Duolite XAD761, sample volume, etc. were investigated.

2. Experimental

2.1. Apparatus

An Agilent model 7500a inductively coupled plasma mass spectrometer was used for the determination of uranium and thorium. The instrument was optimized daily before measurement and operated as recommended by the manufacturers. The conditions are given in Table 1.

A pH meter, WTW Inolab Level 3 Model glass-electrode was employed for measuring pH values in the aqueous phase. The water was purified in Millipore Synergy 185.

2.2. Reagents and solutions

High purity reagents were used for all preparations of the standard and sample solutions. Stock solutions of uranium(VI) and thorium(IV), 1000 mg L⁻¹ (Sigma, St. Louis) was diluted daily for obtaining working solutions. The standard solutions

used for the calibration procedures were prepared before use by dilution of the stock solution with 1 mol L⁻¹ HNO₃. Stock solutions of diverse elements were prepared from the high purity compounds (99.9%, E. Merck, Darmstadt).

A solution of 9-phenyl-3-fluorone (%0.05 m/v) was prepared by dissolving 0.05 g of 9-phenyl-3-fluorone (Sigma, St. Louis, MO, USA) in 1 mL of 0.1 mol L⁻¹ NaOH and diluting to 100 mL with water.

Duolite XAD761 is cross-linked phenol-formaldehyde polymer that was purchased from Sigma Chem. Co., St. Louis, USA. Its surface area is 300 m² g⁻¹. It was used for the removal of proteins, high MW colorants, organic impurities and is useful for the purification of pharmaceuticals [27,28]. A glass column containing 700 mg of Duolite XAD761 in water suspension was 10 cm long and 1.0 cm in diameter. The bed height in the column was approximately 2.5 cm. The resin on the column was preconditioned with pH 5.0 buffer solution prior to percolation of the sample.

2.3. Test studies for solid phase extraction

The presented procedure was checked with test solutions. An aliquot of test solution containing 0.5 μg U(VI) and Th(IV) ions was transferred into a beaker and 0.5 mL of 0.05% (m/v) 9-phenyl-3-fluorone solution was added. The pH of the solution was adjusted to working pH by the addition of diluted NH₃ or HCl. The solution was diluted to 20–30 mL with water and left at room temperature for 10 min for the formation of U(VI) and Th(IV) chelates. The sample solution was permitted to flow through the column under gravity. Then, the column was washed firstly with the blank solution that containing related buffer solution; the retained analytes were eluted with 5 mL of 2 mol L⁻¹ HCl at a flow rate of 4 mL min⁻¹. The metal concentration in the solution was determined by ICP-MS.

2.4. Analysis of real samples

0.1 g of NIST-SRM 2710 Montana I Soil standard reference material was digested with aqua regia (12 mL concentrated hydrochloric acid and 4 mL of concentrated nitric acid) at room temperature then it was heated to 95 °C. After the evolution of NO₂ fumes had ceased, the mixture was evaporated almost to dryness on a sand-bath and mixed with 8 mL of aqua regia. Then the mixture was again evaporated to dryness. After evaporation 8–9 mL of distilled water was added and the sample was mixed. The resulting mixture was filtered through a blue band filter paper. The filtrate was diluted to 25 mL with distilled water. pH of this solution was adjusted to 5 by the addition of 1 mol L⁻¹ NH₃. Then the preconcentration procedure given above was applied.

Water samples analyzed were filtered through a cellulose membrane filter (Millipore) of 0.45 μm pore size. One hundred and fifty millilitres of water sample was transferred to a beaker. Then 0.5 mL of 0.05% (m/v) 9-phenyl-3-fluorone solution was added. The pH of this solution was adjusted to 5.0. After 10 min waiting for complex formation, the sample was passed through the Duolite XAD761 column. The 9-phenyl-3-fluorone chelates

Table 1
Operating conditions of ICP-MS

Inductively coupled plasma	Agilent 7500 a
Nebulizer	Babington
Spray chamber	Quartz, double pass
RF power	1260 W
Frequency	27.12 MHz
Sampling depth	7.0 mm
Plasma gas flow rate	15 L min ⁻¹
Auxiliary gas flow rate	1.0 L min ⁻¹
Carrier gas flow rate	1.15 L min ⁻¹
Sample uptake rate	0.3 mL min ⁻¹
Detector mode	Auto
Integration time	0.10 s
Number of replicates	3
Analytical masses	²³⁸ U, ²³² Th
Internal standard	²⁰⁹ Bi

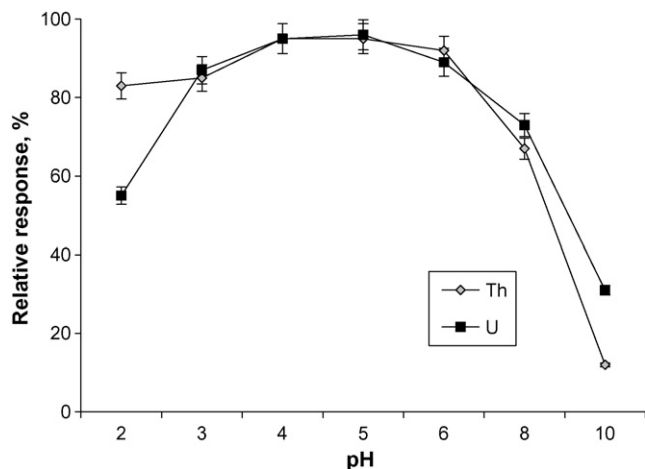


Fig. 1. Influence of pH on the recovery of U(VI) and Th(IV) on Duolite XAD761 (eluent: 2 mol L^{-1} HCl, $N=3$).

adsorbed on Duolite XAD761 were eluted with 5 mL 2 mol L^{-1} HCl. The levels of U(VI) and Th(IV) in the samples were determined by ICP-MS.

3. Results and discussion

3.1. Effect of pH of the aqueous solution on the retention of thorium(IV) and uranium(VI) on Duolite XAD761

As the pH of the working media is one of the important parameters for the quantitative retentions of analytes in the solid phase extraction studies, the influence of the pH of the aqueous solution containing $0.5 \mu\text{g}$ U(VI) and Th(IV) on the quantitative adsorption of analytes on Duolite XAD761 resin were investigated in the pH range of 2.0–10.0. The adjustments of pH of the solutions were performed by the addition of diluted NH_3 or HCl. The results are shown in Fig. 1. U(VI) and Th(IV) as 9-phenyl-3-fluorone chelates were quantitatively recovered in the pH range of 4.0–6.0. The recovery below pH 4 was not quan-

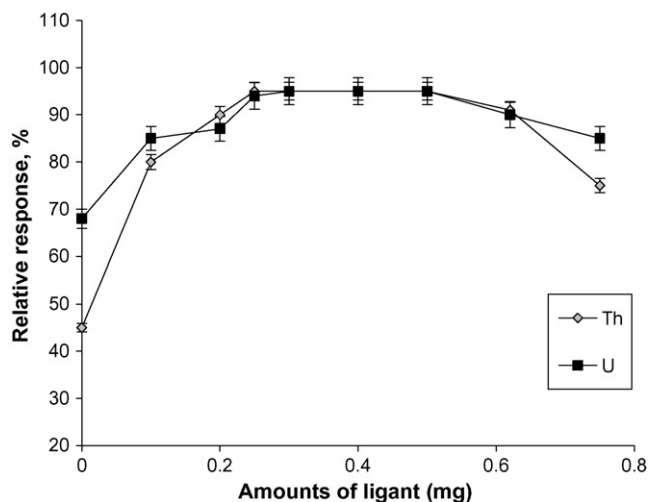


Fig. 2. Effect of amounts of 9-phenyl-3-fluorone on the recovery of uranium and thorium ions (eluent: 2 mol L^{-1} HCl, $N=3$).

Table 2

Effects of various eluents on the recoveries of Th(IV) and U(VI) from the column ($N=3$)

Eluent	Recovery (%)	
	Th(IV)	U(VI)
2 mol L^{-1} HNO_3	92 ± 1	92 ± 1
1 mol L^{-1} HCl	90 ± 1	91 ± 2
2 mol L^{-1} HCl	97 ± 1	95 ± 1
1 mol L^{-1} HNO_3 in acetone	72 ± 2	88 ± 2
2 mol L^{-1} HNO_3 in acetone	91 ± 3	87 ± 2

titative. Therefore, for all subsequent works, pH 5 was fixed as the optimum for the quantitative separation-preconcentration.

3.2. Influence of amount of 9-phenyl-3-fluorone

Prior to adsorption of uranium and thorium ions on a solid phase for preconcentration, generally they were converted to a suitable form including metal chelates or metal inorganic complexes. Phenylfluorones are widely used organic chelating agent that has a larger formation constant with metal ions [29,30]. They are used in chemical enrichment-separation and spectrophotometric determination of some metal ions by various preconcentration techniques prior to their determination [31–33]. In this context, in the present work, 9-phenyl-3-fluorone was selected as chelating agent. Different amounts of 9-phenyl-3-fluorone were added to test solutions containing $0.5 \mu\text{g}$ U(VI) and Th(IV). These solutions passed then through Duolite XAD761 column. The results are shown in Fig. 2. Quantitative recovery was obtained for thorium(IV) and uranium(VI) ions in the 0.25–0.60 mg range of 9-phenyl-3-fluorone. Because of insufficient ligand amounts in the solutions, the recovery of analytes was not quantitative when less than 0.25 mg of 9-phenyl-3-fluorone was used. At concentration higher than 0.60 mg of 9-phenyl-3-fluorone, the recovery was below 95%, due to competition on the adsorption between 9-phenyl-3-fluorone chelates and excess 9-phenyl-3-fluorone in the solution. In further work, 0.25 mg of 9-phenyl-3-fluorone was added to the solutions.

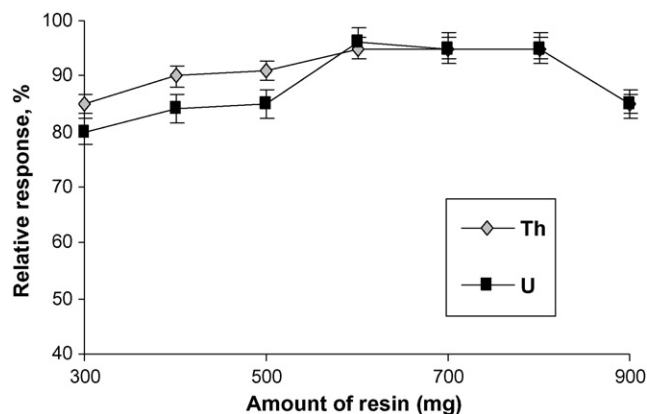


Fig. 3. Effect of amount of Duolite XAD761 on the recovery of uranium and thorium ions ($N=3$).

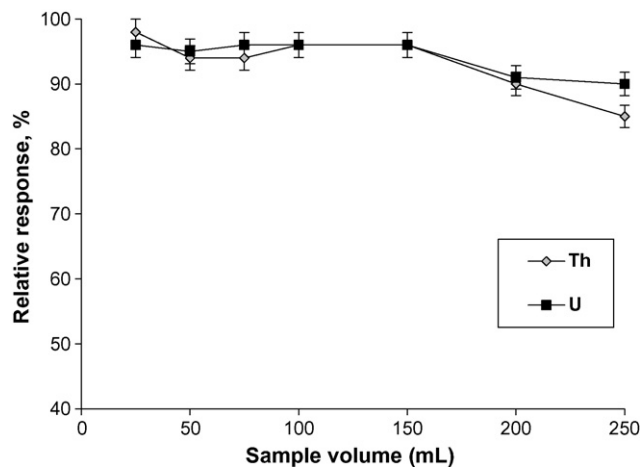


Fig. 4. Effects of sample volume on the recovery of uranium and thorium ions ($N=3$).

3.3. Effect of eluent type

The influence of eluent type on desorption of the analytes from the column was investigated. Various eluents given in Table 2 were used for elution of retained thorium(IV) and uranium(VI) chelates on the Duolite XAD761 column. Quantitative recovery was obtained by using 5 mL of 2 mol L⁻¹ HCl. Under optimized conditions, for all further works, 5 mL of 2 mol L⁻¹ HCl was used.

3.4. Resin amount

As another important analytical factor for the quantitative recovery of analytes on the solid phase extraction of metal ions is the amount of solid phase extractant, the influence of amount of Duolite XAD761 on the recovery of thorium(IV) and uranium(VI) was also investigated. The results are depicted in Fig. 3. The recovery values for analytes were found quantitative in the resin amounts of 600–800 mg. At higher amounts, the retained uranium and thorium could not be eluted completely with 10 mL of 2 mol L⁻¹ HCl. In all further studies, the mini column was filled with 700 mg of Duolite XAD761 for preconcentration.

Table 5

The results for tests of addition/recovery for uranium and thorium determinations in (sample volume: 150 mL, final volume: 5 mL, $N=5$)

Analyte	Added (μg)	Tap water		Mineral water	
		Found (μg)	Recovery (%)	Found (μg)	Recovery (%)
Th(IV)	0	LOD	–	LOD	–
	0.12	0.11 \pm 0.02	93 \pm 3	0.12 \pm 0.01	94 \pm 3
	0.25	0.25 \pm 0.03	100 \pm 3	0.24 \pm 0.02	96 \pm 2
	0.38	0.36 \pm 0.02	97 \pm 3	0.36 \pm 0.02	96 \pm 2
U(VI)	0	LOD	–	LOD	–
	0.12	0.12 \pm 0.01	94 \pm 2	0.12 \pm 0.01	99 \pm 2
	0.25	0.26 \pm 0.02	103 \pm 3	0.25 \pm 0.01	100 \pm 3
	0.38	0.38 \pm 0.03	101 \pm 4	0.37 \pm 0.02	98 \pm 3

LOD: Below the detection limit.

Table 3

Influence of matrix ions on the recovery of uranium and thorium ions ($N=3$)

Concomitant ion	Added as	Concentration (mg L ⁻¹)	Recovery (%)	
			Th(IV)	U(VI)
Na ⁺	NaCl	5000	94 \pm 1	94 \pm 2
K ⁺	KCl	1000	98 \pm 1	99 \pm 2
Ca ²⁺	CaCl ₂	2500	96 \pm 3	94 \pm 1
Mg ²⁺	MgCl ₂	1000	93 \pm 2	95 \pm 1
SO ₄ ²⁻	Na ₂ SO ₄	2500	96 \pm 1	93 \pm 2
NO ₃ ⁻	KNO ₃	2500	99 \pm 2	99 \pm 2
CO ₃ ²⁻	Na ₂ CO ₃	2500	97 \pm 3	96 \pm 2
HPO ₄ ²⁻	Na ₂ HPO ₄ ·7H ₂ O	2500	99 \pm 2	94 \pm 2
Cl ⁻	NaCl	5000	101 \pm 4	93 \pm 2
Al ³⁺	Al ₂ (SO ₄) ₃ ·18H ₂ O	5	100 \pm 5	85 \pm 2
Cr ³⁺	Cr(NO ₃) ₃ ·9H ₂ O	20	101 \pm 4	97 \pm 5
Fe ³⁺	Fe(NO ₃) ₃ ·9H ₂ O	5	105 \pm 3	90 \pm 2
Zn ²⁺	ZnI ₂	10	95 \pm 1	94 \pm 2
Ni ²⁺	NiCl ₂ ·6H ₂ O	5	94 \pm 2	94 \pm 3
Pb ²⁺	PbCl ₂	5	99 \pm 2	99 \pm 2
Co ²⁺	CoCl ₂ ·6H ₂ O	5	97 \pm 5	100 \pm 2
Cu ²⁺	Cu(NO ₃) ₂ ·3H ₂ O	20	96 \pm 2	99 \pm 6

Table 4

Uranium(VI) and thorium(IV) levels of Montana I Soil CRM (NIST-SRM 2710) after application presented separation and preconcentration procedure ($N=4$)

	Certified value ($\mu\text{g g}^{-1}$)	Our value*	Relative error (%)
Th(IV)	13	13.4 \pm 1.9	+ 3.1
U(VI)	25	24.1 \pm 2.2	- 3.6

* $P: 0.95, \bar{X} \pm ts/\sqrt{N}$.

3.5. Sample volume

The effect of the volume of sample solution on the adsorption of thorium(IV) and uranium(VI) was studied by passing 25–250 mL volume. The results are shown in Fig. 4. The adsorption of thorium(IV) and uranium(VI) chelates with 700 mg Duolite XAD761 was not affected by sample volume below 150 mL. Above 150 mL, the percent sorption decreased for U(VI) and Th(IV). The recovery values of analyte ions decreased probably due to the excess analytes loaded over the column capacity with increasing sample volume above 150 mL. Therefore, 150 mL of sample solution was adopted for the separation/preconcentration

Table 6
Levels of uranium and thorium ions in mineral water samples from Turkey (sample volume: 150 mL, final volume: 5 mL, N=5)

Sample	Concentration ($\mu\text{g L}^{-1}$) [*]	
	Th(IV)	U(VI)
Haymana mineral water	0.91 ± 0.09	0.23 ± 0.04
Tekirdag mineral water	0.22 ± 0.03	0.33 ± 0.03
Gokova mineral water	0.36 ± 0.06	0.73 ± 0.04

* P: 0.95, $\bar{X} \pm ts/\sqrt{N}$.

of U(VI) and Th(IV). The adsorbed metals can be eluted with 5.0 mL of 2 mol L⁻¹ HCl and a preconcentration factor of 30 is achieved.

3.6. Flow rate of sample and eluent solutions

The influence of the flow rates of sample and eluent solutions on the recoveries was investigated in the range of 2–8 mL min⁻¹. In the examination of the effects of sample and eluent solutions, 2 mol L⁻¹ HCl was used as eluent. The quantitative recovery values were obtained in the flow rate range of 2–4 mL min⁻¹ for sample and in the flow rate range of 2–8 mL min⁻¹ for eluent solution. After 4 mL min⁻¹ of sample solution, the recovery values of U(VI) and Th(IV) ions were below 95%. Four millilitres per minute was selected as a flow rate for both flow rates of sample and eluent solutions.

3.7. Matrix effect

The influence of possible matrix ions in the environmental samples and some transition metals was also examined. The effect of potential interfering ions on the determination of thorium(IV) and uranium(VI) was investigated by adding known concentrations of each ion in a solution containing analytes and then determining the latter. The results are summarized in Table 3. The tolerated amounts of each ion were the concentration values tested that caused less than 5% the absorbance alteration. The ions normally present in water do not interfere under the experimental conditions used. Also, some of the transition metals at mg L⁻¹ levels did not affect on the recovery of the analyte ions. These results show that the proposed preconcentration/separation method could be applied to the highly saline samples and other environmental samples that contain some transition metals at mg L⁻¹ levels.

3.8. Figures of merit

The limits of detection (LOD) of the proposed method for the determination of analyte elements were studied under the optimal experimental conditions [34]. The detection limits based on three times the standard deviations of the blank (N=15, $X_L = X_b + 3s$, X_L : limit of detection, X_b : blank value) for thorium(IV) and uranium(VI) were found to be 6.3 and 4.5 ng L⁻¹, respectively. The instrumental detection limits for ICP-MS were 0.030 $\mu\text{g L}^{-1}$ for thorium(IV) and 0.16 $\mu\text{g L}^{-1}$ for uranium(VI).

Table 7
Comparative data from some recent solid phase extraction studies on uranium(VI) and thorium(IV) preconcentration

Technique	Analytes	Solid phase	Eluent	PF	Detection limit	R.S.D. (%)	Reference
UV-visible	U(VI), Th(IV)	Calix[4]arene anchored chloromethylated polystyrene	2 mol L ⁻¹ HCl	143–153	6.14–4.29 $\mu\text{g L}^{-1}$	<2	[1]
UV-visible	U(VI), Th(IV), La(III)	Grafting Merrifield chloromethylated resin	1 mol L ⁻¹ (NH ₄) ₂ CO ₃	400–500	10–80 ng mL ⁻¹	<4	[2]
ICP-MS	U(VI), Th(IV)	U/TEVA resin	0.05 mol L ⁻¹ NH ₄ HC ₂ O ₄	4	0.02–0.03 ng L ⁻¹	<2	[3]
ICP-MS	U(VI), Th(IV)	Actinide-specific extraction resin (TRU-spec)	0.1 mol L ⁻¹ NH ₄ HC ₂ O ₄	–	0.015–0.006 ng mL ⁻¹	<6	[23]
UV-visible	U(VI), Th(IV)	Malonamide grafted polymer	0.5 mol L ⁻¹ (NH ₄) ₂ CO ₃	400–350	20–50 ng mL ⁻¹	<4	[26]
Fluorescence spectrometry	U(VI), Th(IV)	AXAD-16-3,4-dihydroxy benzoyl methyl phosphonic acid C ₁₈	6 mol L ⁻¹ HCl	333	10 ng mL ⁻¹	<4	[35]
UV-visible	U(VI)	Quinoline-8-ol anchored chloromethylated polymeric resin	Methanol	325	300 ng L ⁻¹	–	[36]
UV-visible	U(VI)	Quinoline-8-ol anchored chloromethylated polymeric resin	0.1 mol L ⁻¹ Na ₂ CO ₃	100	5 $\mu\text{g L}^{-1}$	<4	[37]
ICP-MS	U(VI), Th(IV)	Duolite XAD761	2 mol L ⁻¹ HCl	30	4.5–6.3 ng L ⁻¹	<4.5	Present work

The analytical performance of the procedure can be calculated from the results of ICP-MS. The reproducibility of the method was evaluated by 25 mL of solution containing analyte ions ($N=10$). The relative standard deviations (R.S.D.) of these determinations were 2.3% for uranium and 4.5% for thorium.

3.9. Analysis of real samples by the proposed method

The validation of the presented procedure is performed by the analysis of Montana I Soil certified reference material (CRM) (NIST-SRM 2710). The certified and observed values for NIST-SRM are given in Table 4. The results found were in good agreement with the certified values of CRM.

Different amounts of thorium(IV) and uranium(VI) ions were spiked in a tap water and a mineral water to estimate the accuracy of the procedure. The resulting solutions were submitted to the presented procedure. The results are given in Table 5. Good agreement is obtained between the added and found analyte content using the recommended procedure. The recovery values for the analyte ions are in the range of 93–103%. The standard deviation values for the spiked samples are in the range of 2–4%. These values are quantitative and show that the presented method can be applied for the separation/preconcentration of analyte ions in natural waters. The solid phase extraction procedure presented for U(VI) and Th(IV) ions was applied to three different mineral water samples from Turkey. The results were given in Table 6.

4. Conclusion

The proposed method has the following advantages: simple, rapid and low analysis cost. Instead of the use of fresh solvent as an extracting phase for each sample, the reusability of Duo-lite XAD761 was as high as greater than 300 cycles without any loss in its sorption behavior. The analytical performance of the presented method is comparable with other preconcentration methods. Comparative information from some recent studies on solid phase extraction of uranium(VI) and thorium(IV) for the figure of the merits is given in Table 7. The analytical performance of the presented method is comparable with other works. The matrix effects with the method were reasonably tolerable. The good features of the proposed method showed that it is a convenient and low cost one. The method applied provides good precision with relative standard deviations lower than 5% and high accuracy obtained with the quantitative recovery of spiked U(VI) and Th(IV). Thus, it may be concluded that the method is an effective approach in preconcentration and selective separation of analytes from the natural waters.

Acknowledgments

F.A. Aydin would like to thank to DSI, The Technical Research and Quality Control Department and director of Test-

ing Laboratory for taking the time to work in laboratory. The authors are grateful for the financial support of the Unit of the Scientific Research Project of Erciyes University (Project no.: EÜBAP-FBT 05 15).

References

- [1] V.K. Jain, R.A. Pandya, S.G. Pillai, P.S. Shrivastav, *Talanta* 70 (2006) 257.
- [2] Ch. Siva Kesava Raju, M.S. Subramanian, *Talanta* 67 (2005) 81.
- [3] K. Benkhedda, V.N. Epov, R.D. Evans, *Anal. Bioanal. Chem.* 381 (2005) 1596.
- [4] S. Dadfarnia, C.W. Mcleod, *Appl. Spectrosc.* 48 (1994) 1331.
- [5] M.S. Hu, S. Chinese, *J. Anal. Chem.* 33 (2005) 173.
- [6] D. Prabhakaran, M.S. Subramanian, *Anal. Lett.* 36 (2003) 2277.
- [7] V.G. Torgov, M.G. Demidova, A.I. Saprykin, I.V. Nikolaeva, T.V. Us, E.P. Chebykin, *J. Anal. Chem.* 57 (2002) 303.
- [8] D. Dojozan, M.H. Pournaghi-Azar, J. Toutouchi-Asr, *Talanta* 46 (1998) 123.
- [9] T. Miura, T. Morimoto, K. Hayano, T. Kishimoto, *Bunseki Kagaku* 49 (2000) 245.
- [10] K. Kato, M. Ito, K. Watanabe, *Fresenius J. Anal. Chem.* 366 (2000) 54.
- [11] J.R. Pretty, G.J. Van Berkel, D.C. Duckworth, *Int. J. Mass Spectrom.* 178 (1998) 51.
- [12] M. Ghaedi, M.R. Fathi, A. Shokrollahi, F. Shajarat, *Anal. Lett.* 39 (2006) 1171.
- [13] S.Y. Tolmachev, J. Kuwabara, H. Noguchi, *J. Radioanal. Nucl. Chem.* 261 (2004) 125.
- [14] S. Baytak, A. Balaban, A.R. Turker, B. Erk, *J. Anal. Chem.* 61 (2006) 476.
- [15] T.H. Zhang, X.Q. Shan, R.X. Liu, H.X. Tang, S.Z. Zhang, *Anal. Chem.* 70 (1998) 3964.
- [16] M. Ghaedi, E. Asadpour, A. Vafaie, *Bull. Chem. Soc. Jpn.* 79 (2006) 432.
- [17] V.A. Lemos, G.T. David, L.N. Santos, *J. Braz. Chem. Soc.* 17 (2006) 697.
- [18] T.P. Rao, P. Metilda, J. Mary Gladis, *Talanta* 68 (2006) 1047.
- [19] T. Seki, K. Oguma, *Bunseki Kagaku* 53 (2004) 353.
- [20] R.K. Dubey, A. Bhalotra, M.K. Gupta, B.K. Puri, *Ann. Chim.* 88 (1998) 719.
- [21] M. Shamsipur, A.R. Ghiasvand, Y. Yamini, *Anal. Chem.* 71 (1999) 4892.
- [22] J.M. Gladis, T.P. Rao, *Anal. Bioanal. Chem.* 373 (2002) 867.
- [23] E.R. Unsworth, J.M. Cook, S.J. Hill, *Anal. Chim. Acta* 442 (2001) 141.
- [24] P. Metilda, J.M. Gladis, T.P. Rao, *Radiochim. Acta* 93 (2005) 219.
- [25] A.R. Ghiasvand, K. Mottaabed, *Asian J. Chem.* 17 (2005) 655.
- [26] C.S.K. Raju, M.S. Subramanian, *Microchim. Acta* 150 (2005) 297.
- [27] <http://www.rohmhaas.com/ionexchange/nutrition/doc/us/XAD761.pdf>.
- [28] N. Zouari, *J. Chem. Technol. Biotechnol.* 73 (1998) 297.
- [29] Z. Marzenko, *Separation and Spectrophotometric Determination of Elements*, Wiley, Chichester, 1986.
- [30] W. Winkler, F. Buhl, A. Arenhövel-Pacula, U. Hachula, *Anal. Bioanal. Chem.* 376 (2003) 934.
- [31] L. Zaijun, P. Jiaomai, T. Jian, *Anal. Bioanal. Chem.* 374 (2002) 1125.
- [32] L. Zaijun, P. Jiaomai, J. Tang, *Analyst* 126 (2001) 1154.
- [33] H.W. Gao, W.G. Liu, *Bull. Korean Chem. Soc.* 21 (2000) 1090.
- [34] IUPAC, Analytical Chemistry Division, *Spectrochim. Acta* 33B (1978) 242.
- [35] M.A. Maheswari, M.S. Subramanian, *React. Funct. Polym.* 62 (2005) 105.
- [36] P.A. Greene, C.L. Copper, D.E. Berv, J.D. Ramsey, G.E. Collins, *Talanta* 66 (2005) 961.
- [37] R.S. Praveen, P. Metilda, S. Daniel, T. Prasada Rao, *Talanta* 67 (2005) 960.

Effect of eluent composition and pH and chemiluminescent reagent pH on ion chromatographic selectivity and luminol-based chemiluminescence detection of Co^{2+} , Mn^{2+} and Fe^{2+} at trace levels

Denis Badocco, Paolo Pastore*, Gabriella Favaro, Carlo Maccà

Department of Chemical Sciences, University of Padova, Via Marzolo 1, 35131 Padova, Italy

Received 22 May 2006; received in revised form 12 October 2006; accepted 19 October 2006

Available online 28 November 2006

Abstract

The alkaline-luminol/ H_2O_2 -based chemiluminescent (CL) detection of Fe^{2+} , Co^{2+} , and Mn^{2+} , separated with a Dionex CS5A ion chromatographic phase was studied by means of a multi-pump flow system allowing the variation of the post-column solution composition. A perchlorate gradient at pH 1.9 (with HCl) was used to separate cations partially complexed with 5.6 mM oxalate present in the eluent and necessary for the chosen separation phase. A 0.91 mM luminol, 3.3 mM H_2O_2 in 0.25 M carbonate buffer at pH 10.5 composition was chosen as CL reagent solution. The chosen pH value warrants signal repeatability and wider linearity range although absolute signal is not maximum. The CL signal was related to the pH of the two post-column mixing solutions. Calibration plots of Co^{2+} and Fe^{2+} were linear in the chosen concentration range whilst a parabolic model was the best fit for Mn^{2+} . Detection limits were 0.24, 0.50 and 375 nM for Co^{2+} , Fe^{2+} and Mn^{2+} , respectively. The method was used to determine Co^{2+} at trace level in commercial copper chelates used for animal feeding. A comparison with a chromatographic method with spectrophotometric detection was made giving results comparable both in absolute values and accuracy.

© 2006 Elsevier B.V. All rights reserved.

Keywords: Luminol chemiluminescence; Transition metal determination; Ion chromatography; Post-column reactions

1. Introduction

The high sensitivity of the CL reaction between luminol (3-aminophthalhydrazide) and hydrogen peroxide (or dioxygen [1]), catalyzed by several metal ions such as Fe^{2+} [2], Co^{2+} [3], Cu^{2+} [4], Mn^{2+} [5], Zn^{2+} , Cd^{2+} [6], and Ti^{3+} [7] is well known. When H_2O_2 and luminol are in excess, CL emission is proportional to the metal ion amount in a wide concentration range. The reaction may, therefore, be used for determining very low concentration levels of the mentioned metal ions in different matrices such as environmental [8–11], food [12,13], and clinic [14] ones. In clinical tests, copper and iron may be used as indicators of various blood diseases such as leukaemia (Cu) and anaemia (Fe); zinc and manganese are very important co-factors for various enzymes and abnormally low concentration levels of Mn in blood are found in diabetic patients. A more selective detection may be achieved by choosing particu-

lar experimental conditions. Iron, for instance, has very different chemiluminescent behaviour in its two forms, Fe^{2+} and Fe^{3+} for the mechanism involved and their amount can be affected by the presence of Cu^{2+} [15].

At present all the mentioned metals can be determined at trace and ultra-trace levels by atomic absorption and inductively coupled plasma-atomic emission spectroscopy [16,17] and by amperometric techniques [18]. Coupling of ion chromatography (IC) with spectrophotometric detection after a post-column complexation of the metal ions with 4-(2-pyridylazo)resorcinol (PAR) [19,20] is also used, but detection limits are usually higher.

Flow injection analysis with CL detection (FIA/CL) [21] designed with optimized multi-pumping system for delivering reagents [11] may be useful because the very low detection limits (nano-molar or lower [22,23]) make pre-concentration unnecessary. Detection limits, however, are greatly increased if ligands are present in solution (such as tartrate, oxalate, citrate, succinate, etc.). In fact, luminol emission is strongly enhanced by the catalysis of the free cations able to coordinate and activate peroxidic species [1]. The catalytic effect lies in the metal/hydrogen

* Corresponding author. Tel.: +39 049 8275182; fax: +39 049 8275175.
E-mail address: Paolo.pastore@unipd.it (P. Pastore).

peroxide complex, which is the intermediate essential for chemiluminescence. Any factor that affects the metal/peroxide complex concentration similarly affects the initial chemiluminescence intensity. The catalytic effect is, therefore, inhibited if the free cation concentration is decreased by interfering ligands [3]. Consequently, if an ion chromatographic separation is needed to simultaneously determine various cations at very low concentration levels, the presence of complexing agents in the eluent solution, often necessary to improve column selectivity [19], must be accurately taken into consideration to keep CL detection at the required performance. Chromatography/CL coupling has been already proposed [24,25] but the use of weakly selective columns did not allow suitable separation. At present, the availability of mixed beads columns ensures greater chromatographic selectivity by using ligand species in the eluent, which varies the nature of the metal ionic form. In this paper, we will study the influence of different experimental parameters on luminol/H₂O₂ CL used as detection technique of Co²⁺, Fe²⁺, and Mn²⁺. In particular, the effects of eluent composition in terms of ligand concentration (oxalate) and pH and luminol/H₂O₂ pH will be evaluated also in the context of the IC separation. The investigation output can help, besides the customary scopes quoted above, investigating the fate of said metals administered as nutrient mineral cations in animal feed supplements. Cobalt amount in four commercial copper chelates used for animal feeding will be determined and results compared with HPLC/VIS detection.

2. Experimental

2.1. Reagents

Luminol (5-amino-2,3-dihydro-1,4-phthalazinedione) \geq 98.0% Fluka was kept in dark to limit decomposition. Hydrogen peroxide \geq 30% was Fluka. Sodium chloride was purified according to [26] to eliminate traces of metal ions. Sodium hydrogen carbonate, sodium perchlorate, sodium hydroxide, hydrochloric acid, oxalic acid dihydrate, manganese(II) sulphate monohydrate \geq 98%, cobalt(II) chloride hexahydrate \geq 99.0%, iron(II) ammonium sulfate hexahydrate \geq 99.0%, were all analytical grade ACS reagents supplied by Fluka (Milan,

Italy) and were used as received, after verifying that the small amounts used could not introduce appreciable amounts of impurities. Ultrapure water (resistivity 18.2 M Ω cm) obtained with a MilliQ Plus System (Millipore, Milan, Italy) was used for preparing all solutions. Batch solutions (1 mM) of all metals were prepared in 0.01 M HCl, and suitably diluted with 0.01 M HCl for injection. All solutions were kept under nitrogen.

The CL detection was tested for determining the Co²⁺ amount in four commercial Copper chelates used for animal feeding, here indicated as A–D with declared Cu amount ranging from 5 to 10% (w/w).

2.2. Apparatus

The chromatographic/CL apparatus is schematically illustrated in Fig. 1. Three HPLC pumps were used, for the alkaline luminol solution, for H₂O₂ (at neutral pH to limit decomposition [27]), and for the eluent solution, respectively. The first two were 350T Biorad pumps (Richmond, CA, USA) and delivered the two reagent solutions at 1.0 and 0.1 ml/min, respectively; the third one was a four solvents Dionex gradient pump (Sunnyvale, CA, USA) delivering the eluent solution at 1.0 ml/min. A 650 μ l injection loop was used. IONPAC CG5A guard column and IONPAC CS5A analytical column were used as separators; a dark box was used to shield external light. The CL cell (20 μ l) was built in our laboratory according to [23]. Tubing size was 0.013 cm. A Hamamatsu (Shimokanzo, Japan) mod. 5600-04 photomultiplier powered up at 900 V was used as light detector and the output signal was recorded with a PC controlled LeCroy 9350, 500 MHz oscilloscope (Geneva, Switzerland). Solution pH was measured with a Crison mod. 2002 pH-meter equipped with an Ingold mod. 405-57/120 glass electrode.

2.3. Preliminary tests

Preliminary experiments to evaluate the effect of luminol pH on the CL emission were made by using luminol at fixed concentration (1.0 mM) dissolved in hydrogen carbonate solutions ranging from 0.1 to 1 M and adjusted with sodium hydroxide at various pH values from 9.5 to 13.5. A 44.0 mM hydrogen per-

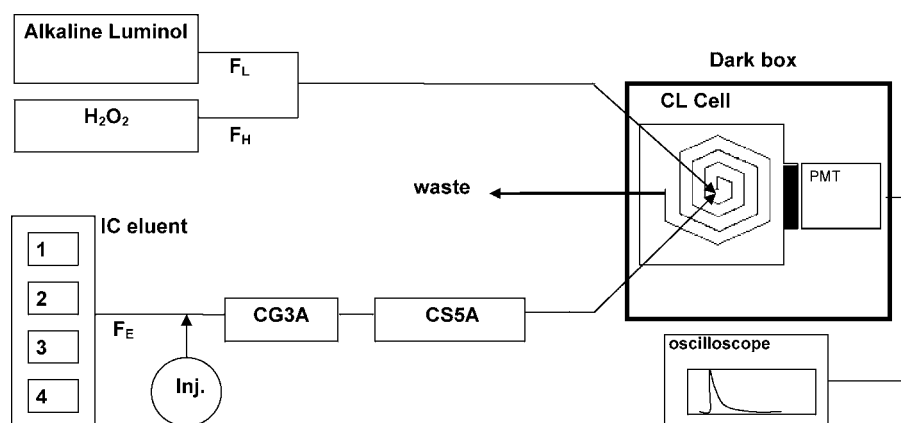


Fig. 1. IC/CL system. Alkaline luminol, H₂O₂ and eluent solutions were delivered at F_L, F_H and F_E flow rates, respectively (see Tables 1 and 2). Tubing size is 0.013 cm and the flow cell volume is 20 μ l.

Table 1
IC mobile phase and CL reagents for the evaluation of luminol and eluent solutions pH effect on CL emission

	Line	Components	C (mM)	% ^a
Eluent ($F_E = 1.0$ ml/min)	1	H ₂ Ox + HCl	14 + 250	0–40
	2	H ₂ Ox (NaCl)	14 + 250	40–0
	3	NaClO ₄	640	60
Reagent A ($F_L = 1.0$ ml/min)	L	Luminol	1	
		NaHCO ₃ (pH adjusted with NaOH)	100–1000	
		pH	9.5–13.5	
Reagent B ($F_H = 0.1$ ml/min)	H	H ₂ O ₂	44.0	

Column 2 (“Line” heading) indicates the gradient pump lines used for reagents and eluent delivering, L and H refer to luminol and H₂O₂ delivering according to Fig. 1. F_L , F_H and F_E are the flow rates of luminol, H₂O₂, and eluent, respectively. Injected amount, 650 μ l. H₂Ox = oxalic acid.

^a The linear gradient develops in 8 min from $t = 0$ min.

oxide neutral solution was added with a “T” junction just before the mixing point with the eluent solution (composition, see Section 2.4), in order to minimise its permanence at alkaline pH, thus reducing self-decomposition of H₂O₂ [27]. Luminol and H₂O₂ concentrations were chosen according to [24]. Eluent and alkaline luminol/H₂O₂ solutions were mixed inside the CL cell (see Fig. 1).

Experiments to evaluate the effect of eluent and luminol pH values on the final pH of the solution were made by holding constant all the other parameters according to the experimental scheme reported in Table 1. Eluent pH was changed by changing the percent of lines 1 and 2.

2.4. Procedures

The optimized formulation of IC mobile phase and of injected reagent for CL detection is summarised in Table 2. The eluent solution contained oxalic acid, HCl, NaCl and NaClO₄. The effective eluent was NaClO₄ and a linear 8 min gradient was used according to the conditions reported in Table 2. The influence of oxalic acid concentration on CL emission and retention times was studied by changing oxalic acid concentration delivery rate of line 1 (x values ranging from 0 to 11%) and using line 2 to

keep NaCl + HCl constant during elution. The optimized x value was 9% corresponding to an eluent solution of 5.6 mM oxalic acid in HCl at pH 1.9.

The commercial Cu chelates were mineralized by boiling 1 g sample in 10 ml concentrated HNO₃ and evaporating to 2 ml, adding 2 ml concentrated HClO₄ and evaporating again to 1 ml. After dilution to 100 ml the solution was filtered on 0.22 μ m. For the HPLC-CL detection, solutions were diluted 10⁴ times before injection. The HPLC-VIS detection method described in the literature [19] was used for comparing results.

3. Results and discussion

3.1. IC separation

Organic ligands, as shown in Section 1, are necessary to improve the column selectivity, but do adversely affect the CL emission, that is detection sensitivity. Consequently, the choice of ligand nature and concentration together with pH conditions becomes critical. A quite popular ligand used for the separation under study is oxalate [19]; indeed, preliminary tests (data not shown) confirmed its superior behaviour respect to succinate, tartrate and citrate. With succinate, CL emission was comparable to oxalate, but analytes separation was insufficient. Tartrate and citrate yielded both very poorer CL emission and IC separation.

Fig. 2 shows the effect of oxalate concentration in the eluent on analytes retention time and on CL response. The elution sequence is Co²⁺, Fe²⁺, and Mn²⁺. On increasing oxalate dilution, retention times are increased and detection sensitivity is improved, while resolution only decreases very moderately. Further dilution, however, causes rapid deterioration of the chromatographic separation so that all peaks finally merge into one. The inset in Fig. 2 shows the dependence of capacity factors (k') of Co²⁺, Fe²⁺, and Mn²⁺ on oxalic acid concentration. The k' parameter increases by decreasing oxalate concentration; regression lines of Fe²⁺ and Mn²⁺ are essentially parallel with slope close to 0.15, while Co²⁺ has a slope of 0.2.

Emission of all cations increases more rapidly than the oxalate concentration decrease owing to the higher and higher concentration of free metal ion in solution responsible of a larger catalytic effect. Fig. 3 compares the experimental CL emission

Table 2
IC mobile phase and CL reagents in the final formulation

	Line	Components	C (mM)	% ^a	% ^a
Eluent ($F_E = 1.0$ ml/min)	1	H ₂ Ox + NaCl + HCl	140 + 200 + 200	13– x	13– x
	2	NaCl + HCl	200 + 200	x	x
	3	LiClO ₄	320	10	80
	4	H ₂ O		77	7
Reagent A ($F_L = 1.0$ ml/min)	L	Luminol	1.0		
		NaHCO ₃	250 (pH 10.5)		
Reagent B ($F_H = 0.1$ ml/min)	H	H ₂ O ₂	44.0		

Column 2 (“Line” heading) shows the gradient pump line used for reagent delivering; L and H refer to luminol and H₂O₂ delivering according to Fig. 1. F_L , F_H and F_E are the flow rates, of luminol, H₂O₂, and eluent, respectively. The x value (columns 5 and 6) was varied from 0 to 11 to study the effect of oxalic acid concentration; the optimized value was $x = 9$. Injected amount: 650 μ l.

^a The linear gradient develops in 8 min from $t = 0$ min.

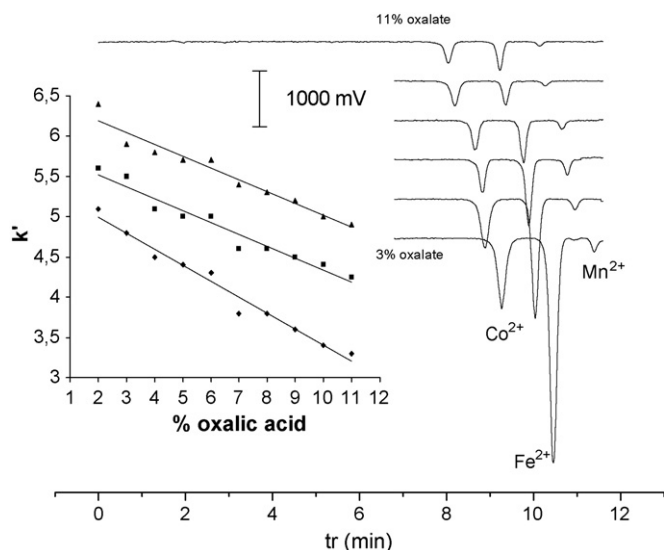


Fig. 2. IC separation of Co^{2+} , Fe^{2+} and Mn^{2+} with different % oxalic acid. Chromatographic conditions: see Table 2. Oxalate percentage, from top to bottom: x (as defined Table 2) = 1, 3, 5, 7, 9, and 11%. Analyte concentrations: 5 nM Co^{2+} , 10 nM Fe^{2+} and 500 nM Mn^{2+} . Injected amount, 650 μl . Inset: capacity factors k' of (◆) Co^{2+} , (■) Fe^{2+} , (▲) Mn^{2+} vs. % oxalic acid (x values in Table 2). Regression parameters for a linear model, $k' = a + b$ (% oxalic acid): (▲) $a = 6.487$ (0.084), $b = -0.147$ (0.012), $R^2 = 0.95$; (■) $a = 5.818$ (0.083), $b = -0.148$ (0.012), $R^2 = 0.95$; (◆) $a = 5.392$ (0.078), $b = -0.199$ (0.011), $R^2 = 0.98$. Standard deviations are in parenthesis.

(symbols) with the free cation concentrations (lines) computed from the stability constants of the oxalate complexes and the experimental oxalate concentration, under the hypothesis that other competitive reactions are absent. Emission and computed concentrations were normalized at the most concentrated oxalate concentration. Indeed, CL takes place after the mixing of the acidic eluent and the alkaline luminol/ H_2O_2 solutions; thus, the final pH is alkaline, so that metal precipitation as hydroxide might occur. Shapes of Co^{2+} do agree pretty well. In contrast, Fe^{2+} emits less at low oxalate concentration because its Cl^-

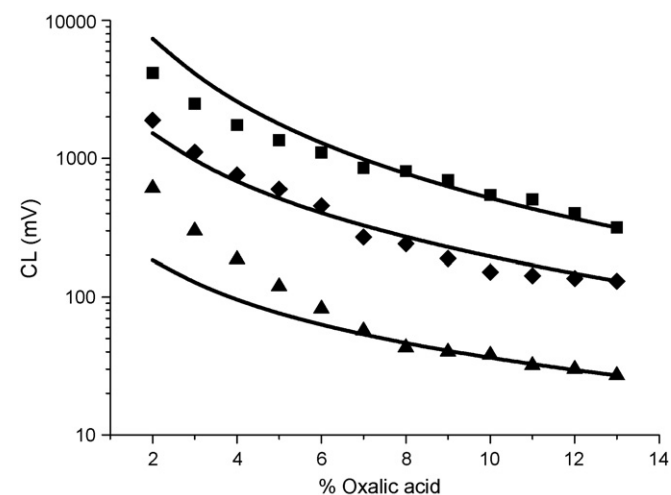


Fig. 3. CL intensity in logarithmic scale of (◆) Co^{2+} , (■) Fe^{2+} , (▲) Mn^{2+} vs. % oxalic acid compared to the theoretical amount of free ion. Data are normalized at the highest oxalate concentration. Chromatographic conditions are as in Fig. 2.

complexes may play a significant role. Mn^{2+} emits more than expected at low oxalate concentrations possibly because Mn^{2+} is oxidized in the peroxide environment, producing species with higher catalytic effect [2] and consequently higher CL emission. Nevertheless our results evidence that a correlation between emission and the calculated free metal concentration does exist, thus showing that the kinetics of catalysis are more rapid than any competing reaction (complexation and, in case, precipitation) able to decrease the free metal ion after final mixing of line fluxes.

On the basis of the above results, our choice of oxalate concentration was 5.6 mM (corresponding to 4% in Table 2), because it yielded better peak repeatability both in terms of retention time and CL emission, while providing a very good compromise between CL response and chromatographic resolution.

3.2. Emission optimization: pH control

According to the relevant literature, the luminol CL is optimal at alkaline pH [5]. In principle, best performance should be achieved at pH close to 10 for homogeneous solutions. For CL detection, the acidic eluate from IC separation (see former section) must therefore be mixed with a luminol/ H_2O_2 solution with a base content suitable to properly adjust the final pH, which is crucial to ensure detection repeatability and low noise. This adjustment, however, is more conveniently made on an empirical basis, because, the mixing kinetics and, consequently, the effective pH inside the CL cell are hardly predictable. In Fig. 4, the CL emission is reported against the pH of the luminol solution in 0.1 M carbonate adjusted with sodium hydroxide between 12 and 13.6 (line L in Fig. 1). The pH producing the most intense CL emission is 13.2 for all metal ions as well as for background, thus giving evidence that the emission process is always the same. It must be pointed out that repeatability is not good in this experimental conditions. A very good repeatability can be

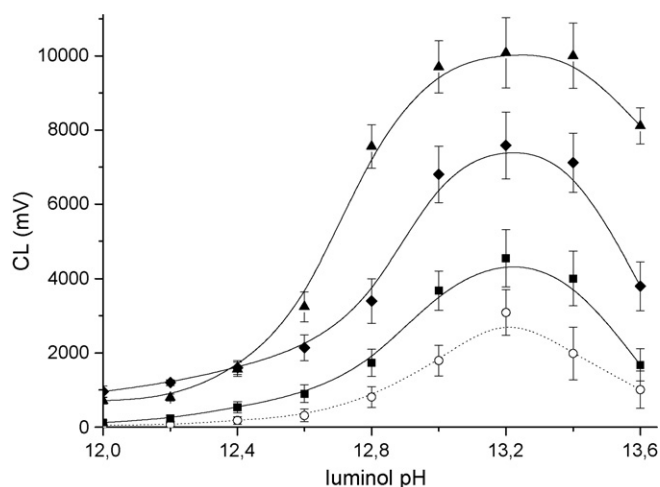


Fig. 4. CL emission as a function of the luminol pH value in 0.1 M carbonate buffer. Eluent solution is at pH 1.9. Other chromatographic conditions are as in Table 1. (○) Background; (◆) 5 nM Co^{2+} , (■) 1 nM Fe^{2+} , (▲) 1000 nM Mn^{2+} . Error bars refer to 95% confidence interval.

observed at $\text{pH} < 12.5$ where signal is low but still enough to give good sensitivity. Nevertheless, it was deemed that a theoretical forecast of CL emitting solution pH could provide a better understanding of the system at hand. The contributions of both luminol/ H_2O_2 (lines L and H in Table 1, $F_L + F_H$ in Fig. 1) and eluent (lines 1 + 2 + 3 + 4 in Table 1, F_E in Fig. 1) pH values on the final pH, including dilution effect, were taken into account. Fig. 5 reports the calculated pH value of luminol/ H_2O_2 in 0.1 M (Fig. 5a) and 1 M (Fig. 5c) carbonate buffer resulting after mixing with eluent at various pH values in the range 0.99–2.28 calculated according to the hydrodynamic scheme of Table 1. Fig. 5a (0.1 M NaHCO_3^- + variable NaOH up to pH 14) and Fig. 5c (1 M NaHCO_3^- + NaOH) clearly show that only solutions with higher buffer power, i.e., either with 1 M $\text{HCO}_3^-/\text{CO}_3^{2-}$ pair at pH around 10.3 ($=\text{p}K_2$) or with $\text{pH} > 13.2$, do warrant a sufficient pH control; only in these conditions, indeed, all curves are close one another. According to these results, the following compositions of Reagent A were tested for CL emission: (1) luminol in 0.1 M carbonate + sodium hydroxide at pH 13.2 and 2) luminol in 1 M carbonate buffer at $\text{pH} = 10.5$. The former

solution, with a lower content of carbonate, should provide the highest emission [28]. The latter solution, allowing a better pH control, should warrant higher repeatability and wider linearity range, although at the cost of lower sensitivity. Emission measurements on background and after injection of Co^{2+} , Mn^{2+} or Fe^{2+} in both conditions are reported in Fig. 5b and d, respectively, as a function of eluent pH. The difference is remarkable: under condition 1, the signal is greatly decreased by increasing eluent acidity, whilst in condition 2 the signal is less affected by eluent pH and with an opposite trend. It is noteworthy that, at highest eluent acidity, solution 2 gives a stronger emission than solution 1. The positive emission trend suggests that the overall emission kinetics are faster than the oxalate complexation. In other words, free cation present in the acidic eluent solution (larger concentration at lower pH in the presence of oxalate) reacts more rapidly with the species leading to emission than to complexation or precipitation. This evidence agrees well with the considerations reported above in the discussion of Fig. 3 and is also supported by the background emission. In fact, the absolute background emission is low and cannot justify the emission

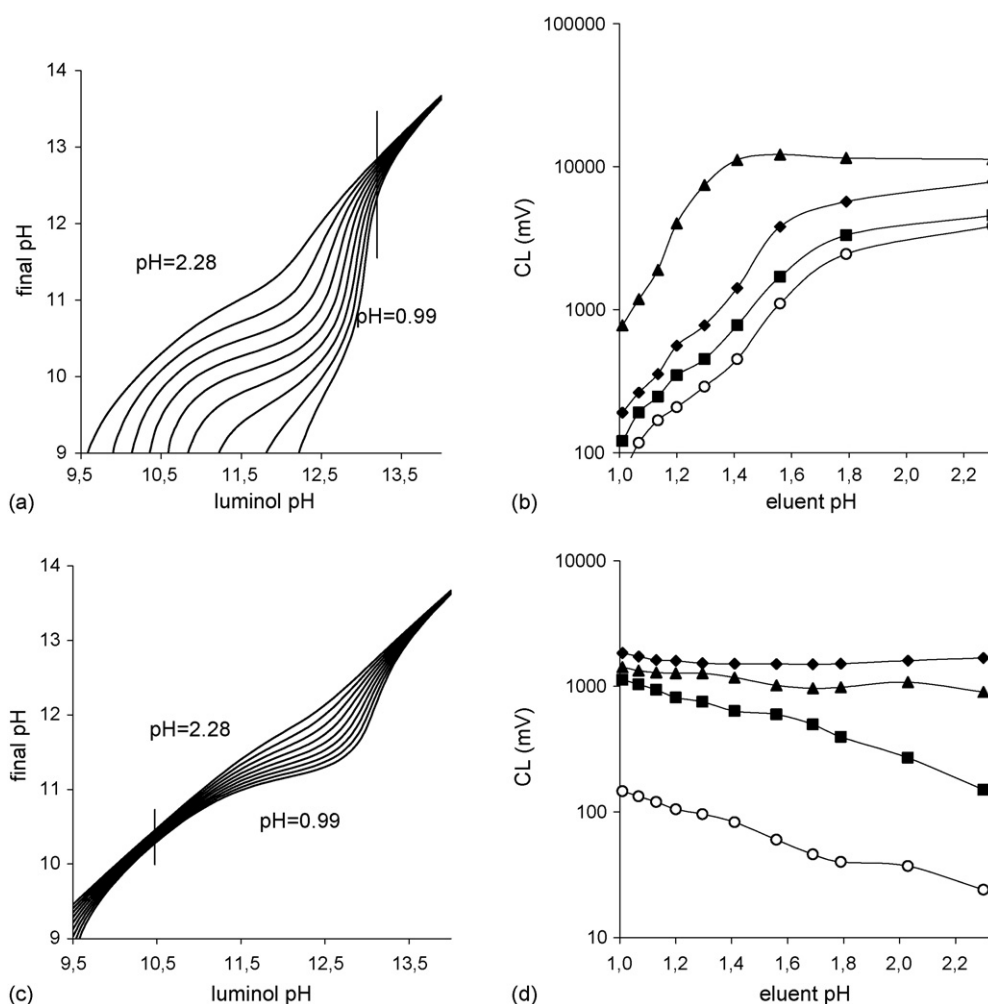


Fig. 5. Calculated pH in the measuring cell as a function of luminol solution pH with (a) 1 mM luminol in 0.1 M carbonate buffer and (c) 1 mM luminol in 1 M carbonate buffer. Curves correspond to an eluent pH of 2.28, 1.77, 1.54, 1.39, 1.28, 1.18, 1.11, 1.05, and 0.99. Vertical lines refer to the chosen pH values. Graphs (b) and (d) refer to the effect of eluent pH value on CL emission. Chromatographic conditions are as in Table 2. (b) 0.1 M carbonate luminol solution at pH 13.5. (d) 1.0 M carbonate luminol solution at pH 10.5. (○) Background (◆) 5 nM Co^{2+} , (■) 1 nM Fe^{2+} , and (▲) 1000 nM Mn^{2+} .

increment recorded in the presence of the analytes. An eluent pH = 1.9 was chosen to work in the emission plateau. Calculation of the pH decrease of luminol solution in alkaline buffer at pH 10.5 at 1.0, 0.5, 0.25, and 0.1 M after mixing with the eluent at acidic pH showed that 0.25 M $\text{HCO}_3^-/\text{CO}_3^{2-}$ has a buffer power sufficient to keep the pH near to the optimal value. Therefore, eluent at pH 1.9 and luminol at pH 10.5 in 0.25 M carbonate buffer were chosen as the final experimental parameters for both separation and detection.

3.3. Quantitative analysis

The studied method was statistically tested in order to evaluate its performances for quantitative application. The investigated metal ions exhibited different behaviours, respectively obeying to a linear (Co^{2+} and Fe^{2+}) and a quadratic ($\text{Mn}(\text{II})$) response model. Three repetitions at five very low concentration levels were made for each species to obtain the regression parameters for each calibration model and to compute the lower detection limit (DL).

3.3.1. Cobalt and iron

For Co^{2+} , regression parameters, according to the linear calibration model, $\text{CL} = a + bC$, (CL (mV), C (nM)) were: $a = 52$ (57) mV, $b = 1577$ (46) mV/nM, $R^2 = 0.99$, (standard deviations in brackets). DL was computed by means of the Schwartz method [29] instead of the popular Hubaux–Vos method [30], because a Bartlett test demonstrated that the variances of repeated measurements at the five concentration levels were not homoscedastic (Test-Bartlett = $14.322 > 9.5 = \chi_{\text{critical}}^2$ ($\nu = 4$; $\alpha = 0.05$)). The Schwartz method accounts for the prediction bands built with a weighed linear model. The computed DL was 0.24 nM. Calibration plot of Fe^{2+} is characterized by the following parameters: $a = 32$ (47) mV, $b = 1677$ (76) mV/nM, $R^2 = 0.99$. The response to Fe^{2+} differs from the Co^{2+} one by poorer signal repeatability, thus increasing the DL to 0.5 nM.

3.3.2. Manganese

As already mentioned, manganese may be present in solution in various forms having different catalytic effects. This may be the cause of the quadratic calibration graph obtained for this element. The regression parameters for the quadratic model $y = a + bx + cx^2$ were: $a = 2.2$ (3.4) 10^2 mV, $b = 2.1$ (2.3) mV/nM, $c = 1.10$ (0.31) 10^{-2} mV/(nM) 2 , $R^2 = 0.97$. Also in this case the variances were not homoscedastic; the Schwartz method yielded DL = 375 nM.

3.4. Application to real samples

The described method was used to determine Co^{2+} at trace level in four commercial Cu chelates used for animal feeding. Table 3 reports the obtained data. The results obtained with the two methods agree quite well both in found values and accuracy. It must be noted that samples injected for CL detection were 100 times more diluted with respect to the same sample detected by VIS spectroscopy. This fact allowed a selective detection as Cu,

Table 3
Quantification of Co^{2+} amount in four commercial copper chelates

Cu Chelate	Co in label (% w/w)	HPLC/545 nm (% w/w)	Luminol CL (% w/w)
A	Not declared	0.30 ± 0.05	0.39 ± 0.06
B	0.10	0.16 ± 0.05	0.23 ± 0.05
C	Not declared	0.0029 ± 0.0004	0.0024 ± 0.0006
D	Not declared	0.0089 ± 0.0004	0.0076 ± 0.0006

Fe and other metal ions did not give CL signal. Consequently, the chromatograms, developed in these very selective conditions were composed of the single peak of the most sensitive cation, i.e., cobalt.

4. Conclusions

In the present study the alkaline-luminol/ H_2O_2 -based CL detection of Fe^{2+} , Co^{2+} , and Mn^{2+} after separation with a mixed bead ion chromatographic phase was investigated. Organic ligands, required for improving separation, did decrease CL emission; it was therefore, necessary to formulate a compromise reagents composition. A perchlorate gradient at pH 1.9 was used to separate cations in the presence of 5.6 mM oxalate as a moderate complexing agent suitable to provide good chromatographic selectivity without quenching the CL signal. The signal is also related to the pH of the two post-column mixing solutions, namely, eluent (acidic) and luminol/ H_2O_2 (alkaline). The choice composition of the latter solution was 0.91 mM luminol, 3.3 mM H_2O_2 in 0.25 M carbonate buffer at pH 10.5. Calibration plot of Co^{2+} and Fe^{2+} were linear whilst was parabolic for Mn^{2+} . Detection limits were 0.24, 0.5 and 375 nM, respectively. The described method was successfully used to determine Co^{2+} at trace level in four commercial Cu chelates used for animal feeding obtaining results comparable with VIS detection both in absolute values and accuracy.

Acknowledgement

This research was supported by the Italian Ministry of University and Research (PRIN 2004).

References

- [1] L.L. Klopff, T.A. Nieman, *Anal. Chem.* 55 (1983) 1080.
- [2] W. Seitz, D. Hercules, *Anal. Chem.* 44 (13) (1972) 2143.
- [3] G. Burdo, W.R. Seitz, *Anal. Chem.* 47 (1975) 1639.
- [4] K.E. Haapakka, J.J. Kankare, *Anal. Chim. Acta* 118 (1980) 333.
- [5] J.L. Burguera, A. Townshend, *Talanta* 28 (1981) 731.
- [6] J.L. Burguera, A. Townshend, *Anal. Chim. Acta* 127 (1981) 199.
- [7] A. Alwarthan, A. Townshend, *Anal. Chim. Acta* 196 (1987) 135.
- [8] S. Hirata, Y. Hashimoto, *Fresenius J. Anal. Chem.* 355 (1996) 676.
- [9] D. Lannuzel, J. de Jong, V. Schoemann, A. Trevena, J.L. Tison, L. Chou, *Anal. Chim. Acta* 556 (2006) 476.
- [10] A.R. Bowie, E.P. Achterberg, P.N. Sedwick, S. Ussher, P.J. Worsfold, *Environ. Sci. Technol.* 36 (2002) 4600.
- [11] V. Cannizzaro, R. Bowie, A. Sax, *Analyst* 125 (2000) 51.

- [12] F. Watanabe, E. Miyamoto, *J. Liquid Chromatogr.* 25 (2002) 1561.
- [13] R. Banerjee, S.W. Ragsdale, *Annu. Rev. Biochem.* 72 (2003) 209.
- [14] X.Y. Huang, J.C. Ren, *Trends Anal. Chem.* 25 (2006) 155.
- [15] D. Lannuzel, J. de Jong, V. Schoemannb, A. Trevena, J.L. Tison, L. Choua, *Anal. Chim. Acta* 556 (2006) 476–483.
- [16] S.J. Hill, T.A. Arowolo, O.T. Butler, J.M. Cook, M.S. Cresser, *J. Anal. Atom. Spectrom.* 19 (2004) 301.
- [17] V.Z. Paneva, K. Cundeva, T. Stafilov, *Spectrochim. Acta B* 60 (2005) 403.
- [18] X.D. Xie, D. Stueben, Z. Berner, *Anal. Lett.* 38 (2005) 2281.
- [19] M.C. Bruzzoniti, N. Cardellicchio, S. Cavalli, C. Sarzanini, *Chromatographia* 55 (2002) 231.
- [20] A. Rahmalan, M. Zahari Abdullah, M. Marsin Sanagi, M. Rashid, *J. Chromatogr. A* 739 (1996) 233.
- [21] C.A. Marquette, L.J. Blum, *Anal. Bioanal. Chem.* 385 (2006) 546.
- [22] C. Zhang, S. Zhang, Z. Zhang, *Analyst* 123 (1998) 1383.
- [23] D.W. King, H.A. Lounsbury, F.J. Millero, *J. Environ. Sci. Technol.* 29 (1995) 818.
- [24] H. Sakai, T. Fujiwara, M. Yamamoto, T. Kumamaru, *Anal. Chim. Acta* 221 (1989) 249.
- [25] P. Jones, T. Williams, L. Ebdon, *Anal. Chim. Acta* 217 (1989) 157.
- [26] V. Di Marco, A. Tapparo, G.G. Bombi, *Ann. Chim. (Rome)* 89 (1999) 397.
- [27] J.M. Aubry, *J. Am. Chem. Soc.* 107 (1985) 5844.
- [28] D.W. King, *J. Environ. Sci. Technol.* 32 (1998) 2997.
- [29] L.M. Schwartz, *Anal. Chem.* 49 (1977) 2062.
- [30] A. Hubaux, G. Vos, *Anal. Chem.* 42 (1970) 849.

Application of the Bahe's pseudolattice-theory to water—1-butyl-3-methylimidazolium tetrafluoroborate (bmimBF₄) mixtures at 298.15 K

Part I. Autoprotolysis constants

I. Bou Malham, P. Letellier, M. Turmine*

Université Pierre et Marie Curie-PARIS6, CNRS-ENSCP, UMR7575, Energétique et Réactivité aux Interfaces, UPMC, case 39, 4 place Jussieu, 75252 Paris cedex 05, France

Received 5 June 2006; received in revised form 4 October 2006; accepted 5 October 2006
Available online 7 November 2006

Abstract

The autoprotolysis constants (K_s) of water – 1-butyl-3-methylimidazolium tetrafluoroborate (bmimBF₄) mixtures were determined at 298 K over the composition range of 0 to 77.43 vol.% bmimBF₄ using potentiometric method with a glass electrode. A slight increase in the autoprotolysis constant was observed when the salt was added to the water. The value of the ionic product of the medium then decreases as the bmimBF₄ content increases from about 20 vol.%. The acid–base properties of these media were perfectly described by Bahe's approaches that were completed by Varela et al. concerning structured electrolyte solutions with large short-range interactions.

© 2006 Elsevier B.V. All rights reserved.

Keywords: 1-Butyl-3-methylimidazolium tetrafluoroborate; Autoprotolysis constant; Solvent mixture

1. Introduction

For many years, chemists have become increasingly interested in ionic liquids as reaction media. Ionic liquids can be used pure (molten salt at room temperature) [1], or mixed with water [2] or other solvents [3]. The increasing number of publication and feature revues on these liquids [4–6] attests to this interest. Ionic liquids have low vapour pressures and are considered as green solvents [7–12]. Therefore, they are excellent candidates for replacing organic solvents in many industrial processes. However, their main advantage is the possibility of modulating and adjusting their physicochemical properties. This currently occupies the main body of work on these media. However, only a few studies have investigated the physicochemical extents likely to affect the reactivity, such as, for example, their acid–base properties, particularly for imidazolium salts. Acid–base studies of imidazolium salts, such as 1-butyl-3-methylimidazolium tetrafluoroborate (bmimBF₄), are complicated by their being

aprotic solvents and thus even trace amounts of water substantially modifies their properties [13]. Thus, before we considered the properties of a pure ionic liquid, we began by studying the acid–base properties of water—bmimBF₄ mixtures with an approach previously used for water–ethylammonium nitrate (EAN) mixtures at 298 K [14]. Unlike imidazolium salts, EAN is a protic solvent having an autoprotolysis constant, pK_s , of 10.2. Recently, we measured vapour pressures of water above the same media. We showed that between 0 and 77.43 vol.% of bmimBF₄, the water activity is close to one. Thus, we wondered about the behaviour of H⁺ and OH[−] ions in the same composition range. Furthermore, bmimBF₄ salt forms aggregates in water at a concentration of 1 mol L^{−1} [15], leading to a very structured concentrated electrolyte media with short-range ion–ion interactions. We decided to test the validity of the pseudolattice theory introduced by Bahe [16] to describe the behaviour of these particular media.

2. Theory

There have been many studies of the physicochemical properties of solvent mixtures showing that hydro-organic media can be

* Corresponding author. Tel.: +33 1 44 27 36 76; fax: +33 1 44 27 30 35.
E-mail address: turmine@ccr.jussieu.fr (M. Turmine).

characterized by an autoprotolysis constant. In these mixtures, the co-solvents can be protic (methanol [17], isopropanol [18] ethanolamine [19], butylamine [20], pyridine [21], etc.) or aprotic (dimethylsulfoxide [22], dioxane [23], dimethylformamide [24], etc.).

Adding an organic co-solvent to water extends the acidity domain of the medium when the co-solvent is non-protic or restricts it when the co-solvent has acid–base properties (acetic acid [25], butylamine [20]), and in particular, it allows molecular species to be solubilised. For water–EAN (which is protic molten salt) mixtures, the observed solubilising capacity is close to that of a water–70% methanol mixture. Moreover, when only a small amount of EAN was added to water, a strong decrease in the pK_s by four units was observed because EAN is a stronger acid than water and thus liberates protons. The pK_s value then stabilises at value close to 10 for all compositions. As imidazolium salts are aprotic solvents, a completely different behaviour would be expected because only the water can exchange protons. Thus, we can specify the equilibrium conditions of autoprotolysis.

Consider a mixture, S, characterised by a molar fraction of salt, x . The water autoprotolysis equilibrium in this medium is:



where H^+ and OH^- are the solvated species. The equilibrium condition in the medium S can be written as:

$${}^S\mu_{H^+} + {}^S\mu_{OH^-} - {}^S\mu_{H_2O} = 0 \quad (1)$$

where ${}^S\mu_{H^+}$, ${}^S\mu_{OH^-}$ and ${}^S\mu_{H_2O}$ are, respectively, the chemical potentials of the proton, hydroxide ion and water in the mixture. The chemical potential of the ions can be considered in terms of concentration according to their standard state in medium, S,

$${}^S\mu_{H^+(C)}^\theta + {}^S\mu_{OH^-(C)}^\theta + RT \ln {}^S a_{H^+(C)} {}^S a_{OH^-(C)} - {}^S\mu_{H_2O} = 0 \quad (2)$$

In the medium, S, the chemical potential of water has a fixed value. So,

$$\ln {}^S a_{H^+(C)} {}^S a_{OH^-(C)} = \frac{{}^S\mu_{H_2O} - {}^S\mu_{H^+(C)}^\theta - {}^S\mu_{OH^-(C)}^\theta}{RT} \quad (3)$$

The standard chemical potentials terms are thermodynamic constants that are characteristic of the medium, S, and thus the product of activities of H^+ and of OH^- are also constant. An autoprotolysis product can be defined as:

$$K_S = {}^S a_{H^+(C)} {}^S a_{OH^-(C)} \quad (4)$$

By convention, the proton activity in the solvent S is linked to the quantity:

$$pS^+ = -\log {}^S a_{H^+(C)} \quad (5)$$

and

$$pK_S = -\log K_S$$

In this definition of the autoprotolysis product, the water behaviour taken as a reference for expressing its chemical potential is the same as it has in the medium, S. In other words, we can consider the water activity in S as being equal to one.

Consequently, the autoprotolysis product is thermodynamically defined. It is a characteristic constant for the medium, S, which can change as the mixture composition changes. However, the obvious problem is linking the activities of diluted species to their concentrations by means of a deviation rule to the behaviour “at infinite dilution”. Thus, we can write for the medium S:

$$K_S = {}^S\gamma_{H^+(C)} {}^S\gamma_{OH^-(C)} \{C_{H^+}\} \{C_{OH^-}\} \quad (6)$$

where ${}^S\gamma_{H^+(C)}$ and ${}^S\gamma_{OH^-(C)}$ are the activity coefficients of H^+ and of OH^- in S in terms of concentration, and $\{C_{H^+}\}$ and $\{C_{OH^-}\}$ are the concentration values of H^+ and of OH^- . As the ionic strength of the salts in this media are strong, other electrolytes present in the solution do not affect this relationship. We will suppose, for the medium S, that H^+ and OH^- activity coefficients are equal to one,

$${}^S\gamma_{H^+(C)} = {}^S\gamma_{OH^-(C)} = 1 \quad (7)$$

and

$$K_S = \{C_{H^+}\} \{C_{OH^-}\}$$

This approximation must be carefully validated during the experimental study. The autoprotolysis product in the medium S can be related to that in pure water by introducing its characteristic extents, we can write:

$$pK_S = pK_W - \log a_{H_2O} + \frac{{}^S\mu_{H^+(C)}^\theta - {}^W\mu_{H^+(C)}^\theta}{2.3RT} + \frac{{}^S\mu_{OH^-(C)}^\theta - {}^W\mu_{OH^-(C)}^\theta}{2.3RT} \quad (8)$$

with

$$pK_W = -\log K_W$$

The standard Gibbs energies of transfer and the transfer activity coefficients of the H^+ and OH^- ions are defined by the following relationships:

$$\frac{{}^S\mu_{H^+(C)}^\theta - {}^W\mu_{H^+(C)}^\theta}{2.3RT} = \frac{\Delta_t G_{W \rightarrow S(H^+)}^\theta}{2.3RT} = \log \gamma_{t(H^+)} \quad (9)$$

$$\frac{{}^S\mu_{OH^-(C)}^\theta - {}^W\mu_{OH^-(C)}^\theta}{2.3RT} = \frac{\Delta_t G_{W \rightarrow S(OH^-)}^\theta}{2.3RT} = \log \gamma_{t(OH^-)} \quad (9')$$

The expression for the autoprotolysis product in the medium S can thus be written as

$$pK_S = pK_W - \log a_{H_2O} + \frac{\Delta_t G_{W \rightarrow S(H^+)}^\theta}{2.3RT} + \frac{\Delta_t G_{W \rightarrow S(OH^-)}^\theta}{2.3RT} \quad (10)$$

or,

$$pK_S = pK_W - \log a_{H_2O} + \log \gamma_{t(H^+)} \gamma_{t(OH^-)} \quad (11)$$

These equations have been established from a characteristic formalism of a mixed medium [26]. We could also have chosen to describe the behaviour of electrolyte aqueous solutions using the more usual formalism that always refers to behaviour in pure

water. Thus, for the proton, its chemical potential is, for example, written as:

$$\begin{aligned} {}^S\mu_{\text{H}^+} &= {}^W\mu_{\text{H}^+(\text{C})}^\theta + RT \ln\{\text{C}\} + RT \ln {}^W\gamma_{\text{H}^+(\text{C})} \\ &= {}^S\mu_{\text{H}^+(\text{C})}^\theta + RT \ln\{\text{C}\} + RT \ln {}^S\gamma_{\text{H}^+(\text{C})} \end{aligned} \quad (12)$$

where ${}^W\gamma_{\text{H}^+(\text{C})}$ is the activity coefficient of the proton in the concentrated salt solution, taking its behaviour at the standard state at infinite dilution in water as the reference. ${}^S\gamma_{\text{H}^+(\text{C})}$ is the activity coefficient of proton in the concentrated salt, taking its behaviour at the standard state at infinite dilution in the medium S as the reference. The following general relations can then be written:

$$\ln {}^W\gamma_{\text{H}^+(\text{C})} = \frac{{}^S\mu_{\text{H}^+(\text{C})}^\theta - {}^W\mu_{\text{H}^+(\text{C})}^\theta}{RT} + \ln {}^S\gamma_{\text{H}^+(\text{C})} \quad (13)$$

or

$$\ln {}^W\gamma_{\text{H}^+(\text{C})} = \ln \gamma_{\text{t}(\text{H}^+)} + \ln {}^S\gamma_{\text{H}^+(\text{C})} \quad (13')$$

As previously stated, for concentrated salt media, the values of ${}^S\gamma_{\text{H}^+(\text{C})}$ are close to one, which allows the activity coefficients of the ions, referenced to the ideal dilute behaviour of the solute in water in terms of concentration, to be identified with the transfer activity coefficients. Then,

$$\ln {}^W\gamma_{\text{H}^+(\text{C})} = \ln \gamma_{\text{t}(\text{H}^+)} \quad (14)$$

and

$$\ln {}^W\gamma_{\text{OH}^-(\text{C})} = \ln \gamma_{\text{t}(\text{OH}^-)} \quad (14')$$

This identification is useful for describing the activity coefficients of ions from the various approaches used in studies by Bahe or Pitzer to explain the behaviour of concentrated electrolyte solutions. The formalism can be completed by writing the mean extents of transfer activity coefficients as:

$$\begin{aligned} \ln {}^W\gamma_{\text{H}^+(\text{C})} {}^W\gamma_{\text{OH}^-(\text{C})} &= \ln \gamma_{\text{t}(\text{H}^+)} \gamma_{\text{t}(\text{OH}^-)} = 2 \ln {}^W\gamma_{\pm(\text{C})} \\ &= 2 \ln \gamma_{\text{t}(\pm)} \end{aligned} \quad (15)$$

This convention allows Eq. (11) to be written in a simple form:

$$\text{p}K_{\text{S}} = \text{p}K_{\text{W}} - \log a_{\text{H}_2\text{O}} + 2 \log \gamma_{\text{t}(\pm)} \quad (16)$$

In this equation, the values of $\text{p}K_{\text{S}}$ and $\text{p}K_{\text{W}}$ can be experimentally determined potentiometrically. The water activity with reference to the behaviour of pure component can be obtained from vapour pressure measurements of water above pure liquid water, ${}^W P_{\text{H}_2\text{O}}$, and above the solution S, ${}^S P_{\text{H}_2\text{O}}$, according to

$$a_{\text{W}} = \frac{{}^S P_{\text{H}_2\text{O}}}{{}^W P_{\text{H}_2\text{O}}} \quad (17)$$

In hydro-organic mixtures, the water activity is always less than one and decreases as more organic solvent is added to the mixture. This generally implies that this term positively contributes to the variation in $\text{p}K_{\text{S}}$, becoming larger as the medium

Table 1

Values of water activities in water–bmimBF₄ mixtures according to Katayanagi et al. [27] and our recent measurements*

X_{bmimBF_4}	bmimBF ₄ (vol.%)	($a_{\text{H}_2\text{O}}$) [27]	($a_{\text{H}_2\text{O}}$) [*]
0	0	1.0000	1.0000
0.0157	14.26	0.9862	1.0173
0.0407	30.67	0.9844	1.0374
0.1748	68.83	0.9368	1.0289
0.3125	82.57	0.8258	0.9486
0.4379	89.04	0.6863	0.8251
0.5641	93.10	0.5300	0.6589
0.7079	96.19	0.3544	0.5411
0.8755	98.65	0.1593	0.3294
0.889	98.82	0.2432	0.2375

becomes richer in organic solvent. For water–bmimBF₄ mixtures, unusual water behaviour was observed between 0 and 77.43 vol.% of salt (molar fraction $X=0.2470$), with the water activity remaining almost equal to one, slightly lower according to Katayanagi [27], and slightly higher according to our recent measurements, although the water content of the solution becomes weaker. Table 1 shows the activities of these mixtures.

As can be seen in Table 1, the participation of the water activity to the value of $\text{p}K_{\text{S}}$ is negligible until 77.43 vol.% of salt, and any changes to the autoprotolysis constant come almost exclusively from changes to the stability of H⁺ and OH[−] in the medium.

3. Materials and products

3.1. Products

3.1.1. Chemicals

Sodium tetrafluoroborate (98%), 1-methylimidazole (99%) and 1-bromobutane (99%) were from Acros Organics. Acetone (Normapur) was from Prolabo, ethyl acetate (purex for analysis) and dichloromethane were from SDS.

Sodium hydroxide (1 M, titrinorm, without carbonate), hydrochloric acid (1 M, titrinorm) and buffer solutions (pH 4, pH 7, pH 10) were from VWR Prolabo.

All mixtures were prepared in ultrapure water (all water used was distilled and filtered with an ELGA UHQ II system, $\kappa=18 \text{ M}\Omega$). All imidazolium salts were synthesised according to standard methods [28].

3.1.1.1. Synthesis of 1-butyl-3-methylimidazolium bromide (bmimBr). An excess of 1-bromobutane was slowly added to a stirred solution of 1-methylimidazole in ethyl acetate. The mixture was then heated at reflux for 24 h. The reaction was stopped when two phases were formed. The top phase, containing unreacted starting material in ethyl acetate, was decanted and discarded. The bottom phase contained the butylimidazolium bromide. This was washed three times with ethyl acetate to remove any unreacted reagents (particularly 1-methylimidazole). Residual ethyl acetate was removed by heating (70 °C) under vacuum (12 h). bmimBr was obtained as colourless hygroscopic solid. The structure

of the resulting salt was confirmed by ^1H NMR spectroscopy (400 MHz, CDCl_3 , δ/ppm relative to TMS) = 0.94 (t, $J = 7.4$ Hz, $\text{NCH}_2\text{CH}_2\text{CH}_2\text{CH}_3$); 1.35 (m, $J = 7.5$ Hz, $\text{NCH}_2\text{CH}_2\text{CH}_2\text{CH}_3$); 1.88 (m, $J = 7.6$ Hz, $\text{NCH}_2\text{CH}_2\text{CH}_2\text{CH}_3$); 4.10 (s, NCH_3); 4.31 (t, $J = 7.4$ Hz, $\text{NCH}_2\text{CH}_2\text{CH}_2\text{CH}_3$); 7.41 (s, $\text{CH}(\text{ring})$); 7.52 (s, $\text{CH}(\text{ring})$); 10.39 (s, $\text{CH}(\text{ring})$).

3.1.1.2. Synthesis of 1-butyl-3-methylimidazolium tetrafluoroborate (bmimBF₄). A solution of NaBF_4 in acetone was slowly added to a rapidly stirred solution of the appropriate bmimBr. The mixture was stirred at room temperature for four days and then filtered through celite. The acetone was removed on the rotary evaporator. The resultant viscous liquid was dissolved in dichloromethane (CH_2Cl_2) and washed with small volumes of distilled water (3:1, v/v) until no precipitation of AgBr occurred in the aqueous phase on addition of a concentrated AgNO_3 solution. The CH_2Cl_2 was then evaporated. Traces of water and other volatile solvents were removed by freeze-drying just before starting the experiment. bmimBF₄ was obtained as colourless, very viscous, hydrophilic liquid. The structure was confirmed by ^1H and ^{13}C NMR spectroscopy.

^1H NMR spectroscopy (400 MHz, D_2O , δ/ppm relative to TMS) = 0.82 [t, $J = 7.4$ Hz, $\text{NCH}_2\text{CH}_2\text{CH}_2\text{CH}_3$]; 1.21 [m, $J = 7.5$ Hz, $\text{NCH}_2\text{CH}_2\text{CH}_2\text{CH}_3$]; 1.75 [m, $J = 7.6$ Hz, $\text{NCH}_2\text{CH}_2\text{CH}_2\text{CH}_3$]; 3.79 [s, NCH_3]; 4.10 [t, $J = 7.4$ Hz, $\text{NCH}_2\text{CH}_2\text{CH}_2\text{CH}_3$]; 7.34 [s, $\text{CH}(\text{ring})$]; 7.35 [s, $\text{CH}(\text{ring})$]; 8.60 [s, $\text{CH}(\text{ring})$]; ^{13}C NMR spectroscopy (300 MHz, D_2O , δ/ppm relative to TMS) = 15.37 [$\text{NCH}_2\text{CH}_2\text{CH}_2\text{CH}_3$]; 21.52 [$\text{NCH}_2\text{CH}_2\text{CH}_2\text{CH}_3$]; 34.04 [$\text{NCH}_2\text{CH}_2\text{CH}_2\text{CH}_3$]; 38.35 [NCH_3]; 52.04 [$\text{NCH}_2\text{CH}_2\text{CH}_2\text{CH}_3$]; 124.97 [$\text{C}(\text{ring})$]; 126.25 [$\text{C}(\text{ring})$]; 138.60 [$\text{C}(\text{ring})$]. ElectroSpray mass spectrometry (ESI positive): bmimBF₄, $m/z = 139.04$ (bmim⁺).

3.1.2. Properties of room temperature molten salt and its mixtures with water

As the molar weight of the salt, $M_2 = 226.04$ g mol⁻¹, is much higher than that of water, $M_1 = 18.01$ g mol⁻¹, the molar fraction variation of the salt was small even for high volume percentages of salt. The pure salt concentration is $C_{\text{salt}} = 5.31$ mol L⁻¹. Therefore, we will generally use the concentration or volume percentage (pure salt volume in cm³ for 100 cm³ of solution) for the composition variations of the solution. Different composition scales in the studied range are given in Table 2.

Table 2
Relation between the composition scales of various water–1-butyl-3-methylimidazolium tetrafluoroborate (bmimBF₄) mixtures in the studied domain

X_{bmimBF_4}	C_{bmimBF_4}	vol.% bmimBF ₄
0	0	0
0.0231	1.038	19.80
0.0389	1.545	29.75
0.0569	2.032	38.67
0.0856	2.573	49.48
0.1208	3.081	58.97
0.1707	3.579	68.28
0.2470	4.069	77.43

3.2. Materials

3.2.1. Proton-specific electrodes: hydrogen electrode and glass electrode

We attempted to measure acidity levels with a hydrogen electrode classically prepared according to Bates [29] and used in many studies, particularly for concentrated salt mixtures [30,31]. We checked the validity of the responses of the prepared electrodes in water–DMSO mixtures [22]. However, the hydrogen electrode was not stable in water–molten salt mixtures, possibly because ammonium ions poison the catalytic surface of platinum on the Pt electrode [32]. The same problem was encountered in our studies of water–EAN mixtures. Thus, potentiometric methods for determining the acidity levels in media with low autoprotolysis constants are limited by the difficulty in using a thermodynamic hydrogen electrode. Glass electrodes (membrane electrodes) do not have the same potentials. However, various studies have shown that glass electrodes can measure $\text{p}K_s$ values up to about 16 [33,34]. Thus, we attempted this study with “high alkalinity” glass electrode made by Inforlab Chimie.

3.2.2. Reference electrode and electromotive force measurements

The pH glass electrode was used in a potentiometric cell in conjunction with a KCl-saturated calomel reference electrode (Radiometer Analytical). The electromotive force (emf) of this cell was measured using a Radiometer Analytical millivoltmeter (LPH530T).

3.3. Measurement cell

We tested the junction between the measurement compartment containing the solution being studied and the reference compartment by testing three different electrochemical set-ups, all of which gave the same values of $\text{p}K_s$. The first set-up used a leak junction, the second, an agar–agar gel salt bridge and the third, a ceramic junction. The studied and reference solutions were contained in double-walled measurement cells that allowed water to circulate from a thermostated bath. The temperature was maintained at a constant 298.15 ± 0.10 K.

3.3.1. Electrochemical cell

The glass electrode was soaked in a thermostated compartment containing the solution being studied and the KCl-saturated calomel electrode (SCE) was immersed in 2 M NaBr solution. We chose this electrolyte instead of KCl to avoid precipitation of the molten salt ions. Potassium tetrafluoroborate is slightly soluble in water, whereas NaBF_4 is completely soluble. The junction between the two compartments was either:

- a glass striped tap that allows a continuous flow of the solutions in the two compartments. This set-up was used to study the $\text{p}K_s$ constants in hydro-organic medium [35]. Through mixing, the solutions maintain the electrical continuity of the electrochemical cell. Once mixed, the mixture drips into a flask. This allows an extremely stable junction between both

compartments to be established with no risk of polluting the solutions.

- a salt bridge consisting of a capillary Teflon tube filled with saline gel of 2 M NaBr in agar–agar. This junction limits ion diffusion phenomena and pollution of the solution. The junction was regenerated after each series of measurement by cutting the end of the saline bridge. This junction was also shown to be steady over time.
- a glass salt bridge junction ending with a ceramic and filled with 2 M NaBr solution. This is obviously the most practical set-up. However, there is the possibility of diffusion of the electrolytes from one compartment to the other and a risk of polluting the solutions. Undoubtedly, diffusion is very limited because the potential of the junction does not vary during measurements. As a precaution, we renewed the NaBr solution before each series of measurements.

The electrochemical cell used can be described as follows:

Cu	KCl-saturated calomel electrode	2 M aqueous NaBr solution	water–bmimBF ₄ mixture	High alkalinity glass electrode	Cu
φ_{M_1}	φ_{cal}	φ_{ref}	cell 1: ΔE_a : H ⁺ , Ca cell 2: ΔE_b : OH ⁻ , Cb	φ_v	φ_{M_2}

Taking account of the electrical continuity of the cell, the emf (ΔE) is written:

$$\begin{aligned} \Delta E &= \varphi_{M_2} - \varphi_{M_1} \\ &= (\varphi_{M_2} - \varphi_{sol}) + (\varphi_{sol} - \varphi_{ref}) + (\varphi_{ref} - \varphi_{M_1}) \end{aligned} \quad (18)$$

and:

$$\Delta E = E_{mes} + E_j - E_{ref} \quad (19)$$

where $E_{mes} = \varphi_{M_2} - \varphi_{sol}$ is the potential difference between the millivoltmeter terminal and the solution. The glass electrode is a membrane electrode with a potential that follows the Eisenman-Nikolsky's equation [36]

$$E_{mes} = cste + m \log \left(a_{H^+} + k_M \sum a_M \right) \quad (20)$$

where a_{H^+} is the proton activity in solution, a_M is the interfering cation activities and k_M is the selectivity coefficient, m is the experimental slope of the electrode. In the concentrated saline solutions, the activities, with reference to the infinite diluted state in the medium, are given in terms of the concentration. As will be shown in the experimental study, the imidazolium cation interferes very little with the electrode response.

$E_j = \varphi_{sol} - \varphi_{ref}$ is the junction potential between the two compartments. Its value depends only on the concentration of the two electrolytes involved: the molten salt and the 2 M NaBr solution. This potential can be assumed not to vary with the concentration of the acids and bases introduced into the solution. Thus, E_j is considered as constant.

$E_{ref} = \varphi_{M_1} - \varphi_{ref}$ is the potential difference between the millivoltmeter terminal M_1 and the NaBr solution. This potential difference is constant providing the junction between the KCl-saturated calomel electrode and the NaBr solution does not

change. Diffusion between these two solutions at this junction was avoided by means of a Teflon capillary filled with 2 M NaBr solution in agar–agar gel. Under these conditions, the liquid-junction potential, E_{ref} , was found to be stable over time (to within ± 0.1 mV). If the imidazolium ion does not interfere, the emf of this cell will be:

$$\begin{aligned} \Delta E &= \varphi_{M_2} - \varphi_{M_1} = cste + m \log a_{H^+} + E_j - E_{ref} \\ &= A + m \log a_{H^+} \end{aligned} \quad (21)$$

3.3.2. Determination of pK_s

We prepared solutions of the same concentration, C , of HCl (C_a), and NaOH (C_b): $C = C_a = C_b$. We then measure the emf of the corresponding cells. In acidic medium, the emf was:

$$\Delta E_a = A + m \log \{C_a\} \quad (22)$$

In basic medium, the base concentration C_b is implied from

$$\begin{aligned} \Delta E_b &= A + m \log a_{H^+} = A + m \log \frac{K_s}{\{C_b\}} \\ &= A - mpK_s - m \log \{C_b\} \end{aligned} \quad (23)$$

For the same concentration $C = C_a = C_b$, pK_s was calculated from the following relationship:

$$\frac{\Delta E_a - \Delta E_b}{m} - 2 \log \{C\} = pK_s \quad (24)$$

3.4. Solvent preparation

Despite all possible experimental precautions, we were unable to prepare a strictly neutral salt. This was mainly due to the presence of traces of acid in the sodium tetrafluoroborate used for the ionic liquid synthesis. We were unable to remove these traces despite repeated recrystallisation. Thus, we decided to neutralise the salt before studying it, according to a procedure proposed by Fischer and Byé [37]. Thus, 5 mL of a given water–bmimBF₄ aqueous solution was titrated with concentrated sodium hydroxide solution to limit dilution phenomenon. The position of the equivalent point was then determined using a Gran-like graphical method. We assumed that the aqueous solution of the molten salt contained a residual strong acid, AH, of unknown concentration (C_{AH}). V_{AH} is the initial volume of the solution containing this residual acid. The acid solution was titrated with a solution of strong base (NaOH) having a concentration C_b . The volume, V_b , of the basic solution was added and the pH of the titrated solution was followed with a calibrated pH meter. For this purely analytical application, we adopt the following approximation $[H^+] = 10^{-pH} \text{ mol L}^{-1}$.

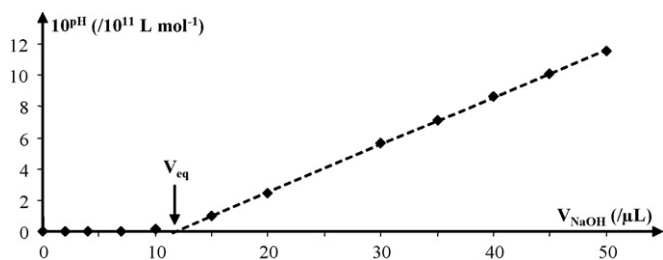


Fig. 1. Titration of 5 mL aqueous 1-butyl-3-methylimidazolium tetrafluoroborate (bmimBF₄) solution at 19.8 vol.% with 1 M NaOH. The equivalent volume is about 12 μL.

By considering more particularly the electrode responses after the equivalent point (i.e., when the proton concentration is low) and that $V_b \ll V_{AH}$, we establish the following Gran-type relationship:

$$\frac{1}{[H^+]} = 10^{pH} = \frac{C_b}{K_s V_{AH}} (V_b - V_{eq}) \quad (25)$$

For all pH values, the plot of 10^{pH} versus V_b gives a horizontal line before the equivalent point and a straight line of slope $C_b/K_s V_{AH}$ after this point. These two lines intercept on the x-axis at $V_b = V_{eq}$. An example of a titration is given in Fig. 1.

Once calculated, the aqueous salt solution was neutralised by adding the necessary quantity of base. Thus, the salt solution is neutral from an acid–base point of view, which was verified by a second titration. The principal criticism of this procedure is that a small quantity of a salt NaA corresponding to the residual quantity of acid present in the solution is added to the salt solution. This quantity is very small and is assumed to have no effect on the medium properties.

4. Results

For various water–salt mixtures, we measured the emf of the previously described cells at 298.15 K in acidic medium (ΔE_a), and basic medium (ΔE_b) by respectively varying the concentrations of HCl and NaOH (Fig. 2). For the medium at 68.28 vol.% salt, ΔE_b slowly evolved in the basic medium for NaOH concentrations greater than 10^{-2} mol L⁻¹. For the medium at 77.43 vol.% bmimBF₄, ΔE_b did not stabilize for NaOH concen-

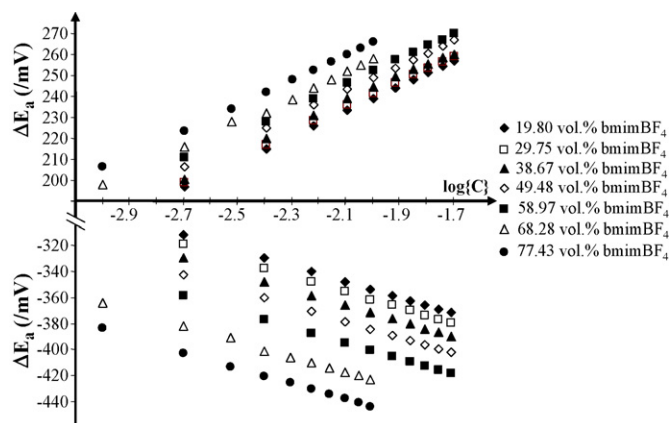


Fig. 2. Plots of ΔE_a and ΔE_b against the logarithm of the concentration for a series of acid and base solutions of same concentration in media containing bmimBF₄ in the range between 19.80 and 77.43 vol.% at 298.15 K.

trations greater than 10^{-2} mol L⁻¹. Tests at 86.47 vol.% showed that the emf, ΔE_b , did not stabilise for any value of C_b . For these three media, we can suppose that we have reached the working limits of the glass electrode toward protons in basic medium, with the autoprotolysis constant of these media becoming undoubtedly very weak.

In all the studied mixtures, we observed an excellent linearity in the electrode response (Fig. 2). The slopes are about 60 ± 1 mV per decade for acid media and about -60 ± 1 mV per decade for basic media. For each medium and for all concentrations, the pK_s values were calculated according to Eq. (27). An example of some of these results is given in Table 3 for aqueous mixtures containing 49.48 and 77.43 vol.% salt.

As can be seen, the standard deviation of pK_s is close to 0.01. For all studied water–bmimBF₄ mixtures, pK_s values are given in Table 4.

Fig. 3 shows the variation of the autoprotolysis constants of water–bmimBF₄ mixtures with respect to the salt concentration at 298.15 K. The variations in pK_s for water–NaClO₄, water–NaCl [30,38], and water–Me₄NCl [34] systems are also given for comparison.

The variations in pK_s for these four salts have the same form. However, the concentration scale in x-axis gives a distorted picture. This is due to the large differences between the molecular

Table 3
Calculation of pK_s for two mixtures containing 49.48 and 77.43 vol.% bmimBF₄ at 298.15 K

49.48 vol.% bmimBF ₄ m = 60.3				77.43 vol.% bmimBF ₄ m = 59.8			
ΔE_a	ΔE_b	$\log\{C\}$	pK_s	ΔE_a	ΔE_b	$\log\{C\}$	pK_s
206.4	-342.9	-2.70	14.509	206.7	-383.5	-3.00	15.870
225.2	-360.4	-2.40	14.511	223.5	-402.6	-2.70	15.869
236	-371	-2.22	14.515	234.2	-413.1	-2.52	15.873
243.5	-378.6	-2.10	14.517	241.8	-420.6	-2.40	15.876
249	-384.4	-2.00	14.513	248	-425.5	-2.30	15.869
253.6	-389.1	-1.93	14.510	252.4	-430.3	-2.22	15.865
257.4	-393.2	-1.86	14.509	256.5	-434.4	-2.16	15.869
260.6	-396.6	-1.80	14.504	260	-437.8	-2.10	15.869
263.8	-399.9	-1.75	14.511	263.1	-441	-2.05	15.873
266.9	-402.4	-1.70	14.515	265.8	-443.7	-2.00	15.873

|m| is the absolute value of the slope of the electrode response.

Table 4

Values of ionic products of water–bmimBF₄ mixtures determined with glass-electrode at 298.15 K

% (Volume) bmimBF ₄	pK _s ± 0.01
19.80	13.76
29.75	13.96
38.67	14.21
49.48	14.51
58.97	14.89
68.28	15.45
77.43	15.87

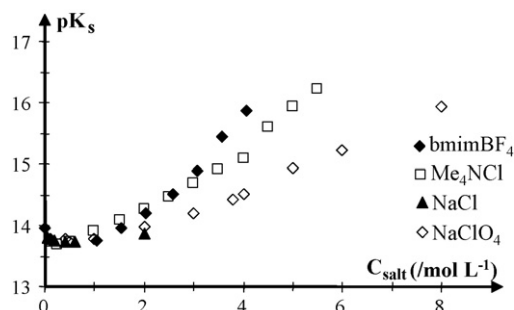


Fig. 3. Variations of autoprotolysis constants for water–bmimBF₄ (this study), water–NaClO₄, water–NaCl [30,38] and water–tetramethylammonium chloride (Me₄NCl) [34] mixtures as a function of the concentration of the electrolyte at 298.15 K.

weight of these salts. A 5.31 M bmimBF₄ solution corresponds to the pure salt, which is not the case for the other electrolytes. However, up to a concentration of 3 mol L⁻¹, the two ammonium salts exhibit a very similar behaviour.

5. Discussion

All of our experimental data allow calculating the mean transfer activity coefficients for H⁺ and OH⁻ ions for the different water–salt mixtures (Table 5).

The mean transfer activity coefficients are positive for bmimBF₄ concentrations greater than 1 M, which corresponds to a decrease in stability of the ions (or an increase in their standard chemical potential). Thus, with the water activity remaining almost constant, the decrease in the autoprotolysis constant of the medium is essentially due to the destabilisation of the H⁺ and OH⁻ ions.

Table 5

Mean transfer activity coefficients of ($\gamma_{\pm(C)}$) with respect to concentration and the autoprotolysis products (pK_s) for the different water–bmimBF₄ mixtures

X _{bmimBF₄}	C _{bmimBF₄}	% Vol. bmimBF ₄	pK _s	a _w	log{a _w }	log{ $\gamma_{\pm(C)}$ }
0	0	0	13.96	1	0	0
0.0231	1.038	19.80	13.76	1.0232	0.0099	-0.09502
0.0389	1.545	29.75	13.96	1.0371	0.0158	0.00791
0.0569	2.032	38.67	14.21	1.0489	0.0207	0.135367
0.0856	2.573	49.48	14.51	1.0599	0.0253	0.287632
0.1208	3.081	58.97	14.89	1.0619	0.0261	0.478042
0.1707	3.579	68.28	15.45	1.0472	0.0200	0.755015
0.2470	4.069	77.43	15.87	0.9961	-0.0017	0.954151

The water activities (a_w) are recently determined by water vapour pressure measurements.

We tried to account for this by considering the properties inherent in highly concentrated electrolytes solutions. Various studies on water–bmimBF₄ mixtures have shown that these media are strongly structured [39] for salt concentrations greater than 1 mol L⁻¹. Surface tensions studies [40], C_p measurements [41] or surface thermal coefficient, b_{T,P}, measurements [42] have shown that the salt aggregates, inducing structure to the medium. Thus, we were interested in the approach taken by Bahe [16] for concentrated electrolyte solutions (quasi-lattice theory) using short-range ion–ion interaction model that assumes that the electrolyte ions adopt a face-centred cubic structure in solution. Several studies have shown that this approach works for concentrated salt solutions up to concentrations as high as 3 or 4 M [43–45], and also when determining the standard extents at the infinitely diluted state [16]. Bahe suggested that for an electrolyte, MX, the mean activity coefficient for a molar fraction can be written with respect to the salt concentration in solution according to:

$$\log \gamma_{\pm(x)S} = -AC^{1/3} + bC \quad (26)$$

where A is a calculated parameter having the value of 0.28894 at 298 K in water. The parameter b is calculated from experiment. Bahe gave a mean value of 0.065 for 1:1 electrolytes. Varela et al. [46] showed that for very high salt concentrations, above 4 M, this relationship should take a C² term to take into account the strong short-range interactions between ions. Thus, they proposed the following relationship:

$$\log \gamma_{\pm(x)S} = -AC^{1/3} + bC + cC^2 \quad (27)$$

Obviously, water–bmimBF₄ mixtures fulfil all these criteria and we tried to judge validity of these approaches to explain how the autoprotolysis constant evolves. Our reasoning consists of two steps.

The first is to consider how the transfer activity coefficients of the H⁺ and OH⁻ ions vary with the nature of the medium. If we introduce a very small quantity of HCl in the structured solution of bmimBF₄, the H⁺ and Cl⁻ ions are included in the existing structure without modifying it. Thus, the state of these ions will be identical to those of the solvent [47]. The activity coefficients for H⁺ and OH⁻ are then assumed to be described by the same rules as those concerning bmim⁺ and BF₄⁻, thus:

$$\gamma_{I(H^+)} = \gamma_{bmim^+(c)} \quad (28)$$

$$\gamma_{I(OH^-)} = \gamma_{BF_4^-(c)}$$

Or by introducing the mean extents:

$$\gamma_{I(\pm)} = \gamma_{\pm(c)} \quad (29)$$

Variations of mean transfer activity coefficients for H^+ and OH^- ions will then be the same as the mean activity coefficient of the salt with respect to the concentration.

The second step in our reasoning requires linking the mean activity coefficient for the molar fraction of the salt to that with respect to the concentration. For notational convenience, the salt $bmim^+BF_4^-$ will be represented by M^+X^- . n_2 moles of MX salt are introduced in n_1 moles of water. The chemical potential of the salt is the sum of the chemical potentials of the ions, $\mu_{MX} = \mu_{M^+} + \mu_{X^-}$. In the obtained solution, the chemical potential of MX can be expressed with respect to the concentration referenced to the ideal dilute behaviour in water as:

$$\mu_{MX} = \mu_{MX(c)}^\theta + RT \ln\{C_{M^+}\}C_{X^-} + RT \ln \gamma_{M^+(c)}\gamma_{X^-(c)} \quad (30)$$

where $\gamma_{M^+(c)}$ and $\gamma_{X^-(c)}$ are the respective activity coefficients of M^+ and X^- with respect to the concentration referenced to the ideal dilute behaviour in water. The concentrations of M^+ and X^- are equal to C , so,

$$\mu_{MX} = \mu_{MX(c)}^\theta + 2RT \ln\{C\} + 2RT \ln \gamma_{\pm(c)} \quad (31)$$

where $\gamma_{\pm(c)}$ is the mean activity coefficient with respect to the concentration. The chemical potentials can be also written for the molar fractions,

$$\mu_{MX} = \mu_{MX(x)}^\theta + RT \ln(x_{M^+}x_{X^-}) + 2RT \ln \gamma_{\pm(x)} \quad (32)$$

where $\gamma_{\pm(x)}$ is the mean activity coefficient for the molar fraction. The molar fractions of M^+ and X^- must take into account the real number of particles in the system, that is, M^+ , X^- and water. So:

$$x_{M^+} = \frac{n_2}{n_1 + 2n_2} = x_{X^-} \quad (33)$$

This quantity can be related to the molar fraction of the salt (x_s):

$$x_{M^+} = x_{X^-} = \frac{x_s}{1 + x_s} \quad (34)$$

with

$$x_s = \frac{n_2}{n_1 + n_2}$$

leading to the following expression for the chemical potential of MX :

$$\mu_{MX} = \mu_{MX(x)}^\theta + 2RT \ln \frac{x_s}{1 + x_s} + 2RT \ln \gamma_{\pm(x)} \quad (35)$$

This relationship is valid over all compositions, even at the limits. At infinite dilutions, when x_s and C tend towards 0, the mean activity coefficients with respect to mole fraction and concentration are both equal to one. Thus, we have established a simple relationship between the standard states of the salt for

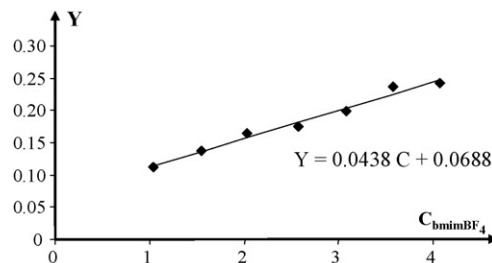


Fig. 4. Variation of Y vs. the concentration of $bmimBF_4$ in water at 298.15 K.

both composition scales:

$$\begin{aligned} \mu_{MX(x)}^\theta + 2RT \ln x_s &= \mu_{MX(c)}^\theta + 2RT \ln \frac{n_2 V_1^*}{n_1 V_1^*} \\ &= \mu_{MX(c)}^\theta + 2RT \ln\{C\} \end{aligned} \quad (36)$$

and by identification,

$$\mu_{MX(x)}^\theta + 2RT \ln\{V_1^*\} = \mu_{MX(c)}^\theta \quad (37)$$

This relationship allows us to link together the activity coefficients for the two scales as:

$$\log \gamma_{\pm(x)} = \log \frac{V_1^* C(1 + x_s)}{x_s} + \log \gamma_{\pm(c)} \quad (38)$$

This relationship can be inserted into that proposed by Varela et al. (Eq. (27)) thus:

$$\log \gamma_{\pm(c)} = \log \frac{x_s}{V_1^* C(1 + x_s)} - AC^{1/3} + bC + cC^2 \quad (39)$$

By identifying the transfer activity coefficients for H^+ and OH^- ions with those of $bmimBF_4$, the variations in the pK_s of the medium are described by:

$$\begin{aligned} pK_s &= pK_w - \log aw \\ &+ 2 \left(\log \frac{x_s}{V_1^* C(1 + x_s)} - AC^{1/3} + bC + cC^2 \right) \end{aligned} \quad (40)$$

We can thus plot the following using our experimental data:

$$\begin{aligned} Y &= \frac{pK_s - pK_w + \log aw - 2(\log(x_s/V_1^* C(1 + x_s)) - AC^{1/3})}{2C} \\ &= b + cC \end{aligned} \quad (41)$$

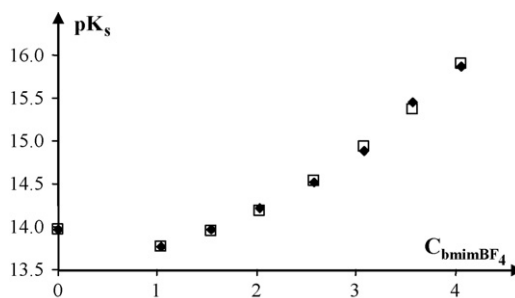


Fig. 5. Variations of the autoprotolysis constant (pK_s) of water- $bmimBF_4$ mixtures vs. the concentration of $bmimBF_4$; the open squares are the pK_s values from the experimental data, the closed diamonds are the calculated values.

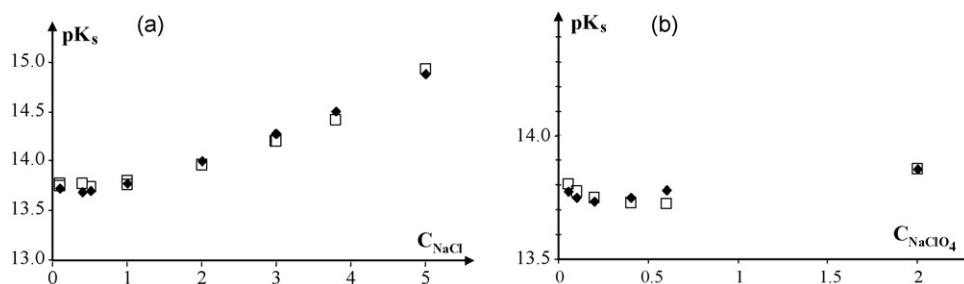


Fig. 6. Variations of the autoprotolysis constant (pK_s) of water– NaClO_4 (a) and water– NaCl (b) mixtures vs. the concentration of the salt. The open squares are the experimental pK_s values [30], and the closed diamonds are the calculated values.

Table 6

Experimental autoprotolysis constants (pK_s) of water– NaCl and water– NaClO_4 mixtures [30,38] and the pK_s values calculated from Eq. (40)

Water– NaClO_4 $b=0.1859$; $c=-0.0023$			Water– NaCl $b=0.2993$; $c=-0.0705$		
C_{NaClO_4} (mol L^{-1})	pK_s [30,38]	pK_s calc. Eq. (40)	C_{NaCl} (mol L^{-1})	pK_s [30,38]	pK_s calc. Eq. (40)
1	13.77	13.77	0.05	13.805	13.777
3	14.22	14.28	0.1	13.775	13.750
0.1	13.78	13.73	0.2	13.749	13.736
0.5	13.74	13.70	0.4	13.773	13.751
1	13.80	13.77	0.6	13.727	13.781
2	13.97	14.00	2	13.866	13.869
2.99	14.20	14.28			
3.8	14.42	14.51			
0.1	13.75	13.73			
0.4	13.78	13.69			
1	13.77	13.77			
3	14.2	14.28			
5	14.94	14.88			

We obtain a good-fitting straight line with an intercept $b=0.0688 \text{ L mol}^{-1}$ close to the mean value proposed by Bahe (0.065 L mol^{-1} for 1:1 electrolytes) and a slope $c=0.0438 \text{ L}^2 \text{ mol}^{-2}$, which is of the same order but slightly higher than that proposed by Varela et al. for different concentrated mineral electrolytes (LiNO_3 , $c=0.0047$, NaCl , $c=0.0028 \text{ L}^2 \text{ mol}^{-2}$) (Fig. 4).

The pK_s values can be now calculated from Eq. (40) and compared with experimental values (Fig. 5).

There is a very good fit between the experimental and calculated values, confirming that the approach of Bahe is relevant for describing the autoprotolysis constants. This approach is also general as we could describe, using literature values, the pK_s variations for water– NaClO_4 and water– NaCl mixtures [30,38] (Fig. 6).

Table 6 gives the experimental autoprotolysis constants (pK_s) of water– NaClO_4 and water– NaCl mixtures [30,38] and the pK_s values calculated from Eq. (40).

6. Conclusion

This study of water– bmimBF_4 mixtures at 298 K has revealed some experimental difficulties inherent in determining acid–base properties in ionic liquid media, but has also suggested some solutions. The synthesis of ionic liquids, except for ethy-

lammonium nitrate (EAN), rarely leads to perfect neutral salts. For EAN, the nitric acid was neutralised with a small excess of ethylamine. As ethylamine is very volatile, it is eliminated along with water when the salt is concentrated [48]. However, for imidazolium salts, this is not possible and thus we had to titrate and neutralise the medium before any acid–base measurements. The method we described was rapid and efficient.

For the measurements, imidazolium salts do not allow the use of hydrogen electrode classically prepared according to Bates' procedure. Measurements using a glass pH electrode were limited to pK_s values less than about 16. This poses an obvious problem for determine the pK_s of media containing more than 77.43 vol.% of bmimBF_4 , as the pK_s value for the more concentrated salt media strongly increases as the water activity decreases. One solution is to use the approach of Hammett, in which coloured indicators and buffer solutions are used over all acidities. We are currently undertaking this in our laboratory.

For the behaviour of these media, we obtained an excellent description of the acid–base properties of water– bmimBF_4 mixtures using the approach of Bahe completed by Varela et al. In this approach, we consider the electrolyte solutions to be structured with large short-range interactions between ions.

The second part of this paper deals with variations of the dissociation constant (pK_a) of different acid–base couples in the same media to establish an acidity scale in water– bmimBF_4 mixtures.

References

- [1] J. Zhang, A.J. Ragauskas, *Carbohydr. Res.* 340 (2005) 2812.
- [2] Y.B. Zhao, Z.Y. Yan, Y.M. Liang, *Tetrahedron Lett.* 47 (2006) 1545.
- [3] M.A. Klingshrin, S.K. Spear, J.D. Holbrey, R.D. Rogers, *J. Mater. Chem.* 15 (2005) 5174.
- [4] K.J. Cavell, D.S. Mc Guinness, *Coord. Chem. Rev.* 248 (2004) 671.
- [5] A.D. Headley, S.R.S.S. Kotti, J. Nam, K. Li, *J. Phys. Org. Chem.* 18 (2005) 1018.
- [6] C. Chiappe, D. Pieraccini, *J. Phys. Org. Chem.* 18 (2005) 275.
- [7] J.D. Holbrey, K.R. Seddon, *J. Chem. Soc., Dalton Trans.* 13 (1999) 2133.
- [8] P. Bonhôte, A.P. Dias, N. Papageorgiou, K. Kalyanasundaram, M. Grätzel, *Inorg. Chem.* 35 (1996) 1168.
- [9] G. Law, P.R. Watson, *Langmuir* 17 (2001) 6138.
- [10] H.L. Ngo, K. LeCompte, L. Hargens, A.B. McEwen, *Thermochim. Acta* 357–358 (2000) 97.
- [11] J.G. Huddleston, A.E. Visser, W.M. Reichert, H.D. Willauer, G.A. Broker, R.D. Rogers, *Green Chem.* 3 (2001) 156.
- [12] P. Izak, N.M.M. Mateus, C.A.M. Afonso, J.G. Crespo, *Sep. Purif. Technol.* 41 (2005) 141.
- [13] C. Thomazeau, H. Olivier-Bourbigou, L. Magna, S. Luts, B. Gilbert, *J. Am. Chem. Soc.* 125 (2003) 5264.
- [14] N. Benlhima, D. Lemordant, P. Letellier, *J. Chim. Phys.* 86 (1989) 1919.
- [15] J. Bowers, C.P. Butts, P.J. Martin, M.C. Vergara-Gutierrez, *Langmuir* 20 (2004) 2191.
- [16] (a) L.W. Bahe, *J. Phys. Chem.* 76 (1972) 1062;
(b) L.W. Bahe, *J. Phys. Chem.* 76 (1972) 1608;
(c) L.W. Bahe, D. Parker, *J. Am. Chem. Soc.* 97 (1975) 5664;
(d) L.W. Bahe, K.A. Jung, *Can. J. Chem.* 54 (1976) 824.
- [17] C.H. Rochester, *J. Chem. Soc., Dalton trans.* 1 (1972) 5.
- [18] R. Gaboriaud, R. Schaal, O. Fillaux, *J. Chim. Phys.* 66 (1969) 730.
- [19] R. Gaboriaud, *C.R. Acad. Sci.: Ser. C Chem.* 263 (1966) 282.
- [20] R. Gaboriaud, J.L. Brisset, *J. Chim. Phys.* 67 (1970) 1715.
- [21] J.L. Brisset, D. Meeroff, *J. Chim. Phys.* 10 (1971) 1506.
- [22] J.C. Halle, R. Gaboriaud, R. Schaal, *Bull. Soc. Chim. Fr.* 6 (1969) 1851.
- [23] E. Kilic, N. Aslan, *Microchim. Acta* 151 (2005) 89.
- [24] G. Demange-Guerin, *Talanta* 17 (1970) 1075.
- [25] R. Gaboriaud, *C. R. Acad. Sci.: Ser. C Chem.* 265 (1967) 425.
- [26] R. Gaboriaud, *J. Chim. Phys.* 65 (1968) 1155.
- [27] H. Katayanagi, K. Nishikawa, H. Shimozaki, K. Miki, P. Westh, Y. Koga, *J. Phys. Chem. B* 108 (2004) 19451.
- [28] P.A.Z. Suarez, J.E.L. Dullius, S. Einloft, R.F. De Souza, J. Dupont, *Polyhedron* 15 (1996) 1217.
- [29] R.G. Bates, *Determination of Ph, Theory and Practice*, second ed., J. Wiley, New York, 1973, p. 327.
- [30] I. Kron, S.L. Marshall, P.M. May, G. Hefter, E. Konigsberger, *Monatshefte für Chemie* 126 (1995) 819.
- [31] H.S. Harned, W.J. Hamer, *J. Am. Chem. Soc.* 55 (1933) 219.
- [32] G. Charlot, J. Badoz-Lambling, B. Tremillon, *Les Réactions Electrochimiques, Méthodes Electrochimiques d'Analyses*, Ed. Masson et Cie, Paris, 1958. pp. 117, 147, 155.
- [33] M.L. Turonek, P.M. Hefter, P.M. May, *Talanta* 45 (1998) 931.
- [34] P. Sipos, I. Bodi, P.M. May, G.T. Hefter, *Talanta* 44 (1997) 617.
- [35] J.C. Hallé, R. Harivel, R. Gaboriaud, *Can. J. Chem.* 52 (1974) 1774.
- [36] J. Koryta, *Principles of Electrochemistry*, J. Wiley, New York, 1987.
- [37] R. Fischer, J. Byé, *Bull. Soc. Chim. Fr.* 11 (1964) 2920.
- [38] V.M. Lobo, J.L. Quaresma, *Electrolyte Solutions: Literature Data On Thermodynamics And Transport Properties*, Volume II, Coimbra (Portugal) 1981. pp. 439, 773.
- [39] J. Bowers, C.P. Butts, P.J. Martin, M.C. Vergara-Gutierrez, *Langmuir* 20 (2004) 2191.
- [40] J. Sung, Y. Jeon, D. Kim, T. Iwahashi, T. Iimori, K. Seki, Y. Ouchi, *Chem. Phys. Lett.* 406 (2005) 495.
- [41] L.P.N. Rebelo, V. Najdanovic-Visak, Z.P. Visak, M. Nunes da Ponte, J. Szydowski, C.A. Cerdeirina, J. Troncoso, L. Romani, J.M.S.S. Esperança, H.J.R. Guedes, H.C. de Sousa, *Green Chem.* 6 (2004) 369.
- [42] I. Bou Malham, P. Letellier, M. Turmine, *J. Phys. Chem.* 110 (2006) 14212.
- [43] I. Ruff, *J. Chem. Soc., Faraday trans.* 2 73 (1977) 1858.
- [44] (a) J.L. Gomez Estevez, V. Torra, *An. Quim.* 79 (1983) 49;
(b) J.L. Gomez Estevez, V. Torra, *An. Quim.* 79 (1983) 359.
- [45] J.L. Gomez Estevez, V. Torra Ferre, *Calorim. Anal. Therm.* 13 (1982) III.1.1.
- [46] L.M. Varela, M. Garcia, F. Sarmiento, D. Attwood, V. Mosquera, *J. Chem. Phys.* 107 (1997) 6415.
- [47] I. Ruff, *J. Chem. Soc., Faraday trans.* 2 75 (1979) 1.
- [48] M. Hadded, M. Biquard, P. Letellier, R. Schaal, *Can. J. Chem.* 63 (1985) 565.

Comparison of slurry sampling and microwave-assisted digestion for calcium, magnesium, iron, copper and zinc determination in fish tissue samples by flame atomic absorption spectrometry

Raquel Alonso Bugallo, Susana Río Segade*, Esperanza Fernández Gómez

Departamento de Química Analítica y Alimentaria, Área de Química Analítica, Universidad de Vigo, Facultad de Ciencias de Ourense, As Lagoas s/n, 32004 Ourense, Spain

Received 27 March 2006; received in revised form 24 August 2006; accepted 27 September 2006

Available online 1 November 2006

Abstract

The development of a slurry sampling method for the determination of calcium, copper, iron, magnesium and zinc in fish tissue samples by flame atomic absorption spectrometry is described. In comparison with microwave-assisted digestion, the proposed method is simple, requires short time and eliminates total sample dissolution before analysis. Suspension medium was optimized for each analyte to obtain quantitative recoveries from fish tissue samples without matrix interferences. Nevertheless, iron recoveries higher than 46% were not found. Treatment of samples slurried in nitric acid by microwave irradiation for 15–30 s at 75–285 W permitted to achieve efficient recoveries for calcium, iron, magnesium and zinc. Further improvement in the matrix effects for iron determination was accomplished by the use of an additional step of short microwave-assisted suspension treatment. However, standard addition method was required for calcium and copper determination, being necessary hydrochloric acid as suspension medium for the last one. Although copper could not be determined in the certified reference material using microwave-assisted digestion, the accuracy of the slurry sampling method was verified for all the investigated analytes. Detection limits were 22.8 ± 8.0 , 0.884 ± 0.092 , 5.07 ± 0.76 , 35.5 ± 0.7 and $1.17 \pm 0.04 \mu\text{g g}^{-1}$ for calcium, copper, iron, magnesium and zinc, respectively. The standard deviations obtained using slurry sampling method and microwave-assisted digestion were not significantly different, and the mean relative standard deviation of the over-all method ($n = 3$) of the slurry sampling method for different concentration levels was below 12%.

© 2006 Elsevier B.V. All rights reserved.

Keywords: Slurry sampling; Microwave-assisted digestion; Calcium, magnesium, iron, copper and zinc determination; Fish tissue samples; Flame atomic absorption spectrometry

1. Introduction

The most time consuming step in solid materials analysis is often sample treatment. Several procedures have been developed for elements determination by atomic spectrometric techniques, in order to short the analysis time and to minimize the problems associated with solid sample treatment (conventional wet acid digestion and dry-ashing), such as sample contamination and analyte loss. So, alkaline [1–3] and acid [3–11] digestion methods assisted by microwave [3–8,10,11] or ultrasound [2–4,8,9]

energy (involve complete or partial matrix solubilization) permit to short the time required for sample treatment. Furthermore, direct solid sampling offers several advantages, including the minimization of the sample handling and, as a consequence, the reduction of the risks previously mentioned [12–15].

The slurry sampling technique has been extensively used for the determination of trace elements in biological and environmental solid samples by electrothermal atomic absorption spectrometry (ETAAS) [4,6,8,16–20]. This approach combines the advantages of both liquid and direct solid sampling. However, it is important to emphasize that slurry homogeneity must be preserved during the time required for sample introduction into the atomizer. Furthermore, the particle size affects accuracy and precision. Anyway, literature has been also published in the last years on the analysis of biological [8,21,22] and inorganic [23–26] solid samples by slurry sampling flame atomic absorp-

* Corresponding author. Present address: Estación de Viticultura y Enología de Galicia, Ponte San Clodio s/n, Leiro, 32427 Ourense, Spain.

Tel.: +34 988 488033; fax: +34 988 488191.

E-mail address: evgado2@cesga.es (S.R. Segade).

tion spectrometry (FAAS) in spite of the continuous aspiration of the slurry, which affects atomization efficiency. In this context, some investigations have been realized in order to improve the transport of the solid particles to the flame and, therefore, the atomization efficiency of the analytes from the slurry. The four principal proposals were the use of special nebulizers [21,27], the addition of wetting agents [28], the acid extraction of analyte into the liquid phase [21] or the use of flow injection systems for the introduction of slurried solid samples into the flame [22,23,25,26].

Most of the methods for determining elements in biological samples by FAAS are based on microwave-assisted acid digestion. In this paper, a method has been developed for the determination of calcium, copper, iron, magnesium and zinc in fish tissue samples by slurry sampling FAAS, using a conventional nebulizer. Very few works have been reported in relation to the analysis of fish tissue samples by the combination of both techniques [8]. The main aims proposed were to short the time required for sample treatment, to avoid the problems related with sample decomposition and to achieve quantification limits suitable for the determination of element concentration present in fish from high sea. The effect of the suspension medium and a novel microwave-assisted slurry treatment was studied, being tested not only the most commonly used acid medium, but also alkaline medium and a complexing agent. Moreover, the influence of the addition of glycerol as wetting agent and the slurry concentration was also evaluated. The results so obtained for all the tuna samples analyzed were compared with those obtained by means of microwave-assisted acid digestion in order to emphasize the advantages of the proposed method.

2. Experimental

2.1. Instrumentation

The slurry treatment was performed with a Moulinex (Barcelona, Spain) 900 W microwave oven. A Selecta (Barcelona, Spain) Model Agimatic-N magnetic stirrer was used to homogenize the slurry. A Kubota (Tokyo, Japan) Model 5100 centrifuge was employed for the separation of the liquid phase from the slurried samples. The solid materials were also acid digested in a Parr (Moline, IL, USA) Model 4782 medium-pressure reactor heated by the above-mentioned microwave oven. A Perkin-Elmer (Norwalk, CT, USA) Model 2380 atomic absorption spectrometer equipped with an acetylene-air flame was used for element determination. Cathodeon hollow-cathode lamps were used as the radiation source. The instrumental parameters used were those recommended by the manufacturer.

2.2. Reagents, samples and reference material

All chemicals used were of analytical reagent grade (Merck, Darmstadt, Germany) and deionized water was used throughout the experiments. The stock standard solutions (1000 mg l^{-1}) were prepared from pure metal (copper, iron, magnesium and zinc) or from high purity calcium carbonate salt (calcium). Working standard solutions were prepared daily by appro-

riately diluting the stock standard solutions. Diluted nitric acid, diluted hydrochloric acid, disodium ethylenediaminetetraacetate solution, sodium hydroxide solution and diluted hydrogen peroxide were used for the slurry preparation by adding glycerol as dispersing agent. Concentrated nitric acid was also used in combination with hydrogen peroxide for solid samples digestion.

The comestible part of the tuna samples (I–III) was oven dried at 50°C for 48 h to constant weight and ground. The powdered sample with particle size less than $70 \mu\text{m}$ was selected by sieving (nylon sieves) for analysis and stored at room temperature in polyethylene bottles in a desiccator. A certified reference material was used to validate the proposed method. The NCS ZC 80006 (prawn) was obtained from the China National Analysis Center for Iron and Steel.

2.3. Microwave-assisted acid digestion procedure

A microwave-assisted wet decomposition of fish tissue samples was performed according to a slightly modified procedure [29]. About 0.1 g of tuna sample were digested with 4 ml of concentrated nitric acid in a Parr reactor by heating in a microwave oven at 510 W for 60 s. After cooling to room temperature in an ice bath, the reactor was opened and the digested sample was after treated with 2 ml of concentrated hydrogen peroxide in the closed reactor by microwave irradiation at 510 W for 120 s. The resulting solution was partially evaporated and quantitatively transferred into a 10 ml calibrated flask, where it was diluted to volume with deionized water. Blanks were prepared with the same reagents undergoing a similar treatment. Finally, all solutions were stored in polyethylene bottles at 4°C .

2.4. Slurry preparation procedure

A 3–300 mg portion of tuna sample was weighed into a 50 ml polyethylene tube and 10–50 ml of $0.1\text{--}3 \text{ mol dm}^{-3}$ hydrochloric acid, $0.07\text{--}1.5 \text{ mol dm}^{-3}$ nitric acid, $0.05\text{--}1 \text{ mol dm}^{-3}$ sodium hydroxide, $0.05\text{--}3\%$ (m/v) disodium ethylenediaminetetraacetate or $1\text{--}5\%$ (m/v) hydrogen peroxide containing $0.1\text{--}3\%$ (v/v) glycerol were added. The slurry was homogenized by magnetic stirring for 5 min. When nitric acid was employed as suspension medium, the slurry was microwave irradiated at $75\text{--}400 \text{ W}$ for $5\text{--}60 \text{ s}$ and, before aspirating, again homogenized by magnetic stirring. The supernatant liquid was separated from the slurried tuna sample by centrifugation at 2500 rpm for 5 min in order to check extraction efficiency of the suspension medium. Blanks were prepared with the same reagents undergoing a similar treatment.

3. Results and discussion

3.1. Optimization of suspension medium

The atomization efficiency for the elements studied from slurried tuna samples was evaluated by comparison of the absorbance values with those obtained from an aqueous standard. The tuna sample suspended in deionized water and the

Table 1
Initial and optimum parameters for calcium, copper, iron, magnesium and zinc determination using slurry sampling

Parameter	Ca	Cu	Fe	Mg	Zn
Initial					
Suspension medium	HNO ₃	HNO ₃	HNO ₃	HNO ₃	HNO ₃
Medium concentration (mol dm ⁻³)	0.15	0.15	0.15	0.15	0.15
Suspension medium volume (cm ³)	10	10	10	50	10
Glycerol concentration (% v/v)	0.3	0.3	0.3	0.3	0.3
Sample amount (mg)	100	150	150	50	100
Optimum					
Suspension medium	HNO ₃	HCl	HNO ₃	HNO ₃	HNO ₃
Medium concentration (mol dm ⁻³)	0.15	0.10	0.15	0.15	0.15
Suspension medium volume (cm ³)	10	10	10	50	10
Microwave time (s)	15	–	30	15	15
Microwave power (W)	123	–	285	75	75
Glycerol concentration (% v/v)	0.3	0.3	0.3	0.3	0.3
Sample amount (mg)	40	150	150	3	100

aqueous standard solution were prepared to contain the same analyte concentration. The absorbance signals obtained for all elements from slurried tuna sample were less than those corresponding to the aqueous standard, except for magnesium. The effect of nebulization flow-rate and air/acetylene flow-rates relation on the atomization efficiency from the slurry was investigated. Maximum atomization efficiency from both the slurry and the aqueous standard was 0.1, 0.02, 0.2, 0.9 and 0.08 for calcium, copper, iron, magnesium and zinc, respectively. The instrumental conditions selected were those corresponding to maximum sensitivity for all elements from aqueous standard solutions.

Some investigators have reported that partial extraction of several analytes into the liquid phase improves the precision and accuracy of slurry sampling ETAAS [30]. Moreover, slurry sampling could be replaced by supernatant liquid sampling when the analytes were quantitatively extracted in the suspension medium. Further advantages were the elimination of stirring systems and stabilizing agents since a homogeneous distribution of solid particles was not necessary [31].

In this sense, suspension medium was evaluated in order to establish: (i) the percentage of analyte recovered by the slurry sampling technique in relation to the analyte concentration determined using the microwave-assisted acid digestion procedure; (ii) the extraction efficiency of analyte from the slurry into the liquid phase; (iii) the presence of matrix effects. The initial parameters are shown in Table 1. The suspension medium investigated was hydrochloric acid (as acid medium), sodium hydroxide (as alkaline medium) and disodium ethylenediaminetetraacetate (as complexing medium). All determinations were carried out by triplicate using a tuna sample.

Fig. 1 shows that quantitative calcium recovery was achieved using either disodium ethylenediaminetetraacetate concentrations equal to or less than 0.5% (m/v) or hydrochloric acid concentrations comprised between 0.5 and 1 mol dm⁻³. Taking into account that both the greatest slopes of standard addition lines corresponded to the use of disodium ethylenediaminetetraacetate (0.00758–0.01131 mg⁻¹) and absorbance values obtained for reagent blank increased with increasing complexing agent concentration from 0.5% (m/v), the suspension medium selected

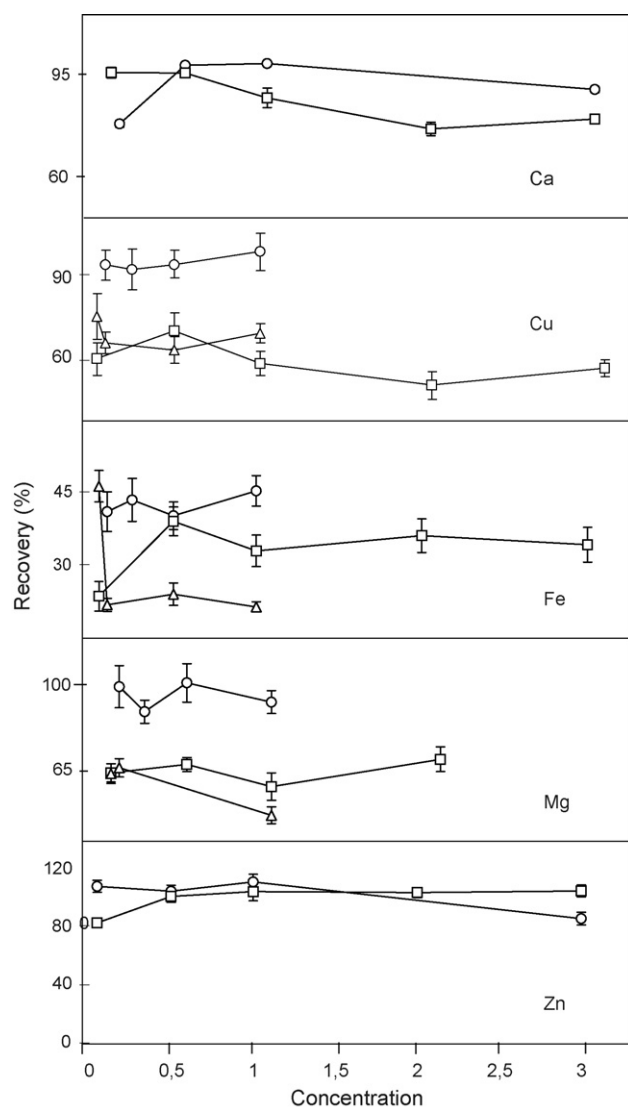


Fig. 1. Effect of %disodium ethylenediaminetetraacetate (m/v) (□), hydrochloric acid (mol dm⁻³) (○) and sodium hydroxide (mol dm⁻³) (Δ) on recovery of calcium, copper, iron, magnesium and zinc.

was 0.05% (m/v) disodium ethylenediaminetetraacetate. Furthermore, the influence of pH value of disodium ethylenediaminetetraacetate on calcium recovery was also investigated. So, an increase in pH value caused calcium amount recovered to decrease, obtaining a calcium recovery of 68% for a pH value of 9. This effect was verified by the use of ammonium chloride/ammonium hydroxide buffer solution or sodium hydroxide concentrations higher than 0.05 mol dm⁻³ as suspension medium, which gave calcium recoveries of 41 and 74%, respectively.

The effect of disodium ethylenediaminetetraacetate and sodium hydroxide concentrations on copper recovery was not significant. Moreover, pH value of disodium ethylenediaminetetraacetate solution had no influence on copper amount recovered. Fig. 1 shows quantitative copper recoveries only for hydrochloric acid concentrations ranging from 0.1 to 1 mol dm⁻³. As the maximum slope of standard addition line was attained using 0.1 mol dm⁻³ hydrochloric acid (0.131 l mg⁻¹), this suspension medium was chosen.

The maximum iron recovery (~42%) corresponded to hydrochloric acid concentrations comprised between 0.1 and 1 mol dm⁻³, 0.05 mol dm⁻³ sodium hydroxide or 0.5% (m/v) disodium ethylenediaminetetraacetate, as can be observed in Fig. 1. The alkalization of the complexing agent or the use of sodium hydroxide concentrations higher than 0.05 mol dm⁻³ caused an important reduction of iron amount recovered. The slopes of external calibration and standard addition lines obtained for iron were not statistically different (*t*-test; *p*=0.05) for the sample slurried in 0.5–1 mol dm⁻³ hydrochloric acid or 0.05–3% (m/v) disodium ethylenediaminetetraacetate (0.0383–0.0400 l mg⁻¹). Therefore, 0.5 mol dm⁻³ hydrochloric acid could be selected as optimum suspension medium.

Fig. 1 shows that magnesium recovery depended on the suspension medium used. Quantitative recoveries were obtained for hydrochloric acid concentrations comprised between 0.1 and 1 mol dm⁻³, followed by those (67%) corresponding to the use of disodium ethylenediaminetetraacetate concentrations ranging from 0.05 to 2% (m/v). The last ones were maintained practically constant when the solution was alkalized. However, sodium hydroxide concentrations within the range 0.05–0.1 mol dm⁻³ or ammonium chloride/ammonium hydroxide buffer solution permitted to obtain magnesium recoveries of 68%. On the other hand, insignificant absorbance signals corresponding to reagent blank and no significant difference (*t*-test; *p*=0.05) between the slopes of external calibration and standard addition lines (0.647 l mg⁻¹) were found when low hydrochloric acid concentrations were used as suspension medium. Thus, the suspension medium chosen was 0.1 mol dm⁻³ hydrochloric acid.

The influence of suspension medium on zinc recovery is shown in Fig. 1. So, the use of disodium ethylenediaminetetraacetate concentrations equal to or higher than 0.5% (m/v) or hydrochloric acid concentrations equal to or less than 1 mol dm⁻³ permitted to achieve quantitative recoveries for zinc. The alkalization of disodium ethylenediaminetetraacetate solution caused the diminution of zinc amount recovered, which was verified by the suspension of the sample in either sodium hydroxide or ammonium chloride/ammonium

hydroxide buffer solution. The slope of standard addition line obtained for both acid and complexing suspension medium was 0.162 l mg⁻¹. Taking into account that low absorbance values were obtained for reagent blank when 0.1 mol dm⁻³ hydrochloric acid was employed, this suspension medium was selected.

The concentrations found in the tuna slurry are in accordance with those found in the supernatant liquid for all analytes determined, achieving recoveries higher than 96% in the last one in relation to the concentrations determined in the slurried samples.

3.2. Microwave-assisted suspension treatment

The low recoveries obtained for iron and the presence of matrix interferences for calcium, copper and zinc led to the optimization of a microwave-assisted treatment of slurried tuna sample in order to achieve greater matrix decomposition degree. Nitric acid is adequate for microwave-assisted treatments, because of its capability to absorb efficiently microwave energy and it is one of the most widely used reagents for biological samples treatment because of its oxidant properties.

The effect of nitric acid concentration on calcium, copper, iron, magnesium and zinc recovery was investigated and the results can be seen in Fig. 2. Calcium, copper and magnesium recovery remained practically constant for nitric acid concentrations between 0.07 and 0.7 mol dm⁻³. Although magnesium recovery was quantitative for a nitric acid concentration of 1.5 mol dm⁻³, the absorbance values obtained for reagent blank were also high. On the other hand, iron recovery decreased slightly and zinc recovery increased markedly when nitric acid concentration was increased from 0.07 to 0.15 mol dm⁻³ and both recoveries kept constant for higher nitric acid concentrations. Thus, the slopes of standard addition lines obtained using nitric acid as suspension medium were 0.00935, 0.139, 0.0280, 0.668 and 0.195 l mg⁻¹ for calcium, copper, iron, magnesium and zinc, respectively. The slopes of external calibration and standard addition lines were significantly different (*t*-test; *p*=0.05) for calcium, copper and iron. 0.15 mol dm⁻³ (1%, v/v) nitric acid was selected for further experiments. The same concentration was previously used by other authors for metals determination in human scalp hair by slurry sampling FAAS [21].

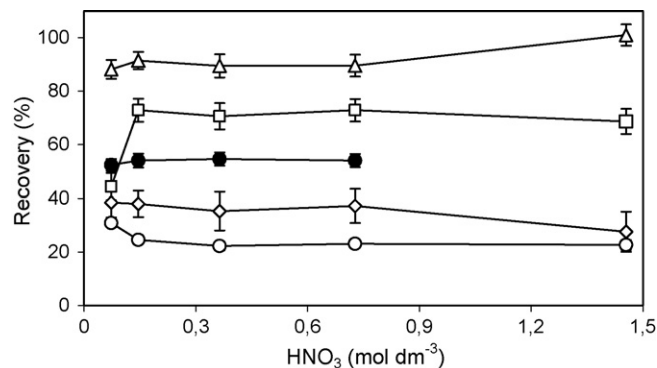


Fig. 2. Effect of nitric acid concentration on recovery of: calcium (●), copper (◇), iron (○), magnesium (△) and zinc (□).

Microwave heating times between 5 and 60 s were optimized at 75 W power. Calcium and iron recoveries increased with increasing microwave time up to 15 and 30 s, respectively. However, the effect of microwave time on copper, magnesium and zinc recoveries was not significant. Then, in another experiment the influence of different microwave powers (75–400 W) on analyte recovery revealed that maximum recoveries were obtained for calcium (88.1%), copper (55.1%), iron (94.5%), magnesium (85.6%) and zinc (97.9%) when microwave powers ranging 123–285, 75, 285–400, 75–170 and 75–170 W, respectively, were employed. The microwave-assisted slurry treatment permitted to avoid matrix interferences for iron because of both slopes of external calibration and standard addition lines were in good agreement (*t*-test; *p* = 0.05). Furthermore, the slope of standard addition line for copper increased when microwave energy was applied to the slurry heating.

The effect of the addition of hydrogen peroxide to nitric acid suspension medium was also investigated for calcium, copper, iron, magnesium and zinc. However, recoveries and slopes of standard addition lines remained practically constant for all ones when hydrogen peroxide in the range of concentrations from 1 to 5% (m/v) was added.

After selecting the optimum conditions for each element (Table 1), glycerol concentration (0.1–3%, v/v) and sample amount slurried (3–300 mg) were evaluated. Thus, the effect of wetting agent concentration on recovery and slope of standard addition line for all elements studied was not significant. While the sample amount slurried negatively affected to magnesium and zinc recoveries for values higher than 6 and 100 mg, respectively, or to calcium and zinc sensitivity for values higher than 45 and 100 mg, respectively. On the other hand, an analyte extraction percentage into the liquid phase of the slurry close to 100% was reached for all elements.

3.3. Validation of the method

The proposed method was validated by the analysis of one biological reference material using the optimum experimental conditions described in Table 1. External calibration with a series of aqueous standards was applied to iron, magnesium and zinc determination. However, standard addition method was applied to calcium and copper determination because of the slope of external calibration line was significantly different with that corresponding to standard addition line (*t*-test; *p* = 0.05). The sample was analyzed 10 times. The results obtained for calcium, copper, iron, magnesium and zinc concentration in the certified reference material by slurry sampling method and the certified values are shown in Table 2. It can be observed that the concentrations found of each ones were in good agreement with the certified values (*t*-test; *p* = 0.05).

3.4. Analysis of fish tissue samples

Three tuna tissue samples (I–III) were analyzed by triplicate using both microwave-assisted digestion and slurry sampling methodologies. The results obtained for calcium, copper, iron, magnesium and zinc determination are shown in Table 3. Recov-

Table 2

Calcium, copper, iron, magnesium and zinc concentration ($\mu\text{g g}^{-1}$) in the certified reference material using microwave-assisted digestion and slurry sampling methods

Element	Certified value ^a	Obtained value ^{a,b,c}	Obtained value ^{a,b,d}
Ca	3040 ± 60	3100 ± 50	3008 ± 25
Cu	4.66 ± 0.23	4.58 ± 0.19	<LOD
Fe	19.8 ± 0.4	19.6 ± 0.3	19.4 ± 0.2
Mg	1600 ± 30	1602 ± 7	1586 ± 6
Zn	60.8 ± 1.4	60.5 ± 0.6	61.2 ± 0.7

^a Average value ± standard deviation.

^b *n* = 10.

^c Results obtained using the slurry sampling.

^d Results obtained using the microwave-assisted digestion.

ery was calculated as quotient between concentrations determined using slurry sampling and microwave-assisted digestion methodologies.

Absorbance signals for copper in microwave-assisted digested tuna samples were not detected by the FAAS technique owing to the necessity for the treatment of little sample amounts in pressurized reactors. So, copper concentrations determined using both methodologies could not be compared. The mean relative standard deviation of the over-all method (*n* = 3) for different concentration levels was 11.1%. The slopes of standard addition lines (0.125–0.1621 mg⁻¹) were significantly higher than those corresponding to external calibration lines (*t*-test; *p* = 0.05), which permitted to determine lower concentrations of copper.

There were not significant differences between calcium, iron, magnesium and zinc concentrations obtained using both slurry sampling and microwave-assisted digestion methodologies

Table 3

Calcium, copper, iron, magnesium and zinc concentration ($\mu\text{g g}^{-1}$) in three tuna tissue samples using microwave-assisted digestion and slurry sampling methods

Element	Obtained value ^{a,b,c}	Obtained value ^{a,b,d}	Recovery (%)
Sample I			
Ca	283 ± 18	277 ± 11	102 ± 6
Cu	12.0 ± 1.5	<LOD	–
Fe	21.0 ± 1.8	22.0 ± 3.3	95.5 ± 8.2
Mg	1708 ± 25	1741 ± 5	98.1 ± 1.4
Zn	16.7 ± 0.9	15.0 ± 1.2	111 ± 6
Sample II			
Ca	233 ± 10	243 ± 8	95.9 ± 4.1
Cu	6.99 ± 0.63	<LOD	–
Fe	48.1 ± 2.5	47.6 ± 5.2	101 ± 5
Mg	1304 ± 20	1331 ± 7	98.0 ± 1.5
Zn	16.2 ± 1.1	16.6 ± 0.6	97.6 ± 6.6
Sample III			
Ca	713 ± 37	728 ± 15	97.9 ± 5.1
Cu	3.73 ± 0.44	<LOD	–
Fe	58.8 ± 2.7	59.4 ± 2.1	99.0 ± 4.6
Mg	1224 ± 10	1174 ± 13	104 ± 1
Zn	37.2 ± 0.9	34.9 ± 1.9	107 ± 3

^a Average value ± standard deviation.

^b *n* = 3.

^c Results obtained using the slurry sampling.

^d Results obtained using the microwave-assisted digestion.

(*t*-test; *p* = 0.05). Furthermore, the standard deviations obtained for calcium, iron, magnesium and zinc using both methodologies were not significantly different (*F*-test; *p* = 0.05) and mean relative standard deviations of the over-all method (*n* = 3) for different concentration levels were 5.3, 6.1, 1.3 and 4.9% for calcium, iron, magnesium and zinc, respectively, by slurry sampling. Calcium, iron, magnesium and zinc recoveries were greater than 95%. Finally, 10 tuna tissue samples were analyzed using slurry sampling and standard addition method in order to check the absence of matrix interferences on iron, magnesium and zinc determination by comparing the slopes associated with standard addition lines and with external calibration lines. The differences between both slopes were only significant (*t*-test; *p* = 0.05) for iron determination in some tuna samples (0.0251–0.03891 mg⁻¹). As expected, external calibration with aqueous standards can be used for magnesium and zinc determination. The slopes of standard addition lines for calcium varied between 0.00881 and 0.01861 mg⁻¹.

The detection limits based on the amount necessary to yield a net signal equal to three times the standard deviation of the blank were 22.8 ± 8.0, 0.884 ± 0.092, 5.07 ± 0.76, 35.5 ± 0.7 and 1.17 ± 0.04 μg g⁻¹ for calcium, copper, iron, magnesium and zinc determination, respectively. It should be noted that the detection limits obtained by the proposed method for copper and zinc are 3–4 times less than those reported for other slurry sampling FAAS approaches [21]. Therefore, the slurry sampling method proposed in this work permits to spread the application field to the analysis of fish samples from high sea containing lower copper and zinc concentrations than those found in human scalp hair samples.

4. Conclusions

Slurry sampling was compared with microwave-assisted acid digestion for the determination of calcium, copper, iron, magnesium and zinc in fish tissue samples by flame atomic absorption spectrometry. The main advantages of using slurry sampling are the elimination of a tedious and time-consuming step of sample dissolution and quantitative extraction of all analytes studied into the liquid phase of the slurry. Unlike the microwave-assisted digestion method, in which sample amount is limited, long times are required for cooling the digestion vessel after the microwave irradiation and concentrated acids are used, involving high blank values, sampling of the liquid phase present in slurried samples, after microwave irradiation except for copper, does not require stabilizing agents nor finely ground material without nebulizer blockage. The accuracy of both methods was checked using a certified reference material. The results obtained were in good agreement with the certified values for all chosen analytes when slurry sampling method was used. The precision (R.S.D.) was less than 5.3, 11.1, 6.1, 1.3 and

4.9% for calcium, copper, iron, magnesium and zinc at concentration ranging of 233–713, 3.73–12.0, 21.0–58.8, 1224–1708 and 16.2–37.2 μg g⁻¹, respectively. Furthermore, the results obtained using slurry technique were not significantly different with those corresponding to microwave-assisted digestion for calcium, iron, magnesium and zinc in the fish samples analyzed.

References

- [1] D. Pozebon, V.L. Dressler, A.J. Curtius, *J. Anal. Atom. Spectrom.* 13 (1998) 1101.
- [2] R.G.L. Silva, S.N. Willie, R.E. Sturgeon, R.E. Santelli, S.M. Sella, *Analyst* 124 (1999) 1843.
- [3] L.M. Costa, S.T. Gouveia, J.A. Nobrega, *Anal. Sci.* 18 (2002) 313.
- [4] E.C. Lima, F. Barbosa Jr., F.J. Krug, M.M. Silva, M.G.R. Vale, *J. Anal. Atom. Spectrom.* 15 (2000) 995.
- [5] P.R.M. Correia, E. Oliveira, P.V. Oliveira, *Anal. Chim. Acta* 405 (2000) 205.
- [6] B. Pérez Cid, C. Silva, C. Boia, *Anal. Bioanal. Chem.* 374 (2002) 477.
- [7] J. Sastre, A. Sahuquillo, M. Vidal, G. Rauret, *Anal. Chim. Acta* 462 (2002) 59.
- [8] P. Bermejo Barrera, A. Moreda Piñeiro, A. Bermejo Barrera, *Talanta* 57 (2002) 969.
- [9] M.C. Yebra, A. Moreno Cid, R.M. Cespon, S. Cancela, *Atom. Spectrosc.* 24 (2003) 31.
- [10] K. Eilola, P. Perämäki, *Analyst* 128 (2003) 194.
- [11] E.C. Lima, J.L. Brasil, A.H.D.P. Santos, *Anal. Chim. Acta* 484 (2003) 233.
- [12] E. Lückner, K. Failing, T. Schmidt, *Fresen. J. Anal. Chem.* 366 (2000) 137.
- [13] E.M.M. Flores, A.B. da Costa, J.S. Barin, V.L. Dressler, J.N.G. Paniz, A.F. Martins, *Spectrochim. Acta* 56B (2001) 1875.
- [14] M.G.R. Vale, M.M. Silva, B. Welz, R. Nowka, *J. Anal. Atom. Spectrom.* 17 (2002) 38.
- [15] E.M.M. Flores, J.N.G. Paniz, A.P.F. Saidelles, E.I. Müller, A.B. da Costa, *J. Anal. Atom. Spectrom.* 18 (2003) 769.
- [16] E.C. Lima, F.J. Krug, A.T. Ferreira, F. Barbosa Jr., *J. Anal. Atom. Spectrom.* 14 (1999) 269.
- [17] M. González, M. Gallego, M. Valcárcel, *Talanta* 48 (1999) 1051.
- [18] P. Bermejo Barrera, A. Moreda Piñeiro, J. Moreda Piñeiro, T. Kauppila, A. Bermejo Barrera, *Atom. Spectrosc.* 21 (2000) 5.
- [19] S.J. Huang, S.J. Jiang, *Analyst* 125 (2000) 1491.
- [20] E.C. Lima, F. Barbosa, F.J. Krug, *J. Fresenius, Anal. Chem.* 369 (2001) 496.
- [21] P. Bermejo Barrera, A. Moreda Piñeiro, J. Moreda Piñeiro, A. Bermejo Barrera, *Fresen. J. Anal. Chem.* 360 (1998) 707.
- [22] P. Jacob, H. Berndt, *J. Anal. Atom. Spectrom.* 17 (2002) 1615.
- [23] M.A. Bautista, C. Pérez Sirvent, I. López García, M. Hernández Córdoba, *Fresen. J. Anal. Chem.* 350 (1994) 359.
- [24] J.H. Brown, J.E. Vaz, Z. Benzo, M. Velosa, *Analyst* 120 (1995) 1215.
- [25] M.D. de Almeida, K.C. Leandro, C.V. da Costa, R.E. Santelli, M. de la Guardia, *J. Anal. Atom. Spectrom.* 12 (1997) 1235.
- [26] J.A. Sweileh, *Anal. Chim. Acta* 448 (2001) 151.
- [27] N. Mohamed, R.C. Fry, *Anal. Chem.* 53 (1981) 450.
- [28] J. Stupar, R. Ajlec, *Analyst* 107 (1982) 144.
- [29] S. Río Segade, C. Bendicho, *Ecotoxicol. Environ. Saf.* 42 (1999) 245.
- [30] N.J. Miller-Ihli, *J. Anal. Atom. Spectrom.* 9 (1994) 1129.
- [31] I. Lavilla, J.L. Capelo, C. Bendicho, *Fresen. J. Anal. Chem.* 363 (1999) 283.

Enzyme inhibition-based biosensor for the electrochemical detection of microcystins in natural blooms of cyanobacteria

Mònica Campàs^{a,*}, Dorota Szydłowska^b, Marek Trojanowicz^b, Jean-Louis Marty^a

^a BIOMEM group, Université de Perpignan, 52 Avenue Paul Alduy, 66860 Perpignan Cedex, France

^b Laboratory of Flow Analysis and Chromatography, Department of Chemistry, University of Warsaw, Pasteura 1, PL-02-093 Warsaw, Poland

Received 20 June 2006; received in revised form 29 September 2006; accepted 5 October 2006

Available online 13 November 2006

Abstract

An electrochemical biosensor for the detection of microcystin has been developed based on the inhibition of the protein phosphatase 2A (PP2A) by this cyanobacterial toxin. The enzyme has been immobilised by entrapment using a poly(vinyl alcohol) azide-unit pendant water-soluble photopolymer (PVA-AWP). Electrode supports and immobilisation conditions have been optimised by colorimetric assays, the highest immobilisation yields being obtained with screen-printed graphite electrodes and the 1:2 PP2A:PVA ratio. Catechyl monophosphate (CMP), α -naphthyl phosphate (α -NP) and 4-methylumbelliferyl phosphate (4-MUP) have been used as phosphorylated substrates to monitor the protein phosphatase activity by electrochemical methods, the former providing the highest chronoamperometric currents at appropriate working potentials (+450 mV *versus* Ag/AgCl). Incubation with standard microcystin solutions has demonstrated the inhibition of the immobilised enzyme, proportional to the toxin concentration. The standard inhibition curve has provided a 50% inhibition coefficient (IC_{50}) of $83 \mu\text{g L}^{-1}$, a limit of detection (LOD; 35% inhibition) of $37 \mu\text{g L}^{-1}$, and 100% inhibition at about $1000 \mu\text{g L}^{-1}$. Real samples of cyanobacterial blooms from the Tarn River (Midi-Pyrénées, France) have been analysed using the developed amperometric biosensor and the toxin contents have been compared to those obtained by a conventional colorimetric protein phosphatase inhibition (PPI) assay and high-performance liquid chromatography (HPLC). The results clearly justify the use of the developed amperometric biosensor as screening method for microcystin detection.

© 2006 Elsevier B.V. All rights reserved.

Keywords: Microcystin (MC); Protein phosphatase 2A (PP2A); Poly(vinyl alcohol) azide-unit pendant water-soluble photopolymer (PVA-AWP) Entrapment; Inhibition; Catechyl monophosphate (CMP); Electrochemical detection

1. Introduction

Microcystins (MCs) are cyanobacterial toxins usually produced in freshwaters throughout the world. Cyanobacteria (blue-green algae) growth and toxin production are associated to several factors: (a) eutrophication, *i.e.* the presence of excessive nutrients coming from agricultural run-off, deforestation and urban pollution; (b) low flow regimes, with the corresponding long retention times; (c) high light intensity, necessary for the photosynthesis; (d) warm water temperatures, which explains why most blooms occur in summer; (e) the presence of trace metals [1,2]. MCs are cyclic heptapeptides, with five constant amino acids and two variable ones. More than 70 variants are known, showing variations in structure and toxicity [3,4]. Microcystin-

LR (MC-LR) was the first MC chemically identified and it is known to be the most toxic and frequently found.

MCs are potent hepatotoxins. The peculiar hydrophobic Adda (3-amino-9-methoxy-2,6,8-trimethyl-10-phenyldeca-4,6-dienoic acid) chain allows them to penetrate the hepatocytes, where MCs irreversibly bind to serine/threonine protein phosphatases type 2A (PP2A) and type 1 (PP1), inhibiting their enzymatic activity [5–8]. These enzymes are involved on the dephosphorylation of proteins. Consequently, their inhibition results in hyperphosphorylation and reorganisation of the microfilaments, promoting tumours and liver cancer [9]. Apart from the 60 patients of a renal dialysis unit who died due to an accidental intravenous uptake [10–12], no other human fatalities due to MCs have been documented. In fact, MCs are not likely to be ingested in lethal doses by humans due to the repulsive aspect of contaminated water. However, numerous cases of human illnesses and lethal poisoning of animals have been reported [13–22]. The main human exposure routes to MC are the oral

* Corresponding author. Tel.: +33 468 66 22 53; fax: +33 468 66 22 23.
E-mail address: campas@univ-perp.fr (M. Campàs).

consumption of contaminated drinking water and the dermal contact with poisoned recreational water. Although to a lower extent, other human exposure routes are the inhalation of aqueous aerosols [23,24] and the consumption of toxic cyanobacterial dietary supplements [25], vegetables irrigated by contaminated water [26], and poisoned animals [27–29]. The high chemical stability of MCs conferred by their cyclic structure, together with their water solubility, explain their environmental persistence and the difficulty to be degraded or removed. The potential risk for the public health has led the World Health Organisation (WHO) to adopt a provisional guideline value of $1 \mu\text{g L}^{-1}$ for MC-LR in drinking water [30].

To minimise the potential risk to human health, it is necessary to develop fast, sensitive and reliable methods to detect MCs. Several biological screening methods and also more sophisticated analytical techniques are currently in use. The first screening method to detect MCs was the mouse bioassay [31,32]. This assay gives an indication of the toxicity of the sample, but suffers from low sensitivity, lack of reliability and ethical implications. Another screening method is the protein phosphatase inhibition (PPI) assay [7,33–38]. Like the mouse bioassay, this method informs about the toxicity of the sample (although it is necessary to mention that *in vivo* toxicities may not be directly correlated to *in vitro* PP inhibition), but is not specific to MCs and positive results may indicate the presence of other enzyme inhibitors. Nevertheless, this method is sensitive to subnanogram levels. Enzyme-linked immunosorbent assays (ELISAs) based on antibodies are also highly specific but they are not selective and usually have problems of cross-reactivity among MC and even nodularin congeners [39–41]. Apart from these screening methods, more sophisticated identification and quantification techniques have been applied to MC detection. The most widespread is high performance liquid chromatography (HPLC), usually coupled to a UV detector and preferably to a photodiode array (PDA) detector, due to its inherent high sensitivity and selective detection [42,43]. However, only a few standards are commercially available and it requires trained personnel, expensive equipment and sample pre-treatment, resulting in long analysis times. Liquid chromatography/mass spectrometry (LC/MS) enables the simultaneous separation and identification of MCs in a mixture [43,44]. This analysis technique has been coupled to several ionisation technologies, i.e. fast atom bombardment (FAB) [45], electrospray ionisation (ESI) [46] and matrix assisted laser desorption ionisation time of flight (MALDI-TOF) [47]. Alternative analytical methods are thin-layer chromatography (TLC) [48], suitable as screening method due to its simplicity and low cost; capillary electrophoresis (CE), which achieves appropriate detection limits when coupled with fluorescence detection [49] or ESI/MS [50]; the detection of 2-methyl-3-methoxy-4-phenyl-butyric acid (MMPB), an oxidation product of MCs, by gas chromatography/mass spectrometry (GC/MS) [51] or fluorescence [52]; and the electrochemical detection of the arginine and tyrosine aminoacids [53,54], only valid for the variants with electroactive residues. The choice of the detection method depends on the purpose. They can be used in combination to exploit their complementarities and obtain a complete identification.

Screening techniques for an initial evaluation of MC in cyanobacterial samples should be improved, the ideal method being simple, robust, reliable and sensitive. Biosensors offer themselves as bioanalytical tools potentially able to fulfil all these requirements. Most of the PPI-based assays are colorimetric and in order to develop a biosensor, other transduction techniques should be found. Electrochemistry has been widely used in biosensors because of the simplicity, ease of use, portability, disposability and cost-effectiveness of the electrochemical devices. For the first time, our group has developed an electrochemical approach for the detection of the PP inhibition by cyanobacterial hepatotoxins. This electrochemical biosensing strategy has led to the development of an amperometric biosensor for MC screening, with significant advantages over current analytical methods in respect to analysis time, cost and simplicity.

2. Materials and methods

2.1. Reagents and materials

MC-LR was purchased from Sigma (St. Quentin Fallavier, France). MC standard solutions were firstly prepared in 50:50 methanol:water and subsequently diluted in a buffer solution at pH 8.4 containing 30 mM Tris-HCl, 2 mM ethylene diamine tetraacetic acid (EDTA) and 20 mM MgCl_2 . Protein phosphatase 2A (PP2A) was obtained from Upstate Biotechnology (New York, USA). PP2A is isolated as the heterodimer of 60 kDa (A) and 36 kDa (C) subunits from human red blood cells. The activity of the stock solution was 1100–2000 U mL^{-1} , 1 unit being defined as the amount of enzyme required to hydrolyse 1 nmol of *p*-NitroPhenyl Phosphate (*p*-NPP) in 1 min at 37 °C. *p*-NPP, α -Naphthyl Phosphate (α -NP), 4-MethylUmbelliferyl Phosphate (4-MUP) and components of buffers were purchased from Sigma. All solutions were prepared using Milli-Q water. Catechyl MonoPhosphate (CMP) was synthesised according to the method given by Kreuzer et al. [55]. Poly(vinyl alcohol) azide-unit pendant water-soluble photopolymer (PVA-AWP) (solid content 6 wt %, pH 6–6.5) was provided by Toyo Gosei Kogyo Co. (Chiba, Japan). Gold and platinum foils were purchased from Sigma (St. Quentin Fallavier, France). Copper chips were obtained from Biosentec (Toulouse, France). Silver (Electrodag PF 410), graphite (Electrodag 423 SS) and silver/silver chloride (Electrodag 418 SS) inks were obtained from Acheson (Erstein, France). The insulating layer was a Dulux Valentine paint (Asnières, France). PVC sheets (200 mm \times 100 mm \times 0.5 mm), supplied by SKK (Denzlingen, Germany), were used as support for the screen-printed electrodes. Microtiter plates were obtained from Nunc (Roskilde, Denmark). Real samples of cyanobacteria from the Tarn River (Midi-Pyrénées, France) were kindly provided by CRITT Bio-Industries (Toulouse, France).

2.2. Apparatus

Colorimetric measurements were performed with a Beckman DU520 UV/Vis spectrophotometer (Beckman Coulter France, S. A., Roissy CDG, France) or a Labsystems Multiskan EX

microtiter plate reader (Thermo Life Sciences, Cergy-Pontoise, France). Cyclic voltammeteries and chronoamperometric measurements were performed with an AUTOLAB PGSTAT12 potentiostat interfaced to a PC. Screen-printed 3-electrode systems, with graphite as working and counter electrodes and Ag/AgCl as reference electrode (on Ag conductive tracks), were fabricated using a DEK 248 screen-printing system (Weymouth, UK) as previously reported for screen-printed 2-electrode systems [56]. MC separation was carried out using an HPLC system (Merck, Whitehouse Station, USA), which consisted of a pump (type L-7100), an autosampler (L-7250) with a 20- μ L loop and a UV detector (L-7400). Data were collected and evaluated by HSM 4.1 chromatographic software from Merck.

2.3. Extraction of MCs from cyanobacterial samples

Forty milligrams of lyophilised cyanobacterial cells were extracted three times with 1.5 mL of 75:25 methanol:water by sonication for 5 min and centrifugation for 10 min. The three supernatants were mixed together and passed through a 0.2- μ m cut-off Acrodisc[®] syringe filter (Pall Corporation, Saint-Germain-en-Laye, France). After evaporation of the solvent in a Speed VAC concentrator (Organomation Associates, Inc., Berlin, USA) under nitrogen at room temperature, the residue was resuspended in 500 μ L of 30 mM Tris-HCl, 2 mM EDTA and 20 mM MgCl₂, pH 8.4, containing 10% (v/v) methanol.

2.4. Enzyme immobilisation and colorimetric optimisation

PP2A was immobilised by entrapment with poly(vinyl alcohol) azide-unit pendant water-soluble photopolymer (PVA-AWP), following the same protocol than with poly(vinyl alcohol) bearing styrylpyridinium groups, also named Poly(vinyl alcohol)-stilbazolium quaternary (PVA-SbQ) [57–63]. The stock enzyme solution was mixed with the polymer in a 2:1, 1:2 or 1:3 PP2A:PVA ratio on a Vortex mixer. Controls without enzyme were also performed. After homogenisation, 3 μ L of this solution were dropped on screen-printed graphite electrodes, gold or platinum foil, and copper chips. The supports were then exposed to neon light (two 15-W lamps) for 3 h at 4 °C to allow entrapment of the enzyme by polymerisation. Finally, the supports were dried for 22 h at 4 °C and rinsed with water prior use. The amount of entrapped enzyme was calculated to be 3.8 U when using stock PP2A solution in a 2:1 ratio, 1.9 U when using stock PP2A solution in a 1:2 ratio, and 1.4 U when using PP2A solution in a 1:3 ratio.

Activity assays were performed in order to study the possible enzyme leakage during the toxin incubation. To this end, the electrode supports with immobilised PP2A were introduced into microtiter wells containing 270 μ L of buffer solution at pH 8.4 with 30 mM Tris-HCl, 2 mM DTT, 2 mM EDTA, 0.2 mg mL⁻¹ BSA and 20 mM MgCl₂, and incubated for 30 min (the time subsequently used for the MC incubation) at room temperature. The supports were then rinsed with water and transferred to new microtiter wells containing fresh buffer. Thirty microliters of the colourless 100 mM *p*-NPP solution were added and after 1 h at room temperature, 200 μ L of solution were trans-

ferred to fresh microtiter wells to measure the absorbance of the yellow *p*-NP produced with the microtiter plate reader. The enzymatic activity arising from the incubation buffer was also measured. Controls without enzyme were always performed. Assays were performed in triplicate. Results were compared to those obtained with supports that had not been incubated in the buffer for 30 min.

2.5. Electrochemical enzymatic assays

The enzymatic activity of PP2A towards phosphorylated compounds was investigated by electrochemical methods with the purpose to develop an amperometric biosensor for MC detection. Electrochemical experiments were performed at room temperature using a single-drop configuration on a horizontally supported screen-printed 3-electrode system. The enzymatic substrates Catechyl MonoPhosphate (CMP), α -Naphthyl Phosphate (α -NP) and 4-MethylUmbelliferyl Phosphate (4-MUP) were dissolved in a buffer solution at pH 8.4 containing 30 mM Tris-HCl, 2 mM EDTA, 20 mM MgCl₂ and 100 mM KCl. Preliminary experiments were performed with alkaline phosphatase in solution, used as model enzyme (results not shown).

- (a) Cyclic voltammetry: 80 μ L of buffer were placed on the 3-electrode system with PP2A immobilised on the working electrode. Three scans were performed in the quiescent solution between +100 and +700 (for CMP), 0 and +600 (for α -NP), and +300 and +1000 mV (*versus* Ag/AgCl) (for 4-MUP) at 50 mV s⁻¹ and one at 5 mV s⁻¹. Afterwards, 10 μ L of 50 mM phosphorylated substrate were injected and mixed, and after 20 min one scan was performed again at 5 mV s⁻¹. Controls without enzyme were always performed. Assays were performed in triplicate.
- (b) Steady-state chronoamperometry: 90 μ L of buffer and 10 μ L of 50 mM phosphorylated substrate were placed on the 3-electrode system with PP2A immobilised on the working electrode. After 20-min incubation, the corresponding working potential (+450, +300 and +700 mV *versus* Ag/AgCl when using, respectively, CMP, α -NP and 4-MUP, according to the oxidation peaks obtained by cyclic voltammetry) was applied for 1 min in the quiescent solution and the current was measured at the end point. Controls without enzyme were always performed. Assays were performed in triplicate.

2.6. MC detection in real cyanobacterial samples

After extraction of MC from cyanobacterial cells, samples were analysed by a colorimetric PPI assay and with the developed amperometric biosensor. In both techniques, the standard curves for the enzyme inhibition were firstly plotted. Results were also compared to those obtained by HPLC, the most widespread method for MC analysis.

- (a) Colorimetry (*enzyme in solution*): the colorimetric assays for the inhibition of the enzyme in solution were performed by the addition of 20 μ L of pure, 10-, 100- and 1000-fold

diluted real samples or MC standard solutions at different concentrations into microtiter wells containing 160 μL of enzyme solution (0.3 U mL^{-1} final concentration in the well after the addition of all reagents) in 30 mM Tris–HCl, 2 mM EDTA, 20 mM MgCl_2 and 100 mM KCl buffer, pH 8.4. After 30-min pre-incubation at room temperature, 20 μL of 100 mM *p*-NPP solution were added and after 1 h, the absorbance was measured using the microtiter plate reader. Controls without enzyme and without MC were always performed. Assays were performed in triplicate.

- (b) Electrochemistry–steady-state chronoamperometry (*immobilised enzyme*): 80 μL of 30 mM Tris–HCl, 2 mM EDTA, 20 mM MgCl_2 and 100 mM KCl buffer, pH 8.4, and 10 μL of pure and 100-fold diluted real samples or MC standard solutions at different concentrations were placed on the 3-electrode system with PP2A immobilised on the working electrode. After 30-min incubation, 10 μL of 50 mM CMP were added and incubated for 20 min. Enzyme inhibition was then detected by steady-state chronoamperometry, by applying a potential of +450 mV *versus* Ag/AgCl for 1 min in the quiescent solution and measuring the current value at the end point. Controls without enzyme and without MC were always performed. Assays were performed in duplicate.
- (c) HPLC: Separation of cyanobacterial samples (prepared in 50:50 methanol:water) was performed on a Phenomenex C18(2) Luna 3- μm analytical column (150 mm \times 4.6 mm i.d.) using a 20 μL injection volume at a flow rate of 0.75 mL min^{-1} with a mixture of acetonitrile and water both containing 0.05% trifluoroacetic acid, using the following linear gradient: 30% of acetonitrile at 0 min, 35% of acetonitrile at 10 min, 70% of acetonitrile at 40 min, 100% of acetonitrile at 42 min and 30% of acetonitrile at 46 min. UV detection was performed at 238 nm. All the assays were performed in triplicate.

3. Results and discussion

3.1. Choice of the appropriate enzyme:polymer ratio and the electrode support

As demonstrated in our previous work [57], the immobilisation of PP2A using the entrapment method improves the stability of the enzymatic activity, when compared to the enzyme in solution. In this work, a water-soluble polymer with pendant photosensitive azide units has been used as cross-linked matrix. Its biocompatibility characteristics make it appropriate for enzyme immobilisation and biosensor construction.

Different electrode materials (gold, platinum, copper and graphite) were tested in order to choose the best support for PP immobilisation, *i.e.* the support that provides higher immobilisation yields. The 1:2 PP2A:PVA ratio was chosen to carry out this study. When gold and platinum foils were used, the activity assays of the incubated electrodes did not result in any colour development. In fact, it was noticed that the polymer was not adsorbed on the surface and that it was removed by rinsing. When copper chips were used, the polymer was also desorbed.

These results do not demonstrate the lack of retention of the enzyme into the polymer network, but the poor adsorption of the polymer on those materials. It is interesting to note that if the supports were not rinsed prior the colorimetric assay (consequently, the totality of the deposited enzyme was in the microtiter well, either immobilised or free in solution), the activity assays showed colour development for gold and platinum foils, but no response from copper chips. This result may be explained by the inhibitory effect of the copper metal on the PP enzymatic activity, already demonstrated when using 0.2 mM Cu^{2+} salt with PP from bacteriophage lambda [64]. When graphite electrodes were used, the activity assays of the incubated electrodes showed 62% (relative standard deviation (R.S.D.) = 17%, $n = 3$) of the response of non-incubated electrode controls. The missing 38% could be due to the leakage of the enzyme from the network during the 30-min incubation step required for the subsequent MC incubation and/or to its partial inactivation during that period. In fact, the “leaked” enzymatic activity (arising from the incubation buffer) was not 38%, but 8% (R.S.D. = 8%, $n = 3$). The fact that the balance does not close can be explained by the partial enzyme inactivation, higher for the enzyme in solution. Although this result is far from ideal, the response was high enough to continue with the development of the electrochemical biosensor.

After the electrode material optimisation, several PP2A:PVA ratios were investigated for the immobilisation on graphite electrodes. A high polymer proportion may provide a high enzyme immobilisation yield, however, it may also restrict the enzyme freedom and flexibility, decreasing or totally inhibiting the enzymatic activity. Therefore, a compromise needs to be found between a high immobilisation yield and a measurable signal. Similarly, a high enzyme proportion may provide higher responses, however the sensitivity of the inhibition assay decreases as the enzyme activity increases. Hence another compromise needs to be found between a significant response and a low limit of detection. The absorbance values of the activity assays of the incubated electrodes were 0.041 (R.S.D. = 9%, $n = 3$), 0.259 (R.S.D. = 17%, $n = 3$) and 0.189 AU (R.S.D. = 15%, $n = 3$) for, respectively, the 2:1, 1:2 and 1:3 PP2A:PVA ratios. Although the enzyme amount used in the 1:2 ratio (1.9 U) was lower than that in the 2:1 ratio (3.8 U), the colorimetric response was higher, indicating that the enzyme was better immobilised and/or retained in that matrix. The 2:1 ratio was discarded, as the maximum absorbance (0.041 AU) was too low to perform an inhibition experiment. Compared to the 1:3 ratio (1.4 U), the 1:2 ratio provides only slightly higher absorbance values. Like the 0.259 AU value, the 0.189 AU value could also be appropriate for inhibition experiments. Looking at the immobilisation and/or retention yields, the activity assays of the incubated electrodes for the 2:1, 1:2 and 1:3 PP2A:PVA ratios, respectively, showed 16 (R.S.D. = 9%, $n = 3$), 62 (R.S.D. = 17%, $n = 3$) and 41% (R.S.D. = 15%, $n = 3$) of the response of non-incubated electrode controls. The “leaked” enzymatic activity was 16 (R.S.D. = 6%, $n = 3$), 8 (R.S.D. = 8%, $n = 3$) and 3% (R.S.D. = 5%, $n = 3$). Once again, the balances do not close due to the partial enzyme inactivation. The results demonstrate that the 1:2 PP2A:PVA ratio provides the higher immobilisation and/or

retention (during MC incubation) yield. Although looking at the absorbance values, both the 1:2 and 1:3 PP2A:PVA ratios could be used, the 62% of retention and/or immobilisation in front of the 41% induced us to chose the 1:2 ratio for the subsequent electrochemical enzyme inhibition experiments.

3.2. Choice of the appropriate substrate for PP2A activity electrochemical detection

Most of the enzymes participating in electrochemical biosensors are redox enzymes and, consequently, the electron transfer is guaranteed by the enzyme itself (direct electron transfer) or by the inclusion of redox mediators that react with the enzyme and with the electrode surface (mediated electron transfer). In this work, the enzyme used for the MC detection is not electrochemically active and other electrochemical transduction pathways should be found. The use of an enzymatic substrate electrochemically active only after dephosphorylation by the enzyme would be the solution. In order to choose the optimum phosphorylated substrate to monitor the PP2A activity by electrochemistry, CMP, α -NP and 4-MUP were tested. Preliminary experiments using alkaline phosphatase in solution as model enzyme demonstrated the possibility to detect the dephosphorylated products both by cyclic voltammetry and steady-state chronoamperometry.

Cyclic voltammetry experiments with PP2A in solution demonstrated the ability of the PP2A to dephosphorylate the three substrates. Fig. 1A shows an oxidation peak at approximately +450 mV (*versus* Ag/AgCl), corresponding to the catechol coming from the reaction between CMP and PP2A. The reaction between α -NP and PP2A resulted in an oxidation peak at approximately +300 mV (*versus* Ag/AgCl) (Fig. 1B). Although in the development of electrochemical biosensors, low oxidation peaks are preferred, as they lower the working potential and decrease the interference level, CMP was preferred to α -NP due to the less pronounced electrode fouling [57]. The reaction between 4-MUP and PP2A resulted in an oxidation peak at approximately +700 mV (*versus* Ag/AgCl) (Fig. 1C). Despite the high currents obtained with this substrate, the oxidation potential was too high to be used as working potential in an amperometric biosensor. In the chronoamperometric experiments, the background-subtracted steady-state oxidation currents were 637 (R.S.D. = 18%, $n = 3$), 98 (R.S.D. = 20%, $n = 3$)

and 429 nA (R.S.D. = 25%, $n = 3$) for, respectively, CMP, α -NP and 4-MUP. The CMP provides not only the highest oxidation currents but also the highest reproducibility. However, this reproducibility should be improved, as it compromises the reliability of the assay. As the rough graphite surface may be responsible for the high R.S.D. values, other types of electrodes are currently under study in our group. In conclusion, both voltammetric and amperometric results led us to choose CMP as phosphorylated substrate for the subsequent electrochemical enzyme inhibition experiments.

3.3. MC detection in real cyanobacterial samples

Real samples of cyanobacterial blooms from the Tarn River (Midi-Pyrénées, France) were tested using the developed amperometric biosensor. Electrochemical results were compared to those obtained by a colorimetric PPI assay with the enzyme in solution and by HPLC. Firstly, calibration curves with MC standard solutions were plotted for both the colorimetric (Fig. 2A) and the electrochemical (Fig. 2B) approaches. Whereas the R.S.D. values for the colorimetric assay were always less than 7%, the biosensor showed much higher values (R.S.D. = 35%), due to the less steeper slope of the curve (which induces a higher uncertainty on the concentration values), but also to reproducibility problems associated to the electrode construction and to the fouling phenomena. The regression equations obtained for the linear regions ($y = 88.462 \ln(x) - 47.312$, $R^2 = 0.9962$, and $y = 18.344 \ln(x) - 31.077$, $R^2 = 0.9968$, for the colorimetric and the electrochemical strategies, respectively), subsequently used for quantification of MC concentrations in the real samples, indicate 50% inhibition coefficients (IC_{50}) of 3 and $83 \mu\text{g L}^{-1}$. The limit of detection (LOD) in the colorimetric approach, considered as 10% inhibition, was $2 \mu\text{g L}^{-1}$. In the electrochemical approach, the LOD was considered to be 35% inhibition (due to the lower reproducibility values, which compromise the reliability of the MC determination) and it was $37 \mu\text{g L}^{-1}$. The curves show 100% inhibition at about 10 and $1000 \mu\text{g L}^{-1}$, for the colorimetric and the electrochemical strategies, respectively. Thus the colorimetric method is almost 20 times more sensitive, but the electrochemical strategy provides a larger working range. This larger working range is very useful for screening purposes, since when unknown samples are analysed, subsequent dilutions have to be performed to meet the linear section of the calibration

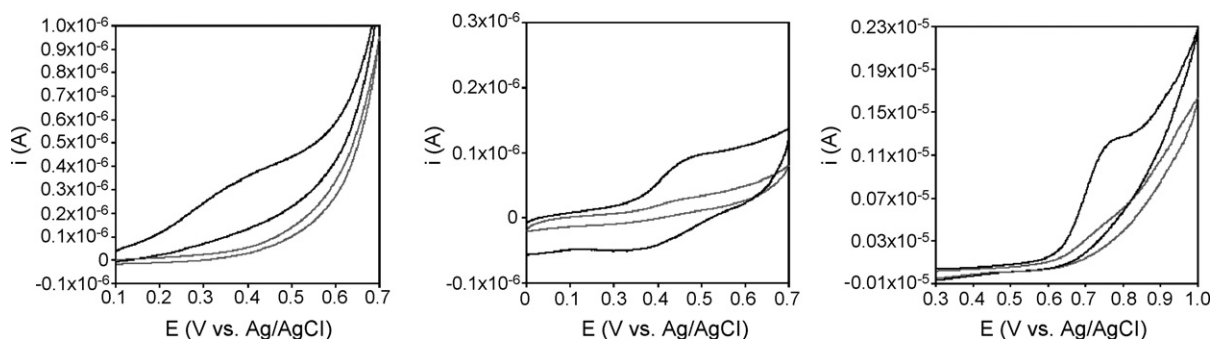


Fig. 1. Cyclic voltammogram of 1.1 U PP2A (grey line) and 1.1 U PP2A + 5 mM substrate (CMP for 1A, α -NP for 1B and 4-MUP for 1C; black line) at 5 mV s^{-1} using a single-drop configuration on a horizontally supported screen-printed 3-electrode system.

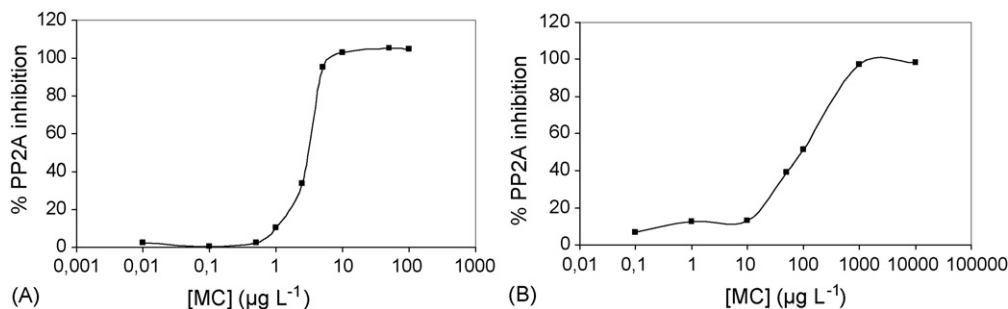


Fig. 2. Colorimetric (enzyme in solution) (A) and electrochemical (immobilised enzyme); (B) standard curves for the inhibition of PP2A by MC-LR. Inhibition is expressed as percentage of the control (no MC). Concentrations refer to the initial MC standard solutions. R.S.D. values are not shown for clarity (for more details, see in the text).

curve. Although electrochemical techniques are usually more sensitive than colorimetric assays, in this case problems associated to the reproducibility between electrodes derived from the screen-printing process and the partial electrode fouling have restricted the sensitivity of the biosensor. As previously mentioned, work is in progress to improve both the reproducibility and the limits of detection by the use of new types of electrodes. At this moment, since the determination level of the biosensor ranges from 37 to 188 $\mu\text{g L}^{-1}$ (from 35 to 65% inhibition), the biosensor is not directly applicable to natural water samples and a prior concentration step is necessary. However, in the analysis of microcystin content in algae, the residue resuspension step may include this concentration step.

MC-LR equivalent contents in natural blooms of cyanobacteria obtained by the colorimetric PPI assay, with the amperometric PPI-based biosensor and by HPLC are summarised in Table 1. From the 7 real samples tested, all of them contained MC at levels detectable by the amperometric biosensor, 6 by the colorimetric assay and 5 by HPLC. The correlation between the two enzymatic methods is very good (Fig. 3A), but always with higher toxin levels when analysed with the biosensor. Taking into account that when MC standard solutions were used, the colorimetry assay showed lower limits of detection, it seems that the electrochemical biosensor gives an overestimation of the toxin content compared to the colorimetric assay. This effect could be due to the fouling of the electrode by some of the cell extract components, which would decrease the steady-state oxidation currents, simulating an enzymatic inhibition. HPLC

correlations with the colorimetric assay (Fig. 3B) and the electrochemical biosensor (Fig. 3C) are poorer. HPLC indicates slightly higher toxin contents for samples 1, 2, 4 and 6 when compared with both PPI-based techniques. Since all the real samples had MC-LR as main or only component, this slight underestimation of the enzymatic techniques is not certainly due to the presence of a MC variant less active than MC-LR (although only three MC variants – MC-LR, MC-LF and MC-RR – were used as standards). Neither to the presence of intracellular PPs, first because cells were lyophilised and second because the methanol used in the extraction process would have neutralised their activity. The explanation to the underestimation should be found in the potential matrix effects. Work is in progress to evaluate them. Sample 3 presented slightly higher toxin contents than those

Table 1

MC-LR equivalent concentrations (ng mg^{-1} dry weight) in cyanobacterial blooms derived by the colorimetric PPI assay, the amperometric PPI-based biosensor and HPLC (MC variant composition obtained by HPLC is provided)

Sample	Colorimetric	Electrochemical	HPLC
1	4.0 (7.4)	10.2 (1.4)	28.7 (0.6) 100% MC-LR
2	6.1 (8.3)	14.3 (21.8)	15.7 (1.1) 100% MC-LR
3	32.4 (1.9)	149.7 (18.3)	83.3 (0.9) 99% MC-LR 1% MC-LF
4	–	0.5 (9.6)	4.1 (1.4) 100% MC-LR
5	3.5 (2.5)	9.2 (25.3)	–
6	0.1 (6.3)	0.3 (16.5)	5.9 (3.5) 100% MC-LR
7	0.4 (2.9)	2.5 (19.6)	–

In parentheses, the R.S.D. (%) values are given.

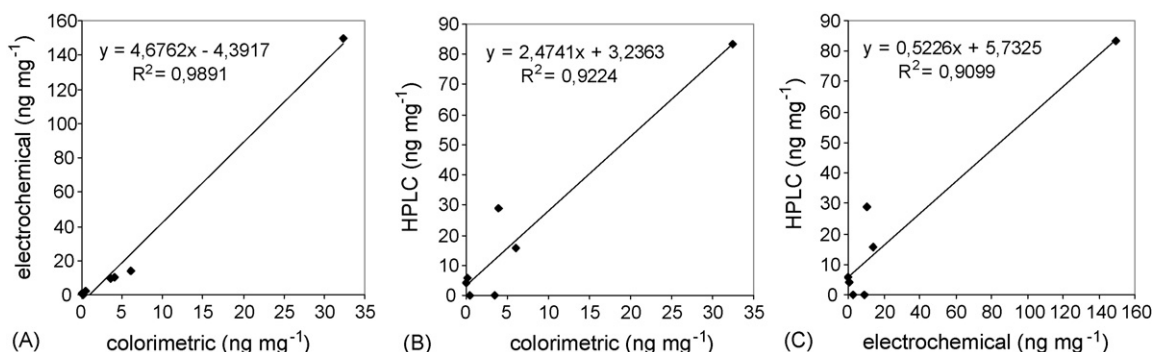


Fig. 3. Correlations of MC-LR equivalent concentrations (ng mg^{-1} dry weight) in cyanobacterial blooms derived by the colorimetric PPI assay, the amperometric PPI-based biosensor and HPLC. The regression lines and equations are shown.

determined by colorimetry but lower than those determined with the biosensor. This result clearly demonstrates the biosensor overestimation, more evident at high toxin concentrations. Samples 5 and 7 were indicated to contain MC by PPI at levels that should have been detected by HPLC. The non-detectable contents by HPLC could be due to the fact that only MC-LR, MC-LF and MC-RR were used as standards and other variants, whose standards were not tested or are not commercially available, could be present in those samples. In fact, because the PPI-based techniques detect all inhibitory MC variants at the same time, its sensitivity compared to HPLC is further enhanced. One can not ignore the fact that the MC presence detected in samples 5 and 7 by the enzymatic methods could be a false positive due to the presence of PP2A inhibitors others than microcystins, such as nodularins, okadaic acid and its derivatives, cantharidin, tautomycin, calyculin A; however, only nodularins can be present in cyanobacterial cells, which, in any case, are less spread in the world than microcystins.

Although there was a poor correlation between HPLC and the electrochemical device, the high sensitivity, the simplicity and the broad working range of the approach justify the use of the amperometric biosensor as screening and monitoring tool to roughly estimate the microcystin content in sample. In positive samples, the use in parallel of other analytical techniques, such as LC/UV or LC/MS, would eliminate the possibility of having other inhibiting compounds, would provide accurate MC determination and would enable the identification of the variant/s.

4. Conclusions

The enzymatic methods for MC detection present the advantage over HPLC of being more sensitive and less expensive and do not require trained personnel. Although enzymatic assays are not specific to MCs, they give the microcystin content expressed into a MC-LR equivalent concentration. In this work, a PPI-based amperometric biosensor for MC detection has been developed for the first time, combining the advantages of the PPI assays and the electrochemical transducers. The low working potential required, provided by the lab-made CMP enzyme substrate, avoids the oxidation of interferences that might be present in real samples. Despite the overestimation of the toxin content, potentially due to the electrode fouling by some cell extracts components, the applicability of the biosensor to rapidly assess the environmental and health risk due to MCs is demonstrated. To minimise the risk of false positive results or if accurate toxin determination and quantification are desired, the amperometric biosensor should be used in parallel with other analytical techniques. The simplicity of both the biosensor construction and the electrochemical measurement, together with the electrode disposability and the possibility to be used *in situ*, make the amperometric biosensor attractive as screening tool for rapid and early MC detection.

Acknowledgements

Dr. Campàs acknowledges the “Secretaría de Estado de Educación y Universidades” and the “Fondo Social Europeo”

for financial support. Mrs. Szydłowska acknowledges the project “ACI, Nouvelles méthodologies analytiques et capteurs”, CNRS, for financial support. The authors are grateful to Toyo Gosei Kogyo Co. for kindly providing the PVA-AWP polymer and CRITT Bio-Industries for the real cyanobacterial samples.

References

- [1] M.J. Pearson, A.J.D. Ferguson, G.A. Codd, C.S. Reynolds, J.K. Fawell, R.M. Hamilton, S.R. Howard, M.R. Attwood, Toxic blue-green algae, Report of the National Rivers Authority, Water Quality, Series no. 2. London, 1990.
- [2] R. Resson, F.S. Soong, J. Fitzgerald, L. Turczynowicz, O. El Saadi, D. Roder, T. Maynard, I.R. Falconer, Health Effects of Toxic Cyanobacteria (Blue-green Algae), National Health and Medical Council, Australian Government Publishing Service, Canberra, 1994.
- [3] W.W. Carmichael, Sci. Am. 270 (1994) 78.
- [4] K. Sivonen, G. Jones, in: I. Chorus, J. Bartram (Eds.), Toxic Cyanobacteria in Water—A Guide to their Public Health Consequences, Monitoring and Management, E&FP Spon, London, 1999, pp. 41–112.
- [5] R.M. Dawson, Toxicol. 36 (1998) 953.
- [6] T. Kuiper-Goodman, I.R. Falconer, J. Fitzgerald, in: I. Chorus, J. Bartram (Eds.), Toxic Cyanobacteria in Water—A Guide to their Public Health Consequences, Monitoring and Management, WHO, E&FP Spon, London, 1999, pp. 113–153.
- [7] C. MacKintosh, K.A. Beattie, S. Klumpp, P. Cohen, G.A. Codd, FEBS Lett. 264 (1990) 187.
- [8] S. Yoshizawa, R. Matsushima, M.F. Watanabe, K. Hard, A. Ichihara, W.W. Carmichael, H. Fujiki, J. Cancer Res. Clin. Oncol. 116 (1990) 609.
- [9] J.E. Eriksson, D. Toivela, J.A.O. Meriluto, H. Karaki, Y.G. Han, D. Harstshorne, Biochem. Biophys. Res. Commun. 173 (1990) 1347.
- [10] W.W. Carmichael, S.M.F.O. Azevedo, J.S. An, R.J.R. Molicca, E.M. Jochimsen, S. Lau, K.L. Rinehart, G.R. Shaw, G.K. Eaglesham, Environ. Health Perspect. 109 (2001) 663.
- [11] E.M. Jochimsen, W.W. Carmichael, J.S. An, D.M. Cardo, S.T. Cookson, C.E.M. Aholmes, M.B. Antunes, D.A. de Melo, T.M. Lyra, V.T. Spinelli, S.M.F.O. Azevedo, M.D. Jarvis, N. Engl. J. Med. 338 (1998) 873.
- [12] S. Pouria, A. de Andrade, J. Barbosa, R.L. Cavalcanti, V.T.S. Barreto, C.J. Ward, W. Preiser, G.K. Poon, G.H. Neild, G.A. Codd, Brazil Lancet 352 (1998) 21.
- [13] W.W. Carmichael, J. Appl. Bacteriol. 72 (1992) 445.
- [14] I. Chorus, I.R. Falconer, H.J. Salas, J. Bartram, J. Toxicol. Environ. Health, B 3 (2000) 323.
- [15] G.A. Codd, W.P. Brooks, L.A. Lawton, K.A. Beattie, in: D. Wheeler, M.L. Richardson, J. Bridges (Eds.), Watershed '89, The Future for Water Quality in Europe, vol. II, Pergamon, Oxford, 1989, pp. 211–220.
- [16] G.A. Codd, Ecol. Eng. 16 (2000) 51.
- [17] I.R. Falconer, Phycologia 35 (1996) 6.
- [18] I.R. Falconer, Quality and Treatment of Drinking Water II in: J. Hrubec (Ed.), The Handbook of Environmental Chemistry, vol. 5 (Part C), Springer-Verlag, Berlin, 1998, pp. 54–72.
- [19] B.C. Hitzfeld, S.J. Hoger, D.R. Dietrich, Environ. Health Perspect. 108 (2000) 113.
- [20] L.S. Pilotto, R.M. Douglas, M.D. Burch, S. Cameron, M. Beers, G.R. Rouch, P. Robinson, M. Kirk, C.T. Cowie, S. Hardiman, C. Moore, R.G. Attewell, N. Zealand, J. Public Health 21 (1997) 562.
- [21] S.-Z. Yu, in: Z.Y. Tang, M.C. Wu, S.S. Xia (Eds.), Primary Liver Cancer, China Academic Publishers, Spring-Verlag, Berlin, 1989, pp. 30–37.
- [22] S.-Z. Yu, J. Gastroenterol. Hepatol. 10 (1995) 674.
- [23] R.B. Fitzgeorge, S.A. Clark, C.W. Keevil, in: G.A. Codd, T.M. Jefferies, C.W. Keevil, E. Potter (Eds.), Detection Methods for Cyanobacterial Toxins, The Royal Society of Chemistry, Cambridge, 1994, pp. 69–74.
- [24] T.W. Lambert, C.F.B. Holmes, S.E. Hrudefy, Environ. Rew. 2 (1994) 167.
- [25] D.J. Gilroy, K.W. Kauffman, R.A. Hall, X. Huang, F.S. Chu, Environ. Health Perspect. 108 (2000) 435.
- [26] G.A. Codd, J.S. Metcalf, A.B. Kenneth, Toxicol. 37 (1999) 1181.

- [27] I.R. Falconer, M. Dornbusch, G. Moran, S.K. Yeung, *Toxicon* 30 (1992) 790.
- [28] I.R. Falconer, M.D. Burch, D.A. Steffensen, M. Choice, O.R. Coverdale, *Environ. Toxicol. Water Qual.* 9 (1994) 131.
- [29] E.E. Prepas, E.G. Kotak, L.M. Campbell, J.C. Evans, S.E. Hrudey, C.F.B. Holmes, *Can. J. Fish. Aquat. Sci.* 54 (1997) 41.
- [30] WHO, *Guidelines for Drinking-Water Quality*, second ed., WHO, Geneva, 1998 (addendum to vol. 1, recommendations).
- [31] D.L. Campbell, L.A. Lawton, K.A. Beattie, G.A. Codd, *Environ. Toxicol. Water Qual.* 9 (1994) 71.
- [32] I.R. Falconer, in: I.R. Falconer (Ed.), *Algal Toxins in Seafood and Drinking Water*, Academic Press, London, 1993, pp. 165–175.
- [33] J.S. An, W.W. Carmichael, *Toxicon* 32 (1994) 1495.
- [34] N. Bouaïcha, I. Maatouk, G. Vincent, Y. Levi, *Food Chem. Toxicol.* 40 (2002) 1677.
- [35] T. Heresztyn, B.C. Nicholson, *Water Res.* 35 (2001) 3049.
- [36] C. Rivasseau, P. Racaud, A. Deguin, M.-C. Henion, *Anal. Chim. Acta* 394 (1999) 243.
- [37] B.S.F. Wang, P.K.S. Lam, L. Xu, Y. Zhang, B.J. Richardson, *Chemosphere* 38 (1999) 1113.
- [38] C.J. Ward, K.A. Beattie, E.Y.C. Lee, G.A. Codd, *FEMS Microbiol. Lett.* 153 (1997) 465.
- [39] W.P. Brooks, G.A. Codd, *Environ. Technol. Lett.* 9 (1988) 1343.
- [40] F.S. Chu, X. Huang, R.D. Wei, *J. Assoc. Off. Anal. Chem.* 73 (1990) 451.
- [41] S. Nagata, H. Soutome, T. Tsutsumi, A. Hasegawa, M. Sekijima, M. Sugamata, K.-I. Harada, M. Sukanuma, Y. Ueno, *Nat. Toxins* 3 (1995) 78.
- [42] L.A. Lawton, C. Edwards, G.A. Codd, *Analyst* 119 (1994) 1525.
- [43] K. Tsuji, S. Naito, F. Kondo, M.F. Watanabe, S. Suzuki, H. Nakazawa, M. Suzuki, T. Shimada, K.-I. Harada, *Toxicon* 32 (1994) 1251.
- [44] C. Edwards, L.A. Lawton, K.A. Beattie, G.A. Codd, S. Pleasance, G.J. Dear, *Rapid Commun. Mass Spectrom.* 7 (1993) 714.
- [45] F. Kondo, Y. Ikai, H. Oka, N. Ishikawa, M.F. Watanabe, M. Watanabe, K.-I. Harada, M. Suzuki, *Toxicon* 30 (1992) 227.
- [46] M. Barco, J. Rivera, J. Caixach, *J. Chromatogr. A* 959 (2002) 103.
- [47] M. Welker, J. Fastner, M. Erhard, H. von Döhren, *Environ. Toxicol.* 17 (2002) 367.
- [48] A. Pelander, I. Ojanperä, K. Lahti, K. Niinivaara, E. Vuori, *Water Res.* 10 (2000) 2643.
- [49] P.C.H. Li, L.A. Lawton, P.K. Robertson, *Environ. Sci. Technol.* 37 (2003) 3214.
- [50] H. Sirèn, M. Jussila, H. Liu, S. Peltoniemi, K. Sivonen, M.-L. Riekkola, *J. Chromatogr. A* 839 (1999) 203.
- [51] K. Tsuji, H. Masui, H. Uemura, Y. Mori, K.-I. Harada, *Toxicon* 39 (2001) 687.
- [52] T. Sano, K. Nohara, F. Shiraishi, K. Kaya, *Int. J. Environ. Anal. Chem.* 49 (1992) 163.
- [53] J. Meriluoto, B. Kincaid, M.R. Smyth, M. Wasberg, *J. Chromatogr. A* 810 (1998) 226.
- [54] F. Yan, M. Ozsoz, O.A. Sadik, *Anal. Chim. Acta* 409 (2000) 247.
- [55] M.P. Kreuzer, C.K. O'Sullivan, G.G. Guilbault, *Anal. Chim. Acta* 393 (1999) 95.
- [56] S. Andreescu, L. Barthelmebs, J.-L. Marty, *Anal. Chim. Acta* 464 (2002) 171.
- [57] M. Campàs, D. Szydłowska, M. Trojanowicz, J.-L. Marty, *Biosens. Bioelectron.* 20 (2005) 1520.
- [58] T. Noguer, J.-L. Marty, *Enzyme Microb. Technol.* 17 (1995) 453.
- [59] T. Noguer, J.-L. Marty, *Anal. Lett.* 30 (1997) 1069.
- [60] T. Noguer, J.-L. Marty, *Anal. Chim. Acta* 347 (1997) 63.
- [61] T. Noguer, A. Gradinaru, A. Ciucu, J.-L. Marty, *Anal. Lett.* 32 (1999) 1723.
- [62] T. Noguer, A.-M. Balasoïu, A. Avramescu, J.-L. Marty, *Anal. Lett.* 34 (2001) 513.
- [63] T. Noguer, A. Tencaliec, C. Calas-Blanchard, A. Avramescu, J.-L. Marty, *J. AOAC Int.* 85 (2002) 1383.
- [64] S. Zhuo, J.C. Clemens, D.J. Hakes, D. Badford, J.E. Dixon, *J. Biol. Chem.* 268 (1993) 17754.

Determination of atenolol at a graphite–polyurethane composite electrode

Priscila Cervini, Luiz Antônio Ramos, Éder Tadeu Gomes Cavalheiro*

Universidade de Sao Paulo, Instituto de Quimica de Sao Carlos, Av. do Trabalhador Sancarlense, 400, 13566-590 Sao Carlos, SP, Brazil

Received 13 July 2006; received in revised form 9 October 2006; accepted 13 October 2006
Available online 17 November 2006

Abstract

A bare graphite–polyurethane composite was evaluated as an alternative electrode in the determination of atenolol (ATN) in pharmaceutical formulations. Using a DPV procedure, a linear analytical curve was observed in the 4–100 $\mu\text{mol L}^{-1}$ range with a LOD = 3.16 $\mu\text{mol L}^{-1}$, without need of surface renewing between successive runs, with recoveries between 95.5 and 108%. Interference of other antihypertensive drugs was observed, but not from the usual components of tablets. The results of the proposed method agreed with HPLC ones within 95% confidence level.

© 2006 Published by Elsevier B.V.

Keywords: Atenolol; Graphite–PU composite electrode; DPV

1. Introduction

Atenolol (ATN) [4-[2-hydroxy-3-isopropylaminopropoxy]-phenylacetamide] is a hydrophilic β_1 -receptor blocking agent. This β -adrenoceptor blocking drug is of therapeutic value in the treatment of various cardiovascular disorders, such as angina pectoris, cardiac arrhythmia and hypertension [1]. With chronic treatment, it reduces mortality in hypertension and prolongs survival in patients with coronary heart disease [2]. β -Blockers are exceptionally toxic and most of them acts in a narrow therapeutic range; the differences between the lowest therapeutic and the highest tolerable doses are small [3]. Common effects associated with atenolol overdose are lethargy, disorder of respiratory drive, wheezing, sinus pause, bradycardia, congestive heart failure, hypotension, bronchospasm and hypoglycemia [4,5]. This is the reason that analysis of ATN is of great importance in pharmaceutical research. In the literature, few methods have been reported for the determination of ATN in pharmaceutical formulations. Most of them relying on the use of chromatographic techniques, like gas chromatography (GC) with mass spectrometry or electron capture detector [3,6] and high performance liquid chromatography (HPLC) [7,8]. Electrochemical determination

of atenolol was performed using both C_{60} —modified glassy carbon (GC) electrode [9] and nanogold modified indium tin oxide electrode [10]. In these works limits of detection such as 0.16 mmol L^{-1} and 0.13 $\mu\text{mol L}^{-1}$ were described, respectively. Due to the importance of ATN, it is interesting to develop a rapid screening method for its determination in pharmaceutical formulations.

Therefore, the purpose of this work is to investigate the voltammetric behavior of ATN using a 60% (graphite, w/w) composite graphite–polyurethane (PU) electrode, without modification. This new composite was recently proposed [11] and showed to be sensitive and useful in differential pulse voltammetry (DPV), square wave voltammetry (SWV) techniques [12] and as an amperometric detector in flow injection analysis [13].

2. Experimental

2.1. Apparatus

Voltammetric experiments were performed using an AUTO-LAB PGSTAT-30 (Ecochemie, The Netherlands) potentiostat/galvanostat coupled to a personal computer and controlled with GPES 4.9 software. A three-electrode cell with 20 mL total capacity was used with a saturated calomel electrode (SCE) and

* Corresponding author. Tel.: +55 16 3373 8054; fax: +55 16 3373 9987.
E-mail address: cavalheiro@iqsc.usp.br (É.T.G. Cavalheiro).

a platinum wire as the reference and counter electrodes, respectively. The 60% (graphite, w/w) composite [11] was used as working electrode. All measurements were performed at room temperature.

2.2. Reagents and solutions

All reagents were of analytical grade and used as received. Solutions were prepared with water bi-distilled in quartz stiller.

ATN was purchased from Natural Pharma (Brazil) and a 1 mmol L^{-1} stock solution was prepared in universal buffer pH 10.

2.3. Preparation of the composite electrode

The 60% (graphite, w/w) composite graphite–PU electrode was prepared as previously described [11]. Briefly, adequate amounts of the polyol, hardener (Poliqual, Brazil) and graphite (Aldrich, USA) were mixed in a mortar for 5 min in order to obtain a mixture with 60% of graphite (w/w). The resulting mixture was inserted in a manual press and extruded as 3.0 mm diameter rods. The composite was cured for 24 h at room temperature and cutted in 1.0 cm long rods. A copper wire (\varnothing , 1.0 mm) was attached to these rods with the help of a silver epoxy (EPO-TEK 410E, Epoxy Technology, USA), conducting resin in order to reach electric contact. This set was then inserted in a 5.0 mm i.d. glass tube and sealed with the unmodified PU resin. The electrodes were let to cure for 24 h.

After curing, the excess of polymer was removed using a 600-grit sand paper, polished with $1 \mu\text{m } \gamma\text{-Al}_2\text{O}_3$ suspension in an APL-2 polishing wheel (Arotec, Brazil), and sonicated in isopropyl alcohol during 5 min.

2.4. Procedures

Voltammetric measurements were performed after deaeration with N_2 bubbled during at least 5 min, using the 60% (graphite, w/w) composite and glassy carbon electrodes for comparison.

For recording differential pulse voltammograms, aliquots of a freshly prepared ATN stock solution were diluted in 10 mL of universal buffer pH 10 inside the voltammetric cell.

DPV is a pulse technique dependent of the pulse amplitude (a) and scan rate (v), these parameters were optimized from a set of values $a = 10$ and 50 mV , and $v = 5$ and 50 mV s^{-1} , according to a factorial planning 2^n , in a total of four experiments, in universal buffer pH 10.

2.5. Procedures for pharmaceutical formulation analysis

According to the Brazilian Pharmacopea recommendations [14], 20 tablets were weighed and powdered. Accurately weighed portions of powder equivalent to 100, 50, 50 and 25 mg of generic Atenolol (1) (Medley, Brazil), Atenol (Astra Zeneca, Brazil), generic Atenolol (2) (Biossintética, Brazil) and Angipress (Biossintética, Brazil), respectively, were dissolved in 25 mL of universal buffer pH 10 to obtain solutions correspondent to 15.0, 7.5, 7.5 and 3.7 mmol L^{-1} in ATN, respectively.

The solutions were sonicated for 10 min to complete the dissolution of the analyte. After decantation, suitable volumes of the supernatant of these solutions were transferred to the voltammetric cell containing 10 mL of universal buffer pH 10, to obtain concentrations ca. $1.1 \times 10^{-4} \text{ mol L}^{-1}$ for all samples. Then, single additions [15] of $400 \mu\text{L}$ of standard solution of ATN 10 mmol L^{-1} were made and differential pulse voltammograms were recorded.

2.6. Comparison method [16]

In the HPLC comparison method, the mobile phase was composed of acetonitrile (solvent A) and phosphate buffer (solvent B), with 0.2% (w/v) of triethylamine, with the pH adjusted to 3 with orthophosphoric acid 85% (0.067 mol L^{-1} 10:70 v:v, pH 3). The flow rate was 0.8 mL min^{-1} . The injection volume was $20 \mu\text{L}$. The UV detection was accomplished at 225 nm.

Working solutions were obtained by suitable dilution from standard stock ATN solutions prepared in 0.25 mg mL^{-1} in phosphate buffer (pH 7.4, 0.067 mol L^{-1}). The concentration range of the analytical curves was $25\text{--}1.56 \mu\text{g mL}^{-1}$. Solutions of the pharmaceutical formulations were prepared to be $6.25 \mu\text{g mL}^{-1}$ in ATN.

3. Results and discussion

The resulting voltammograms are presented in Fig. 1, from which is possible to observe the ATN oxidation at ca. 760 mV (versus SCE), with better peak definition at $a = 50 \text{ mV}$ and higher sensitivities at $v = 50 \text{ mV s}^{-1}$. Using $a = 10 \text{ mV}$, very low sensitivity was achieved. Thus, 50 mV and 50 mV s^{-1} was used as pulse amplitude and scan rate, respectively, in further studies.

The effect of the pH varying from 2 to 12 on the voltammetric response of ATN at the 60% (graphite, w/w) composite electrode was also evaluated. Only at pH 8, 10 and 12 it was observed a signal.

This electrochemical response for the ATN in pH up to 8 is blocked by the acid-base equilibrium of the amino group, whose $pK_a = 9.4$ [17], as represented in Eq. (1).

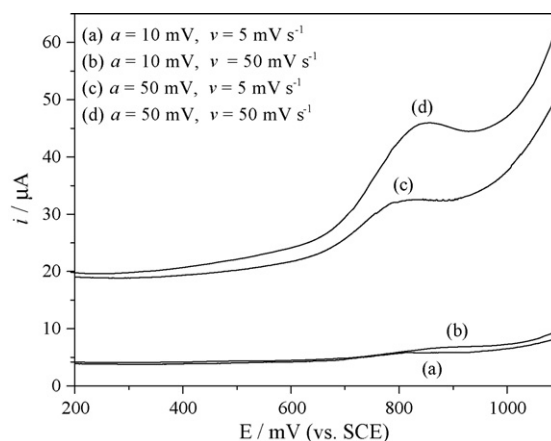
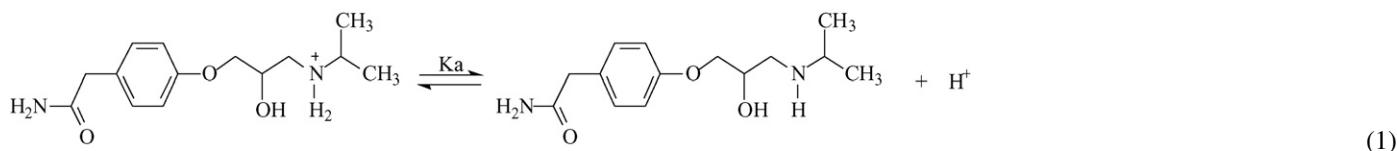


Fig. 1. DPV voltammograms obtained at 60% (graphite, w/w) composite electrode using $1.0 \times 10^{-3} \text{ mol L}^{-1}$ ATN in universal buffer pH 10.



The obtained results suggest that the 60% (graphite, w/w) composite electrode is a suitable tool to be used in DPV procedures for the determination of ATN in pH 8–10, but the last one presents better response. At pH 12, the electrode response became noisy as expected to the higher basic medium [11].

Using these optimized conditions an analytical curve was obtained in the 1.0×10^{-6} to 2.3×10^{-3} mol L⁻¹ ATN range. The results are presented in Fig. 2, whose curves were obtained with no need of surface renewing between successive determinations.

The DPV voltammograms showed successive enhancement of peak current on increasing ATN concentration. In the investigated interval two linear regions were determined. The first between 4 and 100 μmol L⁻¹, obeying the linear equation:

$$I_p = 0.55 \mu\text{A} + 0.15 \mu\text{A mmol L}^{-1} [\text{ATN}], \quad (n=8, R=0.999) \quad (2)$$

The second linear region obtained was between 0.49 and 2.3 mmol L⁻¹, obeying the linear equation:

$$I_p = 15.6 \mu\text{A} + 0.01 \mu\text{A mmol L}^{-1} [\text{ATN}], \quad (n=5, R=0.996) \quad (3)$$

The limit of detection (LOD) obtained in the interval 4.0–100 μmol L⁻¹ was 3.16 μmol L⁻¹, determined as three times the standard deviation of the blank (*S_d*) divided by the angular coefficient of straight line (b) [18]:

$$\text{LOD} = \frac{3S_d}{b} \quad (4)$$

An analytical curve for ATN was also obtained at a glassy carbon electrode (GC) using the same conditions employed in the

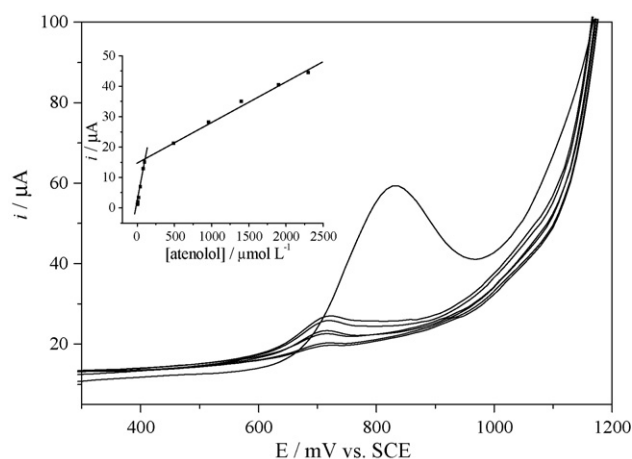


Fig. 2. Dependence of the DPV voltammograms with ATN concentration from 4.0 μmol L⁻¹ to 2.3 mmol L⁻¹ in universal buffer, pH 10, *a* = 50 mV, *v* = 50 mV s⁻¹ at the 60% (graphite, w/w) composite electrode. In the inset, the analytical curve with two linear dynamic ranges described in the text.

experiments at the 60% (graphite, w/w) composite electrode for comparison. Therefore, it was observed only one linear region between 0.49 and 1.4 mmol L⁻¹, obeying the linear equation:

$$I_p = 2.30 \mu\text{A} + 3.48 \times 10^{-3} \mu\text{A mmol L}^{-1} [\text{ATN}], \quad (n = 3, R = 0.999) \quad (5)$$

For concentrations higher than 1.4 mmol L⁻¹ a practically constant current was observed, suggesting a saturation of the active sites of the electrode. The LOD obtained with Eq. (4) in the interval 0.49–1.4 mmol L⁻¹ was 41.55 μmol L⁻¹.

These data permit to conclude that the composite electrode is much more sensitive and presented a lower LOD than the GC and the C₆₀—modified glassy carbon electrode described in reference [9]. However, is higher than the LOD for the nanogold modified indium tin oxide electrode described in reference [10]. Concluding, it is possible to say that the advantages of the proposed method are the higher sensitivity without electrode modification, no need of surface renewing between experiments, long useful live of the electrode and its low cost.

Single point standard additions for solutions of the pharmaceutical formulations showed recoveries between 95.50 and 107.5% for additions of ATN as presented in Table 1.

3.1. Application of the method

The performance of the proposed method in the determination of ATN in tablet samples was evaluated. For the voltammetric determination of the ATN amount present in the pharmaceutical formulations samples, the single standard addition method was used.

The voltammograms were recorded at 60% (graphite, w/w) composite electrode in DPV. The conditions for the determination of ATN were those optimized as above.

The results obtained by DPV were compared those obtained by a HPLC procedure. Results summarized in Table 2 show that the content for all assayed tablets falls within the claimed amount. The DPV results agree with those from the HPLC procedure within 95% of confidence level.

Table 1
Recovery of ATN in four pharmaceutical formulations

Sample	Added (10 ⁻⁴ mol L ⁻¹)	Found (10 ⁻⁴ mol L ⁻¹)	Recovery (%)
Atenolol (G1) ^a	1.11	1.06	95.5
Atenol	1.10	1.11	101
Atenolol (G2) ^a	1.09	1.07	98.2
Angipress	1.07	1.15	108

^a G, generic.

Table 2
Determination of ATN in pharmaceutical formulations using both the DPV at 60% (graphite, w/w) composite electrode proposed and HPLC procedure

Sample	Atenolol (mg g ⁻¹)			E ₁ (%)	E ₂ (%)
	Labeled	DPV ^b	HPLC ^c		
Atenolol (G1) ^a	100.00	95.88 ± 0.82	93.92	+2.09	-4.12
Atenol	50.00	51.00 ± 0.78	48.98	+4.12	+2.00
Atenolol (G2) ^a	50.00	49.14 ± 0.34	48.94	+0.41	-1.72
Angipress	25.00	26.77 ± 0.93	25.06	+6.82	+7.08

$E_1 = [(DPV - HPLC)/HPLC] \times 100\%$; $E_2 = [(DPV\text{-labeled})/labeled] \times 100\%$.

^a G, generic.

^b Result ± standard deviation ($n = 3$).

^c 1 determination.

3.2. Interference study

The interference study was carried out in order to investigate the effect of other anti-hypertensive drugs like propranolol and furosemide on the voltammetric response of ATN. DPV experiments were carried out for 0.25 mmol L⁻¹ ATN in presence of 0.12, 0.25 and 0.50 mmol L⁻¹ of propranolol and furosemide. Interference was observed in both cases. In the presence of propranolol, two oxidation peaks were found in the DPV voltammograms with a current increase in the ATN response when the interferent concentration was increased in the cell. Furosemide caused an increase in the ATN current without appearing of a new peak in the voltammogram.

ATN is formulated in single as well as multi-component tablets. As any interference was observed by the components of the tablets it is possible to use the standard addition procedure to quantify the ATN in these formulations, using the 60% (graphite, w/w) composite electrode. In this sense, it is possible to suppose that standard addition can be also a useful strategy to determine ATN in the presence of other anti-hypertensive drugs.

4. Conclusions

According to these results it can be concluded that the composite 60% (graphite, w/w) electrode represents an interesting

alternative to be used in DPV for the determination of ATN with a detection limit in the $\mu\text{mol L}^{-1}$ level without modification. The method has been satisfactorily applied to determination of ATN in pharmaceutical formulations.

Acknowledgments

The authors are indebted to the Brazilian agencies CNPq and CAPES for PC fellowship, FAPESP for financial support (05/04297-1) and Programa PROCONTES/USP.

References

- [1] H. Winkler, W. Ried, B. Lemmer, J. Chromatogr. Biomed. Appl. 228 (1982) 223.
- [2] A.N. Wadworth, D. Murdoch, R.N. Brogden, Drugs 42 (1991) 468.
- [3] H. Siren, M. Saarinen, S. Hainari, M.L. Riekkola, J. Chromatogr. Biomed. Appl. 632 (1993) 215.
- [4] C.P. Snook, K. Sigvaldason, J. Kristinsson, J. Toxicol. Clin. Toxicol. 38 (2000) 661.
- [5] I.A. Abbasi, S. Sorsby, Clin. Pharm. 5 (1986) 836.
- [6] M. Ervik, K. Kylberg-Hanssen, P.O. Lagerström, J. Chromatogr. Biomed. Appl. 182 (1980) 341.
- [7] M.S. Leloux, F. Dost, Chromatographia 32 (1991) 429.
- [8] M.T. Rosseel, A.M. Vermeulen, F.M. Belpaire, J. Chromatogr. Biomed. Appl. 568 (1991) 239.
- [9] R.N. Goyal, S.P. Singh, Talanta 69 (2006) 932.
- [10] R.N. Goyal, V.K. Gupta, M. Oyama, N. Bachheti, Electrochem. Commun. 8 (2006) 65.
- [11] R.K. Mendes, S. Claro-Neto, E.T.G. Cavalheiro, Talanta 57 (2002) 909.
- [12] R.K. Mendes, P. Cervini, E.T.G. Cavalheiro, Talanta 68 (2006) 708.
- [13] P. Cervini, L.A. Ramos, E.T.G. Cavalheiro, ACAI 2 (2006) 187.
- [14] Farmacopéia Brasileira, 4ed-Parte I, Atheneu Editora São Paulo LTDA, São Paulo, 1988.
- [15] M. Bader, J. Chem. Educ. 57 (1980) 703.
- [16] P. Modamio, C.F. Lastra, E.L. Marino, J. Pharm. Biomed. Anal. 17 (1998) 507.
- [17] V. Martínez, M.I. Maguregui, R.M. Jiménez, R.M. Alonso, Pharm. Biomed. Anal. 23 (2000) 459.
- [18] G.L. Long, J.D. Winefordner, Anal. Chem. 55 (1983) 712A.

Short communication

Long pathlength, three-dimensional absorbance microchip

Greg E. Collins^{a,*}, Qin Lu^a, Nicholas Pereira^a, Peter Wu^b

^a Naval Research Laboratory, 4555 Overlook Ave., S.W., Chemistry Division, Code 6112, Washington, DC 20375-5342, United States

^b Southern Oregon University, Department of Physics, 1250 Siskiyou Blvd., Ashland, OR 97520, United States

Received 11 August 2006; received in revised form 11 October 2006; accepted 11 October 2006

Available online 20 November 2006

Abstract

A long pathlength, three-dimensional U-type flow cell was microfabricated and evaluated for improved absorbance detection on a glass microdevice. A small diameter hole (75 μm) was laser etched in a thin glass substrate whose thickness (100 μm) defined much of the pathlength of the cell. This substrate was thermally bonded and sandwiched between two different glass substrates. The top substrate contained a typical injection cross and separation microchannel. Projecting out of the plane of the separation device was a 126 μm pathlength flow cell as defined by the laser etched hole and the attached microchannels. The flow cell was connected to a microchannel on the bottom substrate that led to a waste reservoir. The planar, flat windows on the top and bottom of this device made light introduction and collection a simple matter using a light emitting diode (LED) and microscope objective. The experimentally obtained detection limit for rhodamine B was determined to be 0.95 μM , which is nearly identical to the theoretical limit calculated by Beer's Law. A separation of three fluorescent dyes was performed, and direct comparisons were made between the transmittance changes through the narrow pathlength separation microchannel and the adjacent long pathlength, three-dimensional U-type flow cell.

© 2006 Elsevier B.V. All rights reserved.

Keywords: Capillary electrophoresis microchip; Absorbance; Long pathlength; Three dimensional

1. Introduction

Despite the wide applicability of absorbance detection and more than a decade of research since the first introduction of the lab on a chip platform, there continues to be few examples of absorbance detection on capillary electrophoresis (CE) microchip devices. The predominant reason for this is their inherently short pathlengths, and the resulting poor sensitivity this engenders. Jindal and Cramer demonstrate, for example, that the trapezoidal-shaped microchannels etched in glass substrates result in an effective pathlength that is approximately 50% that of the etched depth [1]. For a typical microchannel depth of 10 μm , reducing this to an effective pathlength of $\sim 5 \mu\text{m}$ becomes a serious sensitivity issue for absorbance detection.

Several researchers have examined methods for increasing the pathlength on a CE microchip. Harrison and co-workers have investigated the application of a microfabricated U-cell within

the plane of the glass device (120–140 μm long) [2]. Disadvantages associated with this approach include difficult positioning of optical fibers within the planar device, and the requirement of a laser to prevent stray light effects. Alternatively, a multireflection cell was microfabricated on a microdevice by depositing an aluminum mirror above and below a separation microchannel, adding entrance and exit apertures positioned 200 μm apart in the top mirror [3]. This technique, however, required a laser whose angle of incidence was carefully controlled to define the resulting pathlength. Kutter and co-workers have fabricated optical waveguides into a silicon, planar microchip device containing a 750 μm U-cell, but the multistep fabrication process and applied laser make this approach unpractical for many [4]. Finally, Collins and Lu have examined 100 μm deep microchannels for absorbance detection, although the wide channels necessitate non-aqueous buffer compositions to prevent Joule heating effects [5,6].

The three-dimensional approach applied to absorbance detection in microfluidic systems was an idea first put forth by Caliper Technologies as a patent application in 2002, however, to our knowledge, the viability of this technique has never been verified in the literature [7]. The microfabricated absorbance flow

* Corresponding author. Tel.: +1 202 404 3337; fax: +1 202 404 8119.
E-mail address: greg.collins@nrl.navy.mil (G.E. Collins).

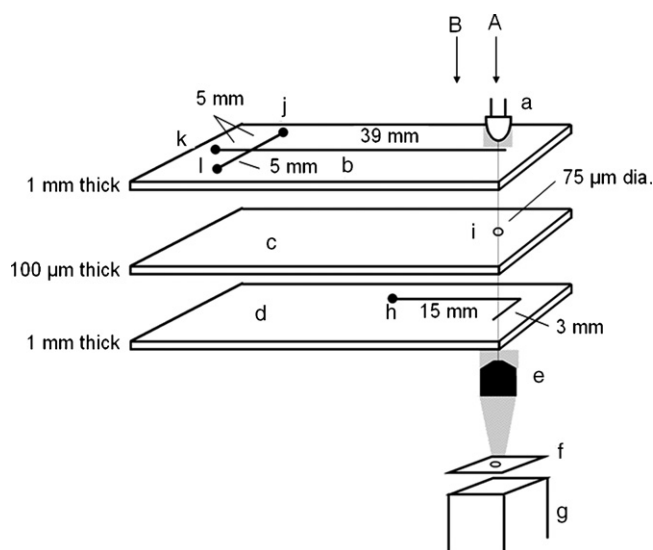


Fig. 1. Design for the long pathlength, three-dimensional absorbance microchip. All three glass substrates are bonded together, creating a sandwich microchip device whose total absorbance pathlength is defined by the thickness of the middle substrate and the etch depth of the channels superpositioned above and below the laser etched hole: (A) long optical pathlength point of detection, (B) short optical pathlength point of detection: (a) light emitting diode, (b) separation microchip substrate, top (c) thin glass substrate, middle, (d) waste microchip substrate, bottom, (e) microscope objective, (f) circular slit, (g) photomultiplier tube, (h) buffer waste reservoir, (i) laser etched hole, (j) sample reservoir, (k) buffer reservoir, (l) sample waste reservoir.

cell discussed here can be considered to be a U-type flow cell that projects out of the plane of the separation microdevice in the third dimension (see Fig. 1). A typical cross injector and separation microchannel pattern was etched into a top glass substrate, and thermally bonded to a thin glass substrate containing a laser etched, small diameter hole. The bottom substrate, containing a microchannel pattern that connected the flow cell to a waste reservoir, was thermally bonded to the middle substrate. The advantages of this type of microchip flow cell are: (1) that the planar top and bottom of the microchip can now be used as easily accessible, flat windows for monitoring the flow cell, for example, with an inexpensive, stable light emitting diode (LED) light source and a microscope objective and (2) that the flow channel does not need to be widened in order to increase the pathlength, e.g. bubble cells, thereby, allowing the separation efficiency to be maintained as resolved bands enter the flow cell.

2. Experimental

2.1. Chemicals

Rhodamine B, sulforhodamine G, eosin Y and *N*-(2-hydroxyethyl)piperazine-*N'*-(2-ethanesulfonic acid) (HEPES) were obtained from Sigma (St. Louis, MO) and utilized as received. Stock solutions for each fluorescent dye (100 μM) were prepared in 25 mM HEPES buffer and adjusted to pH 7.0. Subsequent dilutions of the stock were made in an identical buffer composition.

2.2. Device microfabrication

Wet chemical etching of 1 mm thick, soda lime chrome photomask blanks (Telic, Santa Monica, CA) was performed utilizing standard lithographic procedures [8]. Microchannels etched on the top and bottom substrate each had a depth of 13 μm. The top substrate was a standard cross design with dimensions of 5 mm from each reservoir to the intersection point, 39 mm from the injection cross to the absorbance flow cell and 100 μm in width. The bottom substrate had an L-shaped pattern, which was 18 mm in total length from the absorbance flow cell to the buffer waste reservoir and 200 μm in width. The middle substrate consisted of a 100 μm thick soda lime glass (Mark's Optics, San Diego, CA) bearing a 75 μm diameter laser etched hole (Continuum Minilite Q-switched Nd:Yag laser, frequency quadrupled to 266 nm, 100 mJ/cm²). The beam was focused at the point of ablation using a microscope objective to a diameter of 3 μm, giving a peak fluence of ~100 mJ/cm². A video camera allowed real time visual monitoring of the ablation process. The glass plate was mounted on a two-axis linear translational stage, allowing movement in a plane normal to the incident beam. The hole was drilled by manually moving the plate and repeatedly pulsing the laser on it until the desired shape and size of the hole is achieved. Reservoir access holes (2 mm) were drilled prior to bonding using diamond tipped drill bits. Low temperature bonding of the device was achieved using a high pressure press (Carver Model 3912, Wabash, IN) operated at elevated temperature (200 °C), and performed in a sequential manner, first bonding the bottom substrate to the middle substrate, followed by the top substrate. Glass reservoirs were epoxied to each access hole; the bottom reservoir required a curved length of glass tubing that extended above the plane of the device, ensuring that each reservoir was filled to the same height with buffer and preventing hydrodynamic flow.

2.3. Instrumentation

A green LED (525 nm, Allied Electronics) was oriented directly above the absorbance flow cell, nearly touching the top substrate. Light passing through the microchannel was collected using a microscope objective (Newport, U-27X) and directed through a circular slit (1 mm) positioned at the objective's focal point and onto a miniature, red-shifted photomultiplier tube (Hamamatsu, Model H5784). The photomultiplier had a built in current to voltage convertor, and the voltage signal was monitored using LabView (National Instruments, Austin, TX). The high voltage switching apparatus has been described previously [9]. A floating load mode was utilized for sample injection, wherein a potential of 476 V was applied between the sample and sample waste reservoirs, while both the buffer and buffer waste reservoirs were allowed to float. A field strength of 530 V/cm was applied for separation of the dye mixture.

3. Results and discussion

The design for the three dimensional, long pathlength absorbance microchip is shown in Fig. 1. The key compo-

ment to this design is the thin, glass substrate in the middle that defines the predominant length of the flow cell (in this case, 100 μm). The hole in the glass plate is drilled using laser ablation. Bellouard et al. have published a detailed explanation of the effectiveness of laser etching in glass substrates [10]. It is this hole or channel, which connects the separation microchannel on the top substrate to the L-shaped microchannel leading to the waste reservoir on the bottom substrate. Following sequential low temperature bonding of these separate, planar glass substrates into a single, three-dimensional microchip device, the pathlength was further extended by the etched depth of the microchannels on the top and bottom substrates (in this case, total pathlength = 13 μm (bottom) + 100 μm (middle) + 13 μm (top) = 126 μm). In general, all three substrates comprising this microchip, including the middle substrate, must be identical in material (soda lime glass, in this case) to avoid degradation of separation performance due to the presence of two chemically distinct surfaces within the separation channel.

Fluorescent dyes were utilized to characterize the sensitivity of the absorbance microchip due to their high molar absorptivity coefficients, to enable comparison to other absorbance microchip designs evaluated with fluorescent dyes and because all fluorescence from these dyes can be effectively ignored at the low light levels and dye concentrations being employed. Taking into account the molar absorptivity of rhodamine B (4.4×10^4 l/mol/cm), the effective pathlength of the U-cell ($b_{\text{eff}} \sim 113$ μm when we include the trapezoidal losses described by Jindal and Cramer [11]), and the minimum absorbance change detectable on our system (4.8×10^{-4} assuming a signal to noise ratio of 3:1), the theoretical detection limit calculated using Beer's Law was 0.96 μM . This assumes, of course, that a large enough plug has been injected onto the microchip in order to eliminate dispersion effects due to diffusion. The experimentally obtained limit of detection for rhodamine B on this microdevice was 0.95 μM , verifying the accuracy of this theoretically determined value.

Shown in Fig. 2 is the separation and detection of three fluorescent dyes, which were monitored through the long pathlength flow cell (Fig. 2A), as well as through the narrow pathlength, separation microchannel adjacent to this U-type flow cell (Fig. 2B). The mixture of three dyes analyzed consisted of one neutral dye, rhodamine B, which migrated with electroosmotic flow (EOF), and two negatively charged dyes, sulforhodamine G and eosin Y, which migrated against EOF. Discussion will first center on the long pathlength cell. In order to achieve well resolved bands for this mixture, a floating mode of injection was utilized to give small injection plug sizes that approximated the dimensions of the injection cross, 100–200 μm , depending upon the extent of diffusion at the injection cross. Rhodamine B, as the EOF marker, underwent minimal band dispersion, and, therefore, resulted in the best detection limits, 1.9 μM , for this particular injection. This detection limit was two times higher than the theoretical detection limit described above, due to smaller injection plug size and the geometry of this microdevice. The cross-sectional area of the trapezoidal separation microcolumn was 1300 μm^2 , while the cross-sectional area of the

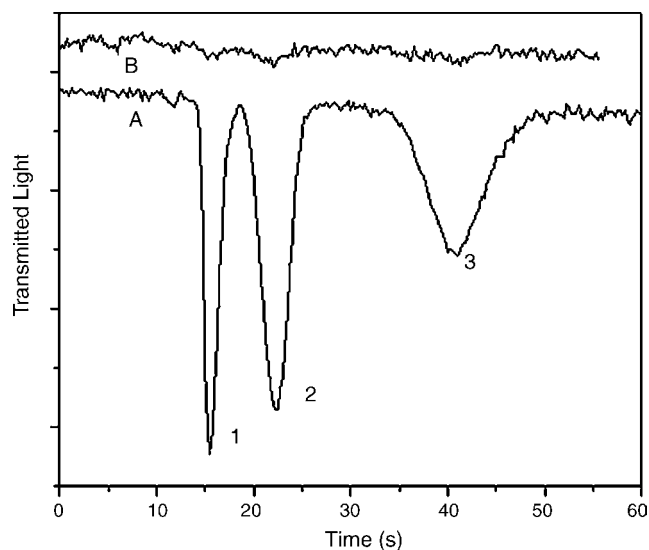


Fig. 2. Electropherograms obtained for the separation of three fluorescent dyes, rhodamine B (1, 20.3 μM), sulforhodamine G (2, 23.0 μM) and eosin Y (3, 27.5 μM): (A) detection through long pathlength flow cell, 126 μm and (B) detection through 13 μm deep separation microchannel just prior to long pathlength, laser etched flow cell. Conditions utilized were 25 mM HEPES buffer, pH 7.0, floating injection, field strength of 530 V/cm.

U-type flow cell was 4420 μm^2 . Completely filling the 126 μm long absorbance flow cell required a ~ 430 μm long separation band. The rhodamine B separation band encountered a dilution factor upon introduction to the flow cell, resulting in reduced sensitivity. The simplest method for eliminating this effect is to reduce the diameter of the laser etched hole from 75 μm down to 41 μm , a capability currently under investigation in our laboratory. Sulforhodamine G and eosin Y gave detection limits of 2.5 and 6.4 μM , respectively, which are factors of 7 and 13 times higher than theoretical calculations based on Beer's Law and their molar absorptivities (1.2 and 0.87×10^5 l/mol/cm, respectively). Diffusion of these injected plugs beyond the dimensions of the absorbance flow cell resulted in substantial deviations from the detection limits achievable with larger injection plug sizes. As a demonstration of the significant sensitivity enhancement gained by using the long pathlength flow cell, when the LED and objective were shifted over to monitor transmittance through the narrow pathlength separation microchannel, detection limits were a factor of 24 times higher (Fig. 2A). This loss in sensitivity is due primarily to the significantly shorter pathlength (b_{eff} for the long pathlength cell was 113 μm and b_{eff} for the short pathlength microchannel was 6.5 μm).

In conclusion, we have demonstrated the benefits of a three-dimensional microchip approach for increasing the pathlength of a microchip absorbance flow cell, enhancing the resultant sensitivity and maintaining the instrumental simplicity associated with performing detection in a direction perpendicular to the plane of the microchip. While soda lime microchips can be operated down to 330 nm, our future goal is to enable UV detection on quartz or UV-extended polymethylmethacrylate microchips.

Acknowledgment

The authors gratefully acknowledge financial support of this work through a grant from the Food and Drug Administration. Its contents are solely the responsibility of the authors and do not necessarily represent the official views of the National Institutes of Health (NIH).

References

- [1] R. Jindal, S.M. Cramer, *J. Chromatogr. A* 1044 (2004) 277.
- [2] Z. Liang, N. Chiem, G. Ocvirk, T. Tang, K. Fluri, D.J. Harrison, *Anal. Chem.* 68 (1996) 1040.
- [3] H. Salimi-Moosavi, Y. Jiang, L. Lester, G. Mckinnon, D.J. Harrison, *Electrophoresis* 21 (2000) 1291.
- [4] K.B. Mogensen, N.J. Petersen, J. Hübner, J.P. Kutter, *Electrophoresis* 22 (2001) 3930.
- [5] G.E. Collins, Q. Lu, *Anal. Chim. Acta* 436 (2001) 181.
- [6] G.E. Collins, Q. Lu, *Sens. Actuators B* 76 (2001) 244.
- [7] R.-L. Chien, J.A. Wolk, M. Spaid, R.J. McReynolds, U.S. Patent Application US 2002-76136 20020214.
- [8] Z.H. Fan, D.J. Harrison, *Anal. Chem.* 66 (1994) 177.
- [9] Q. Lu, G.E. Collins, T. Evans, M. Hammond, J. Wang, A. Mulchandani, *Electrophoresis* 25 (2004) 116.
- [10] Y. Bellouard, A. Said, M. Dugan, P. Bado, *Opt. Express* 12 (2004) 2120.

Combining synchronous fluorescence spectroscopy with multivariate methods for the analysis of petrol–kerosene mixtures

O. Divya, Ashok K. Mishra*

Department of Chemistry, Indian Institute of Technology, Chennai-36, India

Received 10 August 2006; received in revised form 25 September 2006; accepted 26 September 2006

Available online 7 November 2006

Abstract

Synchronous fluorescence spectroscopy (SFS) is a rapid, sensitive and nondestructive method suitable for the analysis of multifluorophoric mixtures. The present study demonstrates the use of SFS and multivariate methods for the analysis of petroleum products which is a complex mixture of multiple fluorophores. Two multivariate techniques principal component regression (PCR) and partial least square regression (PLSR) have been successfully applied for the classification of petrol–kerosene mixtures. Calibration models were constructed using 35 samples and their validation was carried out with varying composition of petrol and kerosene in the calibration range. The results showed that the method could be used for the estimation of kerosene in kerosene-mixed petrol. The model was found to be sensitive, detecting even 1% contamination of kerosene in petrol. © 2006 Elsevier B.V. All rights reserved.

Keywords: SFS; Synchronous fluorescence; Principal component regression; Partial least squares regression

1. Introduction

Analytical multivariate techniques are increasingly used in spectroscopic data for the development of classification and estimation methods. Of a variety of spectroscopic methods available, significant amount of work has been done by combining multivariate techniques with UV–vis spectroscopy and near infrared (NIR) spectroscopy as evidenced by some recent reviews on the topics [1–4] but much less work has been reported with nuclear magnetic resonance (NMR) [5] and fluorescence spectroscopy [6]. Synchronous fluorescence spectroscopy (SFS) is often considered as a convenient technique for simultaneous determination of multifluorophoric samples like polycyclic aromatic compound (PAC) mixtures, without pre-separation [7,8]. A synchronous fluorescence spectrum is obtained by scanning both the excitation and emission monochromators simultaneously keeping a fixed wavelength interval ($\Delta\lambda$) between them. It gives a narrower and simpler spectrum. For the SFS technique, the selection of wavelength interval is one of the most important experimental parameter and the parameter $\Delta\lambda$ is needed to be optimized which is carried out by measuring the spectra at

various $\Delta\lambda$. SFS along with multivariate regression methods has been recently used in areas like food industry [9], biological samples [10], and environmental samples [11]. Sikorska et al. used principal component analysis (PCA) along with SFS data for the classification of beer samples stored at various conditions [9]. Damiani et al. used partial least squares regression (PLSR) as a multivariate tool for the simultaneous determination of naproxen and salicylate in human serum [10]. Guiteras et al. did a comparative study between three different multivariate calibration methods, classical least squares (CLS), principal component regression and partial least squares regression (PLSR) [11]. Thus, various multivariate calibration techniques are available for the treatment of SFS data, in order to quantify the compounds present in a mixture. Among these, PLSR and PCR appears to be the best suited for multicomponent spectral analysis [11]. PLSR is considered to be superior over PCR as it uses both the concentration data and spectral data for creating mathematical models, while the latter uses only the spectral data [12]. Therefore, PLSR is found to be more robust than PCR and it yields models of lower dimensionality. Products of petroleum crude like petrol and kerosene contain PACs, which are highly fluorescent. The hydrocarbon composition of petroleum crudes vary remarkably depending on the crude source, refining process and distillation procedure. In spite of their complexities and differences, petroleum products show a systematic behavior with respect to

* Corresponding author. Tel.: +91 44 22574207; fax: +91 44 22574202.
E-mail address: mishra@iitm.ac.in (A.K. Mishra).

fluorescence parameters [13]. The large difference between the pricing of petrol and kerosene in some southeast Asian countries has led to an extensive problem of adulteration of petrol by kerosene [14,15]. This causes a decrease in performance of petrol engines and possibly other serious environmental problems like higher levels of emission.

Finding convenient methods for the adulteration analysis have been a topic of much interest. Investigations on petrol adulteration started in 1966 when Babitz and Rocker used semimicro-chromatography to address the problem [16]. Octane number comparison test [17], phase titration method [15], distillation [18] and gas chromatographic analysis [19] are some of the methods currently adopted. Despite the fact that petroleum products have complex mixtures of PACs absorbing and emitting at different wavelengths and that complex energy-degrading interaction exists between the fluorophores at higher concentration, there exists a systematic synchronous spectral response to various petroleum products. This has been shown in a series of works by Patra et al. and it was possible to introduce some analytical methods based on synchronous fluorescence techniques [13,20–23]. A recent report by Abbas et al. describes a novel approach for identification and discrimination of the geographic origin of petroleum oils by chemometric treatment of synchronous ultraviolet fluorescence. They adopted PCA for classification of crude oils and PLSR for predicting the geographic origin of oils and reservoir rocks when geochemical data is provided [24]. Thus, there is a distinct possibility that multivariate methods can be applied to SF spectral data of petroleum product mixtures.

The aim of the present work is to use synchronous fluorescence spectroscopy along with chemometric multivariate techniques for quantitative examination of the adulteration of petrol by kerosene. Application of two multivariate techniques, PCR and PLSR, to the SFS data of petrol–kerosene mixtures and evaluation of the prediction level of the two methods, is the specific focus of this work. To the best of our knowledge, this is the first attempt to use SFS with multivariate regression methods for estimating the amount of kerosene in petrol.

2. Experimental

2.1. Apparatus

Fluorescence spectra were obtained on a Hitachi F-4500 spectrofluorimeter with a 100 W xenon lamp as excitation source. For SFS measurement, the scan speed was 240 nm/s and PMT voltage was fixed at 700 V. Band pass for both excitation and emission monochromators were kept at 5 nm. Conventional right-angle geometry was used for all the measurements since such a geometry have been shown to give better SF spectral resolution [20]. SFS was measured in the excitation wavelength range 250–600 nm.

2.2. Reagents and procedure

Petrol and kerosene were collected from the authorized local vendors in Chennai. Petrol samples with different relative

kerosene fractions (% v/v) were prepared by adding appropriate volumes of neat kerosene to neat petrol. A calibration set of 35 samples and an independent validation set of 8 samples containing varying amounts of petrol and kerosene were prepared. Relative kerosene fraction (% v/v) in the samples varies from 0 to 100%.

2.3. Data analysis

Pre-processing of the raw data obtained from fluorimeter and all calculations were performed with a Pentium 4 Personal Computer using the algorithms from the PLS_Toolbox 3.5 written in MATLAB language.

Multivariate calibration is the process of constructing a mathematical model that relates a property, such as concentration to absorbance or fluorescence intensity of a set of known reference samples at more than one wavelength. It usually involves a calibration step in which the relationship between spectra and component concentrations is estimated from a set of reference samples, and a prediction step in which the results of the calibration are used to estimate the component concentrations from an unknown sample spectrum [25]. Among the available multivariate calibration procedures, principal component regression (PCR) and partial least squares regression (PLSR) are widely used for multicomponent analysis.

PCR is a two-step multivariate calibration method. In the first step, a principal component analysis (PCA) is performed, which is a statistical tool used for data compression and information extraction. The main aim of PCA is to reduce the large number of variables to a much lesser number of principal components (PCs) that explain majority of variance in the data. This reduces the dimensionality of the data considerably enabling effective visualization, regression and classification of multivariate data [26]. Thus, the measured variables (e.g. SFS intensity at different wavelengths) are converted into new ones (scores on latent variables). In the second step of PCR a multiple linear regression (MLR) is performed on the scores obtained in the PCA step. PLSR is another quantitative spectral decomposition technique that generalizes and combines features from PCA and MLR and performs the data analysis in one step [27]. PLSR is based on the simultaneous decomposition of two blocks of variables, X and Y which may contain spectral and concentration data, respectively. Thus, in PLSR which is a single step decomposition and regression, scores are directly related to constituents of interest, whereas PCR, being a two-step process scores are related to the largest common spectral variation [28,29].

The regression model was evaluated using the correlation coefficient, R^2 and the parameter root mean square error of calibration (RMSEC). It helps to estimate the average deviation of the model from the data and tells about the validity of the model to the calibration data. It is defined as:

$$\text{RMSEC} = \sqrt{\frac{\sum_{i=1}^n (y_{\text{pred}} - y_{\text{obs}})^2}{n}} \quad (1)$$

where y_{pred} and y_{obs} are the predicted and reference values of sample i in the calibration set, respectively, and ' n ' is the number of samples used for calibration.

The optimum dimensionality of the method was obtained from the prediction error sum of squares function (PRESS), which was done by cross-validation method (i.e. leave one out method). It is defined as:

$$\text{PRESS} = \sum_{i=1}^n (y_{\text{pred}} - y_{\text{obs}})^2 \quad (2)$$

where y_{pred} and y_{obs} are the predicted and reference value of sample i in the cross-validation set, respectively, and ' n ' is the number of samples in cross-validation set.

The ability of a model to predict new sample is expressed in terms of root mean square error of cross-validation (RMSECV) which is given by:

$$\text{RMSECV} = \sqrt{\frac{\text{PRESS}}{n}} \quad (3)$$

when the model is applied to a new set of data, it is possible to calculate a root mean square error of prediction (RMSEP) provided, the reference values for the new data set are known. RMSEP is expressed as:

$$\text{RMSEP} = \sqrt{\frac{\sum_{i=1}^n (y_{\text{pred}} - y_{\text{obs}})^2}{n}} \quad (4)$$

where y_{pred} and y_{obs} are the predicted and reference value of sample i in the prediction set, respectively, and ' n ' is the number of samples used in prediction set.

3. Results and discussion

3.1. Synchronous fluorescence

The variation of SFS maximum ($\lambda_{\text{SFS}}^{\text{max}}$) at different wavelength interval ($\Delta\lambda$) for petrol and kerosene is studied by Patra et al. [23] and they have shown that $\Delta\lambda$ 40 nm is the best for petrol. Fig. 1. shows the SFS of petrol–kerosene mixtures at $\Delta\lambda$

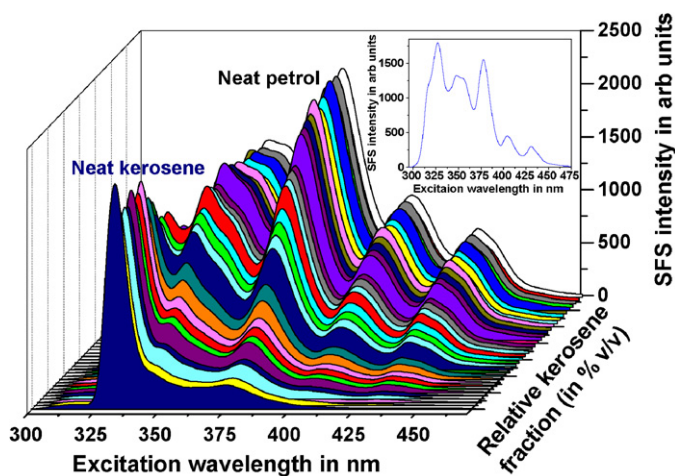


Fig. 1. Synchronous fluorescence spectra of petrol kerosene mixtures at $\Delta\lambda$ 40 nm. Inset shows the SF spectrum of neat petrol.

40. As it is seen (Fig. 1, inset) the SF spectrum has many well resolved spectral features. There is a regular and appreciable variation of peaks at 331, 351, 377, 405, 431 nm wavelengths. Peak positions get slightly blue shifted on increasing the relative kerosene fraction (% v/v).

3.2. Data pre-processing

To proceed with the multivariate regression process, data were arranged into a matrix characterized by samples as rows and synchronous fluorescence intensities as columns. To find out the best pre-processing technique, analysis was performed with and without pre-processing and the one with the minimum prediction error, RMSEP was chosen. Different pre-processing methods adopted were AUTO, MNCN and SAVGOL combined with MSC and SNV [30].

AUTO, autoscales a matrix to mean zero and unity variance. MNCN, mean center data matrices. The Savitzky–Golay smoothing method (SAVGOL) essentially performs a local polynomial regression to determine the smoothed value for each data point on a matrix of row vectors y . At each increment a polynomial of order 2 is fitted to the number of points with width 21 surrounding the increment. An estimate for the value of the function (deriv = 0) at the increment is calculated from the fit resulting in a smoothed function $y1$, where:

$$y1 = \text{savgol}(y, \text{width}, \text{order}, \text{deriv})$$

SAVGOL was performed with various window widths like 5, 7, 11, 15 and 21. With each output the model was built and the RMSEP values were compared and it was observed that there was a remarkable reduction in RMSEP for the window width 21. MSC does multiplicative scatter correction on a input of matrix $y1$. Standard normal variate scaling (SNV), scales rows of the matrix $y1$ to mean zero with unity standard deviation. This is same as autoscaling the transpose of $y1$.

$$x = \text{snv}(y1)$$

The RMSEP values obtained for PCR with three principal components (PCs) and PLSR with three latent variables (LVs) are given in Table 1. Since SAVGOL and SNV produce the lowest RMSEP value, this method was chosen as the best pre-processing method.

3.3. Optimum number of components to build the model

The first step involved in the multivariate regression method is the determination of optimum number of factors that allow

Table 1

The RMSEP values of PLSR and PCR method with three LVs and three PCs, respectively

Pre-processing method	PLSR (RMSEP)	PCR (RMSEP)
None	0.0644	0.0658
Auto scaling	0.0305	0.0492
Mean centering	0.0214	0.0217
SAVGOL and MSC	0.0212	0.0213
SAVGOL and SNV	0.0207	0.0208

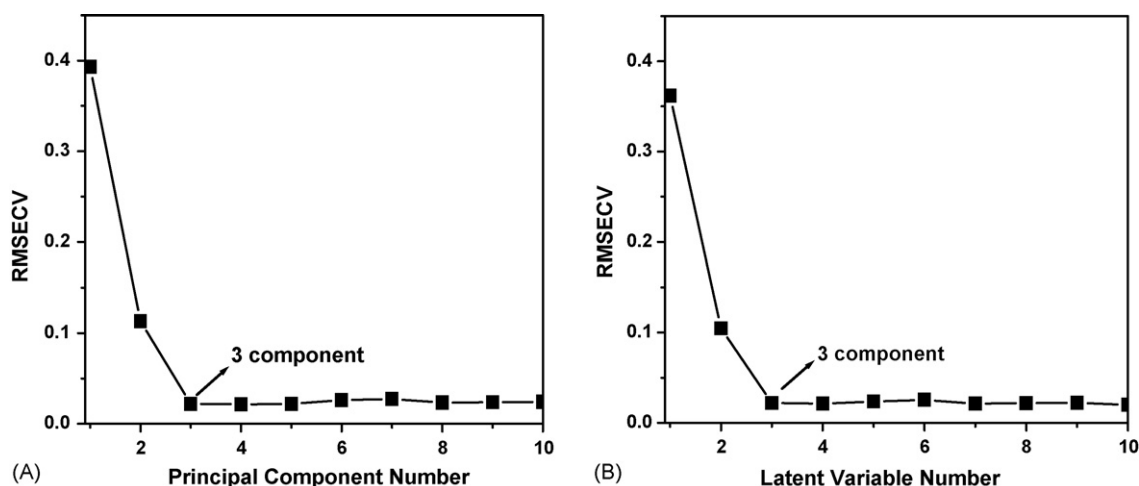


Fig. 2. Value of PRESS vs. the number of factors. (A) PCR model, (B) PLSR model.

the system to be modeled without overfitting the concentration data. For this purpose a cross-validation method, leaving out one sample at a time, was used [30]. For a calibration set with N standards, the PLSR or PCR calibration was carried out with $N - 1$ standards, and the data thus obtained were used to calculate the concentration of the left out sample. This process was repeated for the N standards and the prediction error sum of squares (PRESS) was calculated. The number of components giving a minimum PRESS is the right number of factors that give optimal prediction. PRESS plot represents the RMSECV value against number of factors and is given in Fig. 2.

The optimum number of factors obtained is 3 for both PCR and PLSR models. So, further analysis and development of model were carried out by taking into account that the maximum variation will be carried by first three PCs or LVs.

3.4. Developing mathematical models using the pre-processed data

PCR allows visualizing the information of the data set in a few principal components retaining the maximum possible vari-

ability. PCR was performed on the pre-processed fluorescence data obtained from a batch of 35 samples. The first three PCs were found to explain 99.97% of the variance in the spectra (91.56% PC1, 7.84% for PC2 and 0.57% of PC3). The first two PC scores are plotted in a scatter diagram shown in Fig. 3A. PLSR also was performed on the pre-processed data set and it was found to explain 99.98% of the variance in the spectra (91.22% LV1, 8.18% for LV2 and 0.58% of LV3). The first two LV scores are plotted in a scatter diagram shown in Fig. 3B.

Score plot gives information about samples. When the spectra were projected (using their scores as coordinates) in the space of the first and second components, the natural grouping of the samples into two groups was observed. The first group, which is having a negative score value represents the samples with more of petrol like character (less kerosene contamination) and the second group, which is having a positive score value contains samples with more of kerosene like character (more kerosene contamination).

It is observed that the model obtained by PCR method is not able to differentiate the samples having more petrol like

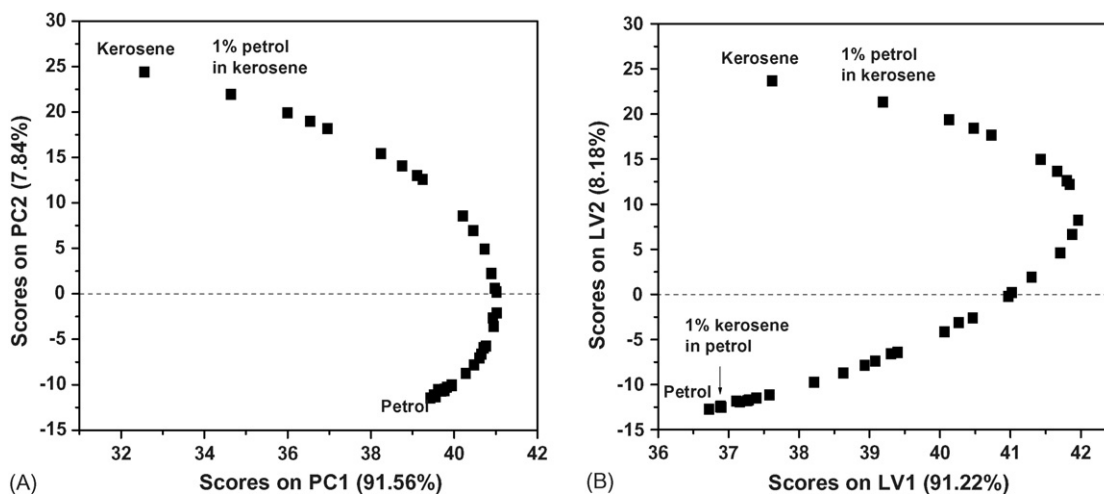


Fig. 3. (A) First two principal component scores for PCR model, (B) first two latent variable score for PLS model.

character (negative quadrant) in an efficient way. But, PLSR makes the differentiation in a better way and better separation of samples having more of petrol character (negative quadrant) is achieved using this method. From the experimental data it is not possible to differentiate petrol from slight amount of kerosene adulterated petrol (Fig. 4). But, with PLSR method even 1% contamination of kerosene in petrol is very obvious, while it is not very clear in PCR modeling.

3.5. Accuracy and prediction ability of the model

To evaluate the accuracy and reliability of the model, the reference values of concentration is plotted against the concentration values predicted by the model (Fig. 5). It should be noted that in Fig. 5, the axes are normalized to unity, the value 1 representing 100% pure petrol. Both PCR and PLSR methods shows very good correlation between the measured and predicted concentrations with correlation coefficients of 0.997 which shows a good linear fit (Fig. 5). The RMSECV values for PLSR and PCR are 0.0219 and 0.0220, respectively. These low RMSECV values indicate the accuracy of model prediction using cross-validation.

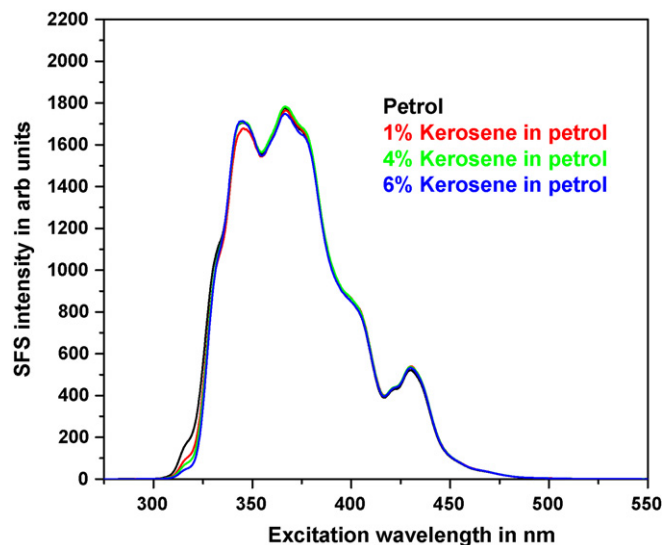


Fig. 4. Synchronous fluorescence spectra of petrol and kerosene-adulterated petrol.

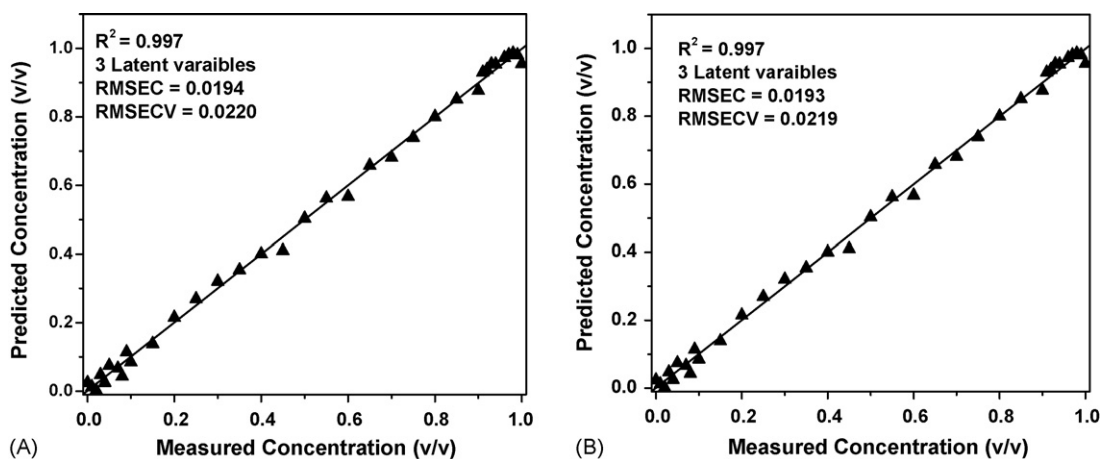


Fig. 5. Measured vs. predicted concentrations of petrol kerosene mixtures based on full cross-validation. (A) PCR model, (B) PLSR model. The axes have been normalized, 1.0 representing 100% petrol.

Table 2

Relative kerosene fraction of the samples used in the calibration dataset (reference value) and the concentration validated by model (predicted value)

Normalized relative kerosene fraction (% v/v)/100					
Reference value	Predicted value	Reference value	Predicted value	Reference value	Predicted value
0	0.002	0.25	0.269	0.85	0.850
0.01	0.011	0.30	0.320	0.90	0.876
0.02	0.019	0.35	0.353	0.91	0.929
0.03	0.047	0.40	0.400	0.92	0.937
0.04	0.044	0.45	0.410	0.93	0.933
0.05	0.066	0.50	0.503	0.94	0.953
0.07	0.074	0.55	0.562	0.95	0.962
0.08	0.083	0.60	0.567	0.97	0.980
0.09	0.114	0.65	0.657	0.98	0.985
0.10	0.085	0.70	0.681	0.99	0.980
0.15	0.139	0.75	0.739	1.00	0.955
0.20	0.215	0.80	0.799	–	–

Table 3
Normalized reference value and predicted value of kerosene (% v/v)/100 present in the adulterated mixture

Normalized relative kerosene fraction (%, v/v)/100 (reference value)	PLSR		PCR	
	Predicted concentration	Prediction error	Predicted concentration	Prediction error
0	0.015	0.015	0.015	0.015
0.080	0.036	0.044	0.036	0.044
0.150	0.134	0.016	0.134	0.016
0.400	0.399	0.001	0.399	0.001
0.650	0.660	0.010	0.660	0.010
0.800	0.803	0.003	0.803	0.003
0.920	0.941	0.021	0.941	0.021
0.980	0.988	0.008	0.988	0.008
Overall RMSEP	0.0195		0.0195	

Table 2 represents the calibration dataset (reference value) and the values obtained on validation (predicted value) by cross-validation (leave-one-out) method.

A test set of eight samples of known concentrations is used to test the prediction ability of the model. Quantitative determination of amount of kerosene present in the mixture was achieved, which shows very close agreement with the reference value (Table 3). Samples with very low value of relative kerosene fraction (0–10% relative kerosene fraction, %, v/v) show a small deviation from the reference value. The error value of prediction, RMSEP, for both PLSR and PCR method, is 0.0195.

4. Conclusion

The proposed method of combining SFS with multivariate technique is found to be more efficient for the quantitative determination of kerosene present in petrol kerosene mixture. This is achieved by selecting proper pre-processing methods and developing suitable mathematical models using methods like PCR and PLSR. Both PCR and PLSR gives same prediction (RMSEP value). However PLSR is found to be superior to PCR with regard to better discrimination of the samples (scores plot). The model building is applicable for detection of adulteration due to kerosene in petroleum mixtures and the model was found to be very sensitive to detect low contamination of kerosene (1% relative kerosene fraction (% v/v)) in mixture.

Acknowledgements

Divya thanks Council of Scientific and Industrial Research (CSIR) New Delhi for financial assistance. The authors thank Mr. V. Venkataraman, Scientist (CEERI Centre, CSIR complex, Chennai) for valuable suggestions and help.

References

- [1] P. Geladi, E. Dabakki, J. Near Infrared Spectrosc. 3 (1995) 119.
- [2] S. Macho, M.S. Larrechi, Trends Anal. Chem. 21 (2002) 799.
- [3] M.K. Boysworth, S.K. Booksh, Practical Spectroscopy (Handbook of Near-Infrared Analysis), 27, second ed., CRC Press, 2001, p. 209.
- [4] J. Workman Jr., Spectroscopy, 4, Duluth, MN, United States, 1989, p. 10.
- [5] J.R. Harmer, T.G. Callcott, M. Maeder, B.E. Smith, Fuel 80 (2000) 1341.
- [6] R. Ferrer, J.L. Beltran, J. Guiteras, Talanta 45 (1998) 1073.
- [7] J.B.F. Lloyd, Nat. Phys. Sci. 231 (1971) 64.
- [8] T. Vo-Dinh, P.R. Martinez, Anal. Chim. Acta 125 (1981) 13.
- [9] E. Sikorska, T. Gorecki, I.V. Khmelinskii, M. Sikorski, D. De Keukeleire, Food Chem. 96 (2006) 632.
- [10] P.C. Damiani, M.D. Borraccetti, A.C. Olivieri, Anal. Chim. Acta 471 (2002) 87R.
- [11] J. Guiteras, J.L. Beltran, R. Ferrer, Anal. Chim. Acta 361 (1998) 233.
- [12] D.M. Haaland, E.V. Thomas, Anal. Chem. 60 (1988) 1193.
- [13] D. Patra, A.K. Mishra, Trends Anal. Chem. 21 (2002) 787.
- [14] V.P. Bhatnagar, J. Acoust. Soc. Ind. 9 (1981) 19.
- [15] M.S. Bahari, W.J. Criddle, J.D.R. Thomas, Analyst 115 (1990) 417.
- [16] M. Babitz, A. Rucker, Isr. J. Technol. 4 (1966) 271.
- [17] M. Goodger, Hydrocarbon Fuels: Production, Properties and Performance of Liquids and gases, Macmillan, London, 1975, p. 173.
- [18] M. Goodger, Hydrocarbon Fuels: Production, Properties and Performance of Liquids and Gases, Macmillan, London, 1975, p. 80.
- [19] L.S.M. Wiedemanna, L.A. d'Avila, D.A. Azevedo, Fuel 84 (2005) 467.
- [20] D. Patra, A.K. Mishra, Analyst 125 (2000) 1383.
- [21] D. Patra, A.K. Mishra, J. Sci. Ind. Res. 59 (2000) 300.
- [22] D. Patra, A.K. Mishra, Talanta 53 (2001) 783.
- [23] D. Patra, A.K. Mishra, Anal. Bioanal. Chem. 373 (2002) 304.
- [24] O. Abbas, C. Rebufa, N. Dupuy, A. Permanyer, J. Kister, D.A. Azevedo, Fuel 85 (2006) 2653.
- [25] H. Martens, T. Naes, Multivariate Calibration, Wiley, Chichester, 1989.
- [26] J.E. Jackson, J. Qual. Tech. 12 (1980) 201.
- [27] P. Geladi, B. Kowalski, Anal. Chim. Acta 185 (1986) 1.
- [28] R.G. Brereton, Chemometrics Data Analysis for the Laboratory and Chemical Plant, Wiley, Chichester, 2003.
- [29] R. Kramer, Chemometric Techniques for Quantitative Analysis, Marcel Dekker, New York, 1998.
- [30] B.M. Wise, N.B. Gallagher, R. Bro, J.M. Shaver, PLS_Toolbox 3.5, Eigenvector research (2005).

Application of headspace solvent microextraction to the analysis of mononitrotoluenes in waste water samples

Homeira Ebrahimzadeh^{a,*}, Yadollah Yamini^b, Fahimeh Kamarei^a,
Mohammadreza Khalili-Zanjani^b

^a Department of Chemistry, Shahid Beheshti University, Evin, Tehran, Iran

^b Department of Chemistry, Tarbiat Modarres University, P.O. Box 14115-175, Tehran, Iran

Received 29 June 2006; received in revised form 11 October 2006; accepted 11 October 2006

Available online 21 November 2006

Abstract

The possibility of applying headspace solvent microextraction (HSME) for determination of mononitrotoluenes (MNTs) in waste water samples is demonstrated. A drop of *n*-amyl alcohol containing naphthalene as an internal standard was suspended from the tip of a microsyringe needle over the headspace of stirred sample solutions for a predescribed extraction period. The drop was then injected directly into a gas chromatograph. Optimization of experimental parameters such as the nature of extracting solvent, microdrop and sample volumes, sampling temperature, stirring rate, ionic strength of the solution, pH and extraction time on HSME efficiency were investigated. Then enrichment factor, dynamic linear range (DLR), limit of detection (LOD) and precision of the method were evaluated by water samples spiked with MNTs. Finally, the method was successfully applied to the extraction and determination of the mononitrotoluenes in waste waters of both P.C.I. Company and Research Center of Azad University.

© 2006 Elsevier B.V. All rights reserved.

Keywords: Headspace solvent microextraction; Mononitrotoluenes; Gas chromatography

1. Introduction

Isomers of mononitrotoluenes (MNTs) are widely presented in the aquatic environment due to their vast spread of uses in several industrial and chemical manufacturing applications. In toluene nitration, three isomers are produced in a ratio of about 58.8% *o*-nitrotoluene, 36.8% *p*-nitrotoluene, and 4.4% *m*-nitro toluene. MNTs are used in the synthesis of intermediates for production of dyes, rubber chemicals, pesticides, drugs, resin modifiers, optical brighteners, suntan lotions, and photographic developing agents [1]. Nitrotoluenes are highly toxic compounds in low concentrations. Moreover, the aromatic amines formed by biodegradation are suspected to be carcinogenic. Consequently, there is increasing interest in the determination of concentrations of MNTs at part per billion (ppb) levels in various matrices [2].

Determination of MNTs in water samples involves an initial sample pretreatment step for isolation of target analytes, using

liquid–liquid extraction (LLE) or solid-phase extraction (SPE) techniques prior to gas chromatography or high-performance liquid (HPLC) chromatographic analyses [2,3]. But these techniques have many disadvantages as they are tedious, labor-intensive and time consuming. LLE in particular requires the use of large amounts of high-purity solvents, which are often hazardous and result in the production of toxic laboratory waste. LLE and also SPE require solvent evaporation, in order to pre-concentrate the analytes. During evaporation step, loss and/or deterioration of target analytes has been reported [4].

Recently, other extraction techniques such as solid-phase microextraction (SPME) and solvent microextraction (SME) have successfully been developed for extraction of MNTs from environmental matrixes in order to reduce the extraction time and also the amount of solvent used [5,6].

SPME is solvent-free, simple, and fast and sampling can be carried out directly under field conditions. The main drawbacks of SPME are: its fibers are expensive and when reused, there is a potential for sample carry over between runs, which could invalidate the results. SPME's life time is limited because the solid-phase materials degrade with usage. Moreover, the partial

* Corresponding author. Tel.: +98 21 29902891; fax: +98 21 22403041.
E-mail address: h-ebrahim@sbu.ac.ir (H. Ebrahimzadeh).

loss of SPME fiber stationary phase can result in peaks that may co-elute with the analytes [7,8].

SME is a LLE type in which the analytes distribute between the bulk aqueous phase and a very small volume of organic solvent. SME is very inexpensive, because it requires only simple laboratory equipments and 1–3 μl of solvent. Moreover, it does not suffer from carry over between extractions that may be experienced when using SPME. Other advantages of SME include simplicity, speed, potential for easy automation and low consumption of solvent [9]. In addition, it overcomes the problem of fiber degradation and relatively slow desorption of analytes in SPME when coupled with GC [7]. SME suffers from some major disadvantages such as: the method can only be used for liquid samples; only water immiscible solvents are applicable in this method; it is a suitable method for extraction of non-polar and moderately polar analytes; also high molecular mass and other non-volatile interfaces which are extracted by the microdrop; matrix has an important effect on the extraction process. These drawbacks can be eliminated if microdrop is used in the headspace of solution. Headspace solvent microextraction (HSME) is a sample preparation technique that has been utilized by Theis et al. in 2001 as a means of direct determination without interference from the sample matrix [10]. In this method extraction of analytes occurs via suspending a microdrop of a proper non-aqueous solvent from the tip of a microsyringe that is located in the headspace of sample. HSME integrates extraction, concentration and sample introduction into a single step. The objective of the present study was to investigate the feasibility of HSME to the extraction and determination of isomers of MNTs from waste water samples produced by P.C.I. Company (Iran) and Research Center of Azad University. Several variables were studied on the method performance.

2. Experimental

2.1. Reagents and materials

Methanol, *p*-nitrotoluene, *m*-nitrotoluene, *o*-nitrotoluene (Merck, Darmstadt, Germany), *n*-amyl alcohol (Fluka, Busch, Switzerland), naphthalene (Merck), were all reagent grade and were used without further purification. Sodium chloride, sodium bicarbonate, sodium carbonate, sodium sulfate and sodium bisulfate were purchased from Merck Company. Waste water samples were obtained from P.C.I. Company and Research Center of Azad University and were kept in polyethylene bottles at the ambient temperature and were used without dilution.

2.2. Apparatus

The extraction and injection procedures were carried out using a 10 μl microsyringe (Code: 5B-7) and 13 ml extraction vial. Stirring of the solution was carried out with a magnetic stirrer (Heidolph MR 3001 K) and an 8 mm \times 1.5 mm magnetic stirring bar. A water bath was used for controlling the sample temperature.

Separation and quantification of three isomers of MNTs were carried out using a Varian 3800 CP gas chromatography

equipped with a flame ionization detector and a CP-Sil-5 fused-silica capillary column (25 m \times 0.32 mm i.d. and 0.52 μm film thickness). The GC split valve was opened and nitrogen was used as a carrier gas at the constant flow rate of 3.0 ml/min. The column oven was initially held at 60 $^{\circ}\text{C}$ for 4 min, programmed to 200 $^{\circ}\text{C}$ at a rate of 10 $^{\circ}\text{C}/\text{min}$ and then to 250 $^{\circ}\text{C}$ at 20 $^{\circ}\text{C}/\text{min}$.

2.3. Procedure

A fixed concentration of naphthalene (10 mg/l) as internal standard was prepared in *n*-amyl alcohol as the extracting solvent. Naphthalene has similar retention time to MNTs' in GC chromatogram and also at 10 mg/l the intensity of its peak is similar to that of preconcentrated MNTs. A stock standard solution of MNTs (1000 $\mu\text{g}/\text{ml}$) was prepared in methanol. All of standard solutions were stored in a refrigerator (4 $^{\circ}\text{C}$) and brought to the ambient temperature just prior to use. A 5 ml of the sample solution was placed in 13 ml vial with an 8 mm magnetic stir bar. After the uptake of 3 μl of extraction solvent, the needle of the syringe pierced the vial septum, and the syringe needle was fixed so that the tip of the needle was located in a constant position in the headspace. After extraction for a prescribed time, the syringe plunger was withdrawn and the microdrop was retracted into the microsyringe and injected into the GC for the analysis. Finally, all quantifications made in this study were based on the relative peak area of analyte to the internal standard (naphthalene) from the average of three replicate measurements.

3. Results and discussion

In this study, parameters related to the headspace solvent microextraction (HSME) were optimized by utilizing the univariate method for simplifying the optimization procedure.

3.1. Solvent selection

The choice of an appropriate solvent has a main role in this method in order to achieve good sensitivity, precision and selectivity of the target compounds.

The extraction solvent has to meet three requirements: to extract analytes well, to be separated from analyte peaks in the chromatogram and to have low volatility [7]. It is well known that three isomers of mononitrotoluene are soluble in alcohols and ethers, so in order to select a proper solvent, several alcohols including 1-propanol, 1-butanol, 1-octanol, 1-nonanol, 1-decanol, 1-undecanol, 1-heptanol, 1-hexanol, *n*-amyl alcohol, and benzyl alcohol were examined. Solvent selectivity was evaluated for the extraction of a 5 ml sample containing 200 $\mu\text{g}/\text{l}$ of MNTs in deionized water. The stirred solution (200 $\mu\text{g}/\text{l}$) was sampled for 15 min using 3 μl of appropriate organic solvent. Among different solvents examined, *n*-amyl alcohol gave the best extraction efficiency and its peak was easily separated from the sample peaks. Therefore, *n*-amyl alcohol was chosen as the extracting solvent in this investigation.

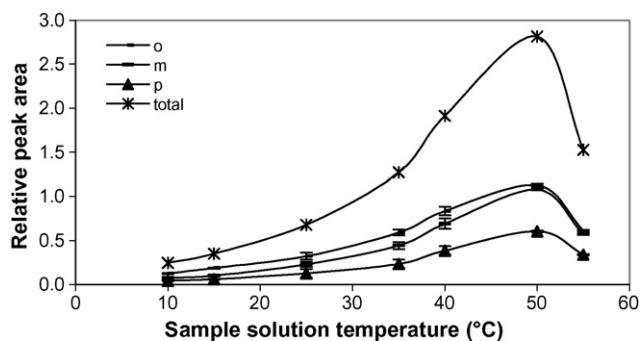


Fig. 1. Effect of sample solution temperature on the extraction efficiency. Conditions: microdrop volume, 3 μl ; sample volume, 5 ml; stirring speed, 400 rpm; extraction time, 15 min; pH 5.05; without salt addition.

3.2. Sample temperature

The effect of sample temperature was investigated by suspending a drop of *n*-amyl alcohol from the tip of a microsyringe fixed above the surface of solution in a sealed vial for 15 min in the headspace while varying the sample temperature in the range of 10–55 $^{\circ}\text{C}$. Measurements were performed on aqueous solution containing 200 $\mu\text{g/l}$ of each analyte. Fig. 1 shows that temperature has a significant effect on the extraction. Usually, increasing temperature increases the evaporation of analytes from the sample matrix to the headspace. This can be explained by the fact that at higher temperatures vapor pressures of the analytes and their concentration in headspace increase. At elevated temperatures the amount of the extracted analyte decreases; probably, due to the decrease of partition coefficient of the analyte in the extraction phase, especially for the analytes with small distribution constants. On the other hand, by increasing the temperature of the solution, evaporation of microdrop was observed. Therefore, the extraction temperature of 45 $^{\circ}\text{C}$ was considered as the optimum temperature in the following experiments.

3.3. Microdrop volume

The influence of microdrop's volume on the extraction efficiency of the system was studied in the range of 1–3 μl and the results are shown in Fig. 2. As it was expected an increase in the

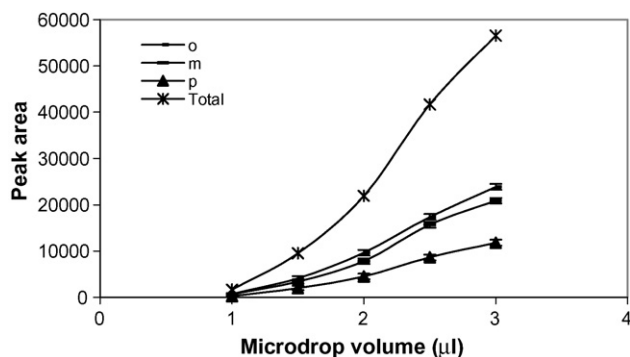


Fig. 2. Effect of microdrop volume on the extraction efficiency. Conditions: sample temperature, 45 $^{\circ}\text{C}$; sample volume, 5 ml; stirring speed, 400 rpm; extraction time, 15 min; pH 5.05; without salt addition.

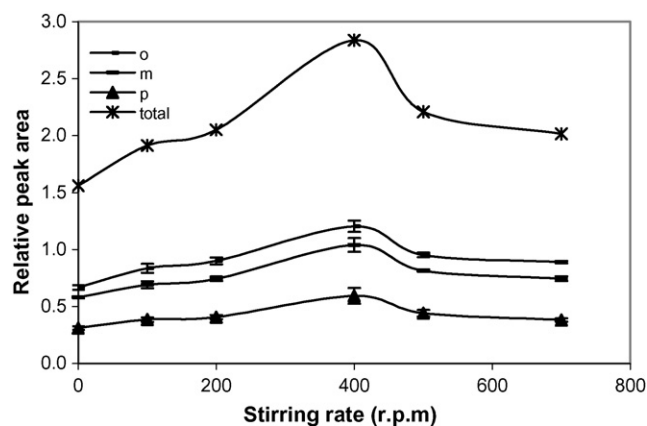


Fig. 3. Effect of stirring rate on the extraction efficiency. Conditions: sample temperature, 45 $^{\circ}\text{C}$; sample volume, 5 ml; extraction time, 15 min; pH 5.05; without salt addition.

volume of the microdrop (up to 3 μl) resulted in a sharp increase in the extraction efficiency of MNTs. Increasing the microdrop's volume higher than 3 μl revealed a great tendency of the drop to fall down from the tip of the microsyringe. Therefore, in other extractions a microdrop with volume of 3 μl was used.

3.4. Stirring rate

In HSME mass transfer in the headspace is assumed to be a fast process because diffusion coefficients in the gas phase are typically 10^4 times greater than corresponding diffusion coefficients in condensed phase [11]. Sampling agitation enhances extraction and reduces extraction time because the equilibrium between the aqueous and vapor phases can be achieved more rapidly and enhances the diffusion of the analytes toward the microdrop [12]. Effect of the stirring rate on the extraction efficiency of the system was studied in the range of 100–700 rpm and the results are shown in Fig. 3. Three replicate extractions were performed at five different stirring rates. The peak areas of all analytes increase when increasing the stirring rates up to 400 rpm. At higher stirring rates due to the type of the sample vial and the volume of the solution, splattering of solution occur which damages the drop and causes the signal to decrease; hence a stirring rate of 400 rpm was chosen for further studies.

3.5. Ionic strength of the solution

The effect of salt concentration on the extraction efficiency was studied with NaCl concentrations in the range of 0.0–4.0 mol/l (Fig. 4). The results revealed that the presence of salt significantly increases the extraction efficiency. In fact the presence of salt increases the ionic strength of solution and decreases the solubilities of the organic analytes due to the salting out phenomena [13,14]. Thus, further extractions were carried out in the presence of 4 M of NaCl.

3.6. pH of the sample solution

The pH of the sample solution is known to play a key role in the headspace extraction of ionizable analytes [15,16]. Ionizable

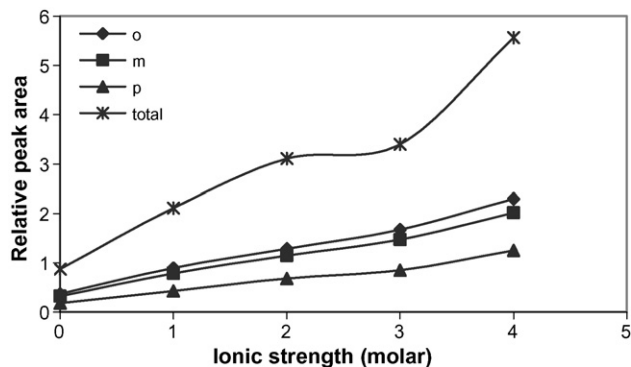


Fig. 4. Effect of ionic strength on the extraction efficiency. Conditions: sample temperature, 45 °C; sample volume, 5 ml; stirring speed, 400 rpm; extraction time, 15 min; pH 5.05.

analytes should be changed to their neutral form in order to reach to maximum extraction efficiency. In the present study, the pH of the solution varied in the range of 3–12 and the procedure was followed by examining pH influence on the extraction efficiency. Fig. 5 reveals that extraction efficiencies of the analytes increase significantly by increasing the pH of the sample solution. Probably this is due to the interaction of electron cloud of benzene ring analytes and protons at lower pHs. Based on this investigation, the pH of the solutions was adjusted at 12 for further studies.

3.7. Sample volume

In HSME when using constant volume vials, sample volume influences the magnitude of the headspace volume and thus might influence the extraction efficiency. The combination of k_{mh} (microdrop/head space distribution constant) and k_{hs} (head space/sample distribution constant) determines the magnitude of the sample volume's effect on the amount of the extracted analyte into the microdrop. An increase in the sample volume and consequently a decrease in the headspace volume enhance the extracted amount of analytes, which improves the sensitivity [17,18]. The effect of sample volume on the extracted amounts of MNTs was investigated as follows. A set of experiments were performed using a 13 ml vial with different volumes of the aque-

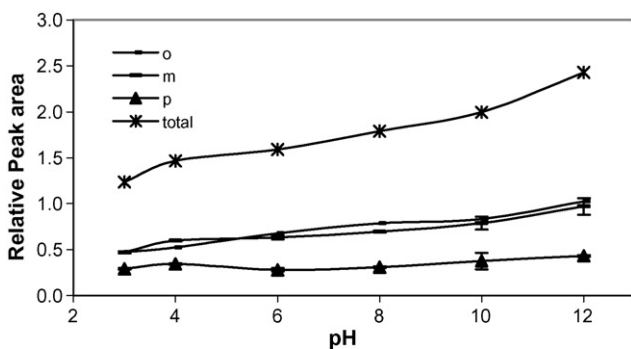


Fig. 5. Effect of pH on the extraction efficiency. Conditions: sample temperature, 45 °C; sample volume, 5 ml; stirring speed, 400 rpm; extraction time, 15 min; without salt addition.

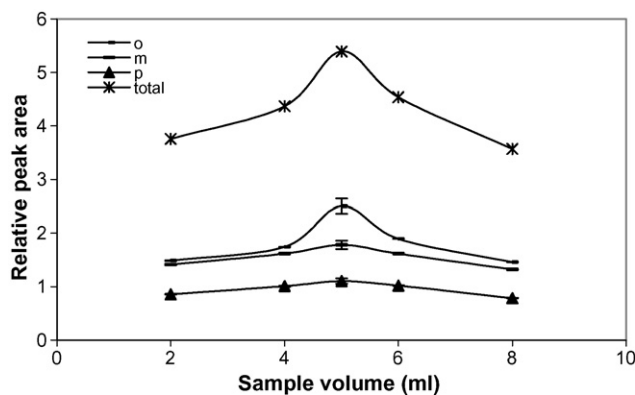


Fig. 6. Effect of sample volume on the extraction efficiency. Conditions: sample temperature, 45 °C; stirring speed, 400 rpm; extraction time, 15 min; pH 5.05; ionic strength, 4 M of NaCl.

ous phase in the range of 2–8 ml. Fig. 6 shows that the extraction efficiency increases by increasing the sample volume up to 5 ml. At higher volumes a decrease in the signal occurs. These observations can be explained by the fact that the percentage of the headspace decreases because of an increase in sample volume, which accelerates the diffusion of the analytes into the microdrop. On the other hand, by stirring the solution at a fixed rate with a large volume, the convection is not as good as in the aqueous phase and takes more time to transfer analytes from the liquid phase to the headspace. Thus, the response begins to decrease at higher sample volumes.

3.8. Extraction time

The profiles of the extraction time were studied by monitoring the variation of relative peak area of analyte with exposure of the time under the following conditions: MNTs solution with concentration of 200 $\mu\text{g/l}$, was stirred at 400 rpm, solution temperature 45 °C, drop volume 3 μl , pH 12 and NaCl concentration of 4 M. In Fig. 7 one can see the amount of MNTs extracted into *n*-amyl alcohol (containing 10 $\mu\text{g/ml}$ naphthalene as an internal standard) rises by increasing the exposure time in the range of

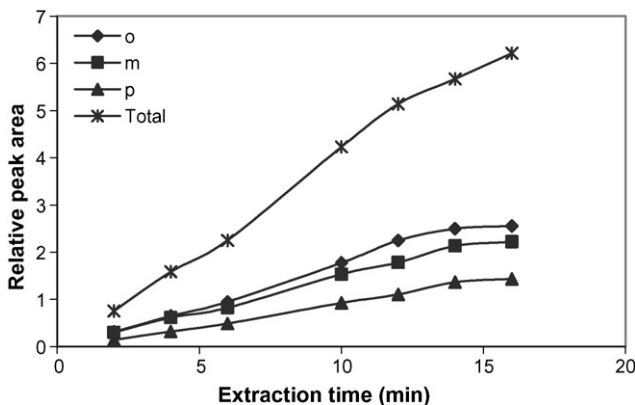


Fig. 7. Effect of extraction time on the extraction efficiency. Conditions: sample temperature, 45 °C; sample volume, 5 ml; stirring speed, 400 rpm; pH 5.05; ionic strength, 4 M of NaCl.

Table 1
Limit of detections, regression equations, correlation coefficients, dynamic linear ranges and enrichment factors for HSME of MNTs

Analyte	LOD ($\mu\text{g/l}$)	R^2	Regression equation	DLR ($\mu\text{g/l}$)	Enrichment factor ^a
<i>o</i> -Nitrotoluene	0.06	0.9994	$A = 0.0112C (\mu\text{g/l}) - 0.0027$	1–600	142
<i>m</i> -Nitrotoluene	0.03	0.9986	$A = 0.0098C (\mu\text{g/l}) + 0.0514$	1–600	128
<i>p</i> -Nitrotoluene	0.02	0.9994	$A = 0.0061C (\mu\text{g/l}) + 0.0038$	3–600	103

^a Enrichment factors were calculated based on extraction of 200 $\mu\text{g/l}$ of MNTs.

2–15 min. Longer times were not studied because by increasing the exposure time, the drop volume increases significantly, due to the hydrophilicity of *n*-amyl alcohol and microdrop falls of due to the gravity force. HSME is not an exhaustive extraction method and analytes are partitioned between the bulk aqueous phase and the organic microdrop. For quantitative analysis, it is necessary to allow sufficient mass transfer into the microdrop in an exact reproducible extraction time. Therefore, a sample extraction time of 15 min was chosen for further studies.

3.9. Evaluation of the method performance

Under optimum conditions, limits of detection (LODs), regression equations, correlation coefficients (R^2), dynamic linear ranges (DLRs), and enrichment factors were obtained (Table 1). Calibration curves for the MNTs were tested in the concentration range of 0.3–800 $\mu\text{g/l}$ and DLRs obtained in the range of 1–600 $\mu\text{g/l}$ for *o*-nitrotoluene and *m*-nitrotoluene and 3–600 for *p*-nitrotoluene.

In order to calculate the enrichment factor of each analyte, three replicate extractions were performed at optimal conditions from aqueous solution containing 200 $\mu\text{g/l}$ of analytes. The enrichment factor was calculated as the ratio of the final concentration of analyte in the microdrop and its concentration in the original solution. The standard solutions of MNTs were prepared in *n*-amyl alcohol as solvent and the calibration curves were drawn in the concentration range of 1–40 $\mu\text{g/ml}$ with three replicate direct injections. The actual concentration of each extracted analyte in *n*-amyl alcohol was calculated from the calibration curves and the enrichment factors were determined and summarized in Table 1.

Finally, the applicability of the extraction method to real samples was examined by extraction and determination of MNTs from waste water of P.C.I. Company, Research Center of Azad University and also one further water sample. A chromatogram of the standard solution (100 $\mu\text{g/l}$) of analytes after headspace extraction with a 3 μl drop of *n*-amyl alcohol containing 10 $\mu\text{g/ml}$ naphthalene as internal standard is shown in Fig. 8A and a chromatogram of waste water sample of P.C.I. Co after headspace extraction at the same conditions is shown in Fig. 8B. The determination of MNTs was performed using the standard addition method. At least four points were applied for obtaining needed calibration curve for each MNT. Table 2 shows that the results of four replicate analysis of each sample obtained by the proposed method and the amount added are satisfactory. Percent errors for determination of MNTs in different

water samples are located in the range of 5.2–20.0. The precision of the proposed method is very similar to the SPME and SDME methods reported for the extraction and subsequent GC analysis of MNTs in water samples [5,6]. On the other hand, the proposed method revealed suitable reproducibility with R.S.D. values in the range of 2.6–12.9%. Similar R.S.D.s (3.4–11.3) were reported for extraction and determination of MNTs in water samples [5,6]. It is worthy to note that using solvent microextraction methods for extraction of ppb levels of analytes from water samples high R.S.D.s are acceptable. For example R.S.D.s in the range of 4.5–18.8 and 8.2–11.3 for HSME of alcohols [19] and trihalomethanes [20], 2.5–10.8 and 2.7–12.3 and 4.9–17.7 for SDME of polychlorinated biphenyls [21], benzodiazepines [22] and endosulfans [23] have been obtained, respectively.

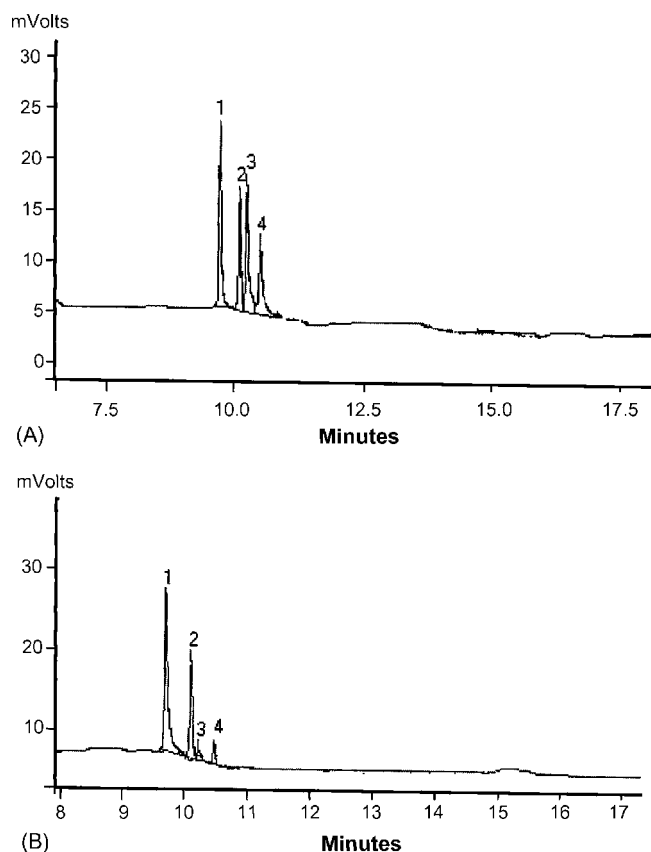


Fig. 8. (A) Chromatogram of standard solution (100 $\mu\text{g/l}$) of MNTs after HSME at optimum conditions. Peak: (1) *o*-nitrotoluene, (2) naphthalene, (3) *m*-nitrotoluene, and (4) *p*-nitrotoluene. (B) Chromatogram of waste water of P.C.I. Co after HSME at optimum conditions. Peak: (1) *o*-nitrotoluene, (2) naphthalene, (3) *m*-nitrotoluene, and (4) *p*-nitrotoluene.

Table 2
Determination of MNTs in waste water of P.C.I. Company (Tehran, Iran), Research Center of Azad University (Tehran, Iran) and well water

Sample	Analyte											
	<i>o</i> -Nitrotoluene				<i>m</i> -Nitrotoluene				<i>p</i> -Nitrotoluene			
	<i>C</i> _{added} ($\mu\text{g/l}$)	<i>C</i> _{found} ($\mu\text{g/l}$)	% R.S.D.	% <i>E</i>	<i>C</i> _{added} ($\mu\text{g/l}$)	<i>C</i> _{found} ($\mu\text{g/l}$)	% R.S.D.	% <i>E</i>	<i>C</i> _{added} ($\mu\text{g/l}$)	<i>C</i> _{found} ($\mu\text{g/l}$)	% R.S.D.	% <i>E</i>
Waste water of (P.C.I. Co.)	–	173.5 ^a	12.5	–	–	4.5	11.9	–	–	49.3	11.7	–
	175.0	362.7	12.9	8.1	5.0	8.5	12.5	–20.0	50.0	96.7	12.6	–5.2
Waste water of (R.C.)	–	192.0	7.8	–	–	4.0	12.0	–	–	87.0	12.5	–
	192.0	366.0	8.1	–9.4	16.0	21.6	12.7	10.0	100.0	198.0	12.9	11.0
Well water	–	–	–	–	–	–	–	–	–	–	–	–
	100.0	118.0	2.6	18.0	100.0	115.7	3.1	15.7	100.0	118.0	6.6	18.0

^a Mean value of four replicate measurements.

4. Conclusions

The results of this work showed that the proposed HSME is a very fast and simple method for preconcentration and determination of $\mu\text{g/l}$ concentration of MNTs in waste water samples, which uses very low volumes of an organic solvent. The consumption of toxic organic solvents is very low (1–3 μl). There is no need of dedicated and expensive apparatuses for the proposed method. Simplicity and cost-effectiveness of HSME makes it quite attractive when compared to SPME and LLE or SPE. A comparison between single-drop microextraction (SDME) [5] and HSME for extraction of MNTs revealed that both methods have similar capabilities in terms of precision, speed of analytes and detections, but the major advantage of present method is direct determination of analytes without interference from the sample matrix (while SDME has interference from the sample matrix). DLR of the proposed method is in the range of 1–600 $\mu\text{g/l}$ and for SDME is in the range of 20–1000 $\mu\text{g/l}$ [5]. The proposed procedure was successfully applied with satisfactory accuracy and reproducibility to the extraction and determination of MNTs from waste water of P.C.I. Company and Research Center of Azad University. No significant differences were observed in the quantification of the analytes between the different types of samples tested. Also occurrence of MNTs in Iranian waste waters required further revisiting of these substances in various water samples through sensitive and selective extraction and determination methods as presented in this work.

Acknowledgement

This study was supported by the Vice Research of Shahid Beheshti University for financial support. Professor M. Semnani-Rahbar is gratefully acknowledged for his support.

References

- [1] P.H. Groggins (Ed.), *Unite Process in Organic Synthesis*, 5th ed., Mc Graw Hill, New York, 1958.
- [2] M.E. Walsh, T.A. Raney, Determination of Nitroaromatic, Nitramine, and Nitrate Ester Explosives in Water using SPE and GC/ECD; Comparison with HPLC, Special Report 98-2, US Army Cold Regions Research and Engineering Laboratory, Hanover, NH, 1998.
- [3] SW-846, Method 8330, Nitroaromatics & Nitramines by High Performance Liquid Chromatography (HPLC), US Environmental Protection Agency, Office of Solid Waste and Emergency Response, Washington, DC, 1994.
- [4] M.R. Darrach, A. Chutjian, G.A. Plett, *Environ. Sci. Technol.* 32 (1998) 1354.
- [5] E. Psillakis, N. Kalogerakis, *J. Chromatogr. A* 907 (2001) 211.
- [6] E. Psillakis, N. Kalogerakis, *J. Chromatogr. A* 938 (2001) 113.
- [7] S. Shariati-Feizabadi, Y. Yamini, N. Bahramifar, *Anal. Chim. Acta* 489 (2003) 21.
- [8] K.G. Karaisz, N.H. Snow, *J. Microcolumn Sep.* 13 (2001) 1.
- [9] S. de Jager, R.J. Andrews, *Analyst* 125 (2000) 1943.
- [10] A.L. Theis, A.J. Waldack, S.M. Hansen, M.A. Jeannot, *Anal. Chem.* 73 (2001) 5651.
- [11] E.L. Culssler, *Diffusion and Mass Transfer in Fluid System*, Cambridge University Press, Cambridge, 1984 (Chapters 4 and 5).
- [12] E. Psillakis, N. Kalogerakis, *Trends Anal. Chem.* 22 (2003) 565.
- [13] D.C. Leggett, T.F. Jenkins, P.H. Miyares, *Anal. Chem.* 62 (1990) 1355.
- [14] Y. Yamini, M. Hojjati, M. Hajihoseini, M. Shamsipur, *Talanta* 62 (2004) 265.
- [15] L.S. de Jager, A.R.J. Andrews, *J. Chromatogr. A* 911 (2001) 97.
- [16] B.H. Hwang, M.R. Lee, *J. Chromatogr. A* 898 (2000) 245.
- [17] T. Gorecki, J. Pawliszyn, *Analyst* 122 (1997) 1079.
- [18] M. Liompart, K. Li, M. Fingas, *Talanta* 48 (1999) 451.
- [19] A. Tankeviciute, R. Kazlauskas, V. Vickackaite, *Analyst* 126 (2001) 1674.
- [20] R.S. Zhao, W.J. Lao, X.B. Xu, *Talanta* 62 (2004) 751.
- [21] C. Basheer, H.K. Lee, J.P. Obbard, *J. Chromatogr. A* 1022 (2004) 161.
- [22] H.G. Uglund, M. Krogh, K.E. Rasmussen, *J. Chromatogr. B* 749 (2000) 85.
- [23] M.C. Lopez-Blanco, S. Blanco-Cid, B. Cancho-Grande, J. Simal-Gandara, *J. Chromatogr. A* 984 (2003) 245.

Off-line chromatographic assessment of Fe(II) in seawater

A.C. Fischer*, T.G. Verburg, H.Th. Wolterbeek

*Faculty of Applied Sciences, Department of Radiation, Radionuclides and Reactors, Delft University of Technology,
Mekelweg 15, 2629 JB Delft, The Netherlands*

Received 16 February 2006; received in revised form 11 September 2006; accepted 27 September 2006

Available online 13 November 2006

Abstract

The speciation of iron in seawater is receiving much attention worldwide, and several methods have been developed to measure its various chemical species. Although probably the most important in algal iron accumulation, Fe(II) is very unstable in seawater, is rapidly oxidised to Fe(III), thus the time between collection of the samples and the actual Fe(II) assessment may have significant impact on the obtained results. Especially for kinetic analysis, where radiotracer methods ask for off-line counting, waiting times should be taken into account.

The present paper presents a model to account for waiting time in off-line Fe(II) assessment. The model comprises Fe(II) oxidation in a reducing environment ($\sim 1 \times 10^{-5}$ M Na₂SO₃ in filtered seawater) and binding to column-associated ferrozine, for use with ferrozine preloaded SepPak® C₁₈ cartridges. The model is essentially based on mathematical treatment of transport in micro-vessels and uses known rate factors for the oxidation and reduction of Fe. In off-line chromatographic Fe(II) assessment, the model was shown to account for variances in Fe(II) recoveries ranging from 10 to 54%, and for waiting times ranging from 2 to 80 min. The presented data shows that waiting time resulted in underestimation up to a factor 10 as measured by direct recovery counting of loaded Fe(II). As excess amounts of ferrozine were used for these experiments, this underestimation will be mainly caused by the oxidation of ferrous iron during this waiting time. The data also suggests that time-modelling may account for all effects, thus permitting off-line counting of Fe(II) without loss of data quality.

© 2006 Elsevier B.V. All rights reserved.

Keywords: Off-line Fe(II) assessment; Oxidation; Waiting time; Iron; Ferrozine

1. Introduction

The speciation of iron is an important factor controlling its bioavailability for phytoplankton [1,2]. Much attention has been given to the chemistry of iron in seawater, especially in the high-nutrient low-chlorophyll (HNLC) regions of the ocean, where this chemical parameter is considered as a limiting nutrient [3–6]. Several methods are known for iron speciation analysis, such as voltammetry [7,8], flow-injection analysis [9–11] and chromatography [12,13]. Determination of low iron concentrations in seawater, typically 50–200 pM in the open surface waters [14], demands very precise measurements and presents a high risk of contamination of the samples.

The pre-dominant iron species in seawater are organic iron–ligand complexes, over 99% of the iron present is bound by naturally occurring ligands that have a high affinity for

iron (conditional stability constants reported as $\log K'_{\text{FeL}} = 18\text{--}21$ [15,16]). It is unclear if algae can take up these large iron–ligand complexes, as different reports show different results. For example, the fungal siderophore desferrioxamine B (DFOB), which has a high affinity for iron, was tested for its uptake by phytoplankton. Maldonado and Price [17] showed that Fe–DFOB complexes can be taken up by phytoplankton, whereas Hutchins et al. [18] and Wells [19] both showed a reduction of biological Fe uptake when DFOB was added to their medium.

But, if iron uptake by phytoplankton is similar to uptake mechanisms by terrestrial plants [20], the Fe(II) species may be of importance for phytoplankton. The ocean being an oxidising environment, Fe(II) concentrations are usually extremely small due to rapid transformation into Fe(III). The oxidation rate of Fe(II) is known to be in the order of minutes [21,22] although there may be some organic ligands present in seawater that can extend the lifetime of Fe(II) [23]. For Fe(II) measurements, in-line measurements are preferred, although there is always a minimum amount of time due to sample loops before

* Corresponding author.

E-mail address: science@astrid.thatsme.nl (A.C. Fischer).

Nomenclature

a	volume-flow (L s^{-1})
c_1	$k_{\text{red}}\{[\text{Fe}_{\text{total}}] - [\text{FeL}]\}[\text{SO}_3]$
c_2	$((k_{\text{ox}}/[\text{SO}_3] + k_{\text{red}})[\text{SO}_3]$
k_{FZ}	rate constant for the formation of the Fe(II)Ferrozine complex (s^{-1})
k_{ox}	rate constant for the oxidation of Fe(II) to Fe(III) (s^{-1})
k_{red}	rate constant for the reduction of Fe(III) to Fe(II) by Na_2SO_3 ($\text{mol L}^{-1} \text{s}^{-1}$)
T	time (s)
T_w	waiting time before V_v is introduced onto the cartridge (s)
V_k	volume of the cartridge (L)
V_v	volume of a sample (L)

the actual measurement takes place. However, this time is often considered to be negligible [24,10].

In bioavailability, not only the speciation of metals, but also the kinetics of metal speciation (the rates of change in speciation), should be considered as important. Kinetic studies using radiotracers could give us valuable information on the actual processes happening, as it has recently been shown that the widely accepted CLE-AdSV method for the determination of iron in seawater has its kinetic limitations [25]. Although for conventional Fe(II) analysis there are now several in-line measurement techniques available [26–31], the measurement of the kinetics requires the use of radiotracers with an off-line separation and counting approach [32]. In these approaches, waiting times between sampling and assessment will be increased, and cannot be neglected. In the present paper, we present a model that describes the effect of waiting time (caused by, e.g. sample loops) on measurement of Fe(II) on a ferrozine preloaded cartridge [24]. The model is essentially based on modelling of transport in micro-vessels [33], and uses known rate factors for the binding of Fe to ferrozine [34] and for the reduction and oxidation of iron in seawater [35].

2. Materials and methods

2.1. Counting

The radioisotope $^{55}\text{FeCl}_3$ in 0.1 M HCl solution (Isotope Products Laboratory, BLASEG GmbH, Waldburg, Germany) was used to measure recoveries of Fe(II) when different waiting times were applied. ^{55}Fe (specific activity 3300 GBq/g at time of purchase) has a half-life of 2.7 years and decays via electron capture, while emitting low energy X-rays (~ 5 keV). Fifteen milliliters of Ultima Gold AB scintillation cocktail was added to each 5-mL sample. The samples were subsequently counted on a liquid scintillation counter (Packard Tri-carb 2750 TR/LL LSC) in an energy window from 2 to 25 keV. The counting time was set on a counting error of 1% or maxi-

mally 30 min. Background radiation, as measured with blanks (counting time 1 h), is approximately 1 cps for ^{55}Fe in the energy regions chosen. The efficiency of the ^{55}Fe measurement via LSC can vary due to quenching (decrease in the signal due to chemical or optical shielding of the scintillations). The efficiency of LSC-counting was determined with a known amount of radioactivity and 1-nitroso-2-naphthol as a shielding agent. The measured efficiency varied from 25 to 60%, depending on the degree of quenching. For this study an amount of radiotracer (containing both radioactive and non-radioactive iron) was used corresponding to a concentration of 0.1–1 nM iron.

2.2. Experiments

Several experiments, with different waiting times T_w , were carried out to examine the effect of T_w on Fe(II) oxidation, as described in Fig. 1. A sample with volume V_v , and an iron radiotracer concentration of $[\text{FeII}]_0$ is taken at $t = t_0$. In the sample the Fe(II) present will oxidise to Fe(III) with an oxidation constant k_{ox} . Also, the Fe(III) will be reduced to Fe(II) – in presence of SO_3^- – with a reduction constant k_{red} . The SO_3^- is in excess and therefore the concentration is considered to be constant. At $t = T_w$ the sample is brought onto the cartridge with a volume V_k and is eluted at a volume-flow a . This will cause a flow linear velocity v in the cartridge. The iron in the cartridge will bind to the ferrozine with binding constant k_{FZ} . Because of the excess amount of ferrozine at the cartridge, the Fe(II) will be complexed at the cartridge and there should be no further oxidation [34]. At $t = T$ the sample has been eluted completely. The experiments were carried out with seawater from the Bay of Biscay (salinity = 35, pH 8). This sea-

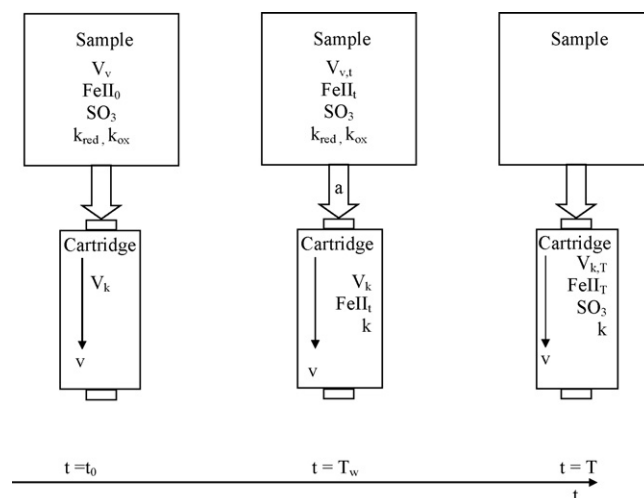


Fig. 1. Schematic representation of the model parameters. A sample with volume V_v , and an iron radiotracer concentration of $[\text{FeII}]_0$ is taken at $t = t_0$. In the sample the Fe(II) present will oxidise to Fe(III) with an oxidation constant k_{ox} . Also, the Fe(III) will be reduced to Fe(II) – in presence of SO_3^- – with a reduction constant k_{red} . The SO_3^- is in excess and therefore the concentration is considered to be constant. At $t = T_w$ the sample is brought onto the cartridge with a volume V_k and is eluted at a volume-flow a . This will cause a flow linear velocity v in the cartridge. The iron in the cartridge will bind to the ferrozine with binding constant k_{FZ} . At $t = T$ the sample has been eluted completely.

Table 1
Experimental data used for modelling

T (s)	a (L s^{-1})	V_v (L)	T_w (s)	$[\text{SO}_3]$ (mol L^{-1})	$[\text{Fe(II)}]_0$ (mol L^{-1})	Recovery (%)
558	6.8E–05	0.024	138	1.7E–05	7E–10	18
1340	6.7E–05	0.023	920	1.7E–05	7E–10	13
2102	8E–05	0.029	1682	1.7E–05	7E–10	10
3843	6.9E–05	0.024	3423	1.7E–05	2E–10	24
4513	6.9E–05	0.024	4093	1.7E–05	2E–10	25
5126	8.2E–05	0.03	4706	1.7E–05	2E–10	21
695	7.4E–05	0.027	269	1.9E–05	5E–10	50
1326	6.4E–05	0.022	906	1.9E–05	5E–10	54
1882	7.7E–05	0.028	1456	1.9E–05	5E–10	45
455	7.4E–05	0.019	130	1.1E–05	1E–09	40
990	7.9E–05	0.02	672	1.1E–05	1E–09	33
1460	8.8E–05	0.022	1159	1.1E–05	1E–09	31
395	5.4E–05	0.016	105	2E–05	5E–10	48
896	4.4E–05	0.02	420	2E–05	5E–10	42
1215	8.6E–05	0.025	930	2E–05	5E–10	43

T , the total experiment time (s), a , the flow rate of the sample over the cartridge (L s^{-1}), V_v , the sample volume (L), T_w , the waiting time (s), $[\text{SO}_3]$ and $[\text{Fe(II)}]_0$ concentrations are in mol L^{-1} . Recoveries of ^{55}Fe are given as the percentage (%) of added $^{55}\text{Fe(II)}$.

water was sampled after a phytoplankton bloom [36] and was stored in an acid-cleaned and seawater-rinsed polypropylene cubic metre vessel at room temperature. We filtered this seawater successively over two polycarbonate filter systems (Sartobran, Sartorius). The first filter system had an entrance pore size of $0.7 \mu\text{m}$ and an exit pore size of $0.45 \mu\text{m}$, and the second one ranged from 0.45 to $0.2 \mu\text{m}$. The filtered seawater (FSW) was stored in a pre-cleaned 10 L polypropylene bottle at 4°C (no acidification). The pre-cleaning of the materials consisted of two steps: first cleaning with a Laviton soap solution to remove organic material followed by three rinses with milliQ[®] water. A second cleaning step involved a 6 M HCl solution to remove all trace metals, followed by three rinses with milliQ[®] water. This second cleaning step was repeated three times. Because of possible damage by 6 M HCl, this cleaning step was performed as quickly as possible. Prior to use in experiments the iron content of this seawater was determined by flow-injection analysis [10] and ligand concentrations were measured by voltammetric analysis with 2-(2-thiazolylazo)-*p*-cresol (TAC) as a competing ligand [7]. The filtered seawater used in our experiments therefore contains $1.3 \pm 0.4 \text{ nM}$ of total dissolved Fe and $3.4 \pm 0.5 \text{ nM}$ of natural occurring organic ligands with a conditional stability constant of $\log K(\text{Fe}^{3+}\text{L}) = 22.49 \pm 0.16$ or $\log K(\text{Fe}^{\text{II}}\text{L}) = 13.59 \pm 0.16$ (Gerringa, personal communication). For this present study, we used the methods described by Fischer et al. [32], which are an adaptation of a method developed by King et al. [24]. The cartridge volume used in these experiments is 7 mL, and with an average flow velocity of 0.024 L s^{-1} (see also Table 1 for all other parameters used) the process of fully loading the cartridge will be nearly instantaneous compared to the waiting times chosen for these experiments. Waiting time, flow and seawater volumes were varied and recoveries of the ^{55}Fe were measured. In all the experiments the radiotracer was added as $^{55}\text{Fe(II)}$. This radio-iron species was made according to Millero et al. [35], which involves reduction by an excess of Na_2SO_3 (analytical grade) solution.

3. Results and discussion

In previous experiments [32] the direct recovery of Fe(II) on ferrozine (FZ) preloaded cartridges was observed as $85 \pm 7\%$ (recovery defined here as the amount of found radiotracer as percentage of the originally added Fe(II) radiotracer). However, fractional recoveries largely varied with time between sampling and start-up of chromatographic separation (Fig. 2). Therefore, effects of waiting time on Fe(II) assessment should be regarded as important, and should be taken into account in any off-line Fe(II) analysis. The present paper focuses on the necessary modelling of Fe behaviour in the procedures of off-line Fe(II) assessment: changing FZ-preloaded columns for any other chromatographic approach would give no principal differences in the lines of reasoning leading to the presently adopted model.

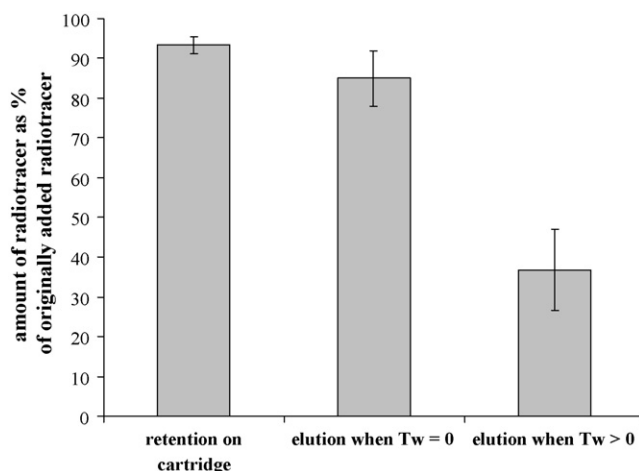


Fig. 2. The effect of waiting time on measurement, as percentage (%) of the amount of radiotracer originally added to the seawater sample. Retention of Fe(II) on the FZ-preloaded cartridge; elution of the cartridge, after direct measurement (no sample loops), thus without waiting time (T_w); elution of the cartridge, after a waiting time varying from 7.5 to 85 min before sampling.

Our model presents the column transport as a longitudinal transport of Fe chemical forms, with Fe(II) being withdrawn both by binding to immobilised FZ and by oxidation to Fe(III). Approaches in modelling are largely adopted from Horwitz [33], and in line with Helfferich [37]. Fig. 1 shows the experimental approach: Fe(II), in a sampled volume V_v , is retained for a waiting time T_w , during which the concentration [Fe(II)] depends on both processes of oxidation to Fe(III) and back-reduction to Fe(II), the latter affected by added Na_2SO_3 , as

$$\frac{d[\text{Fe(II)}]}{dt} = -k_{\text{ox}}[\text{Fe(II)}] + k_{\text{red}}[\text{Fe(III)}][\text{SO}_3] \quad (1)$$

$$[\text{Fe(III)}] = [\text{Fe}_{\text{total}}] - [\text{FeL}] - [\text{Fe(II)}] \quad (2)$$

Substituting (2) in (1) results in:

$$\begin{aligned} \frac{d[\text{Fe(II)}]}{dt} &= -k_{\text{ox}}[\text{Fe(II)}] + k_{\text{red}}([\text{Fe}_{\text{total}}] - [\text{FeL}] - [\text{Fe(II)}])[\text{SO}_3] \\ \frac{d[\text{Fe(II)}]}{dt} &= k_{\text{red}}([\text{Fe}_{\text{total}}] - [\text{FeL}])[\text{SO}_3] - (k_{\text{ox}} + k_{\text{red}} \cdot [\text{SO}_3])[\text{Fe(II)}] \end{aligned} \quad (3)$$

As $[\text{SO}_3]$, $[\text{Fe}_{\text{total}}]$ and $[\text{FeL}]$ are available in excess compared to $[\text{Fe(II)}]$, these concentrations are regarded as constants. Based on these constants and on the reaction rate constants (k_{ox} and k_{red}), Eq. (3) can be rewritten as:

$$\frac{d[\text{Fe(II)}]}{dt} = c_1 - c_2[\text{Fe(II)}] \quad (4)$$

where

$$\begin{aligned} c_1 &= k_{\text{red}}\{[\text{Fe}_{\text{total}}] - [\text{FeL}]\}[\text{SO}_3] \quad \text{and} \\ c_2 &= ((k_{\text{ox}}/[\text{SO}_3]) + k_{\text{red}})[\text{SO}_3] = (k_{\text{ox}} + k_{\text{red}}[\text{SO}_3]) \end{aligned}$$

[Fe(II)] at every time t can be derived from Eq. (4) as:

$$[\text{Fe(II)}] = \frac{c_1}{c_2} + \left([\text{Fe(II)}]_0 - \frac{c_1}{c_2} \right) e^{-c_2 t} \quad (5)$$

with $[\text{Fe(II)}] = [\text{Fe(II)}]_0$ for $t = 0$.

It should be noted here that Eq. (4) is integrated over time t and not over T_w , which implies that oxidation–reduction are assumed to be equal in open solution and in the cartridge.

Apart from oxidation and reduction, Fe(II) will be affected by formation of Fe-ferrozine (Fe(II)FZ) in the cartridge. Following Horwitz [33], the net formation of Fe(II)FZ can be described by the function $e^{-k(V/a)}$, thus:

$$\begin{aligned} \frac{d[\text{Fe(II)FZ}]}{dt} &= k[\text{Fe(II)}] e^{-k(V/a)} \\ &= k \left\{ \frac{c_1}{c_2} + \left([\text{Fe(II)}]_0 - \frac{c_1}{c_2} \right) e^{-c_2 t} \right\} e^{-k(V/a)} \end{aligned} \quad (6)$$

with V , cartridge volume; a , volume-flow (in L s^{-1}); k , first-order rate constant (s^{-1}) for the formation of FeFZ₃ on the cartridge. It should be noted here that Eq. (6) considers formation of Fe(II)FZ as first order, whereas Lin and Kester [34] suggested the rate

of formation to be co-governed by $[\text{FZ}]^3$. This means that the presently obtained k value could be interpreted as:

$$k = k_{\text{FZ}}[\text{FZ}]^3 \quad (7)$$

making k dependent of $[\text{FZ}]$. However, considering that cartridge FZ is in excess to loaded Fe(II), $[\text{FZ}]$ may be regarded as constant in time, in other words $[\text{FZ}] \sim [\text{FZ}]_0$. Therefore, k will be constant in time.

The total *absolute* amount of Fe(II)FZ complex formed in time t can be derived from integrating Eq. (6) over time ($T - T_w$), volume V_k , and waiting time T_w as:

$$\begin{aligned} \text{Fe(II)FZ}_{V_k, T} &= \int_0^{V_k} \int_{T_w}^T k[\text{Fe(II)}] e^{-k(V/a)} \\ &= k \left\{ \frac{c_1}{c_2} + \left([\text{Fe(II)}]_0 - \frac{c_1}{c_2} \right) e^{-c_2 t} \right\} \\ &\quad \times e^{-k(V/a)} dt dV \Leftrightarrow \text{Fe(II)FZ}_{V_k, T} \\ &= a \{ (e^{-c_2 T} - e^{-c_2 T_w}) (\text{FeII} c_2 - c_1) \\ &\quad - c_1 c_2 (T - T_w) \} \frac{e^{-k(V/a)} - 1}{c_2^2} \end{aligned} \quad (8)$$

The formed Fe(II)FZ thus depends on the flowrate a , the reduction and oxidation of Fe(II) via $c_1 = k_{\text{red}}\{[\text{Fe}_{\text{total}}] - [\text{FeL}]\}[\text{SO}_3]$ and $c_2 = ((k_{\text{ox}}/[\text{SO}_3]) + k_{\text{red}})[\text{SO}_3]$, the waiting time T_w , the binding constant of Fe(II) to ferrozine (k) and the cartridge volume V_k .

The recovery of sampled Fe(II) can then be defined as the Fe(II)FZ recovered as percentage of then the original concentration $[\text{Fe(II)}]_0$ in sample volume V_v :

$$\text{recovery} = \frac{100a \{ (e^{-c_2 T} - e^{-c_2 T_w}) (\text{FeII} c_2 - c_1) - c_1 c_2 (T - T_w) \} (e^{-k(V_k/a)} - 1) / c_2^2}{\text{FeII}_0 V_v} \quad (9)$$

It should be noted that in Eq. (8) assumes $T \gg V_k/a$, which means that the time needed to reach the outlet of the cartridge is very short relative to the total time T . In effect, the assumption implies that the total cartridge capacity is available for the total elution period. If this is not the case, the integration should not be over T , but over $T - (V_k/a)$, so that the time needed for the sample front to reach the outlet of the cartridge is considered.

The experimental data are given in Table 1, and indicate that for the present paper $T \gg V_k/a$ may be assumed, thus substantiating the use of Eq. (8).

The literature value for k_{red} was chosen from a study [35] that, similar to this one, made use of SO_3 . Although the oxidation for Fe(II) may not be first order [38], for low Fe(II) concentrations pseudo-first-order kinetics are observed and therefore this was assumed here. The values for k_{ox} , k_{red} [22,39] were taken in data processing as fixed values, denoting $k_{\text{red}} = 0.35 \text{ L mol}^{-1} \text{ s}^{-1}$ (as calculated with Fe(III) and SO_3 concentrations as given in Table 1) and $k_{\text{ox}} = 2.0\text{E}-05 \text{ s}^{-1}$, respectively. In doing so, all fitting-uncertainty was dedicated to the derived constant k , or k_{FZ} . As can be seen in Fig. 3 there is good agreement between the actual (10–50%) and the calculated recoveries although at

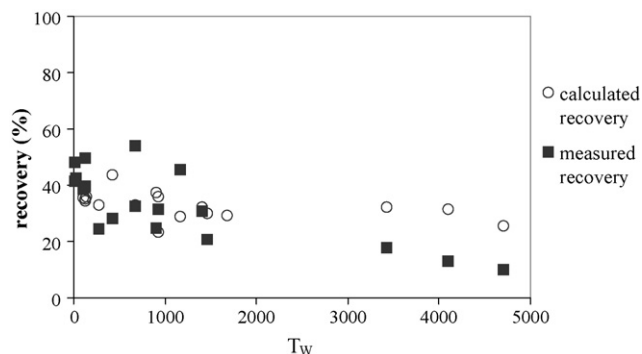


Fig. 3. Measured recovery vs. modelled recovery for Fe(II) added and eluted in a Ferrozine preloaded cartridge, for different radioactive iron concentrations, flow rates, waiting time and sample volumes. Recoveries of ^{55}Fe in the eluted methanol solution are given as the percentage (%) of added $[^{55}\text{Fe}]\text{Fe(II)}$.

higher waiting times the model shows some deviation. However, this may be caused by a small analytical error in the determination of the original radio-iron concentration added, as these are all points measured for an added radio-iron concentration of 0.25 nM. This is a systematic error for this concentration due to the low Fe(II) concentration used. The calculated recoveries are based on the proposed model (Fig. 3; Table 2). Table 2 therefore gives k_{ox} and k_{red} as the adopted literature data, and presents k fitted as $3.5\text{E}-02\text{ s}^{-1}$. Comparing this latter outcome with results obtained by Lin and Kester ([34], see their Eq. (3) and their Table 1) shows that the present k ($3.5\text{E}-02\text{ s}^{-1}$ or 2.1 min^{-1}) fits within their results, although theirs are in correspondence to FZ applied at $50\text{--}60\text{ }\mu\text{mol/L}$ [34]. It should be noted that Lin and Kester [34] derived unidirectional rate constants for complexation, while in the present paper the k value denote the *net* rate of complexation, that is the resultant of simultaneous build-up and breakdown of the Fe(II)–FZ complex. The presently obtained k is fitted from experiments for which the cartridges were FZ-loaded up to 11.4 mmol/L , that is FZ concentrations of circa $200\times$ higher compared to the concentrations used by Lin and Kester [34]. Recalculating k into k_{FZ} , following Lin and Kester ([34], see also Eq. (8) of the present paper), yields $k_{\text{FZ}} = \approx 10^{11}\text{ L}^3\text{ mol}^{-3}\text{ s}^{-1}$ [34] and $\approx 10^4\text{ L}^3\text{ mol}^{-3}\text{ s}^{-1}$ (present results).

Apart from reasoning in net fluxes (see above) the large difference between these two values may be associated to the third-order function of FZ concentration in Fe(II) complexation, as assumed in Eq. (8), which was adopted by Lin and Kester [34] in free solution experiments. In contrast, however, in the present column set-up, FZ is bound to the Si-backbone of the SepPak[®] cartridge, inferring that the formation of Fe(II)FZ₃ asks for the presence of three nearby but fixed FZ molecules. In a number of

Table 2

Kinetic parameters used for modelling of the data: k_{ox} (s^{-1} , Millero et al. [22,39]), k_{red} ($\text{L mol}^{-1}\text{ s}^{-1}$, Millero et al. [35]) and k (s^{-1} , fitted from the present data)

k_{ox} (s^{-1})	2.0E–5
k_{red} ($\text{L mol}^{-1}\text{ s}^{-1}$)	0.35
k (s^{-1})	3.5E–02

reports, fixed groups are interpreted as possibly leading to first-ordered binding functions of metal^{z+} to z nearby ligands[–], which infers that metal bonding is regarded as first-ordered towards ligand/ z [40,41]. Therefore, in the present experiments Fe(II) may have associated into Fe(II)FZ _{x} for $x < 3$ stoichiometries. In addition, Lin and Kester [34] performed their experiments under a N₂/CO₂ mixture, whereas the present experiments were performed in a flow bench under ambient laboratory conditions.

It should be noted that the adopted literature values [35,42] are based on seawater which was different from the seawater presently used in experiments, thus possibly different in its occurrence of natural ligands. These organic ligands are place-dependent as they are at least partly excreted by the marine bacteria [43]. Naturally occurring ligands are known to affect the rate of oxidation and even the formation of the Fe(II)FZ₃ complex [38,44]. Whereas previous studies have made use of Surface Sargasso Seawater [34], Gulf Stream Seawater [35] and Funka Bay (Japan) Seawater [42], the present study made use of water from the Bay of Biscay. The present paper adopted the reported redox constants without further adaptation, and the presented results show that reduction–oxidation and waiting time can have significant effects on the measured Fe(II) concentrations, even in induced reducing conditions where oxidation to Fe(III) should be minimal.

Lin and Kester [34] showed that Fe(II) could be measured by ferrozine analysis and that an excess amount of ferrozine could ensure a complete Fe(II) complexation. But in off-line analysis of Fe(II) the waiting time before this complexation has taken place can significantly alter the outcomes. The present study suggests that waiting time is a highly significant factor that cannot be neglected in any Fe(II) research that includes off-line separation, counting, or time-consuming sample loops. Even at relatively small waiting times our experiments showed the recovery of Fe(II) to be significantly affected by these factors, consequently the present study underlines the necessity of accounting for these factors by time-modelling of overall iron-behaviour. This study gives a mathematical model that can be applied to account for these indiscrepancies.

Acknowledgement

The Netherlands Society for Scientific Research funded this research (NWO), via the Netherlands AntArctic Programme (NAAP, grant 85120004).

References

- [1] M. Chen, R.C.H. Dei, W.X. Wang, G. Laodong, Mar. Chem. (2003) 177.
- [2] L.J.A. Gerringa, H.J.W. De Baar, K.R. Timmermans, Mar. Chem. 4 (2000) 335.
- [3] R.F. Nolting, L.J.A. Gerringa, M.J.W. Swagerman, K.R. Timmermans, H.J.W. De Baar, Mar. Chem. 3–4 (1998) 335.
- [4] K.H. Coale, K.S. Johnson, S.E. Fitzwater, S.P.G. Blain, T.P. Stanton, T.L. Coley, Deep-Sea Res. Part II–Topical Stud. Oceanogr. 6 (1998) 919.
- [5] P.L. Croot, P. Laan, Anal. Chim. Acta 2 (2002) 261.
- [6] J.H. Martin, K.H. Coale, K.S. Johnson, S.E. Fitzwater, R.M. Gordon, S.J. Tanner, C.N. Hunter, V.A. Elrod, J.L. Nowicki, T.L. Coley, R.T. Barber, S. Lindley, A.J. Watson, K. Vanscoy, C.S. Law, M.I. Liddicoat, R. Ling, T. Stanton, J. Stockel, C. Collins, A. Anderson, R. Bidigare, M. Ondrusek,

- M. Latasa, F.J. Millero, K. Lee, W. Yao, J.Z. Zhang, G. Friederich, C. Sakamoto, F. Chavez, K. Buck, Z. Kolber, R. Greene, P. Falkowski, S.W. Chisholm, F. Hoge, R. Swift, J. Yungel, S. Turner, P. Nightingale, A. Hatton, P. Liss, N.W. Tindale, *Nature* 6493 (1994) 123.
- [7] P.L. Croot, M. Johansson, *Electroanalysis* 8 (2000) 565.
- [8] M. Gledhill, C.M.G. Van den Berg, *Mar. Chem.* 1 (1994) 41.
- [9] A.R. Bowie, E.P. Achterberg, R.F.C. Mantoura, P.J. Worsfold, *Anal. Chim. Acta* 3 (1998) 189.
- [10] J.T.M. de Jong, M. Boye, V.F. Schoemann, R.F. Nolting, H.J.W. De Baar, *J. Environ. Monit.* 5 (2000) 496.
- [11] D.A. Weeks, K.W. Bruland, *Anal. Chim. Acta* 1 (2002) 21.
- [12] K.S. Johnson, K.H. Coale, H.W. Jannasch, *Anal. Chem.* 22 (1992) A1065.
- [13] M.J.A. Rijkenberg, A.C. Fischer, J.J. Kroon, L.J.A. Gerringa, K.R. Timmermans, H.Th. Wolterbeek, H.J.W. De Baar, *Mar. Chem.* (2005) 119.
- [14] R.M. Gordon, K.H. Coale, K.S. Johnson, *Limnol. Oceanogr.* 3 (1997) 419.
- [15] E.L. Rue, K.W. Bruland, *Mar. Chem.* 1–4 (1995) 117.
- [16] A.E. Witter, D.A. Hutchins, A. Butler, G.W. Luther, *Mar. Chem.* 1–2 (2000) 1.
- [17] M.T. Maldonado, N.M. Price, *Deep-Sea Res. Part II—Topical Stud. Oceanogr.* 11–12 (1999) 2447.
- [18] D.A. Hutchins, A.E. Witter, A. Butler, G.W. Luther, *Nature* 6747 (1999) 858.
- [19] M.L. Wells, *Limnol. Oceanogr.* 4 (1999) 1002.
- [20] J.F. Briat, I. FobisLoisy, N. Grignon, S. Lobreaux, N. Pascal, G. Savino, S. Thoirion, N. Vonwiren, O. Van Wuytswinkel, *Biol. Cell* 1–2 (1995) 69.
- [21] D.W. King, H.A. Lounsbury, F.J. Millero, *Environ. Sci. Technol.* 3 (1995) 818.
- [22] F.J. Millero, S. Sotolongo, *Geochim. Cosmochim. Acta* 8 (1989) 1867.
- [23] P.L. Croot, A.R. Bowie, R.D. Frew, M.T. Maldonado, J.A. Hall, K.A. Safi, J. La Roche, P.W. Boyd, C.S. Law, *Geophys. Res. Lett.* 18 (2001) 3425.
- [24] D.W. King, J. Lin, D.R. Kester, *Anal. Chim. Acta* 1 (1991) 125.
- [25] H.P. Van Leeuwen, R.M. Town, *Environ. Sci. Technol.* (2005) 7217.
- [26] J.T.M. De Jong, M. Boye, V.F. Schoemann, R.F. Nolting, H.J.W. De Baar, *J. Environ. Monit.* 5 (2000) 496.
- [27] A.R. Bowie, E.P. Achterberg, S. Blain, M. Boye, P.L. Croot, H.J.W. De Baar, P. Laan, G. Sarthou, P.J. Worsfold, *Mar. Chem.* (2003) 19.
- [28] S. Blain, P. Treguer, *Anal. Chim. Acta* (1995) 425.
- [29] A.R. Bowie, E.P. Achterberg, P.N. Sedwick, S. Ussher, P.J. Worsfold, *Environ. Sci. Technol.* 21 (2002) 4600.
- [30] E.P. Achterberg, C.M.G. Van den Berg, *Anal. Chim. Acta* 3 (1994) 213.
- [31] C.M.G. Van den Berg, E.P. Achterberg, *Trac-Trends Anal. Chem.* 9 (1994) 348.
- [32] A.C. Fischer, H.T. Wolterbeek, J.J. Kroon, L.J.A. Gerringa, K.R. Timmermans, J.T. Van Elteren, T. Teunissen, *Sci. Total Environ.* (2005).
- [33] L. Horwitz, *Plant Physiol.* 2 (1958) 81.
- [34] J. Lin, D.R. Kester, *Mar. Chem.* (1992) 283.
- [35] F.J. Millero, M. Gonzalezdavila, J.M. Santanacasio, *J. Geophys. Res.-Atmospheres D4* (1995) 7235.
- [36] K.R. Timmermans, M. Gledhill, R.F. Nolting, M.J.W. Veldhuis, H.J.W. De Baar, C.M.G. Van den Berg, *Mar. Chem.* 3–4 (1998) 229.
- [37] F. Helfferich, *Ion Exchange*. McGraw-Hill Series in Advanced Chemistry, McGraw-Hill Book Company, Inc., New York, 1962, 624 pp.
- [38] A.L. Rose, T.D. Waite, *Environ. Sci. Technol.* 3 (2002) 433.
- [39] F.J. Millero, S. Sotolongo, M. Izaguirre, *Geochim. Cosmochim. Acta* (1987) 793.
- [40] H. Sentenac, C. Grignon, *Plant Physiol.* (1981) 415.
- [41] H.T. Wolterbeek, M. De Bruin, P. Bode, *Cell Environ.* (1987) 297.
- [42] K. Kuma, S. Nakabayashi, K. Matsunaga, *Water Res.* 6 (1995) 1559.
- [43] H.M. Macrellis, C.G. Trick, E.L. Rue, G. Smith, K.W. Bruland, *Mar. Chem.* 3 (2001) 175.
- [44] J.M. Santana-Casiano, M. Gonzalez-Davila, M.J. Rodriguez, F.J. Millero, *Mar. Chem.* 1–3 (2000) 211.

Microwave-enhanced electro-deposition and stripping of palladium at boron-doped diamond electrodes

Mohamed A. Ghanem^{a,1}, Harriet Hanson^a, Richard G. Compton^b,
Barry A. Coles^b, Frank Marken^{a,*}

^a Department of Chemistry, University of Bath, Bath BA2 7AY, UK

^b Physical and Theoretical Chemistry Laboratory, Oxford University, South Parks Road, Oxford OX1 3TU, UK

Received 8 April 2006; received in revised form 14 September 2006; accepted 27 September 2006

Available online 30 October 2006

Abstract

In situ microwave activation has been applied to the electro-deposition and stripping of palladium metal (which is widely used as a catalyst) at cavitation resistant boron-doped diamond electrodes. Focused microwave radiation leading to heating, boiling, and cavitation is explored as an option to improve the speed and sensitivity of the analytical detection procedure. The deposition and anodic stripping of palladium by linear sweep voltammetry in 0.1 M KCl (pH 2) solution and at boron-doped diamond electrodes is shown to be strongly enhanced by microwave activation due to both (i) the increase in mass transport and (ii) the increase in the kinetic rate of deposition and stripping.

The temperature at the electrode surface is calibrated with the reversible redox couple $\text{Fe}(\text{CN})_6^{4-}/\text{Fe}(\text{CN})_6^{3-}$ and found to be reach 380 K. In the presence of microwave radiation, the potential of onset of the deposition of palladium is strongly shifted positive from -0.4 to $+0.1$ V versus SCE. The optimum potential for deposition in the presence of microwaves is -0.4 V versus SCE and the anodic stripping peak current is shown to increase linearly with deposition time. Under these conditions, the stripping peak current varies linearly with the palladium concentration down to ca. $2 \mu\text{M}$. At concentration lower than this a logarithmic variation of the stripping peak current with concentration is observed down to ca. $0.1 \mu\text{M}$ (for 5 min pre-concentration in presence of microwave radiation).

© 2006 Elsevier B.V. All rights reserved.

Keywords: Microwave; Boron-doped diamond; Linear sweep voltammetry; Palladium; Deposition; Stripping; Sensor

1. Introduction

Over the recent years several methods have been proposed to introduce in situ thermal activation into electrochemical experiments. These methods have been based on (i) laser pulse heating [1], (ii) rf-heating of microelectrodes [2] or macroelectrodes [3], (iii) “hot wire” electrodes [4], and thin film heating [5,6]. They have in common that only the electrode or a very small solution volume in the vicinity of the electrode is heated in order to minimize sample degradation and handling while improving sensitivity and speed. The benefits of thermal activation in electroanalytical processes have been exploited for example in analytical stripping voltammetry [7].

The activation of electrochemical processes by focused microwave radiation has been proposed to achieve both a high rate of mass transport and highly localized heating in a small solution phase region within the diffusion layer at electrode–solution interface. Both, dielectric heating of the solution phase (for metal electrodes) and direct heating of the electrode (for non-metallic electrodes) has been observed and models have been developed to account for the temperature effects and the electrochemical current enhancements [8–10]. It has been demonstrated that in the high temperature zone at the electrode surface, mass transport is enhanced in approximately equal amounts by (i) the temperature effect on rate of diffusion and (ii) by additional convection in the presence of temperature and viscosity gradients. Microwave activation of electrochemical processes has been studied in aqueous solutions [11,12], in organic solvents [13], in ionic liquids [14], and in micellar solutions [15]. Various types of electrodes such as platinum, gold, glassy carbon, or boron-doped

* Corresponding author. Tel.: +44 1225 383694.

E-mail address: f.marken@bath.ac.uk (F. Marken).

¹ Permanent address: Science & Math. Department, Faculty of Petroleum & Mining Engineering, Suez, Egypt.

diamond have been employed [16] as well as array electrode systems [17]. One particular benefit of microwave activation in electroanalysis is that only highly localized effects occur and that conventional equipment, electrodes, and procedures are employed which are readily interfaced to a microwave source.

Palladium is a catalytically active component released from automotive catalytic converters [18,19] or potentially introduced into synthetic products such as drugs via synthetic catalysts. Palladium has the ability to undergo bioaccumulation [20]. The release of palladium for example from diesel engines has been estimated as 250 ng palladium per kilometer [21] for new engines. Anodic stripping methods can be very sensitive and have been developed to determine palladium in the presence of gold [22] or in the presence of other platinum group metals [23]. Usually, several metals such as palladium, rhodium, and platinum are found together and determined individually. In this study we only consider palladium as a model system for this group of analytes and we explore the effects introduced by microwave heating. The stripping voltammetry method is employed based on a pre-concentration step (by electrodepositing the metal) followed by a detection step (quantitative anodic stripping). Low detection limits as well as relatively inexpensive instrumentation makes electrochemical stripping analysis an important and commonly used tool for the trace metal determination [24] and it is demonstrated here that the application of focused microwave heating can further improve this methodology.

In this report we explore the effects of microwave activation on the electro-deposition and stripping of palladium on boron-doped diamond electrodes which are relatively inert towards cavitation erosion [25]. Due to their inert surface characteristics and wide potential window, boron-doped diamond electrodes have been increasingly used for metal pre-concentration and anodic stripping processes. They offer advantages over other type of carbon-based electrode materials due to their mechanical strength and extreme hardness which can resist any damage caused by boiling liquid and cavitation in the presence of microwave radiation [26].

The effect of microwave activation has been previously investigated for cadmium accumulation in mercury [27], for copper electro-deposition onto platinum [28], and for the stripping voltammetry of Pb and PbO₂ using boron-doped diamond electrodes [29,30]. In this paper we report the effect of microwaves on the pre-concentration and stripping of Pd metal using cyclic voltammetry. Both, the electro-deposition and stripping processes are shown to be enhanced at boron-doped diamond of 500 μm × 500 μm size. The nucleation and growth of palladium on boron-doped diamond is strongly affected and detrimental effects of hydrogen evolution are shown to ultimately limit the efficiency of the process under microwave conditions. Without further optimization, detection of palladium down to concentrations of 0.1 μM were readily achieved using linear sweep voltammetry in the presence of microwave activation and accumulation times of 5 min.

2. Experimental

2.1. Chemical reagents

PdCl₂, KCl, HCl, potassium ferrocyanide, and potassium ferricyanide were obtained from Aldrich and used without further purification. Demineralised and filtered water of resistivity not less than 18 MΩ cm was taken from an Elga water purification system. Argon (Pure shield, BOC) was employed for de-aeration of electrolyte solutions.

2.2. Instrumentation

Scanning electron microscopy images were obtained on a JEOL JSM6310 system. A conventional three-electrode micro-Autolab III potentiostat system (Eco Chemie, NL) was employed to control the potential at the working electrode. A boron-doped diamond electrode (BDD) of 500 μm × 500 μm area was employed (supplied by Element Six Ltd., UK). In order to prepare the electrode, a boron-doped diamond rod 5 mm long was connected to a copper wire using silver paint and then coated with a thin layer of Torr Seal ceramic epoxy (Varian, USA) followed by sealing into heat resistant two-component epoxy E14A and E14B (Bondmaster, UK) and mounted in 5 mm diameter glass tube. The electrode was polished with 1 micron diamond abrasive to expose the boron-doped diamond electrode surface. A saturated calomel electrode (SCE, Radiometer) was used as the reference electrode and platinum gauze as the counter electrode in a flow through configuration reported elsewhere [31]. Only the working electrode placed in a small volume Teflon cell is exposed to microwave radiation. Details of the cell design; vacuum degassing, and application of microwaves have been reported previously [24]. The flow rate was typically 0.65 mL min⁻¹ and did not affect the voltammetric current measurements. Prior to each experiment the working electrode was polished with aqueous slurries of 1 μm diamond on a polishing cloth followed by thorough rinsing with deionised water. In order to remove any diamond particles left on the surface, the electrode was further polished on a clean, wet polishing cloth (Buehler, UK) and again rinsed with water. A Panasonic multi-mode microwave oven (NN-3456, 2.45 GHz) with modified power supply, a water energy sink, and a port for the electrochemical cell was used [24]. The microwave intensity was controlled via the anode current of the magnetron. Special care is required when metal objects are placed into a microwave cavity. Before and during operation, the system was tested for leaking microwave radiation with a radiation meter.

3. Results and discussion

3.1. Temperature and mass transport calibration for boron-doped diamond electrodes in the presence of microwaves

Microwave radiation induces primarily localized temperature effects which then lead to convection and mass transport phenomena. These effects can be investigated and “calibrated”

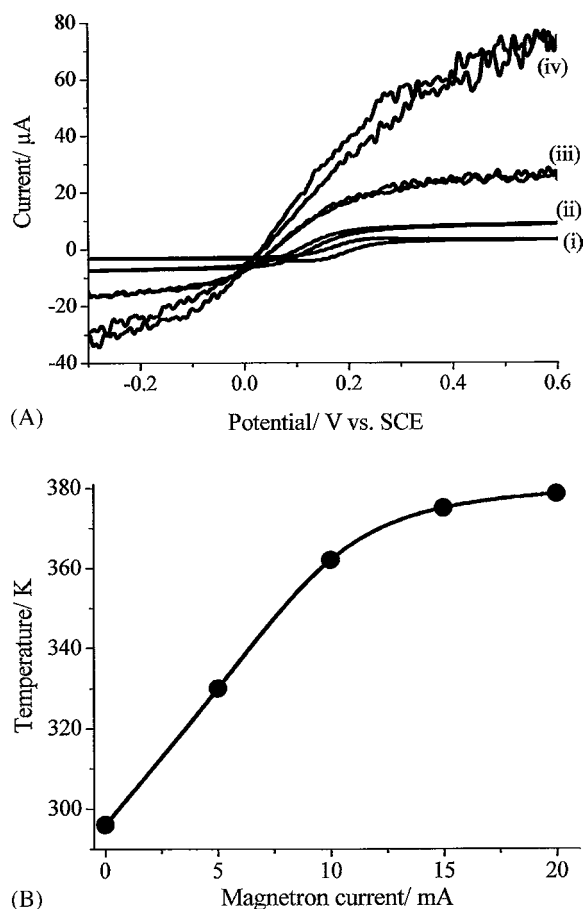


Fig. 1. (A) Cyclic voltammograms (scan rate 50 mV s^{-1}) for the oxidation and reduction of $5 \text{ mM Fe(CN)}_6^{4-}/5 \text{ mM Fe(CN)}_6^{3-}$ in aqueous 0.1 M KCl , pH 2, obtained at a $500 \mu\text{m} \times 500 \mu\text{m}$ diameter BDD electrode in the presence of microwave radiation (magnetron current (i) 0 mA , (ii) 5 mA , (iii) 10 mA , (iv) 15 mA). (B) Plot of the variation of $T_{\text{electrode}}$ as a function of microwave intensity at BDD disc electrode in solution of $5 \text{ mM Fe(CN)}_6^{4-}/5 \text{ mM Fe(CN)}_6^{3-}$ and 0.1 M KCl (pH 2).

for each type of electrode with a suitable reversible redox system [24]. The calibration of the boron-doped diamond electrode surface temperature, $T_{\text{electrode}}$, was achieved here by monitoring the equilibrium potential of the $\text{Fe(CN)}_6^{3-/4-}$ redox system. Fig. 1A shows that the application of microwave radiation to a solution containing the $\text{Fe(CN)}_6^{3-/4-}$ redox system enhances the magnitude of anodic and cathodic currents and causes a equilibrium potential shift to more negative potentials as the temperature increases. The microwave enhancement is dependent on electrode type and material [24]. Fig. 1A shows typical current responses in the absence and in the presence of microwave radiation at boron-doped diamond electrode (area = $500 \mu\text{m} \times 500 \mu\text{m}$) for the oxidation of $5 \text{ mmol dm}^{-3} \text{ Fe(CN)}_6^{4-}$ and for the reduction of $5 \text{ mmol dm}^{-3} \text{ Fe(CN)}_6^{3-}$ in $0.1 \text{ mol dm}^{-3} \text{ KCl}$ aqueous solution (pH 6.5). At room temperature and in the absence of microwave radiation, the oxidation or reduction currents are typically $3.0 \mu\text{A}$. In the presence of low and moderate microwave intensities (curves (ii) and (iii)) a significant shift in the equilibrium potential (the potential at zero current) and an enhancement of the mass transport current (10-fold) was observed. At higher microwave intensities

(curve (iv)), only a slight further shift in equilibrium potential occurs while a considerable further increase in mass transport (30-fold) is achieved [32]. The shift in equilibrium potential may be measured more accurately by zero current potentiometry and employed to obtain an estimate of the temperature at the boron-doped diamond electrode surface, $T_{\text{electrode}}$. By external calibration (with conventional heating and employing the same cell) the relationship $dE_{\text{equilibrium}}/dT = -1.8 \pm 0.2 \text{ mV K}^{-1}$ is obtained for aqueous ferricyanide/ferricyanide in 0.1 M KCl consistent with earlier results [8]. Fig. 1B shows the estimated electrode temperature, $T_{\text{electrode}}$, as a function of the applied microwave power (expressed as magnetron anode current). The boron-doped diamond electrode surface temperature reached approximately 380 K at a microwave radiation intensity generated by 15 mA magnetron anode current, consistent with the onset of solution boiling. This is confirmed by the enhanced noise level observed superimposed on limiting currents for curves (iii) and (iv). Mass transport effects are further increased upon increasing the microwave power due to more violent boiling. These effects are observed only when a suitable vacuum degassing system is employed (see Section 2).

3.2. Palladium deposition and stripping processes at boron-doped diamond electrodes in the presence of microwaves

Palladium ions, Pd(II) , in acidic chloride aqueous media exist as PdCl_4^{2-} complex anions [33] and are reduced at boron-doped diamond electrodes in a two-electron process (Eq. (1)) [34]:



Fig. 2 shows a typical set of cyclic voltammograms obtained for the reduction and anodic stripping of $100 \mu\text{M PdCl}_4^{2-}$ in aqueous 0.1 M KCl (pH 2) at a boron-doped diamond electrode in the absence and in the presence of different intensities of microwave radiation. The results show that in the absence of microwave radiation (dashed curve (i)) the Pd deposition commences at ca -0.4 V versus SCE and hydrogen evolution onset is at -0.5 V versus SCE. The limiting reduction current for PdCl_4^{2-} ($3.0 \mu\text{A}$) and the anodic Pd stripping peak (peak at 0.5 V versus SCE) are hardly visible without microwave activation. Upon application of microwave activation (curves (ii)–(iv)) a significant positive shift of the onset of Pd deposition (to $+0.17 \text{ V}$ versus SCE at 10 mA magnetron current) is observed. This shift in deposition potential is due to an enhancement in the nucleation kinetics. The ratio of the charge under anodic region to the cathodic region is typically 85% which may be attributed to some loss of efficiency due to the hydrogen evolution process. The deposition as well as the anodic stripping peak are significantly affected by microwave activation (vide infra). Also the onset of the hydrogen evolution process in the presence of microwave radiation is significantly shifted to more positive potential (to -0.2 V versus SCE at 10 mA magnetron current, see Fig. 2Aiv).

Both the enhanced deposition current (due to fast mass transport) and the faster nucleation process (due to the increase in

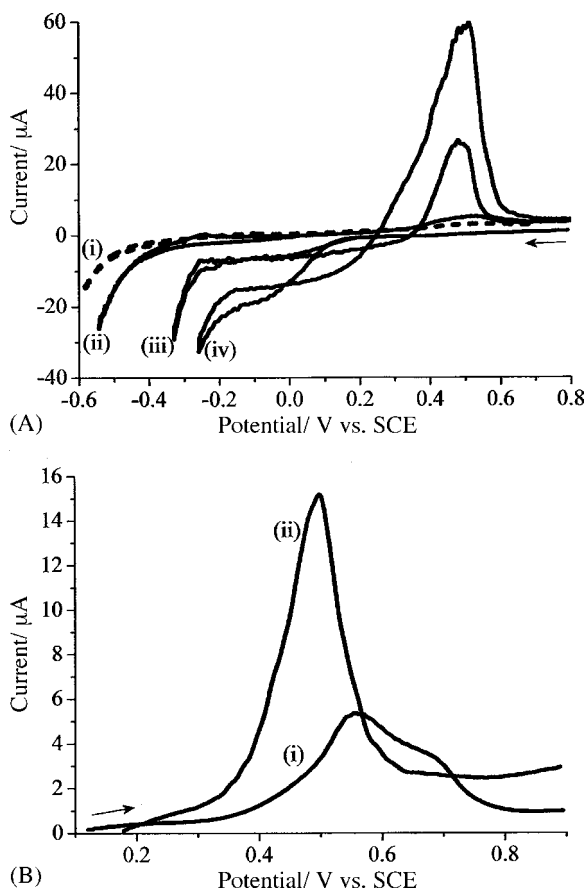


Fig. 2. (A) Cyclic voltammograms (scan rate 50 mV s^{-1}) for the pre-concentration and stripping of $100 \mu\text{M PdCl}_4^{2-}$ in aqueous 0.1 M KCl (pH 2) at a $500 \mu\text{m} \times 500 \mu\text{m}$ diameter diamond disc electrode in the presence of microwave radiation (magnetron current (i) 0 mA , (ii) 3 mA , (iii) 5 mA , (iv) 10 mA). (B) Cyclic voltammograms (scan rate 50 mV s^{-1}) for the microwave effect on the stripping of Pd deposited at diamond electrode, accumulation potential at -0.4 V vs. SCE for 5 min in presence of 10 mA microwave power. Deposition solution $100 \mu\text{M PdCl}_4^{2-}$ in aqueous 0.1 M KCl (pH 2), magnetron current (i) 0 mA , (ii) 10 mA .

temperature) result in more effective anodic stripping analysis. In addition, the Pd stripping peak becomes well-defined in the presence of microwaves. Fig. 2B shows stripping voltammograms obtained for the same type and amount of palladium and with (ii) and without (i) microwave radiation (deposited from $100 \mu\text{M PdCl}_4^{2-}$ in 0.1 M KCl (pH 2) at -0.4 V versus SCE for 5 min in presence of microwaves produced by a 10 mA magnetron current). The application of microwave activation remarkably accelerates the Pd metal dissolution process and a three-fold higher stripping peak current was recorded. Also the area under the stripping peak is increased in the presence of microwaves presumably due to faster removal of palladium metal from the electrode surface.

A typical SEM image of the resulting palladium deposit is shown in Fig. 3 (deposited from $10 \text{ mM PdCl}_4^{2-}$ in 0.1 M KCl (pH 2) at -0.4 V versus SCE for 10 min in presence of microwave intensity produced by 10 mA magnetron current). A thin polycrystalline palladium film is coated onto the $500 \mu\text{m} \times 500 \mu\text{m}$ electrode which is slightly protruding. The “edge-diffusion” effect is responsible for more extensive growth of palladium at the electrode edges. A pattern of non-uniform thickness is apparent and this is consistent with boron-doped diamond crystal grains creating heterogeneous reactivity across the electrode surface. Fig. 3C shows that palladium grown in the absence of microwaves forms poorly crystalline and much thinner deposit.

3.3. Optimization of the palladium deposition and stripping processes at boron-doped diamond electrodes in the presence of microwaves

Next, the palladium deposition conditions are optimized in order to improve the signal from the anodic stripping process. The dependence of anodic stripping peak current on the deposition potential applied to the boron-doped diamond electrode was investigated in presence of microwave radiation and over the potential range from 0.0 to 0.8 V versus SCE. The plots shown in Fig. 4A show the relation between the Pd deposition potential

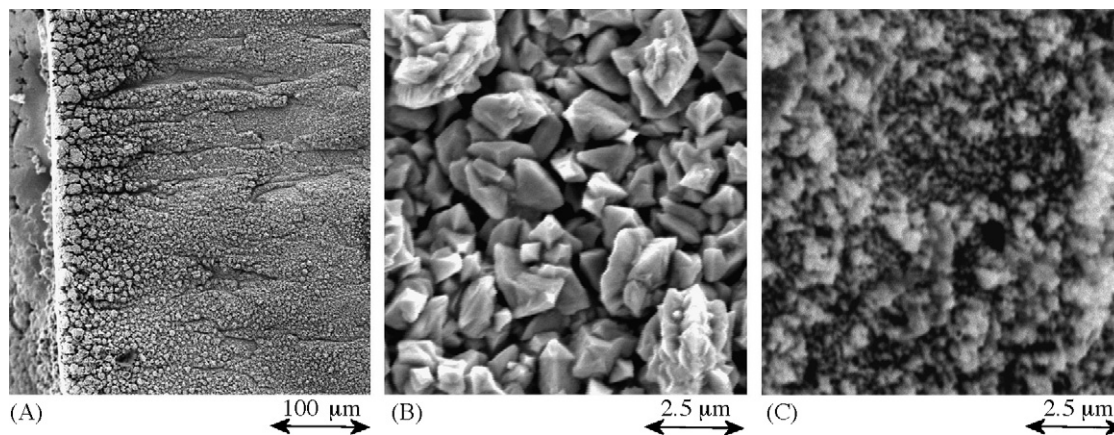
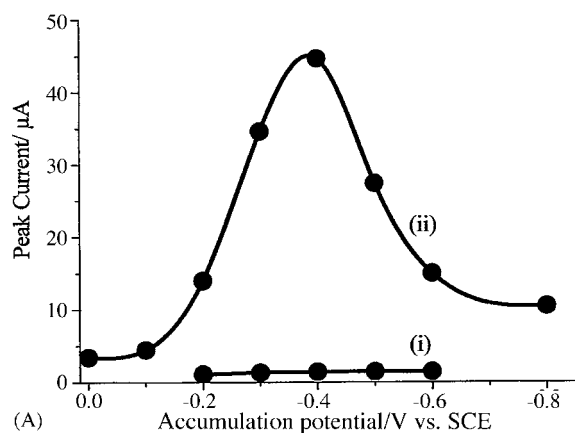
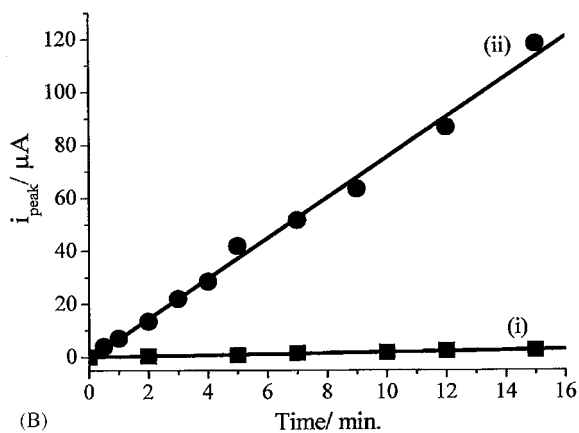


Fig. 3. SEM surface images for Pd deposited onto $500 \mu\text{m} \times 500 \mu\text{m}$ boron-doped diamond with (A) low magnification and (B) high magnification obtained in the presence of microwave power generated by 10 mA magnetron current (deposition time 10 min at -0.4 V vs. SCE , $10 \text{ mM PdCl}_4^{2-}$ in 0.1 M KCl at pH 2). (C) shows the Pd deposit obtained without microwave activation with otherwise identical conditions.



(A)

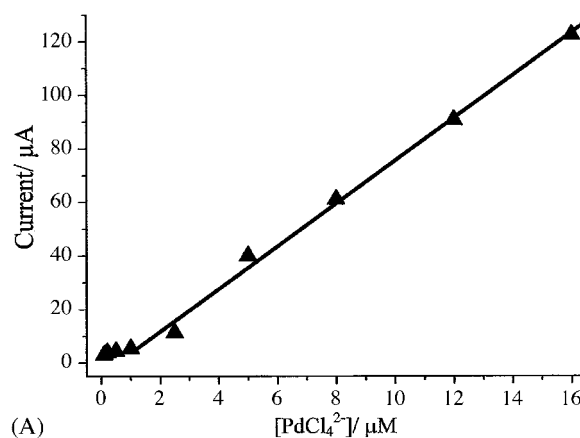


(B)

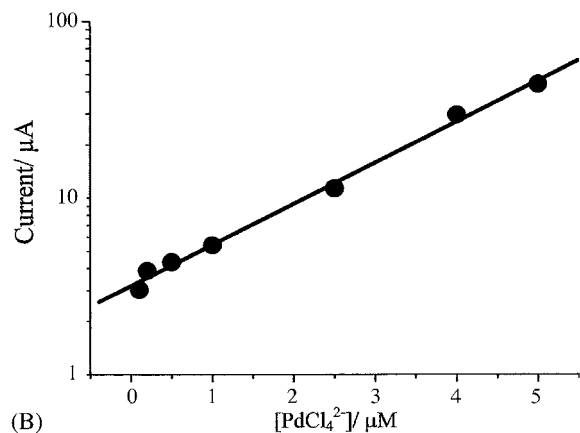
Fig. 4. (A) Effect of accumulation potential on the stripping peak current in absence (i) and in presence (ii) of microwave radiation generated by 10 mA magnetron current. Pd was deposited for 5 min from $5 \mu\text{M PdCl}_4^{2-}$ in 0.1 M KCl (pH 2). (B) Relation between the accumulation time and the stripping peak current (i) in the absence and (ii) in the presence of microwave radiation (obtained with 10 mA magnetron current) observed at a $500 \mu\text{m} \times 500 \mu\text{m}$ boron-doped diamond electrode immersed in $5 \mu\text{M PdCl}_4^{2-}$ in 0.1 M KCl at pH 2 (deposition potential at -0.4 V vs. SCE).

and stripping peak current obtained in the absence (curve (i)) and in the presence (curve (ii)) of microwaves (intensity generated by 10 mA magnetron current). The deposition was performed from a solution containing $5 \mu\text{M PdCl}_4^{2-}$ in 0.1 M KCl (pH 2) and a deposition (accumulation) time of 5 min was employed. The plots clearly show that in presence of microwave radiation, the stripping peak currents increase sharply reaching a maximum at -0.4 V versus SCE. When the deposition potential was chosen more negative than -0.4 V versus SCE, the peak current decreased rapidly, which may be attributed to the fact that the hydrogen evolution reaction interferes with the deposition process. In the absence of microwave radiation, the anodic stripping peak current was approximately constant, $2 \mu\text{A}$, over this potential range. It is interesting to note that the maximum at -0.4 V versus SCE is well into the hydrogen evolution region (compare Fig. 2Aiv) and may actually result from the effect of hydrogen gas bubble formation.

Fig. 4B shows the dependence of the anodic stripping peak current on the deposition (accumulation) time in absence (curve (i)) and in presence (curve (ii)) of microwave intensity generated



(A)



(B)

Fig. 5. Plots of (A) the peak current for the Pd stripping response vs. concentration and (B) for lower concentrations, the logarithm of the peak current for the Pd concentration vs. the concentration (conditions as in Fig. 4).

by 10 mA magnetron current. The plot shows a good linear relationship between accumulation time and stripping peak current with a slope of 7.6 and 0.17 in presence and absence of microwave radiation, respectively. This difference is consistent with a combination of mass transport and kinetic effects.

The concentration dependence of the anodic stripping peak for palladium is linear as expected. This allows conventional standard addition procedures to be employed. Fig. 5A shows the peak current as a function of concentration over a wide range of concentrations. Only for palladium concentrations lower than $5 \mu\text{M}$ a deviation from linearity is observed. However, as shown in Fig. 5B, for the concentration range from 0.1 to $5 \mu\text{M}$, the logarithmic plot of the Pd stripping peak current versus PdCl_4^{2-} concentration appears to be linear (at a deposition potential of -0.4 V versus SCE and an accumulation time of 5 min in presence of microwave generated by 10 mA magnetron current). The unusual logarithmic relationship, which allows the limit of detection to be further reduced, is likely to reflect slow initial nucleation-growth kinetics and competition to hydrogen evolution at very low concentrations of palladium. Literature methods for the electroanalytical palladium determination based on suitable complexing agents have been reported with limits of detection approaching 500 nM [22] and even below 50 nM [23], but the simple microwave-enhanced anodic stripping procedure with 5 min accumulation described

here is already approaching a similar level of trace level sensitivity without additional reagents.

Although a considerable effect of microwave radiation on the deposition and stripping of palladium on boron-doped diamond has been demonstrated, further work will be required to optimize the methodology (type and diameter of electrode, electrolyte composition, etc.) for specific applications.

4. Conclusions

It has been shown that microwave radiation applied to boron-doped diamond electrodes strongly affects the deposition and stripping processes for palladium. Both temperature and mass transport effects are observed and exploited. The relatively simple introduction of localized thermal activation via microwave radiation into electrochemical systems and sensors provides a general future platform for the improvement of electroanalytical procedures and it is suggested that in particular with low power focused microwave devices a wider range of analytical problems may benefit.

Acknowledgements

This work was funded by the EPSRC (GR/S06349/01) and undertaken as part of the EU sponsored COST Programme (Action D32, working group D32/005/04, "Microwave and Ultrasound Activation in Chemical Analysis"). W.L. Gore & Associates (UK) Ltd. are gratefully acknowledged for the generous supply of porous PTFE degassing tubing.

References

- [1] F.L. Qiu, R.G. Compton, F. Marken, S.J. Wilkins, C.H. Goeting, J.S. Foord, *Anal. Chem.* 72 (2000) 2362.
- [2] A.S. Baranski, *Anal. Chem.* 74 (2002) 1294.
- [3] B.A. Coles, M.J. Moorcroft, R.G. Compton, *J. Electroanal. Chem.* 513 (2001) 87.
- [4] P. Gründler, D. Degenring, *J. Electroanal. Chem.* 512 (2001) 74.
- [5] O. Korb, M. Buckova, P. Tarapcik, J. Labuda, P. Gründler, *J. Electroanal. Chem.* 506 (2001) 143.
- [6] G.U. Flechsig, O. Korb, S.B. Hocevar, S. Thongngamdee, B. Ogorevc, P. Gründler, J. Wang, *Electroanalysis* 14 (2002) 192.
- [7] G.U. Flechsig, O. Korb, P. Gründler, *Electroanalysis* 13 (2001) 786.
- [8] F. Marken, Y.C. Tsai, S.L. Matthews, R.G. Compton, *New J. Chem.* 24 (2000) 653.
- [9] R.G. Compton, B.A. Coles, F. Marken, *Chem. Commun.* (1998) 2595.
- [10] F. Marken, S.L. Matthews, R.G. Compton, B.A. Coles, *Electroanalysis* 12 (2000) 267.
- [11] U.K. Sur, F. Marken, N. Rees, B.A. Coles, R.G. Compton, R. Seager, *J. Electroanal. Chem.* 573 (2004) 175.
- [12] U.K. Sur, F. Marken, R.G. Compton, B.A. Coles, *New J. Chem.* 28 (2004) 1544.
- [13] Y.C. Tsai, B.A. Coles, R.G. Compton, F. Marken, *J. Am. Chem. Soc.* 124 (2002) 9784.
- [14] U.K. Sur, F. Marken, B.A. Coles, R.G. Compton, J. Dupont, *Chem. Commun.* (2004) 2816.
- [15] M.A. Ghanem, R.G. Compton, B.A. Coles, A. Canals, F. Marken, *Analyst* 130 (2005) 1425.
- [16] U.K. Sur, F. Marken, R. Seager, J.S. Foord, A. Chatterjee, B.A. Coles, R.G. Compton, *Electroanalysis* 17 (2005) 385.
- [17] M.A. Ghanem, F. Marken, B.A. Coles, R.G. Compton, *J. Solid State Electrochem.* 9 (2005) 809.
- [18] C. Locatelli, *Electroanalysis* 17 (2005) 140.
- [19] B. Sures, S. Zimmermann, J. Messerschmidt, A. Von Bohlen, *Ecotoxicology* 11 (2002) 385.
- [20] S. Zimmermann, B. Sures, *Environ. Sci. Poll. Res.* 11 (2004) 194.
- [21] M. Palacios, M.M. Gomez, M. Moldovan, G. Morrison, S. Rauch, C. McLeod, R. Ma, J. Laserna, P. Lucena, S. Caroli, A. Alimonti, F. Petrucci, B. Bocca, P. Schramel, S. Lustig, M. Zischka, U. Wass, B. Stenbom, M. Luna, J.C. Saenz, J. Santamaria, *Sci. Total Environ.* 257 (2000) 1.
- [22] Y.X. Zhang, C.M. Wang, Y.M. Qu, *Mikrochim. Acta* 1 (1984) 291.
- [23] C. Locatelli, *Anal. Chim. Acta* 557 (2006) 70.
- [24] J. Wang, *Stripping Analysis: Principal, Instrumentation and Application*, VCH Publishers, Dearfield Beach, USA, 1985.
- [25] R.G. Compton, J.S. Foord, F. Marken, *Electroanalysis* 15 (2003) 1349.
- [26] K.B. Holt, J. Del Campo, J.S. Foord, R.G. Compton, F. Marken, *J. Electroanal. Chem.* 513 (2001) 94.
- [27] Y.C. Tsai, B.A. Coles, R.G. Compton, F. Marken, *Electroanalysis* 13 (2001) 639.
- [28] U.K. Sur, F. Marken, B.A. Coles, R.G. Compton, *New J. Chem.* 28 (2004) 1544.
- [29] Y.C. Tsai, B.A. Coles, K. Holt, S. Foord, F. Marken, R.G. Compton, *Electroanalysis* 13 (2001) 831.
- [30] F. Marken, Y.C. Tsai, A.J. Saterlay, B.A. Coles, D. Tibbetts, K. Holt, C.H. Goeting, J.S. Foord, R.G. Compton, *J. Solid State Electrochem.* 5 (2001) 313.
- [31] F. Marken, U.K. Sur, B.A. Coles, R.G. Compton, *Electrochim. Acta* 51 (2006) 2195.
- [32] The asymmetry observed for anodic, and cathodic limiting currents observed at boron-doped diamond under microwave conditions is unexplained (see Fig. 1A) and not observed at platinum electrodes. The effect occurs for several redox systems and remains to be further investigated.
- [33] D.T. Ritchens, *The Chemistry of Aqua Ions*, Wiley, New York, 1997, p. 499.
- [34] C. Batchelor-McAuley, C.E. Banks, A.O. Simm, T.G.J. Jones, R.G. Compton, *Analyst* 131 (2006) 106.

Voltammetric determination of anabolic steroid nandrolone at gold nanoparticles modified ITO electrode in biological fluids

Rajendra N. Goyal^{a,*}, Munetaka Oyama^b, Anuradha Tyagi^a, Sudhanshu P. Singh^a

^a Department of Chemistry, Indian Institute of Technology Roorkee, Roorkee 247 667, India

^b Division of Research Initiatives, International Innovation Center, Nishikyo-Ku, Kyoto 615-8520, Japan

Received 13 September 2006; received in revised form 3 October 2006; accepted 3 October 2006

Available online 13 November 2006

Abstract

The electrochemical behavior of nandrolone decanoate (ND) at gold nanoparticles modified indium tin oxide (ITO) electrode was investigated. Oxidation of ND has been carried out in phosphate containing supporting electrolyte in the pH range 2.1–9.2 and a well-defined oxidation peak was noticed. The peak potential (E_p) of the oxidation peak decreases linearly with increasing pH. Linear calibration curve is obtained over the nandrolone decanoate concentration range of 50 nM to 1.5 μ M at pH 7.2 with a detection limit of 1.36×10^{-7} M. The proposed method is effectively applied to detect the concentration of ND in human blood serum and urine samples after 24 and 72 h of intramuscular injection. The method is rapid and does not require any pre-treatment.

© 2006 Elsevier B.V. All rights reserved.

Keywords: Gold nanoparticles modified ITO electrode; Nandrolone decanoate; Voltammetric detection; Biological fluids

1. Introduction

Nandrolone is an anabolic steroid that differs from testosterone by lacking a methyl group that attached to carbon 10 of the steroid nucleus. Two ester derivatives of nandrolone, viz., nandrolone decanoate (ND) of half life 6 days and nandrolone phenylpropionate (NP) of half life 4.3 h are well known. The esters of steroids are normally used to increase their half lives. NP has moderate duration of action and is used in the treatment of metastatic breast cancer and severe growth retardation in children. However, ND has long duration of action and is used in the treatment of HIV-AIDS related wasting diseases [1–5] resulted in greater increase in fat free mass (FFM). It also has anabolic effects that are more pronounced than its androgenic effect and hence enhances the bone mineral density (BMD) [6–8], haemoglobin levels and muscle mass [9–10] in human. Apart from this ND is also one of the popular doping agent among athletes and body builders [10,11] as it increases muscle mass. It is effective for the treatment of several types of osteoporosis [12–15] and also regulates neuromuscular activity

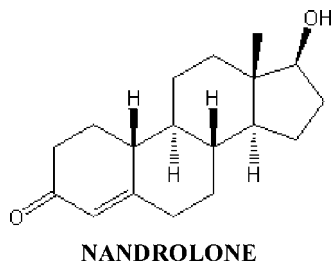
[16–18] in human system. ND reduces lipoprotein concentration in hemodialysis patients [14,19,20], induces erythropoiesis [21,22] and hence effective in the treatment of anemia. High doses of ND reduce volume of testis and length of seminiferous tubules in male rats [23] and affect the sexual cycle in female rats [24].

In view of the medicinal importance and increased abuse of ND by athletes, it is desirable to estimate its concentration in human urine and blood samples. In recent years, several chromatographic–spectrometric techniques [25–28] are generally used to detect doping agents and their metabolites in athletes urine. Although these methods are extremely powerful, require extensive pretreatment of urine [29] and time consuming extraction steps. Derivatization is an unavoidable requirement for GC–MS analysis of urine samples.

Electrochemical determination has shown to be a powerful method for the detection of a wide range of analytes including steroids. Jin et al. [11] have carried out adsorption voltammetry of nandrolone phenylpropionate (NP) at hanging mercury drop electrode (HDME). Use of gold nanoparticles modified ITO electrode could be beneficial since it renders certain advantages such as decrease of the oxidation potential required for the electrochemical reaction to occur and enhancement of the sensitivity due to catalytic activity [30,31]. The aim of the present

* Corresponding author. Tel.: +91 1332 285794; fax: +91 1332 273560.
E-mail address: mngcyfcy@iitr.ernet.in (R.N. Goyal).

work is to develop a simple and sensitive voltammetric method that could be adopted for the detection of ND in body fluids such as blood serum and urine. In the present method differential pulse voltammetry (DPV), one of the popular techniques for the analysis of trace amounts has been used to determine ND.



2. Experimental

2.1. Reagents

Nandrolone decanoate (ND) Injection I.P (Clinical ampoules) were purchased from Ind-Swift Limited (H.P) India. A new injection of ND was used each day before starting each set of experiments.

2.2. Apparatus and procedure

The differential pulse voltammetric experiments were carried out at room temperature ($27 \pm 2^\circ\text{C}$) using three-electrode single compartment cell equipped with a gold nanoparticles modified ITO (geometric area $\sim 0.0314\text{ cm}^2$) working electrode, platinum wire counter electrode and Ag/AgCl (3 M NaCl) reference electrode (Model BAS MF-2052 RB-5B). Gold nanoparticles modified ITO electrodes were prepared by the method reported in the literature [32]. Phosphate buffers in the pH range 2.1–9.2, ionic strength ($\mu = 1.0\text{ M}$) were prepared according to the method reported by Christian and Purdy [33]. BAS (Bioanalytical systems, West Lafayette, USA) CV-50W Voltammetric analyzer controlled via a computer by its own software was used for measurements. Optimized differential pulse voltammetry (DPV) parameters used were: sweep rate 20 mV/s, pulse amplitude 5 mV, sample width 20 ms, pulse width 50 ms, pulse period 200 ms, quiet time 2 s, sensitivity 100 nA/V, initial potential 0 mV, final potential 1000 mV. Concentration of ND in one clinical ampoule was 58 mM (25 mg/1 mL) and was diluted with double distilled water to prepare stock solution of 4 mM.

2.3. Sample preparation

Urine and blood samples from the patients undergoing treatment with ND were obtained from the local hospital of the Institute. The blood with EDTA as anticoagulant was ultra centrifuged (1000 rpm for 10 min) and the supernatant blood serum was used to determine ND concentration using voltammetric technique. Urine as well as blood samples were used after dilution with buffer of pH 7.2 by 100 times.

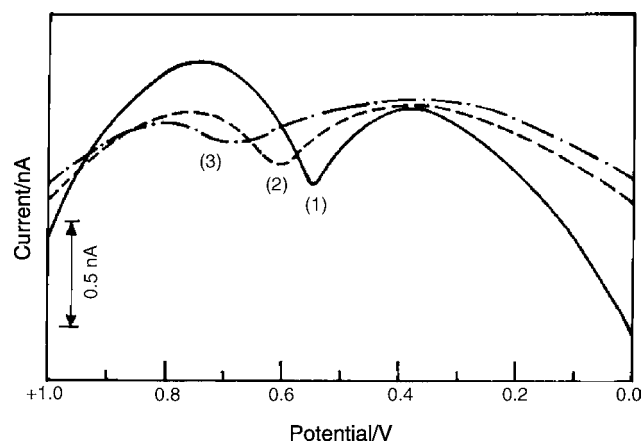


Fig. 1. Differential pulse voltammograms of ND at pH 7.2 at (1) gold nanoparticles modified ITO electrode (—), (2) bare Au electrode (---) and (3) bare ITO electrode (— · —).

3. Results and discussion

To characterize the surface of modified ITO for the deposition of nanogold particles, field emission scanning electron micrographs were recorded at low and high magnification. It was found that spherical nanogold particles (diameter 50–60 nm) were evenly dispersed on the surface of ITO. Differential pulse voltammograms of ND were recorded at gold nanoparticles modified ITO electrode. A single well-defined, oxidation peak was obtained over the entire pH range studied. A comparison of voltammograms at bare ITO, bare Au and gold nanoparticles modified ITO electrode is presented in Fig. 1 and clearly suggests that the nanogold modified electrode catalyzes the oxidation of ND by increasing peak current and shifting the E_p to less positive potential.

3.1. Effect of pH

Effect of pH was studied on the peak potential (E_p) of oxidation peak of ND (2 mM) in the pH range 2.1–9.2 at a sweep rate 20 mV/s a typical differential pulse voltammograms observed for ND is presented in Fig. 1. The E_p of oxidation peak of ND occurs at a potential of $\sim 570\text{ mV}$ at pH 7.2. The peak potential of ND was found to be dependent on pH and shifted to less positive potential with increasing pH (Fig. 2). The linear dependence of the peak potential (E_p) of oxidation peak on pH at gold

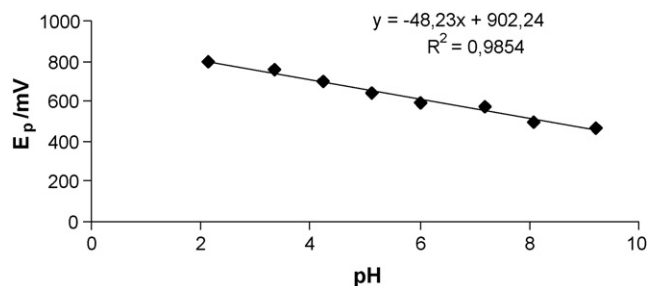


Fig. 2. Observed dependence of peak potential (E_p) on pH for 1.0 mM ND at gold nanoparticles modified ITO electrode.

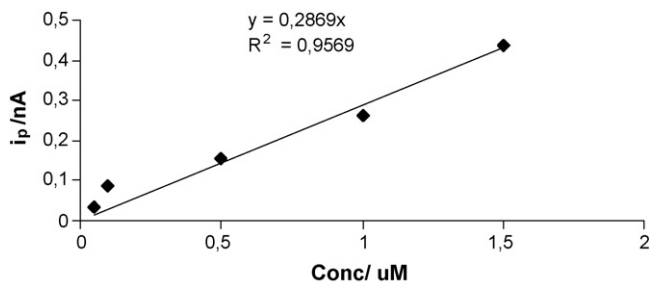


Fig. 3. Calibration plot observed for ND at gold nanoparticles modified ITO electrode at pH 7.2.

nanoparticles modified ITO electrode can be represented by the relation given in Eq. (1):

$$E_p[2.1-9.2] = [902.24-48.23 \text{ pH}] \text{ mV versus Ag/AgCl} \quad (1)$$

having correlation coefficient 0.985. The slope of E_p versus pH plot is 48.23 mV and suggests the number of protons as 1.6 for 2e process. Hence, it is concluded that equal number of electrons and protons are participating in the electrochemical process.

3.2. Effect of concentration

The dependence of the oxidation peak current (i_p) signal at gold nanoparticles modified ITO electrode on increasing concentration of ND is presented in Fig. 3. Peak current of oxidation peak increases linearly in the concentration range 50 nM to 1.5 μM . The dependence of the peak current (after background current correction in peak current) on concentration of ND can be expressed by Eq. (2):

$$i_p \text{ (nA)} = 0.2869C \quad (2)$$

where the term C represents micromolar (μM), concentration. The relation has a correlation coefficient of 0.957. The slope of the calibration plot (Fig. 3) corresponds to the sensitivity, which is equal to 0.003 nA/nM. From such sensitivity, detection limit based on the $3\sigma/m$ criterion was calculated, where σ is the blank standard deviation and m is the sensitivity and is found to be 1.36×10^{-7} M.

3.3. Effect of sweep rate

The effect of sweep rate (ν) on peak potential (E_p) of 1.0 μM ND was studied in the sweep range 10–50 mV/s at pH 7.2. Studies at sweep rate greater than 50 mV/s could not be carried out because the oxidation peak merged with the background. It was found that the peak potential shifted to more positive potential with an increase in sweep rate. The nature of the plot of E_p versus $\log \nu$ was linear as represented in Fig. 4 and the dependence of E_p on $\log \nu$ can be expressed by Eq. (3) having correlation coefficient 0.987:

$$E_p \text{ (mV)} = 263.39 + 163.53 \log \nu \quad (3)$$

The high tafel slope obtained from the plot of E_p versus $\log \nu$ herein seems to suggest strong adsorption of the nandrolone to the electrode surface. It has been well documented [34] that

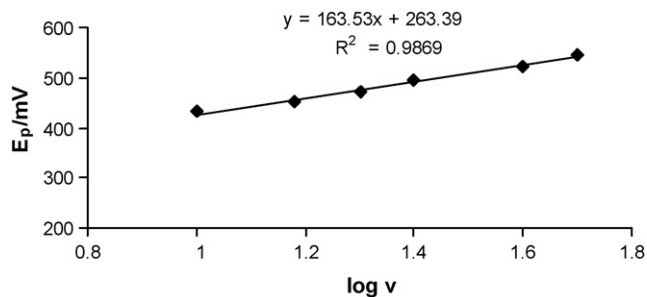


Fig. 4. Plot of E_p vs. logarithm of sweep rate (ν) of 1.0 μM ND at pH 7.2 at gold nanoparticles modified ITO electrode.

to achieve slightly slower oxidation rate in the human system, esters of nandrolone are normally used and as soon as ND comes in blood stream, ester is hydrolyzed and the base nandrolone is rendered active. The hydrolysis time depends on the conditions used and in the present studies appear to be ~ 30 min at pH 7.2. The 17th position in nandrolone contains $-\text{OH}$ group, and is the prime target for the oxidation, hence, oxidation would convert this secondary alcohol of 17th position to cyclic keto group in 2e, 2H⁺ process.

4. Analytical applications

To establish the usefulness of the developed method for determination of ND in the urine and blood serum of the doped athletes, attempts were made to detect ND after 1 day and 3 days of intramuscular injection.

4.1. Human blood serum

The gold nanoparticles modified ITO electrode has been utilized to detect ND content in human blood serum sample. The determination of ND concentration was performed by standard addition method. Prior to analysis, the sample was diluted 100 times with pH 7.2 phosphate buffer solution and a well-defined peak of ND was noticed ($E_p \sim 564$ mV) together with several other peaks in the voltammograms. However, no attempt was made to characterize other peaks noticed. These peaks were due to the presence of interfering species such as ascorbic acid, uric acid, dopamine and serotonin, etc. Research papers from our laboratory suggest that the observed peak at ~ 358 mV is due to dopamine, peak at ~ 467 mV is due to serotonin and peak around ~ 780 mV could be either due to ascorbic acid or uric acid. The results for ND concentration observed are presented in Table 1.

Table 1
Observed concentration of ND in human blood serum and urine after ND injection

Sample	Observed concentration (μM)	
	1 day	3 days
Blood serum	0.25	0.48
Urine	0.42	0.76

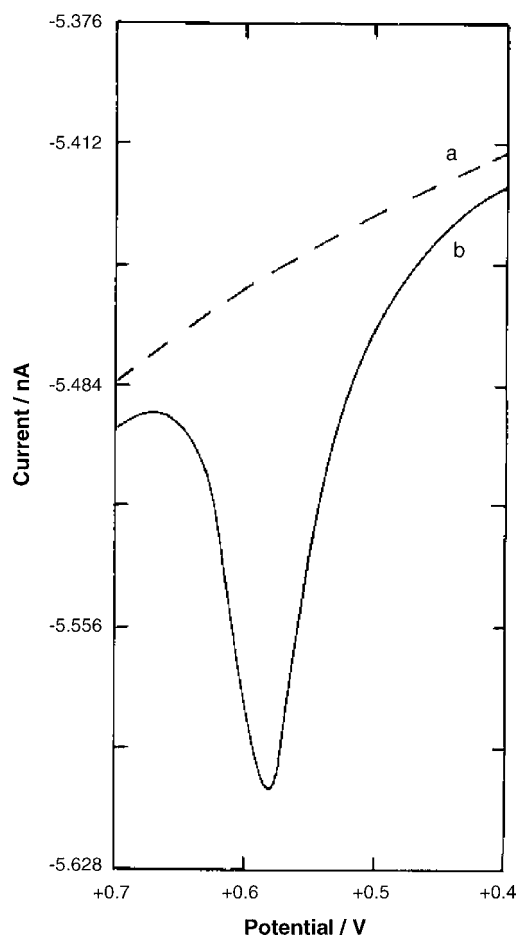


Fig. 5. Differential pulse voltammogram of (a) background (---) and (b) human urine sample (—) at pH 7.2 at gold nanoparticles modified ITO electrode after 24 h of nandrolone injection.

4.2. Human urine

The practical analytical application of the proposed method was further established by estimation of ND in human urine without pretreatment. Human urine samples were obtained from the same patient and were diluted 100 times. The analysis was then carried out. A typical DPV of the sample at gold nanoparticles modified ITO electrode is shown in Fig. 5 and the results obtained are listed in Table 1. A threshold concentration at 2 $\mu\text{g/L}$ urinary nandrolone metabolites is advocated by the International Olympic committee for the detection of doping [11] in human urine.

5. Conclusions

Gold nanoparticles modified ITO electrode allowed the successful determination of ND in the concentration range 50 nM to 1.5 μM with a detection limit of 0.136 $\mu\text{g/L}$. The proposed method provides faster, simpler and more economical alternative for the detection of doping substances in International Olympics. The use of above method would indeed drastically reduce the pretreatment and purification procedure required for urine samples, which is pre-requisite for the use of GC–MS techniques.

The proposed method also does not require the chemical derivatization of the biological samples.

Literature survey revealed that the screening of diuretics is carried out in an antidoping laboratory either by GC–MS or by HPLC [35] and the amount of ND greater than 2 $\mu\text{g/L}$ in urine is considered as an athlete doped. The concentration of ND in human blood serum and urine samples by the proposed method is found to be in the micromolar (μM) range. Hence, on the basis of present investigations it can be concluded that determination of ND can be safely carried out in the range 50 nM to 1.5 μM . The method is proved to be an economical, highly sensitive, fast and effective for the determination of concentration of ND and related steroids in body fluids such as human blood serum and urine.

Acknowledgements

One of the authors (A. Tyagi) is thankful to the Council of Scientific and Industrial Research, New Delhi for awarding Senior Research Fellowship and to the hospital, Indian Institute of Technology Roorkee for providing blood and urine samples. The authors (R.N.G. and M.O.) like to thank the bilateral program between the Indian National Science Academy (INSA) and the Japan Society for the promotion of Science (JSPS) joint program for the support of cooperative research.

References

- [1] J. Gold, et al., Abstract PL7.5. Proceedings of the Seventh International Congress on Drug Therapy in HIV Infection, November 14–18, Glasgow, UK, 2004.
- [2] J. Gold, M.J. Batterham, H. Rekers, M.K. Harms, T.B.P. Geurts, P.M.E. Helmyr, M.J. de Silva, L.H.F. Carvalho, G. Panos, A. Pinchera, F. Ajuti, C. Lee, A. Horban, J. Gatell, P. Phanuphak, W. Prasithsirikul, B. Gazzard, M. Bloch, S.A. Danner, *HIV Med.* 7 (2006) 146–155.
- [3] T.W. Storer, L.J. Woodhouse, F. Sattler, A.B. Singh, E.T. Schroeder, K. Beck, M. Padero, P. Mac, K.E. Yarasheski, P. Geurts, A. Willemsen, M.K. Harms, S. Bhasin, *J. Clin. Endocrinol. Metab.* 90 (2005) 4474–4482.
- [4] F.R. Sattler, E.T. Schroeder, M.P. Dube, S.V. Jaque, C. Martinez, P.J. Blanche, *Am. J. Physiol.* 283 (2002) E1214–E1222.
- [5] M.J. Batterham, R. Garsia, *Int. J. Androl.* 24 (2001) 232–240.
- [6] H.W. Durbeck, C.G.B. Frischkorn, I. Buker, H.E. Frischkorn, W. Leymann, B. Scheulen, H. Schlimper, B. Telin, *Fresenius Z. Anal. Chem.* 311 (1982) 404.
- [7] R.R. Perez, M.A.M. Lobo Silva, F.L.S.B. Varzim, S. Bonci de Oliveira, T. Erica, *Ciencia Rural* 35 (2005) 589–595.
- [8] R.Y. Huang, L.M. Miller, C.S. Carlson, M.R. Chance, *Bone (New York, NY, United States)* 30 (2002) 492–497.
- [9] A. Bisschop, G. Gayan-Ramirez, H. Rollier, P.N.R. Dekhuijzen, R. Dom, V.D. Bock, M. Decramer, *J. Appl. Physiol.* 82 (1997) 1112–1118.
- [10] W.D.V.M. Lichtenbelt, F. Hartgens, B.B.J. Vollaard, S. Ebbing, H. Kuipers, *Med. Sci. Sports Exerc.* 36 (2004) 484–489.
- [11] W.R. Jin, Y.H. Zheng, Xia Chen, *Electroanalysis* 9 (1997) 498–499.
- [12] G.P. Lyritis, C. Androulakis, B. Magiatis, Z. Charalambaki, N. Tsakalakis, *Bone Miner.* 27 (1994) 209–217.
- [13] A.J. Frisoli, P.H.M. Chaves, M.M. Pinheiro, V.L. Szejnfeld, J. Gerontol, *Ser. A: Biol. Sci. Med. Sci.* 60A (2005) 648–653.
- [14] G. Lippi, G. Guidi, O. Ruzzenente, V. Braga, S. Adami, *J. Clin. Lab. Invest.* 57 (1997) 507–511.
- [15] L. Flicker, J.L. Hopper, R.G. Larkins, M. Lichtenstein, G. Buirski, J.D. Wark, *Osteopor. Int.* 7 (1997) 29–35.
- [16] P.J. Steensland, F. Nyberg, L. Chahi, *Eur. J. Neurosci.* 15 (2002) 539–544.

- [17] D.M. Crist, P.J. Stackpole, G.T. Peake, *J. Appl. Physiol.* 54 (1983) 366–370.
- [18] W.L.G. Cavalcante, M.D.P. Silva, M. Gallacci, *Comparative Biochem. Physiol., Part C: Toxicol. Pharmacol.* 139C (2004) 219–224.
- [19] J.L. Teruel, M.A. Lasuncion, M. Rivera, A. Aguilera, H. Ortega, A. Tato, R. Marcen, J. Ortuno, *Am. J. Kidney Dis.* 29 (1997) 569–575.
- [20] A. Ghorbanihaghjo, H. Argani, M. Rohbaninoubar, N. Rashtchizadeh, *Lipids Health Dis.* 3 (2004) 16.
- [21] S. Kurling, A. Kankaanpaae, S. Ellermaa, T. Karila, T. Seppaelae, *Brain Res.* 1044 (2005) 67–75.
- [22] H. Sheashaa, W. Abdel-Razek, A.E. Hussein, A. Salim, N. Hassan, T. Abbas, H.E. Askalani, M. Sobh, *Nephron* 99 (2005) c102–c106.
- [23] A. Noorafshan, S.K. Doust, F.M. Ardekani, *APMIS* 113 (2005) 122–125.
- [24] J.R. Gerez, F. Frei, I.C.C. Isabel, *Contraception* 72 (2005) 77–80.
- [25] A. Solans, M. Carnicero, R. de la Torre, J. Segura, *J. Anal. Toxicol.* 19 (1995) 104.
- [26] P. Hemmersbach, R. de la Tooe, *J. Chromatogr. B* 687 (1996) 221–238.
- [27] M. Tsivou, N.K. Fougia, E. Lyris, Y. Aggelis, A. Fragkaki, X. Kiouisi, P. Simitsek, H. Dimopoulou, I.P. Leontiou, M. Stamou, M.H. Spyridaki, C. Georgakopoulos, *Anal. Chim. Acta* 555 (2006) 1–13.
- [28] J. Segura, in: S.B. Karch (Ed.), *Drug Abuse Handbook*, CRC Press, Boca Raton, 1998, pp. 641–726.
- [29] R.D. Mc Dowall, *J. Chromatogr.* 492 (1989) 3.
- [30] R.N. Goyal, M. Oyama, A. Tyagi, *Anal. Chim. Acta*, in press.
- [31] R.N. Goyal, V.K. Gupta, M. Oyama, N. Bachheti, *Electrochem. Commun.* 8 (2006) 65–70.
- [32] A. Ali Umar, M. Oyama, *Cryst. Growth Des.* 5 (2005) 599–607.
- [33] G.D. Christian, W.C. Purdy, *J. Electroanal. Chem.* 3 (1962) 363.
- [34] H.P. Wijnand, A.M.G. Bosch, C.W. Donker, *Acta Endocrinol.* 110 (1985) 19–30.
- [35] R. Ventura, J. Segura, *J. Chromatogr. B* 687 (1996) 127–144.

Manganese (II) selective PVC based membrane sensor using a Schiff base

Vinod K. Gupta*, Ajay K. Jain, Gaurav Maheshwari

Department of Chemistry, Indian Institute of Technology Roorkee, Roorkee 247667, India

Received 2 September 2006; received in revised form 26 September 2006; accepted 26 September 2006

Available online 13 November 2006

Abstract

N,N',N'',N'''-1,5,8,12-tetraazadodecane-bis(salicylaldiminato)(**H₂L**) has been used as ionophore for preparing Mn²⁺ selective sensor. Membranes of different composition with regard to ratio of **H₂L**:PVC:NPOE:NaTPB have been prepared and investigated. The best performance was obtained with the membrane of composition 10:150:150:10 (**H₂L**:PVC:NPOE:NaTPB) (w/w; mg). This membrane generated linear potential response in the concentration range of 5.0×10^{-6} to 1.0×10^{-1} M with a Nernstian slope of 30.0 mV/decade of activity and fast response time (10 s). Hydrogen ion does not effect to the performance of sensor in the pH range 3.0–6.5. The sensor was found to be sufficient selective for Mn²⁺ over a number of alkali, alkaline and heavy metal ions and could therefore be used for the determination of manganese in various samples by direct potentiometry.

© 2006 Published by Elsevier B.V.

Keywords: Schiff base; Manganese selective sensors; Potentiometry; Nernstian slope

1. Introduction

Manganese is used in various products such as batteries, fertilizers, pesticides, ceramics, gasoline additive and dietary supplements. Thus, it is found in soil, water, plants and animals. Though, manganese is essential micronutrient for various organisms [1], but is toxic at higher concentration level [2]. The manganese toxicity can result in neurological disorder with symptoms similar to Parkinson's disease [3]. Consequently, the determination of manganese in environmental samples becomes important to monitor manganese in environmental samples. A number of techniques such as X-ray fluorescence [4], atomic absorption spectrometry (AAS) [5], anodic stripping voltammetry [6–9] and inductive coupled plasma atomic emission spectrometry (ICP-AES) have been used for manganese determination. These methods give accurate results but are not very convenient for large scale monitoring as they require good infrastructure back up and expertise. For this purpose ion selective sensors are the best tool as they permit quick and convenient determination at low cost. In spite of this important requirement,

only little work on manganese selective electrodes has been done [10–14]. The reported sensors generally show a narrow working concentration range and significant interference to number of metals. This requires further work to develop manganese sensor of higher selectivity. Keeping in this view we have prepared PVC based membranes of a Schiff base *N,N',N'',N'''*-1,5,8,12-tetraazadodecane-bis(salicylaldiminato) [**H₂L**] and studied it as manganese selective sensor. The results reported in the present communication show that the membranes act as sufficiently selective manganese (II) sensor.

2. Experimental

2.1. Reagent

All reagents and chemical used were of analytical grade and used without further purification. Salicylaldehyde (CDH (P) Ltd., India), *N,N'*-bis(3-aminopropyl)ethylenediamine (Lancaster, England), sodium tetraphenyl borate (NaTPB) (BDH, UK), 2-nitrophenyl octyl ether (NPOE) (ACROS Organics, USA), dibutylphthalate (DBP) (Reidel, India), chloronaphthalene (CN) (Merck, Germany), tri-*n*-butylphosphate (TBP) (BDH, England) and high molecular weight poly(vinyl chloride) (PVC) (Aldrich, USA) were used. The multivitamin and multimineral

* Corresponding author. Tel.: +91 1332 285801; fax: +91 1332 285043.
E-mail address: vinodfcy@iitr.ernet.in (V.K. Gupta).

tablet Daily was obtained from Amway, India. Solutions of metal (nitrates) were prepared in double distilled water and standardized by the reported methods where ever necessary. Working solutions of different concentrations were prepared by diluting 0.1 M stock solutions.

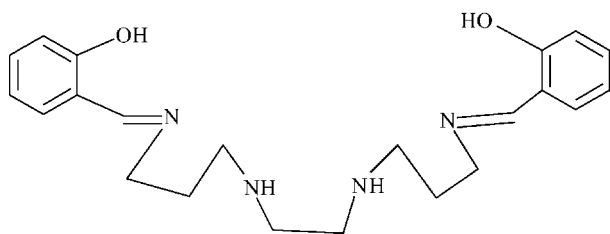
2.2. Equipments

The melting point of the ligand (**H₂L**) was determined on JSGW apparatus. Microanalysis (C, H and N) was performed using Elemental NLR Vario (III) (Germany) analyzer. FT-IR (200–4000 cm⁻¹) spectra were obtained on a Nicole (USA) spectrometer using KBr pellets. The potential measurements were carried out at 25 ± 0.1 °C with a digital pH meter (Model 5652 A, ECIL, India) and microvoltmeter, model CVM 301, Century (India) by setting up the following cell assembly, employing saturated calomel electrodes (SCE) as a reference electrodes.

SCE/internal solution(0.1 M, Mn²⁺)/membrane/
test solution/SCE

2.3. Synthesis and characterization of the ligand dihydrogen [N,N',N'',N'''-1,5,8,12-tetraazadodecane-bis(salicylaldiminato)] [H₂L]

The ligand was synthesized as per reported procedure [15]. Thus, 0.01 mol of N,N'-bis(3-aminopropyl)ethylenediamine was added to 0.02 mol of ethanolic solution of salicylaldehyde and the yellowish orange solution obtained was refluxed for 1 h. The cooling of this solution resulted in the precipitates of the ligand, which was filtered and re-crystallized in ethanol. The product was dried under reduced pressure to obtain solid shiny yellow crystals. (Yield = 81%): m.p.: (30 °C), C₂₂H₃₀N₄O₂ (382.51); Calc.: C, 69.08; H, 7.90; N, 14.65%; Found C, 68.80; H, 7.82; N, 14.10%. Infrared spectrum; 1634 cm⁻¹ (C=N).



Dihydro gen[N, N', N'', N'''-1, 5, 8, 12-tetraazadodecane-bis (salicylaldiminato)][H₂L]

2.4. Sample preparation

A Daily tablet (1.2844 g) containing 2.5 mg (as per literature supplied) manganese was digested with HCL and HNO₃ mixture. After digestion the residue was dissolved in HNO₃ and solution made up to 100 mL with distilled water.

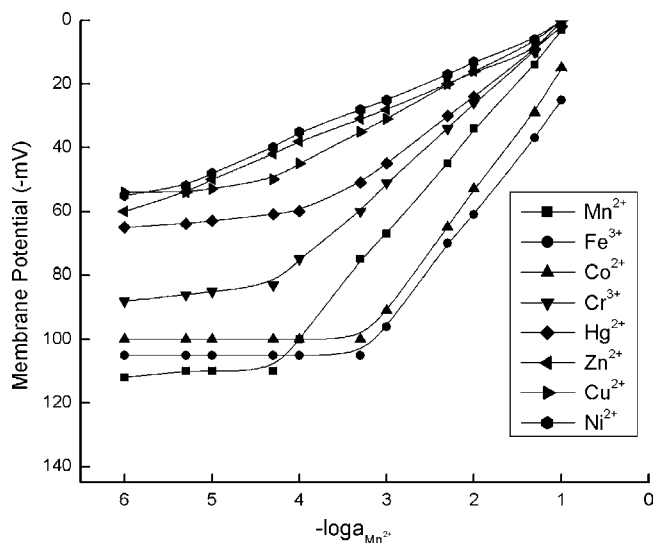


Fig. 1. Potential response of various ion selective sensors based on Schiff base.

2.5. Membrane preparation

The PVC based membranes were prepared by dissolving appropriate amounts of ligand (**H₂L**), anion excluder NaTPB, solvent mediators: NPOE, DBP, CN and TBP and PVC in THF (5–10 mL). After complete dissolution of all the components and thorough mixing, homogeneous mixture was poured into polyacrylates rings placed on a smooth glass plate. THF was allowed to evaporate for about 24 h at room temperature. The transparent membranes of 0.4 mm thickness were removed carefully from the glass plate. A 5 mm diameter piece was cut out and glued to one end of a “Pyrex” glass tube. The membranes thus prepared were equilibrated for 4 days in 0.5 M Mn²⁺ solution. Membranes of different compositions were prepared and investigated. Those, which gave reproducible results and best performance characteristics, were selected for detailed studies.

3. Results and discussion

3.1. Response to heavy metals

In preliminary experiments, response of the PVC based membranes of the ionophore to various metals was looked into and the potential generated are shown in Fig. 1. It is seen that the membrane performs best with regard to Mn²⁺ as the response is linear over a wide concentration. Thus, membranes were studied only as Mn²⁺ sensor.

3.2. Working concentration range and slope of Mn²⁺ sensor

Before starting any experimentation, the membranes were equilibrated with 0.5 M Mn²⁺ solution. The experiments have shown that 4 days equilibration time is required for generating reproducible and stable potential. The potential of the cells employing membranes of different composition is shown in

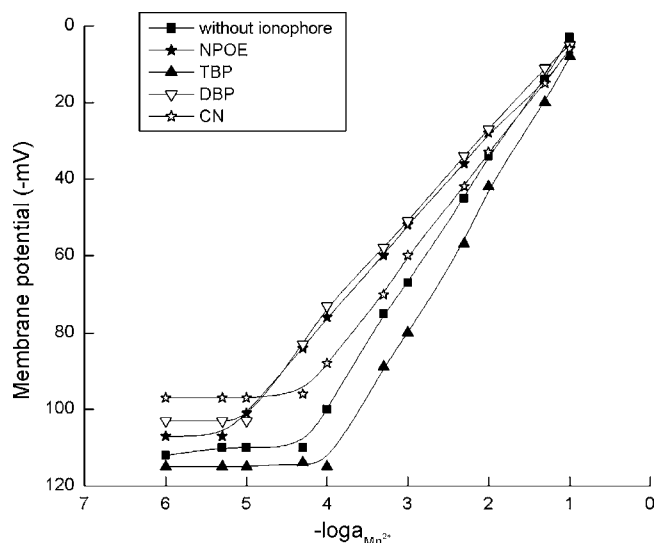


Fig. 2. Variation of membrane potential of PVC based membranes of Schiff base with varying concentrations of Mn^{2+} ions: without plasticizer, with NPOE; TBP; DBP and CN.

Fig. 2. The working concentration range and slope have been evaluated from these plots and summarized in Table 1. It is seen from Fig. 2 that the membrane without plasticizer (sensor no. 1) having composition $H_2L:PVC:NaTPB$ (w/w; mg) exhibits linear response to Mn^{2+} in the concentration range 1.0×10^{-5} to 1.0×10^{-1} M with a slope of 31.5 mV/decade of activity. Different plasticizers and NaTPB were added to the membranes with aim to improve the performance. It is seen from Table 1 and Fig. 2 that the addition of TBP reduces the working concentration range and the slope enhanced to 39.0 mV/decade of activity whereas the performance of the membrane with CN plasticizer (sensor no. 4) is almost same as that of membrane without plasticizer (sensor no.1). However, the addition of NPOE and DBP improves the performance of the membrane significantly as the working concentration range is increased and response becomes faster. The best performance is obtained with NPOE plasticizer with membrane (sensor no. 2) having composition 10:150:150:10 ($H_2L:PVC:NPOE:NaTPB$) (w/w; mg). This sensor exhibits wide working concentration range of 5.0×10^{-6} to 1.0×10^{-1} M with a near-Nernstian slope of 30.0 mV/decade of activity and fast response time (10 s). Standard deviation obtained with this sensor was found to 0.10 mV over the entire working concentration range. It was further seen that the blank membrane generated negligible potential.

Table 1
Composition of PVC membrane of (H_2L) and performance characteristics of Mn^{2+} selective sensors based on them

Sensor no.	Components in membranes (w/w)							Working concentration range (M)	Slope(\pm mV/decade of activity)	Response time (s)
	H_2L	PVC	NaTPB	NPOE	DBP	CN	TBP			
1.	10	150	10	–	–	–	–	5.0×10^{-5} to 1.0×10^{-1}	31.5	20
2.	10	150	10	150	–	–	–	5.0×10^{-6} to 1.0×10^{-1}	30.0	10
3.	10	150	10	–	150	–	–	1.0×10^{-5} to 1.0×10^{-1}	32.2	15
4.	10	150	10	–	–	150	–	5.0×10^{-5} to 1.0×10^{-1}	31.0	18
5.	10	150	10	–	–	–	150	1.0×10^{-4} to 1.0×10^{-1}	39.0	25

Table 2

Effect of partially non-aqueous medium on the working of Mn^{2+} selective sensors (sensor no. 2)

Non-aqueous content (v/v%)	Slope (\pm 0.2 mV/decade of activity)	Working concentration range (M)
0	30.0	5.0×10^{-6} to 1.0×10^{-1}
Methanol		
5	30.0	5.0×10^{-6} to 1.0×10^{-1}
10	30.0	6.0×10^{-6} to 1.0×10^{-1}
20	31.2	1.0×10^{-5} to 1.0×10^{-1}
Ethanol		
5	30.0	5.0×10^{-6} to 1.0×10^{-1}
10	30.2	8.5×10^{-6} to 1.0×10^{-1}
20	31.5	1.8×10^{-5} to 1.0×10^{-1}
Acetone		
5	30.0	5.0×10^{-6} to 1.0×10^{-1}
10	30.0	5.0×10^{-6} to 1.0×10^{-1}
20	30.0	8.9×10^{-6} to 1.0×10^{-1}

3.3. Response and lifetime

Response time (time taken to attain the steady potential) of all the membranes is given in Table 1. Membrane without plasticizer (sensor no.1) generated stable potentials in 20 s and addition of plasticizers decrease the response time of membranes to 10–15 s. The fastest response time (10 s) was shown by the membrane (sensor no. 2) incorporating NPOE as plasticizer. Other membranes having plasticizers DBP, CN and TBP showed a response time of 15, 18 and 25 s, respectively. The lifetime of the sensor was found to be 2.5 months. During this period, the membrane did not show any significant change in working concentration range and the slope.

3.4. pH and solvent effect

The pH dependence of the membrane sensor no. 2 was investigated at two concentrations of Mn^{2+} (1.0×10^{-3} and 1.0×10^{-4} M) and the results obtained are given in Fig. 3. It is seen from this figure that the potential remains constant over a pH range of 3.0–6.5. The sharp change in potential below pH 3.5 may be due to co-fluxing of H^+ with Mn^{2+} while above 6.5 due to hydrolysis of Mn^{2+} ions.

The performance of the sensor was further assessed in partially non-aqueous media, i.e. methanol–water, ethanol–water and acetone–water mixtures. The results obtained are compiled

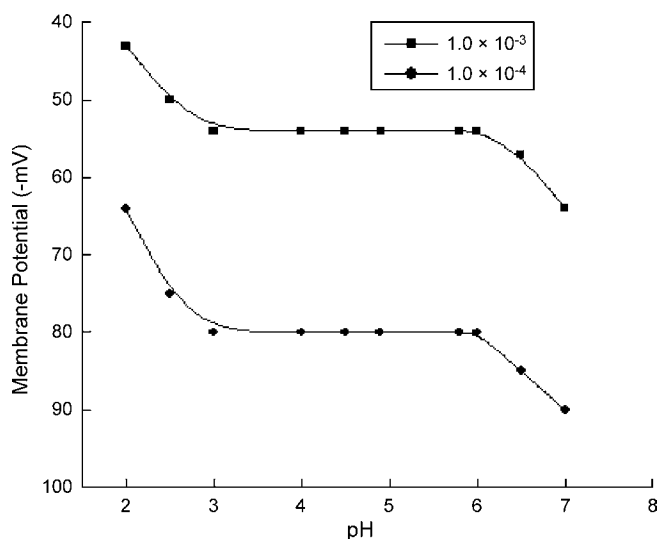


Fig. 3. Effect of pH on membrane potential: $[\text{Mn}^{2+}] = 1.0 \times 10^{-3}$ and 1.0×10^{-4} M.

Table 3
Selectivity coefficient values $[K_{\text{Mn}^{2+},\text{B}}^{\text{Pot}}]$ for Mn^{2+} selective sensor by matched potential method

Interfering ion (B)	Selectivity coefficients $[K_{\text{Mn}^{2+},\text{B}}^{\text{Pot}}]$
K^+	2.0×10^{-4}
Na^+	4.2×10^{-4}
NH_4^+	6.1×10^{-4}
Cd^{2+}	8.1×10^4
Pb^{2+}	3.0×10^{-4}
Cu^{2+}	1.0×10^{-4}
Hg^{2+}	1.0×10^{-4}
Ni^{2+}	8.0×10^{-4}
Zn^{2+}	1.3×10^{-4}
Co^{2+}	3.9×10^{-4}
Fe^{3+}	1.0×10^{-3}
Cr^{3+}	6.5×10^{-4}

in Table 2. It is seen that with increase in aqueous content, the slope is slightly increased but the working concentration range is reduced. Thus, the sensor can be used in partially non-aqueous media containing up to 20% methanol, ethanol and acetone. Above this non-aqueous content, the decrease in concentration range is significant.

Table 4
Analysis of Mn(II) in pharmaceutical preparation and waste water by use of the proposed sensor and comparison with the atomic absorption spectrometry (AAS)

Sample	Reported amount	Sensor no. 2 ^a	AAS ^a
Daily multivitamin and multimineral (mg/tablet)	2.5	2.30 ± 0.05	2.45 ± 0.03
Waste water (mg/L)	2.0	2.20 ± 0.03	2.35 ± 0.05

^a Number of samples = 5.

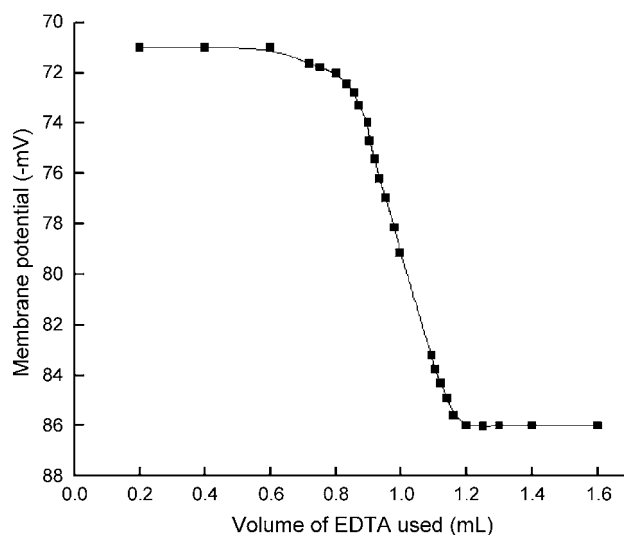


Fig. 4. Potentiometric titration curve of Mn^{2+} ion (1.0×10^{-3} M, 10.0 mL) with EDTA (1.0×10^{-2} M), using the proposed sensor as an indicator electrode.

3.5. Potentiometric selectivity

The selectivity is the most important characteristics, as it determines the extent of utility of a sensor in real sample measurement. The selectivity coefficient values were determined by Matched Potential Method (MPM), which was proposed by Gadzekpo and Christian [16] to overcome difficulties in obtaining selectivity coefficient values when ions of unequal charges are involved. In this procedure, the selectivity coefficient $K_{\text{Mn}^{2+},\text{B}}^{\text{Pot}}$ is calculated by the expression

$$K_{\text{Mn}^{2+},\text{B}}^{\text{Pot}} = \frac{a'_{\text{Mn}^{2+}} - a_{\text{Mn}^{2+}}}{a_{\text{B}}} = \frac{\Delta a_{\text{Mn}^{2+}}}{a_{\text{B}}}$$

where $a_{\text{Mn}^{2+}}$ is the initial activity of the primary ion which is then increased to $a'_{\text{Mn}^{2+}}$ resulting in some change in potential, a_{B} is the activity of the interfering ion which added to $a_{\text{Mn}^{2+}}$ causes the same change in potential as observed when $a_{\text{Mn}^{2+}}$ was increased to $a'_{\text{Mn}^{2+}}$. The values determined by MPM method are given in Table 3. A value of selectivity coefficient equal to 1.0 indicates that the sensor responds equally to primary as well as interfering ion. However, values smaller than 1.0 indicate that membrane sensor is responding more to primary ion than to interfering ions and in such a case the sensor is said to be selective to primary ion over interfering ion. Further, smaller is the selectivity coefficient, higher is the selectivity order. A perusal of Table 3 shows that selectivity coefficient values for the present sensor are much smaller than 1.0 over a number of mono-, di- and trivalent cations studied. Hence, the sensor is sufficiently selective over these ions and can therefore be used to estimate manganese in presence of these ions by direct potentiometry.

4. Analytical application of sensor

The analytical application of the sensor was investigated by using it as an indicator electrode in the potentiometric estimation of Mn^{2+} solution by titrating 10 ml of 1.0×10^{-3} M $\text{Mn}(\text{NO}_3)_2$

Table 5
Comparison of the proposed ion selective sensor with the existing sensors

Ref. no.	Working concentration range (M)	Slope (mV/decade of activity)	pH range	Response time	Interference	Lifetime (days)
10	1.0×10^{-5} to 1.0×10^{-1}	29.5	2.0–8.5	<40 s	NM	NM
11	1.0×10^{-5} to 1.0×10^{-1}	NM	NM	~20 min	NM	120
12	5.0×10^{-5} to 1.0×10^{-1}	Nernstian	4 (acetate medium)	NM	Pb ²⁺	NM
13	1.0×10^{-6} to 1.0×10^{-1}	NM	2.3–8.8	35 s	Co ²⁺ , Pb ²⁺	NM
14	1.2×10^{-5} to 1.0×10^{-1}	29.5	3.0–8.0	20 s	Cu ²⁺ , Ni ²⁺ , Zn ²⁺ , Hg ²⁺ , La ³⁺	120
Proposed sensor	5.0×10^{-6} to 1.0×10^{-1}	30.0	3.0–6.5	10 s	Good	75

NM, not mentioned.

against 1.0×10^{-2} M EDTA solution. The pH of the solution was maintained at 6.0 throughout the titration. The titration plot obtained (Fig. 4) is of standard sigmoid shape and the end point corresponds to 1:1 stoichiometry of Mn–EDTA complex.

Further, the utility of the sensor has been checked by determining Mn²⁺ in real samples by direct potentiometry. The proposed sensor was used to quantify Mn²⁺ in pharmaceutical preparation of Daily tablet and waste water and comparison of the results with that obtained by atomic absorption spectrometry is shown in Table 4. It is clear that the determinations by sensor are in close agreement with those obtained by AAS.

5. Conclusions

Of the several membranes prepared, one with the composition 10:150:150:10 (H2L:PVC:NPOE:NaTPB) exhibits best performance characteristics. Its potential response to Mn²⁺ is linear in the range 5.0×10^{-6} to 1.0×10^{-1} M with Nernstian slope 30.0 mV/decade of activity. Useful pH range of this sensor is 3.0–6.5 and it shows fast response time of 10 s with lifetime of 2.5 months. This sensor is superior to many reported electrodes (Table 5) in terms of working concentration range [10,11,12,14]. There is only electrode [13] which shows slightly better working concentration range [13] than the proposed sensor but shows significant interference to Co²⁺ and Pb²⁺ and slow response time (35 s). The present sensor shows no interference to Co²⁺ and Pb²⁺ and is fast in response. Thus, it even superior to this best reported sensor [13]. Hence, it is reasonable to say that the

sensor prepared is superior to reported electrodes and is therefore a meaningful contribution to the family of Mn²⁺ sensor. Its potentiality has been demonstrated by determining Mn²⁺ in pharmaceutical preparation.

Acknowledgement

The authors are highly thankful to Ministry of Human Resource and Development (MHRD), New Delhi, India, for providing funds to undertake the work.

References

- [1] B.H.-J. Rehm, G. Reed, *Microb. Degrad.* 8 (1986) 408.
- [2] G.M. Gadd, A.J. Griffiths, *Microb. Ecol.* 4 (1978) 303.
- [3] N.V. Hue, S. Vega, J.A. Silva, *J. Am. Soil Sci. Soc.* 65 (2001) 153.
- [4] H. Bilinski, Z. Kwokal, M. Branica, *Water Res.* 30 (1996) 495.
- [5] C. Sarzanini, O. Abollino, E. Mentasti, *Anal. Chim. Acta* 435 (2001) 343.
- [6] O.M.S. Filipe, C.M.A. Brett, *Talanta* 61 (2003) 643.
- [7] C.M.A. Brett, M.M.P.M. Neto, *J. Electroanal. Chem.* 258 (1989) 345.
- [8] G.V. Dijk, F. Verbeek, *Anal. Chim. Acta* 54 (1971) 475.
- [9] D. Monnier, E. Martin, W. Haerdi, *Anal. Chim. Acta* 34 (1966) 346.
- [10] U.S. Lal, M.C. Chattopadhyaya, K. Ghosh, A.K. Dey, *Indian Agriculturist (Spec. Vol.)* (1982) 139.
- [11] Y. Su, *Fenxi Huaxue* 11 (1983) 905.
- [12] D. Midgley, D.E. Mulcahy, *Talanta* 32 (1985) 7.
- [13] V. Agarwala, M.C. Chattopadhyaya, *Anal. Lett.* 22 (1989) 1451.
- [14] A.K. Singh, P. Saxena, A. Panwar, *Sens. Actuators, B* 110 (2005) 377.
- [15] A. Panja, N. Shaikh, S. Gupta, R.J. Butcher, P. Banerjee, *Eur. J. Inorg. Chem.* (2003) 1540.
- [16] V.P. Gadzekpo, G.D. Christian, *Anal. Chim. Acta* 164 (1984) 279.

Derivatization procedures and determination of levoglucosan and related monosaccharide anhydrides in atmospheric aerosols by gas chromatography–mass spectrometry

Ching-Lin Hsu^a, Chin-Yuan Cheng^a, Chung-Te Lee^b, Wang-Hsien Ding^{a,*}

^a Department of Chemistry, National Central University, Chung-Li 32054, Taiwan

^b Graduate Institute of Environmental Engineering, National Central University, Chung-Li 32054, Taiwan

Received 25 June 2006; received in revised form 12 October 2006; accepted 12 October 2006

Available online 27 November 2006

Abstract

This study evaluated the derivatization procedures for detecting the three most commonly monosaccharide anhydrides (MAs) (levoglucosan, mannosan and galactosan) in atmospheric aerosols using gas chromatography–mass spectrometry (GC–MS). Various silylating agents, mainly trimethylsilylating agents (TMS), were compared and the effects of various contents of trimethylchlorosilane (TMCS, as a stimulator) were evaluated to optimize the conditions for detecting these compounds in aerosol samples. Differences among the abundances of the derivatives were caused by the sterical hindrance of three hydroxyl groups in the structures of monosaccharide anhydrides. The effects of the reaction time and temperature were also examined. The optimal reaction time and temperature were 60 min and 80 °C with 1% TMCS plus 0.2% 1,4-dithioerythritol (DTE). Under these conditions, the percentages of formation of bis-*O*-TMS derivatives (as by-products) were 23, 29 and 10% for galactosan, mannosan and levoglucosan, respectively. The concentrations of galactosan, mannosan and levoglucosan in particles of smoke samples ranged from 29 to 88, 23 to 69 and 77 to 380 ng/m³, respectively; and in particles of atmospheric aerosols ranged from 0.06 to 0.75, n.d. to 0.49 and 1.6 to 132 ng/m³, respectively. Levoglucosan was the dominant MAs detected in both type of samples. Less than 10% quantitation difference was obtained when bis-*O*-TMS derivatives were included in the calculation.

© 2006 Elsevier B.V. All rights reserved.

Keywords: Monosaccharide anhydrides; Aerosols; Derivatization; GC–MS

1. Introduction

Recent investigations on aerosol water-soluble organic compounds (WSOCs) formed by burning biomass have become increasingly concerned with the role of these compounds in atmospheric chemistry and their effect on climate, because they have great potential to influence cloud formation, precipitation and climate on both global and regional scales [1–5]. Of these compounds, levoglucosan and its stereoisomers (mannosan and galactosan, as shown in Fig. 1) have attracted the most interest because of their properties as specific tracers for the burning of biomass [5–8]. These monosaccharide anhydrides (MAs) are produced exclusively during the combustion and pyrolysis of cellulose and hemicellulose [9].

Routinely, trimethylsilylation with GC–MS or GC–MS–MS is extensively used in the analysis of MAs [5–12]. Although, LC tandem MS techniques with electrospray ionization (LC-ESI–MS–MS) or LC-HRMS (LC-ESI-TOFMS) currently represent a powerful method for determining MAs [13–15], they required expensive equipment that needs maintenance, and is not readily available. GC–MS not only is more readily available in many analytical laboratories, but also provides a higher chromatographic resolution with a capillary column as well as greater sensitivity. However, information on the derivatization of these compounds with sterical hindrance in the multiple hydroxyl groups is lacking. Procedures for forming suitable TMS derivatives of MAs are important in developing comprehensive methods of determining amounts of this class of chemicals in atmospheric aerosol samples. Since these MAs are present at ng/m³ levels in aerosol samples, the primary requirement of derivatization is to produce a single derivative with a mass spectrum that reveals ions of high diagnostic value, which

* Corresponding author. Tel.: +886 3 4227151x65905; fax: +886 3 4227664.
E-mail address: wding@cc.ncu.edu.tw (W.-H. Ding).

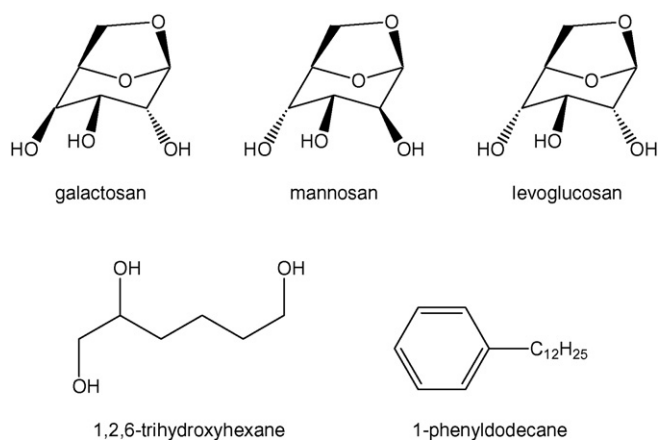


Fig. 1. Chemical structures of galactosan, mannosan, levoglucosan, surrogate 1,2,6-trihydroxyhexane and the internal standard 1-phenyldodecane.

are preferred to maximize the sensitivity and specificity while maintaining high reproducible yield.

This study evaluated various trimethylsilyl derivatization conditions and the role of a stimulator in the derivatization of trimethylsilyl MAs. The goal is to elucidate a method of forming derivatives with sufficient efficacy and selectivity that it can be employed to identify the MAs in atmospheric aerosol samples at trace levels. The quantitation difference between the major “total-substituted” derivatives alone and that including other minor “by-product” derivatives, was also examined.

2. Experimental

2.1. Chemicals and reagents

Unless noted otherwise all high purity chemicals and solvents were purchased from Aldrich (Milwaukee, WI, USA), Tedia (Fairfield, OH, USA) and Merck (Darmstadt, Germany), and were used without further purification. Standards of levoglucosan (1,6-anhydro- β -D-glucopyranose),

mannosan (1,6-anhydro- β -D-mannopyranose) and galactosan (1,6-anhydro- β -D-galactopyranose) were obtained from Sigma (St. Louis, MO). 1,2,6-Trihydroxyhexane (as a surrogate) and 1-phenyldodecane (as an internal standard) were supplied by Aldrich. 1,4-Dithioerythritol (DTE) was purchased from Fluka (Riedel-de Haën, Hannover, Germany). Stock solutions of each monosaccharide anhydride (1000 μ g/ml) were prepared in dichloromethane. Mixtures of three monosaccharide anhydrides for working standard preparation and sample fortification were also prepared in dichloromethane. All stock solutions and mixtures were stored at -4°C in the dark. *N,O*-bis-(trimethylsilyl) trifluoroacetamide (BSTFA), *N*-methyl-*N*-trimethylsilyl trifluoroacetamide (MSTFA) and trimethylchlorosilane (TMCS) were purchased from Pierce & Warriner (Chester, UK).

2.2. Sampling collection

Particles of smoke samples from burning of specific plant species or mixed plant litter were collected by aerosol sampler (10 l/min) at the roof of the Graduate Institute of Environmental Engineering building in National Central University (Chung-Li, Taiwan). Sampling time was 1 h. Samples of atmospheric aerosols were obtained by the same sampler of size segregated (<2.5 μ m diameter) particles at the Mount Lulin (120°52'E, 23°28'N, H = 2862 m) Telescope Observatory in central Taiwan. Sampling time was 12 h. The major sources of atmospheric aerosols at this site are expected via long-range transport of dust storms, pollutant and/or background air masses from Asian continent. The aerosol sampler and sampling procedures acquired to determine levoglucosan and related monosaccharide anhydrides have been described elsewhere [10,16,17]. Particles and aerosol samples were collected on Pallflex quartz fiber filters (o.d. 102 mm).

2.3. Derivatization procedures

Adequate volume of each working standard solution were added to Reacti-Vial (Pierce & Warriner) and evaporated to dry-

Table 1
Effect of simulator on derivatives of MAs formed and their respective percent abundances

Derivatizing agents	Galactosan	Mannosan	Levoglucosan
BSTFA ^a	Tris- <i>O</i> -TMS (100%)	Tris- <i>O</i> -TMS (100%)	Tris- <i>O</i> -TMS (100%)
	Bis- <i>O</i> -TMS (43%)	Bis- <i>O</i> -TMS (61%)	Bis- <i>O</i> -TMS (27%)
BSTFA + 1% TMCS	Tris- <i>O</i> -TMS (100%)	Tris- <i>O</i> -TMS (100%)	Tris- <i>O</i> -TMS (100%)
	Bis- <i>O</i> -TMS (28%)	Bis- <i>O</i> -TMS (40%)	Bis- <i>O</i> -TMS (13%)
BSTFA + 10% TMCS	Tris- <i>O</i> -TMS (100%)	Tris- <i>O</i> -TMS (100%)	Tris- <i>O</i> -TMS (100%)
	Bis- <i>O</i> -TMS (32%)	Bis- <i>O</i> -TMS (33%)	Bis- <i>O</i> -TMS (12%)
MSTFA ^b	Tris- <i>O</i> -TMS (100%)	Tris- <i>O</i> -TMS (100%)	Tris- <i>O</i> -TMS (100%)
	Bis- <i>O</i> -TMS (47%)	Bis- <i>O</i> -TMS (65%)	Bis- <i>O</i> -TMS (35%)
MSTFA + 1% TMCS	Tris- <i>O</i> -TMS (100%)	Tris- <i>O</i> -TMS (100%)	Tris- <i>O</i> -TMS (100%)
	Bis- <i>O</i> -TMS (28%)	Bis- <i>O</i> -TMS (37%)	Bis- <i>O</i> -TMS (20%)
MSTFA + 10% TMCS	Tris- <i>O</i> -TMS (100%)	Tris- <i>O</i> -TMS (100%)	Tris- <i>O</i> -TMS (100%)
	Bis- <i>O</i> -TMS (30%)	Bis- <i>O</i> -TMS (33%)	Bis- <i>O</i> -TMS (21%)

Relative abundances expressed as a percentage of the most abundant derivative (estimated as 100%).

^a Reaction conditions: 70 $^{\circ}\text{C}$ and 30 min.

^b Reaction conditions: 80 $^{\circ}\text{C}$ and 60 min.

ness under nitrogen at 60 °C. Then the residue was derivatized by adding 100 μ l of the silylating agents (containing various amounts of TMCS) and 0.2% of DTE. The vial was vortex mixed and heated at 80 °C for 60 min (among 30, 45 and 60 min, 60 min being chosen, see Section 3). After cooling, the derivatized solu-

tion was evaporated to dryness, and the residue was redissolved in CH₂Cl₂ (100 μ l) containing 5 ng/ μ l of 1-phenyldodecane (as an internal standard). The TMS derivatives of three monosaccharide anhydrides were then made ready for GC–MS analysis.

Table 2

Effect of reaction temperature on derivatives of MAs formed and their respective percent abundances

Temperature (°C)	Galactosan	Mannosan	Levoglucosan
60	Tris- <i>O</i> -TMS (100%) Bis- <i>O</i> -TMS (37%)	Tris- <i>O</i> -TMS (100%) Bis- <i>O</i> -TMS (48%)	Tris- <i>O</i> -TMS (100%) Bis- <i>O</i> -TMS (16%)
70	Tris- <i>O</i> -TMS (100%) Bis- <i>O</i> -TMS (28%)	Tris- <i>O</i> -TMS (100%) Bis- <i>O</i> -TMS (40%)	Tris- <i>O</i> -TMS (100%) Bis- <i>O</i> -TMS (13%)
80	Tris- <i>O</i> -TMS (100%) Bis- <i>O</i> -TMS (25%)	Tris- <i>O</i> -TMS (100%) Bis- <i>O</i> -TMS (36%)	Tris- <i>O</i> -TMS (100%) Bis- <i>O</i> -TMS (11%)

Relative abundances expressed as a percentage of the most abundant derivative (estimated as 100%).

Reaction conditions: BSTFA + 1% TMCS + 0.2%DTE and 30 min.

Table 3

Effect of reaction time on derivatives of MAs formed and their respective percent abundances

Time (min)	Galactosan	Mannosan	Levoglucosan
30	Tris- <i>O</i> -TMS (100%) Bis- <i>O</i> -TMS (28%)	Tris- <i>O</i> -TMS (100%) Bis- <i>O</i> -TMS (40%)	Tris- <i>O</i> -TMS (100%) Bis- <i>O</i> -TMS (13%)
45	Tris- <i>O</i> -TMS (100%) Bis- <i>O</i> -TMS (25%)	Tris- <i>O</i> -TMS (100%) Bis- <i>O</i> -TMS (33%)	Tris- <i>O</i> -TMS (100%) Bis- <i>O</i> -TMS (11%)
60	Tris- <i>O</i> -TMS (100%) Bis- <i>O</i> -TMS (23%)	Tris- <i>O</i> -TMS (100%) Bis- <i>O</i> -TMS (29%)	Tris- <i>O</i> -TMS (100%) Bis- <i>O</i> -TMS (10%)

Relative abundances expressed as a percentage of the most abundant derivative (estimated as 100%).

Reaction conditions: BSTFA + 1% TMCS + 0.2%DTE and 80 °C.

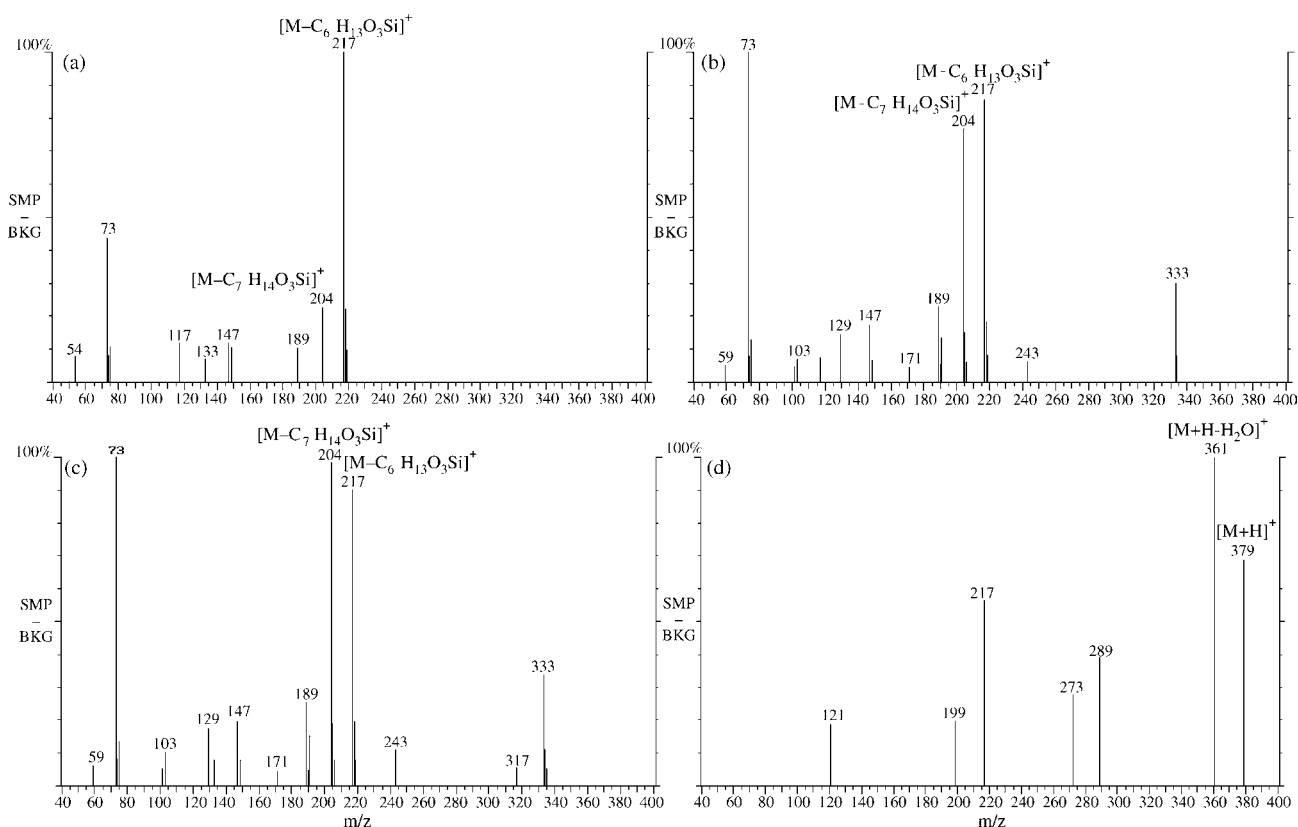


Fig. 2. EI mass spectra of TMS derivatives of (a) galactosan, (b) mannosan, (c) levoglucosan and CI mass spectrum of (d) levoglucosan.

2.4. Sample preparation

The procedure used to extract three monosaccharide anhydrides from the aerosol samples under ultrasonic agitation has been described by Zdráhal et al. [10], and was used with minor modifications. The aerosol samples underwent solvent extraction under ultrasonic agitation. Before extraction, a surrogate (1,2,6-trihydroxyhexane) was added to monitor the recovery of the sample preparation procedures. The surrogate was added on the filter 12 h before extraction, and the spiked sample was maintained frozen until extraction. The spiked filter was extracted three times, each for 30 min using 15 ml of dichloromethane under ultrasonic agitation in 25-ml Pyrex glass flasks with Teflon-lined stoppers. The first extraction step was conducted under acidic conditions by adding acetic acid (200 μ l). The combined dichloromethane extracts were reduced with a rotary evaporator to a volume of around 1 ml. Then, the concentrated extract was filtered through a Teflon syringe filter and completely dried under a stream of nitrogen. Finally, the dried sample was redissolved in pyridine (50 μ l), and this solution (or an aliquot) was immediately derivatized and made ready for GC–MS analysis.

2.5. GC–MS analysis

Analyses were carried out on a Varian 3800CX gas chromatograph directly connected to a Saturn 2000 ion-trap mass spectrometry (Varian, Walnut Creek, CA, USA) at unit resolution. A ChromatoProbe and a temperature-programmed injector (Varian) with a 3.4 mm i.d. liner, was used to introduce a large-volume sample (10 μ l), as described elsewhere [18,19]. A DB-5MS capillary column (30 m \times 0.25 mm i.d., 0.25 μ m film, J&W, USA) was used. Helium carrier gas flow rate was 1.0 ml/min. The injector temperature was set at 280 $^{\circ}$ C. GC temperature program was as follows: 60 $^{\circ}$ C for 3 min, followed by a temperature ramp at 10 $^{\circ}$ C/min to 190 $^{\circ}$ C, then 30 $^{\circ}$ C/min to 300 $^{\circ}$ C, and hold for 5 min. The transfer line to the mass spectrometer was set at 280 $^{\circ}$ C. Saturn revision 5.2 software was used for full-scan EI data acquisition, and acquired under the following conditions: mass range 50–550 m/z , scan time 1 s, solvent delay 13.5 min, manifold temperature 160 $^{\circ}$ C, emission current 10 μ A (70 eV), multiplier voltage 1950 V, automatic gain control (AGC) target 20000.

For low-pressure PICI mass spectrum analysis, methanol was used as CI reagent gas in the selected ejection chemical ionization mode (SECI) to evaluate their sensitivity and stability. Reagent ions were ionized for a variable duration set by automatic reaction control (ARC) of the instrument. The CI full-scan data was acquired under the following conditions: mass range 100–550 m/z ; scan time, 1 s; solvent delay, 13.5 min; manifold temperature, 80 $^{\circ}$ C; and ion trap temperature, 160 $^{\circ}$ C. The optimal conditions of ARC parameters was used as following: 0.1-ms ARC ionization time, 2.0 ms CI maximum ionization time, 40- μ s CI maximum reaction time, 15- m/z CI ionization storage level, 19- m/z CI reaction storage level, 55- m/z CI background mass, and 15-V reagent ion eject amplitude. The autotune program was used to set most instrument parameters with target

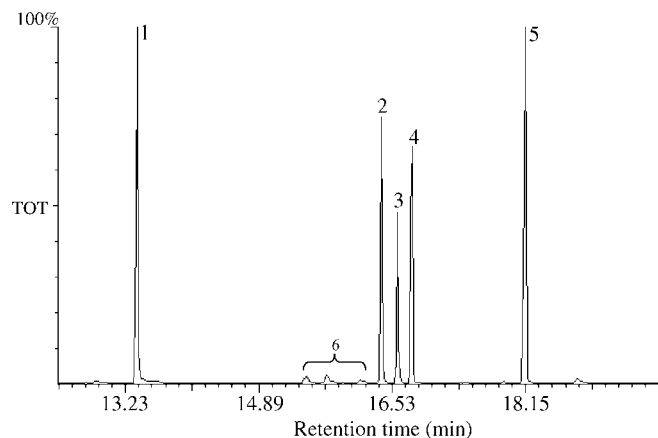


Fig. 3. TIC of the TMS derivatives of the standard. Peak identification: (1) 1,2,6-trihydroxyhexane, (2) galactosan, (3) mannosan, (4) levoglucosan, (5) 1-phenylododecane and (6) bis-*O*-TMS derivatives.

10,000 at a filament current of 10 μ A. The pressures of reagent gases in the ion trap were approximately 2×10^{-5} Torr.

3. Results and discussion

3.1. Evaluation of derivatization conditions

Derivatization is critical to analyzing MAs by GC–MS. Three hydroxyl groups, amenable to derivatization, may yield numer-

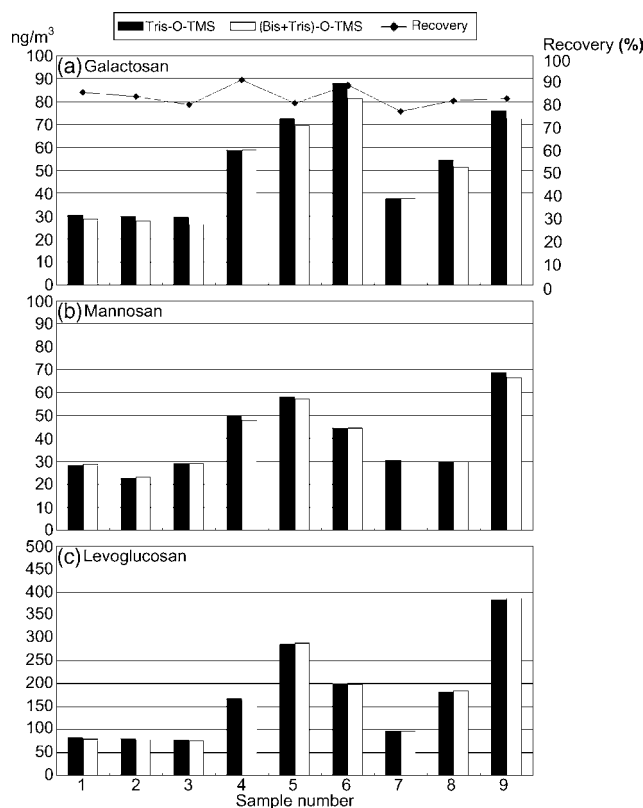


Fig. 4. The surrogate recovery rates (—●—), the concentrations of MAs based on tris-*O*-TMS derivatives alone (■), and those based on tris-*O*-TMS plus bis-*O*-TMS derivatives (□), as well as their quantitation difference detected in particles of smoke samples formed by burning mixed plant litters.

ous derivatives. Theoretically, the formation of a single derivative with a mass spectrum of ions of high diagnostic value is required to maximize sensitivity and specificity. Hence, the first series of experiments was to evaluate the various derivatization conditions of MAs and to optimize the conditions for detecting these compounds in aerosol samples. Tables 1–3 present the main derivatives obtained under each set of derivatization conditions and their respective abundant derivative. Here, tris-*O*-TMS derivatives of MAs were set as 100% abundance. When reacted with derivatizing agent BSTFA alone at 70 °C and 30 min, large fractions of the corresponding bis-*O*-TMS derivatives (as by-products) were formed (Table 1). These results may be due to the sterical hindrance of three hydroxyl groups in the structures. Similar results were also obtained for MSTFA as the lone derivatizing agent at 80 °C and 60 min. To increase the derivative efficiency for multiple hydroxyl analytes, the addition of

a stimulator in BSTFA or MSTFA agent was recommended [10–12,20,21]. Trimethylchlorosilane is one of the commonly used stimulators in TMS derivatives [10–12,20,21]. Clearly, the presence of the TMCS is important for these analytes, more than 40% of bis-*O*-TMS derivatives abundance was reduced when 1% TMCS solution was added with BSTFA or MSTFA (Table 1). However, no significant increase in the silylation efficiency was observed when 10% TMCS was added. Thus, BSTFA or MSTFA with 1% TMCS as derivatization solution was selected, although still has more than 33% of bis-*O*-TMS-mannosan was produced. The effect of reaction temperature was then evaluated. Table 2 shows that the abundances of bis-*O*-TMS derivatives were decreased when reaction temperature increased from 60 °C to 80 °C. The lower temperature was not studied in detail, since 60–80 °C is a temperature range appropriate for most practical purposes. The influence of reaction

Table 4
Detection characteristics, linear range, linearity and instrumental detection limits

Compound	Retention time (min)	Quantitation ions (<i>m/z</i>)	Linear range (µg/ml)	Linearity (r^2)	IDL (pg)
1,2,6-Trihydroxyhexane (surrogate)	13.82	145,103			
Galactosan	16.43	204,217	0.062–1.997	0.994	34
Mannosan	16.62	204,217	0.054–1.741	0.995	68
Levoglucozan	16.75	204,217	0.146–4.659	0.992	29
1-Phenyldodecane (internal standard)	18.15	246,133,92			

Table 5
Surrogate recovery and the concentrations of MAs detected in atmospheric aerosols from long-range transport particles

Sample	Surrogate recovery (%)	Derivatives	Galactosan	Concentration (ng/m ³) Mannosan	Levoglucozan	Difference (%)
1	81	Tris- <i>O</i> -TMS	0.06	0.13	4.08	–
		Tris + bis- <i>O</i> -TMS	0.06	0.13	4.08	
2	81	Tris- <i>O</i> -TMS	0.27	0.16	4.00	–
		Tris + bis- <i>O</i> -TMS	0.27	0.16	4.00	
3	77	Tris- <i>O</i> -TMS	0.75	0.49	124	2.7 ^a
		Tris + bis- <i>O</i> -TMS	0.73	0.49	125	0.6 ^b
4	86	Tris- <i>O</i> -TMS	0.63	0.34	132	
		Tris + bis- <i>O</i> -TMS	0.63	0.34	130	1.5 ^b
5	79	Tris- <i>O</i> -TMS	0.27	0.12	50	
		Tris + bis- <i>O</i> -TMS	0.27	0.12	47	5.0 ^b
6	78	Tris- <i>O</i> -TMS	0.22	n.d.	6.9	–
		Tris + bis- <i>O</i> -TMS	0.22	n.d.	6.9	
7	86	Tris- <i>O</i> -TMS	0.74	0.47	130	6.8 ^a
		Tris + bis- <i>O</i> -TMS	0.69	0.47	128	1.5 ^b
8	81	Tris- <i>O</i> -TMS	0.23	0.15	45	–
		Tris + bis- <i>O</i> -TMS	0.23	0.15	45	
9	85	Tris- <i>O</i> -TMS	0.11	n.d.	2.4	–
		Tris + bis- <i>O</i> -TMS	0.11	n.d.	2.4	
10	84	Tris- <i>O</i> -TMS	0.13	n.d.	6.4	–
		Tris + bis- <i>O</i> -TMS	0.13	n.d.	6.4	
11	76	Tris- <i>O</i> -TMS	0.1	0.08	1.6	–
		Tris + bis- <i>O</i> -TMS	0.1	0.08	1.6	

(–), No quantitation difference for these MAs.

^a Percentage difference for galactosan.

^b Percentage difference for levoglucozan.

time was also examined. Table 3 shows that the abundances of bis-*O*-TMS derivatives did not significantly decrease over the three reaction times (30, 45 and 60 min), except for mannosan, the bis-*O*-TMS derivative was decreased from 40 to 29% at 60 min. Comparison with Tables 1–3, the BSTFA-TMCS (1%) mixture appeared to be more reactive than MSTFA-TMCS (1%), as the percentages of formation of bis-*O*-TMS derivatives were smaller in the former case, although still has 29% of bis-*O*-TMS-mannosan was detected. Here, a small amount of DTE was also added to stabilize the derivatization solution and enhance the peak abundance, as suggested by Smets et al. [22]. The final derivatization conditions chosen were: 100 μ l BSTFA with 1%TMCS plus 0.2% DTE as derivatization solution added to the dried residue and heated for 60 min at 80 °C.

3.2. Mass spectra of derivatives

Fig. 2 displays the profiles of EI mass spectra of tris-*O*-TMS derivatives. These derivatives showed some common fragmentation pathway. The molecular ions were not detected in all cases. Two relative intense ions, m/z 217 and 204, were observed and were tentatively attributed to the loss of $C_6H_{13}O_3Si$ and $C_7H_{14}O_3Si$ from the molecular ion, respectively [11,12,23]. These two characteristic ions were used as the quantitation ions to obtain maximum detection sensitivity and specificity. The relative abundant ion m/z 333 was observed and was tentatively attributed to the loss of a C_2H_5O from the molecular ion of levoglucosan or mannosan. All derivatives displayed ion at m/z 73 [$(CH_3)_3Si$] $^+$ which was characteristic of the TMS group and commonly observed in all TMS derivatives. The protonated molecular signals $[M + 1]^+$ of these derivatives MAs were in accordance with the GC-CI-MS analysis using methanol as reagent gas. The CI mass spectrum of tris-*O*-TMS levoglucosan is characterized by the protonated molecular signal at m/z 379, which then eliminates water to give an intense ion at m/z 361 (Fig. 2(d)).

Fig. 3 displays the total ion chromatogram of derivatives of MAs standard solution with an internal standard and a surrogate under optimal derivatization conditions. Three principal peaks of tris-*O*-TMS derivatives are observed with three smaller peaks of bis-*O*-TMS derivatives. These bis-*O*-TMS derivatives of MAs have been confirmed by CI-MS as described above. Protonated molecular signals $[M + 1]^+$ (m/z 307) and intense ion $[M + 1 - H_2O]^+$ (m/z 289) of bis-*O*-TMS derivatives MAs were detected. Most quantitative studies of MAs are based on the tris-*O*-TMS derivatives [5–12], but over 29% of MA isomers are sometimes excluded from the quantitation results. Therefore, the quantitation difference should be examined when bis-*O*-TMS derivatives MAs are considered.

3.3. Method performance and applications

The analytical characteristics of the method, such as linear response range, reproducibility and quantitation limits, were investigated to evaluate the efficiency of the method and the possibility of the method application to environmental aerosol

samples. Table 4 presents an overview of the GC-MS detection characteristics (retention time and quantitation ions), linear response range, linearity and instrumental detection limits (IDL) for these derivatives (tris-*O*-TMS alone). The quantitation of these derivatives was calculated from the five-level calibration curve (or average response factor, RF) covering the range as shown in Table 4, each divided by the fixed concentration of internal standard (1-phenyldodecane). The calibration curves were linear with coefficients of determination $r^2 \geq 0.992$. The curve covered a range equivalent to the concentration of the analytes in environmental aerosol samples after the extract was concentrated to 100 μ l. The instrumental detection limits, defined as the amount that yielded an S/N of higher than or equal to 3, ranged from 29 to 68 pg (Table 4).

Fig. 4 presents the surrogate recovery rates, the concentrations of MAs based on tris-*O*-TMS derivatives alone, and those based on tris-*O*-TMS plus bis-*O*-TMS derivatives, as well as their quantitation difference detected in particles of smoke samples formed by burning mixed plant litters. The peaks of the derivatives were identified by comparison with the retention time and the CI-MS spectra of the standard solutions, and the corresponding quantities were calculated using response factors. The surrogate recoveries of 1,2,6-trihydroxyhexane ranged from 76 to 89% (average $82 \pm 4\%$, $n = 9$). The measured concentrations of galactosan, mannosan and levoglucosan in particles of smoke samples ranged from 29 to 88, 23 to 69 and 77 to 380 ng/m^3 ,

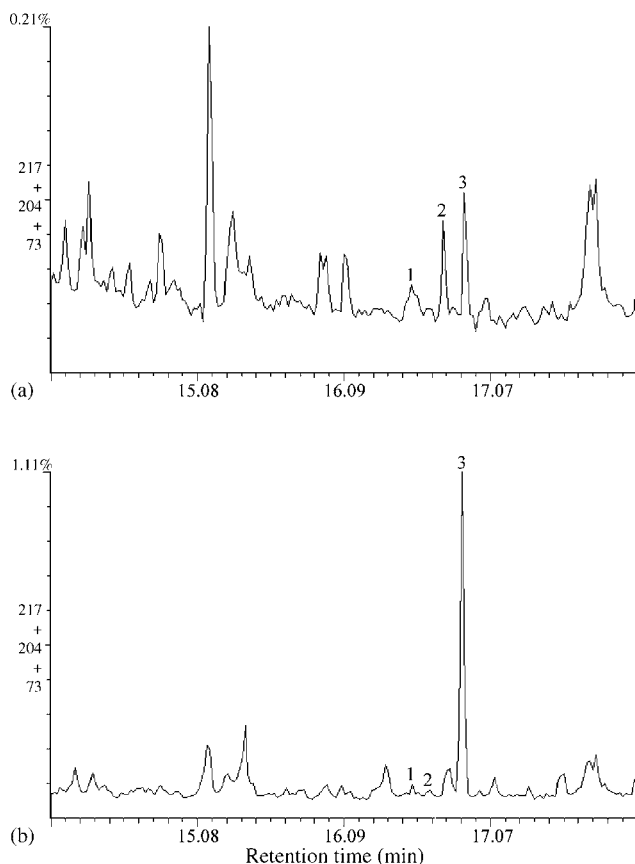


Fig. 5. EI-MS extracted ion chromatograms of MAs detected in particles of (a) an atmospheric aerosol sample and (b) a smoke sample.

respectively. Levoglucosan was the dominant MAs detected in particles of smoke samples, according to this method. The quantitation difference is under 10% when bis-*O*-TMS derivatives were included in the quantitation.

Table 5 lists the surrogate recovery and the concentrations of MAs detected in atmospheric aerosols from particles that were transported over a long-range distance. Fig. 5 displays the EI-MS extracted ion chromatograms of MAs detected in (a) particles of smoke samples and (b) atmospheric aerosol samples. The surrogate recoveries in atmospheric aerosols ranged from 76 to 86% (average $81 \pm 4\%$, $n = 11$). The concentrations of galactosan, mannosan and levoglucosan in particles of atmospheric aerosols ranged from 0.06 to 0.75, n.d. to 0.49 and 1.6 to 132 ng/m³, respectively. Levoglucosan was also the dominant MAs detected in atmospheric aerosols from particles that were transported over a long-range distance. The results indicate that quantitation difference is observed in 4 of 11 samples, and 6.8% is the most difference when bis-*O*-TMS derivatives were considered in the calculation of the concentration of MAs in atmospheric aerosols.

4. Conclusion

Reliable derivatization conditions, including the derivatizing reagent and the stimulator, should be imposed to prevent the formation of numerous derivatives in compounds with multiple hydroxyl groups (i.e., monosaccharide anhydrides). A stimulator must be employed to increase the derivatization efficiency. The results of this study indicate that BSTFA with 1% TMCS exhibited a stronger trimethylsilylation power as described elsewhere. However, small amounts of bis-*O*-TMS derivatives were always present under the optimal derivatization conditions. Based on two calibration curves (tris-*O*-TMS alone and tris-*O*-TMS plus bis-*O*-TMS), less than 10% quantitation difference was observed in the calculation the concentration of MAs in particles of smoke samples or atmospheric aerosols. Although the percentage is insignificant, the difference is a matter of concern.

Acknowledgment

The authors would like to thank the National Science Council of Taiwan for financially supporting this research under contract No. 94-2113-M-008-013.

References

- [1] T. Novakov, J.E. Penner, *Nature* 365 (1993) 823.
- [2] T. Novakov, C.E. Corrigan, *Geophys. Res. Lett.* 23 (1996) 2141.
- [3] R.J. Charlson, J.H. Seinfeld, A. Nenes, M. Kulmala, A. Laaksonen, M.C. Facchini, *Science* 292 (2001) 2025.
- [4] P.M. Fine, G.R. Cass, B.R.T. Simoneit, *Environ. Eng. Sci.* 21 (2004) 387.
- [5] J.J. Schauer, W.F. Rogge, L.M. Hildemann, M.A. Mazurek, G.R. Cass, B.R.T. Simoneit, *Atmos. Environ.* 30 (1996) 3837.
- [6] M.P. Fraser, K. Lakshmanan, *Environ. Sci. Technol.* 34 (2000) 4560.
- [7] B.R.T. Simoneit, V.O. Elias, *Mar. Chem.* 69 (2000) 301.
- [8] C.G. Nolte, J.J. Schauer, G.R. Cass, B.R.T. Simoneit, *Environ. Sci. Technol.* 35 (2001) 1912.
- [9] B.R.T. Simoneit, J.J. Schauer, C.G. Nolte, D.R. Oros, V.O. Elias, M.P. Fraser, W.F. Rogge, G.R. Cass, *Atmos. Environ.* 33 (1999) 173.
- [10] Z. Zdráhal, J. Oliveira, R. Vermeylen, M. Claeys, W. Maenhaut, *Environ. Sci. Technol.* 36 (2002) 747.
- [11] V. Pashynska, R. Vermeylen, G. Vas, W. Maenhaut, M. Claeys, *J. Mass Spectrom.* 37 (2002) 1249.
- [12] D. Fabbri, G. Chiavari, S. Prati, I. Vassura, M. Vangelista, *Rapid Commun. Mass Spectrom.* 16 (2002) 2349.
- [13] P. Palma, A. Cappiello, E. de Simon, F. Mangani, H. Truffelli, S. Decesari, M.C. Facchini, S. Fuzzi, *Ann. Chim.* 94 (2004) 911.
- [14] C. Dye, K.E. Yttri, *Anal. Chem.* 77 (2005) 1853.
- [15] K.E. Yttri, C. Dye, L.H. Slørdal, O.A. Braathen, *J. Air Waste Manage. Assoc.* 55 (2005) 1169.
- [16] C.T. Chang, C.J. Tsai, C.T. Lee, S.Y. Chang, M.T. Cheng, H.M. Chein, *Atmos. Environ.* 35 (2001) 5741.
- [17] C.Y. Lin, S.C. Liu, C.C.K. Chou, T.H. Liu, C.T. Lee, C.S. Yuan, C.J. Shiu, C.Y. Young, *Terr. Atmos. Ocean. Sci.* 15 (2004) 839.
- [18] W.H. Ding, C.T. Chen, *J. Chromatogr. A* 857 (1999) 359.
- [19] W.H. Ding, P.C. Tsai, *Anal. Chem.* 75 (2003) 1792.
- [20] L. Damasceno, R. Ventura, J. Ortuno, J. Segura, *J. Mass Spectrom.* 35 (2000) 1285.
- [21] E.M. Chambaz, G. Defaye, C. Madani, *Anal. Chem.* 45 (1973) 1090.
- [22] F. Smets, C. Vanhoenackere, G. Pottie, *Anal. Chim. Acta* 275 (1993) 147.
- [23] C.Y.M. dos Santos, D. de Almeida Azevedo, F.R. de Aquino Neto, *Atmos. Environ.* 36 (2002) 3009.

Solid-matrix luminescence of heterocyclic aromatic amines in several new sugar-glass systems

Sara E. Hubbard, Robert J. Hurtubise*

Department of Chemistry, University of Wyoming, Laramie, WY 82071-3838, United States

Received 1 August 2006; received in revised form 2 October 2006; accepted 3 October 2006

Available online 7 November 2006

Abstract

Several new sugar glasses were investigated for their potential in solid-matrix luminescence. Both solid-matrix fluorescence (SMF) and solid-matrix phosphorescence (SMP) properties were obtained, and two heterocyclic aromatic amines were employed as model compounds. In addition to glucose glasses, which were investigated previously, fructose, ribose, xylose, galactose, maltose, and glucose with poly(acrylic acid) (PAA) were studied. Detailed experimental conditions were obtained for each sugar-glass system. In addition, NaI was investigated as a heavy-atom salt in the sugar-glass systems to enhance the SMP of the heterocyclic aromatic amines. The SMF intensity was the strongest in maltose and glucose with PAA for 2-amino-1-methyl-6-phenylimidazo[4,5-b]pyridine (PhIP) and in maltose for 2-amino-9H-pyrido[2,3-b]indole (A α C). The largest SMP signals for PhIP with and without NaI were acquired in glucose with PAA. For A α C with NaI, the strongest SMP signal was obtained in maltose. Limits of detection were obtained for PhIP in the several sugar-glass systems, and the lowest limit of detection was 0.04 pmol/mg of PhIP in maltose with NaI present. An extensive study was carried out using both SMF and SMP to determine if neutral and/or protonated species of PhIP and A α C were in the sugar-glass systems. General guidelines such as glass transition temperature and solubility are discussed for selecting a sugar glass as a solid matrix.

© 2006 Elsevier B.V. All rights reserved.

Keywords: Solid-matrix fluorescence; Solid-matrix phosphorescence; Sugar glasses; Heterocyclic aromatic amines

1. Introduction

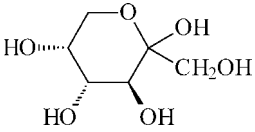
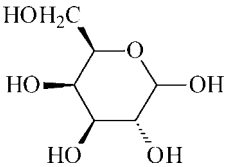
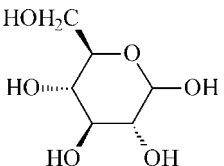
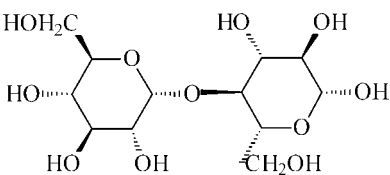
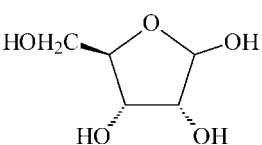
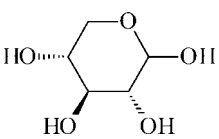
Over the past several decades, solid-matrix luminescence (SML) has been widely used for trace organic analysis [1,2]. The most common solid phase used is filter paper, which is a very effective matrix for many compounds [3–6]. Glucose glasses have been shown to be very effective solid matrices with unique properties from which both solid-matrix fluorescence (SMF) and solid-matrix phosphorescence (SMP) can be obtained at room temperature [7,8]. Recently, there have been some interesting applications of solid-matrix luminescence published. SMP was employed by Rojas-Duran et al. [9] for the detection of aflatoxin produced by *Aspergillus* molds. Rupcich et al. [10] used SMF to monitor the catalytic activity of an enzyme, and SMP was utilized by Liu et al. [11] in the determination of DNA. Nylon was used as a novel solid matrix by Correa and

Escandar [12] for the determination of thiabendazole in water samples via SMP. Wei et al. [13] employed SMP for the determination of purine compounds in urine, and Salinas-Castillo et al. [14] determined benzo(a)pyrene in water samples using SMP.

Carbohydrates and their glasses have a number of uses in practical applications. One well-known use is the encapsulation of pharmaceuticals for human consumption. Sugar glasses are also used in the preservation of liposomes and proteins during the drying process [15–19]. As shown by Wang and Hurtubise [7,20], and more recently by Mendonsa and Hurtubise [8,21,22], glucose glasses can be very effective solid matrices for obtaining SMF and SMP from heterocyclic aromatic amines (HAAs). Mendonsa and Hurtubise [8] have demonstrated that glasses formed from glucose melts, with and without the heavy-atom salt NaI, are particularly useful solid matrices for the detection of HAAs. These sugar glasses were rigid and clear, easy to work with, and gave reproducible data and low limits of detection. Other sugars that have been used as solid matrices for SML are trehalose and sucrose [23].

* Corresponding author. Tel.: +1 307 766 6241; fax: +1 307 766 2807.
E-mail address: hurtubis@uwyo.edu (R.J. Hurtubise).

Table 1
Structures, molecular weights, and glass-transition temperatures of sugars used as solid matrices

Sugar glass	Structure	MW (g/mol)	T_g (K)
Fructose		180	275
Galactose		180	297
Glucose		180	284
Maltose		344	311
Ribose		150	257
Xylose		150	277

T_g values were obtained in this work.

Because sugar glasses have uses in many areas, it is important to understand their behavior. Over the years, there have been numerous reports on the properties of sugars. From 1928 to 1934, Parks et al. [24–26] reported the heat capacities of glucose in the crystalline, glassy, and undercooled liquid states as a function of temperature, glass-transition temperatures, and viscosities. Since then, many other researchers have also attempted to better understand the properties of sugars. For example, Slade and Levine [27,28] and Levine and Slade [29] related the ratio of melting point to glass-transition temperature of sugars (T_m/T_g) to the free-volume of the sugar glass. Others have been interested in the structural relaxation and molecular motion of sugar glasses [30,31].

In this work, five sugars with different physical properties were selected as solid matrices and compared to the glucose solid matrix using two heterocyclic aromatic amines (HAAs) as model compounds. HAAs are a class of carcinogenic/mutagenic compounds found in various foods [32,33]. They have been linked to breast, liver, and intestinal cancers [34,35]. The main goal of the research was to determine if these five solid matrices

were more effective in obtaining SML than glucose glasses. The sugars studied were fructose, galactose, maltose, ribose, and xylose. Their structures are shown in Table 1. Also, glasses formed from glucose with a small amount of poly(acrylic acid) (PAA) present were investigated to determine if PAA would lead to more rigid glasses. Glasses were also prepared with 10% of the heavy-atom salt NaI and glucose/PAA blends. 2-Amino-1-methyl-6-phenylimidazo[4,5-b]pyridine (PhIP) and 2-amino-9H-pyrido[2,3-b]indole (A α C) were selected as the model HAAs. SMF and SMP intensities and spectra were obtained for PhIP and for A α C in all of the sugar-glass systems both with and without NaI. Limits of detection for PhIP in several of the glasses were also acquired.

2. Experimental

2.1. Instrumentation

Luminescence data were obtained on a Spex Fluorolog 2 spectrometer with DataMax Version 4.09 software (Jobin Yvon,

Inc., Edison, NJ). A 450 W xenon arc lamp and an RS928 photomultiplier tube were used to acquire fluorescence data. A 150 W pulsed xenon lamp and an RS928 photomultiplier tube were used to obtain phosphorescence data. The microwave oven used for drying glasses was a Panasonic model NN-6475A domestic microwave oven with an output power of 925 W (Matsushita Electric Corporation of America, Secaucus, NJ). The differential scanning calorimeter used for acquiring T_g values was a TA 2920MDSC with TA Thermal Advantage (Version 1.0 F) software, TA Universal Analysis (Version 2.6 D) software, and liquid nitrogen cooling accessory (TA Instruments, New Castle, DE). For the SMF of PhIP and of A α C, the excitation and emission slits were set to 1.0 and 0.5 mm, respectively. For the SMP of PhIP, the excitation and emission slits were all set to 5.0 mm, the delay time (t_d) to 1 ms, and the gate time (t_g) to 10 ms. For the SMP of A α C, the excitation and emission slits were all set to 5.0 mm, the delay time (t_d) to 3 ms, and the gate time (t_g) to 5 ms. The excitation and emission wavelengths used for PhIP and A α C were somewhat different depending on the sugar glass used as the matrix.

2.2. Reagents and solutions

PhIP and A α C were purchased from Toronto Research Chemicals, Inc., Ontario, Canada. D-(–)-Fructose (SigmaUltra); D-(+)-galactose (min. 99%); D-(+)-glucose (99.5%); maltose monohydrate (min. 99%); and D-(–)-ribose (min. 99.0%) were purchased from Sigma, St. Louis, MO. D-Xylose (99%) and PAA (M_v 450,000) were purchased from Aldrich Chemical Company, Milwaukee, WI. Sodium iodide (99.999%) was purchased from Alfa Aesar, Ward Hill, MA and from Aldrich. HPLC-grade water and methanol were purchased from EMD Chemicals, Inc., Gibbstown, NJ. Stock solutions of 200 μ g/mL of PhIP or A α C in methanol:water (50:50) were used for the preparation of all sugar glasses.

2.3. Glasses prepared without sodium iodide

The preparation methods for each sugar system varied somewhat to obtain the optimum SMP signal. The conditions are listed in Table 2. For glasses without NaI, a sample of sugar was weighed into a 1 mL volumetric flask. For glasses with poly(acrylic acid), certain masses of glucose and PAA were added to give a total of 600 mg, giving the desired percentage of PAA. To this, an appropriate amount of stock solution was added to achieve the appropriate concentration of HAA in a glass. Methanol:water (50:50) was then added to just below the 1 mL mark. The sugar was dissolved by heating the flask in a boiling hot water bath. The flask was cooled, filled to the 1 mL mark with additional methanol:water (50:50) and shaken to assure homogeneity. An aliquot of the sugar solution (Table 2) was then placed in the well of a quartz plate and heated in the center of the microwave at a heat setting and time particular to that sugar (Table 2) [8,21]. Following heating, the sugar glass was allowed to cool for 5 min at room temperature in the dark in a dessicator.

Table 2
Preparation procedures and drying times for glasses

Solid matrix	Mass ^a (mg)	V_{well}^b (μ L)	Drying conditions ^c
Fructose	600	35	Med-Lo, 28 min
Galactose	400	41	Hi 5.5, min
Glucose	600	35	Med-Lo, 22 min
Maltose	600	37	Med-Hi, 7 min
Ribose	600	35	Med-Hi, 8 min
Xylose	550	35	Med, 17 min
Fructose + NaI	630 + 70	35	Med-Lo, 10 min, 11 min
Galactose + NaI	325 + 36	45	Med-Hi, 3 min, 3 min
Glucose + NaI	630 + 70	35	Med-Lo, 15 min, 15 min
Maltose + NaI	630 + 70	40	Med-Hi, 7 min
Ribose + NaI	630 + 70	35	Med, 7 min, 8 min
Xylose + NaI	540 + 60	35	Med-Lo, 14 min, 17 min
Glucose melt	600	40	Med-Lo, 17 min
Glucose melt + NaI	630 + 70	35	Med-Lo, 15 min, 15 min
Glucose + PAA	594 + 6	40	Med-Lo, 22 min
Glucose + NaI + PAA	626 + 70 + 4	35	Med-Lo, 15 min, 15 min

^a Masses for glasses with multiple components are listed in the same order as the components in column 1.

^b Volume from a 1 mL sugar solution placed into the well of a quartz sample holder [20].

^c Microwave settings and drying times for samples. Multiple drying times indicate first in an off-center position and then a second time in the center position of the rotating plate in the microwave oven.

2.4. Glasses prepared with 10% sodium iodide

For glasses prepared with 10% NaI, a sample of sugar and an appropriate amount of sodium iodide were weighed into a 1 mL volumetric flask. For glasses with NaI and PAA present, specific masses of glucose and PAA were added to give a total mass of 630 mg. Sample preparation was continued as in the paragraph above, but different volumes were required for some of the solutions and the aliquots placed into the quartz plate. Most samples required two heating times, one in an off-center position for a certain time, and another in the center of the microwave for a given time (Table 2). The glasses were cooled as explained above.

3. Results and discussion

3.1. Physical characteristics of sugar glasses

3.1.1. Glass appearances

Most of the sugar systems formed clear, smooth, hard glasses, as determined by eye and by manually applying pressure to the glass with a metal probe. The exceptions were glasses formed from ribose and maltose. Ribose glasses had a yellow tinge and were physically softer than other sugar systems. Maltose glasses tended to contain cracks and were brittle. The application of manual pressure to the maltose glasses led to shattering. Galactose glasses, though clear and hard, frequently had a deep meniscus and/or bubbles present. This occurred because galactose was not as soluble in methanol:water (50:50) as were the other sugars. Glasses formed from fructose, glucose, and xylose were all clear, smooth, and hard glasses.

In general, the addition of the heavy-atom salt NaI improved the physical appearance of the glass compared to glasses without NaI, forming harder, clearer glasses. Galactose was the only glass that was not improved with the addition of NaI. Instead, the occurrences of the deep meniscus and bubbles in the glasses increased due to its low solubility. The addition of a small amount of poly(acrylic acid) to glucose glasses, both with and without 10% NaI present, also exhibited an increase in glass hardness. These glasses were clear and colorless, and very hard when pressure was applied manually with a metal probe. In addition to displaying the most ideal appearances, the glucose glasses containing PAA were easy to work with.

3.1.2. Glass-transition temperatures

Glass-transition temperature (T_g) values were obtained for the sugar-glass systems containing PhIP without NaI present. The glasses were prepared exactly as for the SML experiments (Table 2). T_g values for these sugar systems ranged from 257 K for ribose glass to 311 K for maltose glass (Table 1). The T_g value for the glucose glass was 284 K. The T_g values were typically lower than those listed in the literature for glasses formed by melting the pure sugar [36,37]. The differences obtained in this work were most likely caused by residual water remaining in the glass following solvent evaporation in the microwave. Water is a known plasticizer of sugars, which decreases their T_g values [38].

3.2. Excitation and emission wavelengths for solid-matrix fluorescence

A detailed study was performed to determine the solid-matrix fluorescence (SMF) excitation and emission wavelengths of 6.0 ng/mg PhIP and A α C in the six sugar-glass systems. The wavelengths for the peak maxima obtained for PhIP and A α C in each sugar glass were compared, respectively, to the fluorescence of PhIP and A α C in neutral solutions and in solutions containing 0.1 M HCl [39]. The excitation and emission wavelengths of PhIP in neutral solution were 320 and 370 nm, respectively, and in acidic solution they were 338 and 392 nm, respectively. Both the excitation and emission wavelengths were red-shifted in the acidic solutions compared to the neutral solutions, which showed that PhIP was protonated in the ground state prior to excitation.

In the sugar-glass systems, both the neutral and protonated forms of PhIP were present. The excitation spectra indicated that a fraction of PhIP was protonated in the ground state. The protonated form dominated in fructose, galactose, ribose, and xylose glasses. For example, PhIP in xylose was primarily protonated, with excitation and emission wavelengths of 343 and 389 nm. In the cases of PhIP in glucose and in maltose, the neutral and protonated forms gave equal intensities. The excitation and emission wavelengths for PhIP in glucose were 324 and 368 nm for the neutral form and 335 and 379 nm for the protonated form. Representative SMF spectra of PhIP in a glucose glass with the appropriate excitation and emission wavelengths are shown in Fig. 1. The spectra clearly demonstrate the 10 nm red-shift of both the excitation and emission spectra of the pro-

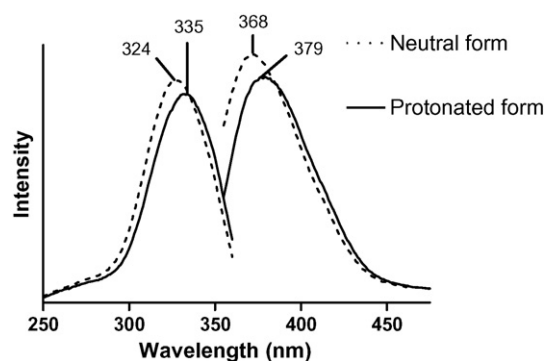


Fig. 1. SMF excitation and emission spectra of the neutral and protonated forms of 6 ng/mg PhIP in glucose without NaI. The numbers near the spectra are the wavelengths of the peak maxima in nm.

tonated form of PhIP in the glucose compared to the spectra of the neutral form of PhIP.

A small amount of HCl solution was added to the six sugar glasses, giving a concentration of 0.0005 M in the sugar solution prior to drying it in the microwave. In the glucose, maltose, xylose, and ribose glasses with the HCl added, the spectra of only the protonated species were obtained. For PhIP in fructose glass, 0.0005 M HCl led to charring during the drying process. The concentration of HCl was decreased to 0.0001 M in the preparation of the fructose glass, which led to full protonation of the PhIP. For PhIP in galactose, the concentration of HCl was increased incrementally to 0.005 M, but the fraction of the neutral form of PhIP in the galactose glass did not change and severe charring occurred.

For A α C, the excitation and emission wavelengths in neutral solution were 339 and 373 nm, respectively, and in acidic solution they were 358 and 404 nm, respectively [39]. As with PhIP, a fraction of the A α C was protonated in the ground state prior to excitation. In all of the sugar glasses, both a neutral and a protonated population were detected for A α C. Depending upon the sugar glass used, either the protonated or the neutral form dominated. For example, the excitation and emission wavelengths of the dominate form of A α C in glucose were 345 and 373 nm, which was the neutral form. A α C in xylose had protonated excitation and emission wavelengths of 372 and 413 nm. As with PhIP, the addition of a small amount of HCl should fully protonate the A α C in these sugar glasses, leading to a single population of only protonated species.

3.3. Excitation and emission wavelengths for solid-matrix phosphorescence

A study similar to the one discussed in the section above was also performed for the solid-matrix phosphorescence (SMP) of PhIP and A α C in the six sugar glasses. SMP spectra were obtained for 10.7 ng/mg PhIP and 12.0 ng/mg A α C in the six systems prepared from sugar glasses. Only the protonated population of PhIP was detected via SMP in the sugar glasses. Fig. 2 gives representative spectra for PhIP. In the six sugar-glass systems, PhIP had excitation wavelengths near 348 nm and emission wavelengths near 485 nm. However, both the protonated and

Table 3
SMF and SMP relative intensities for PhIP in sugar-glass systems with and without the heavy-atom salt NaI (10%)

Sugar system	SMF intensity ^{a,b} (no NaI)		SMP intensity (no NaI) ^{b,c}		SMP intensity (with NaI) ^{b,c}	
	S ^d	S/B ^e	S ^d	S/B ^e	S ^d	S/B ^e
Ribose	1.0	1.4	1.0	4.8	6.8	5.8
Fructose	1.1	1.6	1.0	3.8	14.9	18.9
Xylose	3.2	5.5	2.5	13.6	25.3	84.7
Galactose	3.4	3.5	4.5	40.5	3.6	59.4
Glucose	6.6	25.5	6.0	50.6	75.6	237
Maltose	7.0	13	9.0	94.2	26.1	118
Glucose + PAA ^f	7.0	27	12.2	145	209	140

^a SMF intensities are an average of three or four samples. They are relative to PhIP in ribose and were obtained using the protonated excitation and emission wavelengths near 343 and 390 nm. The actual protonated excitation and emission peak maxima depended on the sugar system used.

^b SMF and SMP intensities are not comparable.

^c SMP intensities are an average of three or four samples and are relative to PhIP in fructose without NaI present. They were obtained using the protonated excitation and emission wavelengths near 348 and 485 nm. The actual protonated excitation and emission peak maxima depended on the sugar system used.

^d Intensity with blank signal subtracted.

^e Signal-to-blank ratio.

^f Glasses prepared with glucose and PAA contained 1.0% PAA when NaI was not present and 0.42% PAA when NaI was present. The excitation and emission wavelengths were 335 and 379 nm for SMF and 345 and 487 nm for SMP, respectively.

neutral forms of A α C could be detected via SMP in many of the glass systems. Also, the neutral form of A α C was the dominate form using SMP, with an excitation wavelength near 348 nm and an emission wavelength near 475 nm.

3.4. Solid-matrix fluorescence intensities

SMF intensities for PhIP (6 ng/mg) and A α C (6 ng/mg) changed depending upon the sugar system used. As shown in Table 3, PhIP in fructose and in ribose showed the lowest SMF intensities without NaI, while PhIP in glucose and in maltose displayed the highest intensities. The highest signal-to-blank ratio was obtained with glucose. The SMF signal was 25.5 times greater than the blank signal. For A α C, a very similar trend to that of PhIP was obtained for SMF intensities and signal-to-blank ratios (Table 4). SMF intensities for A α C were typically twice that of PhIP in the same sugar glass. (The relative SMF intensities in Tables 3 and 4 are not directly comparable.) As shown in Table 4, A α C in fructose exhibited the lowest SMF intensity, and A α C in glucose and maltose gave the highest intensities. For the SMF of A α C, signal-to-blank ratios were 3.6 for fructose and 48.9 for maltose.

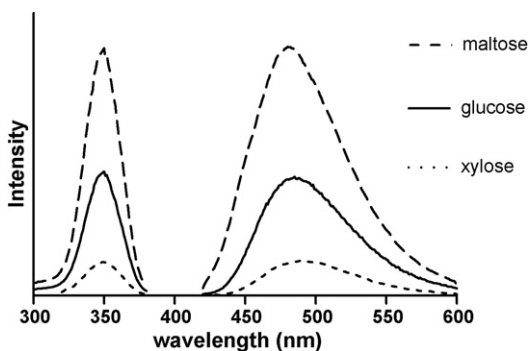


Fig. 2. SMP excitation and emission spectra of 10.7 ng/mg PhIP in maltose, glucose, and xylose without NaI. Excitation and emission wavelengths used were 342 and 482, 345 and 487, and 350 and 487 nm, respectively.

3.5. Solid-matrix phosphorescence intensities

3.5.1. Systems without a heavy-atom salt

The SMP intensities for the HAAs (10.7 ng/mg of PhIP and 12.0 ng/mg A α C) showed considerable change depending upon the sugar system used. The data in Table 3 show that the SMP using protonated wavelengths of PhIP without PAA gave the lowest SMP intensities in fructose and in ribose, and PhIP in maltose displayed the highest intensity, approximately nine times greater than those of PhIP in ribose. With maltose, the highest signal-to-blank ratio was acquired, giving a value of 92.4. The SMP using neutral wavelengths of A α C in ribose and in fructose exhibited the lowest SMP intensities, as shown in Table 4. The SMP intensity values for A α C in galactose and in glucose were 18 and 24 times greater than that of A α C in ribose, respectively. However, A α C in maltose gave the

Table 4
SMF and SMP intensities of A α C in sugar-glass systems without NaI (10%) present

Sugar system	SMF intensity ^{a,b}		SMP intensity ^{b,c}	
	S ^d	S/B ^e	S ^d	S/B ^e
Fructose	1.0	3.6	1.4	5.9
Ribose	2.0	9.3	1.0	8.6
Xylose	2.0	10.7	3.0	20.1
Galactose	2.9	17.7	18.2	69.1
Glucose	4.7	37.3	24.4	90.6
Maltose	5.3	48.9	83.6	224

^a SMF intensities are an average of three or four samples and are relative to the intensity of A α C in fructose. They were obtained using the neutral excitation and emission wavelengths near 345 and 373 nm. The actual neutral excitation and emission peak maxima depended on the sugar system used.

^b SMF and SMP intensities are not comparable.

^c SMP intensities are an average of three or four samples and are relative to the intensity of A α C in ribose. They were obtained by using the neutral excitation and emission wavelengths near 348 and 475 nm. The actual neutral excitation and emission peak maxima depended on the sugar system used.

^d Intensity with blank signal subtracted.

^e Signal-to-blank ratio.

highest SMP intensity, which was 84 times greater than the SMP intensity for PhIP in ribose. This indicated that A α C was held much more rigidly in maltose than in the other sugar-glass systems. The signal-to-blank ratio values for the SMP of A α C were 5.9 in fructose and 224 in maltose.

3.5.2. Systems with a heavy-atom salt

SMP spectra and intensities were obtained for 11.4 ng/mg PhIP in the six sugar systems discussed above with 10% NaI added. It was shown by Wang and Hurtubise [23] that the addition of 10% NaI permitted very strong SMP signals for PhIP in glasses formed from crystalline glucose. Only the protonated species of PhIP was detected, and the same excitation and emission wavelengths were used as for samples without NaI present. The addition of the heavy-atom salt, NaI, to the glasses caused a significant increase in the intensities of PhIP [40].

The increase in SMP intensity with the addition of NaI was different depending upon the sugar glass (Table 3). For example, the SMP intensity of PhIP in maltose increased by a factor of about 3 with the addition of NaI, whereas the intensity of PhIP in fructose increased by a factor of 15. PhIP in glucose gave an increase in SMP intensity of about 13 times with 10% NaI present over that of PhIP in glucose alone. The addition of 10% NaI to galactose glass actually led to a decrease in SMP intensity, due to the decreased solubility of galactose in methanol:water (50:50) in the presence of NaI. The SMP intensities for PhIP in fructose with 10% NaI glass and in ribose with 10% NaI glass remained the lowest, while intensities for PhIP in glucose with 10% NaI glass was the highest. The heavy-atom effect was much stronger in glucose glasses than in the other sugar glasses. This indicated that NaI is situated in a much closer proximity to PhIP in glucose than in the other sugar glasses. Example signal-to-blank ratios for PhIP in these systems were 5.8 for ribose and 237 for glucose (Table 3).

3.6. Glucose-glass systems with poly(acrylic acid)

Small amounts of poly(acrylic acid) were added to glass systems formed from crystalline glucose. The PAA was added to the glass systems because PAA–salt mixtures were previously shown to be effective SMP matrices [41]. The carboxyl group is the main functional group in PAA, and it can form a complex hydrogen-bonding network. This would make the solid matrix more rigid and would favor SMP. The concentrations of PAA in the glucose glasses were 1.0% with only PAA, and 0.42% with PAA and 10% NaI. Concentrations of PAA were experimentally determined to give the greatest increase in SMP intensity. As mentioned previously, glasses formed by these systems were clear and very hard, and not difficult to work with.

3.6.1. Solid-matrix fluorescence

SMF spectra and intensities were obtained for 6.0 ng/mg PhIP in glucose glasses with small amounts of PAA present. The addition of PAA to glucose glasses caused full protonation of the PhIP, leading to only one excitation and one emission band, with peak maxima at 335 and 379 nm. As shown in Table 3, the addition of PAA to the glucose systems only increased the

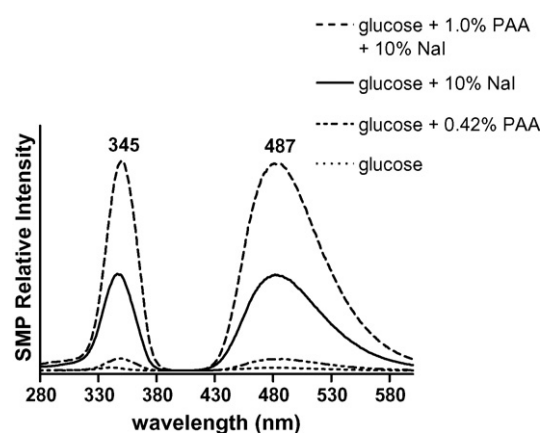


Fig. 3. SMP spectra of PhIP in glucose-glass systems with and without NaI and with and without poly(acrylic acid) (PAA). The numbers near the excitation and emission spectra for glucose with 1.0% PAA and 10% NaI are the excitation and emission wavelengths used to obtain spectra for all of the glucose glasses shown.

SMF intensity of PhIP by a factor of 1.1 compared to PhIP in the glucose systems without PAA. The signal-to-blank ratio also only showed a slight increase compared to that for PhIP in glucose without PAA.

3.6.2. Solid-matrix phosphorescence

SMP spectra and intensities were acquired for 10.7 ng/mg PhIP in glucose with 1.0% PAA and for 11.4 ng/mg PhIP in glucose with 0.42% PAA and 10% NaI. The protonated excitation and emission wavelengths of 345 and 487 nm were used. As shown in Table 3 and Fig. 3, the addition of small amounts of PAA showed a considerable increase in the SMP intensity of PhIP. The SMP intensity of PhIP in glucose with 1.0% PAA was approximately twice the intensity detected for PhIP in glucose alone, with an approximate 3-fold increase in the signal-to-blank ratio. Also, the SMP intensity of PhIP in glucose with 0.42% PAA and 10% NaI was about three times greater than that for PhIP in the same system without PAA. The total increase in SMP intensity for 11.4 ng/mg PhIP in glucose glass with 0.42% PAA and 10% NaI compared to 10.7 ng/mg PhIP in glucose glass with no NaI or PAA was greater than 30-fold. The addition of PAA to glucose glasses gave a more rigid solid matrix than glucose glasses, increasing the probability of phosphorescence.

3.7. Analytical figures of merit

Limits of detection (LODs) were calculated using the IUPAC method (3σ) [42] for PhIP in maltose glasses and in glucose glasses with and without PAA and for A α C in maltose with NaI. The LOD values for PhIP are shown in Table 5. The SMP LODs with maltose were 0.17 pmol/mg without NaI and 0.04 pmol/mg with NaI present. In previous work, Mendonsa and Hurtubise [8] showed that glasses from crystalline glucose gave SMP LODs of 0.26 and 0.16 pmol/mg, without and with NaI, respectively. Mendonsa and Hurtubise [8] demonstrated that glasses from glucose melt gave LODs of 0.06 and 0.04 pmol/mg, without and with NaI, respectively. Thus, with NaI present, maltose gave a LOD comparable to that of glucose melt with NaI and four times less than that of

Table 5
Limits of detection for PhIP in several glass systems

Solid matrix	SMP LOD of PhIP (pmol/mg)	SMF LOD of PhIP (pmol/mg)
Glucose ^a	0.26 ^c	1.4 ^c
Glucose + 10% NaI ^a	0.16 ^c	–
Maltose ^b	0.17	–
Maltose + 10% NaI ^b	0.04	–
Glucose + 1.0% PAA ^a	0.11	0.21
Glucose + 0.42% PAA + 10% NaI ^a	0.44	–

^a Excitation and emission wavelengths used for PhIP in glucose glasses were 335 and 379 nm for SMF and 345 and 487 nm for SMP.

^b SMP excitation and emission wavelengths used for PhIP in maltose glasses were 342 and 482 nm.

^c Obtained from Reference [8].

crystalline glucose with NaI present. The SMP LOD for A α C in maltose with NaI was determined to be 0.09 pmol/mg. Though it does not form a clear glass like glucose, maltose is certainly a useful glass for detection of PhIP and A α C, as demonstrated by the low limits of detection, high SMP and SMF intensities, and the brief amount of time (7 min compared to 22 min for glucose) required for drying these glasses. The lowest LOD in this study was obtained for PhIP in maltose with 10% NaI.

The SMF and SMP LODs for glasses from crystalline glucose with PAA present without heavy atom were 0.21 and 0.11 pmol/mg, respectively. Even though the addition of the heavy-atom salt increased the SMP intensity, it did not decrease the SMP LOD sufficiently due to a relatively high SMP background signal and a high standard deviation when NaI was present with PAA. The SMP LOD for glasses from glucose with PAA and NaI was 0.44 pmol/mg. However, glucose glasses with 1.0% PAA present are effective solid matrices, and both SMF and SMP are useful for the detection of HAAs, because they give reasonably low LODs for PhIP, and form clear, hard glasses that are easy to work with.

Linear ranges for PhIP in glucose with and without the heavy-atom salt, NaI, were determined previously by Mendonsa and Hurtubise [8]. They found linear ranges for PhIP in glucose without NaI to be 0.32–13 ng/mg for SMF and 0.059–40 ng/mg for SMP. They also found that the linear range for the SMP of PhIP in glucose with 10% NaI was 0.036–25 ng/mg. In this current work, six calibration curves were obtained over a limited range to show that linearity could be obtained. Additional work would have to be done to determine the exact concentration at which the calibration curves become non-linear. Some examples of the linear ranges obtained in this work are as follows. The linear ranges for the SMP of PhIP in maltose were 0.037–10.7 ng/mg ($R=0.995$) without NaI, and 0.009–11.4 ng/mg ($R=0.975$) with 10% NaI. Similarly, the linear range for the SMP of A α C in maltose with 10% NaI was 0.016–12.0 ng/mg ($R=0.974$). The SMF calibration curve for PhIP in glucose with 1% PAA gave a linear range of 0.049–6.0 ng/mg ($R=0.994$).

3.8. Guidelines for selecting sugar glasses as solid matrices

The SMP intensities of PhIP in the sugar glasses were compared to the glass-transition temperatures obtained in this work

(Table 1). Samples were prepared as described in Table 2. In sugar glasses with no heavy-atom salt or PAA, the SMP intensity of PhIP increased with the T_g value of the glass. An approximate linear relationship ($R=0.942$) between SMP intensity and T_g was obtained. The lowest intensities were obtained for PhIP in ribose, which had the lowest T_g value (257 K). This glass was not very rigid. PhIP in maltose had both the greatest SMP intensity and the highest T_g value. Therefore, one important physical property to consider when selecting a sugar glass as a solid matrix for room-temperature SMP is the glass-transition temperature. Glasses with T_g values at room-temperature, and higher, hold the phosphor more rigidly at room temperature, and thus the phosphor should have a higher SMP intensity than in glasses with lower T_g values. A sugar glass with a T_g value below room temperature would not be as rigid as a glass with a T_g value near or above room temperature.

It is also important to consider the solubility of the sugar in the solvent. For example, galactose had one of the higher T_g values, and PhIP had a high SMP in this glass. However, galactose was poorly soluble in methanol:water (50:50), and the glass formed tended to have a deep meniscus. The addition of NaI to this glass decreased the solubility further, and thus this glass was not considered acceptable for analytical measurements. Physical properties can play a significant role in the effectiveness of a sugar glass for SMP, and consideration of these properties can aid in obtaining greater SMP intensities and lower limits of detection.

4. Conclusions

Several new sugar-glass systems were optimized and investigated for solid-matrix luminescence using PhIP and A α C as model compounds. SMF and SMP spectra and intensities were obtained with these glass systems. In some of the sugar-glass systems, both the neutral and protonated forms of PhIP and A α C appeared. However, using a weakly acidic solution to prepare these sugar glasses would give the fully protonated form of PhIP and A α C. The different physical properties of the glasses led to a range of intensities for the model compounds and different limits of detection for PhIP. It is very important to consider physical properties such as T_g and solubility in determining which sugars should be effective solid matrices. Maltose, in particular, has a T_g value of 311 K, and was shown to be comparable to the glasses formed from the glucose melt as a solid matrix for PhIP [8]. A very low SMP LOD of 0.04 pmol/mg was obtained for PhIP in maltose with 10% NaI, the lowest LOD obtained in this study.

It was also shown that the addition of small amount of PAA to the glucose-glass systems increased the SMP intensities of PhIP, and glucose with 1.0% PAA lowered the limit of detection for the SMP of PhIP to 0.1 pmol/mg. The limit of detection for the SMF of PhIP in glucose with 1.0% PAA was also very good (0.2 pmol/mg), showing that low levels of PhIP can be detected using both SMP and SMF in this system. However, glasses formed from glucose with 10% NaI and 0.42% PAA did not improve the SMP limit of detection for PhIP, due to increased SMP background signals with PAA present.

From this work, at least two new and interesting sugar-glass systems are available for use as very effective solid matrices for phosphorescence: glasses from maltose with 10% NaI and glasses from glucose with 1.0% poly(acrylic acid). Glucose with 1.0% PAA formed clear, hard glasses. Though maltose with 10% NaI was brittle and tended to crack, this did not affect the reproducibility. Both glass systems were relatively easy to prepare, and displayed high SMF and SMP intensities and low limits of detection for PhIP. Glucose with PAA yielded low LOD values for PhIP using both SMF and SMP. Glucose with PAA and NaI does have the potential to be a useful solid matrix if the SMP background signal can be reduced by purifying the PAA. Also, other polymers added to the glucose glass may form rigid glasses and increase the SMP intensity to a greater degree than PAA.

Acknowledgement

This work was supported by the Chemical Sciences, Geosciences and Biosciences Division, Office of Basic Energy Sciences, Office of Science, U.S. Department of Energy (DE-FG02-04ER15545).

References

- [1] R.J. Hurtubise, *Phosphorimetry: Theory, Instrumentation, and Application*, VCH Publishers Inc., New York, NY, 1990.
- [2] T. Vo-Dinh, *Room Temperature Phosphorimetry for Chemical Analysis*, vol. 68, John Wiley & Sons, New York, 1984.
- [3] A. Thompson, R.J. Hurtubise, *Appl. Spectrosc.* 59 (2005) 126.
- [4] B.W. Smith, R.J. Hurtubise, *Anal. Chim. Acta* 502 (2004) 149.
- [5] R.J. Hurtubise, A. Thompson, S.E. Hubbard, *Anal. Lett.* 38 (2005) 1823.
- [6] R.J. Hurtubise, *Anal. Chim. Acta* 351 (1997) 1.
- [7] J. Wang, R.J. Hurtubise, *Anal. Chem.* 69 (1997) 1946.
- [8] S. Mendonsa, R.J. Hurtubise, *Appl. Spectrosc.* 54 (2000) 456.
- [9] T. Rojas-Duran, I. Sanchez-Barragan, J.M. Costa-Fernandez, A. Sanz-Medal, *Analyst* 131 (2006) 785.
- [10] N. Rupcich, R. Nutiu, Y. Li, J.D. Brennan, *Angew. Chem. Int. Ed.* 45 (2006) 3295.
- [11] J.-M. Liu, T.-L. Yang, F. Gao, L.-X. Hu, H.-X. He, Q.-Y. Liu, Z.-B. Liu, X.-M. Huang, G.-h. Zhu, *Anal. Chim. Acta* 561 (2006) 191.
- [12] R.A. Correa, G.M. Escandar, *Anal. Chim. Acta* 571 (2006) 58.
- [13] Y. Wei, L. Ding, J. Li, Y. Wei, C. Dong, *Anal. Lett.* 37 (2004) 435.
- [14] A. Salinas-Castillo, J.F. Fernandez-Sanchez, A. Segura-Carretero, A. Fernandez-Gutierrez, *Anal. Chim. Acta* 550 (2005) 53.
- [15] J.F. Carpenter, L.M. Crowe, J.H. Crowe, *Biochim. Biophys. Acta* 923 (1987) 109.
- [16] L.M. Crowe, J.H. Crowe, J.F. Carpenter, *BioPharm.* 6 (1993) 28.
- [17] J.H. Crowe, L.M. Crowe, J.F. Carpenter, *BioPharm.* 6 (1993) 40.
- [18] T. Arakawa, S.N. Timasheff, *Biochemistry* 21 (1982) 6536.
- [19] T.E. Honadel, G.J. Killian, *Cryobiology* 25 (1988) 331.
- [20] J. Wang, R.J. Hurtubise, *Appl. Spectrosc.* 50 (1996) 53.
- [21] S. Mendonsa, R.J. Hurtubise, *J. Luminesc.* 97 (2002) 19.
- [22] S. Mendonsa, R.J. Hurtubise, *Appl. Spectrosc.* 55 (2001) 1385.
- [23] J. Wang, R.J. Hurtubise, *Anal. Chim. Acta* 332 (1996) 299.
- [24] G.S. Parks, S.B. Thomas, *J. Am. Chem. Soc.* 56 (1934) 1423.
- [25] G.S. Parks, H.M. Huffman, F.R. Cattoir, *J. Phys. Chem.* 32 (1928) 1366.
- [26] G.S. Parks, L.E. Barton, M.E. Spaght, J.W. Richardson, *Physics* 5 (1934) 193.
- [27] L. Slade, H. Levine, *Pure Appl. Chem.* 60 (1988) 1841.
- [28] L. Slade, H. Levine, *Crit. Rev. Food Sci. Nutr.* 30 (1991) 115.
- [29] H. Levine, L. Slade, *J. Chem. Soc., Faraday Trans.* 84 (1988) 2619.
- [30] S.L. Shamblin, X. Tang, L. Chang, B.C. Hancock, M.J. Pikal, *J. Phys. Chem. B* 103 (1999) 4113.
- [31] S. Yoshioka, Y. Aso, *J. Pharm. Sci.* 94 (2005) 275.
- [32] S. Manabe, K. Tohyama, O. Wada, T. Aramaki, *Carcinogenesis* 12 (1991) 1945.
- [33] P. Pais, C.P. Salmon, M.G. Knize, J.S. Felton, *J. Agric. Food Chem.* 47 (1999) 1098.
- [34] M. Murkovic, *Eur. J. Lipid Sci. Tech.* 106 (2004) 777.
- [35] K.M. Gorlewska-Roberts, C.H. Teitel, J.O.J. Lay, D.W. Roberts, F.F. Kadlubar, *Chem. Res. Toxicol.* 17 (2004) 1659.
- [36] Y. Roos, *Carbohydr. Res.* 238 (1993) 39.
- [37] F. Franks, *Biophys. Chem.* 105 (2003) 251.
- [38] T.R. Noel, R. Parker, S.G. Ring, *Carbohydr. Res.* 282 (1996) 193.
- [39] S. Mendonsa, Ph.D. Dissertation, University of Wyoming, Laramie, WY, 2001.
- [40] N.J. Turro, *Modern Molecular Photochemistry*, University Science Books, Sausalito, CA, 1991.
- [41] R.A. Dalterio, R.J. Hurtubise, *Anal. Chem.* 55 (1983) 1084.
- [42] G.L. Long, J.D. Winefordner, *Anal. Chem.* 55 (1983) 712A.

A high throughput and selective method for the estimation of valproic acid an antiepileptic drug in human plasma by tandem LC–MS/MS

Deepak S. Jain^{a,b}, Gunta Subbaiah^b, Mallika Sanyal^c, Pranav Shrivastav^{a,*}

^a Department of Chemistry, School of Sciences, Gujarat University, Navrangpura, Ahmedabad 380009, India

^b Analytical Development Laboratory, Research Center, Torrent Pharmaceutical Limited, At Village Bhat, Gandhinagar 382428, India

^c Chemistry Department, St. Xaviers' College, Navrangpura, Ahmedabad 380009, India

Received 15 August 2006; received in revised form 27 September 2006; accepted 27 September 2006

Available online 15 November 2006

Abstract

A high throughput liquid chromatography–tandem mass spectrometric (LC–MS/MS) method for the determination of valproic acid, an antiepileptic drug, in human plasma is described. It is a rapid and sensitive isocratic reversed-phase liquid chromatography–tandem mass spectrometric method equipped with turbo ion spray (TIS) source, operating in the negative ion and pseudo selective reaction monitoring (SRM) acquisition mode to quantify valproic acid. The extraction of valproic acid and hydrochlorothiazide (IS) from the plasma involved sample treatment with phosphoric acid followed by solid-phase extraction using Waters hydrophilic–lipophilic balance (HLB) cartridge giving extracts free from endogenous interferences. Sample preparation by this method yielded very good and consistent mean recoveries of 99.73 and 74.47% for valproic acid and IS, respectively. The method was linear over the dynamic range of 2.0–200.0 $\mu\text{g/ml}$ (covering entire therapeutic range) with a correlation coefficient $r \geq 0.9989$. The coefficient of variance (CV, %) was 7.03% at 2.0 $\mu\text{g/ml}$ (LLOQ). This method was fully validated for its accuracy, precision, recovery and matrix effect especially because the pattern of elution of all the analytes may appear as flow injection type. The analyte stability was examined under conditions mimicking the sample storage, handling and analysis procedures. The method was successfully applied for bioequivalence studies in human subject samples after oral administration of 500 mg formulations.

© 2006 Elsevier B.V. All rights reserved.

Keywords: Valproic acid; Pseudo selective reaction monitoring (SRM); Solid-phase extraction; LC–MS/MS; Human plasma

1. Introduction

Valproic acid is an antiepileptic drug with unique anticonvulsant properties and is used in the treatment of primary generalized seizures, partial seizures and myoclonic seizures [1]. Valproate sodium (sodium 2-propylpentanoate) is the sodium salt of valproic acid which dissociates to the valproate ion in the gastrointestinal tract and exists as valproate ion in the blood. Due to changes in valproic acid dose, concomitant medication and/or the clinical condition of the subject, monitoring of valproic levels in patient's plasma is essential. Suitable methods ideally require a small specimen, have a simple sample preparation procedure, meet clinical sensitivity needs while being rugged and offering high throughput.

Number of analytical methods is reported in recent scientific literature for the quantification of valproic acid in biological matrices. High performance liquid chromatographic analysis (HPLC) with UV or fluorescence detection [2–6] has adequate sensitivity but usually requires that the valproate be modified by derivatization prior to analysis to provide a suitable chromophore or fluorophore. Amini et al. [7] were able to estimate valproic acid without derivatization with a quantification limit of 1.25 $\mu\text{g/ml}$ using 1 ml of plasma. Capillary electrophoretic techniques [8,9] have also been employed with UV detection to quantify valproic acid in plasma samples. Desired sensitivity has been achieved using gas chromatography with tandem mass spectrometry (GC/MS/MS) [10–16]; however, prior derivatization limits its suitability for routine sample analysis. Very recently, Zhang and co-workers [17] have developed an in situ derivatization method followed by solid-phase micro extraction and GC/MS detection to achieve a LLOQ of 0.3 $\mu\text{g/ml}$ in human plasma. This sensitive method uses head space extraction

* Corresponding author. Tel.: +91 79 26300969; fax: +91 79 26308545.
E-mail address: pranav_shrivastav@yahoo.com (P. Shrivastav).

and simultaneous concentration using a SPME technique. But the extraction and chromatographic analysis time takes about 55 min, which limits the suitability of the method for high throughput applications.

For the detection of underivatized valproic acid separated by HPLC, mass spectrometry may provide an alternate to UV detection. Such a combination can offer the advantage of the speed of analysis associated with HPLC and the sensitivity and selectivity associated with mass spectrometry. In this context two important communications have appeared in the recent literature describing the use of liquid chromatography–tandem mass spectrometry to quantify valproic acid in human and mouse plasma. Ramakrishna et al. [18] have employed solid-phase extraction for processing 200 μ l of human plasma to achieve a lower limit of quantification of 0.5 μ g/ml. This method is the first on LC/MS detection operating in the single ion monitoring mode, but requires a laborious sample preparation procedure with a run time of 4.5 min. Moreover, with an upper limit of quantification (60 μ g/ml), the method does not span the therapeutic plasma concentration range of valproic acid (50–100 μ g/ml) [19]. Bonelli and co-workers [20] have determined valproic acid in mouse plasma with very high sensitivity (0.15 μ g/ml) using semi-automated sample preparation. The plasma protein precipitation method employed here is very fast to produce analyzable samples, but in terms of cleanliness, the sample is considered crude. This may result in high column back pressure affecting the column life and hence requiring frequent maintenance. This could also be a limitation when it comes to analyzing large number of samples with mass spectrometry. Moreover, the sample injection volume of 20 μ l and analytical run time of 4.5 min is high compared to the present method.

The objective of this study is to develop and validate a high throughput LC–MS/MS method for routine measurement of valproic acid in human plasma in support of clinical findings. We have developed a simple, fast and sensitive LC–MS/MS detection for the analysis of valproic acid with an LLOQ of 2.0 μ g/ml using 200 μ l of human plasma. The SPE eluate (5 μ l) was directly subjected to LC–MS/MS analysis without any prior concentration and reconstitution steps. The run time of 2.0 min described here is particularly suited to high throughput laboratories. The proposed method ensures the estimation of valproic acid up to 72 h with desired accuracy and precision for elimination phase concentration in human volunteers for bioequivalence or bioavailability studies.

2. Experimental

2.1. Materials and reagents

Valproic acid and hydrochlorothiazide standards were procured from Torrent Research Centre (Ahmedabad, India). Water used for the LC–MS/MS was prepared with a Milli-Q water purification system from Millipore (Bangalore, India). Acetonitrile and methanol of HPLC grade were purchased from JT Baker (Phillipsburg, USA). Ammonium formate was of molecular biology grade and obtained from Sigma (Steinheim, Germany), while Suprapure ortho-phosphoric acid was procured

from Merck (Darmstadt, Germany). Oasis HLB[®] SPE cartridges, used for sample preparation, were procured from Waters (Milford, Massachusetts, USA). A 5 mM aqueous ammonium formate, adjusted to pH 8.0 with diluted ammonia solution was used to prepare the mobile phase. Control human plasma was procured from Green cross blood bank (Ahmedabad, India) and was stored at -20°C .

2.2. Liquid chromatography/tandem mass spectrometry instrumentation

An Applied Bio-systems MDS SCIEX (Concord, Ontario, Canada) API-4000 triple Quadrupole mass spectrometer with a turbo ion spray (TIS) ionization probe was interfaced with Perkin-Elmer (Shelton CT, USA) PE 200 series liquid chromatograph. LC system included a vacuum degasser, a quaternary pump, a thermostatted autosampler and column oven compartment. The Analyst Software Version 1.4 package supplied by Applied Bio-systems (MDS SCIEX) was used to control the LC–MS/MS system, as well as for data acquisition and processing. Valproic acid and hydrochlorothiazide (internal standard) were separated on a 5 μ m Thermo Electron (UK) Betabasic C-8 column, 100 mm \times 4.6 mm i.d. (length \times inner diameter) maintained at 45°C . Samples were separated under isocratic conditions with buffer (5 mM ammonium formate pH 8): acetonitrile in ratio of 20:80 (v/v), at a flow rate of 1000 μ l/min flow rate and split ratio of load:waste of 1:3. The autosampler temperature was set at 10°C .

The mass spectrometer was operated in the negative TIS mode with selected reaction monitoring for all the analytes. The focusing of deprotonated precursor molecules were maximized by tuning the declustering potential (DP), and scanned ions were then fragmented to product ions by collision–activation dissociation (CAD) using nitrogen as the collision gas. The mass spectrometer parameters optimized are given in Table 1. The precursor to a stable product ion (in this case the molecular ion) transitions were monitored at m/z 143.0 \rightarrow 143.0 for valproic acid and m/z 296.10 \rightarrow 205.0 for IS. The initial product ion spectrum of valproic acid with molecular structure is shown in Fig. 1 while the product ion spectrum for internal standard is displayed in Fig. 2.

2.3. Preparation of standard stocks and plasma samples (calibration standard and quality control samples)

Stock solutions of 10.0 mg/ml valproic acid and 1.0 mg/ml hydrochlorothiazide (IS) were prepared by dissolving their requisite amounts in a mixture of water:methanol 50:50 (v/v) ratio. These stock solutions were further diluted to get an intermediate concentration of 4.0 mg/ml for valproic acid and 100 μ g/ml for IS, respectively, in water:methanol 50:50 (v/v) ratio. Working solution of valproic acid of different concentrations required for spiking plasma calibration and quality control samples were subsequently prepared in water from the main stock of 10.0 mg/ml and intermediate stock of 4.0 mg/ml. The IS working solution of 30 μ g/ml was prepared from the intermediate stock of 100.0 μ g/ml and was used as internal standard in plasma samples

Table 1
Optimized MS source and compound dependent parameters for valproic acid and hydrochlorothiazide (IS)

Source dependent parameters for		
Valproic acid and hydrochlorothiazide		
Collision activation dissociation (CAD) (psig)	6.00	
Curtain gas (CUR)	25.00	
Gas 1 (GS1)	30.00	
Gas 2 (GS2)	50.0	
Ion spray voltage (IS) (V)	−4200	
Turbo heater temperature (TEM) (°C)	450.00	
Interface heater (Ihe)	ON	
Entrance potential (EP) (V)	−10	
Compound dependent parameters for		
Parameters	Valproic acid	IS
Declustering potential (DP) (V)	−60	−70
Collision energy (CE) (V)	−30	−35
Collision cell exit potential (CXP) (V)	−15	−15
MS detection parameters for		
Valproic acid and hydrochlorothiazide		
Period	1	
Experiment	1	
Scan type	MRM	
Polarity	Negative	
Ion source	Turbo Spray	
Resolution Q1	Unit	
Resolution Q3	Low	
Intensity threshold (cps)	25.00	
Settling time (ms)	0.0	
MR pause (ms)	5.0	
Multiple channel analysis (MCA)	No	
Dwell time (ms)	150.0	
Step size (amu)	0.00	

preparation. All solutions were prepared and stored at 2–8 °C until use. The control samples of blank plasma (free of valproic acid) stored under refrigeration, were completely thawed before use. The spiking (5%, v/v) of these blank plasma was carried out using the working solution of valproic acid to obtain the desired concentration of valproic acid in calibration and quality control samples. The spiked QC samples were stored at −70 °C for stability studies.

2.4. Protocol for sample extraction

Spiked plasma samples were withdrawn from freezer maintained at −70 °C and allowed to thaw at room temperature for 30–45 min. The samples were vortexed adequately using a vortex mixer before dispensing. Using a micropipette, 200 µl of plasma was transferred into eppendorff tubes. To these tubes, 50 µl of working solution (30 µg/ml) of hydrochlorothiazide was added and vortexed to mix. The samples were treated with 10 µl of 10% H₃PO₄ (v/v) followed by addition of 250 µl Milli-Q water and mixed again. Loading of the sample was done thereafter on HLB cartridge previously conditioned with 1 ml methanol followed by 1 ml water. Throughout the extraction

procedure a uniform vacuum of 4 psig was applied to the SPE cartridge. The washing of the cartridge with retained valproic acid and matrix was carried out with 1 ml water and 1 ml, 5% (v/v) aqueous methanol. Further vacuum was applied for 2 min to dry the sorbent. Valproic acid and IS were eluted with 1.0 ml acetonitrile and transferred to an autosampler vial for injection. A 5 µl of eluate was then subjected to LC–MS/MS analysis in partial loop mode.

3. Results

3.1. Selectivity

Selectivity can be defined as the ability of the method to distinguish and quantify the analyte in the presence of endogenous and/or exogenous interferences. The method employed for extraction gave very good selectivity and sensitivity for the analysis of valproic acid and IS in the blank plasma. Fig. 3 represents the blank plasma selectivity, zero standard (plasma sample with only internal standard) and the peak response of valproic acid at LLOQ (2.0 µg/ml, respectively). The ion chromatograms show excellent peak shape for valproic acid and IS. The retention time (RT) was short for both, which makes it suitable for routine analysis. The method gave clean chromatograms free of background interference. Test for selectivity was carried out in 10 lots of blank plasma which included 4 lots of buffered plasma, 4 lots of heparinised plasma, 1 lot of lipemic plasma and 1 lot of haemolysed plasma. The area observed at the RT of valproic acid was less than 20% at the LLOQ (2.0 µg/ml) area, where as the area observed at the RT of IS was less than 5% the area of IS concentration used in sample preparation (Table 2). The aim of performing selectivity check with these different types of plasma samples is to ensure the integrity of volunteers sample analysis.

3.2. Linearity

The linearity of the method was determined by analysis of standard plots associated with nine-point calibration standards in the dynamic range of 2.0–200 µg/ml. Best-fit calibration curves of peak area ratio versus concentration were drawn. The concentration of valproic acid was calculated from the simple linear equation using regression analysis of spiked plasma calibration standard with the reciprocal of the drug concentration as a weighting factor (1/concentration, i.e., 1/x); $y = mx + c$, as indicated in Table 3. The calibration curves were linear from 2.0 to 200.0 µg/ml with mean correlation coefficient of $r = 0.9995$ calculated from five calibrations. The precision values obtained for slopes, and correlation coefficient 'r' from five linearties of valproic acid was 3.81 and 0.05%, respectively. The observed mean back calculated concentration with accuracy (% nominal concentration) and precision (CV, %) of five linearties are given in Table 4.

3.3. Recovery

The percentage recovery of valproic acid was determined by comparing the mean area of five replicates each of extracted

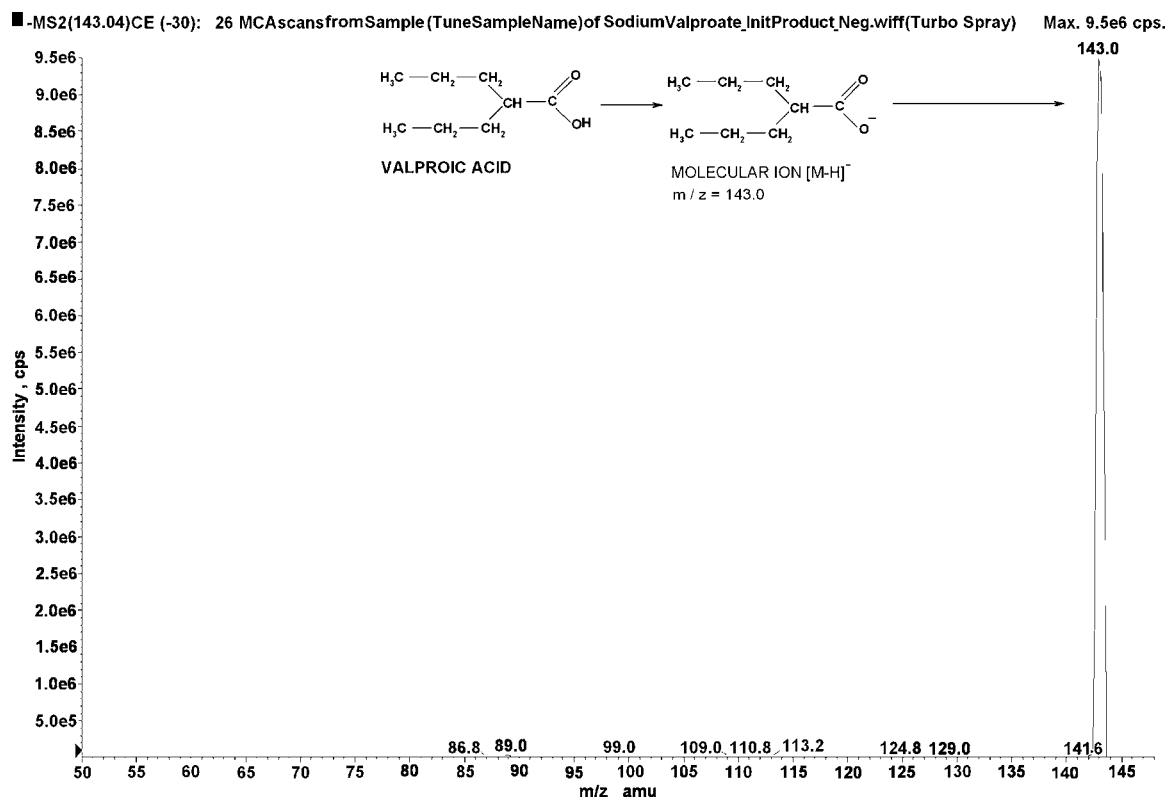


Fig. 1. Product ion of valproic acid is having same m/z as its parent ion even at -30 V collision energy.

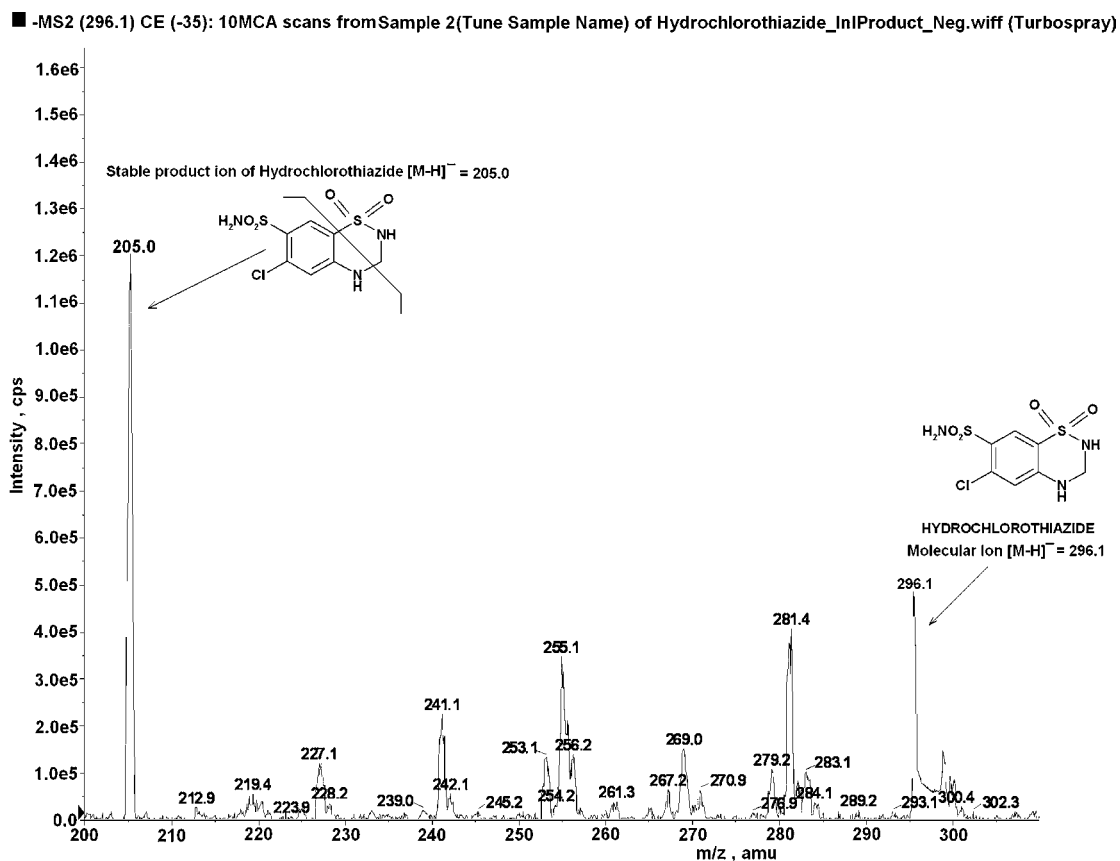


Fig. 2. MS2 of hydrochlorothiazide, with stable product ion with m/z of 205.0.

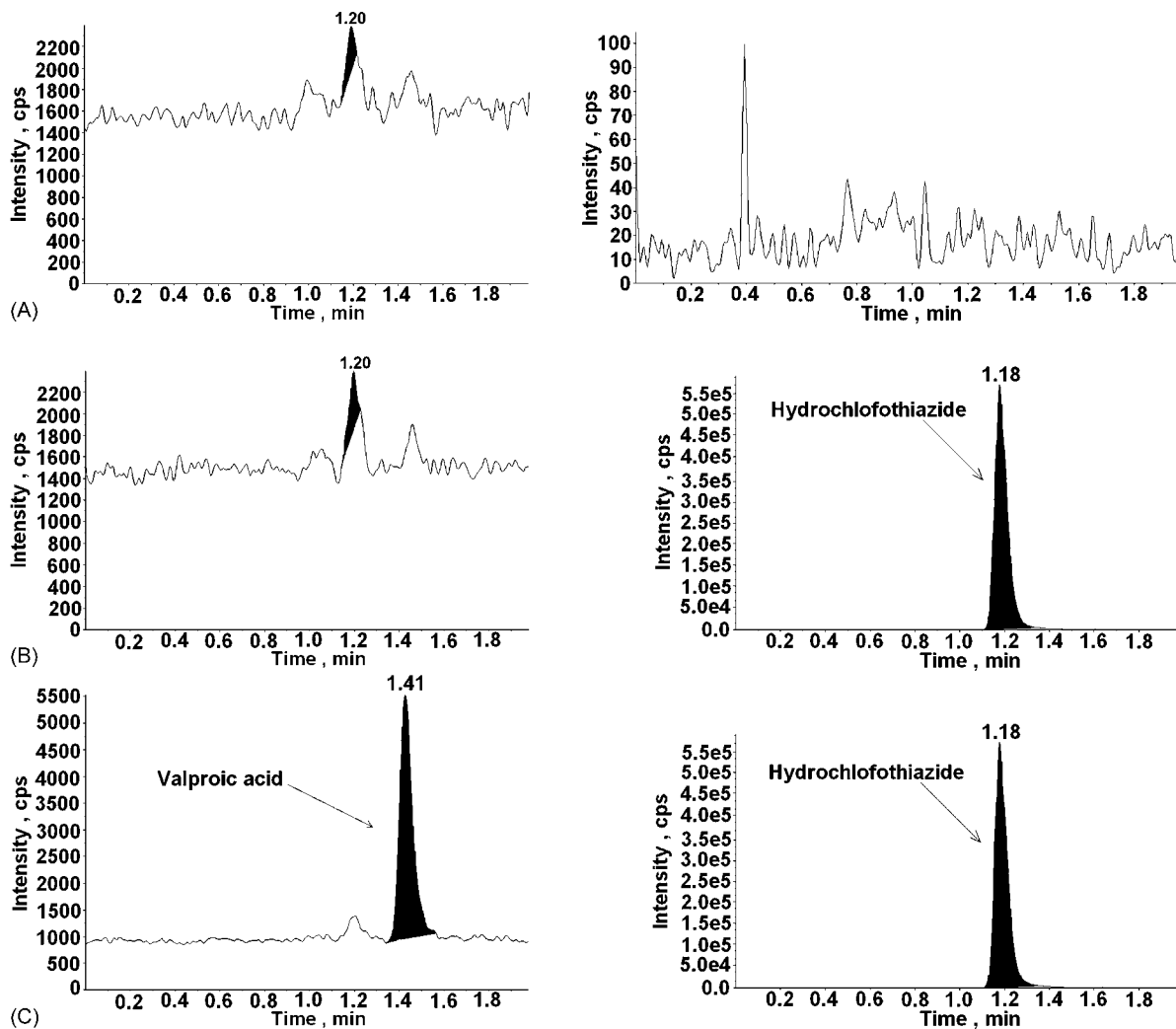


Fig. 3. Representative chromatogram of (A) blank plasma; (B) zero standard and (C) lower limit of quantification (2.0 $\mu\text{g/ml}$) for valproic acid.

quality control samples, i.e., low quality control (LQC), middle quality control (MQC) and high quality control (HQC) samples with mean area of freshly prepared un-extracted LQC, MQC and HQC samples. The overall mean recovery for valproic acid at these levels was 97.15, 101.57 and 100.47%, respectively, with variability (CV, %) between them of 2.71%. The recovery of IS was found to be 74.47%. Thus, the consistency in quantitative recoveries of valproic acid and IS upholds the extraction procedure for its application to routine sample analysis.

3.4. Precision and accuracy

Precision of the method is the degree of agreement among the individual test results when the procedure is applied to multiple samples. The intra-assay precision and accuracy for valproic acid was calculated for LLOQ, LQC, MQC and HQC levels after five replicates, each on the same analytical run while inter-assay precision and accuracy was calculated after repeated analysis in four different analytical runs. The intra-batch and inter-batch coefficient of variation for valproic acid was between 2.78–5.68% and 4.46–7.03%, respectively. The

intra-batch accuracy values for valproic acid were found to be between 92.67 and 109.50% while for inter-batch were between 87.50 and 112.50%. Their comprehensive results for intra- and inter-assay accuracy and precision are given in Table 5.

3.5. Matrix effect assessment

Matrix effect was assessed by post column analyte infusion method. Post column, a combined aqueous plain stock solution of valproic acid and IS of LQC concentration was continuously introduced to source using a 'T' union. This was done with a purpose to raise the background level of valproic ions along with the mobile phase from column. A suppression of valproic acid or IS ions by matrix would result in negative peak and enhancement of valproic acid or IS ions would give rise to a positive peak at the retention time of eluting plasma matrix from column in the dead volume. Further, blank plasma SPE eluate was injected through the autosampler to assess the effect of eluting matrix on valproic acid ionization and its retention time. It was observed that, blank matrix got eluted before the retention time of valproic acid. This led us to conclude that the matrix does not alter the elution and

Table 2
Selectivity in 10 different lots of plasma

Sample name	Valproic acid		Hydrochlorothiazide (IS)	
	Area	Area (%)	Area	Area (%)
LLOQ-1	34,578	NA	1,808,760	NA
LLOQ-2	36,184	NA	1,841,764	NA
LLOQ-3	42,849	NA	2,010,827	NA
LLOQ-4	32,234	NA	1,837,177	NA
LLOQ-5	36,032	NA	1,808,697	NA
Mean	36,375	NA	1,861,445	NA
Blank-1 ^a	985	2.71	0	0.00
Blank-2 ^a	0	0.00	0	0.00
Blank-3 ^a	942	2.59	0	0.00
Blank-4 ^a	853	2.35	0	0.00
Blank-5 ^b	1,072	2.95	0	0.00
Blank-6 ^b	0	0.00	0	0.00
Blank-7 ^b	1,026	2.82	0	0.00
Blank-8 ^b	0	0.00	0	0.00
Blank-9 ^c	779	2.14	0	0.00
Blank-10 ^d	1,154	3.17	0	0.00

NA, not applicable; the area observed at the RT of valproic acid are <20% of the mean area of LLOQ; the mean area observed at the RT of IS are <5% of the mean area of IS.

^a Buffered blank plasma.

^b Heparinised blank plasma.

^c Lipemic blank plasma.

^d Haemolysed blank plasma.

ionization of valproic acid and IS. Further, to study the effect of the matrix on analyte quantification with respect to consistency in signal (ionization), matrix effect was checked in six different lots of heparinised plasma. These lots of plasma comprised of: four lots of normal control plasma, one lot of lipemic control plasma and one lot of haemolysed control plasma. From each of

Table 3
Summary of five different linearity parameters for valproic acid

Linearity	Intercept	Slope	Correlation coefficient (<i>r</i>)
1	−0.00439	0.011	0.9998
2	−0.00377	0.0118	0.9999
3	−0.00527	0.0104	0.9989
4	0.000146	0.00993	0.9998
5	0.000391	0.0096	0.9992
Average		0.0105	0.9995
S.D.		0.0004	0.0005
CV (%)		3.8122	0.0458

Linearity was plotted using weighting factor 1/concentration, i.e., 1/*x*.

these six lots of plasma samples, three samples of LQC and HQC concentrations were prepared and checked for the inaccuracy in all the samples (total 36 QC samples). This was performed with the aim to see the matrix effect of these different lots of plasma on the back calculated value of QC's nominal concentration. The results found were well within the acceptable limits as shown in Table 6. Hence, this proves that the endogenous matrix peaks in the dead volume time did not affect the quantification of valproic acid and IS peak. Thus, the method of extraction of valproic acid from plasma was rugged enough and gave accurate and consistent results when applied to real patient samples.

3.6. Stability study

Plasma being the matrix for extraction encouraged us to give prime consideration for the development of a method, which precisely and quantitatively extracts valproic acid from the stored plasma (stability) samples. Hence, stability experiments were performed thoroughly to evaluate the stability of valproic acid in stock solutions and in plasma samples under differ-

Table 4
Back calculated concentration of calibration standards (CS) from respective calibration curves of valproic acid

Linearity	Concentration (μg/ml)								
	CS-1	CS-2	CS-3	CS-4	CS-5	CS-6	CS-7	CS-8	CS-9
Spiked concentration (μg/ml)	2	5	10	20	40	80	120	160	200
<i>n</i>	5	5	5	5	5	5	5	5	5
Mean (μg/ml)	2.056	5.000	9.842	19.806	39.850	79.696	121.838	157.128	199.548
Accuracy (%)	102.80	100.00	98.42	99.03	99.63	99.62	101.53	98.21	99.77
CV (%)	6.94	4.03	2.49	5.23	2.56	1.23	2.75	3.69	4.15

Table 5
Valproic acid intra-assay and inter-assay precision and accuracy

Quality control samples	Concentration added (μg/ml)	<i>n</i>	Mean concentration found (μg/ml) ^a	Intra-assay			<i>n</i>	Mean concentration found (μg/ml) ^b	Inter-assay		
				RE (%)	S.D.	CV (%)			RE (%)	S.D.	CV (%)
LQC	6	5	5.704	−4.93	0.191	3.36	20	5.824	−2.94	0.325	5.58
MQC	60	5	61.430	2.380	1.705	2.78	20	61.631	2.72	3.157	5.12
HQC	140	5	142.244	1.60	5.206	3.66	20	140.087	0.06	6.25	4.46

RE, relative error; S.D., standard deviation; CV, coefficient of variance; *n*, total number of observations for each concentration.

^a Mean of five replicate observations at each concentration.

^b Mean of 20 observations recorded over 4 different analytical runs (5 replicates/run).

Table 6

Matrix effect in six different lots of normal lots of plasma for valproic acid

	Lot-1	Lot-2	Lot-3	Lot-4	Lot-5	Lot-6
Valproic acid LQC (6.0 $\mu\text{g/ml}$)						
Calculated concentration ($\mu\text{g/ml}$)	6.62	6.12	6.19	6.01	6.09	6.11
RE (%)	10.30	1.99	3.14	0.18	1.57	1.77
Valproic acid HQC (140.0 $\mu\text{g/ml}$)						
Calculated concentration ($\mu\text{g/ml}$)	139.78	140.68	142.63	141.63	142.99	143.05
RE (%)	-0.16	0.48	1.88	1.17	2.13	2.18

RE, relative error.

ent conditions, simulating the same conditions which occurred during study sample analysis in plasma at room temperature, extracted sample stability (process stability), freeze thaw stability and long-term stability. The results obtained were well within the acceptable limit. IS stock solution was also found to be stable.

Stock solution of valproic acid and IS were stable at room temperature for 7 h and at 2–8 °C for 30 days. Valproic acid

in control human plasma at room temperature was stable for at least 10 h. In the final solid-phase extract in autosampler up to 47 h (process stability). Valproic acid was found to be stable for at least three freeze and thaw cycles. The valproic acid spiked plasma samples stored at -70 °C for long-term stability experiment were found stable for at least 150 days. The graphical presentation for the percent change of the above stability experiments are shown in Fig. 4.

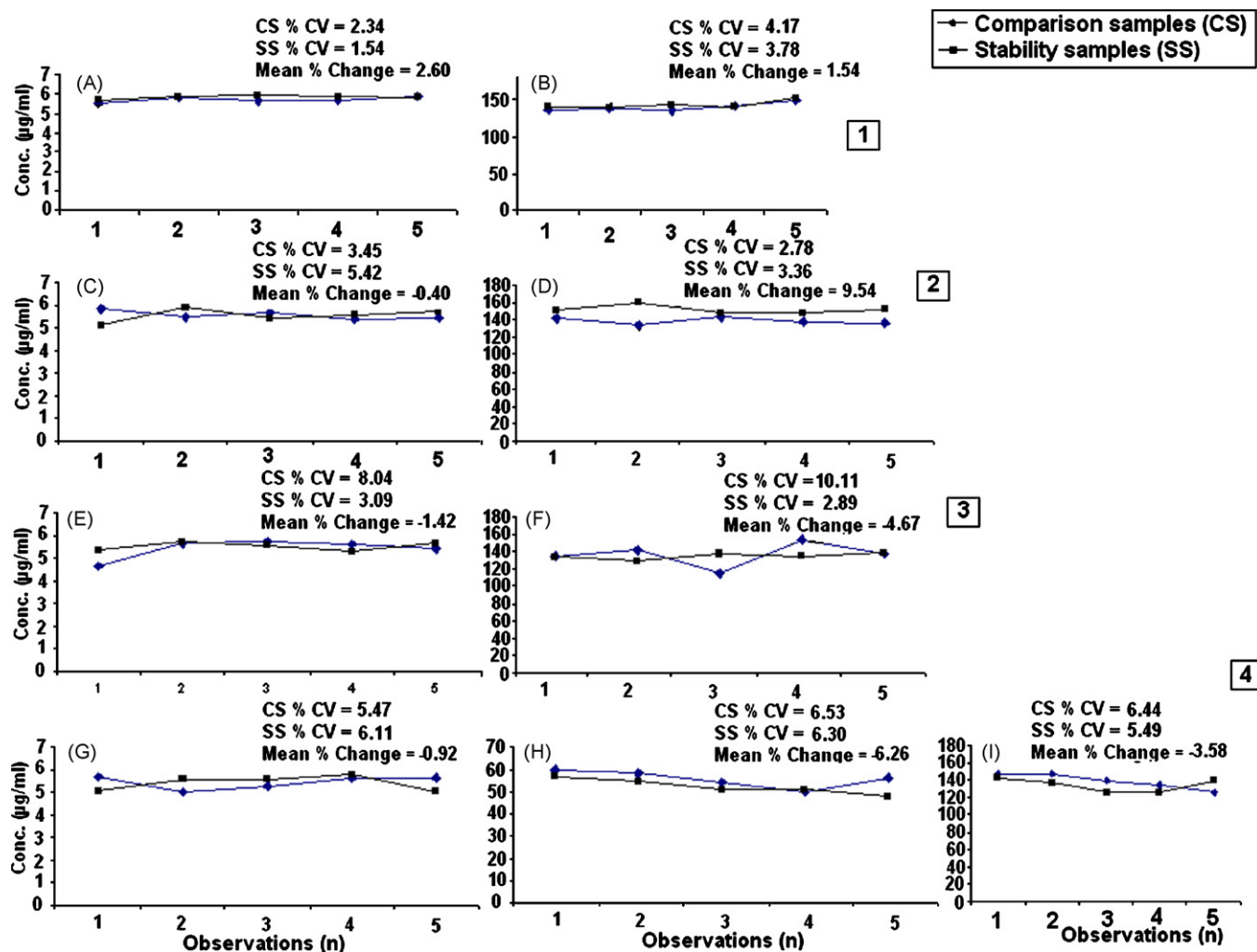


Fig. 4. Graphical representation of different stability studies (1) bench top stability in plasma for 10 h at (A) LQC and (B) HQC levels; (2) process sample stability at 5 °C for 47 h at (C) LQC and (D) HQC level; (3) freeze and thaw stability after third freeze and thaw stability after third freeze and thaw cycle at (E) LQC and (F) HQC level; (4) long-term stability at -70 °C for 150 days at (G) LQC, (H) MQC and (I) HQC levels.

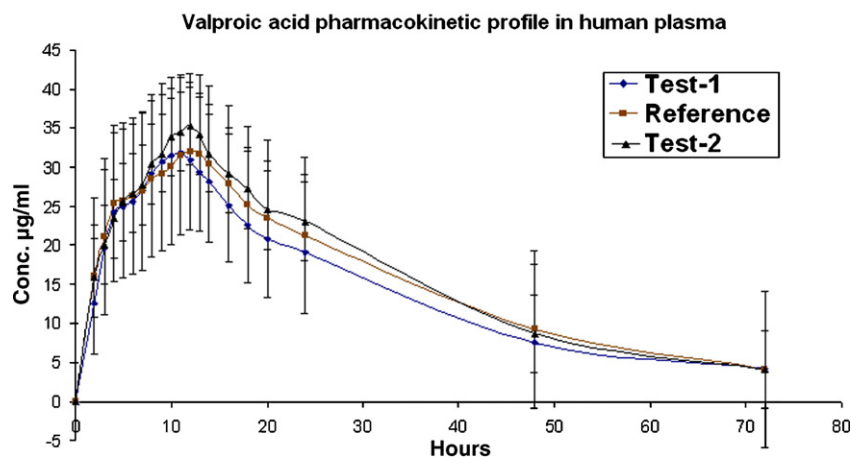


Fig. 5. Mean pharmacokinetic profile of two tests and one reference formulation equivalent to 500 mg valproic acid for 24 volunteers.

3.7. Application of the method to human subjects

The validated method was successfully applied to the assay of valproic acid in healthy human subject samples who received 500 mg sustained release reference and test formulations. The design of the pilot study comprised of “a randomized, open label, single dose, three treatments, three periods, three sequence crossover bioequivalence study of sodium valproate for 500 mg formulation in 24 healthy human subjects”. The subjects were briefed regarding the protocol and risk involved in the study. The study was conducted strictly in accordance with guidelines laid down by International Conference on Harmonization and USFDA [21]. The samples were processed based on the proposed extraction protocol for quantification of valproic acid. The method was sensitive enough to monitor the valproic acid plasma concentration up to 72 h. In all, approximately 1800 samples including the calibration, QC and volunteer samples were run and analyzed in only 6 days and the precision and accuracy for calibration and QC samples were well within the acceptable limits. The mean pharmacokinetic profiles for the treatments are presented in Fig. 5. Thus, the assay procedure for valproic acid in plasma samples with SPE demonstrates the linearity, precision and sensitivity needed for the pharmacokinetic studies of this drug.

4. Discussion

This analytical method was developed and validated for assaying valproic acid in therapeutic concentration range for the analysis of routine samples. To achieve this aim, sample extraction procedure, liquid chromatography conditions and MS detection parameters were optimized. During development, tuning of MS parameters in both positive and negative ionization modes was carried out for valproic acid and hydrochlorothiazide (IS). However, the response found was much higher in negative ionization mode for valproic acid compared to that in positive mode due to its acidic nature. Use of ammonia in the mobile phase to increase the pH of buffer further enhanced the response of valproic acid and IS. Valproic acid being a small aliphatic

molecule did not give stable fragments at very low and high collision energy (CE). Thus initially, setting of the MS parameters for the detection of valproic acid (especially) in pseudo SRM mode was done with the aim to get best specificity with respect to any other available matrix ion with m/z of 143.0 by keeping CE at -1 V. For this, the first quadrupole (Q1) was given a filter for scanning only the molecular ion with m/z of 143.0 with unit resolution and keeping the third quadrupole (Q3) filter to scan the (false) product molecular ion with m/z of 143.0 with low resolution. But this resulted in very high baseline and some other peaks, probably from the endogenous plasma matrix, which interfered with the retention time of valproic acid. Because of this high baseline it was difficult to quantify valproic acid at the desired LLOQ as the molecular ion signal got suppressed by the availability of other continuous competing matrix ions. To reduce the baseline and avoid endogenous matrix interference, sufficient collision gas pressure was applied in second quadrupole (Q2) for CAD along with high collision energy of -30 V instead of -1 V (kept initially for the trial purpose). This helped in fragmenting the possible endogenous matrix at m/z of 143 and not the molecular ion of valproic acid, which does not fragment even at this collision energy. Hence, the specificity and sensitivity of the actual valproic molecular ion was magnified to the desired level. Thus, the optimization of the MS source dependent and compound dependent parameters really augmented this LC–MS method for the quantification of valproic acid.

Efforts were directed towards method development to improve the method ruggedness during the SPE, sample analysis and transferability. The extraction of valproic acid from plasma was tried by liquid–liquid extraction using different solvents, viz., dichloromethane, diethyl ether, tetra butyl methyl ether (TBME), hexane and their mixtures in different ratios, but all resulted in inconsistent and low recoveries, longer extraction time, higher background and hence poor sensitivity. In an attempt to get cleaner extracts, solid-phase extraction was carried out. A plasma volume of 200 μ l was sufficient to obtain quantitative recovery for the analytes. Addition of *o*-phosphoric acid helped in breaking the drug protein binding and contributed significantly in reducing matrix interactions. Subsequent wash-

ings with water resulted in reduced polar matrix interference and increased selectivity. The extraction process was simple and did not involve reconstitution or drying step to achieve the desired sensitivity.

A good internal standard should track the analyte during the extraction and compensate for any analyte on the column and inconsistent response due to matrix effects. Hydrochlorothiazide though belongs to a different chemical class, and a significantly different fragmentation pattern, yet, served as a very good internal standard for valproic acid, since the compound depended parameters optimized for it were very close to that of valproic acid. The selection of hydrochlorothiazide as internal standard in the present study was based on its ready availability, low cost and its unlikely presence in the plasma. The use of short Betabasic C8 column helped in increasing the response for analytes with a short chromatographic run time. The retention times of 1.43 and 1.2 min for valproic acid and IS, respectively, may indicate that they elute in dead volume time. However, the precision at LLOQ for valproic acid demonstrates the consistency of extraction and detection procedure, which was confirmed by the recovery and matrix effect experiments. A mobile phase containing 5 mM aqueous ammonium formate (pH 8.0) buffer and acetonitrile in 20:80 (v/v) ratio gave the best response. The use of only 5 μ l of the final eluate gave an on-column loading of 1 ng/injection for valproic acid. This minimizes matrix interference and suppression of the analyte peak, and helps in extending the lifetime of the column. The column oven temperature of 45 °C was sufficient to obtain a symmetric shape of analyte peaks.

All the significant efforts directed towards the extraction procedure, resulted in achieving the required LLOQ with best selectivity. The limit of quantification (2.0 μ g/ml) for valproic acid achieved is the concentration required for a typical valproic acid pharmacokinetic study with 500 mg formulation. The decision to establish 2.0 μ g/ml as LLOQ was taken only after observing the results of a pilot study, conducted in healthy subjects dosed orally with 500 mg of valproic acid, in which the C_{min} , even at 72 h after administration, was more than 2.0 μ g/ml. This LLOQ can be further lowered by drying and reconstituting the eluate (1.0 ml), as evident from the high area response of ion chromatogram for valproic acid at LLOQ level. The method described is rapid, sensitive and highly reproducible for the analysis of valproic acid in human plasma.

5. Conclusions

The objective of this work was to develop a high throughput and a sensitive method to estimate valproic acid in human plasma, especially in the absorption and elimination phase after oral administration of 500 mg formulation. The method has the advantage of using SPE to obtain clean and consistent extracts with minimum matrix interference. Moreover, the limit of quan-

tification is low enough to monitor at least four half lives of valproic acid concentration with good intra- and inter-assay reproducibility (CV) for the quality controls. The method is useful for the therapeutic drug monitoring, both for analysis of routine samples of single dose or multiple dose pharmacokinetics and also for the clinical trial samples with precision, accuracy and high throughput.

Acknowledgements

The authors are indebted to Dr. Chaitanya Dutt, Director, Torrent Research Centre, for his continuous support and motivation during the course of development and validation of the method. The authors gratefully acknowledge Torrent Research Centre for providing necessary facilities to carry out this work.

References

- [1] L.J. Willmore, *Psychopharmacology* 37 (2003) 43.
- [2] M.-C. Lin, H.-S. Kou, C.-C. Chen, S.-M. Wu, H.-L. Wu, *J. Chromatogr. B* 810 (2004) 169.
- [3] C. Lucarelli, P. Villa, E. Lombardi, P. Prandini, A. Brega, *Chromatographia* 33 (1992) 37.
- [4] J.H. Wolf, L. Veenma-Van der Duin, J. Korf, *J. Chromatogr.* 487 (1989) 496.
- [5] F.A.L. Van der Horst, G.G. Eikelboom, J.J.M. Holthuis, *J. Chromatogr.* 456 (1988) 191.
- [6] M. Nakamura, K. Kondo, R. Nishioka, S. Kawai, *J. Chromatogr.* 310 (1984) 450.
- [7] H. Amini, M. Javan, A. Ahmadiani, *J. Chromatogr. B* 830 (2006) 368.
- [8] V. Pucci, R. Mandrioli, M.A. Raggi, *Electrophoresis* 24 (2003) 2076.
- [9] J.J. Lian, W. Tianalin, F.Y.L. Sam, *Electrophoresis* 20 (1999) 1856.
- [10] M. Nakajima, S. Yamato, K. Shimada, S. Sato, S. Kitagaba, A. Honda, J. Miyamoto, J. Shoda, M. Ohya, H. Miyazaki, *Ther. Drug Monit.* 22 (2000) 716.
- [11] E. Gaetani, C.F. Laureri, M. Vitto, *J. Pharm. Biomed. Anal.* 10 (1992) 193.
- [12] D.J. Speed, S.J. Dickson, E.R. Cairns, N.D. Kim, *J. Anal. Toxicol.* 24 (2000) 685.
- [13] F. Susanto, H. Reinauer, *Chromatographia* 41 (1995) 407.
- [14] J. Darius, *J. Chromatogr. B.* 682 (1996) 67.
- [15] E. Fisher, W. Wittfoht, H. Nau, *Biomed. Chromatogr.* 6 (1992) 24.
- [16] D. Yu, J.D. Gordon, J. Zheng, S.K. Panesar, K.W. Riggs, D.W. Rurak, F.S. Abbott, *J. Chromatogr. B* 666 (1995) 269.
- [17] C. Deng, N. Li, J. Ji, B. Yang, G. Duan, X. Zhang, *Rapid Commun. Mass Spectrom.* 20 (2006) 1281.
- [18] N.V. Ramakrishna, K.N. Vishwottam, S. Manoj, M. Koteswara, M. Santosh, J. Chidambara, B.R. Kumar, *Rapid Commun. Mass Spectrom.* 19 (2005) 1970.
- [19] C.L. Bowden, P.G. Janicak, P. Orsulak, A.C. Swann, J.M. Davis, J.R. Calabrese, P. Goodnick, J. Small, A.J. Rush, S.E. Kaimmel, S.C. Risch, D.D. Morris, *Am. J. Psychiatry* 153 (1996) 765.
- [20] V. Pucci, E. Monteagudo, F. Bonelli, *Rapid Commun. Mass Spectrom.* 19 (2005) 3713.
- [21] FDA Guidance for Industry: Bioavailability Studies for Orally Administered Drug- Products-General Considerations, U.S. Department of Health and Human Services, Food and Drug Administration, Centre for Drug Evaluation and Research (CDER), 2000.

Review

Optical sensors and biosensors based on sol–gel films

Paula C.A. Jerónimo, Alberto N. Araújo*, M. Conceição B.S.M. Montenegro

REQUIMTE – Dpt. Physical-Chemistry, Faculty of Pharmacy, University of Porto, R. Aníbal Cunha 164, 4099-030 Porto, Portugal

Received 26 April 2006; received in revised form 6 September 2006; accepted 27 September 2006

Available online 27 October 2006

Abstract

The sol–gel technology is being increasingly used for the development of optical sensors and biosensors, due to its simplicity and versatility. By this process, porous thin films incorporating different chemical and biochemical sensing agents are easily obtained at room temperature, allowing final structures with mechanical and thermal stability as well as good optical characteristics. In this article, an overview of the state-of-the-art of sol–gel thin films-based optical sensors is presented. Applications reviewed include sensors for determination of pH, gases, ionic species and solvents, as well as biosensors.

© 2006 Elsevier B.V. All rights reserved.

Keywords: Optical sensors; Biosensors; Sol–gel technology; Films

Contents

1. Introduction	13
1.1. Optical fibre chemical sensors	13
1.2. The sol–gel process	14
2. Chemical optical sensors: applications	15
2.1. pH sensors	15
2.2. Gas sensors	17
2.3. Sensors for ionic species	19
2.4. Sensors for determination of solvents	21
2.5. Other applications	21
3. Sol–gel films based optical biosensors	22
4. Conclusions and trends	25
Acknowledgements	25
References	25

1. Introduction

1.1. Optical fibre chemical sensors

A chemical sensor is a device capable of providing continuous real-time chemical information about a sample of interest [1]. Optical sensors, or *optrodes*, represent a group of chemical sensors in which electromagnetic radiation is used to generate

the analytical signal in a transduction element. These sensors can be based on various optical principles (absorbance, reflectance, luminescence, fluorescence), covering different regions of the spectra (UV, visible, IR, NIR) and allowing the measurement not only of the intensity of light, but also of other related properties, such as refractive index, scattering, diffraction and polarization.

Optical fibres are commonly employed in this type of sensors to transmit the electromagnetic radiation to and from a sensing region that is in direct contact with the sample. Besides the advantages in terms of cheapness and ease of miniaturization, a wide variety of sensor designs are made possible [2]. The most common are distal-type sensors, in

* Corresponding author. Tel.: +351 222078940; fax: +351 222004427.
E-mail address: anaraujo@ff.up.pt (A.N. Araújo).

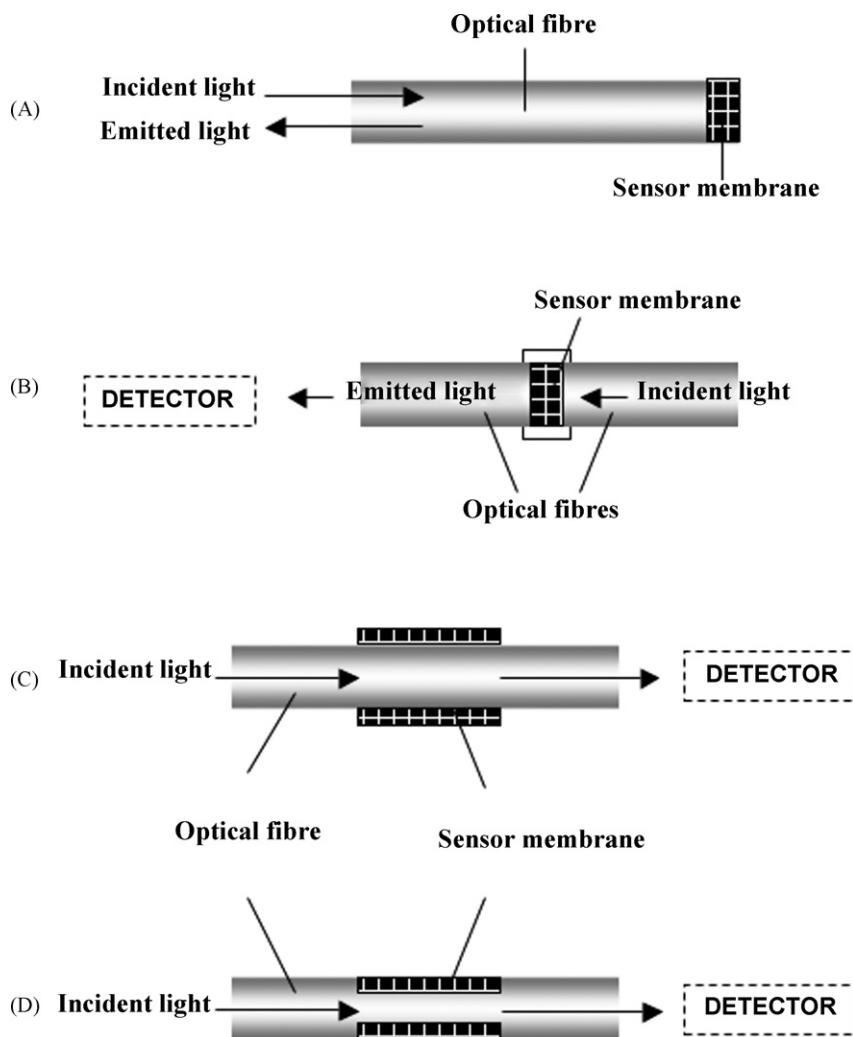


Fig. 1. Typical configurations of optical fibre chemical sensors. A and B are extrinsic type sensors, in which the fibre is used to direct light; C and D are intrinsic sensors, in which the sensor phase modifies the transmission characteristics of the fibre. The sensor membrane can be placed on the tip of the fibre (A and B) or on the side (C); part of the cladding can be removed and leave the fibre core exposed to the chemical interaction medium (D).

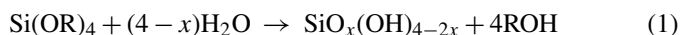
which the indicator chemistry is immobilized at the tip of a single or bifurcated optical fibre. Alternatively, the sensing chemistry can be immobilized along a section of the core of the optical fibre to make an evanescent field sensor. Two sensing configurations are easily recognized: the *extrinsic mode* uses optical fibres to direct the electromagnetic radiation to the sample, and later to the detector; the *intrinsic mode* employs the fibre itself as transduction element. The interaction of light with the sample takes place inside the guiding region, or in the lower refractive index surrounding medium (evanescent field). The basic designs of optical fibre sensors are shown schematically in Fig. 1.

In most optical sensors, the chemical transducer consists of immobilized chemical reagents, placed in the sensing region of the optical fibre either by direct deposition or by encapsulation in a polymeric matrix. The choice of the polymer support may influence the performance of the sensor, namely its selectivity and response time, and is governed by parameters like mechanical stability, permeability to the analyte and suitability

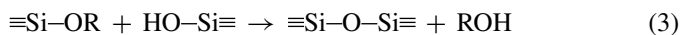
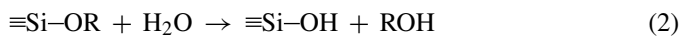
for reagent immobilization. Porous glass-like materials obtained by the sol–gel method present several properties that make them attractive for use in optical chemical sensing applications [3–5]. In particular, sol–gel thin films are now widely recognized as a promising strategy for the effective and low cost mass production of reversible, robust and portable optical chemical sensors and biosensors.

1.2. The sol–gel process

The sol–gel technology [6] is considered one of the fastest growing fields of contemporary chemistry. It offers a low temperature alternative to conventional glass production, enabling final products with high homogeneity and purity. Considering silica alkoxydes as starting materials, the sol–gel process can be represented by the following global chemical equation, in which R is an alkyl group:



The reaction takes place through hydrolysis (2) and condensation (3) of monomeric alkoxyxilanes:



The most frequently used precursors are tetramethoxysilane (TMOS) and tetraethoxysilane (TEOS). In the typical procedure, the precursor is mixed with water and a co-solvent (usually ethanol or methanol), yielding a homogeneous sol. Hydrolysis and polycondensation can be accelerated by employing an appropriate acid or base catalyst. As the reactions proceed, gradual increase of the solution's viscosity occurs and a rigid, porous, interconnected gel is formed. After aging and drying at room temperature, a xerogel is obtained, which may be further densified at high temperatures if a non-porous glass is intended. The physico-chemical properties of the obtained gel depend on the parameters of the process. Factors such as the type of precursor, the pH, the nature and concentration of the catalyst, H₂O:Si molar ratio (R), the type of co-solvent, temperature, method and extension of drying, the presence of doping substances, or even the chemical nature of the gelation vessel, may have a strong influence on the sol-gel glass characteristics: porosity, surface area, refractive index, thickness and mechanical properties. In order to obtain sensing devices, the chemical or biological recognizing elements can be added to the sol during different steps of the process, remaining firmly retained in the matrix, yet sterically accessible to small molecules and ions that may diffuse into the porous structure.

The mild conditions of the process, together with the chemical inertia of sol-gel glass, make these materials ideal for the immobilization of numerous organic, organometallic and biological molecules. Characteristics such as polarity, porosity and ion exchange capacity can be easily tailored by simple modification of the polymerisation protocol. Sol-gel porous matrices in general are thermally and mechanically stable, do not photodegrade and can be transparent to wavelengths above 250 nm, which makes them highly suitable for optical applications. Sol-gel glasses can be obtained in a variety of shapes and configurations (thin films, fibres, monoliths, powders, etc.) and may be easily miniaturized and attached to most other materials.

Thin films (with thickness usually < 1 μm) are obtained by means of spin-coating, dip-coating or spray-coating techniques [7]. They are regarded as the most technologically important sol-gel configuration, representing a key area for the development of optical sensors. Thin films and coatings require only small amounts of precursors and embedded functional molecules, exhibit fast response times and superior transparency, possess mechanical resistance and are less susceptible to crack than monoliths (particularly when exposed to liquids). Sol-gel coatings can also be easily combined with optical fibres or planar waveguides, providing intrinsic evanescent wave sensors; furthermore, thin films have great potential for miniaturisation and also permit the possibility of preparing multi-layer configurations.

In this paper we present an overview of the state-of-the-art of sol-gel thin films-based optical sensors. Sensing devices

reported in the literature until the present moment were divided according to their main application: sensors for determination of pH, gases, ionic species and solvents, as well as other less explored purposes, are described. Finally, special attention is devoted to optical biosensors: this field has been experiencing a rapid growth, as a reflex of the increasing demand for stable, robust and specific devices for application in areas such as food industry, diagnostics, *in vivo* monitoring, environmental control and biotechnology.

2. Chemical optical sensors: applications

2.1. pH sensors

To date, most of the reported sol-gel based optical sensors are related with the measurement of pH, as a consequence of the wide availability of pH-sensitive dyes and the fast diffusion of protons through the sol-gel porous glass. Optical pH sensors can offer significant advantages over commercially available pH electrodes, since electromagnetic interference on the optical signal can be easily overcome, and thus superior signal to noise ratio is obtained. Although typically responding to narrower pH intervals, pH optical sensors usually possess long lasting lifetime. They also exhibit reversible and fast response, durability, low cost, safety, ease of miniaturisation and mechanical robustness. These sensing devices are obtained by simply incorporating a pH indicator into the sol-gel matrix, and their characterization is quite straightforward [8]. Several pH sensitive dyes have been immobilized in sol-gel thin films for attainment of conventional non-waveguided optical sensors, based on fluorescence or absorbance measurements (Table 1).

The easiness by which sol-gel films can be combined with optical fibres and waveguides has led to the development of intrinsic pH sensors, summarized in Table 2. Because the interrogating light remains guided, considerable miniaturisation is achievable, which is advantageous when biological assays or *in situ* remote monitoring are intended; additionally, optical transparency of the sample is not mandatory when the sol-gel/evanescent wave approach is employed. As can be seen in Table 2, most optical fibre-based pH sensors exhibit enlarged response intervals, when compared with the conventional ones, and response times are also typically shorter. For example, the optical fibre sensor proposed by Suah et al. [29], based on bromophenol blue doped sol-gel coatings and relying on artificial neural network for signal processing, presented a dynamic range of 2.0–12.0 pH units, instead of 3.0–5.0 units for the same indicator in solution, and response time of 15–150 s (depending on the pH and amount of immobilized dye). By associating sol-gel layers with optical fibres, *in vivo* determinations in which the sensor must be sterilized before use (for example, in a steam autoclave) are also facilitated. The miniaturised pH sensor developed by McCulloch and Uttamchandani [32], obtained by coating a fluorescein-doped sol-gel film on a submicrometre optical fibre tip, is a good example, and it was applied to pH monitoring in biological media. The optical fibre pH sensor proposed by Grant and Glass [37], based on sol-gel encapsulation of SNARF-1C, was developed specifically for local blood pH measurements,

Table 1
Conventional pH optical sensors based on pH indicators immobilized in sol–gel thin films

pH indicator	Sol–gel precursors	pH range	Response time	Lifetime/stability	Principle of detection	Ref.
Aminofluorescein	TMOS	4.0–9.0	90 s	6 months (stored in distilled water)	Fluorescence	[9]
10-(4-Aminophenyl)-5,15-dimesitylcorrole	TEOS	2.7–10.30	<120 s	1 month	Fluorescence	[10]
Bromocresol green	TEOS + MTES ^a	7.0–10.0	106 s	–	Absorption	[11]
Bromocresol green	TEOS + MTMS/ BTMS/PTMS	5.0–8.0	<60 s	1–2 weeks	Absorption	[12]
Carboxyfluorescein ^b	TMOS	6.0–7.5	<1 s	–	Fluorescence	[13]
Cresol red	TEOS + MTMS/ BTMS/PTMS	7.0–11.0	<60 s	1–2 weeks	Absorption	[12]
Dimethyl yellow	TEOS + MTES	2.9–4.0	200 s (neutral to acid) 2000 s (acid to neutral)	17 h (continuous immersion)	Absorption	[14]
DPO	TEOS	3.0–7.0	4.5 min	<3 months	Fluorescence	[15]
Eriochrome cyanine	TMOS	6.0–8.0; 10.0–12.0	–	20 h	Luminescence	[16]
Europium + terbium complexes	TMOS	6.0–8.0	100 s	–	Luminescence	[17]
Europium complex + BTB	TMOS	5.0–9.0	100 s	5 h (continuous use) 2 months (stored)	Luminescence/fluorescence	[18]
Methyl red	TMOS	6.7–10.0	–	–	Absorption	[19]
Methyl red ^c	TEOS	8.0–14.0	1 min	–	Absorption	[20]
Phenol red	TEOS + PTES	6.0–12.0	<20 s	12 months	Absorption	[21]
Ruthenium(II)polypyridyl	TEOS	3.0–9.0	–	Several months	Fluorescence	[22]
TRH + bromothymol blue	TEOS	–	–	Several days	Fluorescence	[23]

BTMS: Isobutyltrimethoxysilane; DPO: 4-(*p*-*N,N*-dimethylaminophenylmethylene)-2-phenyl-5-oxazolone; MTES: methyltriethoxysilane; MTMS: methyltrimethoxysilane; PTES: phenyltriethoxysilane; PTMS: phenyltrimethoxysilane; TRH: Texas Red Hydrazide.

^a Alkali post-fabrication treatment of the films' surface.

^b Pre-encapsulated in liposomes.

^c Applied to the monitoring of environmental acidity, in liquid and gas phase.

as part of a catheter-based array of sensors to monitor stroke patients.

Another approach for accomplishing sensors with linear response over a broad pH range, simple calibration, as well as

constant sensitivity and precision in the whole response interval, is to use mixtures of multiple pH indicators immobilized in the same sol–gel layer [39–42]; a fibre optic sensing device based on overlapped multiple sol–gel coatings doped with a pH

Table 2
Intrinsic pH sensors based on doped sol–gel films combined with optical fibres

pH indicator	Sol–gel precursors/additives	pH range	Response time	Lifetime/stability	Principle of detection	Ref.
Bromocresol purple	MTES	4.5–8.2	<15 s	2 days	Absorption (ATR)	[24]
Bromophenol blue	TEOS	3.0–6.0	2 s	12 months (stored ambient air)	Absorption (ATR)	[25]
Bromophenol blue	TEOS + MTES	3.0–8.0	20–40 s	–	Absorption	[26,27]
Bromophenol blue	TEOS	4.0–7.5	5 s	–	Absorption	[28]
Bromophenol blue	TEOS + Triton X-100	2.0–12.0	15–150 s	–	Absorption	[29]
Bromophenol blue	TEOS	5.0–7.0	10 s	–	Transmittance	[30]
Cresol red	TEOS	6.5–11.0	5 s	–	Absorption	[28]
Fluorescein	TEOS	4.0–8.0	–	–	Fluorescence	[31]
Fluorescein	TEOS	3.0–10.0	ms	–	Fluorescence	[32]
Fluorescein	^a	7.0–11.0	–	<1 week	Fluorescence	[33]
Fluorescein (FITC)	TEOS + APTES + PDMS (basic catalysis)	4.5–8.0	1.1 ± 0.3 s (increasing pH) 3.5 ± 0.3 s (decreasing)	2 months (stored at pH 2.5)	Fluorescence	[34]
HPTS	TEOS + APTES + PDMS (basic catalysis)	6.0–8.5	13.4 ± 2.4 s	12 months	Fluorescence	[35]
α-Naphtholphthalein	TMOS + CTAB	4.0–11.0	min	–	Absorption	[36]
Phenol red	TEOS	7.5–11.5	5 s	–	Absorption	[28]
SNARF-1C	TMOS	6.8–8.0	<15 s	3 days (continuous use)	Fluorescence	[37]
Thymol blue	TEOS	8.0–12.0	5 s	–	Absorption	[38]

APTES: 3-Aminopropyltriethoxysilane; ATR: attenuated total reflection; CTAB: cetyltrimethylammonium bromide; FITC: fluorescein isothiocyanate; HPTS: hydroxypyrene-3-sulfonic acid; PDMS: polydimethylsiloxane; SNARF-1C: seminaphthorhodamine-1 carboxylate.

^a Not specified.

indicator has also been proposed [43], presenting an increase in sensitivity of 70%.

The entrapment of acid–base indicators in silica thin films obtained by the sol–gel method has also been used for the construction of optical sensors designed particularly for high acidity measurements. These sensors find application in many industrial processes that involve concentrated strong acids, highly pollutant and corrosive, and are proposed as reliable and inexpensive alternatives to classical titration procedures. Allain et al. [44] used sol–gel films doped with bromocresol purple casted on the surface of *Pyrex* glass slides for the determination of HCl in a wide range of concentrations (1–11 M), with short response time (1 s). Noiré et al. [45,46] developed an evanescent wave optical sensor for monitoring of HNO₃ (1–10 M) in nuclear fuel reprocessing systems, based on the immobilization of chromoxane cyanine R in sol–gel membranes coated on the core of unclad optical fibres. Shamsipur and Azimi [47] entrapped the dyes rhodamine B and safranin T in sol–gel porous films, for the determination of HCl and HNO₃ between 1 and 9 M. An optical sensor obtained by immobilization of phenol red in organically modified sol–gel films (TEOS copolymerised with phenyltriethoxysilane) was proposed by Wang et al. [48] for monitoring of HCl in solution and/or gas. This sensing device displayed detection limit to moistured gaseous HCl below 12 ppm, linear response to HCl in solution in the interval 0.01–6 M HCl, response time of 40 s and lifetime of more than 1 year. Recently, Carmona et al. [49] demonstrated the application of these sensing devices to environmental acidity monitoring, as an important tool in the preventive conservation of historical objects. Optical sensors prepared by immobilization of chlorophenol red in sol–gel films were applied to the detection of pH atmospheric changes, as well as SO₂ concentrations at about 10 ppm. Garcia-Heras et al. [50] encapsulated the indicator 2-[4-(dimethylamino)phenylazo]benzoic acid in porous sol–gel films, and the sensor obtained was used for monitoring air acidity in downtown Cracow, Poland. The sensor's detection threshold was found to be 10 µg m⁻³ of SO₂, which corresponded with an estimated pH precision of 0.05. The response was obtained after 1 day of exposure.

Some sol–gel films-based pH sensors have also been applied to ammonia monitoring. Lobnik and Wolfbeis [51] developed an optical sensor for the continuous determination of dissolved ammonia, by incorporating aminofluorescein in organically modified sol–gel films prepared by co-polymerisation of TMOS and diphenyldimethoxysilane. The dynamic range was from 1 to 20 ppm and storage stability (in distilled water) was over 6 months. Malins et al. [52] proposed a compact planar waveguide ammonia sensor for personal monitoring tasks in industrial environments, based on a cyanine dye doped sol–gel film; this sensor was fully reversible, presented limit of detection of 5 ppm and response time of a few seconds. MacCraith and co-workers [53] and, more recently, Cao and Duan [54] as well as Tao et al. [55], used sol–gel films doped with bromocresol purple and coated on unclad optical fibres for detecting gaseous ammonia. The reported results demonstrated that low cost, sensitive and fast response evanescent wave sensors could be attained.

2.2. Gas sensors

Optical sensors for determination of oxygen and other gases are considered more attractive than conventional amperometric devices because they are typically fast, low cost and not easily poisoned by sample constituents. The use of sol–gel films for development of optical gas sensors is becoming increasingly important, as reflected by the significant number of sensing systems reported in the literature [56–86], summarized in Table 3, and even by commercially available devices [87].

Nanocomposites with sensing function have been recently proposed as a new area of interest in the field of optical gas sensors. The electrical resistance or optical transmittance of these materials is changed due to variations of the free electron density as a consequence of physisorption, chemisorption and catalytic reactions of the analyte gas and the surface of the material; since the electrical response to different gases is a surface related phenomenon, the large specific surface area of sol–gel films should enhance the sensor response. Martucci et al. [56,57] prepared SiO₂–NiO and SiO₂–Co₃O₄ nanocomposite films using the sol–gel method. The nanoporosity of the sol–gel matrix provided a path for gas molecules to reach the functional particles embedded, and the films showed a reversible change in resistance to different gases like CO and H₂, as well as a reversible change in the optical transmittance in the vis-NIR range when exposed to CO, providing detection limits of approximately 10 ppm.

Optical sensors for determination of carbon dioxide play an important role in several environmental, industrial and biological processes, where detection limit and moisture insensitivity requirements are often to be considered. Typically, the development of CO₂ sensors is based upon the immobilization of fluorescent or colorimetric pH indicators, which can be used for the detection of the gas in environments where potential interference from other acidic or basic species is negligible. Malins and MacCraith [58] incorporated the deprotonated form of the fluorescent reagent pyranine in an organically modified sol–gel film by means of a phase transfer reagent. Sol–gel films doped with hydroxypyrenetrisulfonic acid (HPTS) [35,59] and thymol blue [60] have also been proposed for CO₂ sensing purposes (see Table 3).

Gas sensors capable of detecting nitrogen dioxide in low concentrations find applications in a variety of industrial processes, environmental and pollution control, biotechnology and bioengineering. Sol–gel coatings are being used in the development of these sensors, showing promising results in terms of sensitivity and detection limit. Worsfold et al. [65] incorporated an azobenzene chromophore in a sol–gel film that demonstrated to be sensitive to NO₂ gas with reproducible response and performance comparable to a Langmuir–Blodgett film of the same chromophore attached to a polysiloxane backbone. Grant et al. [66] proposed two sol–gel-based fibre optic sensors for gaseous NO₂ supported on different chemistries: the first, based on the Saltzman reagent and fluorescent dye acridine orange, demonstrated sensitivity in the ppm range but was irreversible, thus being inadequate for continuous monitoring; the second, containing a ruthenium complex, [Ru(bpy)₃]Cl₂,

Table 3
Optical gas sensors based on sol–gel films

Analyte	Reagent	Sol–gel precursors/additives	Linear range/detection limit	Response time	Lifetime/stability	Principle of detection	Comments	Ref.
CO	NiO and Co ₃ O ₄ nanocrystals	TEOS + MTES; APTES (ligand)	10–500 ppm	–	–	Transmittance (vis-NIR)	–	[56,57]
CO ₂	Pyranine	MTES/ETES, basic catalysis	0–20%	<1 min	6 months (stored ambient)	Fluorescence	–	[58]
CO ₂	HPTS	TEOS + PDMS + APTES	0.023% (gas)/6.6% (dissolved)	8 s (gas)/1–2 min (dissolved)	4–6 months (stored dry)	Fluorescence	–	[35]
CO ₂	HPTS + Ru(dpp) ₃ (reference)	MTES + CTAB	0.08%	20–30 s	>7 weeks	Fluorescence	Modified atmosphere packaging applications	[59]
CO ₂	Thymol blue	MTMS	Full range, except 0.02–0.1%	2 min	–	Absorption	–	[60]
H ₂	NiO and Co ₃ O ₄ nanocrystals	TEOS + MTES; APTES (ligand)	20–850 ppm	–	–	Transmittance (vis-NIR)	–	[57]
H ₂ S	Thionine	TEOS + MTES	0.2–100%	–	6 months (stored)	Absorption	–	[61]
I ₂	–	MTES + DMES + DPDS	100 ppb–15 ppm	<15 s	3 months	ATR	Charge-transfer complex between I ₂ and phenyl groups of modified sol–gel	[62]
NH ₃	–	TiO ₂ –P ₂ O ₅ mesoporous nanocomposite film + TiO ₂ film	100 ppb–10 ppm	60 s, recovery: 90 s	–	Integrated optical polarimetric interferometry	–	[63]
NO	Cobalt-tetrakis(5-sulfothienyl)porphine	–	–	–	–	Absorption	–	[64]
NO ₂	Azobenzene chromophores	TEOS/MTES	–	–	–	Absorption	–	[65]
NO ₂	Ru(bpy) ₃	TMOS	0.5–2% (hundreds ppm level)	15 s	–	Fluorescence	Interference from O ₂	[66]
NO ₂	Acridine orange + Saltzman reagent	TMOS	0.7 ppm	50 min	–	FRET	Irreversible	[66]
NO ₂	Porphyrin dyes	MTES	176 ppb	225 s	–	Absorption	–	[67]
NO ₂	Saltzman reagent	TMOS	ppb level	–	–	Absorption	–	[68]
O ₂	Ru(dpp) ₃	TEOS + MTES/ETES	6 ppb	5 s	6 months	Fluorescence	–	[26,69–76]
O ₂	Pyrene	TEOS	–	–	300 days (stored)	Fluorescence	–	[77]
O ₂	Platinum octaethylporphyrin	TEOS + Triton X-100	0.5–100%	5 s	5 months	Phosphorescence	–	[78,79]
O ₂	Cyclometallated Pt(II) complex	TEOS	–	10 s	–	Luminescence	–	[80]
O ₂	Ru(bpy) ₃	TEOS + Triton X-100	–	–	–	Fluorescence	Regenerable with N ₂	[81]
O ₂	Ru(dpp) ₃	–	–	10 s	–	Luminescence	–	[82]
O ₂	Ru(dpp) ₃	Octyl-triEOS/TEOS	–	–	11 months	Luminescence	–	[83]
O ₂	Erythrosin B	TMOS, basic catalysis	<9.1 mg l ⁻¹ DO	–	–	Phosphorescence	–	[84]
O ₂	Erythrosin B	TEOS + fluoropolymer	–	–	–	Phosphorescence	–	[85]
O ₂	Ru(bpy) ₃	TEOS	0–20%	20 s	–	Fluorescence	<i>In vivo</i> NMR application	[86]

ATR: Attenuated total reflection; DMES: dimethyldiethoxysilane; DO: dissolved oxygen; DPDS: diphenyldiethoxysilane; ETES: ethyltriethoxysilane; FRET: fluorescence resonance energy transfer; HPTS: hydroxyphenyltrisulfonic acid; MTES: methyltriethoxysilane; MTMS: methyltrimethoxysilane; octyl-triEOS: *n*-octyltriethoxysilane; Ru(bpy)₃: tris(bipyridyl)ruthenium(II); Ru(dpp)₃: Ru(II)-tris(4,7-diphenyl-1,10-phenanthroline).

displayed sensitivity in the hundreds ppm range (0.5–2%), with reversibility and rapid response times. A device based on a tetra-substituted porphyrin dye entrapped in a sol–gel thin film was reported by Worsfold et al. [67], presenting response to a concentration of NO₂ as low as 176 ppb at room temperature. Recently, Mechery and Singh [68] developed an optical fibre-based sensor system for selective detection of NO₂ in air samples. A ppb level detection limit was achieved by immobilizing Saltzman reagent (sulfanilic acid and 1-naphthylamine) in a sol–gel film coated on the fibre core, operating as an intrinsic sensor configuration. This device was adequate to monitor harsh environments, with the capability of remote detection; however, unevenly distributed pores of large dimensions seemed to affect sensitivity.

Most of the reported oxygen sensors are based on the quenching of fluorescence from an appropriate chemical species, such as the transition metals photoluminescent complexes. The ruthenium complexes are widely used, due to their highly favourable characteristics: their metal–ligand charge transfer states exhibit high emissions; they possess long unquenched lifetime and strong absorption at blue-green wavelengths. McDonagh, McEvoy and MacCraith's team from Dublin, Ireland, has devoted significant research efforts to this area [23,69–76]. They developed an intrinsic optical fibre oxygen sensor (suitable for both gas-phase and dissolved oxygen) based on sol–gel porous films containing Ru(II)-tris(4,7-diphenyl-1,10-phenanthroline) complex, or Ru(dpp)₃, whose fluorescence is quenched in the presence of oxygen. Most of their work was focused on the optimisation of the sol–gel microstructure, particularly in terms of hydrophobicity and porosity. This, together with the long luminescent period (approximately 6 μs) presented by the ruthenium complex, enabled a highly sensitive sensor, with detection limit of 6 ppb and response time inferior to 5 s. By associating this sensor with low cost optoelectronic components, a portable device was obtained, which represented a progress towards a commercial instrument and made this sensor suitable for a wide scope of applications, from atmospheric control to river pollution monitoring, for example [74]. More recently, the authors proposed a novel miniaturised integrated platform in order to enhance the performance of the sensor and enable multianalyte detection capability [76]. Ru(dpp)₃ doped sol–gel film was deposited on a waveguide; changes in oxygen concentration resulted in a modulation of the output intensity, thereby providing the basis of the sensor. Multimode ridge waveguides were produced using a soft lithography technique. Photocurable sol–gel-derived silica materials were introduced into a poly(dimethylsiloxane) mould and exposed to UV radiation. Sensor spots were then deposited on the resultant ridge waveguides by high-resolution pin-printing. The robust and compact sensor system obtained displayed a resolution of less than 460 ppb over the range 0–9.2 ppm dissolved oxygen. The authors consider that the use of sol–gel technology was a major advantage, since it made possible to tune the sensitivity to specific ranges through correct choice of polymerisation conditions.

Other authors have used Ru(dpp)₃ [82,83] and other ruthenium complexes, namely tris(bipyridyl)ruthenium(II) (Ru(bpy)₃) [81,86] for the development of novel oxygen optical sensors. Other luminescent oxygen-sensitive species, such

as pyrene [77], platinum octaethylporphyrin [78,79], cyclometallated platinum(II) complexes [80] and erythrosine B [84,85] have been immobilized in sol–gel coatings for detection of oxygen either dissolved or in gas-phase. All these sensors are described in Table 3.

2.3. Sensors for ionic species

Silica thin films obtained by the sol–gel process have been used for optical sensing of metal ions [24,88–94]. These sensors, summarized in Table 4, are typically based on the establishment of coloured complexes with several immobilized reagents, such as morin, eriochrome cyanine R [88], xylenol orange [24,89], 8-hydroxyquinoline-5-sulfonic acid [90], porphyrin [92] and 4-(2-pyridylazo)resorcinol (PAR) [91,94]. The sol–gel matrix typically allows the determination of metals with very high sensitivity, due to its dual nature: it simultaneously acts as sensing and pre-concentration element, since it possesses a large surface area with controllable amounts of silanol groups; in addition, it enables the entrapment of significant amounts of indicator molecules. The immobilized ligands must retain considerable freedom to move or reorient, in order to be able to establish complexes with the analyte of interest. Our team has recently confirmed these findings on sol–gel films obtained by physical entrapment of PAR, using a base-catalysed process. The developed optical sensor, which was applied to the direct determination of copper in urine [91] and to the analysis of zinc in injectable insulins [94], exhibited a significant improvement in sensitivity, as pointed above; for both applications, the apparent molar absorptivity of the PAR–metal ion complex was found to be considerably higher than the one reported for the reaction in bulk solution, and low detection limits were obtained (see Table 4).

Besides metal ions, an optical sensor was also proposed for potassium sensing [95]. Ertekin and co-workers immobilized a squaraine dye, the fluoroionophore bis[4-*N*-(1-aza-4,7,10,13,16-pentaoxacyclooctadecyl)-3,5-dihydroxyphenyl]squaraine, in sol–gel films; the sensor was fully reversible within the dynamic range, 10^{−9} and 10^{−6} M K⁺, and the response time was found to be 2 min under batch conditions.

Even though in a smaller scale, sol–gel films have also been the basis for development of optical sensors for anionic species. A cyanide sensor was proposed by Dunuwila et al. [96], prepared by encapsulation of iron(III)porphyrin in a titanium carboxylate thin film obtained by the sol–gel process. Since the reaction between the analyte and the colorimetric dye was irreversible, single-use test-strips were constructed. The use of sol–gel as a matrix support proved to be economically viable and environmentally friendly. The test-strips were stable over a period of 1 month and displayed a detection limit of 10 ppm, with linear response in the range 40–25,000 ppm CN[−] and response time of 15 min. A sol–gel coating containing diphenylcarbazide (DPC) and cetyltrimethylammonium bromide (CTAB) was applied to the determination of chromate, with detection limit as low as 1 ppb [97]. However, this sensor presented a long response time, since the reaction required several steps: pre-extraction of chromate by CTAB, reduction of

Table 4
Optical sensors for determination of metals, based on indicator-doped sol–gel films

Metal	Reagent	Sol–gel precursors	Linear range/detection limit	Response time	Lifetime/stability	Principle of detection	Comments	Ref.
Al ³⁺	Morin	TMOS	4.0–2.0 ppm	–	–	Fluorescence	–	[88]
Bi ³⁺	Xylenol orange	TMOS	125–875 ppb/7.0 ppb	40 s, regeneration: 15 s	200 determinations (4.5 h continuous use)	Absorption	Coupled to flow system and applied to pharmaceutical analysis	[89]
Cd ²⁺	8-Hydroxyquinoline-5-sulfonic acid	–	<ppm	–	–	Absorption	–	[90]
Cu ²⁺	Eriochrome cyanine R	TMOS	0.1 ppm	–	–	Absorption	–	[88]
Cu ²⁺	PAR	TEOS + APTES	5.0–80.0 ppb/3.0 ppb	100 s, regeneration: 100 s	100 determinations (7 h continuous use); 1 year (stored at room temperature)	Absorption	Coupled to flow system and applied to the determination of Cu(II) in urine	[91]
Hg ²⁺	TPPS	TMOS	1.4 ppb	15 min	1 day (continuous use)	Fluorescence	–	[92]
Hg ²⁺	L'	TEOS/PMMA hybrid	–	–	–	Absorption	HgL complex can be used for CN [–] or NH ₃ sensing	[93]
Pb ²⁺	Xylenol orange	MTES	0.01–10,400 ppm/1.04 ppb	240 s	–	Absorption	Film coated on planar integrated waveguide	[24]
Zn ²⁺	PAR	TEOS + APTES	5.0–25.0 ppb/2.0 ppb	100 s, regeneration: 120 s	120 determinations (7.5 h continuous use); 1 year (stored at room temperature)	Absorption	Coupled to flow system and applied to zinc analysis in slow-action insulin	[94]

L': 2-(5-Amino-3,4-dicyano-2H-pyrrol-2-ylidene)-1,1,2-tricyanoethanide; PAR: 4-(2-pyridylazo)resorcinol; TPPS: 5,10,15,20-tetra(*p*-sulfonatophenyl)porphyrin.

Cr(VI) to Cr(III) by DPC, and finally the formation of a purple complex. Jiwan and Soumillion [98] developed a halogen anion (Cl^- , Br^- and I^-) sensor based on the entrapment of a fluorophore, *N*-dodecyl-6-methoxyquinolinium iodide, in a silica sol–gel thin film coated on a glass substrate. The hydrophobicity of the sol–gel membrane enabled a sensor with reduced leaching, suitable for the measurement of chloride in the physiological range (100 mM/3545 ppm), and with response time of less than 1 s. Detection limits for bromide and iodide were approximately 7.5 mM (599 ppm) and 0.5 mM (63.5 ppm), in that order.

2.4. Sensors for determination of solvents

The sol–gel technology has been used as a resource for the development of optical sensors that enable the continuous monitoring of several solvents, with potential applications in the chemical and food industries, as well as in environmental control.

Optochemical sensors for detection of water-miscible organic solvents have been referred in the literature as an alternative to commonly employed mass spectrometry methods. Simon et al. [99] investigated the use of solvatochromic dyes (amino-*N*-methylphthalimide and malachite green) immobilized in sol–gel porous films for the development of optical sensors for determination of ethanol in water. The reversible interaction with ethanol caused a change in the fluorescent properties of the indicators. Films with malachite green were stable over a period of 5 weeks under continuous operation. These sensors presented detection limit of 0.6-vol% ethanol in water, with linear response in the range 0–50 vol% ethanol and response time of 2–4 min. Skrdla et al. [100] proposed an integrated sensor for determination of isopropyl alcohol in aqueous media, using a single-mode planar waveguide coated with a sol–gel film doped with methyl red. This sensing device demonstrated to be potentially useful for on-line monitoring applications, since it exhibited response and regeneration times of less than 1 min, as well as good sensitivity, with detection limit of 0.7% (v/v) and dynamic range of 1–100% (v/v) isopropyl alcohol in water. Preliminary results indicated a stability of 6 months, stored in the dark in air. In a recent report, Hashimoto and co-workers [101] describe an optical sensor based on localized surface plasmon resonance prepared by the evaporation–condensation method combined with the sol–gel technology. Thin silica film prepared by the sonogel method was overcoated on silver particles; cycle performance and sensitivity of the sensor were evaluated for ethanol as well as various liquids with different refractive indices.

Films obtained by sol–gel processing have also been applied to the construction of optical sensors for organic, non-polar solvents, both in solution and in gas phase. Lu et al. [102] developed a sensor suitable for detection of low concentrations of benzene in water, based on attenuated total reflectance-Fourier transformed infrared (ATR-FTIR) spectroscopy. A hydrophobic mesoporous sol–gel film coated on an ATR crystal extracted and pre-concentrated the analyte, allowing enhanced sensitivity and excluding the interference due to water absorption bands. Wallington et al. [88,103] immobilized fluorescent-labelled β -cyclodextrin in porous sol–gel coatings. The cyclodextrin

acted as a molecular receptor, containing the fluorophore in its lipophilic cavity; in the presence of small non-polar solvent molecules, like cyclohexane or toluene, the fluorescent label was displaced and the ensuing decrease in fluorescence intensity was related to the solvent vapour concentration in the range 40–100 ppm. The sensor was reversible and polar solvents such as acetone gave no response. Stability tests were performed for 1 week of continuous exposure to decreasing concentrations of solvent and 2 months storage, with good results. By means of a rather simple approach, Abdelghani et al. [104] developed an optical sensor for detection of trichloroethylene, carbon tetrachloride, chloroform, dichloromethane, propane, butane and hexane vapours, with detection limits of 0.6, 1.5, 1.7, 4, 25, 10 and 5%, respectively. The sensor was based on the deposition of porous TEOS films on unclad portions of optical fibres; by choosing a fixed incident angle, variations of light power transmitted through the fibre were detected as the analyte was sorbed in the silica layer. Sorption and desorption times of the gas molecule onto the silica surface of 2 min and 2.5 min, respectively, were obtained. More recently, the same authors [105] used phenyl-modified silica films as cladding for optical fibres, obtaining higher sensitivity for vapours of aromatic hydrocarbons benzene, toluene and xylene.

2.5. Other applications

Besides the more explored applications presented above, sol–gel films have been used for development of optical sensors with promising applications in several other areas. For example, Skrdla et al. [106] reported a water vapour sensor based on a combination of sol–gel processing and planar optical waveguide technologies. The indicator erythrosin B was entrapped in a sol–gel film, which was deposited onto a sol–gel derived single-mode planar waveguide. The dye exhibited an increase in absorbance in the presence of liquid or gaseous water, which was detected as a decrease in the intensity of the light guided in the waveguide. The sensor was able to detect water vapour concentrations (in inert gas streams) in the low-ppm range with response and reversal times inferior to 1 min.

Lobnik and Čajlaković [107] developed an optical sensor for continuous determination of dissolved hydrogen peroxide, with possible application in industrial processes. This sensor was based on the immobilization of an indicator dye, meldola blue, in sol–gel organically modified layers. It exhibited good selectivity and reversibility, with response time of 120 s over the concentration range of 10^{-8} to 10^{-1} M.

Wen-xu and Jian [108] proposed the continuous monitoring of adriamycin *in vivo* using a sol–gel optical fibre sensor. The fluorescent dye 4-(*N,N*-dioctyl)amino-7-nitrobenz-2-oxa-1,3-diazole, whose fluorescence is quenched by the antibiotic, was incorporated in a sol–gel film fixed on the tip of a 100 μm optical fibre. The carotid artery of rabbits, used as test subjects, was catheterised with a cannula housing the optical fibre, thus allowing the continuous determination of adriamycin with detection limit of $0.057 \mu\text{g ml}^{-1}$.

The application of organically modified sol–gel films to the development of mid-infrared evanescent wave sensors for detec-

tion of nitrated organics in aqueous media was demonstrated by Janotta et al. [109,110]. Sol–gel films obtained by copolymerization of phenyltrimethoxysilane (PTMOS) and TMOS were spin-coated onto ZnSe attenuated total reflection waveguides. The recognition membranes obtained were successfully applied to the determination of the organophosphate pesticides parathion, fenitrothion, paraoxon and nitrobenzene in river water, down to the sub-ppm concentration range. Due to their selectivity, stability (over 2 months) and reproducibility, these sensors were proposed by the authors as a potential alternative to biosensors for detection of organophosphates in environmental analysis.

Recently, Isobe et al. [111] used an optical fibre coated with a porous sol–gel cladding for measurements of critical micelle concentration (CMC) of surfactants. The method for CMC detection was based on an adsorption effect in sample solution, and proved to be quite simple, accurate and cost-effective.

3. Sol–gel films based optical biosensors

One of the main features of the sol–gel technology is that it can be extended to the encapsulation of biological recognizing elements (proteins, enzymes, antibodies, whole cells, etc.) [112,113]. It is now well established that sol–gel immobilized biomolecules retain their structural integrity and full biological functions (molecular recognition, catalysis, cell metabolism and reproduction), and are often significantly stabilized to chemical and thermal inactivation [114]. The ability to produce transparent sol–gels with diverse chemistries and configurations, allied to the broad applicability to the entrapment of many biomolecular dopants, enabled the development of optical biosensors based on this platform.

The prospects of using sol–gel encapsulated biomolecules for development of improved biosensors were greatly advanced by the possibility of preparing thin films of those materials [112,115]. Conventional sol–gel film processing is not suitable for encapsulation of biological agents, because the low pH and high amounts of alcohol used lead to denaturation of most proteins. By using a modified protocol, in which an appropriate buffer is added after acid-catalysed hydrolysis and alcohol is reduced or replaced by sonication, a wide range of biomolecules encapsulated in sol–gel thin films have been employed in the construction of optical biosensors [116–138] (Table 5).

The initial activity on optical sol–gel biosensors was centred on metalloproteins. In particular, the heme proteins are considered excellent model systems because they are chromophoric and they can be readily metalated and metal-exchanged in a reversible manner; additionally, their conformation and ligand binding can be monitored via spectroscopic probing of the active centres. The first optical biosensors built with sol–gel coatings were based on the affinity of haemoglobin, myoglobin or cytochrome *c* for CO and NO [123,124]. The results reported clearly evidenced that sol–gels provide an ideal host matrix for metalloproteins with variable size, showing no adverse effects on their structure or activity. Furthermore, the speed of equilibrium response to changing redox conditions was found to be much faster for spin-coated films than that previously

reported for monoliths: 6 min instead of 15 for a thick sol–gel [124].

Most work on sol–gel biosensors development has focused on the immobilization of enzymes. Besides their unique biocatalytic properties and specificity for a substrate or group of substrates, enzymes allow a wide range of analyte recognition processes by using different combinations of enzymes or enzyme–transducer systems. In fact, most enzymes do not have intrinsic optical properties that undergo a change when they interact with the analyte, so most of these sensors rely on the use of a chemical transducer; its analytical signal can be related to the concentration of the analyte of interest. A wide variety of oxidases have been immobilized in sol–gel films and employed for the monitoring of pesticides, pharmaceuticals, hydrogen peroxide, sugars, lactate, urea, cholesterol, nitrates and nitrites (see Table 5).

The most studied enzyme in the sol–gel context is glucose oxidase (GO_x), which mediates the air oxidation of glucose with generation of hydrogen peroxide. Glucose oxidase is an extremely stable enzyme, commercially available and quite inexpensive, and known to remain active within the sol–gel matrix [112]. Different sensing schemes based on sol–gel films doped with glucose oxidase have been proposed. Narang et al. [127] compared three types of configuration (physisorption, microencapsulation and sol–gel sandwich) and studied their response profiles to glucose. Their results indicated that the sandwich configuration (sol–gel: GO_x :sol–gel) showed the most promise for future biosensor operation. Since the diffusion of the analyte proceeded through the sol–gel top layer, its thickness was adjusted to 0.10 μm in order to obtain response times as short as 30 s. de Marcos et al. [128] immobilized glucose oxidase, firstly covalently bonded to a fluorescein derivative, in a TMOS-based sol–gel film, as the basis of an optical sensor. During the enzymatic reaction, glucose reacted with the labelled GO_x and when the oxygen dissolved in the solution was consumed, an increase in fluorescence intensity was recorded. Wolfbeis et al. [129] developed a reversible glucose optical biosensor by using an oxygen transducer, Ru(dpp), along with glucose oxidase. The sensing scheme was based on the measurement of the amount of oxygen consumed during enzymatic action under steady-state conditions. Three different configurations were tested: sandwich, in which GO_x was placed between a sol–gel layer doped with Ru(dpp) and a second layer of pure sol–gel; two-layer, consisting of a sol–gel film doped with Ru(dpp) covered with sol–gel entrapped GO_x ; powder, for which GO_x plus Ru(dpp)-doped sol–gel powder were dispersed in a sol–gel phase. Sorbitol was added to obtain more porous sol–gel and thus improve diffusion. For all three combinations, storage stability at 4 °C exceeded 4 months. Ertekin et al. [130] combined glucose oxidase with a proton sensitive azlactone derivative, 4-*[p-N,N*-dimethylamino)benzylidene]-2-phenyloxazole-5-one (DPO), in single-layer and two-layer configurations. The monolayer arrangement displayed faster response time but considerable leaching upon prolonged use. The sensor based on the two-layer scheme was fully reversible in the range 0.1–15 mM glucose, with response time of 40 s and working lifetime of at least 90 days.

Table 5
Optical biosensors based on biomolecules encapsulated in sol–gel films

Immobilized biological element (+transducer)	Analyte	Sol–gel precursors	Linear range/detection limit	Response time	Lifetime/stability	Principle of detection	Ref.
Acetylcholinesterase (+FITC-dextran)	Paraoxon	TMOS	152 ppb (30% inhibition)	30 min	–	Fluorescence	[116]
<i>Bacillus licheniformis</i> , <i>Dietzia maris</i> , <i>Marinobacter marinus</i>	BOD	TMOS + DiMe-DMOS (+PVA)	0.2–40 mg l ⁻¹ /0.2 mg l ⁻¹	3 min (10 min recovery)	1 year (stored at 4 °C) ^a	Fluorescence	[117]
<i>Bacillus subtilis</i> (+Ru(dpp) ₃)	BOD	TMOS (+PVA-g-PVP)	0–25 mg l ⁻¹	20 min	2 months (stored in buffered GGA at 4 °C)	Luminescence	[118]
Carbonic anhydrase (+cresol red)	Acetazolamide	TMOS	1.0–10.0 mM/0.2 mM	60 s	3 months (stored room temperature)	Absorption	[119]
Cholesterol oxidase + horseradish peroxidase	Colesterol	TEOS	2–10 mM	10–100 min ^b	8 weeks (stored room temperature)	Absorption	[120]
Cholinesterase (+bromocresol purple)	Carbaryl dichlorvos	TEOS + PTMOS	0.11–0.8 ppm/108 ppb	12 min	3 weeks	Absorption	[121]
Concanavalin-A labelled with FITC	Bacterial endotoxins	TEOS + APTES	5.0–30 ppm/5.2 ppb	–	–	Luminescence	[122]
Cytochrome <i>c</i>	NO and CO	TMOS	–	–	–	Absorption	[123]
Cytochrome <i>c</i>	NO	TMOS	1–25 ppm/1 ppm	6 min	–	Absorption	[124]
Cytochrome <i>cd</i> ₁ nitrite reductase	NO ₂ ⁻	TMOS	3.4–57 ppb/3.4 ppb	5 min	Several months (stored 4 °C)	Absorption	[125]
<i>Escherichia coli</i> (recombinant)	DDT, aldicarb, malathion	TMOS	–	>1 h	Several months	Luminescence	[126]
Glucose oxidase (GO _x)	Glucose	TEOS	5–35 mM/0.2 mM	30 s	2 months (stored ambient)	Absorption	[127]
GO _x labelled with fluorescein	Glucose	TMOS	0.55–55 mM	–	15 days ^c	Fluorescence	[128]
Glucose oxidase (+Ru(dpp) ₃)	Glucose	TMOS + PTMOS/MTMOS	0.1–15 mM ^d	50–150 s ^e	4 months (stored 4 °C)	Fluorescence	[129]
Glucose oxidase (+DPO)	Glucose	TEOS/TEOS + APTES	0.1–15 mM	40 s	90 days (continuous use)	Fluorescence	[130]
Glutathione <i>S</i> -transferase (+bromocresol green)	Atrazine	TEOS + PTMOS	2.52–125 μM/0.84 μM	200 s	1 month (continuous use)	Absorption	[131]
Haemoglobin	NO and CO	TMOS	–	–	–	Absorption	[123]
Horseradish peroxidase	H ₂ O ₂	TEOS	8 × 10 ⁻³ –2 mM	30 s	2 months (continuous use)	Chemiluminescence	[132]
Lactate dehydrogenase (+NADH)	L-lactate	TMOS	0.1–1.0 mM	1 min	3 weeks (stored room temperature, dehumidified cabinet)	Fluorescence	[133]
Lactate dehydrogenase	Piruvate	TEOS	0–1.5 mM/5 × 10 ⁻⁵ M	1 min	30 days (stored 4–10 °C)	Absorption	[134]
Myoglobin	NO and CO	TMOS	–	–	–	Absorption	[123]
Nitrate reductase	NO ₃ ⁻	TMOS	0–1.5 μM/0.125 μM	–	6 months (stored 4 °C)	Absorption	[135]
<i>Pseudomonas fluorescens</i>	Naphthalene; salicylate	TMOS	1.2 mg l ⁻¹ ; 0.5 mg l ⁻¹	–	8 months (continuous use)	Bio-luminescence	[136]
Urease	Urea	TEOS	0.05 mM	10 s	>6 weeks (stored 4 °C)	Absorption	[137,138]

BOD: Biochemical oxygen demand; DiMe-DMOS: dimethyldimethoxysilane; DDT: dichloro-diphenyl-trichloroethane; DPO: 4-[*p*-*N,N*-dimethylamino]benzylidene]-2-phenyloxazole-5-one; FITC: fluorescein isothiocyanate; GGA: glucose-glutamic acid solution; MTMOS: methyltrimethoxysilane; NADH: nicotinamide adenine dinucleotide; PTMOS: phenyltrimethoxysilane; PVA: polyvinyl acetate; PVA-g-PVP: poly(vinyl alcohol)-grafted-poly(4-vinylpyridine); Ru(dpp)₃: ruthenium(II)-tris(4,7-diphenyl-1,10-phenanthroline).

^a Requires reactivation before use after storage.

^b 10 min for physically entrapped films, 30 min for physisorbed and over 100 min for microencapsulated films.

^c 5–6 measurements/day and then stored at 4 °C from 1 day to the next.

^d 0.1–15 mM (sandwich); 0.1–8 mM (two-layer); 0.1–4 mM (powder configuration).

^e 250 s (sandwich); 50 s (two-layer); 150 s (powder configuration).

Besides glucose oxidase, there are several literature reports on the immobilization of other enzymes within sol–gel films. Biosensors based on acetylcholinesterase (AChE) and cholinesterase inhibition have been proposed for screening of organophosphates and carbamates, two major classes of pesticides that find widespread use in agriculture. Doong and Tsai [116] encapsulated AChE and a pH-sensitive fluorophore, fluorescein isothiocyanate-dextran, in a sol–gel film that could be fixed on an optical fibre and integrated with a flow-through reactor for continuous monitoring. The response of the obtained biosensor to acetylcholine was reproducible in the range from 0.5 to 20 mM, and a 30% inhibition was achieved within 30 min when 152 ppb paraoxon was added. Andreou and Clonis [121] developed a portable optical fibre biosensor for the detection of the pesticides carbaryl and dichlorvos based on a three-layer sandwich scheme: the enzyme cholinesterase was immobilized on the outer layer, a hydrophilic modified polyvinylidene fluoride membrane, which was in contact with a sol–gel film doped with bromocresol purple, deposited on an inner glass disk. The same sensing scheme [131] was proposed for development of a biosensor for determination of the herbicide atrazine, using the enzyme glutathione *S*-transferase and bromocresol green. When deteriorated, the bioactive sandwich could be easily replaced on the terminal of the probe.

Our team [119] employed carbonic anhydrase (CA) for development of an optical biosensor for determination of the antiglaucoma agent acetazolamide, suitable for diagnosis and pharmaceutical control purposes. The enzyme and a pH-sensitive dye, cresol red, were entrapped in overlapped sol–gel films, in a dual-layer format. CA catalysed the dehydration of bicarbonate, which was inhibited by acetazolamide. By following the colour transition of cresol red, caused by the change of pH in the microenvironment of the sensor, the enzymatic reaction, as well as its inhibition by acetazolamide, were monitored. The obtained biosensor displayed good sensitivity, reduced leaching, good run-to-run stability and rapid response (60 s). The immobilized enzyme showed activity retention on storage at room temperature after a period of 3 months.

Kumar et al. [120] co-immobilized the enzymes cholesterol oxidase (ChO_x) and horseradish peroxidase (HRP) in a sol–gel film by means of physical adsorption, microencapsulation and physically entrapped sandwich (sol–gel:enzyme:sol–gel) techniques. These systems were used for the spectrophotometric determination of cholesterol, showing increased response time for microencapsulated films. HRP physically immobilized in sol–gel films was also used by Wang et al. [132] in order to obtain a chemiluminescent H_2O_2 sensor with rapid response, good reproducibility and long lifetime.

Aylott et al. [135] demonstrated the feasibility of nitrate reductase immobilized in TMOS-based thick films as a potential sensitive and stable biosensing system for nitrate. The reduction of nitrate by nitrate reductase caused a characteristic change in the UV–vis spectrum of the enzyme, which was quantitatively related with nitrate concentration in the sample. The enzyme did not leach from the sol–gel matrix and retained its activity even after a 6 months storage period. Ferreti et al. [125] encapsulated cytochrome *cd*₁ nitrite reductase between two sol–gel

thin films. This structure enabled the determination of nitrite in environmental waters with detection limits bellow the ones established by the European Union and response times of 5 min, which was a considerable improvement when compared to the 30 min response of the bulk monoliths configuration.

Sol–gel encapsulation of the enzyme lactate dehydrogenase in thin films was employed by Li et al. [133] and Ramanathan et al. [134] to obtain optical biosensors for L-lactate and piruvate, respectively. The lactate sensor, although stable for at least 3 months, was a disposable device, since it used co-immobilized cofactor nicotinamide adenine dinucleotide (NADH), which was not renewable.

Urease has also been entrapped in sol–gel films for development of biosensors for urea detection. Narang et al. [137] proposed the sol–gel:enzyme:sol–gel sandwich architecture which, when compared to previous designs, displayed more rapid response, high storage stability, simplicity in fabrication and did not involve any chemical modification of the enzyme or the use of co-dopants. Ulatowska-Jarza and Podbielska [138] combined urease with a pH indicator, bromothymol blue, and optical fibres.

A common way of using enzymes is through whole cells rather than the purified enzymes. This has been successfully applied in sol–gel films-based optical biosensors for biochemical oxygen demand (BOD) determination, for example. Lin et al. [117] proposed a sensing film consisting of an organically modified silicate film embedded with tri(4,7-diphenyl-1,10-phenanthroline) ruthenium(II) perchlorate and three kinds of seawater microorganisms (*Bacillus licheniformis*, *Dietzia maris*, *Marinobacter marinus*) immobilized on a polyvinyl alcohol sol–gel matrix. The co-immobilized microorganisms maintained their activity even if kept up to 1 year at 4 °C, and the stored sensing film could be employed for BOD measurement after 1 day's reactivation. Kwok et al. [118] constructed a sensing device for parallel multi-sample determination of BOD by immobilizing activated sludge and *Bacillus subtilis* on oxygen sensing films placed on the bottom of glass sample vials. The microorganisms were entrapped in a sol–gel derived film of silica and poly(vinyl alcohol)-grafted-poly(4-vinylpyridine) copolymer. The oxygen film contained Ru(II)-tris(4,7-diphenyl-1,10-phenanthroline) immobilized in a silicone rubber.

Lev and co-workers [126] demonstrated the encapsulation of genetically engineered bioluminescent *Escherichia coli* reporter strains in sol–gel derived silicates. Heat shock, oxidative stress, fatty acids, peroxides and genotoxicity reporting bacteria were incorporated in sol–gel films and maintained the biological properties of the free culture as well as their metrological characteristics including repeatability, shelf life stability, sensitivity and broad range response to a wide class of toxic compounds. This novel whole-cell biosensor is proposed either as a multiple-use sensing element or as part of early warning devices operating in flow conditions. Recently, Trögl et al. [136] immobilized *Pseudomonas fluorescens* HK44, a whole-cell bacterial reporter that responds to naphthalene and salicylate exposure by production of visible light, in sol–gel films that remained mechanically stable for at least 8 months.

Sol–gel materials, due to their biocompatibility and chemical inertia, are also useful matrices for designing optical sensors for monitoring biological species. For example, Kishen and co-workers [139] developed an evanescent wave biosensor for the monitoring of mutans *streptococci* in human saliva. This sensor employed bromophenol blue entrapped in a porous sol–gel film coated on the unclad portion of an optical fibre, which enabled real time monitoring of pH variations in saliva produced by the reactivity of mutans *streptococci* with sucrose.

4. Conclusions and trends

The significant number of applications reported, most of them quite recent, clearly illustrates the growing interest on the sol–gel process to develop optical sensors. There seems to be a rising awareness of the remarkable flexibility of this technology in producing sensors that can be tailored to the needs of a specific application. Optical fibre sensors based on doped sol–gel coatings are easy to prepare, since the sol–gel glass is highly compatible to silica or glass fibres. These sensors are typically inexpensive and provide the possibility of remote sensing and *in vivo* measurements. Through this technology, sensor arrays and sensors containing multiple reagents are easily developed. Additionally, since sol–gel glass is stable, inert and non-toxic, these sensors can be applied to measurements in harsh environments, in medical diagnosis and food industries. The development of optical biosensors based on sol–gel films is also becoming more relevant: the increasing number of applications reported in the literature reflects the unique features of sol–gel bioencapsulation.

However, some critical issues are still to be considered, in order to make mass production and commercialisation viable. A significant number of sensing devices reported exhibit one or more limitations that hinder their continuous use, and some of them (except when specified) were not applied to real samples or practical situations. Many of the works referred, although describing optimisation and, sometimes, showing preliminary results, present insufficient data concerning analytical performance. It is desirable to obtain sol–gel sensors with no reagent leaching and that can be used for a long period of time without changes in sensitivity and response time. Therefore, research in this area places increasing emphasis on the critical issues concerning the sensors' performance – microstructural stability, leaching, reversibility, response time, repeatability, sensitivity and selectivity – instead of simply demonstrating the sensing potential. Once more, the same feature that first attracted attention to this technology – versatility – seems to be the key on achieving this goal.

In the recent years, rapid advances have been made in improving immobilization protocols and overcoming many hurdles of sol–gel technology, as shown in the reports assembled in this review. Novel configurations, such as miniaturised devices and integrated sensors based on planar waveguides, are currently employed and provide high sensitivity, fast response and low costs, as well as an enlarged range of possible applications. Microfabrication techniques, such as soft lithography and photopatternability, enable the production of new microsensors and

bioelectronic devices. Combination of sol–gel glasses with other polymeric matrices, yielding organic–inorganic sol–gels hybrids and composites, results in advanced materials that exhibit the flexibility and functionality of organics and many of the useful properties of inorganics, including stability, hardness and chemical resistance. For example, the fabrication of integrated optics devices using sol–gel precursors and photocurable polymers coatings [140,141] allows the fabrication of a range of sensor configurations on planar substrates, from sensor arrays to micro-total-analysis systems (μ -TAS). New hybrid materials constituted of organic nanocrystals embedded in sol–gel films [142] make possible to control the spatial distribution of nucleation, enabling structures with higher sensitivity and photostability than dispersed dye molecules in a matrix, which gives opportunity to design new 2D arrays of luminescent crystals for chemical and biological multi-sensors.

After decades of theoretical studies devoted to the full understanding of the sol–gel process, it is expected that the future years will witness a variety of new and improved sol–gel films-based sensing applications.

Acknowledgements

One of the authors (P.C.A.J.) gratefully thanks FCT (Fundação para a Ciência e Tecnologia) and FSE (III QCA) for financial support.

References

- [1] A. Hulanicki, S. Glab, F. Ingman, *Pure Appl. Chem.* 63 (1991) 1247.
- [2] O.S. Wolfbeis, *Fiber Optic Chemical Sensors and Biosensors*, CRC Press, Boca Raton, 1991.
- [3] O. Lev, *Analisis* 20 (1992) 543.
- [4] O. Lev, M. Tsionsky, L. Rabinovitch, V. Glezer, S. Sampath, I. Pankratov, *J. Gun, Anal. Chem.* 67 (1995) 22A.
- [5] J. Lin, C.W. Brown, *Trends Anal. Chem.* 16 (1997) 200.
- [6] C.J. Brinker, G.W. Scherer, *Sol-Gel Science: The Physics and Chemistry of Sol-Gel Processing*, Academic Press, New York, 1990.
- [7] L.C. Klein (Ed.), *Sol-Gel Technology for Thin Films, Fibers, Preforms, Electronics, and Specialty Shapes*, Noyes Publications, Park Ridge, 1988.
- [8] C. Rottman, M. Ottolenghi, R. Zusman, O. Lev, M. Smith, G. Cong, M.L. Kagan, D. Avnir, *Mat. Lett.* 13 (1992) 293.
- [9] A. Lobnik, I. Oehme, I. Murkovic, O.S. Wolfbeis, *Anal. Chim. Acta* 367 (1998) 159.
- [10] C. Li, X. Zhang, Z. Han, B. Akermark, L. Sun, G. Shen, R. Yu, *Analyst* 131 (2006) 388.
- [11] F. Ismail, C. Malins, N.J. Goddard, *Analyst* 127 (2002) 253.
- [12] R. Makote, M.M. Collinson, *Anal. Chim. Acta* 394 (1999) 195.
- [13] T. Nguyen, K.P. McNamara, Z. Rosenzweig, *Anal. Chim. Acta* 400 (1999) 45.
- [14] M.A. Villegas, M.A. García, S.E. Paje, J. Llopis, *J. Eur. Ceram. Soc.* 22 (2002) 1475.
- [15] K. Ertekin, C. Karapire, S. Alp, B. Yenigül, S. İçli, *Dyes Pigments* 56 (2003) 125.
- [16] M.A. Villegas, L. Pascual, S.E. Paje, M.A. García, J. Llopis, *J. Eur. Ceram. Soc.* 20 (2000) 1621.
- [17] S. Blair, M.P. Lowe, C.E. Mathieu, D. Parker, P.K. Senanayake, R. Katakay, *Inorg. Chem.* 40 (2001) 5860.
- [18] A. Lobnik, N. Majcen, K. Niederreiter, G. Uray, *Sens. Actuators B* 74 (2001) 200.
- [19] M.A. Villegas, L. Pascual, *Thin Solid Films* 351 (1999) 103.

- [20] M. García-Heras, C. Gil, N. Carmona, J. Faber, K. Kromka, M.A. Villegas, *Anal. Chim. Acta* 540 (2005) 147.
- [21] E. Wang, K. Chow, V. Kwan, T. Chin, C. Wong, A. Bocarsly, *Anal. Chim. Acta* 495 (2003) 45.
- [22] C. Malins, H.G. Glever, T.E. Keyes, J.G. Vos, W.J. Dressick, B.D. MacCraith, *Sens. Actuators B* 67 (2000) 89.
- [23] S.B. Bambot, J. Sipior, J.R. Lakowicz, G. Rao, *Sens. Actuators B* 22 (1994) 181.
- [24] L. Yang, S.S. Saavedra, *Anal. Chem.* 67 (1995) 1307.
- [25] J.E. Lee, S.S. Saavedra, *Anal. Chim. Acta* 285 (1994) 265.
- [26] B.D. MacCraith, C.M. McDonagh, G. O'Keefe, A.K. McEvoy, T. Butler, F.R. Sheridan, *Sens. Actuators B* 29 (1995) 51.
- [27] T.M. Butler, B.D. MacCraith, C. McDonagh, *J. Non-Cryst. Solids* 224 (1998) 249.
- [28] B.D. Gupta, D.K. Sharma, *Opt. Commun.* 140 (1997) 32.
- [29] F.B.M. Suah, M. Ahmad, M.N. Taib, *Sens. Actuators B* 90 (2003) 182.
- [30] E. Alvarado-Méndez, R. Rojas-Laguna, J.A. Andrade-Lucio, D. Hernández-Cruz, R.A. Lessard, J.G. Aviña-Cervantes, *Sens. Actuators B* 106 (2005) 518.
- [31] C.A. Browne, D.H. Tarrant, M.S. Olteanu, J.W. Mullens, E.L. Chronister, *Anal. Chem.* 68 (1996) 2289.
- [32] S. McCulloch, D. Uttamchandani, *IEEE Proc. -Sci. Meas. Technol.* 144 (1997) 241.
- [33] P.A. Wallace, M. Campbell, Y. Yang, A.S. Holmes-Smith, M. Uttamlal, *J. Luminescence* 72–74 (1997) 1017.
- [34] D.A. Nivens, Y. Zhang, S. Michael, *Anal. Chim. Acta* 376 (1998) 235.
- [35] D.A. Nivens, M.V. Schiza, S. Michael, *Talanta* 58 (2002) 543.
- [36] O. Ben-David, E. Shafir, I. Gilath, Y. Prior, D. Avnir, *Chem. Mater.* 9 (1997) 2255.
- [37] S.A. Grant, R.S. Glass, *Sens. Actuators B* 45 (1997) 35.
- [38] O.B. Miled, H.B. Ouada, J. Livage, *Mat. Sci. Eng. C* 21 (2002) 183.
- [39] J.Y. Ding, M.R. Shahriari, G.H. Sigel Jr., *Electron. Lett.* 27 (1991) 1560.
- [40] B.D. Gupta, S. Sharma, *Opt. Commun.* 154 (1998) 282.
- [41] S.T. Lee, B. Aneeshkumar, P. Radhakrishnan, C.P.G. Vallabhan, V.P.N. Nampoori, *Opt. Commun.* 205 (2002) 253.
- [42] J. Lin, D. Liu, *Anal. Chim. Acta* 408 (2000) 49.
- [43] S.T. Lee, J. Gin, V.P.N. Nampoori, C.P.G. Vallabhan, N.V. Unnikrishnan, P. Radhakrishnan, *J. Opt. A: Pure Appl. Opt.* 3 (2001) 355.
- [44] L.R. Allain, K. Soraesene, Z. Xue, *Anal. Chem.* 69 (1997) 3076.
- [45] M.H. Noiré, C. Bouzon, L. Couston, J. Gontier, P. Marty, D. Pouyat, *Sens. Actuators B* 51 (1998) 214.
- [46] M.H. Noiré, L. Couston, E. Douarre, D. Pouyat, C. Bouzon, P. Marty, *J. Sol-Gel Sci. Technol.* 17 (2003) 131.
- [47] M. Shamsipur, G. Azimi, *Anal. Lett.* 34 (2001) 1603.
- [48] E. Wang, K. Chow, W. Wang, C. Wong, C. Yee, A. Persad, J. Mann, A. Bocarsly, *Anal. Chim. Acta* 534 (2005) 301.
- [49] N. Carmona, M.A. Villegas, J.M.F. Navarro, *Sens. Actuators A* 116 (2004) 398.
- [50] M. Garcia-Heras, K. Kromka, J. Faber, P. Karaszkiwicz, M.A. Villegas, *Environ. Sci. Technol.* 39 (2005) 3743.
- [51] A. Lobnik, O.S. Wolfbeis, *Sens. Actuators B* 51 (1998) 203.
- [52] C. Malins, A. Doyle, B.D. MacCraith, F. Kvasnik, M. Landl, P. Simon, L. Kalvoda, R. Lukas, K. Puffer, I. Babusik, *J. Environ. Monit.* 1 (1999) 417.
- [53] C. Malins, T.M. Butler, B.D. MacCraith, *Thin Solid Films* 368 (2000) 105.
- [54] W. Cao, Y. Duan, *Sens. Actuators B* 110 (2005) 252.
- [55] S. Tao, L. Xu, J.C. Fanguy, *Sens. Actuators B* 115 (2006) 158.
- [56] A. Martucci, N. Bassiri, M. Guglielmi, L. Armelao, S. Gross, J.C. Pivin, *J. Sol-Gel Sci. Technol.* 26 (2003) 1573.
- [57] C. Cantalini, M. Post, D. Buso, M. Guglielmi, A. Martucci, *Sens. Actuators B* 108 (2005) 184.
- [58] C. Malins, B.D. MacCraith, *Analyst* 123 (1998) 2373.
- [59] C. von Bültzingslöwen, A.K. McEvoy, C. McDonagh, B.D. MacCraith, I. Klimant, C. Krause, O.S. Wolfbeis, *Analyst* 127 (2002) 1478.
- [60] H. Segawa, E. Ohnishi, Y. Arai, K. Yoshida, *Sens. Actuators B* 94 (2003) 276.
- [61] U.M. Noor, D. Uttamchandani, *Sol-Gel Sci. Technol.* 11 (1998) 177.
- [62] L. Yang, S.S. Saavedra, N.R. Armstrong, *Anal. Chem.* 68 (1996) 1834.
- [63] Z. Qi, I. Honma, H. Zhou, *Anal. Chem.* 78 (2006) 1034.
- [64] K. Eguchi, T. Hashiguchi, K. Sumiyoshi, H. Arai, *Sens. Actuators B* 1 (1990) 154.
- [65] O. Worsfold, C. Malins, M.G. Forkan, I.R. Peterson, B.D. MacCraith, D.J. Walton, *Sens. Actuators B* 15 (1999) 15.
- [66] S.A. Grant, J.H. Satcher Jr., K. Bettencourt, *Sens. Actuators B* 69 (2000) 132.
- [67] O. Worsfold, C.M. Dooling, T.H. Richardson, M.O. Vysotsky, R. Treginning, C.A. Hunter, C. Malins, *J. Mater. Chem.* 11 (2001) 399.
- [68] S.J. Mechery, J.P. Singh, *Anal. Chim. Acta* 557 (2006) 123.
- [69] B.D. MacCraith, C.M. McDonagh, G. O'Keefe, E.T. Keyes, J.G. Vos, B. O'Kelly, J.F. McGilp, *Analyst* 118 (1993) 385.
- [70] G. O'Keefe, B.D. MacCraith, A.K. McEvoy, C.M. McDonagh, J.F. McGilp, *Sens. Actuators B* 29 (1995) 226.
- [71] A.K. McEvoy, C.M. McDonagh, B.D. MacCraith, *Analyst* 121 (1996) 785.
- [72] A.K. McEvoy, C. McDonagh, B.D. MacCraith, *J. Sol-Gel Sci. Technol.* 8 (1997) 1121.
- [73] C. McDonagh, B.D. MacCraith, A.K. McEvoy, *Anal. Chem.* 70 (1998) 45.
- [74] C.M. McDonagh, A.M. Shields, A.K. McEvoy, B.D. MacCraith, J.F. Gouin, *J. Sol-Gel Sci. Technol.* 13 (1998) 207.
- [75] C. McDonagh, P. Bowe, K. Mongey, B.D. MacCraith, *J. Non-Cryst. Solids* 306 (2002) 138.
- [76] C.S. Burke, O. McGaughey, J. Sabattié, H. Barry, A.K. McEvoy, C. McDonagh, B.D. MacCraith, *Analyst* 130 (2005) 41.
- [77] R.A. Dunbar, J.D. Jordan, F.V. Bright, *Anal. Chem.* 68 (1996) 604.
- [78] S.K. Lee, I. Okura, *Analyst* 122 (1997) 81.
- [79] S.K. Lee, I. Okura, *Anal. Chim. Acta* 342 (1997) 181.
- [80] Y.G. Ma, T.C. Cheung, C.M. Che, J. Shen, *Thin Solid Films* 333 (1998) 224.
- [81] M. Ahmad, N. Mohammad, J. Abdullah, *J. Non-Cryst. Solids* 290 (2001) 86.
- [82] S.K. Lee, Y.B. Shin, H.B. Pyo, S.H. Park, *Chem. Lett.* 4 (2001) 310.
- [83] Y. Tang, E.C. Tehan, Z. Tao, F.V. Bright, *Anal. Chem.* 75 (2003) 2407.
- [84] R.T. Bailey, F.R. Cruickshank, G. Deans, R.N. Gillanders, M.C. Tedford, *Anal. Chim. Acta* 487 (2003) 101.
- [85] R.N. Gillanders, M.C. Tedford, P.J. Crilly, R.T. Bailey, *J. Photochem. Photobiol. A* 163 (2004) 193.
- [86] P.A.S. Jorge, P. Caldas, C.C. Rosa, A.G. Oliva, J.L. Santos, *Sens. Actuators B* 103 (2004) 290.
- [87] <http://www.oceanoptics.com/products/foxsystem.asp>.
- [88] S. Wallington, T. Labayen, A. Poppe, N.A.J.M. Sommerdijk, J.D. Wright, *Sens. Actuators B* 38–39 (1997) 48.
- [89] P.C.A. Jerónimo, A.N. Araújo, M.C.B.S.M. Montenegro, D. Satinský, P. Solich, *Anal. Chim. Acta* 504 (2004) 235.
- [90] R. Reisfeld, D. Shamrakov, *Sensors Mat.* 8 (1996) 439.
- [91] P.C.A. Jerónimo, A.N. Araújo, M.C.B.S.M. Montenegro, C. Pasquini, I.M. Raimundo Jr., *Anal. Bioanal. Chem.* 380 (2004) 108.
- [92] M. Plaschke, R. Czolk, H.J. Ache, *Anal. Chim. Acta* 304 (1995) 107.
- [93] A. Panusa, A. Flamini, N. Poli, *Chem. Mater.* 8 (1996) 1202.
- [94] P.C.A. Jerónimo, A.N. Araújo, M.C.B.S.M. Montenegro, *Sens. Actuators B* 103 (2004) 169.
- [95] K. Ertekin, B. Yenigul, E.U. Akkaya, *J. Fluorescence* 12 (2002) 263.
- [96] D.D. Dunuwila, B.A. Torgerson, C.K. Chang, K.A. Berglund, *Anal. Chem.* 66 (1994) 2739.
- [97] M. Zevin, R. Reisfeld, I. Oehme, O.S. Wolfbeis, *Sens. Actuators B* 38–39 (1997) 235.
- [98] J.L.H. Jiwani, J.P. Soumillion, *J. Non-Cryst. Solids* 220 (1997) 316.
- [99] D.N. Simon, R. Czolk, H.J. Ache, *Thin Solid Films* 260 (1995) 107.
- [100] P.J. Skrdla, S.B. Mendes, N.R. Armstrong, S.S. Saavedra, *J. Sol-Gel Sci. Technol.* 24 (2002) 167.
- [101] N. Hashimoto, T. Hashimoto, T. Teranishi, H. Nasu, K. Kamiya, *Sens. Actuators B* 113 (2006) 382.
- [102] Y. Lu, L. Han, C.J. Brinker, T.M. Niemczyk, G.P. Lopez, *Sens. Actuators B* 35–36 (1996) 517.

- [103] S. Wallington, C. Pilon, J.D. Wright, *J. Sol-Gel Sci. Technol.* 8 (1997) 1127.
- [104] A. Abdelghani, J.M. Chovelon, N. Jaffrezic-Renault, M. Lacroix, H. Gagnaire, C. Veillas, B. Berkova, M. Chomat, V. Matejec, *Sens. Actuators B* 44 (1997) 495.
- [105] F. Abdelmalek, J.M. Chovelon, M. Lacroix, N. Jaffrezic-Renault, V. Matejec, *Sens. Actuators B* 56 (1999) 234.
- [106] P.J. Skrdla, S.S. Saavedra, N.R. Armstrong, S.B. Mendes, N. Peyghambarian, *Anal. Chem.* 71 (1999) 1332.
- [107] A. Lobnik, M. Čajlaković, *Sens. Actuators B* 74 (2001) 194.
- [108] L. Wen-xu, C. Jian, *Anal. Chem.* 75 (2003) 1458.
- [109] M. Janotta, M. Karlowatz, F. Vogt, B. Mizaikoff, *Anal. Chim. Acta* 496 (2003) 339.
- [110] M. Janotta, A. Katzir, B. Mizaikoff, *Appl. Spectrosc.* 57 (2003) 823.
- [111] H. Isobe, C.D. Singh, H. Katsumata, H. Suzuki, T. Fujinami, M. Ogita, *Appl. Surface Sci.* 244 (2005) 199.
- [112] I. Gill, A. Ballesteros, *TIBTECH* 18 (2000) 282.
- [113] I. Gill, *Chem. Mater.* 13 (2001) 3404.
- [114] H. Frenkel-Mullerad, D. Avnir, *J. Am. Chem. Soc.* 127 (2005) 8077.
- [115] B. Dunn, J.M. Miller, B.C. Dave, J.S. Valentine, J.I. Zink, *Acta Mater.* 46 (1998) 737.
- [116] R.A. Doong, H.C. Tsai, *Anal. Chim. Acta* 434 (2001) 239.
- [117] L. Lin, L. Xiao, S. Huang, L. Zhao, J. Cui, X. Wang, X. Xen, *Biosens. Bioelectron.* 21 (2006) 1703.
- [118] N.Y. Kwok, S. Dong, W. Lo, K.Y. Wong, *Sens. Actuators B* 110 (2005) 289.
- [119] P.C.A. Jerónimo, A.N. Araújo, M.C.B.S.M. Montenegro, D. Satinský, P. Solich, *Analyst* 130 (2005) 1190.
- [120] A. Kumar, R. Malhotra, B.D. Malhotra, S.K. Grover, *Anal. Chim. Acta* 414 (2000) 43.
- [121] V.G. Andreou, Y.D. Clonis, *Bios. Bioelectron.* 17 (2002) 61.
- [122] A. Hreniak, K. Maruszewski, J. Rybka, A. Gamian, J. Czyzewski, *Optical Mat.* 26 (2004) 141.
- [123] D.J. Blyth, J.W. Aylott, D.J. Richardson, D.A. Russell, *Analyst* 120 (1995) 2725.
- [124] J.W. Aylott, D.J. Richardson, D.A. Russell, *Chem. Mater.* 9 (1997) 2261.
- [125] S. Ferretti, S.K. Lee, B.D. MacCraith, A.G. Oliva, D.J. Richardson, D.A. Russell, K.E. Sapsford, M. Vidal, *Analyst* 125 (2000) 1993.
- [126] J.R. Premkumar, R. Rosen, S. Belkin, O. Lev, *Anal. Chim. Acta* 462 (2002) 11.
- [127] U. Narang, P.N. Prasad, F.V. Bright, K. Ramanathan, N.D. Kumar, B.D. Malhotra, M.N. Kamalasanan, S. Chandra, *Anal. Chem.* 66 (1994) 3139.
- [128] S. de Marcos, J. Galindo, J.F. Sierra, J. Galbán, J.R. Castillo, *Sens. Actuators B* 57 (1999) 227.
- [129] O.S. Wolfbeis, I. Oehme, N. Papkovskaya, I. Klimant, *Biosens. Bioelectron.* 15 (2000) 69.
- [130] K. Ertekin, S. Cinar, T. Aydemir, S. Alp, *Dyes and Pigments* 67 (2005) 133.
- [131] V.G. Andreou, Y.D. Clonis, *Anal. Chim. Acta* 460 (2002) 151.
- [132] K.M. Wang, J. Li, X. Yang, F. Shen, X. Wang, *Sens. Actuators B* 65 (2000) 239.
- [133] C.L. Li, Y.H. Lin, C.L. Shih, J.P. Tsaur, L.K. Chau, *Biosens. Bioelectron.* 17 (2002) 323.
- [134] K. Ramanathan, M.N. Kamalasanan, B.D. Malhotra, D.R. Pradhan, S. Chandra, *J. Sol-gel Sci. Technol.* 10 (1997) 309.
- [135] J.W. Aylott, D.J. Richardson, D.A. Russell, *Analyst* 122 (1997) 77.
- [136] J. Trögl, S. Ripp, G. Kunková, G.S. Slayer, A. Churavá, P. Pařík, K. Demnerová, J. Hálová, L. Kubicová, *Sens. Actuators B* 107 (2005) 98.
- [137] U. Narang, P.N. Prasad, F.V. Bright, *Chem. Mater.* 6 (1994) 1596.
- [138] A. Ulatowska-Jarza, H. Podblieska, *Optica Appl.* 32 (2002) 685.
- [139] A. Kishen, M.S. John, C.S. Lim, A. Asundi, *Biosens. Bioelectron.* 18 (2003) 1371.
- [140] P. Etienne, P. Coudray, Y. Moreau, J. Porque, *J. Sol-Gel Sci. Technol.* 13 (1998) 523.
- [141] S. Aubonnet, H.F. Barry, C. von Bültzingslöwen, J.M. Sabattié, B.D. MacCraith, *Electron. Lett.* 12 (2003) 913.
- [142] E. Botzung-Appert, J. Zaccaro, C. Gourgon, Y. Usson, P.L. Baldeck, A. Ibanez, *J. Cryst. Growth* 283 (2005) 444.

A novel sol–gel-material prepared by a surface imprinting technique for the selective solid-phase extraction of bisphenol A

Xiaoman Jiang, Wei Tian, Chuande Zhao, Haixia Zhang*, Mancang Liu

College of Chemistry and Chemical Engineering, Lanzhou University, Lanzhou, Tianshui Road 222, Lanzhou 730000, PR China

Received 17 May 2006; received in revised form 30 September 2006; accepted 3 October 2006

Available online 15 November 2006

Abstract

A novel and simple imprinted amino-functionalized silica gel material was synthesized by combining a surface molecular imprinting technique with a sol–gel process on the supporter of activated silica gel for solid-phase extraction-high performance liquid chromatography (SPE-HPLC) determination of bisphenol A (BPA). Non-imprinted silica sorbent was synthesized without the addition of BPA using the same procedure as that of BPA-imprinted silica sorbent. The BPA-imprinted silica sorbent and non-imprinted silica sorbent were characterized by FT-IR and the static adsorption experiments. The prepared BPA-imprinted silica sorbent showed high adsorption capacity, significant selectivity and good site accessibility for BPA. The maximum static adsorption capacity of the BPA-imprinted and non-imprinted silica sorbent for BPA was 68.9 and 34.0 mg g⁻¹, respectively. The relatively selective factor value of this BPA-imprinted silica sorbent was 4.5. Furthermore, the difference of the retention characteristics of BPA on the C₈ SPE column and BPA-imprinted silica SPE (MIP-SPE) was compared. The MIP-SPE-HPLC method showed higher selectivity to BPA than the traditional SPE-HPLC method. At last, the BPA-imprinted polymers were used as the sorbent in solid-phase extraction to determine BPA in water samples with satisfactory recovery higher than 99% (R.S.D. 3.7%).

© 2006 Elsevier B.V. All rights reserved.

Keywords: Molecularly imprinted polymers; Bisphenol A; Solid-phase extraction; High performance liquid chromatography

1. Introduction

Molecularly imprinted polymers (MIPs) are an artificially synthesized macromolecular material, which has prearrangement of structure and specific molecular recognition ability [1]. In the last few years, MIPs were widely used for the selective enrichment and pretreatment of target compounds existing in complex matrix [2–4]. And molecular imprinting technology has been expanded to the field of environmental analysis and even reaction media [5].

MIPs can be synthesized following three different imprinting approaches: the non-covalent, the covalent, and the semi-covalent. In all these protocols, a template molecule interacts with an appropriate functional monomer to establish specific interactions [6]. However, the MIPs synthesized by traditional methods exhibit high affinity and selectivity but

poor site accessibility to the target molecules. The kinetics of the sorption/desorption process is unfavorable and the mass transfer is slow [7]. Recently, molecularly imprinted sol–gel materials (MISGMs) have been extensively studied [7–11]. MISGMs are synthesized by a conventional sol–gel process and incorporation of the template molecules into rigid inorganic or inorganic–organic networks. The material with binding sites situated at the surface show many advantages including high selectivity, more accessible sites, fast mass transfer and binding kinetics [12].

In this study, activated silica gel was used as the supporter for organic groups because it was a non-swelling inorganic material being stable under acidic conditions, has high mass exchange characteristics and very high thermal resistance. Bisphenol A (BPA) was studied as the model compound.

BPA is often contained in environmental water and is now attracting attention as an endocrine disturbance. Recently, various analytical methods have been reported for the determination of BPA [2,13–17]. Most of these methods are based on HPLC cooperated with various sample pretreatment techniques. In

* Corresponding author. Tel.: +86 13893105337; fax: +86 931 8912582.
E-mail address: zhanghx@lzu.edu.cn (H. Zhang).

references [2] and [13], trace BPA in complex environmental samples was determined by the method of MIP-SPE-HPLC and showed the good results except using a complex method to synthesize the MIPs.

The purpose of this work was to prepare a new and simple molecularly imprinted amino-functionalized silica gel sorbent with respect to BPA by a surface imprinting technique in combination with a sol–gel process, and to apply in SPE coupled with HPLC for the determination of BPA in water samples. The proposed method presented high selectivity and adsorption capacity for BPA.

2. Experimental

2.1. Materials and chemicals

Silica gel (80–120 mesh, Qingdao Ocean Chemical Company, Qingdao, China) was used as the supporter to prepare the BPA-imprinted functionalized sorbent. 3-Aminopropyltrimethoxysilane (APS), tetraethoxysilane (TEOS) (Qingdao Ocean University Chemical Company, Qingdao, China), bisphenol A (BPA), *D-tert*-butylphenol (BP) (Sinopharm Group Chemical Reagent Co., Ltd., Shanghai, China) were used in this study. The structures of BPA and BP were shown in Fig. 1. Ultra pure water used throughout the experiments was obtained from a purification system (MILLI-Q).

The mobile phase used for HPLC experiments was a mixture of acetonitrile (ACN) and water (70:30, v/v), and was filtered through 0.45 μm filter prior to use.

2.2. Instrumentation

The chromatographic system consisted of a Model 210 HPLC pump and a UV detector (VARIAN PROSTAR). All separations were achieved on an analytical reversed-phase column (Hanbon Science and Technology, C₁₈ column, 4.6 mm \times 150 mm) with a flow rate of 0.8 ml min⁻¹ at room temperature. The UV detector was operated at 278 nm.

The MIP-SPE study was developed in an off-line mode using a solid-phase extraction cartridge supplied by Dalian Institute of Chemical Physics, Chinese academy of sciences. One hundred milligrams of BPA-imprinted silica sorbent and C₈ were packed into this SPE cartridge, respectively.

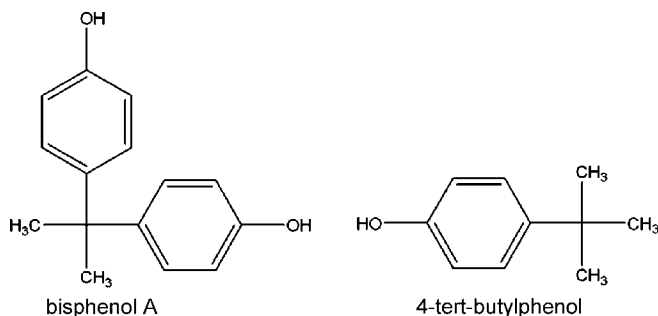


Fig. 1. Structures of BPA and BP.

2.3. Procedures for the preparation of the BPA-imprinted amino-functionalized silica gel sorbent

The silica gel surfaces were activated by refluxing 8 g of silica gel (80–120 mesh) with 60 ml of 6 mol l⁻¹ hydrochloric acid under stirring for 8 h, then the activated silica gel was filtered and washed with ultra pure water to neutral and dried under vacuum at 70 °C for 8 h.

To prepare the BPA-imprinted amino-functionalized silica gel sorbent, 0.4403 g of BPA was dissolved in 5 ml of methanol under stirring, and 2 ml of APS was added into the mixture. After the solution was stirred and refluxed for 30 min, 4 ml of TEOS was added. Stirring for 5 min, 1.0 g of activated silica gel and 1 ml of 1.0 mol l⁻¹ HAc were added. The mixture was stirred for 15 h at room temperature.

The product was filtrated and dried at 100 °C for 12 h. The sorbent was washed with 25 ml of methanol and 25 ml of 1.0 mol l⁻¹ HCl under string for 3 h to remove BPA. The product was recovered by filtration, washed with 50 ml of mixture of methanol and 6 mol l⁻¹ HCl (1:1, v/v) and ultra pure water, neutralized with 0.05 mol l⁻¹ KOH and washed by ultra pure water again. Finally, the sorbent was dried at 100 °C for 12 h. The non-imprinted functionalized silica gel sorbent was also prepared using an identical procedure without adding BPA.

2.4. Static adsorption test

10 ml of various concentrations of BPA were dissolved in methanol, then 50 mg of BPA-imprinted silica sorbent was added. The mixture was shaken for 1 h at room temperature to facilitate adsorption of the BPA onto the BPA-imprinted sorbent. After the solution was centrifuged, the concentrations of the BPA in the supernatants were determined by HPLC.

Adsorption and competitive recognition studies were performed with BPA and structurally similar compounds BP at the 600 mg l⁻¹ level.

2.5. MIP-SPE procedure in extraction of BPA from water samples

2.5.1. Comparison of retention behavior of BPA between C₈ SPE and BPA-imprinted sorbent SPE

For comparative purposes, 100 mg of C₈ and 100 mg of the BPA-imprinted silica sorbent were placed into two empty SPE cartridges, respectively. After they were pretreated with 10 ml methanol and 10 ml pure water, 10 ml of 5 $\mu\text{g ml}^{-1}$ BPA and BP mixture solution was loaded onto the MIP-SPE column and the C₈ SPE column with the speed of 2 ml min⁻¹. Then the C₈ SPE column was eluted with 2 ml methanol and the MIP-SPE column was eluted with 2 ml methanol-acetic acid-water (95:2.5:2.5, v/v/v) solution, respectively. The elution were analysed by HPLC and UV detection at 278 nm.

2.5.2. Cross-sensitivity between BPA and BP

According to the procedure in Section 2.5.1, MIP-SPE column was prepared for the determination of the cross-sensitivity between BPA and BP. Four solutions were prepared with differ-

erent ratios of BPA/BP. Then 10 ml of the mixture solutions were loaded onto the MIP-SPE column and the column was eluted with 2 ml methanol–acetic acid–water (95:2.5:2.5, v/v/v) solution, respectively. The elution were analyzed by HPLC and UV detection at 278 nm.

2.5.3. Determination of BPA in spiked water samples

According the procedure in Section 2.5.1, MIP-SPE column was prepared for the determination of BPA in water samples. Tap water was spiked with BPA at three concentration levels with 5.0, 1.0, and 0.01 $\mu\text{g ml}^{-1}$. Ten millilitres of these BPA

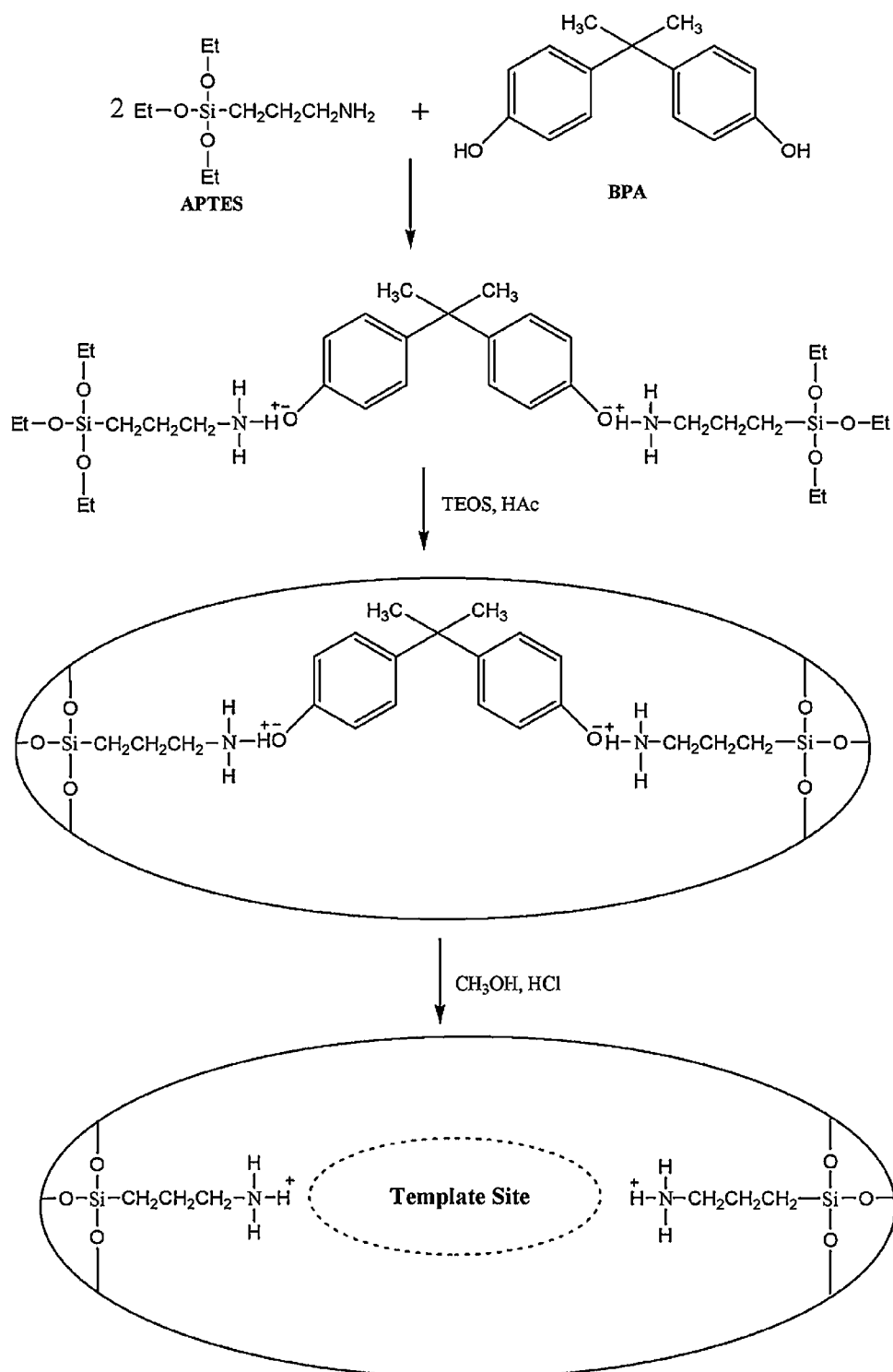


Fig. 2. Preparation protocol of the BPA-imprinted silica sorbent.

solution was introduced onto the MIP-SPE columns at a flow rate of 2 ml min^{-1} .

3. Results and discussion

3.1. Preparation of the BPA-imprinted amino-functionalized silica gel sorbent

Silica gel is an amorphous inorganic polymer having siloxane groups (Si–O–Si) in the bulk and silanol groups (Si–OH) on its surface. The surface silanol groups facilitate the introduction of the organic groups which covalently bind to the silica surface. Because commercial silica gel contains a low concentration of surface silanol groups suitable for modification, the activation of silica gel surface is necessary. In this work hydrochloric acid was used for the activation of silica gel [18].

The complex was formed between BPA and APS, then cohydrolyzed and co-condensed with the activated silica gel. Fig. 2 showed the possible preparation protocol of the BPA-imprinted silica sorbent. The template was thought to be bound using non-covalent interaction owing to the starting functional monomers used and the template functionalities present. Fig. 2 illustrated the proposed monomer–template interaction in this MIP was considered as hydrogen bonding interaction. A similar mechanism has been hypothesized by De-Man Han et al. [7]. After the residue of APS and BPA were removed, the imprinted functionalized silica gel sorbent which contained a tailor-made cavity for BPA was formed.

3.2. Characteristic of the FT-IR spectra

To ascertain the presence of APS in the functionalized silica gel sorbents, FT-IR spectra were obtained from activated silica gel, BPA-imprinted and non-imprinted amino-functionalized silica gel sorbents, respectively. As shown in Fig. 3, the observed features around 1102.32 indicated Si–O–Si and Si–O–H stretching vibrations, respectively. The bands around 807.52 and 469.89 cm^{-1} resulted from Si–O vibrations. A characteristic feature of the BPA-imprinted and non-imprinted silica sorbents compared with activated silica gel is N–H band around 1560.58 cm^{-1} and C–H band around 2976.70 cm^{-1} in Fig. 3b and c. These results suggested that $-\text{NH}_2$ has been grafted onto the surface of silica gel after modification. There was a significant shift in the frequencies of IR spectra of BPA-imprinted and non-imprinted silica sorbents. The C–H band vibration was 2942.28 cm^{-1} in the IR spectra of BPA-imprinted sorbent compared with 2976.70 cm^{-1} of non-imprinted sorbent. Because the presence of the hydrogen bonding in the BPA-imprinted silica sorbent conducted the C–H band stretching vibrations shift to the lower wavenumbers. The shift proved that BPA has been grafted successfully onto the BPA-imprinted polymers too.

3.3. Adsorption capacity of BPA-imprinted sorbent for BPA

The adsorption capacity was an important factor to evaluate the MIPs. The range of BPA solution with the concentration

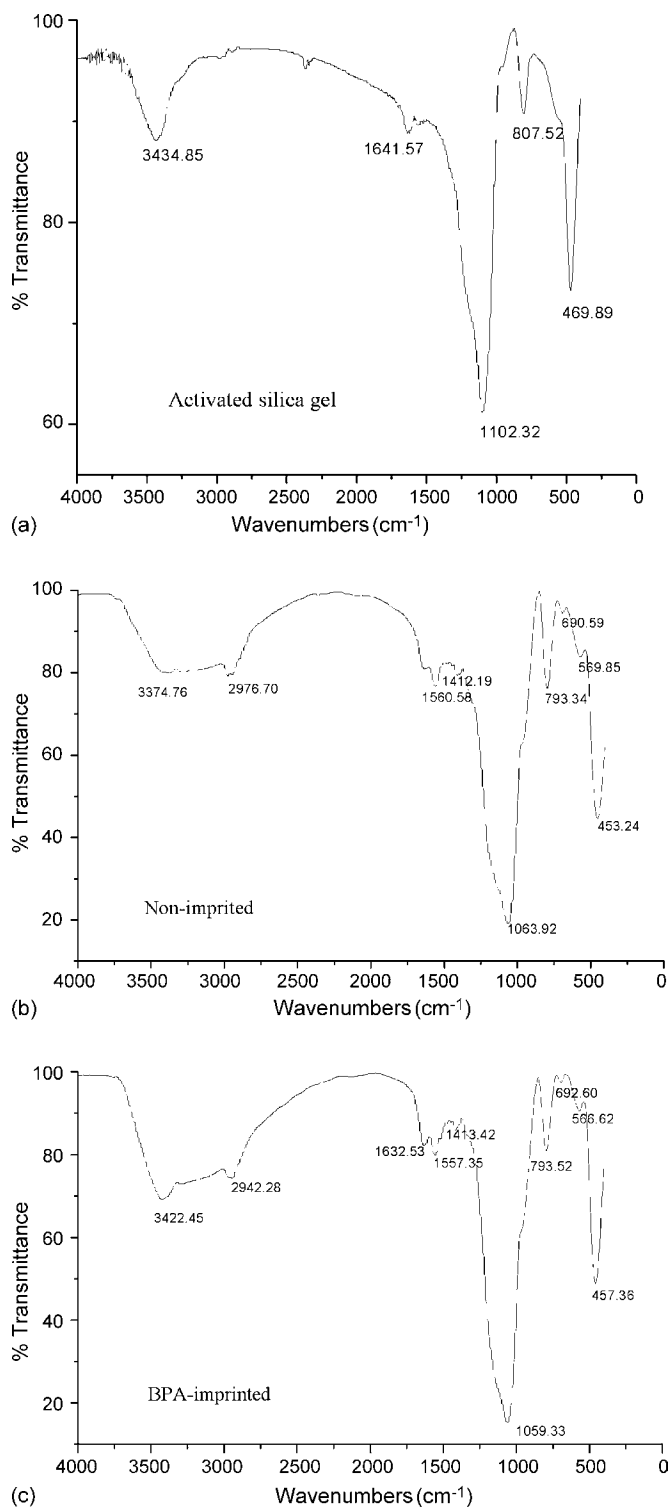


Fig. 3. FT-IR spectra of the activated silica gel, non-imprinted and BPA-imprinted sorbents.

of $200\text{--}2000 \text{ mg l}^{-1}$ was studied. As can be seen in Fig. 4, the amount of BPA adsorbed increased with the increase of the initial concentration of BPA solution. The static adsorption capacity of the BPA-imprinted silica sorbent and non-imprinted silica sorbent for BPA was calculated as 68.9 and 34.0 mg g^{-1} . The static adsorption capacity of the BPA-imprinted silica

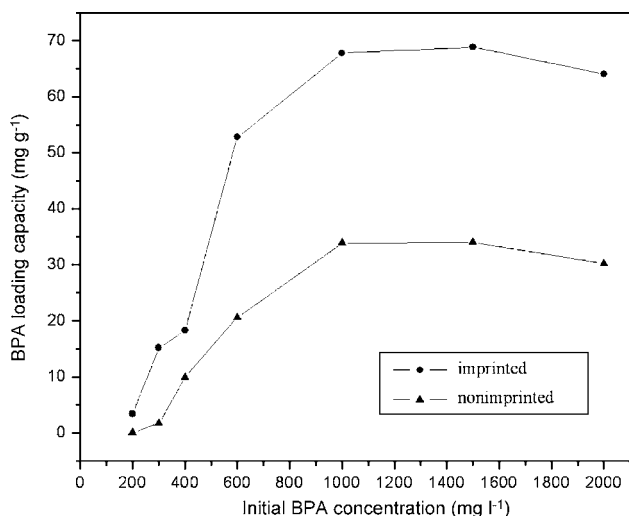


Fig. 4. Loading isotherm of BPA onto the imprinted and non-imprinted sorbents.

sorbent was about two times of non-imprinted silica sorbent. The results showed that the BPA-imprinted silica sorbent had a higher adsorption capacity for BPA than other ordinary sorbents. So, the BPA-imprinted silica sorbent would be better to enrich trace BPA in the samples.

3.4. Selectivity of the imprinted sorbent

The structurally similar compound BP was chosen as the competitive species with BPA for the competitive recognition study. As can be seen in Table 1, distribution coefficient (K_d), selectivity coefficient of the sorbent (k) and the relative selectivity coefficient (k') was obtained in these competitive experiments. Distribution coefficient (K_d) suggested the character of a substance adsorbed by a sorbent, selectivity coefficient of the sorbent (k) suggested the otherness of two substances adsorbed by one sorbent and relative selectivity coefficient (k') suggested the otherness of two sorbents. These factors were calculated as the following formula (1)–(3) [7]. BPA and BP had the similar k_d on the non-imprinted silica sorbent but BPA-imprinted silica showed about five times adsorbed capacity to BPA than to BP. The k (BPA/BP) value of the BPA-imprinted silica sorbent (4.9) was larger than that of non-imprinted silica sorbent (1.1), which showed that the BPA-imprinted silica sorbent had high selectivity for BPA over the structurally similar compounds BP. The k' value was 4.45, which was greater than 1 and showed the BPA-imprinted silica sorbent had higher selectivity than the

non-imprinted silica sorbent

$$K_d = \frac{C_i - C_f}{C_f} \times \frac{\text{volume of solution (ml)}}{\text{mass of gel (g)}} \quad (1)$$

C_i and C_f represent the initial and final concentrations

$$k = K_d \frac{\text{BPA}}{K_d \text{BP}} \quad (2)$$

$$k' = \frac{k_{\text{imprinted}}}{k_{\text{nonimprinted}}} \quad (3)$$

3.5. Application of the BPA imprinted sorbent to selective off-line SPE-HPLC determination of BPA

3.5.1. Comparison of retention behavior of BPA between C₈ SPE and BPA-imprinted sorbent SPE

Chromatograms of the BPA and BP mixture solution from the MIP-SPE and C₈ SPE were shown in Fig. 5. Fig. 5a showed that the directly injection of the standard of the BPA and BP mixture solution. Fig. 5b showed the eluate obtained from C₈ SPE column and Fig. 5c showed the eluate obtained from MIP-SPE column. Peak 1 was identified as BPA and peak 2 was identified as BP. From 5b and 5c, we could find that BPA was retained well on the C₈ SPE column and the MIP-SPE column. The recovery of BPA was 102.89% on the C₈ SPE column and 103.25% on the MIP-SPE column. It means the imprinted silica gel sorbent can be the substitute of the traditional C₈ sorbent and BPA had the similar adsorption behavior on the two sorbents. However, according to Fig. 5b and c, BP was retained well on the C₈ SPE column and retained poorly on the MIP-SPE column. The BPA-imprinted sorbent exhibited high selectivity and molecular recognition function.

Furthermore, the resolving power R_s of the two substances was calculated according to Fig. 5b and c. Fig. 5b showed the R_s was 2.3 and Fig. 5c showed the R_s was 2.8. These results demonstrated that the method of MIP-SPE could reduce the influence of the disturbance and enhance the value of R_s .

3.5.2. Cross-sensitivity between BPA and BP

The cross-sensitivity between BPA and BP was studied according to the Section 2.5.2 under the selected conditions. As shown in Table 2, when the concentration of BP was 50 times of BPA, the average recovery of BPA was 95.47%, which indicated that the BPA-imprinted silica gel sorbent had satisfactory ability of anti-interferences. However, when the concentration of BP was 100 times of BPA, the average recovery of BPA was

Table 1
Competitive loading of BPA and BP by the BPA-imprinted and non-imprinted silica gel sorbents

Sorbents	Initial solution (mg l ⁻¹)		Final solution (mg l ⁻¹)		K_d		k	k'
	BPA	BP	BPA	BP	BPA	BP		
Imprinted	600	600	477	570	51.57	10.52	4.9	4.5
Non-imprinted	600	600	554	558	16.61	15.05	1.1	

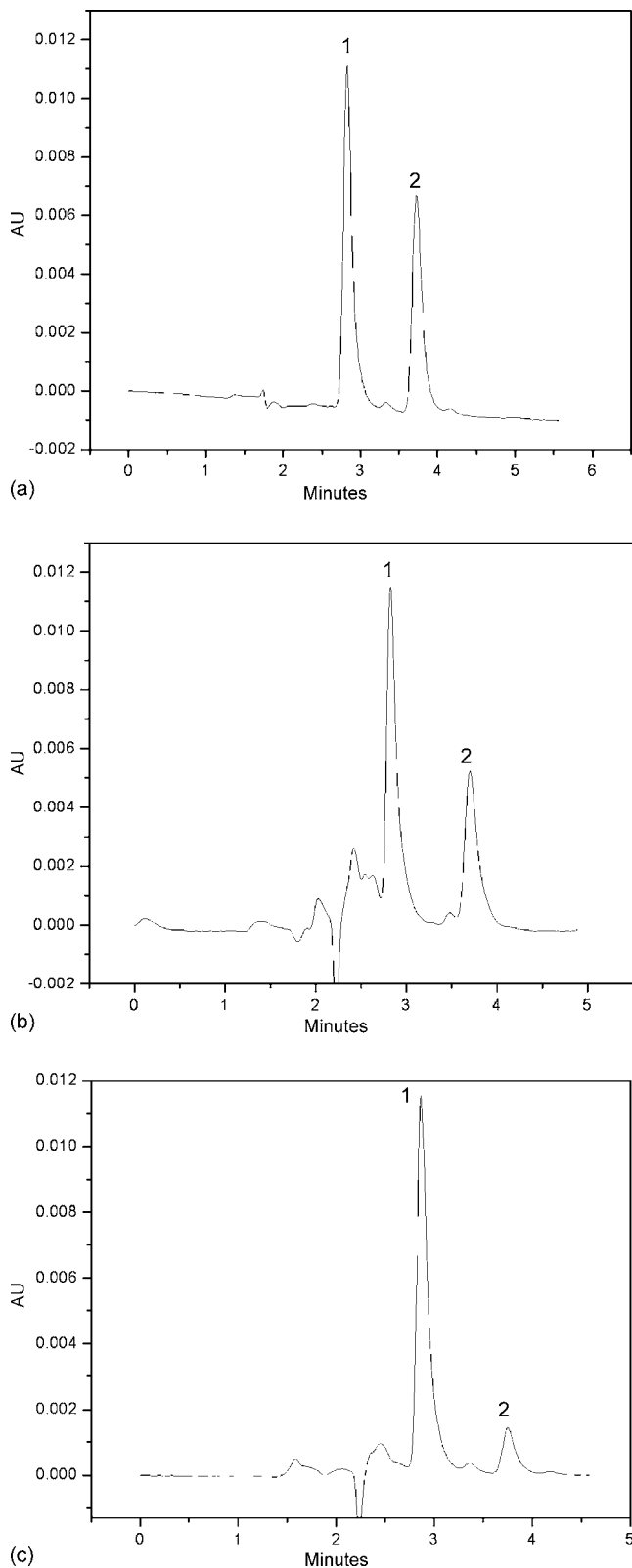


Fig. 5. Chromatograms of the BPA and BP mixture solution from the SPE columns: (a) direct injection of the standard BPA and BP mixture solution, (b) eluate obtained from C_8 SPE column, (c) eluate obtained from MIP-SPE column.

Table 2

Cross-sensitivity between BPA and BP

Initial solution (mg l^{-1})		Recovery (%)		R.S.D. (%)	
BPA	BP	BPA	BP	BPA	BP
1.0	1.0	99.46	73.28	2.3	1.6
1.0	10	97.99	46.58	2.9	3.2
1.0	50	95.47	34.74	3.2	2.7
1.0	100	86.43	18.73	4.1	3.1

Table 3

Recoveries (%) and R.S.D. of BPA after MISPE and NISPE of spiked tap water samples

BPA in water samples ($\mu\text{g ml}^{-1}$)	Recovery (%)		R.S.D. (%)	
	MIP	NIP	MIP	NIP
0.01	101.20	76.5	2.2	1.7
1.0	99.43	75.3	3.6	3.5
5.0	103.25	80.1	5.3	4.8

reduced to 86.43%. So, when the concentration of interference was very high, other sample pretreatment process was necessary.

3.5.3. Determination of BPA in spiked water samples

Tap water was spiked with BPA at three concentration levels with 5, 1 and $0.01 \mu\text{g ml}^{-1}$. The samples were extracted according to Section 2.5. The recoveries and reproducibility of the method were calculated and summarized in Table 3. As can be seen, the average recovery of the MIP-SPE method was 101.3% at the studied levels and the average recovery of the NIP-SPE method was 77.3%. These results demonstrated that the BPA-imprinted silica sorbent had good recovery than non-imprinted silica sorbent. However, the recovery of BPA were decreased when the concentration of BPA solution was higher further. According to the experiment, the dynamic adsorption capacity was concluded that 100 mg of BPA-imprinted silica sorbent could adsorb $40 \mu\text{g}$ of BPA at the speed of 2 ml min^{-1} . When the concentration of BPA was higher than the value, some steps should be adopted, for example, diluted the samples, reduced the analysis speed and increased the amount of sorbent.

4. Conclusions

In this paper, a novel and simple procedure was developed to synthesize BPA-imprinted amino-functionalized silica gel sorbent with a surface molecular imprinting technique. The BPA-imprinted sorbent had high adsorption capacity, selectivity and good site accessibility for BPA. And the polymer was used as a solid-phase extraction sorbent to determine BPA in water samples. The MIP-SPE-HPLC method showed good recoveries and higher selectivity than traditional SPE-HPLC method. The precision and accuracy of the method are satisfactory.

Surface molecular imprinting materials show many advantages including high selectivity, more accessible sites, fast mass transfer and binding kinetics. The surface molecular imprinting technique cooperated with SPE-HPLC would be a powerful tool

for the determination of complex samples such as environmental and biologic samples.

Acknowledgements

The authors thank the National natural Science Foundation of China (NSFC) Fund (No. 20305008), the Huo Yingdong science fund (No. 104038) and the central teacher plan in Lanzhou University for supporting the project.

References

- [1] L.Q. Lin, J. Zhang, Q. Fu, L.C. He, Y.C. Li, *Anal. Chim. Acta* 561 (2006) 178.
- [2] Y. Watabe, K. Hosoya, N. Tanaka, T. Kubo, T. Kondo, M. Morita, *J. Chromatogr. A* 1073 (2005) 363.
- [3] D. Lakshmi, B.B. Prasad, P.S. Sharma, *Talanta* 70 (2006) 272.
- [4] F. Nie, J. Lu, Y. He, J.X. Du, *Talanta* 66 (2005) 728.
- [5] G.L. Yang, H.Y. Liu, M.M. Wang, S.B. Liu, Y. Chen, *React. Function. Polym.* 66 (2006) 579.
- [6] E. Caro, R.M. Marce, F. borruil, P.A.G. Cormack, D.C. Sherrington, *Trends Anal. Chem.* 25 (2006) 143.
- [7] D.M. Han, G.Z. Fang, X.P. Yan, *J. Chromatogr. A* 1100 (2005) 131.
- [8] A. Olwill, H. Hughes, M.O. Riordain, P. Mcloughlin, *Biosens. Bioelectron.* 20 (2004) 1045.
- [9] F.L. Dickert, O. Hayden, *Anal. Chem.* 74 (2002) 1302.
- [10] A. Katz, M.E. Davis, *Nature* 403 (2000) 286.
- [11] K. Sreenivasan, *Talanta* 68 (2006) 1037.
- [12] G.Z. Fang, J. Tan, X.P. Yan, *Anal. Chem.* 77 (2005) 1734.
- [13] Y. Watabe, T. Kondo, M. Morita, N. Tanaka, J. Haginaka, K. Hosoya, *J. Chromatogr. A* 1032 (2004) 45.
- [14] J.F. Liu, J.B. Chao, M.J. Wen, G.B. Jiang, *J. Sep. Sci.* 24 (2001) 874.
- [15] V.P. Joshi, R.N. Karmalkar, M.G. Kullkarni, R.A. Mashelkar, *Ind. Eng. Chem. Res.* 38 (1999) 4417.
- [16] M. Kawaguchi, Y. Hayatsu, H. Nakata, Y. Ishii, R. Ito, K. Saito, H. Nakazawa, *Anal. Chim. Acta* 539 (2005) 583.
- [17] N. Tsuru, M. Kikuchi, H. Kawaguchi, S. Shiratori, *Thin Solid Films* 499 (2006) 380.
- [18] X.J. Chang, N. Jiang, H. Zheng, Q. He, Z. Hu, Y.H. Zhai, Y.M. Cui, *Talanta*, available online 18 April 2006, in press.

Determination of glyphosate using off-line ion exchange preconcentration and capillary electrophoresis-laser induced fluorescence detection

Jiang Jiang, Charles A. Lucy*

Department of Chemistry, Gunning/Lemieux Chemistry Centre, University of Alberta, Edmonton, Alberta, Canada T6G 2G2

Received 24 July 2006; received in revised form 2 October 2006; accepted 2 October 2006

Available online 9 November 2006

Abstract

An enrichment method for the herbicide glyphosate is presented based on ion exchange solid phase extraction (SPE) technique. A 200- μ l micro-pipette tip packed with 50 mg of Bio-Rad AG1-X8 anion exchanger beads was used for offline extraction of glyphosate from 50 ml of spiked river water sample. The retained glyphosate was eluted with 10 mM HCl and then converted quantitatively to the corresponding amine (glycine) using hypochlorite. Subsequent fluorescent labeling using naphthalene-2,3-dicarboxaldehyde (NDA)-cyanide allowed micellar electrokinetic chromatography (MEKC) separation and laser-induced fluorescence detection (LIF) with a violet diode laser. Optimization of the sample clean-up, extraction, elution, conversion and labeling steps enabled analysis of glyphosate in river water in the nanomolar range. Detection limits were 0.04 nM glyphosate in standards and 1.6 nM in spiked river.

© 2006 Elsevier B.V. All rights reserved.

Keywords: Glyphosate; Capillary electrophoresis; Laser-induced fluorescence; Micellar electrokinetic chromatography

1. Introduction

Since its introduction in 1971 by Monsanto Company, glyphosate (*N*-(phosphonomethyl) glycine, Fig. 1) has become one of the most widely used broad-spectrum herbicides. Its market is still growing at an annual rate of 20% because of the expiration of the Monsanto patent in the early 1990s and the introduction of crops genetically engineered to be more glyphosate-tolerant [1]. Due to its strong retention on soil components, high solubility in water and long half-time in the environment (about 47 days) [2], glyphosate may still be detected long after application or even far from the site of application. For decades, the long-term environmental and ecological effects of glyphosate have been the target of research and discussion. A reliable method for the determination of glyphosate in environmental samples is therefore a must for this research and environmental monitoring.

Almost all available analytical methodologies have been applied to the determination of glyphosate, including gas chromatography (GC) [3–13], high performance liquid chro-

matography (HPLC) [14–21], capillary electrophoresis (CE) [22–31], luminescence [32,33] and enzyme-linked immunosorbent assay (ELISA) [19,20,34]. Stalikas et al. have comprehensively reviewed the literature on the analysis of glyphosate and other phosphonic and amino acid group-containing pesticides [35]. To date, most reports were based on chromatographic separations. For example, Grey et al. developed a liquid chromatography/electrospray/mass spectrometry (LC/ES/MS) method for the analysis of glyphosate and its metabolite aminomethylphosphonic acid (AMPA) using isotope-labeled glyphosate as a method surrogate. The reported method detection limits were 0.06 and 0.30 μ g/l, respectively, for glyphosate and AMPA in water matrices [36]. Far fewer CE methods have been reported for glyphosate [22–31]. Cikaló et al. [22] used on-line sample stacking and indirect UV detection to achieve an LOD of 0.06 μ g/l for glyphosate, which were subsequently improved by Corbera et al. using off-line ion exchange preconcentration [37]. Molina and Silva used nonionic surfactant micellar electrokinetic chromatography (MEKC) with laser-induced fluorescence (LIF) detection to determine glyphosate at an LOD of 0.06 μ g/l [29]. Safarpour and Asiaie reported a CE-electrospray ionization mass spectrometry (CE-ESI-MS) method for rapid and selective detection of glyphosate with an LOD of 10 ng/ml and minimal sample handling [31].

* Corresponding author. Tel.: +1 780 492 0315; fax: +1 780 492 8231.
E-mail address: charles.lucy@ualberta.ca (C.A. Lucy).

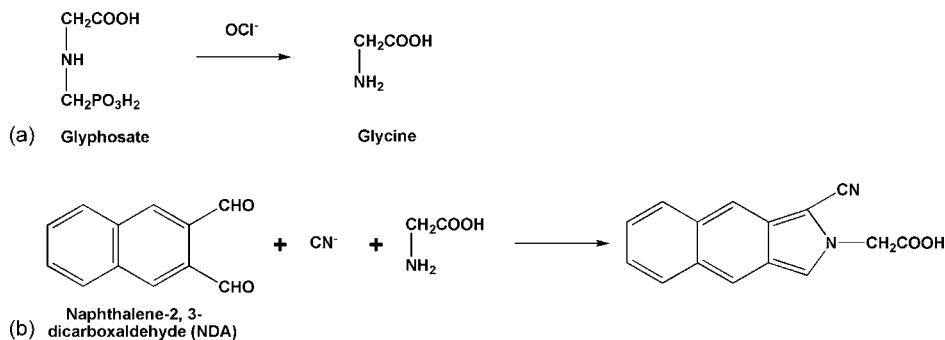


Fig. 1. (a) Oxidative conversion of glyphosate to glycine and (b) subsequent fluorescence labeling reaction.

Ion exchange solid-phase extraction (SPE) preconcentration techniques were utilized prior to the chromatographic or CE separation in many reports [6,37–41] to greatly enhance the detection sensitivity. So far, the most sensitive method was reported by Patsias and coworkers [39]. They coupled a PRP-X100 (polystyrene-divinylbenzene-trimethyl-ammonium) anion exchange cartridge to a cation exchange liquid chromatography separation followed by post-column derivatization and fluorescence detection. By processing 100-ml samples, a detection limit better than 20 ng/l for glyphosate was achieved in river water.

As glyphosate has no chromophore or fluorophore, derivatization is usually required prior to detection. Specifically, for fluorescence detection, most previous reports used hypochlorite to convert glyphosate to glycine and then labeled glycine with *o*-phthalaldehyde (OPA) and 2-mercaptoethanol (ME). In this work, the fluorogenic reagent naphthalene-2,3-dicarboxaldehyde (NDA) was used to label glycine. Like OPA, NDA labels primary amine ($-\text{NH}_2$) groups in the presence of excess cyanide under mild conditions (Fig. 1b). However, the product of the NDA reaction is more strongly fluorescent and more stable than the OPA-ME product [42]. NDA is also suitable for the compact 415 nm violet diode laser used in this work.

In this paper, an anion exchanger SPE method similar to Patsias and coworkers' work [39] was developed for off-line preconcentration of glyphosate at the nM range from water samples. After elution of glyphosate from the SPE device, it is fluorescently labeled with NDA and analyzed by MEKC-LIF. As low as 0.04 nM of glyphosate in standard solutions and 1.6 nM in spiked river water samples can be detected using a 415 nm violet diode laser.

2. Experimental

2.1. Reagents and materials

Sodium glyphosate (GLYP, 97.0%) and sodium dodecyl sulfate (SDS, 99%) were from Fluka (Buchs, Switzerland). Sodium cyanide (99.98%), calcium hypochlorite (available chlorine 65%) and naphthalene-2,3-dicarboxaldehyde (NDA, 98%) were from Aldrich (Milwaukee, WI, USA). Sodium tetraborate was from BDH (Poole, England). Methanol (HPLC grade) was from Fisher (Fair Lawn, NJ, USA). Hydrochloric acid and

sodium hydroxide were from EM Science (an affiliate of Merck KGaA, Darmstadt, Germany). All solutions were prepared with Nanopure 18 M Ω water (Barnstead, Chicago, IL, USA) except NDA which was in methanol.

AG1-X8 strong-base anion exchange resin (50–100 mesh, chloride form) was purchased from Bio-Rad (Richmond, CA, USA). Strong-acid cation exchange resin C-100H ((polystyrene-divinylbenzene)-sulfonate, 16–50 mesh) and macroporous type II strong-base anion exchange resin A-510S ((polystyrene-divinylbenzene)-dimethyl-ethylammonium, 16–50 mesh) were gifts kindly provided by Purolite (Philadelphia, PA, USA). Medium size Maxi-CleanTM solid-phase extraction cartridge and frits/caps were from Alltech (Deerfield, IL, USA). Sixty milliliters of plastic syringes were from Beckton, Dickinson and Company (Franklin Lakes, NJ, USA).

2.2. Analysis procedures

2.2.1. Preconcentration

The sample solution was pumped using a BS-9000-8 syringe pump (Braintree Scientific Inc., Braintree, MA, USA) through a clean-up cartridge followed by a resin preconcentration tip. The clean-up cartridge was a medium size Maxi-CleanTM solid-phase extraction cartridge with 0.2 μm frits, to which 300 mg of a mixture of Purolite A-510S macroporous type II strong base anion exchange resin (chloride form) and Purolite C-100H strong acid cation exchange resin (hydrogen form) at a mass ratio of 60:40 was packed. The resin preconcentration tip was a 200 μl micro-pipette tip, in which 50 mg of Bio-Rad AG1-X8 resin was added. Glass wool was used to avoid loss of AG1-X8 resin when in use. Before use, both the clean-up cartridge and resin preconcentration tip were rinsed with 10 ml of 18 M Ω water.

Fifty milliliters of sample solution was pumped at 5 ml/min through the clean-up cartridge and resin preconcentration tip. After extraction, the clean-up cartridge and resin preconcentration tip were removed and washed separately with 5 ml of 18 M Ω water each. The resin preconcentration tip was eluted with 10 mM HCl at 0.1 ml/min. The first 500 μl of effluent was collected in a 4 ml borosilicate glass vial for subsequent derivatization. After elution, the resin tip was regenerated with 2.5 ml of 1 M HCl at 0.5 ml/min and then 5 ml of 18 M Ω water prior to the next run.

2.2.2. Derivatization and fluorescence labeling

Glyphosate was converted to glycine as per [39]. Briefly, to the 4 ml glass vial containing 500 μ l of effluent, 60 μ l of 200 mM sodium borate buffer (pre-adjusted to pH 10.4 with NaOH) and 40 μ l of 1 mM $\text{Ca}(\text{ClO})_2$ were added. The mixture was vortexed and then placed in a 60 °C water bath for 5 min. Then 20 μ l of 10 mM NaCN and 20 μ l of 2.5 mM NDA were added, mixed thoroughly by vortexing, and allowed to react in the dark at room temperature for 3 min.

2.2.3. MEKC separation

All CE experiments were performed on a P/ACE 2100 capillary electrophoresis system (Beckman Instruments, Fullerton, CA, USA) equipped with a laser-induced fluorescence detector and P/ACE Station software (version 1.2, Beckman) for instrument control and data acquisition. A 415 nm violet diode laser (model LDCU 12/4673, Power Technology Inc., Little Rock, AR, USA) was used as the excitation source [43]. The laser was coupled to the LIF detector through an SMA fiber optic receptacle (Omnichrome, Chino, CA, USA), a 1 m multimode fiber optic patchcord with a 100/140- μ m (core/cladding) diameter and SMA 906 connectors (Polymicro Technologies, Phoenix, AZ, USA). The laser output power was 1 mW as measured at the outlet of optic fiber. An XB84-500DF25 band pass filter (Omega Optical, Brattleboro, V \pm T, USA) was used to collect the fluorescence signal at 500 \pm 12.5 nm. Data were collected at 10 Hz with a detector response time of 0.1 s. The capillary was thermostated to 25 °C.

MEKC separations were performed at 12 kV (normal polarity) across a 37 cm-long (30 cm to the detection window), 50 μ m-i.d. fused-silica capillary (Polymicro Technologies, Phoenix, AZ, USA). Injections were 3 s hydrodynamic at 0.5 psi (1 psi = 6894.76 Pa). The running buffer was 50 mM SDS and 20 mM sodium borate (pH 9.3). Before use each new capillary was conditioned by flushing at 20 psi with 1 M NaOH for 10 min, distilled water for 10 min, 0.1 M NaOH for 5 min and distilled water for 10 min. Between runs the capillary was washed at 20 psi with 0.1 M NaOH for 2 min, distilled water for 2 min and running buffer for 3 min.

2.2.4. Analysis of river water

The river water was taken from North Saskatchewan River and stored in NalgeneTM plastic bottles (Nalge Nunc International, Rochester, NY, USA) at 4 °C for no more than 1 week. The river water sample was spiked with glyphosate for testing the proposed method.

3. Results and discussion

3.1. Derivatization and fluorescent labeling

The first step in derivatization of glyphosate with fluorogenic reagents such as *o*-phthalaldehyde (OPA) or naphthalene-2,3-dicarboxaldehyde (NDA, Fig. 1b) is oxidation of glyphosate to glycine (Fig. 1a). Quantitative yields for this step have been reported using hypochlorite [39,40,44–46]. However, hypochlorite can continue to react with the glycine product and

thus reduce the overall conversion efficiency of glyphosate. Therefore, the derivatization must be carefully optimized to obtain the highest yield of glycine. In this work, the effluent from the resin tip was in 10 mM HCl, and its pH must be made alkaline to be suitable for the subsequent reactions. Addition of 60 μ l of 200 mM sodium borate buffer (pre-adjusted to pH 10.4 by NaOH) to 500 μ l of 10 μ M glyphosate in 10 mM HCl results in a final pH of 9.5, which is the recommended pH for the NDA labeling reaction [42]. However, this may not be the best pH for conversion of glyphosate to glycine [39].

To determine the effect of hypochlorite concentration, 40 μ l of 0.1–7 mM $\text{Ca}(\text{ClO})_2$ (concentration before mixing) were added to 60 μ l of 200 mM sodium borate buffer (pH 10.4) and 500 μ l of 10 μ M glyphosate. Under these conditions there was always a large excess of chlorite ion relative to glyphosate. After oxidation and fluorescence labeling as described in Section 2.2.2, MEKC experiments showed that the glyphosate peak area increased sharply upon addition of hypochlorite and then reached a broad plateau at 0.5–2 mM. At higher $\text{Ca}(\text{ClO})_2$ concentrations, the glyphosate peak area decreased slowly due to the excess hypochlorite converting the glycine into chloramines. Thus 40 μ l of 1 mM $\text{Ca}(\text{ClO})_2$ was used in all further experiments.

Second, at this $\text{Ca}(\text{ClO})_2$ concentration, the effect of oxidative reaction time was examined by mixing 500 μ l of 10 μ M glyphosate, 60 μ l of 200 mM sodium borate buffer (pH 10.4) and 40 μ l of 1 mM $\text{Ca}(\text{ClO})_2$. After reaction at 60 °C and subsequent fluorescence labeling, the glyphosate peak area increased with time up to 7 min and was thereafter constant. A reaction time of 5 min was used throughout this study as a compromise of reaction time and yield.

By comparing the glyphosate results with those obtained by directly labeling glycine, it was determined that 51% of glyphosate was converted to glycine and labeled by NDA at the above optimized conditions while only 9% and 16% of glyphosate were converted at room temperature and 45 °C, respectively. So 60 °C was chosen as the oxidative reaction temperature instead of the 36 °C [39], 43 °C [40] or 48 °C [44] used in previous papers. Higher temperatures were not tested.

Optimization of the NaCN and NDA (Fig. 1b) concentrations were more difficult due to the formation of side-products which causes interference with detection of glyphosate. Fig. 2a shows the electropherogram of a blank experiment in which 20 μ l of 40 mM NaCN and 20 μ l of 10 mM NDA (conditions recommended in most papers [42]) were mixed with 20 mM pH 9.5 sodium borate buffer. Typically 5–7 side product peaks were observed. One of the side-products (at \sim 4 min) co-migrated with the glycine labeling product, regardless of the separation conditions. The peak in Fig. 2a roughly corresponds to 50 nM glycine, but the peak height and area of these side-products were highly irreproducible. These side-reactions were not due to impurities in the NDA, NaCN or any other reagents as their peak area did not increase proportionally with the concentration of these reagents. For example, even a 100-fold increase in NDA or NaCN concentrations resulted in only a 1–2-fold

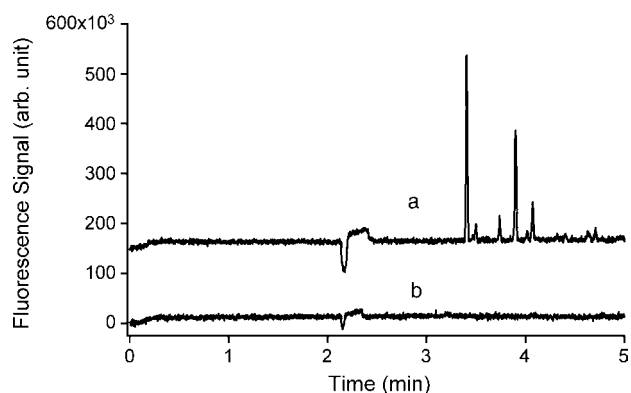


Fig. 2. Typical electropherogram of side-reaction products in blank reaction. 600 μ l of 20 mM pH 9.5 sodium borate was mixed with (a) 20 μ l of 40 mM NaCN and 20 μ l of 10 mM NDA; (b) 20 μ l of 10 mM NaCN and 20 μ l of 2.5 mM NDA. Reaction at room temperature for 3 min. Other reaction conditions are as described in Section 2.2.2.

increase in the side-product peak area. Impurities that may be present in the solvent or glassware were also not responsible for these interfering peaks. Injection of NDA itself or any other reagent did not cause any interference. These side-product peaks only appeared in the presence of both NDA and NaCN and posed severe problems to the detection of glyphosate at nanomolar levels. The side-reaction mechanism is unclear. The only prior report of such side-products in the literature is the PhD thesis of Kwakman in 1991 [46]. However, no mechanistic studies were reported. Rather he just presumed that in principle the formation of benzoin condensation side-products induced by cyanide was possible [47]. These side-product had highly reproducible migration times, but relatively poor peak area reproducibility (peak area RSD > 50%). This made it very difficult to quantitatively study the factors causing the side-products. Also, due to the high salt concentration in the reaction mixture, identification of these side-products was not possible using mass spectrometry. Thus no further efforts were directed towards identifying these side products or their formation mechanism.

However, a number of observations about the side product formation can be made. The side-product formation can be minimized by using very low concentrations of NDA and NaCN (*e.g.*, 2.5 mM and 10 mM, respectively). However, the use of lower reagent concentrations necessitates a large increase in the reaction time. To find a compromise between reaction rate and minimization of side-product peaks, the effect of NDA concentration was examined using 20 μ l of 0.625–10 mM (concentration before mixing). The analytical signal for glyphosate increased up to 2.5 mM NDA, and thereafter was constant. Similarly, the analytical signal increased when using 20 μ l of 5–10 mM NaCN (concentration before mixing) but showed no significant change above 10 mM. Both the NDA and NaCN concentrations were always in great excess, so the effect of reagent concentration on glycine labeling is due to reaction kinetics rather than stoichiometry. The use of 20 μ l of 2.5 mM NDA and 20 μ l of 10 mM NaCN provided maximum analytical signal and negligible formation of side-products

(Fig. 2b). Thus these reaction conditions were used in all further studies.

3.2. Off-line preconcentration

Fifty milliliters of 50 nM glyphosate standard was pumped through the anion exchange column at 1, 3, 5 and 8 ml/min, respectively. The glyphosate was then eluted at 0.1 ml/min 10 mM HCl, derivatized as described in Section 2.2.2 and separated as in Section 2.2.3. No significant change (<3.6%) in peak area was observed. Thus the preconcentration was not affected by the flow rate used for sample loading. Five millimetres per minute was used for all subsequent experiments. On the other hand, elution flow rate did strongly affect glyphosate recovery from the anion exchange preconcentration column. At an elution flow rate of 0.1 ml/min of 10 mM HCl, 88% of the glyphosate was recovered within the first 500 μ l of effluent, whereas at 0.8 ml/min the recovery within the first 500 μ l decreased to 62%. Quantitative recovery (overall $103 \pm 1\%$) of glyphosate was obtained by collecting both the first and second 500 μ l fraction of effluent at 0.1 ml/min. Therefore, to maximize sensitivity, this elution rate was used for analysis.

The HCl concentration for elution of glyphosate from the anion exchange preconcentration column was fixed at 10 mM. A lower HCl concentration would necessitate larger elution volumes and thus lower preconcentration, while higher HCl concentrations would make adjustment of the pH for the derivatization reaction problematic.

However, real samples contain inorganic and organic anions which may compete with glyphosate on the anion exchange resin [40]. For instance when 50 ml of river water sample spiked with 50 nM glyphosate was pumped directly through the anion exchange column, only 7% of the glyphosate was recovered. Following the work of Patsias *et al.* [39], a clean-up cartridge filled with 300 mg of mixture of Purolite A-510S macroporous type II strong base anion exchange resin (chloride form) and Purolite C-100H strong acid cation exchange resin (hydrogen form) at a mass ratio of 60:40 was coupled on-line before the AG1-X8 resin tip. This mixing ratio is selected because both resins have roughly the same exchange capacity. When the spiked river water sample passes through the clean-up cartridge, interfering inorganic ions (and some organic compounds as well) are retained on the cartridge. Glyphosate however is an amphoteric compound with pK_{a1} 0.8 (first phosphonic), pK_{a2} 2.3 (carboxylic), pK_{a3} 6.0 (second phosphonic), and pK_{a4} 11.0 (amine) [2]. As a result, glyphosate is only weakly retained in the mixed resin column. For instance, 55% of the glyphosate was recovered after passing 50 ml of 100 nM glyphosate standard solution through the mixed bed column and then the anion exchange preconcentration column at 5 ml/min. Given that 88% of glyphosate in the AG1-8 preconcentration column was eluted by first 500 μ l of eluent, an overall recovery of 48% was obtained. Seven river water samples could be analyzed using the 300 mg clean-up cartridge (<3% change in peak area for replicate analysis). If more samples were run, a gradual decrease in the glyphosate signal was observed (25% decrease by $n = 13$). To ensure maximal recov-

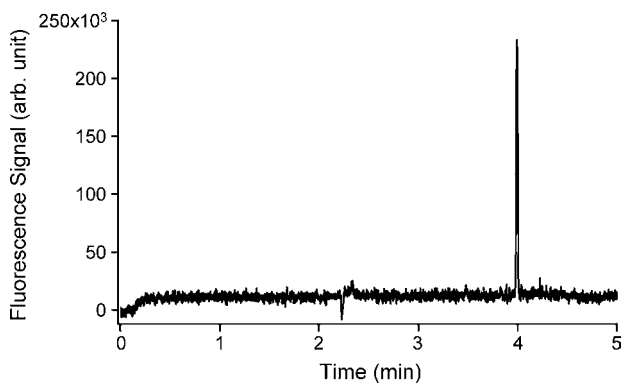


Fig. 3. Electropherogram of 50 ml of a 1 nM glyphosate standard, processed as described in Section 2.2.

ery no more than two samples were processed with a clean up cartridge.

3.3. Quantitative analysis of glyphosate

Under optimized conditions above, 50 ml of 1–100 nM glyphosate was concentrated on the AG1-X8 resin tip. Fig. 3 shows the electropherogram for 50 ml of 1 nM glyphosate standard, processed as described in Section 2.2. Calibration from 1 to 100 nM using peak area resulted in a linear relationship ($R^2 = 0.999$) with an intercept equal to zero within the 95% confidence level. The concentration limit of detection (LOD) based on an S/N ratio of 3 was 0.04 nM. This is superior to LOD achieved using other CE methods. For instance, Goodwin et al. achieved detection limit of 1 μM for water samples using CE-ESIMS [24], while Cikalo et al. achieved an LOD of 10 nM using on-line preconcentration with field-amplified sample injection [22]. With respect to CE-LIF, the LOD is superior to the 0.06 $\mu\text{g/l}$ (0.36 nM) LOD achieved using MEKC of fluorescein isothiocyanate (FITC) derivatives [29] and better than the 1 nM LOD achieved with 5-(4,6-dichlorotriazinylamino) fluorescein (DTAF) derivatization [25]. The 0.04 nM LOD achieved herein is slightly better than the lowest reported 0.02 $\mu\text{g/l}$ (0.1 nM) in the literature achieved using on-line anion exchange solid-phase extraction followed by cation exchange liquid chromatography

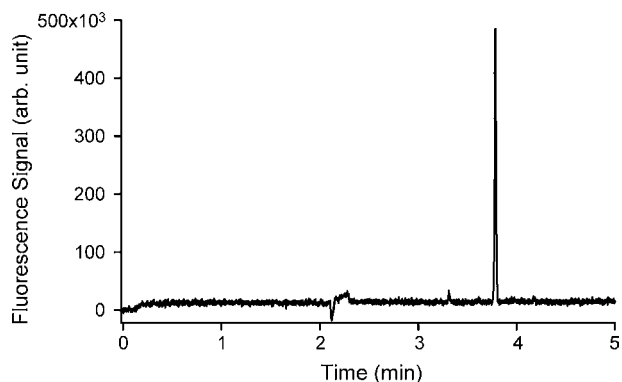


Fig. 4. Electropherogram of 5.0 ml of river water sample spiked with 40 nM glyphosate and processed as described in Section 2.2.

and post-column derivatization [39]. Reproducibility of the peak area for 20 nM glyphosate standards was 4.9% ($n = 9$).

Five milliliters of samples of the river water were spiked glyphosate, diluted 10-fold and processed as in Section 2.2. Fig. 4 is the electropherogram for the 40 nM glyphosate spike. Spike solutions from 40 to 2000 nM (concentrations before 10-fold dilution) yielded linear calibration curves ($R^2 = 0.999$) with an intercept equal to zero within the 95% confidence level. The concentration LOD was 1.6 nM. Reproducibility of peak area measurements at 500 nM was 6.3% RSD ($n = 9$).

4. Conclusions

Off-line clean up using a mixed bed ion exchanger followed by preconcentration using an anion exchange column was used to concentrate glyphosate, prior conversion, fluorescence labeling and MEKC-LIF analysis. It was important to keep the concentration of derivatization reagents low to avoid interfering side-product peaks. As has been reported previously [39], a mixed bed ion exchanger is an effective means of removing inorganic ions which otherwise interfere with anion exchange preconcentration. Using this technique LOD of 0.04 nM glyphosate in standards and 1.6 nM in river water can be achieved.

Acknowledgement

This work was supported by the Natural Sciences and Engineering Research Council of Canada (NSERC) and the University of Alberta.

References

- [1] P. Takacs, P.A. Martin, J. Struger, Pesticides in Ontario, a critical assessment of potential toxicity of agricultural products to wildlife, with consideration for endocrine disruption. Triazine herbicides, Glyphosate, and Metolachlor, vol. 2, 2002.
- [2] Glyphosate Factsheets, (a) <http://www.cetos.org/criticalhabitat/glyphosate.pdf>; (b) <http://www.safe2use.com/poisons-pesticides/pesticides/organo-glyphosate.htm>; (c) http://www.soils.wisc.edu/virtual_museum/glyphosate/content.html.
- [3] P.L. Alferness, Y. Iwata, J. Agric. Food Chem. 42 (1994) 2751.
- [4] F. Hernandez, R. Serrano, M.C. Miralles, N. Font, Chromatographia 42 (1996) 151.
- [5] H. Kataoka, S. Ryu, N. Sakiyama, M. Makita, J. Chromatogr. A 726 (1996) 253.
- [6] P.S. Mogadati, J.B. Louis, J.D. Rosen, J. AOAC Int. 79 (1996) 157.
- [7] N. Sakiyama, H. Kataoka, M. Makita, J. Chromatogr. A 724 (1996) 279.
- [8] A. Royer, S. Beguin, J.C. Tabet, S. Hulot, M.A. Reding, P.Y. Communal, Anal. Chem. 72 (2000) 3826.
- [9] C.D. Stalikas, G.A. Pilidis, J. Chromatogr. A 872 (2000) 215.
- [10] C.D. Stalikas, G.A. Pilidis, M.I. Karayannis, Chromatographia 51 (2000) 741.
- [11] P.L. Alferness, L.A. Wiebe, J. AOAC Int. 84 (2001) 823.
- [12] Y. Hori, M. Fujisawa, K. Shimada, Y. Hirose, J. Anal. Tox. 27 (2003) 162.
- [13] S.H. Tseng, Y.W. Lo, P.C. Chang, S.S. Chou, H.M. Chang, J. Agric. Food Chem. 52 (2004) 4057.
- [14] N.P. Sen, P.A. Baddoo, Int. J. Env. Anal. Chem. 63 (1996) 107.
- [15] J.S. Riddlen, G.J. Klopff, T.A. Nieman, Anal. Chim. Acta 341 (1997) 195.
- [16] R.J. Vreeken, P. Speksnijder, I. Bobeldijk-Pastorova, T.H.M. Noij, J. Chromatogr. A 794 (1998) 187.

- [17] F. Veiga, J.M. Zapata, M.L.F. Marcos, E. Alvarez, *Sci. Total Env.* 271 (2001) 135.
- [18] B. Le Bot, K. Colliaux, D. Pelle, C. Briens, R. Seux, M. Clement, *Chromatographia* 56 (2002) 161.
- [19] E.A. Lee, L.R. Zimmerman, S.S. Bhullar, E.M. Thurman, *Anal. Chem.* 74 (2002) 4937.
- [20] F. Rubio, L.J. Veldhuis, B.S. Clegg, J.R. Fleeker, J.C. Hall, *J. Agric. Food Chem.* 51 (2003) 691.
- [21] T.V. Nedelkoska, G.K.C. Low, *Anal. Chim. Acta* 511 (2004) 145.
- [22] M.G. Cikalo, D.M. Goodall, W. Matthews, *J. Chromatogr. A* 745 (1996) 189.
- [23] J. You, M. Kaljurand, J.A. Koropchak, *Int. J. Env. Anal. Chem.* 83 (2003) 797.
- [24] L. Goodwin, J.R. Startin, B.J. Keely, D.M. Goodall, *J. Chromatogr. A* 1004 (2003) 107.
- [25] M. Molina, M. Silva, *Electrophoresis* 23 (2002) 1096.
- [26] M. Khrolenko, P. Dzygiel, P. Wiczorek, *J. Chromatogr. A* 975 (2002) 219.
- [27] L. Goodwin, M. Hanna, J.R. Startin, B.J. Keely, D.M. Goodall, *Analyst* 127 (2002) 204.
- [28] S.Y. Chang, C.H. Liao, *J. Chromatogr. A* 959 (2002) 309.
- [29] M. Molina, M. Silva, *Electrophoresis* 22 (2001) 1175.
- [30] E.W.J. Hooijschuur, C.E. Kientz, J. Dijkman, U.A.T. Brinkman, *Chromatographia* 54 (2001) 295.
- [31] H. Safarpour, R. Asiaie, *Electrophoresis* 26 (2005) 1562.
- [32] I.D. Meras, T.G. Diaz, M.A. Franco, *Talanta* 65 (2005) 7.
- [33] J.L. Adcock, N.W. Barnett, R.D. Gerardi, C.E. Lenehan, S.W. Lewis, *Talanta* 64 (2004) 534.
- [34] B.S. Clegg, G.R. Stephenson, J.C. Hall, *J. Agric. Food Chem.* 47 (1999) 5031.
- [35] C.D. Stalikas, C.N. Konidari, *J. Chromatogr. A* 907 (2001) 1.
- [36] L. Grey, B. Nguyen, P. Yang, *J. AOAC Int.* 84 (2001) 1770.
- [37] M. Corbera, A. Hidalgo, V. Salvado, P.P. Wiczorek, *Anal. Chim. Acta* 540 (2005) 3.
- [38] C. Hidalgo, C. Rios, M. Hidalgo, V. Salvado, J.V. Sancho, M. Hernandez, *J. Chromatogr. A* 1035 (2004) 153.
- [39] J. Patsias, A. Papadopoulou, E. Papadopoulou-Mourkidou, *J. Chromatogr. A* 932 (2001) 83.
- [40] E. Mallat, D. Barcelo, *J. Chromatogr. A* 823 (1998) 129.
- [41] J.V. Sancho, F. Hernandez, F.J. Lopez, E.A. Hogendoorn, E. Dijkman, P. van Zoonen, *J. Chromatogr. A* 737 (1996) 75.
- [42] P. Demontigny, J.F. Stobaugh, R.S. Givens, R.G. Carlson, K. Srinivasachar, L.A. Sternson, T. Higuchi, *Anal. Chem.* 59 (1987) 1096.
- [43] J.E. Melanson, C.A. Lucy, *Analyst* 125 (2000) 1049.
- [44] M.P. Abdullah, J. Daud, K.S. Hong, C.H. Yew, *J. Chromatogr. A* 697 (1995) 363.
- [45] K.M.S. Sundaram, J. Curry, *J. Liq. Chromatogr. Rel. Tech.* 20 (1997) 511.
- [46] P.J.M. Kwakman, *Derivatization for Column Liquid Chromatography with Peroxyoxalate Chemiluminescence Detection*, Ph.D. Thesis, Vrije University, The Netherlands, 1991.
- [47] A.T. Ternay, *Contemporary Organic Chemistry*, W.B. Saunders, Philadelphia, 1979.

Greener analytical method for the determination of copper(II) in wastewater by micro flow system with optical sensor

Tapparath Leelasattarakul^{a,b}, Saisunee Liawruangrath^{a,*}, Mongkon Rayanakorn^a, Boonsom Liawruangrath^c, Winai Oungpipat^b, Napaporn Youngvises^d

^a Department of Chemistry, Faculty of Science, Chiang Mai University, Chiang Mai 50200, Thailand

^b Division of Analytical Chemistry, Department of Chemical Technology, Rajamangala University of Technology Krungthep, Bangkok 10120, Thailand

^c Department of Pharmaceutical Chemistry, Faculty of Pharmacy, Chiang Mai University, Chiang Mai 50202, Thailand

^d Department of Chemistry, Faculty of Science and Technology, Thammasat University, Pathum Thani 12121, Thailand

Received 29 June 2006; received in revised form 3 October 2006; accepted 3 October 2006

Available online 13 November 2006

Abstract

Greener analytical method using micro flow system for the determination of Cu(II) in wastewater samples was designed and investigated. The micro flow system consisted of a planar glass chip with poly(dimethylsiloxane) (PDMS) top plate and fixed with fiber optic probe as optical sensor for monitoring of Cu(II) that reacted with 2-carboxy-2'-hydroxy-5'-sulfoformazyl benzene (zincon) on the chip at 605 nm. This design gave a satisfied sensitivity with a linear calibration graph over the range of 0.1–3.0 $\mu\text{g mL}^{-1}$ of Cu(II) and correlation coefficient 0.9991. The percentage relative standard deviation was 2.5 for 10-replicate measurements and the limit of detection (LOD) was 0.1 $\mu\text{g mL}^{-1}$. This system has been successfully applied to the determination of Cu(II) in wastewaters from electroplating industry with less reagents and samples consumption and diminutive waste generation.

© 2006 Elsevier B.V. All rights reserved.

Keywords: Green analytical chemistry; Micro flow injection; Optical sensor; Copper(II)

1. Introduction

Nowadays, analytical methods are well established for environmental monitoring. However, a paradoxical situation has emerged because most of the analytical methodologies employed to investigate environmental problems by generating chemical wastes, are resulting in an environmental impact [1]. In some circumstances, the chemicals employed are even more toxic than the species being monitored. As a consequence, the work of some analytical chemists has been focused on the development of chemical processes that minimized or eliminate the use of toxic substances and the generation of toxic wastes in the prevention of environmental pollution and human hazards. Research in this field has been called green chemistry, also named as clean chemistry or environmentally benign chemistry which has focused mainly on the development of new syn-

thetic routes and the replacement or minimization of the use of chemicals. Nowadays, in the development of a new analytical procedure, the amount and toxicity of wastes are as important as any other analytical feature [2].

Flow analysis encompasses a widespread group of analytical techniques that are extensively employed in routine and research laboratories. The developments of these flow-based techniques have brought a new dimension to analytical chemistry, allowing the measurements to be carried out faster with minimum intervention of the analyst. Although there are many reliable flow procedures reported for routine analysis, most of them cannot be considered environmentally friendly, because they produce large amounts of chemical wastes that can be more or less toxic and need to be suitably managed. Despite this, the potentiality to develop greener analytical procedures is inherent to micro flow injection analysis (μFIA) methodology. This can be exemplified by the capability to decrease the reagent consumption and waste generation. Moreover, reagent and sample preparation can be carried out with minimum volumes of solutions [3,4].

* Corresponding author. Tel.: +66 53 943341x126.

E-mail address: Scislwrn@Chiangmai.ac.th (S. Liawruangrath).

Copper(II) determination in waters, is often required in environmental studies. Several analytical techniques are actually available to analyze Cu(II) concentration in environmental water with different matrices, such as atomic absorption spectrometry [5–7], inductively coupled plasma-atomic emission spectroscopy [8,9], stripping voltammetry on a mercury drop [10–13], differential pulse anodic stripping voltammetry [14], X-ray fluorescence [15] and atomic fluorescence spectrometry [16]. Besides the well-known advantages of these instrumental techniques (precision, accuracy, sensitivity, selectivity, etc.), all of them present a series of disadvantages, such as high investment cost, complexity and difficulty in situ application.

A number of flow-based methods for copper(II) determination in water have based on FIA [17–20] and SIA [21]. Recently, a reversed flow injection and sandwich sequential injection methods for the spectrophotometric detection of copper(II) with cuprizone has been reported [22] and a sequential injection analysis coupled with Lab-On-Valve for copper(II) determination has also been developed [23]. Among the above cited flow-based methods, only one FIA procedure [20] and one Lab-On-Valve procedure [23] used zincon as chromogenic reagent.

Micro flow injection provide one solution for portable detection system for environmental analysis due to the advantages of low reagent consumption, low waste production, cost effectiveness and small sample volume which are attractive properties for portable environmental analysis [24]. Micro flow injection techniques have been used for some environmental applications such as nitrites [25], nitrates [26], orthophosphates [27], uric acid [28] and cobalt(IV) [29]. However, no previously published papers have mentioned about Cu(II) determination using such a micro flow device.

In this work, micro flow system with optical sensor was designed, fabricated and investigated for Cu(II) determination based on reaction with zincon on the chip under suitable conditions. Various experimental conditions have been examined to achieve the desired sensitivity, rapidity, cost effectiveness, with minimum sample and/or reagents consumption and waste generation.

2. Experimental

2.1. Chemicals and reagents

All reagents were of analytical grade and Milli-Q (Millipore) double de-ionized water was used throughout the experiment. Standard solutions of 1000 mg L^{-1} Cu(II) (as copper nitrate) were purchased from Merck (Darmstadt, Germany). Working standard solutions of Cu(II) were freshly prepared by appropriate dilution of aqueous 1000 mg L^{-1} standard solutions. Zincon (2-carboxy-2'-hydroxy-5'-sulfoformazybenzene) monosodium salt was purchased from Aldrich, UK. A stock zincon solution (0.10%, w/v) was prepared by dissolving appropriate amounts of solid reagent in 0.01 mol L^{-1} sodium hydroxide and diluting to volume with water. Working solution of zincon was freshly prepared by appropriate dilution of stock zincon solution in universal buffer.

Universal buffer solution was prepared by mixing appropriate volumes of phosphoric, acetic and boric acids, containing 0.04 mol L^{-1} of each acid and sufficient amount of 0.1 mol L^{-1} NaOH solutions is poured into 100 mL of the mixture.

2.2. Apparatus

This system consisted of a planar glass chip and poly(dimethylsiloxane) (PDMS) top plate. The planar glass chip was fabricated using photolithography and wet etching technique [30,31]; the channel was 130 mm long, $200 \mu\text{m}$ wide and $50 \mu\text{m}$ deep. The channel network is shown in Fig. 1. The top plate was made from PDMS (Sylgard 184, Dow Corning) prepared according to instruction, vacuum degassed and then moulded with the reservoirs in place. The PDMS top plate is a clear cubic polymer, which has two small channels. The first channel is for passing the reagent to a glass chip. The second one is for fixing with a small channel PEEK tube with 0.5 mm i.d. size (acted as a flow cell 10 mm path length) for passing the solution out and measures the absorbance by fiber optic probe, which placed on the end of PEEK tube. Absorbance measurements were accomplished via a $600 \mu\text{m}$ UV fiber optic connection to an Ocean Optics SD-2000 CCD spectrophotometer (Ocean Optics, Dunedin, FL) containing a (UV sensitive) grating. The reagent and analyte solution was pumped into the 0.19 mm i.d. tygon tubing (Ismatec, England) by means of a peristaltic pump (Ismatec, Switzerland). The specially developed software in laboratory, "FIA-Studio 6" was used to control the peristaltic pump to mobilize sample and/or standard solutions at the microlitre volume accurately into the reagent channel. FIALab Software Version 5.0 (FIALab Instruments, Medina, WA) was used to control fiber optic spectrometer and also used for data collection and analysis. The light from a tungsten halogen lamp (Ocean Optics Inc.) was carried to the flow cell and then directed to a USB 2000 spectrophotometer for measuring the absorbance. The entire system

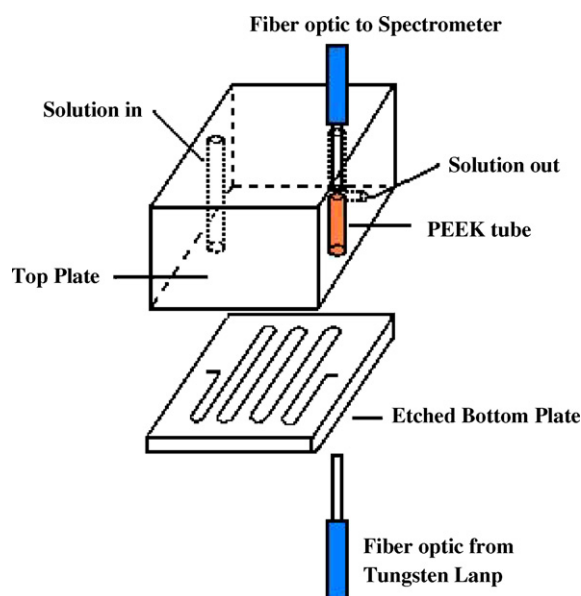


Fig. 1. Schematic diagram of micro flow injection with three-dimensional optical sensor for determination of Cu(II).

was controlled with a personal computer by running the FIAlab Software for Windows.

2.3. Procedure

A micro flow system coupled with a fiber optic spectrometer to obtain a micro flow manifold for the determination of Cu(II) is shown in Fig. 1. The method involved the aspiration of standard or sample solution containing Cu(II) into a reagent stream (zincon) with an appropriate flow rate of 0.01 mL min^{-1} ($10 \mu\text{L min}^{-1}$) using peristaltic pump with the specially desired software to control flow system (time injection, sample volume calculated from aspiration time and flow rate). Zincon and Cu(II) were reacted on a micro reactor producing a blue Cu(II)–zincon complex and then passed through the small channel PEEK tube (acted as flow cell) fixed in PDMS top plate, where the fiber optic probe was placed on the end of PEEK tube (10 mm path length) to measure the absorbance at 605 nm.

3. Results and discussion

3.1. Design of micro flow injection system

A specially designed and fabricated micro flow injection (μFI) system for determining small amounts of Cu(II) is described. The system is claimed to be greener because it uses less reagents and produces less waste than a traditional flow injection system.

Several designs were investigated to find out the best way to detect the signal. Initially, the fiber optic probe was placed in a vertical plane on PDMS top plate 10 mm over the glass chip but reproducible results could not be obtained due to interfering from the stray light and scattering. Therefore, a PEEK tube was inserted in PDMS at the vertical axis 10 mm between the glass chip and fiber optic probe and acted as a flow through cell ($2 \mu\text{L}$). By this design, reproducible signal can be achieved with the low noise signal due to the PEEK tube protected light from outside and reduced the noise from stray light and scattering. The network as coil reaction planar on glass chip is suitable for producing the Cu(II)–zincon complex. The micro flow system with optical sensor is shown in Fig. 1.

The system differs from the traditional FI system in that detection takes place in a monolithic device with machined channels (a micro chip), the flow through cell is a piece of PEEK tubing inserted into a channel in a monolithic device. A peristaltic pump with the small pump tubings is used to deliver the reagent into the μFI system. Sample solutions are introduced into the system by timed based injection using the peristaltic pump controlled by the specially designed software developed in our laboratory termed “FIA studio 6”. This software is capable of controlling the peristaltic pump to mobilize the sample solution through small tubing with accurate volume when an appropriate size of tubing is used. In the present work the sample introduction volumes for replicate injection of 0.5 mg L^{-1} Cu(II) are very accurate with the reproducibility and repeatability (as R.S.D.) of 3.9 and 2.5%, respectively.

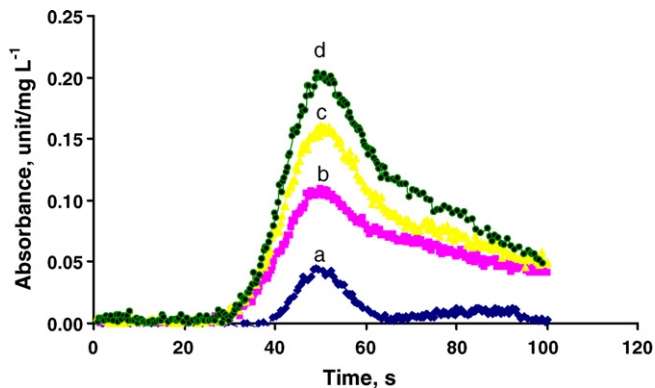


Fig. 2. Analytical signal for the determination of Cu(II) by micro flow system with three-dimensional optical sensor system. Cu(II) concentration: (a) 0.5 mg L^{-1} , (b) 1.0 mg L^{-1} , (c) 1.5 mg L^{-1} and (d) 2.0 mg L^{-1} .

3.2. Optimization of experimental conditions

In this experiment, a set of four standard Cu(II) solutions was measured and the slope of standard curve was determined at different studied parameters. In all experiments, three replicate measurements were performed for each studied parameter. The analytical signal of this system is shown in Fig. 2.

3.2.1. Selecting suitable wavelength

The effect of wavelength on sensitivity (slope of standard curve) was investigated over the range of 580–620 nm to check the performance of micro flow system for determination of copper(II). The results obtained are shown in Fig. 3. It was seen that the sensitivity increases with an increase in the wavelength. At wavelength 605 nm affords the highest sensitivity. On increasing further wavelength, the sensitivity is decreased. Therefore, 605 nm wavelength was chosen as the optimum wavelength and used in subsequent experiment.

3.2.2. The effect of zincon concentration

To obtain the best sensitivity of this method, various zincon concentrations on sensitivity were examined by varying the zincon concentration in the range 0.001–0.009% (w/v). The sensitivity increased with increasing zincon concentration until to

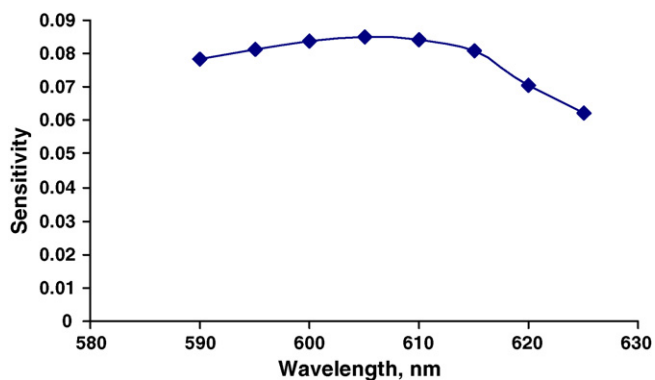


Fig. 3. Effect of varying wavelengths on sensitivity. Conditions: zincon concentration, 0.006% (w/v); pH of zincon solution, 11.0; flow rate, 0.01 mL min^{-1} ; sample volume, $2 \mu\text{L}$.

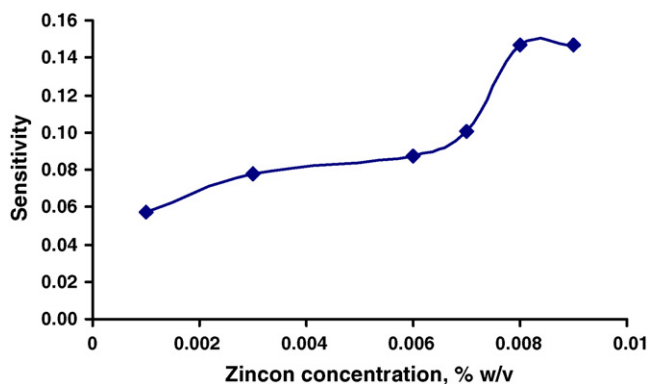


Fig. 4. Effect of varying zincon concentrations on sensitivity. Wavelength, 605 nm; pH of zincon solution, 11.0; flow rate, 0.01 mL min⁻¹; sample volume, 2 μ L.

0.008% (w/v) (Fig. 4). Then the 0.008% (w/v) of zincon was chosen for further study.

3.2.3. The effect of pH

The effect of varying pH values for the determination of Cu(II) was studied by comparing the result of Cu(II) to those of major interference metals, which can react with zincon such as Zn(II), Co(II) and Ni(II). The results obtained are shown in Fig. 5. Although these interfering metals gave the signal in the pH range 4.0–11.0, but the signals of Cu(II) at all pH values studied produce the higher sensitivity than those obtained by other metal ions [Zn(II), Co(II) and Ni(II)]. At pH 9.0 Cu(II) gave the highest signal which was selected throughout the experiment as it gave the highest sensitivity for copper(II) and minimized the effect of other metal interferences.

3.2.4. The effect of flow rate

The influence of flow rate on sensitivity was studied over the range 0.004–0.017 mL min⁻¹. It was found that the higher flow rate was applied, the higher sensitivity was obtained from 0.004–0.010 mL min⁻¹. Further increasing the flow rate, the sensitivity decreased gradually. Therefore, the suitable flow rate was 0.01 mL min⁻¹ (10 μ L min⁻¹) for this micro flow system.

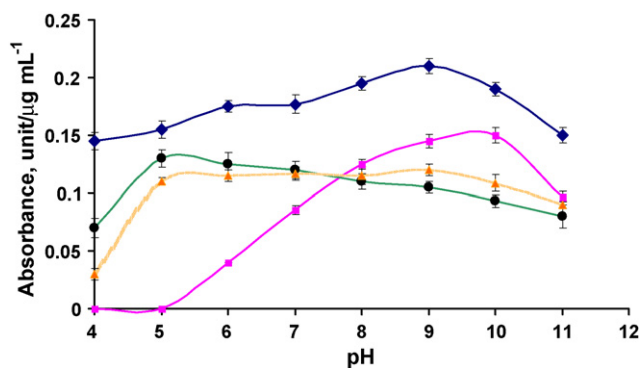


Fig. 5. Effect of varying the pH of zincon solution for the detection of Cu(II) in the presence of other metal. (♦) 2.0 mg L⁻¹ Cu(II); (■) 2.0 mg L⁻¹ Zn(II); (▲) 2.0 mg L⁻¹ Ni(II); (●) 2.0 mg L⁻¹ Co(II).

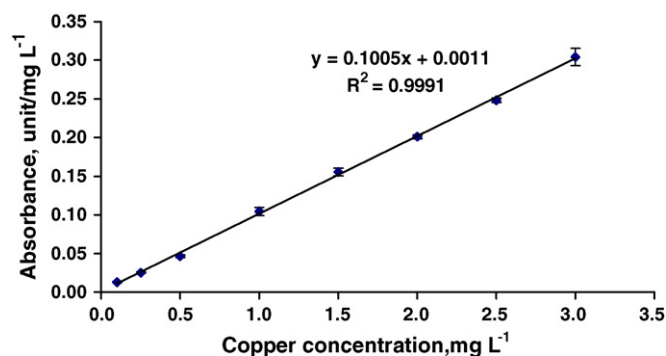


Fig. 6. The calibration curve of Cu(II) determination from micro flow system. Wavelength, 605 nm; zincon concentration, 0.008% (w/v); pH of zincon solution, 9.5; flow rate, 0.01 mL min⁻¹; sample volume, 2 μ L.

3.2.5. The effect of sample volume

The effect of various sample volumes on the sensitivity was investigated by varying the sample volumes in the range 1.0–3.0 μ L. The sensitivity was found to increase when increasing sample volume up to 2.0 μ L. Further increasing in sample volume resulted in less sensitivity probably owing to the effect of dispersion. Therefore, 2.0 μ L sample volume was chosen as the suitable volume.

3.3. Analytical figures of merit

The calibration graph of Cu(II) was studied by measurement of Cu(II) standard solution (0.1–3.0 μ g mL⁻¹) under the suitable conditions (wavelength, 605 nm; zincon concentration, 0.008% (w/v); pH of zincon solution, 9.0; flow rate, 0.01 mL min⁻¹; sample volume 2.0 μ L). The calibration graph was established by plotting peak heights versus various Cu(II) concentrations (Fig. 6). It was found that slope (sensitivity) was 0.1005 absorbance unit/ μ g mL⁻¹, with the intercept of 0.0011 μ g mL⁻¹ and the correlation coefficient (r^2) of 0.9991. The limit of detection (LOD) was evaluated using the blank + 3 $S_{y/x}$ (the error calculated in the y direction) as defined by Miller and Miller [32] and was found to be 0.1 μ g mL⁻¹ at the 95% confidence level. The precision of the method was investigated for the standard Cu(II) solution at concentration 0.5 μ g mL⁻¹. Ten measurements were made with each concentration. Results exhibited very good precision with signal variability of 2.5%.

The LOD of the proposed method (100 ng mL⁻¹) higher than that reported by Richter et al. [20] based on traditional FIA (0.80 ng mL⁻¹) with a continuous preconcentration unit (Chelex 100) to increase sensitivity of the method using zincon as chromogenic reagent. However, the proposed method was operated without any preconcentration micro column leading to poor sensitivity and hence high LOD was obtained. Although the proposed method was not as sensitive as the reported one [20], the proposed method was simple, cost effective and rapid with a sample throughput of 30 samples h⁻¹. The advantages of the proposed μ FI system over the traditional FI system were minimum sample and reagent consumption, minimum waste product, small size of instrumentation and no need of an expensive injection valve.

In contrast to previous report found in the literature on traditional flow injection method for copper(II) determination based on the same chemical reaction [20], the optimum reagent flow rate for the μ FI system is 0.01 mL min^{-1} whereas that of the traditional FI system is 2.0 mL min^{-1} indicating that using the μ FI system the reagent consumption can be reduced 200 times. Regarding the sample injection volume used in both systems, it is clear that the proposed μ FI manifold requires $2 \mu\text{L}$ sample while the traditional FI manifold uses $100 \mu\text{L}$ sample solution. This implies that the former FI method consumes 50 times less sample injection volume than that of the latter FI manifold. Under optimum conditions, minimum waste production can be achieved using the μ FI method. The aim of this research is to develop a fairly sensitive and rapid μ FI system for monitoring of copper(II) in industrial wastewaters containing quite high levels of copper(II) with low sample and/or reagent consumption and minimum waste production. Therefore, in this circumstance, high sensitivity is not needed. With further improvement and/or modification of the μ FI system the more efficient greener analytical methods with reasonable high sensitivity using suitable preconcentration unit will be developed to analyse a wide range of real sample.

3.4. Interference study

The ions present in water samples were examined as possible sources of interferences. A 0.5 mg mL^{-1} Cu(II) solution was used, with increasing concentration of the interfering ion until the usual concentrations in natural waters were reached. Cations at high concentration interfere because they are potentially competing to reach and react with zincon. The tolerable concentration of each foreign metal species was taken as a $<5\%$ relative error in the signal. The tolerable concentration of each interfering metal ion concentration to 0.5 mg L^{-1} Cu(II) was 3 mg L^{-1} for Zn(II) and Co(II), 4 mg L^{-1} for Ni(II), 15 mg L^{-1} for Mn(II) and $>25 \text{ mg L}^{-1}$ for Cd(II), Fe(III), Cr(III), Na(I) and K(I). Although in many real samples most interfering species appear at lower concentration than that of Cu(II). The use of sodium citrate ($2 \times 10^{-3} \text{ mol L}^{-1}$) as the masking agents to avoid the potential interferences from Zn(II), Ni(II) and Cd(II) was investigated. It was clear that $2 \times 10^{-3} \text{ mol L}^{-1}$ sodium citrate could overcome the interference effect from the above three metal ions satisfactorily. In addition, the standard addition procedure was also applied to determine Cu(II) for eliminating matrix effect from other interferences in the polluted wastewater samples studied.

3.5. Sample analysis

In order to demonstrate the applicability of the proposed method to real samples, this designed micro flow system was applied to determine Cu(II) in wastewater from electroplating industry by standard addition method. Comparative determination of copper(II) in the same sample solutions was also carried out by AAS (Table 1). Considering that AAS is usually recognized as a standard technique. As can be observed, the results obtained are in good agreement with those values used

Table 1
Determination of Cu(II) in wastewater samples

Sample	Proposed method ^a ($\mu\text{g mL}^{-1}$)	AAS method ^a ($\mu\text{g mL}^{-1}$)	Relative error (%)
a	$1.86 \pm (0.02)$	$1.88 \pm (0.02)$	-1.06
b	$0.67 \pm (0.02)$	$0.66 \pm (0.01)$	1.52
c	$2.11 \pm (0.03)$	$2.15 \pm (0.03)$	-1.86
d	$1.59 \pm (0.02)$	$1.57 \pm (0.03)$	1.27
e	$1.10 \pm (0.01)$	$1.12 \pm (0.02)$	-1.79

Results expressed as concentration \pm standard deviation.

^a Triplicate analysis.

as reference method. The proposed μ FIA is simple, rapid and inexpensive with low reagent consumption and minimum waste generated and also no flame gases are required. The accuracy of the results was tested by applying the paired *t*-test, which confirmed the absence of systematic errors at the 0.05 level.

4. Conclusions

The specially designed glass chip coupled with PDMS top plate with the sample inlet and the solution outlet tunnels together with an optical sensor in the micro flow system was successfully applied to determine Cu(II) in wastewater. This design is not only a micro reactor but also be a sensor on a chip to provide reliable results. The micro flow system was superior to the conventional method in that it could minimize reagent and sample consumption as well as waste generation with a simple and cost effective technique. It may seem promising as a basis to develop an automatic system to direct monitoring of Cu(II) in the effluent of wastewater form industries.

Acknowledgements

The authors would like to gratefully acknowledge the Thailand Research Fund (TRF), The Royal Golden Jubilee (RGJ) Ph.D. Program for financial support. Thanks are due to Postgraduate Education and Research Program in Chemistry (PERCH) for partial support and also to Graduate School and Chemistry Department, Faculty of Science, Chiang Mai University, for providing all facilities in Ph.D. research. Special thanks are also expressed to Dr. Tom McCreedy, Department of Chemistry, University of Hull, for providing planar glass chip to make this work possible.

References

- [1] P.T. Anastas, Crit. Rev. Anal. Chem. 29 (1999) 167.
- [2] F.R.P. Rocha, J.A. Nobrega, O.F. Filho, Green Chem. 3 (2001) 216.
- [3] S.J. Haswell, Analyst 112 (1997) 1R.
- [4] G.N. Doku, S.J. Haswell, Anal. Chim. Acta 382 (1999) 1.
- [5] W.R. Wolf, K.K. Stewart, Anal. Chem. 51 (1979) 1201.
- [6] K. Fukamachi, N. Ishibashi, Anal. Chim. Acta 119 (1980) 383.
- [7] Z. Fang, S. Xu, S. Zhang, Anal. Chim. Acta 164 (1984) 41.
- [8] A.O. Jacintho, E.A.G. Zagatto, H. Bergamin, F.F.J. Krug, B.F. Reis, R.E. Bruns, B.R. Kowalski, Anal. Chim. Acta 130 (1981) 243.
- [9] E.A.G. Zagatto, A.O. Jacintho, F.F.J. Krug, B.F. Reis, R.E. Bruns, M.C.U. Araujo, Anal. Chim. Acta 145 (1983) 169.
- [10] J. Ruzicka, E.H. Hansen, Anal. Chim. Acta 99 (1978) 37.

- [11] A. Hu, R.E. Dessy, A. Graneli, *Anal. Chem.* 55 (1983) 320.
- [12] L. Anderson, D. Jagner, M. Josefson, *Anal. Chem.* 51 (1982) 1371.
- [13] J. Janata, J. Ruzicka, *Anal. Chim. Acta* 139 (1982) 105.
- [14] G. Gillain, G. Duyckaerts, A. Disteché, *Anal. Chim. Acta* 106 (1979) 23.
- [15] O.W. Lau, S.Y. Ho, *Anal. Chim. Acta* 280 (1993) 269.
- [16] V. Rigin, *Anal. Chim. Acta* 283 (1993) 895.
- [17] N. Pourreza, M. Bebpour, *Anal. Sci.* 14 (1998) 997.
- [18] Q.E. Cao, Y. Zhao, X. Cheng, Z. Hu, Q. Xu, *Food Chem.* 65 (1999) 405.
- [19] B. Puruchat, S. Liawruangrath, P. Sooksamith, S. Rattanaphani, D. Budhasukh, *Anal. Sci.* 17 (2001) 443.
- [20] P. Richter, M. Inés Toral, A. Eugenta, E. Fuenzalida, *Analyst* 122 (1997) 1045.
- [21] I.F. Van Staden, A. Botha, *Talanta* 49 (1999) 1099.
- [22] P. Rumiri, V. Cerdá, *Anal. Chim. Acta* 486 (2003) 227.
- [23] T. Leelasattarathkul, S. Liawruangrath, M. Rayanakorn, W. Oungpipat, B. Liawruangrath, *Talanta* 70 (2006) 656.
- [24] D.R. Reyes, D. Iossifidis, P.A. Auroux, A. Manz, *Anal. Chem.* 74 (2002) 2623.
- [25] G.M. Greenway, S.J. Haswell, P.H. Petsul, *Anal. Chim. Acta* 387 (1999) 1.
- [26] P.H. Petsul, G.M. Greenway, S.J. Haswell, *Anal. Chim. Acta* 428 (2001) 155.
- [27] R.N.C. Daykin, S.J. Haswell, *Anal. Chim. Acta* 313 (1995) 155.
- [28] Y. Lv, Z.J. Zhang, F.N. Chen, *Analyst* 127 (2002) 1176.
- [29] L.J. Nelstrop, P.A. Greenwood, G.M. Greenway, *Lab on a Chip* 1 (2001) 138.
- [30] T. McCreedy, *Trends Anal. Chem.* 19 (2000) 396.
- [31] T. McCreedy, *Anal. Chim. Acta* 427 (2001) 39.
- [32] J.C. Miller, J.N. Miller, *Statistics for Analytical Chemists*, third ed., Ellis Harwood, London, 1994, p. 115.

A consensus least squares support vector regression (LS-SVR) for analysis of near-infrared spectra of plant samples

Yankun Li, Xueguang Shao, Wensheng Cai*

Department of Chemistry, Nankai University, Tianjin 300071, PR China

Received 20 June 2006; received in revised form 26 September 2006; accepted 17 October 2006

Available online 20 November 2006

Abstract

Consensus modeling of combining the results of multiple independent models to produce a single prediction avoids the instability of single model. Based on the principle of consensus modeling, a consensus least squares support vector regression (LS-SVR) method for calibrating the near-infrared (NIR) spectra was proposed. In the proposed approach, NIR spectra of plant samples were firstly preprocessed using discrete wavelet transform (DWT) for filtering the spectral background and noise, then, consensus LS-SVR technique was used for building the calibration model. With an optimization of the parameters involved in the modeling, a satisfied model was achieved for predicting the content of reducing sugar in plant samples. The predicted results show that consensus LS-SVR model is more robust and reliable than the conventional partial least squares (PLS) and LS-SVR methods.

© 2006 Elsevier B.V. All rights reserved.

Keywords: Consensus modeling; Least squares support vector regression (LS-SVR); Near-infrared spectroscopy; Quantitative analysis

1. Introduction

Near-infrared (NIR) spectroscopy has been taking a very important role in the measurement of the composition of complex plant samples due to the characteristics of its rapidity, simplicity and non-destructive measurements [1,2]. However, the presence of the relatively weak and highly overlapping spectral bands in the NIR spectra poses a challenge for extracting sample-specific or component-specific information. It is essential to apply chemometrical methods to preprocess the measured spectra and to build the quantitative model in NIR spectral analysis. Therefore, chemometrical methods have become hot points in quantitative analysis of NIR spectra in recent years. Many multivariate calibration methods, such as multiple linear regression (MLR) [3], principal component regression (PCR) [4], partial least squares (PLS) [5,6,7], artificial neural network (ANN) [8], etc., are widely applied in the analysis of NIR data.

In the analysis of NIR data, a reliable quantitative and qualitative model is a matter of primary importance for prediction of composition contents and characterization of unknown sam-

ples, so it is crucial to study the methods of model construction. Most of the conventional multivariate calibration techniques are based on a single model, which sometimes results in unsatisfactory prediction accuracy and stability when the training set is relatively small. However, in consensus strategy, multiple models are developed by using the training subsets randomly selected from the whole training set [9]. The multiple models are trained individually and then their predictions are combined by simple averaging or by weighted averaging, which would produce higher prediction accuracy and robustness than single model strategies. Consensus strategy has been coupled with PCR [10], ANN [11–13], Decision Tree [9,14], PLS [15], etc., and has been successfully applied in the analysis of multicomponent mixture of constituents with different chemical characteristics [10] and chemical classification [9,11,16], especially in quantitative structure–activity relationship (QSAR) or quantitative structure–property relationship (QSPR) [17,18,19].

In this work, a consensus least squares support vector regression (LS-SVR) method was proposed for building the calibration model of NIR spectra and the routine ingredient of reducing sugar in tobacco samples. Compared with the conventional LS-SVR and PLS method, the predicted results of consensus LS-SVR method are found to be improved significantly in terms of accuracy and robustness.

* Corresponding author. Tel.: +86 22 23503430; fax: +86 22 23502458.
E-mail address: wscail@nankai.edu.cn (W. Cai).

2. Theory and algorithm

2.1. Discrete wavelet transform (DWT)

Wavelet transform (WT) has been found to be a very efficient tool in processing analytical signals [20]. It has been utilized for data compression, data smoothing and denoising, baseline correction, resolution of multicomponent overlapping signals and processing of analytical images [21]. The discrete wavelet transform is a special case of WT that provides a compact representation of a signal in time and frequency and can be computed easily and efficiently. In this study, as a preprocessing tool, DWT is used for data compression, spectral background removal and noise filtration of NIR spectral data.

2.2. LS-SVR

In linear least squares models, the predictions \hat{y} are computed by the equation:

$$\hat{y} = \mathbf{X}\boldsymbol{\beta} + b_0 \quad (1)$$

where \mathbf{X} is a $[n \times p]$ matrix containing the p spectral responses of the n samples, $\boldsymbol{\beta}$ a $[p \times 1]$ vector of regression coefficients and b_0 is the model offset.

The support vector technique proposed by Vapnik [22] is designed to solve the classification problem. Recently support vector machines (SVM) technique has been applied to chemometric issues for nonlinear discrimination and quantitative prediction [23,24]. It has been proved to be a powerful methodology for solving problems in nonlinear classification, function estimation and density estimation [25,26], and has also led to many other recent developments in kernel-based learning methods in general. The basic idea of SVM is, at first, to provide a nonlinear function approximation by mapping the input vectors into high dimensional feature spaces where a special type of hyperplane is constructed, and then, to build a regression model in the hyperplane [27]. There has been several programs for SVM calculation including ν -SVM [28], LS-SVM [29], weighted SVM [30], direct SVM [31], etc.

It has been proved that support vector machine can be used as a candidate for spectral regression purpose, which is called support vector regression (SVR). One of the advantages of SVR is its ability to model nonlinear relationships. SVR is based on a kernel substitution, i.e., in Eq. (1), \mathbf{X} $[n \times p]$ is replaced by an $[n \times n]$ kernel matrix \mathbf{K} , which is defined as:

$$\mathbf{K} = \begin{pmatrix} k_{1,1} & \cdots & k_{1,n} \\ \vdots & \ddots & \vdots \\ k_{n,1} & \cdots & k_{n,n} \end{pmatrix} \quad (2)$$

where $k_{i,j}$ is defined by the kernel function. In this study, the Gaussian radial basis function (RBF) kernel was used:

$$k_{i,j} = e^{-\frac{|\mathbf{x}_i - \mathbf{x}_j|^2}{2\sigma^2}} \quad (3)$$

\mathbf{x}_i and \mathbf{x}_j indicate measured NIR spectra of different samples, σ is the kernel width parameter.

LS-SVR proposed by Suykens is an alternate formulation of SVR [29,32]. In LS-SVM, the ϵ -insensitive loss function (defined using the significance threshold ϵ) is replaced by a classical squared loss function, which constructs the Lagrangian by solving the linear Karush–Kuhn–Tucker (KKT) system:

$$\begin{bmatrix} 0 & \mathbf{I}_n^T \\ \mathbf{I}_n & \mathbf{K} + \boldsymbol{\gamma}^{-1}\mathbf{I} \end{bmatrix} \begin{bmatrix} b_0 \\ \mathbf{b} \end{bmatrix} = \begin{bmatrix} 0 \\ \mathbf{y} \end{bmatrix} \quad (4)$$

where \mathbf{I}_n is a $[n \times 1]$ vector of ones, T means transpose of a matrix or vector, $\boldsymbol{\gamma}$ a weight vector, \mathbf{b} regression vector and b_0 is the model offset. The solution of Eq. (4) can be found by using the most standard methods of solving sets of linear equations. Therefore, LS-SVR are known as a proficient of SVR, complex calculations as in SVR are avoided in LS-SVR. Furthermore, as we can see from Eqs. (3) and (4), only two parameters (γ , σ) are needed for LS-SVR [34]. However, because SVR approach defines the regression error differently by neglecting all regression errors smaller than the ϵ -insensitive loss function [33], the tuning of three parameters (γ , σ , ϵ) is required for SVR computation. Such a difference in error definitions also makes LS-SVR problem computationally much easier than SVR problem.

2.3. Consensus modeling for regression

Consensus modeling combines the results of multiple individual models (called member models hereafter), which are constructed by choosing the different training subsets from the whole training set. The basic idea of consensus modeling is that multiple models will effectively identify and encode more aspects of the relationship between independent and dependent variables than will a single model. It has advantage of reducing dependence on single sample to obtain prediction results by randomly altering training set. Therefore, it can be expected to solve “overfit” or “underfit” problem due to the small training set, thereby, enhance the stability of the predictions.

Theoretically, the error of consensus model $e(\bar{x})$ can be represented by reference [10]:

$$e(\bar{x}) = \bar{e}(\bar{x}) - \bar{a}(\bar{x}) \quad (5)$$

where $\bar{e}(\bar{x})$ is the average error across all member models, while $\bar{a}(\bar{x})$ is the variance of the member models respect to the results of the consensus model. These two terms are defined as:

$$\bar{e}(\bar{x}) = \frac{1}{N_m} \sum_{i=1}^{N_m} (y - \hat{y}_i)^2 \quad (6)$$

$$\bar{a}(\bar{x}) = \frac{1}{N_m} \sum_{i=1}^{N_m} (\hat{y}_i - \hat{y})^2 \quad (7)$$

where N_m is the number of model numbers, \bar{x} the vector of the independent variables (NIR spectral data in this study), y the dependent variable (reducing sugar content modeled in this study), \hat{y}_i the prediction result of the i th member model, while

\hat{y} is the prediction of the consensus model, which is obtained by averaging of the prediction results of multiple member models, i.e.: $\hat{y} = \frac{1}{N_m} \sum_{\alpha=1}^{N_m} \hat{y}_i$.

Clearly, it can be seen from Eq. (5) that the error of consensus model $e(\bar{x})$ can be minimized by a tradeoff between $\bar{\varepsilon}(\bar{x})$ and $\bar{\alpha}(\bar{x})$. The former is a measure of predictive quality of individual member models and the later is a measure of diversity of the member models. Moreover, stability of the model can also be enhanced by increasing the number of member models [9]. Therefore, the consensus modeling can be well performed only if the combined predictors are simultaneously accurate and diverse enough, which requires an adequate tradeoff between those two conflicting conditions [35].

2.4. Consensus LS-SVR calculation

In consensus LS-SVR calculation, member model is selected by a criterion of prediction accuracy and all the accepted models are adopted to predict unknown samples. The accepting criterion is defined by the mean relative error between the prediction results and true results (experimental values) of the assessing set. When the mean relative error is lower than a certain threshold, the constructed model will be accepted as a member model of the consensus method. The final prediction result is an average of the prediction results of all member models. The detailed procedures can be described as follows:

- (1) NIR spectra are firstly preprocessed using discrete wavelet transform. Through comparison of different wavelet filters and decomposition scale, the “sym4” filter (Symmlets wavelet filter with vanishing moment 4) and decomposition scale 9 are adopted. The first five approximation coefficients and the ca. 90% smaller detail coefficients in wavelet domain are eliminated, which correspond to the information of low frequency component of background and high frequency component of noise contained in the spectra, respectively. The rest wavelet coefficients, which are considered to be the sample-specific spectral information, are used for further calculation.
- (2) The compressed NIR spectra are randomly divided into a training set, an assessing set and a predicting set. The training subset for building member models will be randomly selected from the training set, and the assessing subset will be randomly selected from the assessing set in the next step.
- (3) Set parameters for the calculation, including the number of samples (or spectra) of the training subset (N_t), the number of samples of the assessing subset (N_v), number of member models (N_m) and the criterion for accepting the member models (mean relative error in this study). All these parameters will be given in detail in the following sections, some of them are determined with an optimization.
- (4) Build a consensus model with the parameters above. For each member model, N_t samples are randomly selected from the training set and used as a training subset and N_v samples

are randomly selected from the assessing set and used for assessing the model. The constructed model will become a member of the consensus model if its performance in predicting the assessing subset meets an acceptable criterion, otherwise it will be discarded. The process is repeated until the number of member models reaches to the preset number of N_m .

- (5) Predict the samples in the predicting set with the consensus model. In this study, the final prediction of a sample is obtained by a simple average of the results predicted by all the member models in the final consensus LS-SVR model.

3. Experimental

3.1. Experiments

The concentration of the routine components (reducing sugar) was measured on an Auto Analyzer III (BRAN + LUBBE, Germany) following the procedures of the standard method. NIR spectra of 269 tobacco lamina samples were measured on a Vector 22/N FT-NIR System (Bruker, Germany). Each NIR spectrum was recorded in the wavenumber range 4000–9000 cm^{-1} with the digitization interval ca. 4 cm^{-1} , each spectrum is composed of 1296 data points. Due to the large number of samples, only one spectrum was measured for each sample. However, in order to ensure the quality of the measured spectra and avoid the scattering problem, large amount (more than 10 g) ground sample was used and put in a rotating sample vessel with pressure. Furthermore, large scan number (64) was also used in the measurements.

3.2. Calculations

Two hundred and sixty nine samples (or spectra) were arbitrarily divided into three sets. One hundred and sixty one samples were used for training data set, 80 samples were used for assessing data set and the remaining 28 samples were used for prediction data set. The sample number of the training subset (N_t) for building member models will be discussed in the following section, and 30 was used for the sample number of the assessing subset (N_v).

In the comparison of consensus LS-SVR, LS-SVR and PLS methods, the same training set and prediction set are adopted. The LS-SVR parameters σ and γ , and number of principal factor (n_f) in PLS are optimized. $\sigma = 2$, $\gamma = 10^6$ and $n_f = 12$ are used in the calculation. In the optimization of these parameters, the root mean squared error of prediction (RMSEP) of the assessing set is used as an evaluation criterion.

$$\text{RMSEP} = \left[\frac{1}{n} \sum_{i=1}^n (y_i - \hat{y}_i)^2 \right]^{1/2} \quad (8)$$

where \hat{y}_i is the prediction concentration of the i th sample, y_i the true concentration of the i th sample and n is the number of prediction samples.

4. Results and discussions

4.1. Criterion for accepting member models

In the consensus method, an individual model is constructed by randomly selected training subset and becomes a member model when it meets an acceptable criterion. In this study, mean relative error of prediction results of assessing set is used as accepting criterion. According to Eq. (5), the consensus modeling can be well performed only if the combined predictors are simultaneously accurate and diverse enough.

Therefore, different criterion threshold values were investigated. When the threshold is 10, 15, 20, 30, 50 and 100%, the average RMSEPs of 40 runs of prediction are 1.4284, 1.4002, 1.4615, 1.4783, 1.4459 and 1.4461, respectively. It can be seen that the RMSEPs of different threshold are close to each other, which shows the two conflicting factors of the accuracy and diversity of the member models counteract simultaneously. Thus, 15% is chosen as the accepting criterion. By examination of the calculations, it can be found that, with this criterion, only a small fraction of the tested models were rejected.

4.2. Number of training subset

In the consensus method, the multiple models to be combined are developed by different training subset. As indicated by Eq. (5), the optimal prediction of a consensus model is dependent on the tradeoff between the accuracy and diversity of the member models. Clearly, the number of the training subset for each individual model will have an effect on both the quality and the diversity of the member models. Thus, a proper number of training subset must be investigated prior to development of the consensus model.

In this study, the number of training subset is investigated by increasing N_t from 10 to 160 with a step of 10. For each N_t , a consensus LS-SVR model is developed and the model is then used to predict the assessing set. As shown in Fig. 1, RMSEP is large when a small N_t is used, then RMSEP decreases with the increase of N_t . When N_t reaches 80, the variation of RMSEPs

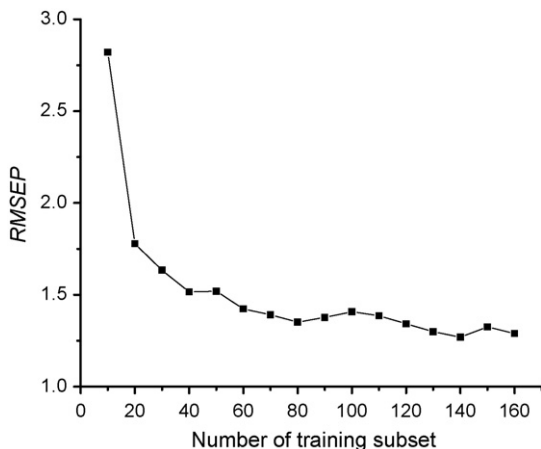


Fig. 1. Variation of RMSEPs with the number of samples used in the training subset.

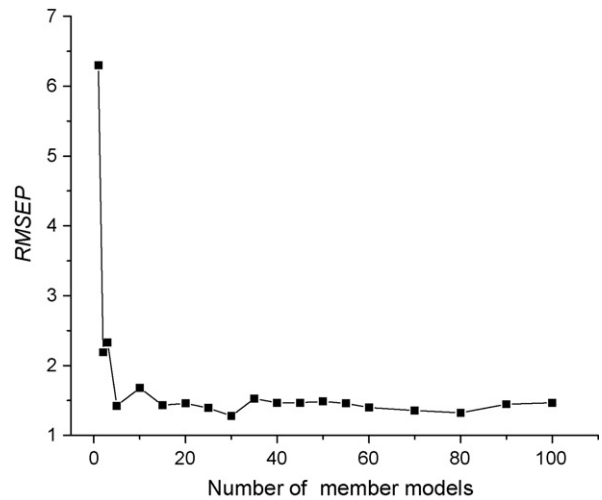


Fig. 2. Variation of RMSEPs with the number of member models in consensus LS-SVM.

tend to be slowed down although there is a little fluctuation and still a trend to decrease. Considering the speed of calculation, 80 was used for N_t in this study.

4.3. Number of member models

The number of member models (N_m) is another important parameter to affect the stability and accuracy of a consensus model. The benefit of combining multiple models can be realized only if individual models give different predictions. An ideal combined system should consist of several accurate models that disagree in prediction as much as possible [9].

In this study, N_m from 1 to 100 was investigated. For each N_m , a consensus LS-SVR model is developed and the model is then used to predict the assessing set. Fig. 2 shows the variation of RMSEPs with different N_m . From the figure, it can be seen that, at the beginning, RMSEP is comparatively large, then, however, with the increase of N_m , RMSEPs reaches almost a constant with little fluctuation. Accordingly, $N_m = 50$ is used for further study.

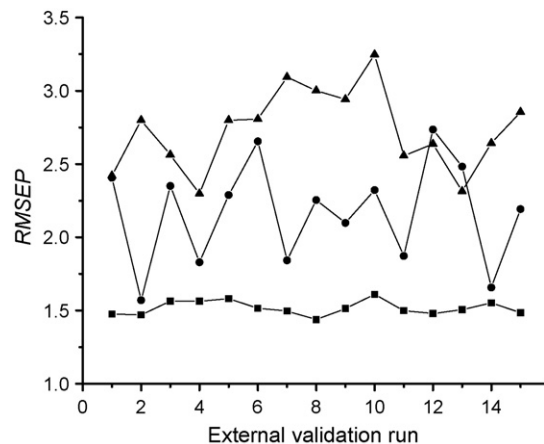


Fig. 3. RMSEPs obtained by consensus LS-SVM (■), LS-SVM (●) and PLS (▲) in 15 runs of prediction.

4.4. Prediction results

With the optimal parameters, a consensus LS-SVR model was developed using the 161 samples in the training set and used to predict the content of reducing sugar of the 28 samples in the predicting set. The process was repeated 15 times and the prediction results were compared with those of LS-SVR model (with the same data sets and same parameters as in consensus LS-SVR) and PLS model (with the same data sets and its optimal parameters). Fig. 3 shows the RMSEPs obtained by the three methods in predicting the same predicting sets. It is clear that, compared with that of LS-SVR and PLS, the RMSEPs of consensus LS-SVR are very low and stable in the 15 runs, which indicates that both the stability and the accuracy of the consen-

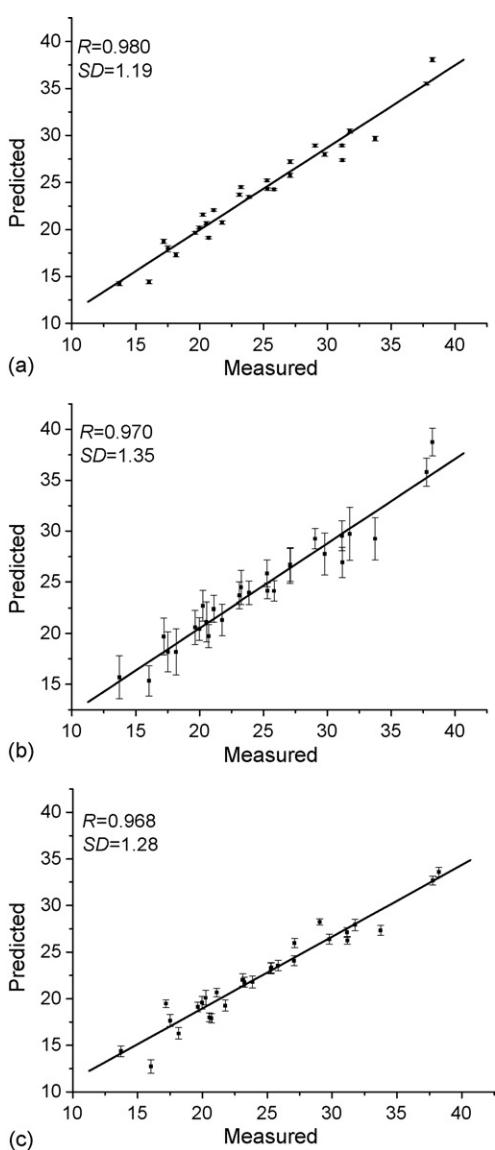


Fig. 4. The relationship between the measured content and the mean values (%) predicted in 15 runs of consensus LS-SVR (a), LS-SVR (b) and PLS (c). Standard deviation of the 15 predicted results for each sample is plotted as an error bar crossing the mean value. The straight line is obtained by a linear regression of the predicted results of the 28 samples in 15 runs with the measured values. R is the correlation coefficient and S.D. is the standard deviation.

sus LS-SVR model are much better than that of LS-SVR and PLS.

For further comparison of the prediction results of the three methods, Fig. 4 shows the relationship between the measured contents and the mean values predicted in 15 runs of consensus LS-SVR, LS-SVR and PLS. In the figure, the standard deviation of the 15 predicted results for each sample is plotted as a error bar crossing the mean value, which clearly shows that prediction stability of consensus LS-SVR is better than those of LS-SVR and PLS. Furthermore, the straight line in Fig. 4 is obtained by a linear regression of the predicted results of the 28 samples in 15 runs with the measured values, the correlation coefficient (R) and standard deviation (S.D.) are also labeled in the figure. It can be seen that, although there is no significant difference in R of the three methods, the S.D. of consensus LS-SVR is the smallest one. Therefore, consensus LS-SVR should be the most robust and accurate one among the compared three methods.

5. Conclusions

Based on the philosophy of consensus modeling, a consensus least squares support vector regression method is proposed and applied to building the quantitative model of NIR spectra of plant samples. Through an optimization of the parameters involved in the modeling, a successful model was acquired for predicting the content of reducing sugar in complex plant samples. By comparison against LS-SVR and PLS models, consensus LS-SVR model gives more stable and accurate prediction results. Therefore, consensus strategy may be a promising way for quantitative modeling of complex samples.

Acknowledgements

This study is supported by National Natural Science Foundation (Nos. 20325517 and 20575031), the Ph.D. Programs Foundation of Ministry of Education (MOE) of China (No. 20050055001) and the Teaching and Research Award Program for Outstanding Young Teachers (TRAPOYT) in High Education Institutions of MOE of China.

References

- [1] A.M. Bruno-soares, I. Murray, R.M. Paterson, J.M.F. Abreu, *Anim. Feed Sci. Technol.* 75 (1998) 15.
- [2] T. Borjesson, B. Stenberg, B. Linden, A. Jonsson, *Plant Soil* 214 (1999) 75.
- [3] I. Ben-Gera, K.H. Norris, *J. Food Sci.* 33 (1968) 64.
- [4] E.V. Thomas, D.M. Haaland, *Anal. Chem.* 62 (1990) 1091.
- [5] P. Geladi, B.R. Kowalski, *Anal. Chim. Acta* 185 (1986) 1.
- [6] D. Chen, B. Hu, X.G. Shao, Q.D. Su, *Anal. Bioanal. Chem.* 381 (2005) 795.
- [7] D. Chen, B. Hu, X.G. Shao, Q.D. Su, *Analyst* 129 (2004) 664.
- [8] C. Borggard, H. Thodberg, *Anal. Chem.* 64 (1992) 545.
- [9] W.D. Tong, H.X. Hong, H. Fang, Q. Xie, R. Perkins, *J. Chem. Inf. Comp. Sci.* 43 (2003) 525.
- [10] J. Aleksander, W. Kazimierz, W. Hanna, *Electroanalysis* 17 (2005) 1477.
- [11] G. Tesaura, D.S. Touretzky, T.K. Leen, *Neural Network Ensembles. Advances in Neural Information Processing Systems 7*, MIT Press, Cambridge, MA, 1995, pp. 231–238.

- [12] M.P. Perrone, L.N. Cooper, R.J. Mammone, *Neural Networks for Speech and Image Processing*, Chapman and Hall, London, 1993, pp. 126–142.
- [13] D.W. Opitz, J.W. Shavlik, *Conn. Sci.* 8 (1996) 337.
- [14] H. Drucker, C. Cortes, *Boosting Decision Trees*, vol. 8, MIT Press, Cambridge, MA, 1996, pp. 479–485.
- [15] P. Geladi, K. Esbensen, *J. Chemometr.* 4 (1990) 337.
- [16] C.A.S. Bergstrom, U. Norinder, K. Luthman, P. Artursson, *J. Chem. Inf. Comp. Sci.* 43 (2003) 1177.
- [17] P. Gramatica, P. Pilutti, E. Papa, *J. Chem. Inf. Comp. Sci.* 44 (2004) 1794.
- [18] N. Baurin, J.C. Mozziconacci, E. Arnoult, P. Chavatte, C. Marot, L. Morin-Allory, *J. Chem. Inf. Comp. Sci.* 44 (2004) 276.
- [19] W.D. Tong, W. Xie, H.X. Hong, L.M. Shi, H. Fang, R. Perkins, *Environ. Health Perspect.* 112 (2004) 1249.
- [20] X.G. Shao, W.S. Cai, *Rev. Anal. Chem.* 17 (1998) 235.
- [21] X.G. Shao, A.K.M. Leung, F.T. Chau, *Acc. Chem. Res.* 36 (2003) 276.
- [22] V. Vapnik, *The Nature of Statistical Learning Theory*, Springer-Verlag, New York, USA, 1995.
- [23] A.I. Belousov, S.A. Verzakov, J. von Frese, *J. Chemometr.* 16 (2002) 482.
- [24] R. Goodacre, *Vib. Spectrosc.* 32 (2003) 33.
- [25] T. van Gestel, J. Suykens, B. Baesens, S. Viaene, J. Vanthienen, G. Dedene, B. de Moor, J. Vandewalle, *Machine Learn.* 54 (2004) 5.
- [26] N. Pochet, F. De Smet, J. Suykens, B. De Moor, *Bioinformatics* 20 (2004) 3185.
- [27] B. Schölkopf, C. Burges, A. Smola, *Three Remarks on the Support Vector Method of Function Estimation in Advanced in Kernel Methods: Support Vector Learning*, The MIT Press, Cambridge, Massachusetts, 1999, pp. 25–43.
- [28] B. Schölkopf, A.J. Smola, R.C. Williamson, P.L. Bartlett, *Neur. Comp.* 12 (2000) 1207.
- [29] J.A.K. Suykens, J. Vandewalle, *Neur. Proc. Let.* 9 (1999) 293.
- [30] J.A.K. Suykens, J. De Brabanter, L. Lukas, J. Vandewalle, *Neurocomputing* 48 (2002) 85.
- [31] D. Roobaert, J. VLSI Signal Process. Syst. Signal Image Video Technol. 32 (2002) 147.
- [32] J.A.K. Suykens, J. Vandewalle, De B. Moor, *Neural Netw.* 14 (2001) 23.
- [33] U. Thissen, B. Ustun, W.J. Melssen, L.M.C. Buydens, *Anal. Chem.* 76 (2004) 3099.
- [34] F. Chauchard, R. Cogdill, S. Roussel, J.M. Roger, V. Bellon-Maurel, *Chemometr. Intell. Lab. Syst.* 71 (2004) 141.
- [35] H.D. Navone, P.M. Granitto, P.F. Verdes, H.A. Ceccatto, *Revista Iberoamericana de Inteligencia Artif.* 12 (2001) 70.

Hydrothermal synthesis of highly luminescent CdTe quantum dots by adjusting precursors' concentration and their conjunction with BSA as biological fluorescent probes

Mengying Li, Yingxin Ge, Qifan Chen, Shukun Xu*, Naizhi Wang, Xiujuan Zhang

Department of Chemistry, P.O. Box 332, Northeastern University, Shenyang 110004, China

Received 21 June 2006; received in revised form 20 September 2006; accepted 29 September 2006

Available online 30 October 2006

Abstract

A study on hydrothermal synthesis of CdTe quantum dots, highly luminescent nanocrystals at a relatively lower temperature, via changing the concentration of the CdTe precursors, is described. The full width at half maximum ranged from 40 to 80 nm and quantum yield (QY) was detected to be 27.4% at room temperature. The as-prepared CdTe QDs were labeled with BSA for fluorescence probes without pretreatment. Conjunction experimental results suggested that the as-prepared CdTe QDs are suitable for the application of biotechnology.
© 2006 Elsevier B.V. All rights reserved.

Keywords: Quantum dots; Precursor; Photoluminescence intensity; Biological fluorescent labeling

1. Introduction

Quantum dots (QDs), which have unique electronic and optical properties such as high quantum yields (QY), narrow emission bands, continuous broad absorption band, and high resistance to photobleaching, receive more concerns in recent years [1,2]. These properties are ascribed to their nanometer scale size, which is smaller than the Bohr radius [3]. Due to their luminescent characteristics which can be tuned by controlling the particle size [4], QDs can provide excitation of several different emission colors using a single excitation wavelength [5], and therefore have a potential application in optoelectronics and bio-labeling [6–11].

Originally, many groups [12–15] tried to synthesize QDs referred above, and succeeded to some extent, through an organic way. The biological applications of these kinds of QDs have been hampered by their inherently low solubility in water, despite they have many advantages in luminescent properties as compared to conventional fluorophore dyes. Then, new chemical strategies have been established to solve this problem. One is to

synthesize in the aqueous solution, with circumfluence at a temperature of lower than 100 °C [16,17]. Indeed, this method gains lots of merits: using water as its medium, less cost, less toxic, and more productive compared to the organic way. However, the full width at half maximum (FWHM) of the QDs' photoluminescent peak is broader; the period of synthesis becomes longer; the QDs prepared in this way need re-processing. In order to obtain high-quality QDs, hydrothermal synthesis, as a modification to former methods, is set up [7]. The key point is, during the hydrothermal synthesis, how to control the surface structure of QDs, which contributes a great influence to their luminescent properties. The hydrothermal synthesis is carried out in two steps: the synthesis of the precursors and the surface flaws' modification of the QDs by heating. Several research groups focus on the first step: try to use the thioglycolic acid or other thiol compounds as stabilizing agent [18,19]. Guo et al. [20] concluded that without any postpreparative treatment, QDs possess excellent luminescent properties via changing the rate of ligand and monomer. Additionally, Zhang et al. [21] concentrated on the relationship between the growth speed of the QDs and variation of heating temperature. As we know, hydrothermal synthesis of high equality QDs, with fixed rate of ligand and monomer in the first section, by adjusting the concentration of the precursors in the second, at a relatively lower temperature, has not been reported so far.

* Corresponding author. Tel.: +86 24 83681343; fax: +86 24 83681343.
E-mail address: xushukun46@126.com (S. Xu).

In this paper, a series of experiments about synthesis of QDs were carried out, in order to lower the temperature for QDs preparation and to improve the quantum yield. It is suggested that, even at 140 °C, CdTe QDs can be obtained with high photoluminescence for almost all colors by fixing the pH value (pH 11.2) and the rate ([ligand]/[monomer] = 0.5:2.4), and adjusting the concentration of the precursors. Thioglycolic acid-stabilized CdTe QDs synthesized in aqueous solution, with a relatively narrower FWHM (40–80 nm), can be effectively bound to a bio-macromolecule via electrostatic interaction, and remain the excellent luminescent properties (i.e. narrow FWHM, high photoluminescence intensity, color purity, and high QY) over 2 years in the sealed recipient. The photoluminescent (PL) QY of CdTe QDs is 27.4%, which was calculated by comparison with Rhodamine 6G in ethanol, assume its PL QY as 95%, at room temperature [22]. The as-prepared CdTe QDs, as fluorescence probes, were labeled with BSA without pretreatment, whose results validated that the as-prepared CdTe QDs are appropriate to biologic conjunction.

2. Experimental

2.1. Instrumentation

The emission spectra were measured on a LS-55 Luminescence Spectrometer (Perkin-Elmer, USA). Absorption spectra were recorded on a UV-2100 UV–vis spectrometer (Rui Li Analytical Instrument Company, Beijing, China). Two cuvettes of 1 cm path length quartz were used to measure the fluorescence spectrum and absorption spectrum separately. All optical measurements were carried out at room temperature under ambient conditions. The pH measurements were made with a PHS-3C pH meter (Hangzhou, China). Transmission electron microscope of Philips EM420 was used to characterize CdTe QDs which were synthesized at 140 °C. During the process of the conjunction with BSA, CdTe QDs and BSA were shaken and mixed by the CHA-S Reciprocating Oscillator (Jintan, Jiangshu, China).

2.2. Reagents and materials

All chemicals, used in the experiments, were of high purity commercially available without further purification. Thioglycolic acid (analytical purity), sodium borohydride (96%), tellurium powder (99.999%) were purchased from the company of chemical reagent in Shanghai. CdCl₂·2.5H₂O (chemical purity) was obtained from the Peking Chemical Plant. NaOH (analytical purity) was obtained from the Shenyang Huabo Company. The aqueous solution of CdCl₂ (0.4 mol l⁻¹) was prepared and diluted only prior to immediate use. The labeled molecules, BAS, were from AOBO Biology Techniques Company in Beijing, China. L-Glycine, used to terminate the conjunction reaction between the CdTe QDs and BAS, was from the Dingguo Biology Techniques Company. N-Hydroxysuccinimide (NHS) was received from Acros Organics, NJ, USA. 0.1 mol l⁻¹ PBS was prepared by dissolving NaH₂PO₄·2H₂O (mass was 1.482 g) and Na₂HPO₄·12H₂O (mass was 17.4 g) in pure water and mak-

ing to 100 ml. The water used in the study was distilled for three times.

2.3. Synthesis of CdTe precursors

CdTe precursors were prepared by utilizing the reaction between Cd²⁺ and sodium hydrogen telluride (NaHTe) solution in the following way, according to the previously reported procedure [21,23]. To be the first, NaHTe solution was produced at 0 °C or below by reaction of sodium borohydride (NaBH₄) with tellurium powder. Then, thioglycolic acid, as a stabilizer, was injected into nitrogen-saturated 2 × 10⁻² mol l⁻¹ CdCl₂ aqueous solution. After that, NaOH solution of 0.01 mol l⁻¹ was used to adjust the pH value of the mixed solution. The whole process was in the circumstance of surrounding with N₂ and ice bath. Finally, CdTe precursors with a concentration of 2.0 × 10⁻² mol l⁻¹ (anywhere in this paper, referring to Cd²⁺) were obtained. And no fluorescence was observed as the precursors were excited.

2.4. Surface flaws' modification of CdTe precursors at temperature from 100 °C to 200 °C

The CdTe precursors (2.0 × 10⁻² mol l⁻¹) were put into a pot of polytetrafluorethylene. The stable photoluminescent CdTe QDs of different sizes were synthesized at temperature controllable cabinet drier via prolonging the heating time. Six typical temperatures (100 °C, 120 °C, 140 °C, 160 °C, 180 °C, 200 °C) were researched in this experiment, as the pH value was fixed at 11.2–11.8 [9].

2.5. Adjusting the concentration of the CdTe precursors

Following the steps above, three samples (sample a, sample b, sample c) of CdTe precursors were prepared with the concentration of 2.0 × 10⁻² mol l⁻¹, 1.0 × 10⁻² mol l⁻¹, and 5.0 × 10⁻³ mol l⁻¹, respectively. The experimental conditions used, such as ice bath, nitrogen surrounding, temperature, pH value fixed at 11.2 ± 0.1, etc., were all the same.

2.6. Preparation of stable photoluminescent CdTe QDs at 140 °C

CdTe precursors with three typical concentrations were put into three pots of polytetrafluorethylene (PTFE), and heated at 140 °C in the cabinet drier mentioned above. With different heating times, the stable CdTe QDs capped by thioglycolic acid were prepared by adjusting the concentration of the CdTe precursors for further use. Their emission maximum wavelengths were at 535 nm, 549 nm, 580 nm, 600 nm, 625 nm, respectively, and their emitted colors ranged from green to red.

2.7. Labeling of BSA with CdTe QDs

One hundred microliters of five kinds of as-prepared CdTe QDs solution was put into five numbered tubules with the concentration of 1.0 × 10⁻³ mol l⁻¹, respectively. As an

activating reagent, 100 μl NHS (5.0 mg ml^{-1}), was added into the five kinds of CdTe QDs solutions and a blank, respectively, and six mixed solutions were shook homogeneously. After 10 min waiting for the reaction of the NHS, appropriate quantity of PBS was added to adjust pH. Then, 100 μl of 1.0 mg l^{-1} BSA was added to each of them, the mixed solution had been shook for 30 min at 37 $^{\circ}\text{C}$ in the oscillator. The reaction was terminated by mingling 100 μl of L-glycine with 0.1 mg ml^{-1} , and then shaking for another 30 min. The pH of reaction system was 7.4. All the samples and blank were stored with ambient temperature of 4 $^{\circ}\text{C}$ overnight for measurement of fluorescent spectrum.

3. Results and discussion

3.1. The growth of $2.0 \times 10^{-2} \text{ mol l}^{-1}$ CdTe QDs at 100–200 $^{\circ}\text{C}$

It had been known that the size of CdTe QDs, with fixed pH value and unaltered ratio(s) of ligand and monomer, was temperature dependent. On varying the heating time at six typical temperatures, CdTe QDs of different sizes were obtained. The evolutional emission peak position of CdTe QDs synthesized at six typical temperatures is shown in Fig. 1. As the clinamen of each curve expressed, the emission peak moved to longer wavelength as the heating time was prolonged. The maximum emission wavelength shifted from 495 nm to 625 nm, and the emission color of CdTe QDs changed from green to red, which could be observed visibly during the experiment. It is ascribed to that quantum dots exhibit an electronic structure intermediate between bands and bonds resulting in a direct correlation between size and band gap energy (emitted wavelength): as the size of the quantum dot increases, the band gap energy decreases. Therefore, we assumed the QDs with the same emitted wavelength as the QDs with the same size and the same photoluminescent properties. Moreover, no further shift of the emission peak occurred when the reaction time was continuously

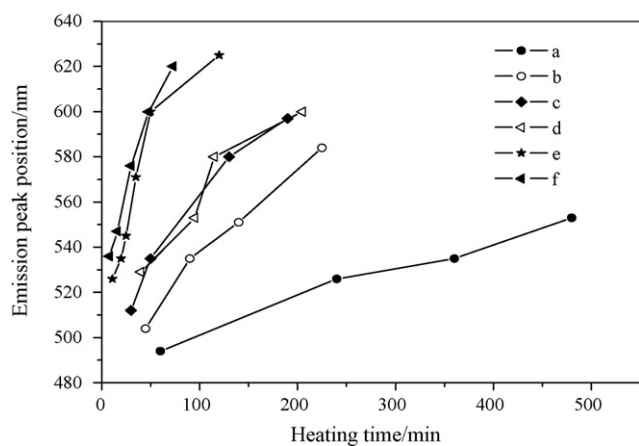


Fig. 1. The emission peak position of CdTe QDs precursors during their growth at six different temperatures. Precursors' concentration was 0.02 mol l^{-1} , the pH value was 11.2–11.8: 100 $^{\circ}\text{C}$ (a); 120 $^{\circ}\text{C}$ (b); 140 $^{\circ}\text{C}$ (c); 160 $^{\circ}\text{C}$ (d); 180 $^{\circ}\text{C}$ (e); 200 $^{\circ}\text{C}$ (f).

prolonged. Meanwhile, the integral tend of the curves evinced that the speed of QDs' growth was faster and faster when the synthesis temperature was raised. The orange/red CdTe QDs with bigger size is hardly synthesized at 100 $^{\circ}\text{C}$ and 120 $^{\circ}\text{C}$, because the lower temperature and the longer period for their growth may be not helpful to the modification of QDs' surface, which determined the photoluminescent properties of CdTe QDs to a certain extent. CdTe QDs in smaller size (wavelength was from 495 nm to 535 nm) grew too fast to form their perfect outer layers, when they were synthesized at the temperature above 180 $^{\circ}\text{C}$. Therefore, it was possible for us to search a series of conditions and synthesize stable CdTe QDs of different sizes with high quality (stronger luminescence, narrow FWHM of the emission spectra) at 140 $^{\circ}\text{C}$.

The temporal evolution of the absorption and luminescent spectra of the CdTe precursors ($2.0 \times 10^{-2} \text{ mol l}^{-1}$), which grew at three typical temperature (100 $^{\circ}\text{C}$; 140 $^{\circ}\text{C}$; 180 $^{\circ}\text{C}$) with different heating times, are shown in Fig. 2. Apparently, the maximum absorption wavelength of CdTe QDs shifted toward lower emitted energy, according to the shift of the emission peak position above. Compared with CdTe QDs synthesized at other temperature, the CdTe QDs prepared at 140 $^{\circ}\text{C}$ had a symmetrical emission peak, good color purity, and narrower FWHM (40–80 nm). The emission color of them nearly covered from green to red as the period of synthesis is not too long. Furthermore, 140 $^{\circ}\text{C}$ was a correspondingly lower temperature which was used in synthesizing CdTe QDs of all colors.

3.2. Photoluminescence properties of CdTe QDs at 140 $^{\circ}\text{C}$

Some references have discussed the growth condition, such as growth temperature, precursor concentration, pH value of the precursor etc in the process of optimizing the spectral properties of the CdTe QDs [24–26]. It was available that the pH value of Cd precursor was generally at 11.2–11.8 [27]. However, PL QY of the CdTe QDs would increase as the pH value of precursors' solution decrease [8]. So, the pH value was fixed at 11.2 ± 0.1 . The optimization of the synthesis condition was carried out by adjusting the concentration of Cd precursors. As the results, CdTe QDs of different colors (from green to red) with high luminescence were prepared at a relatively lower temperature (140 $^{\circ}\text{C}$). The spectra of CdTe QDs grown in samples a–c, are given in Fig. 3. The positions of emission peak were $530 \pm 2 \text{ nm}$. Compared with Rhodamine 6G (the quantum yield is 95%), the quantum yield of CdTe QDs was measured and calculated up to 27.4% [22], with the CdTe QDs diluted to the same concentration ($2.5 \times 10^{-5} \text{ mol l}^{-1}$) before they were detected by the optical instrument. Fig. 3 indicates that the lower concentration of the precursor required less heating time to grow up to CdTe QDs of the same size (emission at $530 \pm 2 \text{ nm}$), and the yielding CdTe QDs had stronger luminescence, symmetrical emission peak, and higher QY. The lower precursor concentration played an important role in preparing highly luminescent CdTe QDs with an emission of green or yellow. It is ascribed to the concentration effects on photoluminescence. The excess cadmium monomers existed in the initial stage of QDs growth, which provided good conditions for the reconstruction of the surfaces of QDs [7,28].

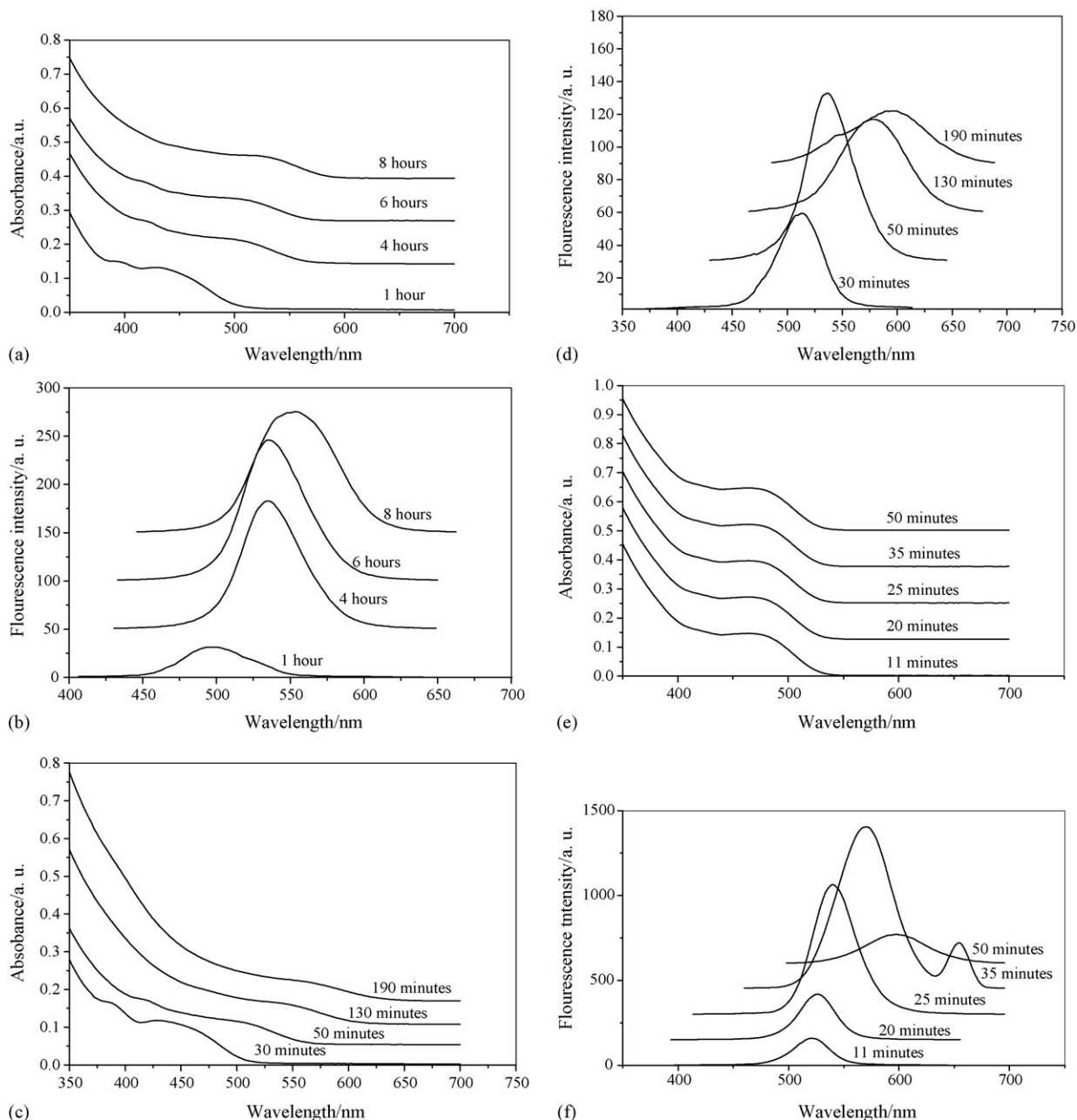


Fig. 2. Temporal evolution of absorption spectra and corresponding emission spectra of CdTe QDs synthesized at different temperatures with different heating times. 100 °C: absorption (a) and emission spectra (b); 140 °C: absorption (c) and emission spectra (d); 180 °C: absorption (e) and emission spectra (f).

Furthermore, the experimental result also suggested that as the concentration of Cd precursors was $1 \times 10^{-2} \text{ mol l}^{-1}$ or even lower, the photoluminescence intensity was enhanced sharply. Additionally, the CdTe QDs growing in sample b and sample c was out of the measurement range of the optical instrument. As a result, there were two platforms (curve b and curve c) shown in Fig. 3. In order to gain the exact maximum wavelength and be more convictive, CdTe QDs prepared in sample b solution, were diluted to the concentration of $1.25 \times 10^{-5} \text{ mol l}^{-1}$, and detected again. The result was shown in curve d. It was well-founded that with the same emission peak position ($530 \pm 2 \text{ nm}$), the same QDs' ratio (s), and the same energy of excitation, CdTe QDs growing in $1 \times 10^{-2} \text{ mol l}^{-1}$ and $5 \times 10^{-3} \text{ mol l}^{-1}$ CdTe

precursor were apparently better than that in $2 \times 10^{-2} \text{ mol l}^{-1}$ CdTe precursor.

The orange/red CdTe QDs were prepared by adjusting the concentration of CdTe precursor, too. The conditions for the CdTe QDs' synthesis and detection were the same as above, except that the excitation wavelength was 390 nm. Here, the disadvantages of the CdTe QDs growing in the precursors of lower concentration were exhibited quickly. As shown in Fig. 4, the emission wavelengths of QDs prepared in precursors sample a ($2.0 \times 10^{-2} \text{ mol l}^{-1}$), b ($1.0 \times 10^{-2} \text{ mol l}^{-1}$) and c ($5.0 \times 10^{-3} \text{ mol l}^{-1}$) were 565 nm, 576 nm, 590 nm, respectively. It can be seen that the photoluminescence intensity of CdTe QDs of growing in the precursor solution of

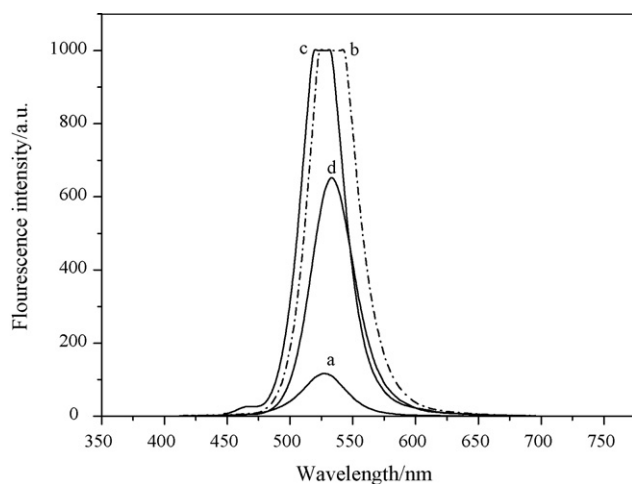


Fig. 3. Typical fluorescence emission spectra of samples a–c with the QDs concentration of $2.5 \times 10^{-5} \text{ mol l}^{-1}$ growing in sample a (a), sample b (b); sample c (c) and $1.25 \times 10^{-5} \text{ mol l}^{-1}$ growing in sample b (d). The fluorescent emission wavelength of CdTe QDs was $530 \pm 2 \text{ nm}$. An excitation wavelength of 400 nm was used.

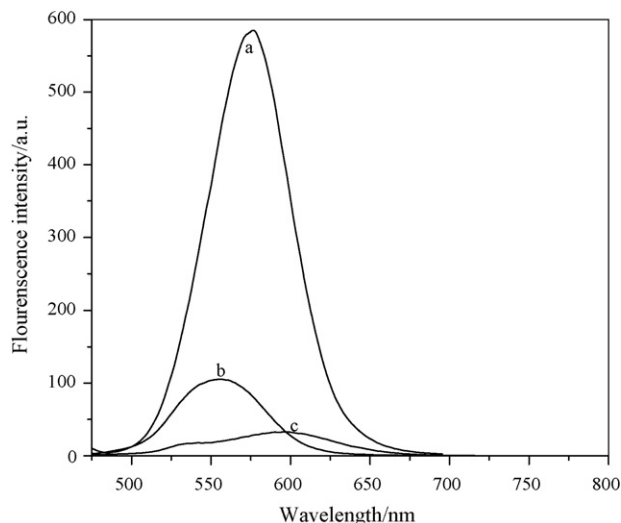
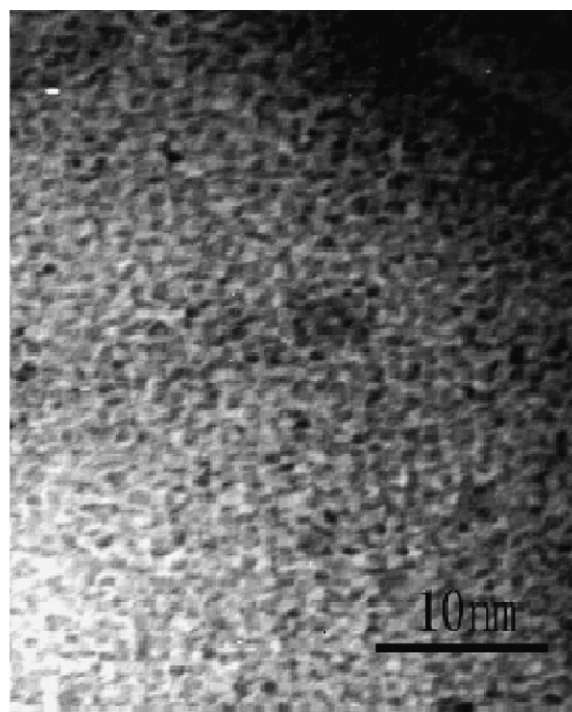


Fig. 4. Typical fluorescence emission spectra of the QDs growing in samples a–c with concentration of $2.5 \times 10^{-5} \text{ mol l}^{-1}$. The emission wavelengths were 565 nm, 576 nm, 590 nm, respectively, with the excitation wavelength of 390 nm.

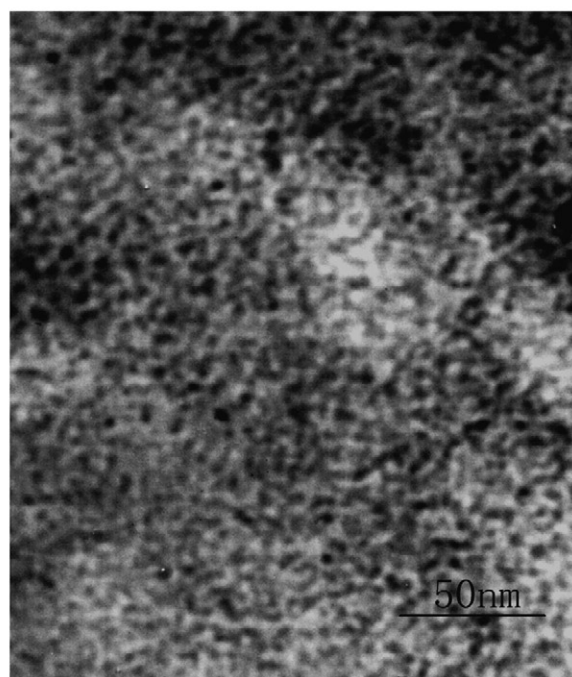
$2.0 \times 10^{-2} \text{ mol l}^{-1}$ (curve a) were better than the others (curve b and curve c). The conclusion that a relative higher concentration of CdTe precursor was more proper to the growth of CdTe QDs emitting fluorescence of longer wavelength was further proved.

3.3. TEM characterization of CdTe QDs synthesized at 140°C

The CdTe QDs synthesized at 140°C were characterized by transmission electron microscopy (TEM) as shown in Fig. 5. It was indicated that CdTe QDs, in narrow particle size distributions, were well dispersed in the solution. On average, the particle size of QDs emitting at 535 nm was $2.0 \pm 0.3 \text{ nm}$ (Fig. 5a), while that of QDs emitting at 625 nm was $6.0 \pm 0.9 \text{ nm}$ (Fig. 5b). It conformed to the previous report [8].



(a)



(b)

Fig. 5. (a) TEM images of CdTe quantum dots with emission of green fluorescence. (b) TEM images of CdTe quantum dots with emission of red fluorescence.

3.4. Characterization of the conjunction between CdTe QDs and BAS

Five kinds of as-prepared CdTe QDs in different sizes, with the highest photoluminescence intensity in each color range, were used to conjunct with BSA. Following the conjunction with BSA, all of their photoluminescence intensities were enhanced accompanying the shift of the emission peak, as shown in Fig. 6. These phenomena were ascribed to the augment of CdTe QDs'

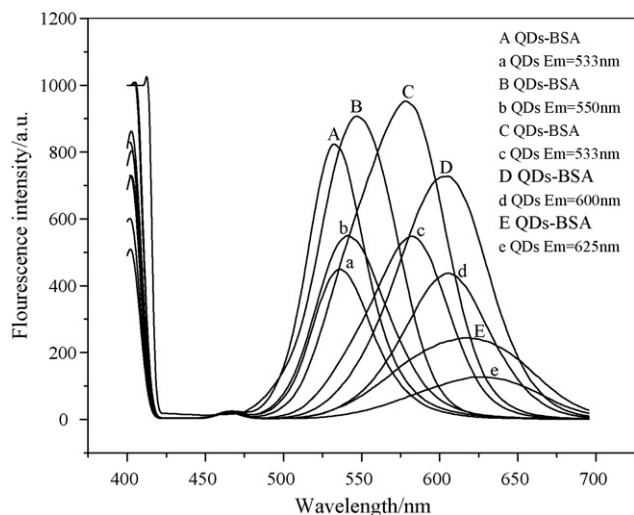


Fig. 6. Luminescence enhancing of $1.0 \times 10^{-3} \text{ mol l}^{-1}$ thiolacetic acid-stabilized CdTe QDs conjunct with BSA.

Stoke's shift, which might occur as CdTe QDs combined with BSA via electrostatic interaction [29], meanwhile the interactions of the dipole between the QDs particles were strengthened due to the reducing of the distance between the QDs particles [30]. According to previous reported results, the obvious variation of QDs suggested that the conjunction of CdTe QDs and BAS succeeded.

3.5. Doubtful points in the experiment

It had been observed that the CdTe QDs presented two peaks sporadically, such as the emission peak of CdTe QDs synthesized at 180°C with 35-min heating, as shown in Fig. 2f, a broader at lower energy and a narrower at the higher energy. The maximum wavelength of the two peaks, a broad one (lower energy emission) and a narrow one (higher energy emission), were away from about 80 nm. Moreover, as the photoluminescence intensity of the broader one decreased, the narrower one tended to be enhanced, vice versa. It may be attributed to the energy transfer between the CdTe QDs. Smaller dots, which have an electric dipole character in the excited state can transfer their excitation energy to nearby larger dots in the ground state via dipole–dipole interaction. A study on the mechanism of this phenomenon involved in the growth of CdTe QDs is undergoing.

4. Conclusions

Hydrothermal synthesis method of CdTe QDs with higher photoluminescence intensity at a relatively lower tempera-

ture (140°C) was developed. A lower concentration ($1.0 \times 10^{-2} \text{ mol l}^{-1}$ or even below) of CdTe QDs precursor provided a good condition to prepare green/yellow CdTe QDs with highly improving of its photoluminescence QY in a shorter time; it was helpful for the orange/red CdTe QDs to grow in the CdTe precursor solution of relatively higher concentration ($2.0 \times 10^{-2} \text{ mol l}^{-1}$). Furthermore, as-prepared CdTe QDs can be used as biological fluorescent probes without any other post-processing.

Acknowledgment

We are grateful for the support from Doctoral Research Found of Education Ministry of China (No. 20021045001) and National Natural Science Foundation of China (No. 20675011).

References

- [1] W. Vastarella, R. Nicastri, *Talanta* 66 (2005) 627.
- [2] Z. Ye, M. Tan, G. Wang, J. Yuan, *Talanta* 65 (2005) 206.
- [3] C. Murphy, J. Coffey, *Appl. Spectrosc.* 56 (2002) 16.
- [4] S.F. Wuister, C.M. Donega, A. Meijerink, *J. Am. Chem. Soc.* 126 (2004) 10397.
- [5] A. Watson, X. Wu, M. Bruchez, *BioTechniques* 34 (2003) 296.
- [6] M.Y. Gao, S.F. Kirstein, *J. Phys. Chem. B* 102 (1998) 8360.
- [7] H. Zhang, L.P. Wang, H.M. Xiong, et al., *Adv. Mater.* 159 (2003) 1712.
- [8] L. Li, H.F. Qian, J.C. Ren, *Chem. Commun.* (2005) 528.
- [9] M. Shingyoji, D. Gerion, D. Pintel, et al., *Talanta* 67 (2005) 472.
- [10] J. Liang, S. Huang, D. Zeng, et al., *Talanta* 69 (2006) 126.
- [11] F. Zhang, C. Li, X. Li, et al., *Talanta* 68 (2006) 1353.
- [12] E. Hao, H. Sun, Z. Zhou, et al., *Chem. Mater.* 11 (1999) 3096.
- [13] T. Rajh, O.I. Mičić, A.J. Nozik, *J. Phys. Chem.* 97 (1993) 11999.
- [14] N. Gaponik, D.V. Talapin, A.L. Rogach, et al., *J. Phys. Chem. B* 106 (2002) 7177.
- [15] L.D. Sun, X.F. Fu, C. Qian, et al., *Chem. J. Chin. Univ.* 22 (2001) 879.
- [16] J. Aldana, Y.A. Wang, X.G. Peng, *J. Am. Chem. Soc.* 12 (2001) 8844.
- [17] J.F. Weng, X.T. Song, L. Li, et al., *Talanta* 70 (2006) 397.
- [18] A.L. Rogach, A. Kornowski, M. Gao, et al., *J. Phys. Chem. B* 103 (1999) 3065.
- [19] N. Gaponik, D.V. Talapin, A.L. Rogach, et al., *J. Phys. Chem. B* 106 (2002) 7177.
- [20] J. Guo, W.L. Yang, C.C. Wang, *J. Phys. Chem. B* 109 (2005) 17467.
- [21] H. Zhang, Z. Zhou, B. Yang, et al., *J. Phys. Chem. B* 107 (2003) 8.
- [22] G.A. Crosby, J.N. Demas, *J. Phys. Chem.* 75 (1971) 991.
- [23] A.L. Rogach, L. Kataskas, A. Kornowski, et al., *J. Phys. Chem.* 100 (1996) 1772.
- [24] L. Qu, Z.A. Peng, X. Peng, et al., *Nano Lett.* 1 (2001) 333.
- [25] A.L. Rogach, D.V. Talapin, E.V. Shevchenko, et al., *Adv. Funct. Mater.* 12 (2002) 653.
- [26] D.V. Talapin, A.L. Rogach, A. Kornowski, et al., *Nano Lett.* 1 (2001) 207.
- [27] H. Zhang, L. Wang, H. Xiong, et al., *Adv. Mater.* 15 (2003) 1712.
- [28] X. Peng, *Chem. Eur. J.* 8 (2000) 334.
- [29] Z.B. Lin, S.X. Cui, H. Zhang, et al., *Anal. Biochem.* 319 (2003) 239.
- [30] Y. Wan, B.Z. Lin, Q.D. Chen, et al., *Anal. Instrum. China* 3 (2004) 41.

Simultaneous determination of three organophosphorus pesticides residues in vegetables using continuous-flow chemiluminescence with artificial neural network calibration

Baoxin Li^{*}, Yuezhen He, Chunli Xu

Department of Chemistry, School of Chemistry and Materials Science, Shaanxi Normal University, Xi'an 710062, PR China

Received 23 June 2006; received in revised form 8 October 2006; accepted 17 October 2006

Available online 20 November 2006

Abstract

In this article, a continuous-flow chemiluminescence (CL) system with artificial neural network calibration is proposed for simultaneous determination of three organophosphorus pesticides residues. This method is based on the fact that organophosphorus pesticides can be decomposed into orthophosphate with potassium peroxodisulphate as oxidant under ultraviolet radiation and that the decomposing kinetic characteristics of the organophosphorus pesticides with different molecular structure are significantly different. The produced orthophosphate can react with molybdate and vanadate to form the vanadomolybdophosphoric heteropoly acid, which can oxidize luminol to produce intense CL emission. The CL intensity of the solution was measured and recorded every 2 s in the range of 0–250 s. The obtained data were processed chemometrically by use of a three-layered feed-forward artificial neural network trained by back-propagation learning algorithm, in which input node, hidden node and output nodes were 65, 21 and 3, respectively. The proposed multi-residue analysis method was successfully applied to the simultaneous determination of the three organophosphorus pesticides residue in some vegetables samples.

© 2006 Elsevier B.V. All rights reserved.

Keywords: Chemiluminescence; Organophosphorus pesticides; Artificial neural network; Simultaneous determination

1. Introduction

Organophosphorus pesticides are essential in modern agriculture, and are now widely used to control pests and to increase harvest productivity. However, it is well known that they do have a high acute toxicity due to prevention of neural impulse transmission by their inhibition of cholinesterase [1]. Because of the potentially dangerous effects on human health, the control of pesticide residue in food is of great importance in order to minimize risk to consumers. So, the fast, reliable and economically viable methods are required for their detection in the environment and in agro-food products.

Many methods have been developed in the last few years for the determination of organophosphorus pesticides. The most widely used methods are gas chromatography (GC) [2–4], liquid chromatography (LC) [5–7] and biosensor [8–10]. The classical GC methods have not been satisfactory in general, due to the

thermal instability of the molecules of these compounds [11], and S- or P-detectors are required. In high performance liquid chromatography (HPLC), the usual UV or electrochemical detectors, which are utilized in the analysis of water samples of different origin as well as of samples from soils and oils, cannot provide enough sensitivity to detect the organophosphorus pesticides residue in the samples. Nowadays, mass spectrometry (MS) is often used as the GC and LC detector for identification and determination of mixtures of organophosphorus pesticides in the developed countries [12,13]. However, the expensive GC–MS and LC–MS instrumentation are rather few and cannot widely used for analysis of organophosphorus pesticides in the developing countries, yet the need for pesticide analysis for the developing countries is arguably even greater than that for the developed countries because agriculture production mainly concentrates in developing countries; furthermore, these chromatographical methods require trained staff, complicated sample pretreatments and are often not suitable for field analysis. The biosensor has now emerged as a popular alternative technique for organophosphorus pesticides, and most of the biosensors are based on the inhibition action of organophosphorus pesticides

^{*} Corresponding author. Tel.: +86 29 85300986; fax: +86 29 85307774.
E-mail address: libx29@hotmail.com (B. Li).

on cholinesterases, and the biosensors are rather rapid, sensitive and suitable for analysis of organophosphorus pesticides on-line and on site. However, the biosensors supply the total amount of organophosphorus pesticides in samples, and cannot distinguish the different kinds of organophosphorus pesticides; the inhibition action of every organophosphorus pesticide on the same cholinesterases is remarkably different [14], and when different organophosphorus pesticide is used as the standard solution, the amount of organophosphorus pesticides in same sample is different with such same biosensor; some heavy metal ions and proteins also inhibit the activity of cholinesterases, so the biosensor lacks enough selectivity [1]; the inhibition action of organophosphorus pesticides on cholinesterases is irreversible, so the lifetime of the biosensor is rather short and the measurement cost increases. Thus, development of reliable and fit-for-purpose methods of analysis for mixtures of organophosphorus pesticides with the use of simple and relatively inexpensive instrumentation is an appropriate objective to strive for.

Chemiluminescence (CL) has been known as a powerful and important analytical technique because the analytical performance of CL detection is better than that of other common spectroscopic detection methods (such as spectrophotometry and fluorescence), higher sensitivity, lower detection limits and wider linear ranges can be achieved with simpler and cheaper instrument (no excitation light source and no spectral resolving system) [15,16]. CL methods have been applied to the determination of pesticides [14,17]. Based on the catalytic effect of organophosphorus pesticides on the luminol–H₂O₂ CL reaction, the luminol–H₂O₂ CL system has been used for the detection of dichlorvos [18], parathion [19], monocrotophos [20] and methyl-parathion [21], respectively. So, these CL methods for organophosphorus pesticides could be applied to the single-residue samples, and the multi-residue samples could not be detected using these CL methods. Nowadays, about 36 organophosphorus pesticides are in use in China [22], and two or three organophosphorus pesticides are often simultaneously used in agriculture production. Therefore, multi-residue analysis method of organophosphorus pesticides is far more important for food safety and environmental protection.

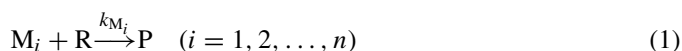
In recent years, the use of some analytical methods combined with multivariate calibration can be considered a promising, faster, direct and relatively less expensive alternative for the multicomponent analysis of mixture [23]. In this kind of situation, where the direct determination of a analyte is difficult due to the presence of one or several other constituents, instead of eliminating the interfering species, e.g. by a separation procedure, the use of multivariate calibration makes possible the quantification of these interferences along with the analyte. Artificial neural networks (ANN) based on artificial intelligence is powerful non-parametric non-linear modeling techniques [24–27]. The ANN calibration is able to acquire information and provide models even when the information and data are complex, noise contaminated, nonlinear and incomplete. They can model nonlinear systems with no prior knowledge of the system concerned or reaction order and reaction rate coefficient of the involved analytical system. This ability makes them particularly attractive for calibration in kinetic mixture

resolution [28]. Simultaneous determination of closely related species is of continuing analytical interest and methods developed for resolving them are important. Multicomponent kinetic determinations are able to resolve these systems by using differences of behavior with respect to a common reagent [29]. The kinetic methods of analysis with some advantages such as selectivity, sensitivity, and determination of species that cannot be resolved by equilibrium-based methods have been developed. These methods can be associated with ANN to resolve multicomponent kinetic systems without requiring their prior separation [30].

This paper describes a simple continuous-flow CL system combined with ANN calibration for simultaneous determination of three organophosphorus pesticides in ternary mixtures without previous separation. This method is based on the fact that organophosphorus pesticides can be decomposed into orthophosphate with potassium peroxodisulphate as oxidant under ultraviolet radiation [31] and that the decomposing kinetic characteristics of the organophosphorus pesticides with different molecular structure are significantly different. The produced orthophosphate can react with molybdate and vanadate to form the yellow vanadomolybdophosphoric heteropoly acid (the chemical formula H₄[PMo₁₁–VO₄₀].xH₂O), which can oxidize luminol to produce intense CL emission [32]. The main organophosphorus pesticides are commonly classified into P–C band organophosphorus pesticides, P–O band organophosphorus pesticides, P–S band organophosphorus pesticides and P–N band organophosphorus pesticides. In the north of China, the three organophosphorus pesticides (P–C, P–O and P–S) are widely used. So, in this paper we chose the dipterex, dichlorvos and omethoate as model molecules of P–C band organophosphorus pesticides, P–O band organophosphorus pesticides and P–S band organophosphorus pesticides, respectively. The CL intensity was measured and recorded at 2-s intervals during the reaction, and the obtained data were processed by ANN calibration. The proposed multi-residue analysis method was successfully applied to the simultaneous determination of the three organophosphorus pesticides residue in some vegetables samples.

2. Theoretical background

Assume that n analytes, M_i ($i = 1, 2, \dots, n$), react with a common reagent R to give the same product P, according to the following scheme:



If the concentration of R is much larger than that of the analytes, the reaction can be conformed to the first or pseudo-first-order kinetics [33], and thus its rate equation can be represented as

$$\frac{dC_P}{dt} = k_{1,t}C_{M_1,t} + k_{2,t}C_{M_2,t} + \dots + k_{n,t}C_{M_n,t} \quad (t = 1, 2, \dots, s) \quad (2)$$

where, $C_{M_i,t}$ is the concentration of M_i at time t , $k_{i,t}$ the rate constant of M_i , and s is the total number of time values at which measurements are made. For this CL system, the CL intensity increases during measurement time. The CL intensity (I) measurement *versus* time can be expressed as:

$$I_t = b_{1,t}C_{M_1} + b_{2,t}C_{M_2} + \cdots + b_{i,t}C_{M_i} + \cdots + b_{n,t}C_{M_n} + b_{0t} \quad (t = 1, 2, \dots, s) \quad (3)$$

where $b_{i,t}$ is the proportional coefficient for component C_{M_i} at a time t , and b_{0t} is the corresponding background. Let $C_{M_0} = 1$, and then $I_0 = b_{0,t}C_{M_0}$. Now, Eq. (3) can further be simplified as:

$$I_t = \sum_{i=0}^n b_{i,t}C_{M_i} \quad (t = 1, 2, \dots, s) \quad (4)$$

If m standard samples are prepared, Eq. (4) can be expressed in matrix form:

$$I_{m \times s} = C_{m \times (n+1)} B_{(n+1) \times s} \quad (5)$$

where the first row in matrix B represents the background vector. According to this equation it is possible to determine the component by a suitable chemometric method. In this paper, the experimental data were collected from experiments and then processed by the ANN calibration method.

3. Experiment

3.1. Chemicals and reagents

All chemicals used were of analytical grade unless stated otherwise, and the water used throughout was deionized and double distilled.

Pesticide standards including dipterex, dichlorvos and omethoate were obtained from Shaanxi Huawei Pesticide Co. Ltd. (Xi'an, China). KH_2PO_4 , $\text{Na}_2\text{B}_4\text{O}_7$, $\text{K}_2\text{S}_2\text{O}_8$, NH_4VO_3 , $(\text{NH}_4)_6\text{Mo}_7\text{O}_{24} \cdot 4\text{H}_2\text{O}$, H_2SO_4 and NaOH were obtained from Xi'an Chemical Plant (Xi'an, China). A $5 \times 10^{-2} \text{ mol l}^{-1}$ luminol stock solution was prepared by dissolving 9.32 g of luminol (Shaanxi Normal University, PR China, >95%) in 20 ml of 0.1 mol l^{-1} NaOH and then diluting to 1 l with water. The luminol solution was stored in the dark for 24 h prior to use ensure that the reagent properties had stabilized.

3.2. Apparatus and software

The continuous-flow CL system used in this work is shown in Fig. 1. There are two HL-2 type peristaltic pumps (Shanghai Huxi Analytical Instrument Plant, China): one was used to deliver the stream (sample + $\text{K}_2\text{S}_2\text{O}_8$) and the stream ($\text{NH}_4\text{VO}_3 + (\text{NH}_4)_6\text{Mo}_7\text{O}_{24} + \text{H}_2\text{SO}_4$) at a flow rate of 0.8 ml min^{-1} (per tube), and another was used to deliver the luminol stream at a flow rate of 0.8 ml min^{-1} (per tube). PTFE tubing (0.8 mm i.d.) was used as connection material in the flow system. The UV source was a rod-shaped high pressure mercury lamp (400 W, Philips) that had a major emission line at 254 nm.

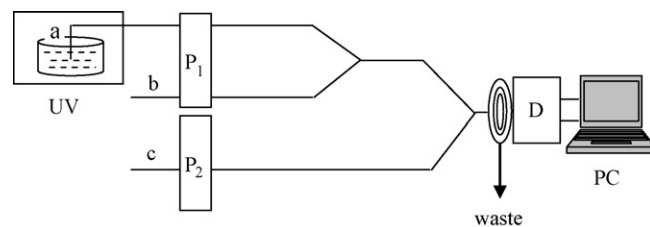


Fig. 1. Schematic diagram of continuous-flow CL system for simultaneous determination of omethoate, dichlorvos and dipterex. P₁ and P₂, peristaltic pump; UV, UV photo-reactor; D, detector; PC, personal computer; (a) pesticides + $\text{K}_2\text{S}_2\text{O}_8$; (b) $\text{NH}_4\text{VO}_3 + (\text{NH}_4)_6\text{Mo}_7\text{O}_{24}$; (c) luminol.

The photoreactor-lamp assembly was housed in a fan ventilated metal box. The flow cell is a flat spiral-coiled colorless glass tube (i.d. 1.0 mm; total diameter of the flow cell, 3 cm, without gaps between loops) and placed close to the window of the photomultiplier tuber (PMT). The CL signal produced in the flow cell was collected with a CR-105 PMT (Hamamatsu, Japan) of the ultra-weak Chemiluminescence Analyzer (Institute of Biophysics, Chinese Academy of Sciences, Beijing). The signal was recorded using an IBM-compatible computer, equipped with a data acquisition interface. Data acquisition and treatment were performed with BPCL software running under Windows 95. The data pretreatment was done with MATLAB for windows (Mathworks, version 6.1). The ANN program for calibration prediction and experimental design was written in MATLAB 6.1 according to the algorithm described by Xu et al. [34].

3.3. Procedures

Transfer 0.25 ml of 0.4 mol l^{-1} $\text{Na}_2\text{B}_4\text{O}_7$ solution and 2.50 ml of 0.1 mol l^{-1} $\text{K}_2\text{S}_2\text{O}_8$ solution into a volumetric flask with the appropriate amounts of dipterex, dichlorvos and omethoate (or the treated sample solution), and dilute to 25 ml. The mixture solution was placed in the photo-reactor. As shown in Fig. 1, flow lines were inserted into mixture solution and luminol solution, respectively. The UV lamp and the pump were started at the same time, and the decomposed pesticide stream was merged with the mixture stream ($\text{NH}_4\text{VO}_3 + (\text{NH}_4)_6\text{Mo}_7\text{O}_{24} + \text{H}_2\text{SO}_4$), and then merged with luminol stream just prior to reaching a spiral flow cell, producing CL emission. The CL intensity of the solution was recorded every 2 s in the range of 0–250 s.

4. Results and discussion

4.1. Photo-oxidation kinetics of organophosphorus pesticides

Preliminary investigations showed that the UV irradiation of solutions of dipterex, dichlorvos and omethoate in the presence of peroxydisulphate or TiO_2 led to the conversion of the organophosphorus compounds into orthophosphate, and that the photochemical reaction using peroxydisulphate as oxidant was faster possibly because the rate of homogenous reaction is higher than its of heterogeneous reaction (using TiO_2 as photo-oxidant).

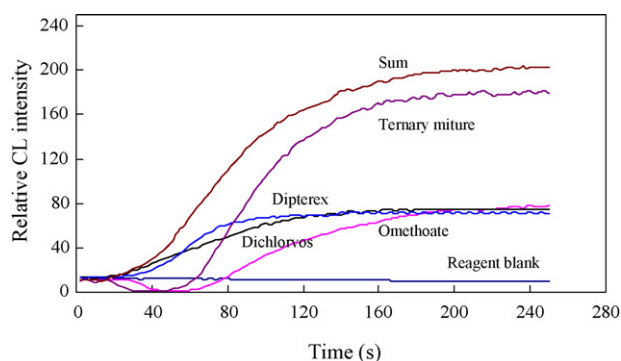


Fig. 2. Kinetic data for omethoate, dichlorvos, dipterex and the reagent blank. Omethoate, 5×10^{-7} g ml $^{-1}$; dichlorvos, 5×10^{-7} g ml $^{-1}$; dipterex, 5×10^{-7} g ml $^{-1}$; $K_2S_2O_8$, 0.05 mol l $^{-1}$; NH_4VO_3 , 4×10^{-4} g ml $^{-1}$; $(NH_4)_6Mo_7O_{24}$, 5×10^{-4} mol l $^{-1}$; H_2SO_4 , 0.01 mol l $^{-1}$; luminol, 5×10^{-4} mol l $^{-1}$; NaOH, 0.06 mol l $^{-1}$.

So, we chose peroxydisulphate as the oxidant. The strong acid or alkaline peroxydisulphate solution was suitable for decomposing organophosphorus compound, but problem arose with the use of peroxydisulphate in acid medium due to the noise caused by gas bubbling generated within sample solution. Alkaline $K_2S_2O_8$ has the advantage that the CO_2 generated by the photo-oxidation of the organophosphorus pesticide is predominantly in the carbonate form and hence problem of bubble is resolved. Sodium tetrahydroborate was selected as photo-oxidation media.

In this system, organophosphorus pesticide is photodegraded quantitatively to PO_4^{3-} , and the produced PO_4^{3-} can react with molybdate and vanadate to form the yellow vanadomolybdophosphoric heteropoly acid, which can oxidize luminol to produce intense CL emission. So, the CL signal of the luminol system can be used to character the process of the photodegradation reaction. Fig. 2 shows the kinetic of the reaction of each of the three pesticides in the presence of excess amounts of other reagents (such as $K_2S_2O_8$ and luminol). The experimental results showed that the reaction rates of the three pesticides were different. In addition, it can also be seen that the intensity response of the ternary mixture of the pesticides is lower than the sum of the intensities recorded for each individual pesticide, probably because of the synergy action of

the three pesticides in the photo-reaction. This observed difference in the kinetic behavior of the three pesticides result form the difference of their molecule structures (Table 1). The order of photo-degradation rate of the three pesticides was dipterex > dichlorvos > omethoate. For omethoate, almost no CL signal was detected at beginning of degradation (0–60 s), possibly because omethoate could not directly transform to orthophosphate, and omethoate would firstly transform to one intermediate, which could not react with molybdate and vanadate to form the vanadomolybdophosphoric heteropoly acid to oxidize luminol, producing CL emission. The different reaction rates in the photo-degradation reaction with $K_2S_2O_8$ provide the possibility for resolving their mixtures and enabling their quantitative analysis. In this system, we chose the ANN calibration for simultaneous determination of the three organophosphorus pesticides.

4.2. Optimization of the photo-reaction conditions

In this system, $K_2S_2O_8$ is oxidant in the photo-degradation of the organophosphorus pesticides, and the concentration of $K_2S_2O_8$ affects the redox reaction. At first, the concentration of $K_2S_2O_8$ must be much more than that of pesticides in order that the reaction can be conformed to the first or pseudo-first-order kinetics. The results showed that the CL intensity increased with increasing $K_2S_2O_8$ concentration, and at the $K_2S_2O_8$ concentration of 0.01 mol l $^{-1}$, there is a relatively high CL intensity of three pesticides. Thus, a $K_2S_2O_8$ concentration of 0.01 mol l $^{-1}$ was selected for simultaneous determination of dipterex, dichlorvos and omethoate. In this photo-reaction, $Na_2B_4O_7$ is the media [31], so the effect of $Na_2B_4O_7$ concentration on the CL intensity was also investigated. It was found that the optimal concentration of was 0.004 mol l $^{-1}$. Therefore, 0.004 mol l $^{-1}$ $Na_2B_4O_7$ was chosen as the reaction media (the pH was about 10.3) in this photo-reaction.

4.3. Optimization of forming condition of vanadomolybdophosphoric heteropoly acid

The concentrations of ammonium molybdate, ammonium vanadate and H_2SO_4 affect the form ratio of vanadomolyb-

Table 1
Chemical structure of the three organophosphorus pesticides

Pesticides	Molecular formula	Structure
Omethoate (OME)	$C_5H_{12}O_4NSP$	
Dichlorvos (DIC)	$C_4H_7O_4PCl_2$	
Dipterex (DIP)	$C_4H_8O_4PCl_3$	

Table 2
Concentration data for different mixtures used for calibration of omethoate, dichlorvos and dipterex

Mixture	Omethoate ($\times 10^{-7}$ g ml $^{-1}$)	Dichlorvos ($\times 10^{-7}$ g ml $^{-1}$)	Dipterex ($\times 10^{-7}$ g ml $^{-1}$)
1	0.83	0.77	0.60
2	0.83	1.82	1.54
3	0.83	5.67	3.95
4	0.83	9.36	8.82
5	1.76	0.77	1.54
6	1.76	1.82	0.60
7	1.76	5.67	8.82
8	1.76	9.36	3.95
9	4.25	0.77	3.95
10	4.25	1.82	8.82
11	4.25	5.67	0.60
12	4.25	9.36	1.54
13	11.80	0.77	8.82
14	11.80	1.82	3.95
15	11.80	5.67	1.54
16	11.80	9.36	0.60

dophosphoric heteropoly acid, on which the oxidation activity of vanadomolybdophosphoric heteropoly acid depends. So the effect of ammonium molybdate concentration was studied over 5×10^{-5} to 1×10^{-3} mol l $^{-1}$. The results showed that the CL response increased up to 7×10^{-4} mol l $^{-1}$ ammonium molybdate, above which the response decreased due to a low acid/molybdate ration [35]. At the same time, the effect of NH₄VO₃ concentration and H₂SO₄ concentration on the CL intensity, and the experimental results showed that the optimal concentrations of NH₄VO₃ and H₂SO₄ were 0.043 and 0.01 mol l $^{-1}$, respectively.

4.4. Optimization of CL reaction condition

As the luminescence reagent in this system, the luminol concentration affects the response. The effect of luminol concentration on the determination of the pesticides was studied over the range 1×10^{-5} to 4×10^{-3} mol l $^{-1}$. The results showed that the CL intensity increased from 1×10^{-5} to 5×10^{-4} mol l $^{-1}$, but no appreciable increase in CL intensity was observed above this concentration due to saturation. A luminol concentration of 5×10^{-4} mol l $^{-1}$ was therefore used for all subsequent experiments. The CL response varied with the age of the luminol solution [36] and therefore it was always prepared 24 h before use.

Luminol chemiluminescence is particularly dependent on the reaction pH [37]. In view of the nature of luminol CL reaction, which is more favoured under basic conditions, an alkaline medium was introduced to improve the sensitivity of the system. Several medium solutions such as NaOH, NaHCO₃–Na₂CO₃, Na₂B₄O₇–NaOH and NH₃–NH₄Cl were studied. The result showed that the strong and stable CL signal was obtained in the NaOH. In the experiments, the alkalinity of the reaction medium was adjusted by preparing luminol with a suitable concentration of sodium hydroxide. The effect of NaOH concentration was also studied in the range 0.02–0.12 mol l $^{-1}$. It was found that 0.07 mol l $^{-1}$ NaOH was optimum reaction media and chosen for further work. In this system, vanadomolybdophosphoric

heteropoly acid formed in 0.01 mol l $^{-1}$ H₂SO₄ media, so some NaOH was first needed to neutralize the acid, resulting in higher concentration NaOH in this system.

4.5. Multivariate calibration

Multivariate calibration methods such as ANN require a suitable experimental design of the standard belong to the calibration set in order to provide good prediction. Two sets of standard solutions were prepared as calibration set and prediction set. The former was used to train the network and the latter was used to validate the learned network. Base on our primary experiment, the CL intensity versus the pesticides concentration was linear in the range 1×10^{-8} to 5×10^{-6} g ml $^{-1}$. The calibration set consisting of 16 standards with different concentrations of omethoate, dichlorvos and dipterex was used. Their concentrations are shown in Table 2. For prediction set, 12 test mixtures in Table 4 were used, and the concentration of the three pesticides solution covered the whole concentration range of the three pesticides in calibration set. The CL intensity of each ternary mixture solution was detected every 2 s from 0 to 250 s. An experimental calibration data matrix with 16 by 125 was prepared.

The kinetic data were processed by ANN, which was trained with the back-propagation of errors learning algorithm. Its basic theory and application to chemical problems can be found in the literature [38]. The neural network performs a non-linear iterative fit of data. The structure of the network is comprised of three node layers: an input layer, a hidden layer and output layer. The node in the input layer transferred the input data to all nodes in the hidden layer. These nodes calculate a weighted sum of the inputs that is subsequently subjected to a non-linear transformation:

$$O_j = f \left(\sum_{i=1}^l s_i w_{ij} \right) \quad (6)$$

where s_i is the input to the node i in the input layer, l the number of nodes in the input layer, w_{ij} (weights) are the connection

Table 3
Statistical data for the optimization matrix using the ANN model

Item	Value
Input nodes	65
Hidden nodes	21
Output nodes	3
Number of iterations	5500
Hidden layer transfer function	Sigmoid
Output layer transfer function	Purelin

between each node i in the input layer and each node j in the hidden layer, O_j the output of node j in the hidden layer, and f is a non-linear function. The output of the network is a weighted sum of the outputs of the hidden layer and it is the calculated concentration. During training (calibration) of the network, the weights are iteratively calculated in order to minimize the sum of the squared difference between the known concentration and the calculated concentration. Overfitting is avoided by using two sample sets; thus weights are calculated from a calibration set while the concentration of another sample set (the test set) is being simultaneously predicted. In addition, the number of the data values used for training must exceed that of weights determined in the network; this entails using a large number of samples for calibration if the number of input variables is also large. In this work, the CL intensity data *versus* the time were centred and normalized with pressed function in MATLAB as the input for ANN, and the output of the network were the calculated concentrations related to the CL intensity data.

For the optimized model, three parameters were selected to test the prediction ability of the chemometric model for each component. The root mean square difference (RMSD), the square of the correlation coefficient (R^2) and the relative error of prediction (REP), which can be calculated for each component as:

$$\text{RMSD} = \left[\frac{1}{n} \sum_{i=1}^n (\hat{c}_i - c_i)^2 \right]^{0.5} \quad (7)$$

Table 4
Prediction results for synthetic mixtures of omethoate, dichlorvos and dipterox

Synthetic mixture	OME ($\times 10^{-7}$ g ml $^{-1}$)		DIC ($\times 10^{-7}$ g ml $^{-1}$)		DIP ($\times 10^{-7}$ g ml $^{-1}$)	
	Added	Found	Added	Found	Added	Found
1	0.91	0.91	0.73	0.75	0.68	0.70
2	0.91	0.89	2.00	1.89	1.86	1.95
3	0.91	0.82	8.70	8.51	7.90	7.76
4	1.62	1.59	0.73	0.71	1.86	1.78
5	1.62	1.53	4.90	5.04	7.90	8.12
6	1.62	1.54	8.70	8.87	4.15	3.98
7	3.75	3.66	2.00	2.08	4.15	4.26
8	3.75	3.60	4.90	5.12	0.68	0.63
9	3.75	3.89	8.70	8.53	1.86	1.76
10	9.50	9.23	0.73	0.76	7.90	7.63
11	9.50	9.63	2.00	1.92	4.15	4.32
12	9.50	9.37	4.90	4.71	0.68	0.68
RMSD		0.1227		0.1368		0.1405
R^2		0.9995		0.9989		0.9987
REP (%)		3.110		3.3509		3.8519

$$R^2 = \frac{\sum_{i=1}^n (\hat{c}_i - \bar{c}_i)^2}{\sum_{i=1}^n (c_i - \bar{c}_i)^2} \quad (8)$$

$$\text{REP}(\%) = \left(\frac{100}{\bar{c}_i} \right) \left[\frac{1}{n} \sum_{i=1}^n (\hat{c}_i - c_i)^2 \right]^{0.5} \quad (9)$$

where c_i is the true concentration of the analyte in the sample i , \hat{c}_i represented the estimated concentration of the analyte in the sample i , \bar{c}_i the mean of the true concentration in the prediction set, and n is the total number of sample used in the prediction set.

To enhance the prediction ability of ANN, neural network models were optimized. Function sigmoid hidden layer functions that can be used to model a variety of relationships were found to be optimum for calculation. The different number of input nodes was changed to sieve the data. The result showed that the relative errors of both calibration set and prediction set gradually decreased when the number of input nodes was increased. When the number of input nodes was 65, the network had the highest degree of approximation. When the number of input nodes exceeded 65, the relative standard error of the calibration set decreased and that of the prediction set increased. Thus the degree of approximation evidently decreased. This result indicates an overfitting phenomenon is affecting the network. Because there are three kinds of pesticides in sample, the output layer contained three neurons. The number of hidden nodes also has great effect on the predictive result. The proper number of nodes in the hidden layer was determined by training ANN with different numbers of nodes in the hidden layer. A minimum in RMSE occurred when 21 nodes were used in the hidden layer. Continued training beyond 5500 iterations frequently resulted in a slight increase in error of prediction as the learning iteration increased whereas the error of calibration leveled off or continued to increase slightly. The construction of these ANN models is summarized in Table 3.

From the CL intensity data of the calibration sets of the above mixtures, whose concentrations were selected randomly,

Table 5
Determination results of organophosphorous pesticides residues in vegetable samples

Sample ^a	Found ($\times 10^{-7}$ g ml ⁻¹) original sample			Added ($\times 10^{-7}$ g ml ⁻¹) addition			Found ($\times 10^{-7}$ g ml ⁻¹) addition			Recovery (%)		
	OME	DIC	DIP	OME	DIC	DIP	OME	DIC	DIP	OME	DIC	DIP
Lettuce												
1 [#]	9.4	7.7	10.5	5.0	5.0	5.0	4.6	5.2	5.0	92	104	100
2 [#]	1.1	4.1	4.8	3.0	3.0	3.0	2.8	2.9	3.2	93	97	107
3 [#]	0.4	1.7	2.0	1.5	1.5	1.5	1.6	1.6	1.5	107	107	100
Rape												
1 [#]	15.3	7.1	5.5	5.0	5.0	5.0	5.3	5.1	4.9	106	102	98
2 [#]	2.5	4.2	2.3	3.0	3.0	3.0	3.3	3.1	3.3	110	103	110
3 [#]	0.9	2.6	0.6	1.5	1.5	1.5	1.4	1.7	1.5	93	113	100
Spinach												
1 [#]	14.6	33.6	13.9	5.0	5.0	5.0	4.8	4.9	5.2	96	98	104
2 [#]	2.7	4.7	1.7	3.0	3.0	3.0	2.8	2.8	2.6	93	93	87
3 [#]	0.7	1.9	0.4	1.5	1.5	1.5	1.6	1.4	1.5	107	93	100
Leek												
1 [#]	18.6	24.7	41.9	5.0	5.0	5.0	5.4	5.1	5.2	108	102	104
2 [#]	3.3	2.1	7.3	3.0	3.0	3.0	3.1	3.2	3.3	103	107	110
3 [#]	1.2	0.4	1.6	1.5	1.5	1.5	1.7	1.6	1.4	113	107	93

^a 1[#], the first eluted solution; 2[#], the second eluted solution; 3[#], the third eluted solution.

the ANN model was optimized and the data of the prediction sets were used to evaluate the performance of the resulting ANN model. The prediction, RMSD, REP, and R^2 are summarized in Table 4. The obtained values of the statistical parameters show the ability of the chosen method for simultaneous determination of analytes.

4.6. Interference studies

The interference of foreign substances was tested by analyzing a standard mixture solution of 1×10^{-7} g ml⁻¹ omethoate, 1×10^{-7} g ml⁻¹ dichlorvos and 1×10^{-7} g ml⁻¹ dipterex. The tolerable concentration ratios for interference at the 5% level were over 1000 for Na⁺, Ca²⁺, K⁺, Mn²⁺, Cl⁻, SO₄²⁻, CO₃²⁻ and NO₃⁻; 100 for Ba²⁺, Pb²⁺, Mg²⁺, Al³⁺ and Zn²⁺; 5 for Cu²⁺, Fe³⁺, Cr³⁺, Co²⁺ and Ni²⁺; and 1 for PO₄³⁻. In this system, some substances with strong reducing property (such as ascorbic acid and SO₃²⁻) did not cause interference because in the photo-oxidation these substances would be oxidized. Although some ions (such as Cu²⁺, Fe³⁺, Cr³⁺, Co²⁺, Ni²⁺, PO₄³⁻) caused interference severely, it could be easily discriminated by the cation-exchange and anion-exchange resins.

4.7. Application of the model to determination of the three pesticides in vegetable sample

Some fresh commercial vegetable samples obtained from a supermarket in Xi'an were free from pesticides. About 2 ml mixture standard solution of 1×10^{-3} g ml⁻¹ omethoate, 1×10^{-3} g ml⁻¹ dichlorvos and 1×10^{-3} g ml⁻¹ dipterex was sprayed on the surface of about 50 g each samples, and the treated vegetables were placed at ventilation cabinet for 2 h at 25 °C. Then the each of vegetables was immersed in 50 ml water to wash the pesticides for 5 min, and the first eluted solution were collected and measured. At last, each of vegetables

samples was again eluted two times using 50 ml water, and the second eluted solution and the third eluted solution were collected and measured, respectively. In order to evaluate the validity of the proposed method for the simultaneous determination of omethoate, dichlorvos and dipterex, recovery studies were carried out on the eluted solutions to which known amounts of omethoate, dichlorvos and dipterex were added. The results are given in Table 5.

5. Conclusions

In this paper, the continuous-flow CL system combined with artificial neural network calibration was successfully applied to simultaneous determination of omethoate, dichlorvos and dipterex in the vegetable samples without any prior separation. The detection limit of the proposed method was less than 1×10^{-8} g ml⁻¹ for the pesticides. Compared with the reported multi-residue analysis methods of organophosphorus pesticides (such as CG and LC), this method offers the potential advantages of high sensitivity, simplicity and rapidity for multi-residue analysis of organophosphorus pesticides. Furthermore, this paper shows the possibilities of the combination of ANN calibration and CL method, and it shows a guide that the CL method is used to synchronously determinate multi-analytes in one sample.

Acknowledgements

This study was supported by the National Natural Science Foundation of China (Grant No. 20405009) and by the Program for New Century Excellent Talents in University.

References

- [1] L. Wang, L. Zhang, H. Chen, Prog. Chem. 18 (2006) 440.
- [2] F. Ahmadi, Y. Assadi, S.M.R. Milani Hosseini, M. Rezaee, J. Chromatogr. A 1101 (2006) 307.

- [3] Q. Xiao, B. Hu, C. Yu, L. Xia, Z. Jiang, *Talanta* 69 (2006) 848.
- [4] D.H. Kim, G.S. Heo, D.W. Lee, *J. Chromatogr. A* 824 (1998) 63.
- [5] X. Zhu, J. Yang, Q. Su, J. Cai, Y. Gao, *J. Chromatogr. A* 1092 (2005) 161.
- [6] T. Pérez-Ruiz, C. Martínez-Lozano, V. Tomás, J. Martín, *Anal. Chim. Acta* 540 (2005) 383.
- [7] C.P. Sanz, R. Halko, Z.S. Ferrera, J.J.S. Rodríguez, *Anal. Chim. Acta* 524 (2004) 265.
- [8] V.B. Kandimalla, H. Ju, *Chem. Eur. J.* 12 (2006) 1074.
- [9] J.M. Abad, F. Pariente, L. Hernández, H.D. Abruña, E. Lorenzo, *Anal. Chem.* 70 (1998) 807.
- [10] M. Shi, J. Xu, S. Zhang, B. Liu, J. Kong, *Talanta* 68 (2006) 1089.
- [11] E.D. Magallona, *Res. Rev.* 56 (1975) 1.
- [12] P.-S. Chen, S.-D. Huang, *Talanta* 69 (2006) 669.
- [13] S. Dulaurent, F. Saint-Marcoux, P. Marquet, G. Lachâtre, *J. Chromatogr. B* 831 (2006) 223.
- [14] P. Moris, I. Alexandre, M. Roger, J. Remacle, *Anal. Chim. Acta* 302 (1995) 53.
- [15] B. Li, D. Wang, J. Lv, Z. Zhang, *Talanta* 69 (2006) 160.
- [16] B. Li, Z. Zhang, Y. Jin, *Anal. Chem.* 73 (2001) 1203.
- [17] L. Gámiz-Gracia, A.M. García-Campaña, J.J. Soto-Chinchilla, J.F. Huertas-Pérez, A. González-Casado, *Trends Anal. Chem.* 24 (2005) 927.
- [18] J. Wang, C. Zhang, H. Wang, F. Yang, X. Zhang, *Talanta* 54 (2001) 1185.
- [19] X. Liu, J. Du, J. Lv, *Luminescence* 18 (2003) 245.
- [20] J. Du, X. Liu, J. Lv, *Anal. Lett.* 36 (2003) 1209.
- [21] Z. Rao, J. Wang, L. Li, X. Zhang, *Chin. J. Anal. Chem.* 29 (2001) 373.
- [22] *Encyclopedia of Chinese Chemical Products*, Chemical Industry Press, Beijing, 2005.
- [23] G.M. Escandar, P.C. Damiani, H.C. Goicoechea, A.C. Olivieri, *Mirochem. J.* 82 (2006) 29.
- [24] A.A. Ensañi, T. Khayanmian, A. Benvidi, E. Mirmomtaz, *Anal. Chim. Acta* 561 (2006) 225.
- [25] B. Li, Y. He, J. Lv, Z. Zhang, *Anal. Bioanal. Chem.* 383 (2005) 817.
- [26] K. Petritis, L.J. Kangas, P.L. Ferguson, G.A. Anderson, L. Psa-Yoli, M.S. Lipton, K.J. Auberry, E.F. Strittmatter, Y. Shao, R. Zhao, R.D. Smith, *Anal. Chem.* 75 (2003) 1039.
- [27] Y. Ni, G. Zhang, S. Kokot, *Food Chem.* 89 (2005) 465.
- [28] S. Ventura, M. Silva, D. Pérez-Bendito, *Anal. Chem.* 67 (1995) 4458.
- [29] B.M. Quencer, S.R. Crouch, *Crit. Rev. Anal. Chem.* 24 (1993) 243.
- [30] Safavi, O. Moradlou, S. Maesum, *Talanta* 62 (2004) 51.
- [31] T. Pérez-Ruiz, C. Martínez-Lozano, V. Tomás, J. Martín, *Anal. Chim. Acta* 442 (2001) 147.
- [32] O.V. Zui, J.W. Birks, *Anal. Chem.* 72 (2000) 1699.
- [33] R.J. Garmon, C.N. Reilley, *Anal. Chem.* 34 (1962) 600.
- [34] D. Xu, Z. Wu, *System Analysis and Design based on Matlab 6X-Neural Network*, Xidian University Press, Xi'an, 2003.
- [35] J.Z. Zhang, C.J. Fischer, P.B. Ortner, *Talanta* 49 (1999) 293.
- [36] W.D. King, H.A. Lounsbury, F.J. Millero, *Environ. Sci. Technol.* 29 (1995) 818.
- [37] K. Robards, P.J. Worsfold, *Anal. Chim. Acta* 266 (1992) 147.
- [38] J. Zupan, J. Gasteiger, *Anal. Chim. Acta* 248 (1991) 1.

Short communication

Characterization of different diamond-like carbon electrodes for biosensor design

R. Maalouf^{a,b,c}, H. Chebib^b, Y. Saikali^b, O. Vittori^c, M. Sigaud^c,
F. Garrelie^d, C. Donnet^d, N. Jaffrezic-Renault^{a,*}

^a Center of Electrical Engineering of Lyon, CEGELY, UMR/CNRS 5005, Ecole Centrale Lyon, 69134 Ecully Cedex, France

^b Laboratory of Chemistry, Lebanese University, Fanar, Beirut, Lebanon

^c Laboratory of Analytical Electrochemistry, Claude Bernard University, Lyon I, 43 Boulevard du 11 Novembre 1918, Villeurbanne Cedex, France

^d Laboratory of Signal Processing and Instrumentation, UMR/CNRS 5516, Jean Monnet University, Saint Etienne, France

Received 6 April 2006; received in revised form 18 October 2006; accepted 19 October 2006

Available online 4 December 2006

Abstract

Diamond-like carbon (DLC) films are gaining big interest in electrochemistry research area. DLC electrodes made with different ratio of sp^3/sp^2 carbon hybridization or doped with different percentages of nickel were characterized electrochemically by cyclic voltammetry and by amperometric measurements towards hydrogen peroxide. SiCAr1 and SiCNi5% were chosen as sensitive transducers for the elaboration of amperometric glucose biosensors. Immobilization of glucose oxidase was carried out by cross-linking with glutaraldehyde. Measurements were made at a fixed potential +1.0 V in 40 mM phosphate buffer pH 7.4. SiCAr1 seems to be more sensitive for glucose, 0.6875 $\mu A/mM$, than SiCNi5%, 0.3654 $\mu A/mM$. Detection limits were 20 μM and 30 μM , respectively. Apparent Michaelis-Menten constants were found around 3 mM. Forty-eight percent and 79% of the original response for 0.5 mM glucose remained after 10 days for both biosensors, respectively. © 2006 Elsevier B.V. All rights reserved.

Keywords: Diamond-like carbon; Biosensors; Glucose oxidase; Amperometric measurements

1. Introduction

Biosensors, combining a selective biological recognition element and a sensitive transducer, are of increasing importance in many areas such as medicine, food quality and safety control, and environmental pollution monitoring. Amperometric enzyme electrodes hold a leading position among biosensor systems presently available and have already found a large commercial market. The most common enzymes used in monoenzymatic systems are oxidases; especially glucose oxidase due to its low price and high stability. Such devices combine the specificity of the enzyme for recognizing a given target analyte, whilst their sensitivity is greatly influenced by the transducer [1–3]. The most employed electrochemical transducers are platinum, gold and carbonaceous materials [4,5]. Carbon electrodes exist in different allotropes and they are widely used in the field of

biosensors. Glassy carbon (GC) electrodes are often used as transducers [6–8] by employing a modified GC electrode or by changing the methods of enzyme immobilisation in the aim to get sensitive, stable and reproducible biosensor. Graphite, porous carbon [9] and carbon films [10,11] electrodes are also used as transducers in the field of biosensors.

Diamond-like carbon films are gaining now big interest. These films are chemically stable, optically transparent and achieve good mechanical properties, low coefficient of friction, and strong wear resistance. Due to these properties, DLC films found application in variety of areas such as electronic, optical, mechanical and biomedical applications. Pulsed laser deposition of diamond-like carbon leads to high purity films with a predominance of sp^3 hybridization (diamond) at low deposition temperature. Since the last ten years, femtosecond lasers have been used in pulsed laser deposition. In this case, the kinetic energy of the ejected particles can be increased up to a few keV, which is much higher than in nanosecond regime. Original properties of these coatings, including lower stress and good adherence, may be related to such a

* Corresponding author. Tel.: +33 4 72 18 62 43; fax: +33 4 78 43 37 17.
E-mail address: Nicole.Jaffrezic@ec-lyon.fr (N. Jaffrezic-Renault).

high value of the kinetic energy. These advantages allow the development of DLC coatings without any adhesion underlayer [12].

Diamond-like-carbon films constitute a new research area in electrochemistry. They have been used as electrodes in electrochemical microgravimetry on quartz crystal electrodes [13], as nitrogenated DLC films (N:DLC) for metal tracing analysis [14] and as coatings for polycarbonate membranes used as permselective barriers in glucose oxidase biosensors [15,16]. We have tested amorphous DLC electrodes in a preliminary work for the development of a glucose amperometric biosensor. It can be seen that DLC films can be used as transducers in the field of biosensors nevertheless they are less sensitive than glucose oxidase/glassy carbon electrodes [17]. Properties of DLC films can be adjusted depending on their application. Thus, the sp^3/sp^2 carbon hybridization ratio may be adjusted and controlled according to the deposition process and conditions. Their conductivity also can be controlled by doping elements such as metals, Si and N.

The present study deals with characterization and the comparison of different diamond-like carbon films as matrices for biosensor design. Some of these films are elaborated with different ratio of sp^3/sp^2 carbon hybridization and others are doped with Ni. Cyclic voltammetry and amperometric measurements aim to see whether properties of DLC films affect their sensitivities towards hydrogen peroxide. The behavior of the most sensitive electrodes for H_2O_2 will be studied for biosensor elaboration by using a conventional glucose oxidase assay system.

2. Experimental

2.1. Materials

Glucose Oxidase (GOD, EC 1.1.3.4, 130 U/mg) was kindly given by the Laboratory of Biomolecular Electronics, IMBG, Kiev, Ukraine. Bovine Serum Albumin (BSA, Fraction V) and α -D(+)-glucose were obtained from Sigma. Glutaraldehyde, 24-wt.% solution in water, was purchased from Acros Organics. Hydrogen peroxide 30% and chemicals used for preparing buffer solution, sodium hydroxide and potassium dihydrogen phosphate were obtained, respectively, from Fluka, Sigma and Prolabo. Glucose standard solutions were elaborated by diluting a 1 M α -D(+)-glucose stock solution prepared 24 h before use to establish the anomeric equilibrium between α and β forms of D-glucose. Ultra-pure water (resistivity > 18.2 M Ω cm, Elga System) was used for the preparation of all solutions.

2.2. Measurements and apparatus

Voltammetric and amperometric experiments were carried out using a Voltalab 10 (PGZ100 & VoltaMaster 4). The electrochemical cell consisted of a three-electrode system with a platinum plate (0.54 cm²) and a saturated calomel electrode (SCE) as counter and reference electrode, respectively. Diamond-like carbon electrodes with an effective surface of 0.15 cm² were used as working electrodes. A magnetic

stirred and a stirring bar provide the convective transport. All potentials were reported versus SCE. The background current was allowed to decay to a steady value before aliquots of substrate solution were added. The biosensor response was measured as the difference between total and residual current.

2.3. Diamond-like carbon films deposition

These films were prepared by the Laboratory of Signal Processing and Instrumentation, Jean Monnet-University, France. Nickel containing DLC films have been deposited by femtosecond pulsed laser deposition by ablating alternatively graphite (purity 99.997%) and nickel (purity 99.9%) targets under vacuum conditions at room temperature onto p-silicon substrates at a target to substrate distance of 36 mm. The femtosecond laser (Concerto, BMI/TCL, Ti-Saphir, $\lambda = 800$ nm, pulse duration 300–350 fs, repetition rate 1 kHz, energy per pulse 1 mJ, energy density 2.6 J/m²) has been alternatively focused on the targets with an incident angle of 45°, by using a shutter rotating at 32 rpm.

Two percentages of nickel have been introduced in diamond-like carbon films according to the conditions mentioned below. For the first sample, six sequences of ablation on each target have been performed alternatively during 89 s for graphite and 1 s for nickel. A similar procedure has been carried out for the second sample, with 16 sequences of ablation on each target during 32 s for graphite and 1 s for the nickel. Taking into account the deposition rate of pure carbon (22 nm/min) and pure nickel (35 nm/min), nickel incorporated DLC film thickness is estimated in the range of 200 nm for both samples. Percentages of nickel in diamond-like carbon films have been determined by X-ray photoelectron spectroscopy (XPS) and Rutherford backscattering spectroscopy (RBS). They showed 2 at.% for the first sample (SiCNi2%) and 5 at.% for the second one (SiCNi5%) [14].

Three other types of DLC films have been elaborated by femtosecond pulsed laser ablation onto p-silicon substrates under argon pressure at room temperature. Normally DLC films made under vacuum show a predominance of sp^3 hybridized carbon [15]. Thus, working under argon pressure and modifying this pressure leads to DLC films with different ratio of sp^3/sp^2 carbon hybridization. $P_{Ar} = 2 \times 10^{-2}$ mbar (SiCAr1), $P_{Ar} = 5 \times 10^{-1}$ mbar (SiCAr2) and $P_{Ar} = 5 \times 10^{-3}$ mbar (SiCAr3) were used, respectively, for the deposition of DLC films by ablation graphite target during 10 min.

All diamond-like-carbon electrodes cited below were cleaned with ultra-pure water and with optical paper before use.

2.4. Enzyme immobilization

Immobilization was carried out by cross-linking with glutaraldehyde. Thus, a mixture of 5% glucose oxidase, 5% BSA and 10% glycerol in phosphate buffer 20 mM pH 7.4 was prepared. The glycerol was used as a plasticizer in order to avoid cracks appearing in the biolayer. DLC electrodes were coated with a thin layer of this mixture and kept 20 min in

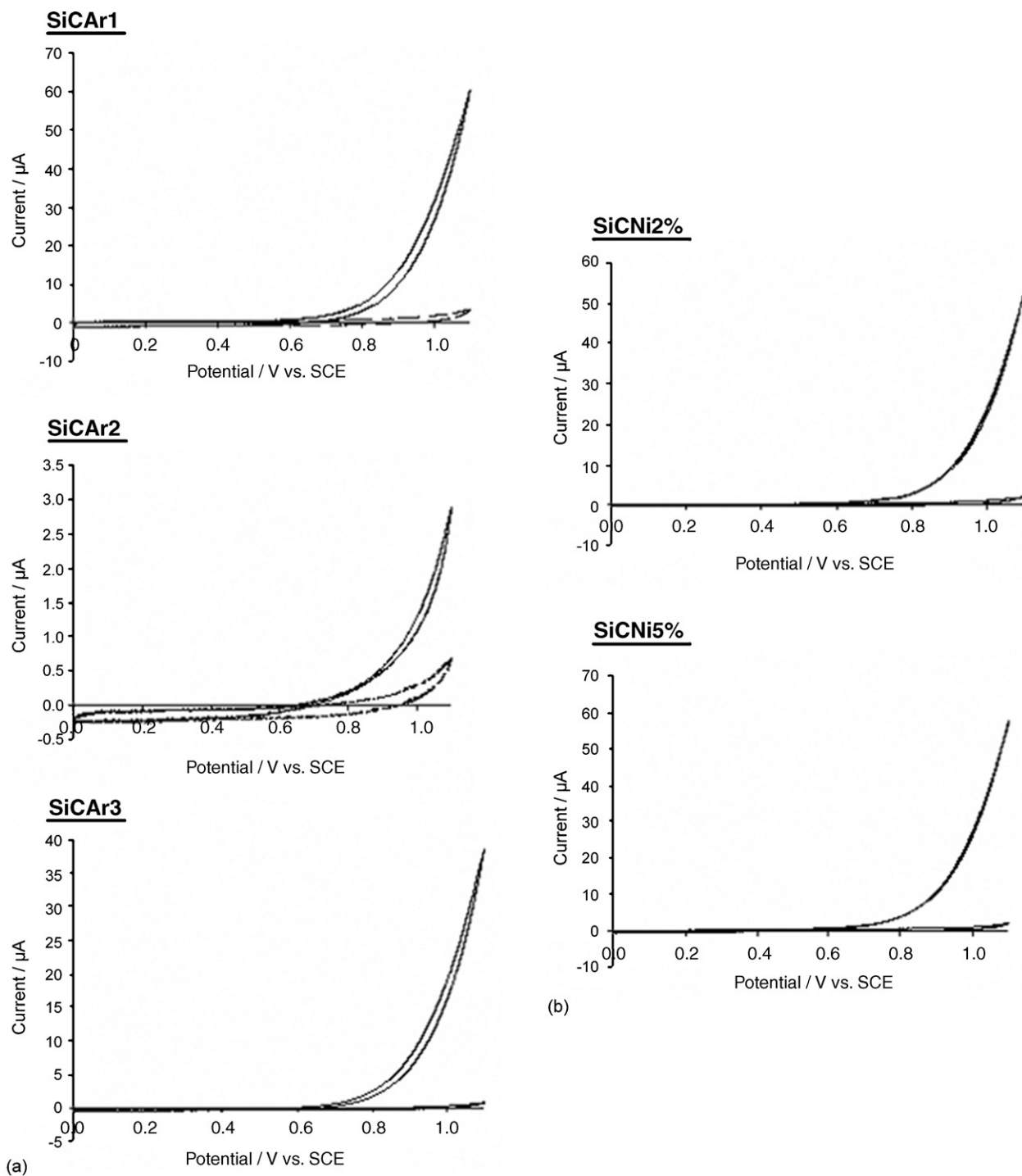


Fig. 1. (a) Cyclic Voltammograms of DLCs films with different ratio of sp^3/sp^2 carbon hybridization in 40 mM PB solution, pH 7.4 with and without 5 mM H_2O_2 . (b) Cyclic Voltammograms of Ni-containing DLCs films in 40 mM PB solution, pH 7.4 with and without 5 mM H_2O_2 .

glutaraldehyde vapor at room temperature. This bifunctional compound ($OHC-(CH_2)_3-CHO$) links covalently from each side to the amine groups of GOD and BSA, respectively, creating a stable biopolymer. The resulting enzyme electrodes were allowed to dry in air and were thoroughly washed and stored in 40 mM phosphate buffer (PB) solution, pH 7.4, at 4 °C when not in use.

3. Results and discussions

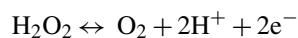
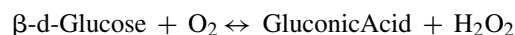
3.1. Hydrogen peroxide detection

Glucose biosensors are based on the fact that glucose oxidase, a flavoenzyme, catalyses the oxidation of glucose to gluconic acid in the presence of oxygen. Since hydrogen peroxide is the

Table 1
Hydrogen peroxide sensitivity of different diamond-like carbon electrodes in 40 mM PB solution, pH 7.4

Electrodes	SiCar1	SiCar2	SiCar3	SiCNI2%	SiCNI5%
Sensitivity ($\mu\text{A}/\text{mM}$)	4.4463	1.1872	2.0397	3.4659	4.6401

co-product of this reaction; its electroactivity can be used to obtain a measurable current signal.



DLC electrodes were initially characterized electrochemically by recording their cyclic voltammograms between 0.0 V and 1.1 V in 40 mM phosphate buffer solution, pH 7.4 with and without 5 mM H_2O_2 . The catalytic voltammograms obtained in the presence of hydrogen peroxide exhibit a greater sensitivity for SiCar1 and SiCNI5% electrodes; no observable plateau was distinguished (Fig. 1a and b). After analysis of these responses, a potential of +1.0 V was chosen for H_2O_2 amperometric detection.

Amperometric measurements were carried out in PB solution at +1.0 V by injecting H_2O_2 aliquots; each addition result in a 0.02 mM increment in concentration. The comparison of DLCs electrodes according to H_2O_2 sensitivity is shown in Fig. 2. Their corresponding sensitivities are presented in Table 1. Since SiCar1 and SiCNI5% electrodes enable a more satisfactory determination of hydrogen peroxide, 4.4463 $\mu\text{A}/\text{mM}$ and 4.6401 $\mu\text{A}/\text{mM}$, respectively, their behavior will be studied for biosensor elaboration by using a glucose amperometric assay system.

3.2. Enzyme measurements

To evaluate the possible application and the behavior of the above-mentioned DLCs electrodes in biosensor construction, glucose biosensors were fabricated following the procedure previously described. Kinetics studies of the immobilized enzyme

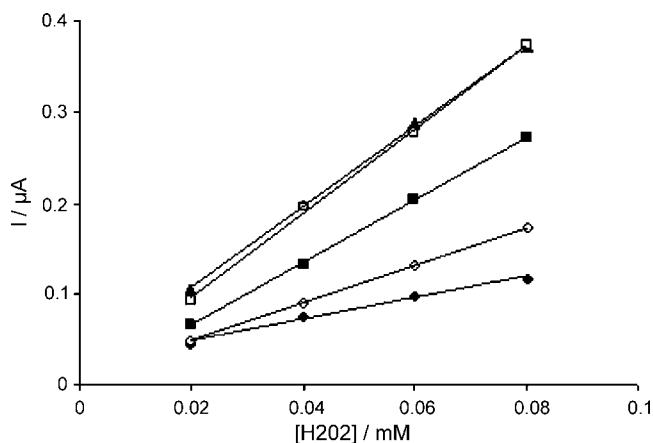


Fig. 2. Hydrogen peroxide calibrations curves for SiCar1 (Δ), SiCar2 (\blacklozenge), SiCar3 (\diamond), SiCNI2% (\blacksquare) and SiCNI5% (\square) electrodes for successive additions of 0.02 mM H_2O_2 in 40 mM PB, pH 7.4.

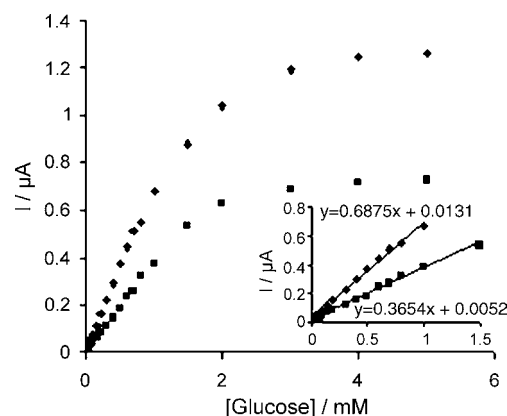


Fig. 3. Glucose Calibration curves for SiCar1 (\blacklozenge) and SiCNI5% (\blacksquare) biosensors for successive additions of glucose in 40 mM PB, pH 7.4.

were carried out by plotting the electrochemical response to increasing concentrations of glucose. Fig. 3 shows the curves of DLCs electrodes, SiCar1 and SiCNI5%, in 40 mM PB, pH 7.4 at a measurement potential of +1.0 V for successive additions of glucose.

The SiCar1 glucose biosensor displays a linearity range up to 1 mM and until 1.5 mM for SiCNI5%. Corresponding detection limits were 20 μM and 30 μM , respectively. Even if these two electrodes have exhibited the same sensitivity for hydrogen peroxide, SiCar1 biosensor shows higher sensitivity for glucose, 0.6875 $\mu\text{A}/\text{mM}$ with $R = 0.9984$, than SiCNI5% biosensor, 0.3654 $\mu\text{A}/\text{mM}$ with $R = 0.9982$. This fact can be explained by the use of two different topographical and constitutional structure electrodes leading to different and various interaction phenomena between the immobilized biopolymer and the electrode surface. From the Lineweaver-Burk plots, apparent Michaelis-Menten constants of 3.38 mM and 3.09 mM were obtained, respectively, for SiCar1 and SiCNI5% biosensors. The apparent K_m which depends on enzyme and not on the substrate is almost the same for both electrodes.

3.3. Operational and storage stability

The stability of enzyme sensors was usually limited by the deactivation and loss of enzyme. The deactivation of enzyme was mainly caused by unsuitable temperature. So, enzyme electrode needs to be kept at 4 $^\circ\text{C}$. The loss of enzyme is highly related to the way the enzyme is fixed to the electrode (adsorption to the electrode, entrapment into a polymer, cross-linking with a bifunctional compound...).

The operational stability during 10 h for SiCar1 and SiCNI5% glucose biosensors and their storage stability were tested in 40 mM phosphate buffer pH 7.4 containing 0.5 mM glucose.

The operational stability of both biosensors during ten working hours is presented in Fig. 4. The current response for 0.5 mM glucose seems to be very stable for SiCar1 while it increases very slowly for SiCNI5%. It may be explained by the swollen of the biolayer with time allowing easily access of glucose to the electrode surface leading therefore to increasing quantity of

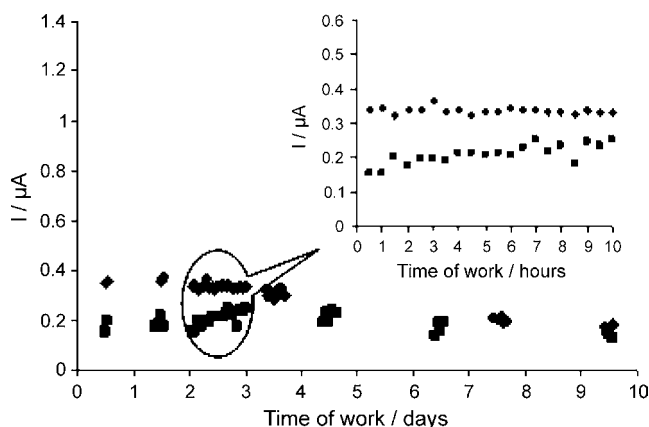


Fig. 4. Operational and storage stability of SiCAr1 (◆) and SiCNi5% (■) biosensors for 0.5 mM glucose concentration.

H₂O₂. It is illustrated in Fig. 4 by the slow increasing of the slope after 10 h of work.

The storage stability of SiCAr1 and SiCNi5% has been examined by checking periodically their activities. The current response of these two biosensors for 0.5 mM glucose remained almost unchanged during the three first days, and ~48% and ~79% of the original response remained after 10 days, respectively (Fig. 4). In fact, it can be deduced from X-ray photoelectron spectroscopy (XPS), near edge X-ray absorption fine structure (NEXAFS) and transmission electron microscope (TEM) that nickel is predominantly present in the metallic form in DLC films. They have the shape of nodules which are dispersed in the carbonaceous matrix [18]. In addition, AFM measurements provide an average roughness (Ra) of 2 nm for non-doped diamond-like carbon electrodes and 32 nm for nickel doped DLC electrodes. Thus, the higher roughness of SiCNi5% electrodes explains the better biolayer immobilization leading therefore to a more stable biosensor.

4. Conclusion

This work has been concerned with the characterization and the comparison of different diamond-like carbon electrodes for biosensor construction. DLC films appear to be very interesting

in the electrochemical biosensor field. Evaluation of these electrodes was carried out by comparing their sensitivities towards hydrogen peroxide. The most sensitive electrodes were explored and studied for the development of a conventional glucose biosensor. SiCAr1 glucose oxidase based biosensor seems to be more sensitive than SiCNi5% but its main drawback is the stability that may be increased by fixing the enzyme differently on the electrode surface.

Acknowledgements

This work was done in the framework of Beyrouth-Rhone-Alpes MIRA program of a Rhone-Alpes Priority Thematic Action and of the Japan-France IRCP Project.

References

- [1] J. Castillo, S. Gaspar, S. Leth, M. Niculescu, A. Mortari, I. Bontidean, V. Soukharev, S.A. Dorneanu, A.D. Ryabov, E. Csöregi, *Sens. Actuators, B* 102 (2004) 179.
- [2] J. Wang, *J. Pharm. Biomed. Anal.* 19 (1999) 47.
- [3] D.G. Georganopoulou, R. Carley, D.A. Jones, M.G. Boutelle, *Faraday Discuss.* 116 (2000) 291.
- [4] J.-J. Xu, H.-Y. Chen, *Anal. Chim. Acta* 423 (2000) 101.
- [5] S. Zhang, N. Wang, H. Yu, Y. Niu, C. Sun, *Bioelectrochemistry* 67 (2005) 15.
- [6] H. Liu, H. Li, T. Ying, K. Sun, Y. Qin, D. Qi, *Anal. Chim. Acta* 358 (1998) 137.
- [7] S. Yabuki, F. Mizutani, *Sens. Actuator, B* 108 (2005) 651.
- [8] Han Nim Choi, Min Ah Kim, Won-Yong Lee, *Anal. Chim. Acta* 537 (2005) 179.
- [9] V.G. Gavalas, N.A. Chaniotakis, T.D. Gibson, *Biosens. Bioelectron.* 13 (1998) 1205.
- [10] M.E. Ghica, C.M.A. Brett, *Anal. Chim. Acta* 532 (2005) 145.
- [11] M. Florescu, C.M.A. Brett, *Talanta* 65 (2005) 306.
- [12] A.S. Loir, PhD thesis, University Jean Monnet, Saint Etienne (2004).
- [13] J.M. Moon, S. Park, Y.K. Lee, G.S. Bang, Y.K. Hong, C. Park, J.C. Jeon, *J. Electroanal. Chem.* 464 (1999) 230.
- [14] L.X. Liu, E. Liu, *Surf. Coat. Technol.* 198 (2005) 189.
- [15] S.P.J. Higson, P.M. Vadgma, *Anal. Chim. Acta* 300 (1995) 85.
- [16] S.P.J. Higson, P.M. Vadgma, *Anal. Chim. Acta* 300 (1995) 77.
- [17] R. Maalouf, O. Vittori, Y. Saikali, H. Chebib, A.S. Loir, F. Garrelie, C. Donnet, N. Jaffrezic-Renault, *Mater. Sci. Eng. C* 26 (2006) 564.
- [18] N. Benchikh, F. Garrelie, C. Donnet, B. Bouchet-Fabre, K. Wolski, F. Rogemond, A.S. Loir, J.L. Subtil, *Thin Solid Films* 482 (2005) 287.

Short communication

Development of a new high performance low pressure chromatographic system using a multisyringe burette coupled to a chromatographic monolithic column

Hilda M. González-San Miguel^a, Jesús M. Alpízar-Lorenzo^b, Víctor Cerdà-Martín^{c,*}

^a *Department of Quality Assurance and Pharmaceutical Technology, Food and Pharmaceutical Sciences Institute, University of Havana, Cuba*

^b *Department of Analytical Chemistry, Faculty of Chemistry, University of Havana, Cuba*

^c *Department of Chemistry, University of the Balearic Islands, Spain*

Received 12 April 2006; received in revised form 14 September 2006; accepted 27 September 2006

Available online 13 November 2006

Abstract

A novel combination of high performance low pressure chromatography with multisyringe flow injection analysis is presented. This system comprises a multisyringe module, three low pressure solenoid valves, a monolithic Chromolith Flash RP-18e column and a diode array spectrophotometer. UV detection is carried out at 250 nm. AutoAnalysis software is used for instrumental control and automated data collection. The results obtained with multisyringe liquid chromatography (MSC) were compared with those obtained with a HPLC system using similar conditions. The chromatographic parameters were calculated from a mixture of anthracene and thiourea using a mobile phase containing acetonitrile–water (60:40) at a flow rate of 2 ml min⁻¹. The proposed MSC system has been successfully applied to the determination of amoxicillin, ampicillin and cephalexin using a mobile phase of sodium acetate buffer (pH 6.2, 0.1 mol l⁻¹)–methanol (90:10) at a flow rate of 2 ml min⁻¹. The low-cost, flexibility and simplicity of MSC should be highlighted.

© 2006 Elsevier B.V. All rights reserved.

Keywords: Multisyringe liquid chromatography; MSC; Monolithic column; Amoxicillin; Ampicillin; Cephalexin

1. Introduction

Most applications of monolithic columns proposed so far are for HPLC. It is clear, however, that monolithic columns have a good potential for use in other chromatographic applications. Recently, a new sequential injection chromatography (SIC) system with a monolithic support and a FIALab system has been developed [1]. In that work, different monolithic columns were tested and the results were compared with those obtained using a similar HPLC system. These systems have been successfully applied to the determination of pharmaceutical products, such as sodium diclofenac, triamcinolone and ambroxol [1–3].

The advantages of the combination of chromatographic techniques with flow techniques are noteworthy. Thus, flow analysis equipments are not extremely expensive, but these methods do

not allow the separation of several analytes in a mixture. On the other hand, HPLC has been widely used in pharmaceutical analysis and analytical research due to its high selectivity. However, it requires very expensive instrumentation with regard to flow techniques. For these reasons, the combination of flow injection analysis (FIA) and sequential injection analysis (SIA) with low pressure chromatographic separations can be regarded as a low-cost methodology that allows to achieve the required selectivity.

FIA has proved to be a suitable technique for on-line analysis because of its low reagent and sample consumption, high sample frequency and easy automation. Multisyringe flow injection analysis (MSFIA) is a novel multicommutated flow technique that has been developed with the aim to combine the advantages of FIA with the versatility and robustness of SIA [4]. The basic element of MSFIA is a multisyringe burette which allows the simultaneous movement of four syringes. These syringes are connected in block to the same stepper motor. The three-way solenoid valve placed on the head of each syringe increases the

* Corresponding author. Tel.: +34 971 173261; fax: +34 971 173426.
E-mail address: victor.cerda@uib.es (V. Cerdà-Martín).

flexibility of the technique and reduces sample and reagent consumption since reagents are injected into the system only when necessary [4,5].

In this work, chromatography has been coupled to a MSFIA system. The chromatographic separation is achieved on a monolithic column. Multisyringe liquid chromatography (MSC) is a novel approach to low pressure high performance chromatography. The chromatographic performance of the proposed MSC system has been tested using thiourea and anthracene as reference analytes [6]. The results have been compared to those obtained using a conventional HPLC configuration. In order to extend this result to pharmaceutical samples, the proposed system has been applied to the separation of amoxicillin, ampicillin and cephalixin. In this sense, several chromatographic methods have been developed for the determination of penicillanic and cephalosporin antibiotics using particulated C-18 as stationary phase and methanol–buffer as mobile phase [7,8].

2. Experimental

2.1. Reagents

All reagents were of analytical-reagent grade and all solutions were prepared in Millipore ultra-pure water (Millipore Corp., New York).

Methanol Chromasolv[®] (HPLC grade, Sigma–Aldrich) and acetonitrile (HPLC—gradient grade PAI-ACS, Panreac) were used to prepare the required mobile phase.

Amoxicillin, ampicillin and cephalixin pharmacopoeial quality were obtained from Laboratory “8 de Marzo”, Cuba. Solutions of amoxicillin (0.2 mg ml⁻¹), ampicillin (0.2 mg ml⁻¹) and cephalixin (0.1 mg ml⁻¹) were prepared in acetic-acetate buffer (pH 6.2; 0.1 mol l⁻¹). The solutions were degassed by sonication when necessary.

2.2. HPLC system and MSC system

The chromatographic system consisted of a Waters 510 pump and a Waters manual injector model U6K (Milford, MA, USA).

The proposed multisyringe liquid chromatography (MSC) system (Fig. 1) comprised a multisyringe burette module (CRISON,¹ Alella, Spain), three additional solenoid valves MTV-3-N1/4UKG (Takasago,² Japan) and a two-way connector that connects syringe S1 to valve V2 (Sciware,³ Palma de Mallorca, Spain). Manifold was constructed with 0.5 and 0.8 mm i.d. poly(tetrafluoroethylene) (PTFE) tubing. The chromatographic separation was achieved on a Chromolith Flash RP-18e, (25 mm × 4.6 mm i.d. column) protected with a Chromolith RP-18e (10 mm × 4.6 mm i.d.) guard column (Merck). A Hewlett Packard 8453 diode array spectrophotometer equipped with an 18 μl inner volume flow-cell (Hellma) was used as detector. Measurements were recorded at 250 nm. Sample volumes of

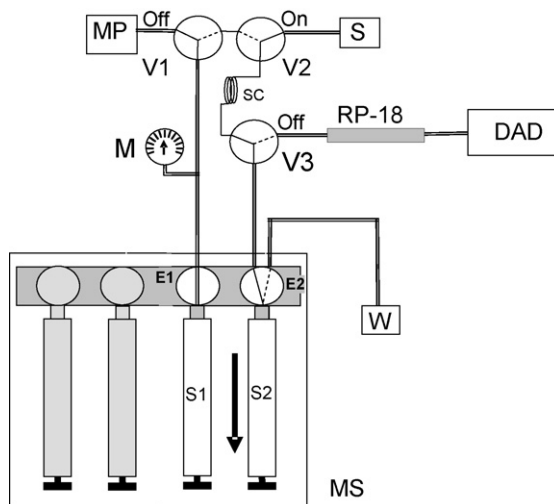


Fig. 1. MSC system for isocratic separation. MS: multisyringe burette, M: manometer, V1–V3: solenoid valves, E1: two-way connector, E2: three-way solenoid valve, MP: mobile phase, S: sample, W: waste, RP-18: monolithic column, DAD: diode array detector, and SC: sample coil.

20 μl and 60 μl were injected into the HPLC and the MLSC system, respectively.

For instrumental control, data acquisition and processing in MSC and HPLC, AutoAnalysis 5.0⁴ software was used [9].

2.3. Mobile phases

The mobile phase used for the evaluation of the chromatographic parameters was acetonitrile–water (60:40) at a flow rate of 2 ml min⁻¹ in HPLC and MSC systems. For the analysis of antibiotics, a mobile phase containing acetic-acetate buffer (pH 6.2, 0.1 mol l⁻¹)–methanol (90:10) was used.

2.4. MSC procedure

In the system, two syringes (S1 and S2) were used. The commutation valve of syringe S1 was replaced by a two-way connector (E1). The position “off” of the three-way solenoid valve E2 connected syringe S2 to waste and the position “on” connected syringe S2 to the system. The syringe S2 was used for loading and dispensing the sample. First, valves E2 and V2 were switched on for loading the sample coil with sample (60 μl). The other valves were in the off position and syringe S1 was filled with mobile phase. Afterwards, the mobile phase was delivered isocratically through the previously filled sample coil and the sample was injected into the chromatographic column (RP-18). Valves E2 and V2 were in the off position whereas valves V1 and V3 were in the on position. The separation products were propelled to the diode-array detector (Table 1).

3. Results and discussion

3.1. Comparison between HPLC and MSC system

The MSC system consisted of a multisyringe module, three additional solenoid valves, a monolithic column and a diode

¹ <http://www.crison.es>.

² <http://www.takasago-elec.co.jp>.

³ <http://www.sciware-sl.com>.

Table 1
Analytical procedure for MSC analysis of antibiotics

Step	Operation	Flow rate (ml min ⁻¹)	Position of the solenoid valves				Description
			E2	V1	V2	V3	
1	Dispense (0.620 ml)	3	Off	On	Off	On	Pre-conditioning of the system
2	Pick up (0.620 ml)	1	On	Off	On	Off	Filling S1 with mobile phase and SC with sample
3	Get measurement						Data acquisition
4	Dispense (5 ml)	2	Off	On	Off	On	Injection of mobile phase (The sample is delivered to the chromatographic column) UV detection
5	Pick up (5 ml)	5	On	Off	On	Off	Adjustment of the piston bar position
6	Dispense (5 ml)	2	Off	On	Off	On	Injection of mobile phase in order to complete chromatographic analysis
7	Stop measurement						Stop data acquisition
8	Pick up (5 ml)	5	On	Off	On	Off	Filling S1 and SC with mobile phase

The volumes and flow rates are referred to syringe 1.

array spectrophotometer. In order to avoid peak broadening, 0.5 mm i.d. PTFE tubing was used for sample loading. 0.8 mm i.d. PTFE tubing was used in the other parts of the system. Multisyringe was both the mobile phase and sample liquid driver. The low-cost of the multisyringe module in comparison with the common binary pump system used in HPLC should be highlighted. On the other hand, the detector used in the proposed system was controlled by AutoAnalysis software so that it was not necessary to acquire a specific HPLC detector. Therefore, the MSC system is quite cheaper than the HPLC one.

Different mobile phases and flow rates were tried in order to study back pressure in MSC system (Table 2).

Column back pressure was measured for each flow rate using mobile phases containing methanol-water. It was observed that the impact of increasing flow-rate on column back pressure was minimal; probably it was a result of similar viscosity of these binary mobile phases. Analogously, column back pressure was not affected by varying the composition of this binary phase. The highest pressure levels (about 9 bar) were obtained during the first stabilization step. These values are much lower

Table 2
Back pressure obtained with different mobile phases and flow rates

Mobile phase	Flow rate (ml min ⁻¹)	Back pressure (bar)
Acetonitrile–water (60:40)	1.0	4.0
	1.5	6.0
	2.0	8.2
	2.5	8.5
Methanol–water (60:40)	1.0	8.0
	1.5	8.0
	2.0	8.0
	2.5	8.0
Methanol–water (40:60)	1.0	8.0
	1.5	8.2
	2.0	8.2
	2.5	8.3
Methanol–water (10:90)	1.0	8.2
	1.5	8.2
	2.0	8.5
	2.5	8.5

than those found in the HPLC system. The pressure decreased rapidly up to 8 bar. By contrast, column back pressure increased as the flow-rate increased when a mobile phase containing acetonitrile–water (60:40) was used, but in this combination all values were under 9 bar.

The results obtained for the chromatographic separation of anthracene and thiourea using MSC were compared to those obtained using HPLC. A mobile phase of acetonitrile–water (60:40) at a flow rate of 2 ml min⁻¹ was used. In this first approach, the efficiency of MSC is lower with regard to HPLC. However, these results could be improved by increasing the flow-rate (Table 3). The influence of the flow rate on the efficiency of the MSC system was studied in the range 0.5–3.0 ml min⁻¹. It was observed that the retention time of anthracene decreased as the flow rate was increased (Fig. 2A). However, it was found that the asymmetry of peaks increased with increasing mobile phase flow rate. This result was compared with the obtained using the empirical Cerdà equation for diagrams [10]. According to Cerdà, the symmetry of peaks increases with decreasing the flow rate as a consequence of diffusion effect. In this work, peak tailing was decreased at higher flow rates. This result is similar to the obtained in a traditional chromatographic separation (Fig. 3).

The relationship between the height equivalent to a theoretical plate (HETP) and flow rate was studied Chromolith columns have a typical Van Deemter response when used in HPLC systems [6] (i.e. the highest efficiency is obtained at a

Table 3
Chromatographic parameters for the separation of anthracene and thiourea using the Chromolith™ Flash RP-18e column and acetonitrile–water (60:40) as mobile phase

	HPLC	MSC ^a	MSC ^b
<i>t</i> _R anthracene (s)	116.4	97.6	45.8
<i>t</i> _R thiourea (s)	65.2	58.2	12.2
Rs ^c	1.9	2.5	2.5
HETP (μm) ^d	113.9	438.1	155.9
As	4	5	3

As: tailing factor for anthracene.

^a MSC: flow rate 2.0 ml min⁻¹.

^b MSC: flow rate 3.0 ml min⁻¹.

^c Rs: separation of anthracene and thiourea.

^d HETP: evaluated for anthracene.

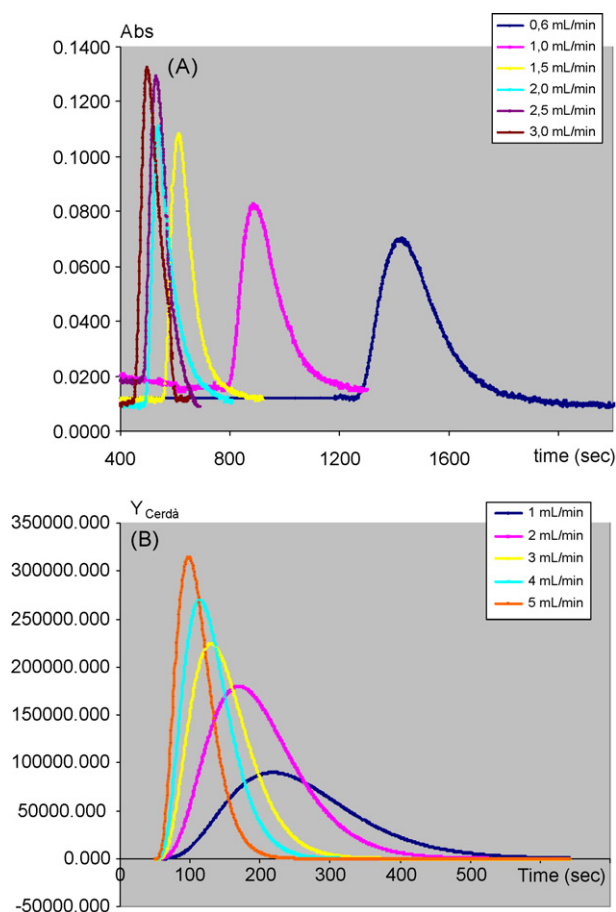


Fig. 2. Behavior of anthracene on the MSC system and typical diagrams. (A) MSC chromatograms of anthracene separation were performed on a Chromolith™ Flash RP-18e column using a mobile Phase containing acetonitrile–water (60:40) at different flow rates. (B) Diagrams obtained using the Cerdà equation at different flow rates [10].

given flow-rate as a consequence of the combination of longitudinal diffusion, mass transfer and multistep effects). By contrast, a different behavior was observed in MSC (Fig. 2). Analogous to FIA, the asymmetry of peaks increases with increasing flow-rate. The prevalence of FIA effects can be attributed to the inner diameter of the tubing used.

3.2. Application to the analysis of antibiotics

Penicilanic and cephalosporin antibiotics have been widely studied in different chromatographic systems using different mobile and stationary phases. Several FIA systems for the determination of these compounds have also been reported [11,12]. In this paper, amoxicillin, ampicillin and cephalexin have been chosen as model analytes in order to demonstrate the possibilities of the MSC system. A conventional HPLC system was also applied to the chromatographic separation of these antibiotics using mobile phases containing different proportions of methanol–sodium acetate buffer pH 6.2 (Fig. 3). The best results were obtained by using sodium acetate buffer pH 6.2, 0.1 mol l⁻¹ – methanol (90:10) as mobile phase. This mobile phase was also selected to analyze these antibiotics with the MSC system. A sat-

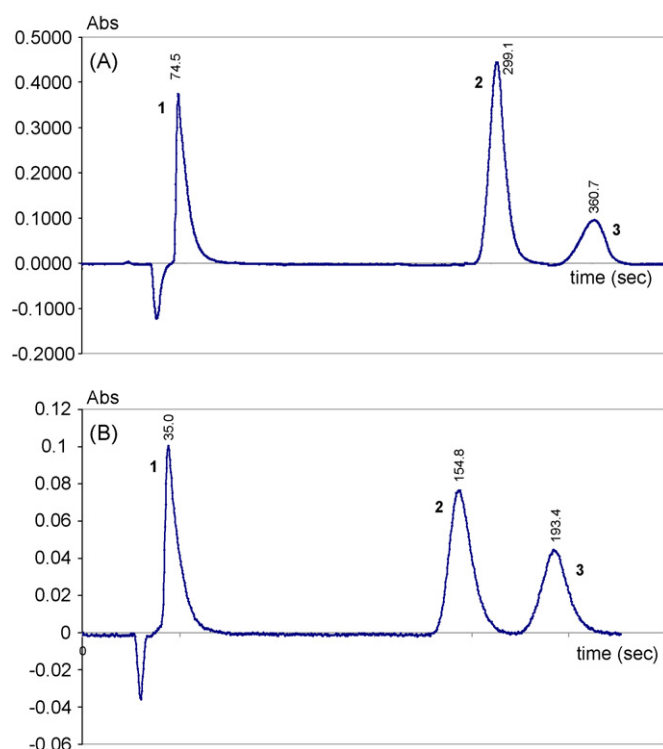


Fig. 3. Chromatographic separation of amoxicillin, cephalexin and ampicillin using a Chromolith RP-18e column as stationary phase. Mobile phase methanol–sodium acetate buffer pH 6.2, 0.1 mol l⁻¹ (10:90). Flow rate 2 ml min⁻¹. Detection at 250 nm. (A) MSC chromatogram; (B) HPLC chromatogram.

isfactory separation of the three antibiotics was achieved in the new chromatographic system. Moreover, the resolution between cephalexin and ampicillin was improved due to the recharge of the syringe (Table 4). A preliminary evaluation of this method showed linearity response in a range of 0.04–0.4 mg/mL with a correlation coefficient of 0.9996 for amoxicillin; for ampicillin and cephalexin regression coefficients upper than 0.99 were obtained in linearity evaluation.

3.3. MSC performances

Our preliminary results show the possibilities of the combination of MSFIA with chromatographic analysis. In the proposed MSC system, AutoAnalysis software was used due to its high

Table 4
Retention time and resolution obtained for antibiotics in HPLC and MSC systems with a mobile phase containing methanol and 0.1 M sodium acetate –0.1 M acetic acid (10:90) pH 6.2

Antibiotic	HPLC	MSC
Amoxicillin (<i>t_R</i> , s)	35.0	74.5
Ampicillin (<i>t_R</i> , s)	154.8	360.7
Cephalexin (<i>t_R</i> , s)	193.4	299.1
Amoxicillin–cephalexin (<i>R_s</i>)	4.7	6.3 (4.6) ^a
Ampicillin–cephalexin (<i>R_s</i>)	1.3	1.3

^a*R_s* value evaluated without death time produce due to syringe recharge of mobile phase.

versatility. This user-friendly software has an open, hardware-independent design. Thus, this software works with dynamic link libraries (DLLs) which allow to develop analytical methods independent from the instrumentation used. All kind of detectors can be incorporated when necessary by creating the corresponding DLLs [9].

On the other hand, the Crison multisyringe module is also very versatile. In this sense, this liquid driver allows the mobile phase delivery, the sample injection and the use of derivatization strategies. Other features of the multisyringe module are robustness and the possibility to use aggressive fluids. In this work, isocratic conditions were maintained during analysis. However, a gradient elution is also feasible when using MSC and Auto-Analysis software.

4. Conclusions

MSC is a novel approach to chromatography and flow analysis. The flexibility of MSC should be pointed out. Its design can be easily modified according to the analyst's needs. The proposed MSC system was compared to a similar HPLC one. Maintained the simplicity, versatility and low-cost equipment of MSC, it can be regarded as an alternative to HPLC using low pressure and it could be a very attractive technique to improve selectivity in flow analytical systems (FIA and SIA). Back pressure was not a limiting factor in MSC. MSC allowed using similar flow-rates to those used in HPLC under the same conditions. Analogous to SIC, the possibilities of MSC have been demonstrated. Therefore, special benefit can be derived from the combination of flow techniques with monolithic columns in car-

rying out low-cost chromatographic separations of compounds of pharmaceutical interest.

Acknowledgments

The authors are grateful to the MCyT (Ministerio de Ciencia y Tecnología) for supporting the project CTQ2004-01201. Hilda M. González thanks to the MEC (Ministerio de Educación y Ciencia) for the allowance of the sabbatical grant SAB-103 2005. We are grateful to María del Carmen Pons for her suggestions.

References

- [1] D. Šatínský, P. Solich, P. Chocholouš, R. Karlíček, *Anal. Chim. Acta* 499 (2003) 205–214.
- [2] D. Šatínský, J. Huclová, P. Solich, R. Karlíček, *J. Chromatogr. A* 1015 (2003) 239–244.
- [3] D. Šatínský, J. Huclová, R.L.C. Ferreira, M.C. Montenegro, P. Solich, *J. Pharm. Biomed. Anal.* 40 (2) (2006) 287–293.
- [4] V. Cerdà, J.M. Estela, R. Forteza, A. Cladera, E. Becerra, P. Altimira, P. Sitjar, *Talanta* 50 (1999) 695–705.
- [5] L.O. Leal, R. Forteza, V. Cerdà, *Talanta* 69 (2006) 500–508.
- [6] Merck, Chromolith columns, General Information and Applications.
- [7] V.F. Samanidou, E.A. Hapeshi, I.N. Papadoyannis, *J. Chromatogr. B* 788 (2003) 147–158.
- [8] H. Liu, H. Wang, V.B. Sunderland, *J. Pharm. Biomed. Anal.* 37 (2005) 395–398.
- [9] E. Becerra, A. Cladera, V. Cerdà, *Lab. Rob. Autom.* 11 (1999) 131–140.
- [10] V. Cerdà, *Introducción a los métodos de análisis en flujo*, Sciware, Palma de Mallorca, 2006.
- [11] M.S. García, C. Sánchez-Pedreño, M.I. Albero, Ródenas, *J. Pharm. Biomed. Anal.* 12 (1994) 1585–1589.
- [12] I.F. Al-Momani, *J. Pharm. Biomed. Anal.* 25 (2001) 751–757.

Voltammetric determination of Cu(II) in natural waters and human hair at a meso-2,3-dimercaptosuccinic acid self-assembled gold electrode

Alireza Mohadesi, Mohammad Ali Taher*

Department of Chemistry, Shahid Bahonar University of Kerman, P.O. Box 76175-133, Kerman, Iran

Received 26 August 2006; received in revised form 28 September 2006; accepted 30 September 2006

Available online 30 October 2006

Abstract

An electrochemical sensor for the detection of copper(II) ions is described using a meso-2,3-dimercaptosuccinic acid (DMSA) self-assembled gold electrode. First in ammonia buffer pH 8, copper(II) ions complex with self-assembled monolayer (SAM) via the free carboxyl groups on immobilized meso-2,3-dimercaptosuccinic acid (accumulation step). Then, the medium is exchanged to acetate buffer pH 4.6 and the complexed Cu(II) ions are reduced in negative potential of -0.3 V (reduction step). Following this, reduced coppers are oxidized and detected by differential pulse (DP) voltammetric scans from -0.3 to $+0.7$ V (stripping step). The effective parameters in sensor response were examined. The detection limit of copper(II) was $1.29 \mu\text{g L}^{-1}$ and R.S.D. for $200 \mu\text{g L}^{-1}$ was 1.06%. The calibration curve was linear for 3 – $225 \mu\text{g L}^{-1}$ copper(II). The procedure was applied for determination of Cu(II) to natural waters and human hairs. The accuracy and precision of results were comparable to those obtained by flame atomic absorption spectroscopy (FAAS).

© 2006 Elsevier B.V. All rights reserved.

Keywords: Self-assembled monolayer; Copper(II); Stripping analysis; Gold electrode; Voltammetric detection

1. Introduction

Self-assembled monolayers (SAMs) have been used in electroanalytical chemistry for some 20 years now as the basis of electrochemical sensors. SAMs are monomolecular layers, which are spontaneously formed upon immersing a solid substrate into a solution containing amphifunctional molecules [1]. Most studies in this area have included the assembly of trialkyl-, trichloro- or trialkoxysilanes on silicon dioxide surfaces, carboxylic acids adsorbing onto aluminum oxide and silver surfaces and thiol compounds chemisorbing to gold surfaces [2,3]. In the latter case (if a thiol molecule is used to modify the gold electrode), the bond of S–H cleaves and that of S–Au will form because of the strong affinity between S and Au. The reaction mechanism between the S–H bond and the Au atom is as follows: $\text{RS-H} + \text{Au} \rightarrow \text{RS-Au} + 1/2\text{H}_2$. On the surface of the gold electrode, the mercapto group will be oxidized to the Au–S bond.

Because of the powerful energy between Au and S atoms (bond energy is 184 kJ mol^{-1}), it is seldom that groups can compete with it; consequently, the selection of this adsorption is assured [4].

Recently, SAM modified electrodes were applied for adsorptive stripping voltammetric determination of metal ions based on preconcentration of these ions on electrode surfaces by complexation between SAM and metal ions [5–22]. The method consists of two steps. The first one is a preconcentration step where a small portion of the unknown metal ion is preconcentrated at the modified electrode surface under opened or closed circuit conditions. The second step involves stripping of the accumulated ion. The technique has been most useful in the determination of trace levels of certain heavy metal ions in solution [23].

Voltammetric detection of Cu(II) ions has been paid special attention by the use of the thiol compounds self-assembled on gold electrodes. Profumo et al. [21] prepared D,L-penicillamine and thiodimethylglyoxime SAMs on gold electrode and characterized by electrochemical measurements. The two sensors exhibited sensitive and selective response to Cu(II), both forming 2:1 complexes. Copper determination at trace level

* Corresponding author.

E-mail address: ma.taher@yahoo.com (M.A. Taher).

(detection limits of 0.2 and $0.3 \mu\text{g L}^{-1}$ for D,L-penicillamine and thiodimethylglyoxime, respectively) was possible with both the electrodes as verified in tap, spring and sea waters. Liu et al. [19] and Yang et al. [11] used the gold cysteine SAM-modified electrode and determined Cu(II) ions in solution with a detection limits of 0.025 and $5 \mu\text{g L}^{-1}$, respectively. The gold 3-mercaptopropionic acid [16] and mercaptoacetic acid [17] SAMs have been used as highly sensitive voltammetric sensor for Cu(II) with the linear range from 0.06 to 63 ng L^{-1} and 50 to $635 \mu\text{g L}^{-1}$ Cu(II), respectively. Employing a different approach, where the tripeptide Gly–Gly–His covalently attached to a 3-mercaptopropionic acid modified gold electrode was used as a recognition element; Liu et al. [12] reported a detection limit of $0.02 \mu\text{g L}^{-1}$ for Cu(II). Zeng et al. [9] described the voltammetric response of glutathione and mercaptopropionic acid SAM-based electrodes to copper ions; they showed that the glutathione/Au electrode exhibited selective response to Cu(II), which was improved in the presence of mercaptopropionic acid. More recently, Shervedani and Mozaffari [22] fabricated novel nanosensor for determination of Cu(II) in subnanomolar concentrations. The sensor was based on gold cysteamine self-assembled monolayer functionalized with salicylaldehyde by means of Schiff's base formation. A wide range linear calibration curve was reported, 0.03 – $317 \mu\text{g L}^{-1}$ Cu(II), by using the EIS and OSWV methods.

Meso-2,3-dimercaptosuccinic acid (DMSA) contains two mercapto groups, and has been previously used for the preparation of SAMs on gold electrodes and applied for voltammetric determination of ascorbic acid and uric acid [24]. In this paper, DMSA was used as the assembled molecule and the DMSA self-assembled gold electrode (DMSA/Au) was prepared. It was found that DMSA can preconcentrate Cu(II) from sample solutions on the electrode surface. A differential pulse (DP) anodic stripping voltammetric method has been developed for determination of Cu(II) concentration.

2. Experiment

2.1. Reagents

All reagents were of analytical reagent grade and used without further purification. Doubly distilled water was used for all experiments. DMSA was purchased from Sigma and used for preparation of a DMSA saturated solution by dissolving 0.05 g of DMSA in 10 mL distilled water. The stock solution of 1000 mg L^{-1} Cu(II) was prepared from $\text{Cu}(\text{NO}_3)_2$ in doubly distilled water.

2.2. Apparatus

All voltammograms were recorded with a three-electrode system consisting of an Ag/AgCl as the reference electrode, a platinum wire as the counter electrode, and a gold electrode (2 mm diameter, Metrohm) as the working electrode. Voltammetric experiments were performed using a Metrohm electro-analyzer (Model 757 VA computrace). The measurements were

recorded using VA Computrace Version 2.0 (Metrohm) running under Windows 98. A Metrohm 710 pH meter was used for pH adjustments. A Zag-Shimi stirrer was applied to stir solutions in the accumulation step. All measurements were carried out at room temperature ($23 \pm 1^\circ\text{C}$).

2.3. Preparation of DMSA/Au electrode

Gold electrodes were polished with an alumina ($3 \mu\text{m}$) water slurry on a polishing cloth, then immersed in a Piranha solution (a mixed solution of 30% H_2O_2 and concentrated H_2SO_4 , volume ratio 1:3), then rinsed well with doubly distilled water and wiped several times with wetted soft tissue. The cleaned electrode was electrochemically treated by cycling five times in $1 \text{ M H}_2\text{SO}_4$ from 0 to 1.8 V at 100 mV s^{-1} scan rate until a stable voltammogram was obtained. Then, the treated electrode washed copiously with doubly distilled water and immersed into the freshly treated aqueous saturated solution of DMSA for 15 h to form SAM of DMSA on the gold surface.

2.4. Stripping determination of Cu(II) on DMSA/Au electrode

Cyclic voltammograms (CVs) were run after purging solutions for at least 5 min with ultra pure nitrogen gas. The CVs were run starting from -0.4 to $+0.6 \text{ V}$ and back (with a 50 mV s^{-1} scan rate) after 10 min preconcentration at the open circuit condition with $250 \mu\text{g L}^{-1}$ Cu(II) in accumulation medium.

For DP anodic stripping voltammetric experiments, the DMSA/Au electrode was immersed in a 20 mL of sample solution (ammonia buffer pH 8) containing a known amount of Cu(II) and the solution was stirred for 15 min . This was followed by medium exchange to a 0.1 M stripping solution (acetate buffer pH 4.6), where the accumulated copper(II) was reduced for 15 s in -0.3 V . Finally, the DP voltammogram was recorded from -0.3 to $+0.7 \text{ V}$ (with 50 mV s^{-1} scan rate, 50 mV pulse amplitude and 4 ms pulse period).

3. Results and discussion

3.1. Electrochemical behavior of Cu(II) at DMSA/Au modified electrodes

The DMSA molecule has two functional groups: mercapto and carboxyl. The mercapto groups have been widely used to construct SAMs on noble metal electrode surfaces [2,3], although these films are low density. The carboxyl functional groups can be used for formation of metal complexes via electrostatic forces [10,16,20]. The ability of a modified gold electrode with SAM of DMSA for chemical accumulation and stripping voltammetry of copper ions was examined.

Fig. 1 presents the cyclic voltammograms of a DMSA/Au electrode in the acetate buffer pH 4.6 after accumulation in the given solutions. With the presence of Cu(II) in accumulation solution, a pair of waves can be observed at about 0.25 and 0.08 V (Fig. 1(a)). However, the DMSA/Au electrode did not exhibit any wave over this potential range in the blank accumulation

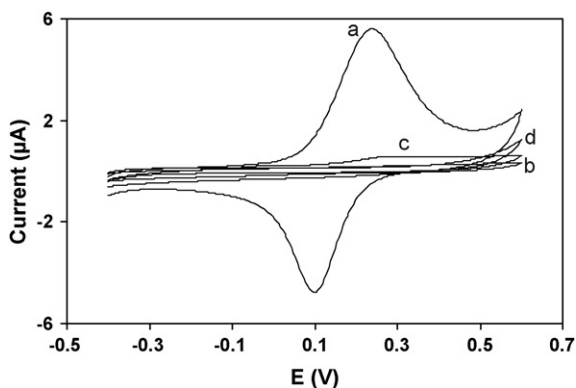


Fig. 1. Cyclic voltammograms in acetate buffer pH 4.6 after open circuit accumulation in ammonia buffer pH 8: (a) DMSA/Au electrode, with $250 \mu\text{g L}^{-1}$ Cu(II) in accumulation medium, (b) DMSA/Au electrode, no Cu(II) in accumulation medium, (c) bare Au electrode, with $250 \mu\text{g L}^{-1}$ Cu(II) in accumulation medium and (d) bare Au electrode, no Cu(II) in accumulation medium. Accumulation time was 10 min and scan rate was 50 mV s^{-1} .

solution (Fig. 1(b)). So, the waves can be described to the redox of Cu(II). Meanwhile, a bare gold electrode was tested but no current peak was observed for it under these conditions. This indicates that the chemical preconcentration of Cu(II) cannot take place on a bare gold electrode but can on the DMSA/Au electrode surface.

3.2. Modification time for preparation of DMSA/Au electrode

We studied the time-dependent adsorption of DMSA at the Au electrode by virtue of the change of DP anodic stripping peak currents of Cu(II). As shown in Fig. 2, the anodic stripping peak currents of Cu(II) increased with time and reached the maximum after about 15 h because of the saturated adsorptive quantity. After that, even if the time was prolonged, the quantity

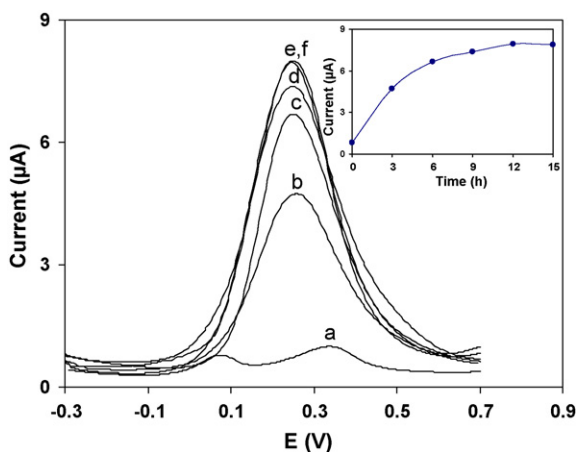


Fig. 2. DP voltammograms of accumulated copper(II) at DMSA/Au electrodes prepared with different modification times. Inset: The relationship between anodic stripping current of Cu(II) and time applied for formation of SAM of DMSA. Conditions: accumulation medium, ammonia buffer pH 8; accumulation time, 15 min; stripping medium, acetate buffer pH 4.6; reduction potential, -0.3 V ; reduction time, 15 s; scan potentials, from -0.3 to $+0.7 \text{ V}$; scan rate, 50 mV s^{-1} .

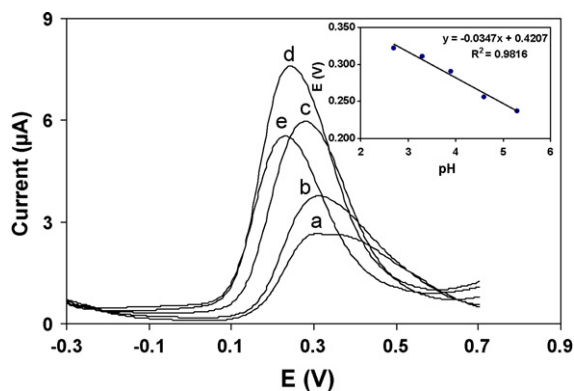


Fig. 3. DP voltammograms of accumulated DMSA/Au electrode at different pHs of stripping solution. DPs (a–e) correspond to pHs of 2.7, 3.3, 3.9, 4.6 and 5.3, respectively. Inset: The relationship between E_{pa} and pH. Other conditions were the same as Fig. 2.

would not increase. Therefore, in this paper, the time of 15 h was adopted as the modification time to assemble the Au electrode.

3.3. pH of stripping and accumulation solution

Complex formation between copper ions in solution and carboxyl groups on DMSA/Au electrode occurs via electrostatic forces. The charge state of carboxyl groups can be controlled by pH values of the accumulation solution. In the present investigation, the stripping peak currents were found to increase as the pH of the accumulation solution (ammonia buffer) was increased. This can be due to an increase in the complexation rate between Cu(II) and the carboxyl groups at higher pHs. The maximum stripping currents are to be expected at pHs between 7.2 and 8.8. pH 8 was applied as the pH of the accumulation medium for copper determination.

The pH dependence of the stripping medium on the electrochemistry of accumulated Cu(II) was evaluated. Fig. 3 shows the influence of pH on DP voltammograms of copper complexed in a DMSA/Au electrode; these data were obtained in a copper-free acetate buffer solution after a preconcentration step. A linear shift to lower potential can be observed as the pH increases (Fig. 3, inset). This is indicative that a protonation/deprotonation step is involved in the overall redox process. The slope of the curve *e* versus pH showed a value of 34 mV, which can indicate that two protons are involved in this step. Also, as seen from Fig. 3, the best choice for the ability to give the best shape and highest current was pH 4.6.

3.4. Accumulation time

The dependence of the anodic stripping peak current on the preconcentration time for two different Cu(II) concentration was studied. The peak current was found to increase with increasing preconcentration time, indicating an enhancement of Cu(II) uptake at the electrode surface. Normally, the increase in the response current will continue until a maximum signal level (presumably corresponding to either saturation or an equilibrium surface coverage) is attained. The results thus obtained

here indicate that the attainment of a steady state accumulation level of Cu(II) at the electrode surface requires an exposure time of 6 min time for $220 \mu\text{g L}^{-1}$ and a 15 min time for $3 \mu\text{g L}^{-1}$ Cu^{2+} . Hence, a 15 min preconcentration time was employed in all subsequent experiments.

3.5. Reduction potential and time

The best reduction potential for copper determination was studied in the interval between +0.5 and -0.8 V. No significant anodic peak currents were observed for more positive reduction potentials of +0.2 V. Increasing the potential from +0.2 to -0.3 V, the anodic peak current increased successively, and then levelled off after -0.3 V. The potentials more negative than -0.6 V led to decreased peak currents. Hence, -0.3 V was employed as an optimum reduction potential for copper(II) determination studies.

The effect of the reduction time on the anodic peak current of copper was examined. The peak currents were found to increase linearly, increasing reduction time up to 15 s. After this time, peak currents remained constant. Therefore, reduction times of 15 s were used for all subsequent measurements.

3.6. Regeneration of electrode

The ability of copper ions to form stable complexes with EDTA formed the basis of the regeneration step. Due to the high concentration of EDTA (0.2 M) employed, the copper ions bound to the electrode surface dissolved in solution as EDTA– Cu^{2+} chelates which are presumably more stable than DMSA– Cu^{2+} chelates. The idea here is to re-use the same DMSA/Au electrode for several experiments. Results shown a used electrode can be completely regenerated after at least 3 min in EDTA solution (see curves a–c, successively in Fig. 4). There is no significant difference in the response of a regenerated electrode compared to a new one (compare voltammograms b and d in Fig. 4).

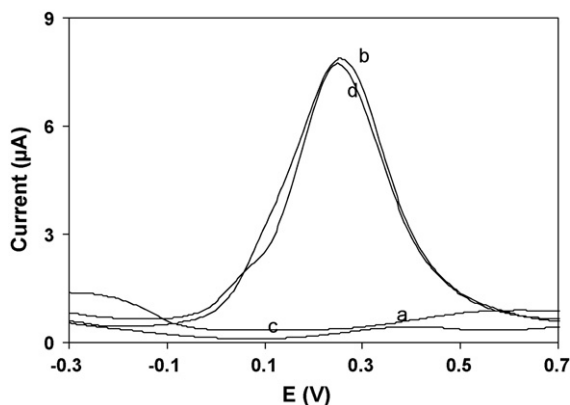


Fig. 4. DP voltammograms of (a) new DMSA/Au electrode without accumulation of Cu^{2+} , (b) new DMSA/Au electrode after 15 min accumulation in $200 \mu\text{g L}^{-1}$ Cu^{2+} , (c) used DMSA/Au electrode after 3 min immersing in 0.2 M EDTA and (d) regenerated DMSA/Au electrode after 15 min accumulation in $200 \mu\text{g L}^{-1}$ Cu^{2+} . Other conditions were the same as Fig. 2.

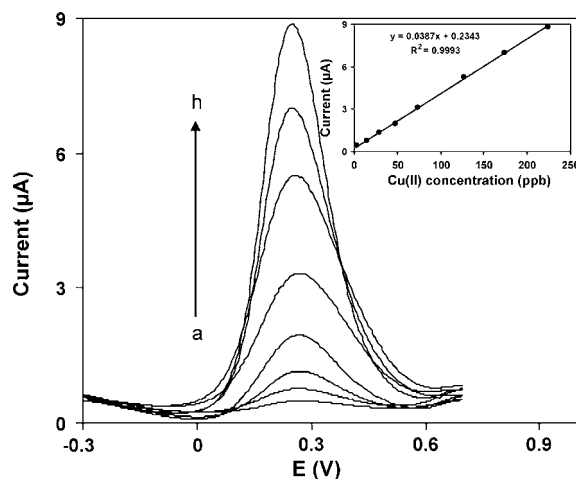


Fig. 5. DP anodic stripping voltammograms of DMSA/Au electrode, concentrations of (a–h): 3.0, 14.7, 29.1, 47.6, 73.8, 126.7, 173.7 and $224.6 \mu\text{g L}^{-1}$ Cu^{2+} in accumulation medium. Inset: The related calibration graph. Other conditions were the same as Fig. 2.

3.7. Calibration curve, detection limit and reproducibility

Standard solutions containing different concentrations of Cu(II) were prepared in pH 8 solutions and adjusted to the optimized anodic stripping voltammetric procedure. Voltammograms at these concentrations are shown in Fig. 5. A linear calibration graph was obtained in the concentration range 3 – $225 \mu\text{g L}^{-1}$ (Fig. 5, inset). The detection limit was found to be $1.3 \mu\text{g L}^{-1}$ Cu(II) and for five successive determinations of $200 \mu\text{g L}^{-1}$ Cu(II) relative standard deviation was 1.06%.

3.8. Co-existing ions

The presence of other metal ions could interfere with Cu(II) determination if they compete for complexation at the carboxyl complexing sites. When the developed procedure was explored for the determination of $200 \mu\text{g L}^{-1}$ Cu(II) with optimum conditions, no interference was encountered for additions of 10 mg L^{-1} each of Hg (II), Ni(II), Mn(II), Co(II), Bi(III), Ag(I), Na(I), Fe(II) and K(I). However, the presence of 10 mg L^{-1} Pb(II), Zn(II) and Cd(II) caused 13, 6 and 17% depressions of the Cu(II) peak, respectively.

3.9. Real sample analysis

The developed method was applied to the determination of Cu(II) in human hair and natural waters. The procedure of wet ashing of human hair is described by Sabermahani and Taher [25]. The hair sample was rinsed with acetone and 4.20 g of dried sample was accurately weighed and burned in a furnace at 700°C until a white powder was obtained. The obtained ash was dissolved in a minimum volume of concentrated nitric acid with heating. The solution was boiled to expel brown fumes, cooled and diluted with distilled water to 20 mL in a calibration flask. A $300 \mu\text{L}$ of this solution added to 20 mL of ammonia buffer with pH 8, and the general procedure was used on the resultant solution. For natural waters, these waters were exchanged with dis-

Table 1
Determination of Cu(II) in natural water and human hair samples

Sample	Present method ^a ($\mu\text{g L}^{-1}$)	FAAS method ^a ($\mu\text{g L}^{-1}$)	Recovery (%)	Spiked Cu ²⁺ ($\mu\text{g L}^{-1}$)	Founded Cu ²⁺ ^a ($\mu\text{g L}^{-1}$)	Recovery (%)
River water	6.63 \pm 0.14	6.75 \pm 0.10 ^b	98.22	100	106.02 \pm 2.01	99.31
Human hair ^c	12.41 \pm 0.59	12.93 \pm 0.06	95.97	–	–	–

^a Mean of three determinations \pm standard deviation.

^b After vacuum evaporator concentration.

^c Results are given in $\mu\text{g g}^{-1}$.

Table 2
Comparison of some properties of the present work with other studies

No.	Self-assembled modifier	t_p ^a (h)	t_a ^a (min)	DL ($\mu\text{g L}^{-1}$)	LR ($\mu\text{g L}^{-1}$)	R.S.D. ^a (%)	Interferences	Real samples	Reference
1	Tripeptide Gly–Gly–His	26	10	0.02	Up to 0.13	12.5	Cr ²⁺ , Cr ³⁺ , Pb ²⁺	Natural waters	[12]
2	L-Cysteine	2	5	5	5–630	1.1	Ni ²⁺ , Ag ²⁺	Natural waters	[11]
3	Cysteine	2	5	0.025	0.05–5	3.2	Ni ²⁺	Reference waters	[19]
4	Mercaptoacetic acid	2	–	–	50–635	10.7	Ni ²⁺ , Co ²⁺	Environmental samples	[17]
5	Thiodimethylglyoxime	2	4	0.3	0.3–30	–	–	Natural waters	[21]
6	3-Mercaptopropionic and glutathione	26	2	–	635–6354	–	–	–	[9]
7	Cysteamine	6	5	0.005	0.03–317	6.6	–	Blood serum	[22]
8	2,3-Dimercaptosuccinic acid	16	15	1.29	3–225	2.1	Cd ²⁺ , Pb ²⁺	Natural waters, human hairs	This work

^a t_p is minimum time spent for preparation of electrode, t_a accumulation time, R.S.D.s are amounts reported in the real samples.

tilled water used for the preparation of an ammonia buffer (pH 8) and the general procedure was used on these resultant solutions. The standard addition method was applied for the determinations of copper. The results obtained by the proposed method were compared with flame atomic absorption spectroscopy (FAAS) method (Table 1) [25–27] by t -test [28]. Statistical comparison at the 95% confidence level showed no significant difference between the results obtained with the proposed procedure and those of the FAAS standard method. Also, the concentration of Cu in human hair sample obtained in the present procedure (12.41 $\mu\text{g g}^{-1}$) is in the same range as the levels that of Sabermahani and Taher (11.59 $\mu\text{g g}^{-1}$) [25], Ramakrishna et al. (13.90 $\mu\text{g g}^{-1}$) [29], Bertazzo et al. (14.89–15.29 $\mu\text{g g}^{-1}$) [30] and Sreenivasa Rao et al. (4.90–22.54 $\mu\text{g g}^{-1}$) [31] reported.

4. Conclusion

It was shown DMSA can attach to a gold surface by its two thiol functional groups and form a SAM on the Au electrode. This SAM can interact with copper ions by free carboxyl groups of attached DMSA. The DMSA/Au electrode was used for DP anodic stripping voltammetry of copper(II). The calibration graph of Cu(II) was shown ideally to be a linear relationship from 3 to 225 $\mu\text{g L}^{-1}$, with a slope factor of 0.038 $\mu\text{A} (\mu\text{g L}^{-1})^{-1}$ and correlation factor of 0.998. The detection limit was 1.29 $\mu\text{g L}^{-1}$. Table 2 shows comparison of current work and some previous works performed by self-assembled monolayer electrodes applied for determination of copper. Although some of these works have reported low detection limits, but preparation methods for these self-assembled monolayers are usually complex and include various synthesis steps [12,22], whereas our elec-

trode is modified simply only dipping gold electrode into the modifier solution. On the other hand, analyzed real samples in these works have the concentration ranges about ppb [12,21,22], therefore, they can be analyzed easily by our method. Also, our work shows a good reproducibility as compared to other studies. Similarly, linear range, modification time and interference effects are comparable with other studies. Also, this electrode can be regenerated easily by dipping it into the EDTA solution for a few times.

References

- [1] J.J. Gooding, F. Mearns, W. Yang, J. Liu, *Electroanalysis* 15 (2003) 81.
- [2] R.K. Smith, P.A. Lewis, P.S. Weiss, *Prog. Surf. Sci.* 75 (2004) 1.
- [3] V. Kriegisch, C. Lambert, *Top. Curr. Chem.* 258 (2005) 257.
- [4] S.F. Wang, D. Du, Q.C. Zou, *Acta Phys. Chim. Sin.* 17 (2001) 1102.
- [5] S. Berchmans, S. Arivukkodi, *Electrochem. Commun.* 2 (2000) 226.
- [6] I. Turyan, D. Mandler, *Anal. Chem.* 66 (1994) 58.
- [7] J. Wang, B.Z. Zeng, C. Fang, X.Y. Zhou, *Electroanalysis* 12 (2000) 763.
- [8] B.Z. Zeng, F.Q. Zhao, X.G. Ding, *Anal. Sci.* 17 (2001) 259.
- [9] B. Zeng, X. Ding, F. Zhao, *Electroanalysis* 14 (2002) 651.
- [10] B. Zeng, X. Ding, D. Pan, F. Zhao, *Talanta* 59 (2003) 501.
- [11] W. Yang, J.J. Gooding, D.B. Hibbert, *J. Electroanal. Chem.* 516 (2001) 10.
- [12] G. Liu, Q.T. Nguyen, E. Chow, T. Bocking, D.B. Hibbert, J.J. Gooding, *Electroanalysis* 18 (2006) 1141.
- [13] W. Yang, E. Chow, G.D. Willett, D.B. Hibbert, J.J. Gooding, *Analyst* 128 (2003) 712.
- [14] E. Chow, D.B. Hibbert, J.J. Gooding, *Analyst* 130 (2005) 831.
- [15] N. Yang, X. Wang, Q. Wan, *Electrochim. Acta* 51 (2006) 2050.
- [16] R.S. Freire, L.T. Kubota, *Electrochim. Acta* 49 (2004) 3795.
- [17] J. Xia, W. Wei, Y. Hu, L. Wu, *Anal. Sci.* 20 (2004) 1037.
- [18] D.W.M. Arrigan, L.L. Bihan, *Analyst* 124 (1999) 1645.
- [19] A.C. Liu, D.C. Chen, C.C. Lin, H.H. Chou, C.H. Chen, *Anal. Chem.* 71 (1999) 1549.

- [20] S. Huan, C. Jiao, Q. Shen, J. Jiang, G. Zeng, G. Huang, G. Shen, R. Yu, *Electrochim. Acta* 49 (2004) 4273.
- [21] A. Profumo, D. Merli, M. Pesavento, *Anal. Chim. Acta* 557 (2006) 45.
- [22] R.K. Shervedani, S.A. Mozaffari, *Anal. Chem.* 78 (2006) 4957.
- [23] A. Mohadesi, M.A. Taher, *Talanta*, in press.
- [24] N.B. Li, L.M. Niu, H.Q. Luo, *Microchim. Acta* 153 (2006) 37.
- [25] F. Sabermahani, M.A. Taher, *Anal. Chim. Acta* 265 (2006) 152.
- [26] T. Galeano Diaz, A. Guiberteau, M.D. Lopez Soto, J.M. Ortiz, *Food Chem.* 96 (2006) 156.
- [27] M.H. Sorouraddin, J.L. Manzoori, M. Iranifam, *Talanta* 66 (2005) 1117.
- [28] J.N. Miller, J.C. Miller, *Statistics and Chemometrics for Analytical Chemistry*, fifth ed., Pearson Prentice Hall, 2005.
- [29] V.V.S. Ramakrishna, V. Singh, A.N. Garg, *Sci. Total Environ.* 192 (1996) 259.
- [30] A. Bertazzo, C. Costa, M. Biasiolo, G. Allegri, G. Cirrincione, G. Presti, *Biol. Trace Elem. Res.* 52 (1996) 37.
- [31] K. Sreenivasa Rao, T. Balaji, T. Prasada Rao, Y. Babu, G.R.K. Naidu, *Spectrochim. Acta B* 57 (2002) 1333.

Differentiation of two Canary DO red wines according to their metal content from inductively coupled plasma optical emission spectrometry and graphite furnace atomic absorption spectrometry by using Probabilistic Neural Networks

Isabel M. Moreno^a, Dailos González-Weller^b, Valerio Gutierrez^c, Marino Marino^d, Ana M. Cameán^a, A. Gustavo González^{e,*}, Arturo Hardisson^b

^a Nutrition, Food Chemistry and Toxicology, Faculty of Pharmacy, University of Sevilla, C/Profesor García González 2, 41012 Sevilla, Spain

^b Obstetrics, Gynaecology, Paediatrics, Preventive Medicine and Public Health, Toxicology and Legal Medicine, Faculty of Medicine, University of La Laguna, Campus de Ofra s/n, 38071 La Laguna, Tenerife, Spain

^c Chemistry Engineering and Pharmacist Technology, Faculty of Chemistry, University of La Laguna, C/Astrofísico Francisco Sánchez s/n, 38071 La Laguna, Tenerife, Spain

^d Laboratory of Public Health, C/Rambla General Franco 53, 38006 Santa Cruz de Tenerife, Tenerife, Spain

^e Analytical Chemistry, Faculty of Chemistry, University of Sevilla, C/Profesor García González no. 1, 41012 Sevilla, Spain

Received 3 July 2006; received in revised form 9 October 2006; accepted 19 October 2006

Available online 28 November 2006

Abstract

The metal content of 54 commercialized wines (30 samples from Tacoronte-Acentejo DO (class T) and 24 Valle de la Orotava DO (class O) wines) was performed by ICP-OES (Al, Ba, Cu, Fe, Mn, Sr, Zn, Ca, K, Na and Mg) and GF-AAS (Ni and Pb). Wine samples were processed by dry ashing followed by solution with 5% nitric acid. Metals were considered as suitable descriptors to differentiate between T and O classes. Supervised learning pattern recognition procedures were applied. Linear discriminant analysis (LDA) led to good results up to about 90% of correct classification. In order to improve the results, another kind of algorithms able to model non-linear separation between classes was considered: Probabilistic Neural Networks. Accordingly, excellent results were obtained, leading to sensitivities and specificities higher than 95% for the two classes.

© 2006 Elsevier B.V. All rights reserved.

Keywords: Wine differentiation; Linear discriminant analysis; Probabilistic Neural Networks; Canary island

1. Introduction

Wine is a widely consumed beverage in the world and has an obvious commercial value and social importance. Therefore, the evaluation of the quality of wines is important for manufacturers, merchants and consumers. Denomination of origin (DO) have been created in Spain, the main purpose of whose Regulating Councils is to guarantee the source and quality of the wines to prevent fraud and to guarantee origin [1]. To attain it, a by far useful tool is the knowledge of the values of several chemical

descriptors that allow a link to be established between the wine samples and their geographical origin.

The quantity of inorganic ions in wine is of great interest, because of their influence on wine technology as well as their toxic effects [2]. However, one of the main interests is to use the mineral content to characterise the wines by their geographical origin taking into account the relationship between the metallic content in samples and soil composition [3]. This differentiation can be carried out by using major, trace and ultra-trace elements [4]. Climatic conditions influence on necessary fungicide treatments of wines that determine the level of copper in grapes, and edaphical features also have influence on metal level such as Na, Ca, K and Fe of grapes [5]. The two major sources of Pb in wine are soil-related and anthropogenic: winery equipment, vine treatment, atmospheric aerosols rich in industrial fumes

* Corresponding author. Tel.: +34 954557173; fax: +34 954557168.
E-mail address: agonzale@us.es (A.G. González).

and exhaust gases. Because of government policies to reduce total Pb emissions and replace old winery equipment, the Pb content in wine is gradually decreasing. The Organisation Internationale de la Vigne et du Vin (OIV) limits Pb amounts in wine to $200 \mu\text{g L}^{-1}$ [6].

Metal elements have been widely used for differentiating Spanish wines according to geographical origin [5,7–13]. In the present work, two Canary DO were studied: Tacoronte-Acentejo and Valle de la Orotava. Particularities of wines from the Canary Island are that they are elaborated with autochthonous varieties that cannot be found elsewhere in the world, the vines are not contaminated by phylloxera and soils are volcanic [14]. With respect to these two growing areas, the production region of wines protected by the Tacoronte-Acentejo DO is located at the north side of the Tenerife Island and is run through by steep mountain-clefts. The district contains nine communities: La Laguna, Tegueste, Tacoronte, El Sauzal, La Matanza de Acentejo, La Victoria de Acentejo, Santa Ursula, El Rosario and Santa Cruz de Tenerife (Anaga). The cultivated area is approximately 2422 ha, distributed among the different communities. The grape and wine-growing region which is currently protected under the DO of Valle de la Orotava comprises a region located at the north side of the Tenerife Island. At present, the planted area inscribed of this DO is 671 ha and includes the cities of La Orotava, Los Realejos and El Puerto de la Cruz.

Tacoronte-Acentejo DO uses grapes belonging to Canary variety Listán Negro and Negramoll. The hills and valleys of this district are covered by grapes, which reach from the sea until almost 1000 m. This area is the biggest wine-district and the one with the most intensive cultivation of the Canary Islands. It represents 40% of the wine cultivation area of the island of Tenerife and 20% of the area of the Canary archipelago. The cultivation is situated at hillsides, which are orientated to the north and the sea. The grounds have a red colour and are rich of organic earth, deficient in lime, but rich in nitrogen, phosphorus and potassium.

El Valle de la Orotava DO employs grapes belonging to the one of the autochthonous varieties above mentioned (Listán Negro). The vines of this district reach from the sea since 250–700 m. The cultivation is situated in a vast valley which is making one's way at the foot of the mountain Teide and spreading out until the sea, showing very different hues according to the distinct terrains and unevenness, vegetation and farming.

Typical vineyard soil is permeable, rich in minerals nutrients and with a slightly acid pH because of its volcanic origin.

The north coast of the island is protected from the African winds and influenced by the September winds and the influence of the altitude causes a mild and pleasant climate which is steady and has almost no notable thermal differences. The yearly temperature is always above 7°C . Although the sky is often cloudy (with an atmospheric humidity of 60%) the rainfalls are few, because the low temperature holds up the condensation of the humidity.

Accordingly, soil differences and, in minor extent, differences in grape varieties could be reflected in the metal content

Table 1

Analytical lines used for each element and the instrumental conditions in the ICP-OES apparatus

Parameter	
RF frequency (MHz)	27.12
Operating power (W)	1350
Coolant Ar flow (L min^{-1})	20
Plasma Ar flow (L min^{-1})	0.6
Carrier Ar flow (L min^{-1})	0.5
Nebulizer type	Babington V
Detection wavelengths (nm^{-1})	
Al	396.152
Ba	233.527
Ca	393.366
Fe	259.940
K	766.490
Mg	280.270
Mn	257.610
Na	589.592
Sr	346.446
Zn	213.856
Cu	324.754

of the two DO wines. Consequently, the aim of the present paper is the determination of the content of Al, Ba, Cu, Fe, Mn, Sr, Zn, Ca, K, Na, and Mg by using inductively coupled plasma atomic emission spectrometry (ICP-OES) and Ni and Pb measured by graphite furnace atomic absorption spectrometry (GFAAS) in red wines to differentiate between the two DO mentioned (Tacoronte-Acentejo and Valle de la Orotava).

For classification and discrimination between wine samples coming from these two producing regions, supervised pattern recognition techniques such as linear discriminant analysis (LDA) [15] and Probabilistic Neural Networks (PNN) [16] were applied.

2. Experimental

2.1. Apparatus

Elemental analyses were carried out on a Thermo Jarrell Ash Atom Scan 25 inductively coupled plasma atomic emission spectrometer (Genesis Laboratory Systems Inc., CO, USA). Table 1 shows the analytical lines used for each element, as well as the instrumental conditions. Moreover, a Perkin-Elmer 4100 ZL Zeeman atomic absorption spectrometer attached to a PE HG 4100 graphite furnace (with a PE AS-70 automatic injector, all from Perkin-Elmer, Norwalk, CT, USA) was employed for quantitation of Pb and Ni by the GFAAS technique. The graphite furnace temperature program is gathered in Table 2.

2.2. Chemical and reagents

Merck (Darmstadt, Germany) CertiPUR[®]. ICP-multielement standard solutions of about 1000 mg L^{-1} were used as stock solution for calibration. Other reagents were of analytical grade. Milli-Q treated water was used throughout.

Table 2
HG 4100 Graphite furnace parameters used for analysis of Ni and Pb in red wines from Tacoronte and Orotava DO

Step	Temperature (°C)		Ramp time (s)	Hold time (s)	
	Ni	Pb		Ni	Pb
1	100	100	10	10	20
2	130	130	25	20	20
3	450	450	15	20	20
4	1350	800	5	20	10
5	2350	1250	0	5 ^a	3 ^a
6	2550	2500	2	4	3

Argon flow rate, 250 mL min⁻¹; injection volume, 20 µL.

^a Gas stop for reading.

2.3. Samples

Thirty samples of red wines of different brands with D.O. trademark “Tacoronte-Acentejo” (code T) and 24 samples of “El Valle de la Orotava” (code O) were purchased in liquor retails and markets. All the samples were from 2004-vintage. The alcoholic content ranged from 12 to 14% (v/v) ethanol for all wine samples.

The plastic containers used for storing and treating the samples were cleaned to avoid contamination of the samples with traces of any metal. Containers were treated with 5% nitric acid during 24 h followed with two washes with Milli-Q water.

Once opened, wines samples were digested according to the following procedure:

The 25 mL of each sample were placed in porcelain crucibles. To avoid contamination and cross-talking between the samples, single used plastic tools were utilised to transfer the material. Each sample was then dried in an oven at a temperature of 50 °C for at least 12 h. The crucibles with the samples were then introduced in muffle ovens and burned to ash at 450 °C. The temperature in the muffle oven was increased at a rate of approximately 50 °C h⁻¹ and maintained at 450 °C during 18–24 h. The white ashes obtained with this procedure were then dissolved in 5% nitric acid to a volume of 25 mL.

2.4. Data analysis

The content of each mineral element was considered as chemical descriptor. Pattern recognition methods were applied to the data matrix, composed of 13 columns (the analysed elements) and 54 rows (red wines). LDA and PNN were applied for differentiation between class T and class O wines. The statistical package, STATISTICA 7 from Statsoft [17] was used for all the chemometric calculations.

3. Results and discussion

3.1. Mineral content in red wine samples

The metal content of the two different DO red wines was determined and carefully scrutinized. The results, expressed in

milligram per litre (except Pb and Ni values, in microgram per litre), were obtained from triplicate measurements and rounded up to the last significant figure associated with random error. Table 3 shows these results. The corresponding descriptive basic statistic for both DO wines samples can be seen in Table 4. Looking at these values, K was the element with a major content in all samples. The mean concentration of K was similar in Tacoronte and Orotava wines samples, with average concentrations of 1363.6 and 1307.2 mg L⁻¹, respectively. Ca, Mg and Na presented lower and similar contents, their average values being 111.6, 107 and 106.6 mg L⁻¹, respectively, in Tacoronte samples and 124.9, 110.7 and 84 mg L⁻¹ in Orotava ones. Nickel was also present with values higher than 10 mg L⁻¹ (37.1 and 31.5 mg L⁻¹ in Tacoronte and Orotava, respectively) and Al was present with values near 10 mg L⁻¹. The other analysed metals mostly appeared with values close to 1 mg L⁻¹, such as Fe, Mn, Sr and Zn, and even lower, being Ba and Cu the metals with the lowest concentration in both class (T and O). All the values obtain for both class of red wines were similar with the exception of Pb which was not detected in the Orotava samples and close to 1 mg L⁻¹ in Tacoronte ones.

3.2. Statistical procedures for classification

Using the mineral content found in the analysed red wines samples as chemical descriptors, statistical methods were applied in order to establish differences between both DO wines samples for classification and authentication purposes. There are a number of display methods for visualizing data trends, such as principal component analysis (PCA) [18] or cluster analysis (CA) [19]. However, our research starts from the a priori knowledge of class membership of the samples to be processed and hence, typical supervised learning pattern recognition methods have to be applied. In our case, two classes were considered, i.e. Tacoronte (T) and Orotava (O) red wines samples. First of all, the method of LDA was applied for building linear frontiers between the two classes. Because of possible non-linear nature of class distribution, Bayesian artificial neural networks such as PNN were also applied.

3.2.1. LDA

Linear discriminant analysis is a typical discriminating method, belonging to the first level of PR, where objects are classified into either of a number of defined classes [20]. Discriminant functions are obtained as linear combination of metal descriptors to maximise the *F*-ratio of between class sum of squares and within class sum of squares. If we have *p* descriptors and *g* classes, the number of uncorrelated discriminant functions are *p* or *g* – 1 whichever is smaller; and so, in our case only one discriminant function can be obtained. The parameter called Wilks’ lambda is the ratio between the within class sum of squares and the total sum of squares, calculated for each descriptor. The discrimination power of a given descriptor is better when its Wilks’ lambda is lesser [21,22]. Thus, after applying standard LDA and according to the Wilks’ lambda, six descriptors, namely Zn, Ba, Pb, Na, Mg and Al, seem to be optimal ones for distinguishing between class

Table 3
 Experimental results^a for determination of elements (mg L⁻¹) in T and O red wines samples by ICP-OES and GFAAS^b

Sample	Code	Pb ^b	Ni ^b	Al	Ba	Cu	Fe	Mn	Sr	Zn	Ca	K	Na	Mg
1	T	2.64	78.66	6.68	0.05	1.30	4.57	2.15	0.73	0.86	94.53	1110.25	145.75	107.88
2	T	1.00	39.94	8.63	0.06	0.12	3.34	1.77	0.48	0.64	76.45	1248.50	79.10	127.33
3	T	0.85	46.16	11.04	0.15	0.03	3.50	2.26	0.71	0.80	103.70	1335.00	84.28	119.05
4	T	1.07	33.22	12.33	0.10	0.15	3.25	1.31	0.67	0.48	102.80	1392.75	81.70	118.88
5	T	0.43	22.47	7.96	0.17	0.31	2.71	0.88	1.24	0.51	112.13	1238.00	108.63	123.75
6	T	2.23	15.24	5.19	0.11	0.53	1.14	2.58	0.81	1.04	95.65	1325.50	127.80	132.23
7	T	ND	42.12	7.31	0.14	0.90	2.99	2.79	0.87	0.78	130.73	980.75	110.38	111.48
8	T	ND	24.08	6.68	0.09	0.12	2.62	3.29	0.68	0.52	118.05	1193.25	102.00	114.05
9	T	ND	40.41	6.86	0.11	0.05	2.83	1.17	0.82	0.52	110.08	1311.50	78.78	113.53
10	T	0.17	44.60	7.02	0.14	0.10	3.60	2.74	1.09	1.01	132.83	1309.25	160.80	134.85
11	T	0.00	29.59	6.94	0.12	0.14	4.00	2.87	0.98	0.97	111.73	1430.50	96.93	123.20
12	T	1.32	34.41	7.28	0.13	1.20	3.19	1.13	0.96	0.65	100.75	1438.50	67.45	99.45
13	T	1.17	58.86	6.70	0.12	0.07	6.70	2.24	0.57	0.66	114.38	1369.50	120.15	136.33
14	T	ND	26.43	7.27	0.15	0.67	2.47	2.31	0.95	0.75	213.28	1826.50	256.03	236.15
15	T	1.07	24.95	5.60	0.14	0.13	2.32	1.67	0.94	0.78	98.85	1408.75	114.18	140.83
16	T	0.81	22.52	5.53	0.12	1.27	2.45	2.02	1.05	0.49	91.10	1474.50	96.43	121.08
17	T	1.15	27.65	5.27	0.10	0.16	2.66	2.57	0.69	0.62	98.75	1205.50	106.80	135.05
18	T	0.62	29.69	12.45	0.14	0.11	2.68	2.67	1.04	0.89	107.05	1395.75	69.28	137.90
19	T	0.83	24.75	5.87	0.10	0.25	2.43	1.63	0.74	0.66	110.45	1169.00	67.75	98.35
20	T	1.42	73.05	6.85	0.10	0.07	2.68	0.87	1.06	0.68	112.55	1322.00	89.80	122.95
21	T	1.22	71.63	5.94	0.08	0.14	2.66	4.08	1.01	0.67	114.40	1356.00	111.30	110.40
22	T	0.88	30.08	8.99	0.12	0.34	4.30	2.51	1.08	0.78	133.70	1595.00	95.45	154.55
23	T	ND	24.92	5.12	0.11	0.17	1.91	2.14	0.75	1.01	114.40	1494.00	124.25	128.10
24	T	7.36	39.76	8.23	0.16	0.22	2.55	0.82	1.12	0.78	115.90	1613.50	174.25	116.45
25	T	1.01	28.57	8.16	0.11	0.14	2.74	1.84	0.80	0.54	114.80	1377.00	75.15	109.55
26	T	0.87	32.97	9.29	0.14	0.30	3.08	0.94	0.97	0.61	98.20	1535.50	114.80	116.70
27	T	ND	39.66	7.85	0.12	0.06	3.16	1.16	1.02	0.67	150.45	1231.00	87.70	108.45
28	T	0.96	31.09	6.23	0.16	0.10	2.57	1.86	0.86	0.64	119.00	1232.50	94.70	129.25
29	T	2.16	44.06	7.66	0.18	0.07	3.29	1.42	0.73	1.03	65.40	1590.00	74.30	117.75
30	T	2.11	40.37	5.10	0.11	0.08	2.03	1.04	0.75	0.69	105.05	1451.00	93.30	112.65
31	O	ND	20.89	9.35	0.11	0.28	2.39	1.85	1.11	0.92	118.28	1224.33	68.90	115.12
32	O	ND	29.06	9.70	0.16	0.22	3.12	0.95	0.97	0.76	91.77	933.17	76.88	102.42
33	O	ND	22.95	8.73	0.15	0.19	3.00	0.99	0.97	0.81	85.78	1607.00	75.38	103.28
34	O	ND	20.42	8.69	0.12	0.06	2.57	1.61	0.82	0.45	99.65	1922.17	63.20	102.45
35	O	ND	31.90	9.00	0.10	0.13	1.93	1.65	0.75	0.69	118.23	1824.25	58.50	100.88
36	O	ND	24.58	6.45	0.09	1.38	2.66	1.89	0.58	0.85	88.85	1259.75	71.10	87.55
37	O	ND	17.86	6.53	0.12	0.10	2.63	1.08	0.50	0.73	100.95	1077.25	83.65	87.33
38	O	ND	15.92	5.15	0.08	0.05	2.73	1.18	0.45	0.91	89.40	1127.50	57.30	88.73
39	O	ND	22.76	5.94	0.05	0.04	2.50	1.95	0.28	0.10	79.73	1371.75	65.85	98.23
40	O	ND	50.87	12.73	0.11	0.37	3.49	3.43	0.88	0.75	118.73	1564.75	78.13	119.30
41	O	ND	22.06	8.63	0.10	0.63	3.00	1.63	0.85	1.01	108.10	1199.50	75.20	120.00
42	O	ND	18.19	11.27	0.11	0.45	2.36	2.10	1.10	0.71	122.23	1385.00	71.33	120.85
43	O	ND	31.09	8.40	0.12	0.04	3.68	1.82	1.22	0.67	127.40	1326.50	106.05	110.63
44	O	ND	27.48	6.09	0.08	0.17	2.93	2.18	0.88	0.77	92.50	1048.25	99.45	96.35
45	O	ND	27.20	7.25	0.11	0.14	3.65	1.72	1.05	0.87	116.25	1113.50	104.80	103.85
46	O	ND	19.69	7.26	0.09	0.21	2.80	2.53	0.83	1.07	102.30	1229.00	71.85	122.33
47	O	ND	36.35	10.30	0.24	3.09	1.82	2.82	1.44	0.00	107.65	1281.50	85.00	127.85
48	O	ND	32.41	10.22	0.20	0.18	5.22	1.61	1.80	0.50	134.40	1577.50	84.40	138.85
49	O	ND	53.51	8.98	0.19	0.14	5.38	2.33	1.31	0.78	119.25	1032.50	86.35	110.45
50	O	ND	41.13	14.34	0.26	1.15	4.69	2.85	1.43	0.13	136.00	1491.00	138.95	136.35
51	O	ND	46.52	12.77	0.28	2.73	2.29	2.36	1.49	ND	111.20	1313.50	105.90	127.20
52	O	ND	64.44	9.99	0.23	0.22	4.12	1.88	1.23	ND	109.45	1350.50	112.55	125.90
53	O	ND	33.76	7.21	0.13	0.05	3.33	1.73	0.79	0.71	105.35	1111.00	123.90	129.60
54	O	ND	35.31	6.45	0.08	0.03	3.02	0.91	0.58	0.83	97.85	732.00	96.45	92.45

ND, not detected.

^a Mean of triplicate determinations.

^b Pb and Ni values were expressed in $\mu\text{g L}^{-1}$.

T and O samples. Evaluation samples are classified from the estimation of an a posteriori probability of class membership using the Bayes' theorem. In order to evaluate the classification performance, the leave-one-out method was used as a validation

procedure, obtaining a prediction ability of 90.7%. This result, albeit fairly good, could be improved by using artificial neural networks that are able to model non-linear frontiers between classes.

Table 4
Metal concentration in Tacoronte red wine samples ($n=30$) and Villa de la Orotava samples ($n=24$)

Element	“Tacoronte samples”			“Orotava samples”		
	Mean \pm S.D. (mg L^{-1})	Median (mg L^{-1})	Range of quantified values (mg L^{-1})	Mean \pm S.D. (mg L^{-1})	Median (mg L^{-1})	Range of quantified values (mg L^{-1})
Al	7.32 ± 1.91	6.94	4.37–13.31	8.79 ± 2.29	8.54	5.15–14.34
Ba	0.12 ± 0.03	0.12	0.042–0.18	0.14 ± 0.06	0.12	0.05–0.29
Ca	111.55 ± 26.79	107.83	64.00–252.45	106.99 ± 17.99	104.45	82.40–172.85
Cu	$0.31 \pm .37$	0.14	0.06–1.34	0.47 ± 0.76	0.18	0.03–2.78
Fe	3.01 ± 0.96	2.72	1.12–6.85	3.10 ± 0.88	2.96	1.77–5.38
K	1363.47 ± 170.62	1354.50	968.00–1887.50	1307.16 ± 290.02	1297.50	732.00–2016.50
Mg	124.94 ± 25.60	120.55	96.55–280.85	110.66 ± 15.52	109.53	70.65–139.80
Mn	2.36 ± 3.29	1.99	0.81–4.01	1.82 ± 0.62	1.76	0.91–3.46
Na	106.58 ± 39.42	96.50	62.05–220.75	83.99 ± 20.29	79.00	54.45–138.95
Ni ^a	37.11 ± 16.21	33.08	14.39–103.4	31.55 ± 13.62	27.57	14.5–69.18
Pb ^a	1.16 ± 1.46	0.95	0.17–7.36	ND	ND	ND
Sr	$0.88 \pm .18$	0.86	0.44–1.24	0.97 ± 0.36	0.95	0.27–1.84
Zn	$0.74 \pm .17$	0.72	0.44–1.05	0.63 ± 0.33	0.71	0.04–1.08

^a Ni and Pb values were expressed in $\mu\text{g L}^{-1}$.

3.2.2. PNN

In this paper, we propose to use Probabilistic Neural Networks (PNNs) for the classification of the two classes of wine. The PNN approach combines both Bayes theorem of conditional probability and Parzen’s method for estimating the probability density functions of the random variables. Unlike other neural network training paradigms, PNNs are characterised by high training speed and their ability to produce confidence levels for their classification decision. The probabilistic neural network was developed by Donald Specht. His network architecture was first presented in two papers, *Probabilistic Neural Networks for Classification, Mapping or Associative Memory and Probabilistic Neural Networks*, released in 1988 and 1990, respectively. This network provides a general solution to pattern classification problems by following an approach developed in statistics, called Bayesian classifiers. Bayes theory, developed in the 1950s, takes into account the relative likelihood of events and uses a priori information to improve prediction. We will outline the PNN performance in the following.

Consider Q classes in the training set, C_1, C_2, \dots, C_Q ; and n_1, n_2, \dots, n_Q the corresponding number of pattern vectors that belongs to each class. The prior probability for that a given pattern vector \mathbf{x} belongs to class C_K can be estimated from Laplace’s rule:

$$P(C_K) = \frac{n_K}{\sum_{j=1}^Q n_j}$$

but if we know the components x_1, x_2, \dots, x_p , this information can be added to the network and calculate the posterior probability by using the Bayes’ theorem:

$$P\left(\frac{C_K}{\mathbf{x}}\right) = \frac{p(\mathbf{x}/C_K)P(C_K)}{p(\mathbf{x})}$$

P refers to the probability and p to the probability density function (PDF). Thus, $p(\mathbf{x}/C_K)$ is the conditional PDF of the pattern vector once it belongs to class C_K . $p(\mathbf{x})$ is the PDF of pattern vectors and plays the role of a normalization factor. The posterior probability $P(C_K/\mathbf{x})$ is the probability that the pattern belongs

to class C_K once their components are known. This probability can be evaluated by choosing the class having the high posterior value:

$$P\left(\frac{C_K}{\mathbf{x}}\right) = \max_{j \in \{1, 2, \dots, Q\}} P\left(\frac{C_j}{\mathbf{x}}\right) \quad (1)$$

Taking into account that $p(\mathbf{x})$ is a normalization factor, we can write:

$$P\left(\frac{\mathbf{x}}{C_K}\right) P(C_K) = \max_{j \in \{1, 2, \dots, Q\}} P\left(\frac{\mathbf{x}}{C_j}\right) P(C_j) \quad (2)$$

The estimation of conditional PDF for every class can be easily done by applying the modified Parzen’s estimator that is the activation function of PNN and acts as a multivariate Gaussian operator:

$$P\left(\frac{\mathbf{x}}{C_K}\right) = \frac{1}{(2\pi)^{p/2} \sigma_K^p n_K} \sum_{i=1}^{n_K} \exp\left(-\sum_{j=1}^p \left(\frac{x_j - x_{ij}^{(K)}}{\sigma_K}\right)^2\right) \quad (3)$$

x_j and x_{ij} are the components of any pattern vector \mathbf{x} and of the pattern vector $\mathbf{x}_i^{(K)}$ belonging to class K . σ_K is the called smoothing factor, which is optimised during training.

PNN are arranged into four layers: input layer, pattern layer, summation layer and decision layer. Fig. 1 shows the corresponding architecture. The input layer is used to store the new samples of the validation set. Pattern vectors of the training set are used to optimise the smoothing factor in the training step. The pattern layer contains as many neurons as pattern vectors of the training set grouped by classes. PNN training is accomplished by simply copying each pattern in the training set to the neurons of the pattern layer. The summation layer consists of one neuron for each class and sums the outputs from all pattern neurons. This gives a measure of the posterior probability density function for each class when an input vector is processed. The decision layer consists of one neuron that search for the maximum posterior probability density function, and assign to the input vector the class with highest probability.

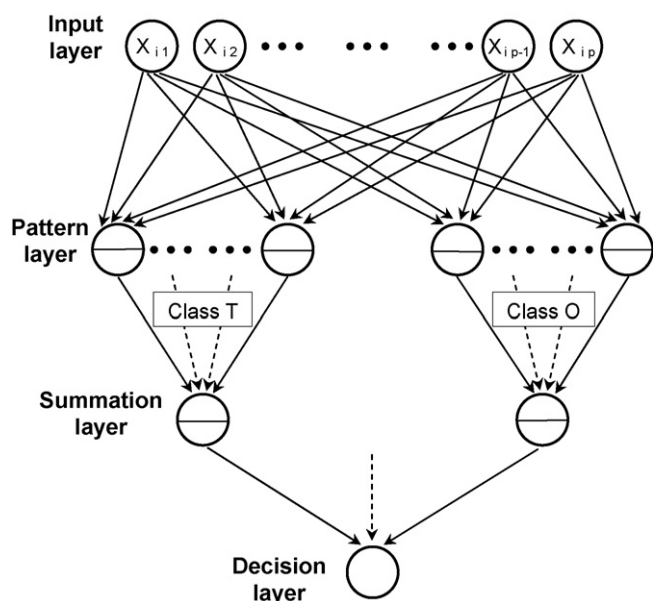


Fig. 1. Architecture of a typical PNN for two classes O and T.

For validation purposes the whole data set is then split randomly into two sets, the training and the evaluation set, each containing about 50% samples of every class. Once the classification rule is developed, some workers consider as validation parameters the recalling efficiency (rate of training samples correctly classified by the rule) and, specially, the prediction ability (rate of evaluation samples correctly classified by the rule). However, these parameters could be misleading because they do not consider the number of false positive and false negative for each class. These two concepts provide a deep knowledge of the classes' space. Accordingly, it seems to be more advisable the use of terms sensitivity (SENS) and specificity (SPEC) for validating the decision rule [23]. The SENS of a class corresponds to the rate of evaluation objects belonging to the class that are correctly classified, and the SPEC of a class corresponds to the rate of evaluation objects not belonging to the class that are correctly considered as belonging to the other classes. This may be explained in terms of the first and second kind of risks associated with prediction. The first kind of errors (α) corresponds to the probability of erroneously reject a member of the class as a non-member (rate of false negative, FN). The second kind of errors (β) corresponds to the probability of erroneously classify a non-member of the class as a member (rate of false positive, FP). Accordingly, for a given class A, and setting n_A as the number of members of class A, \bar{n}_A as the number of non-members of class A, $\langle n_A \rangle$ as the number of members of class A correctly classified as "belonging to class A" and $\langle \bar{n}_A \rangle$ as the number of non-members of class A classified as "not belonging to class A", we have:

$$\text{SENS} = \frac{\langle n_A \rangle}{n_A} = 1 - \alpha = 1 - \frac{\text{FN}_A}{n_A},$$

$$\text{SPEC} = \frac{\langle \bar{n}_A \rangle}{\bar{n}_A} = 1 - \beta = 1 - \frac{\text{FP}_A}{\bar{n}_A}$$

In our case, we have 13 input neurons (one for any metal descriptor), 54 pattern neurons (30 for T class and 24 for O class), 2 summation neurons (the two classes) and 1 decision neuron (the class winner). In this case, and dealing with two classes, it is clear that $\text{FP}_O = \text{FN}_T$ and $\text{FP}_T = \text{FN}_O$.

By suitably adjusting the smoothing factor minimising the training error, we obtain in average $\text{FP} = \text{FN} = 1$ for the two classes. Thus, class O has $\text{SENS} = 95.8\%$ and $\text{SPEC} = 96.7\%$ and class T, conversely, $\text{SENS} = 96.7\%$ and $\text{SPEC} = 95.8\%$. These findings fit very well with the assumption of two classes corresponding to the investigated DO.

4. Conclusion

For differentiation of the considered samples of the Tacoronte and Orotava DO wines, PNN algorithms give excellent results, leading to specificities and sensitivities higher than 95%.

References

- [1] S. Pérez-Magariño, M. Ortega-Heras, M.L. González-San José, Z. Boger, *Talanta* 62 (2004) 983.
- [2] G. González Hernández, A. Hardisson de la Torre, Arias León F.J.J., *Z Lebensm Unters Forsch* 203 (1996) 517.
- [3] S. Frías, J.E. Conde, M.A. Rodríguez, V. Dohnal, J.P. Pérez-Trujillo, *Nahrung/Food* 46 (2002) 370.
- [4] B. Medina, in: P.R. Ashurst, M.J. Dennis (Eds.), *Wine Authenticity, Food Authentication*, London, UK, 1996, pp. 60–107.
- [5] M. Ortega, M.L. Gonzalez-San Jose, S. Beltran, *Quim. Anal.* 18 (1999) 127.
- [6] M. Barbaste, B. Medina, J.P. Pérez-Trujillo, *Food Addit. Contam.* 20 (2003) 141.
- [7] M.S. Larrechi, J. Guasch, F.X. Rius, A. Solé, *Vitis* 26 (1987) 172.
- [8] M. Gonzales-Larraina, A. Gonzales, B. Medina, *Connai. Vigne. Vin.* 21 (1987) 127.
- [9] C. Herrero-Latorre, B. Medina, *Connais. Vigne. Vin.* 24 (1990) 147.
- [10] M.J. Latorre, C. Garcia-Jares, B. Medina, C. Herrero, *J. Agric. Food Chem.* 42 (1994) 1451.
- [11] V. Lizama, J.L. Aleixandre, I. Alvarez, M.J. García, *Riv. Vitic. Enol.* 50 (1997) 29.
- [12] S. Frías, J.P. Perez -Trujillo, E.M. Peña, J.E. Conde, *Eur. Food Res. Technol.* 213 (2001) 145.
- [13] A. Jos, I. Moreno, A.G. González, G. Repetto, A.M. Cameán, *Talanta* 63 (2004) 382.
- [14] J.P. Pérez-Trujillo, M. Barbaste, B. Medina, *Anal. Lett.* 36 (2003) 679.
- [15] D. Coomans, D.L. Massart, L. Kaufman, *O. Anal. Chim. Acta* 112 (1979) 97.
- [16] D. Sprech, *Neural Netw.* 3 (1990) 109.
- [17] StatSoft Inc., *STATISTICA for Windows (Computer Program Manual)*, Tulsa, OK, 2005.
- [18] I.T. Jolliffe, *Principal Component Analysis*, Springer-Verlag, Berlín, 1986.
- [19] N. Bratchell, *Chemom. Int. Lab. Sys.* 6 (1989) 105.
- [20] C. Albano, W. Dunn, U. Edlund, E. Johansson, B. Nordén, M. Sjöström, S. Wold, *Anal. Chim. Acta* 103 (1978) 429.
- [21] D. González-Arjona, A.G. González, *Anal. Chim. Acta* 363 (1998) 89.
- [22] A. Alcázar, F. Pablos, M.J. Martín, A.G. González, *Talanta* 57 (2002) 45.
- [23] D. González-Arjona, G. López-Pérez, A.G. González, *Chemom. Intell. Lab Sys.* 57 (2001) 133.

Comparison of two vibrational procedures for the direct determination of mancozeb in agrochemicals

Javier Moros, Sergio Armenta, Salvador Garrigues*, Miguel de la Guardia

Department of Analytical Chemistry, Universitat de València, Edifici Jeroni Muñoz, 50th Dr. Moliner, 46100 Burjassot, Valencia, Spain

Received 17 April 2006; received in revised form 20 September 2006; accepted 27 September 2006

Available online 27 October 2006

Abstract

The direct determination of mancozeb in agrochemicals has been made by diamond attenuated total reflectance (ATR) Fourier transform infrared spectroscopy in the middle range (DATR-MIR) and diffuse reflectance infrared Fourier transform spectroscopy in the near range (DR-NIR) methods using in both cases a previous identification of the samples using a dendrographic classification and an appropriate partial least squares (PLS) calibration established from a set of nine external standards and optimized for each type of sample. It was analyzed a heterogeneous population of 11 samples obtained from the Spanish market, containing different co-formulated products, such as fosetyl-Al, copper oxychloride, metalaxyl or cymoxanil. High performance liquid chromatography (HPLC) was used as reference method for validation of both vibrational strategies. The close agreement between values found for both, DATR-MIR and DR-NIR methods, and reference HPLC values indicates the accuracy and reliability of the proposed techniques for the direct determination of mancozeb in commercially available formulations.

© 2006 Elsevier B.V. All rights reserved.

Keywords: Mancozeb; Mid infrared; Near infrared; Attenuated total reflectance; Diffuse reflectance; Non-linear; Partial least squares; Pesticide formulations

1. Introduction

The agrochemical sector is the world's major industry area, over 50 percent of the world's population being dependent upon agriculture for its livelihood. It has been evidenced by data reported in 2000 and 2001 that the world pesticide expenditures totalize more than 32.5 billion dollars per year and that the amount used of these products exceeded 5.0 billion pounds per year [1].

The registration and sale of a pesticide formulation implies a number of different controls among which its evaluation, safety and composition are the most important aspects [2].

Mancozeb, a mixture of [[1,2-etenbisdithiocarbamate](2-)] of manganese and zinc is one of the most used pesticides around the world because of its effect against a wide spectrum of fungal diseases, including potato blight, leaf spot, scab (on apples and pears) and rust (on roses) and due to its low oral lethal dose LD₅₀ (greater than 5000 mg/kg to greater than 11,200 mg/kg in rats) [3].

Mancozeb is practically insoluble in common organic and inorganic solvents and indirect methods for its determination include spectrophotometric [4], gas chromatography (GC) [5], headspace solid phase micro-extraction GC [6] or reversed phase ion-pair chromatography [7] determination of the reaction products liberated after reduction, in an acidic medium, to carbon disulfide.

Other methods employed for the determination of ethylenebisdithiocarbamates rely on the measurement of the metallic portion of these compounds, and therefore, many of these methods are similar to those used for determination of inorganic manganese or zinc [8].

Liquid chromatography has been employed after transformation of dithiocarbamates onto water-soluble sodium salts, methylation and ultraviolet detection at 272 nm [9] to determine and distinguish thiocarbamates and dithiocarbamates.

Mancozeb has been also determined in solid pesticide formulations by Fourier transform infrared, FTIR spectrometry based on the use of the ratio between the absorbance of a characteristic band of mancozeb and that of an internal standard measured in the FTIR spectra obtained from KBr pellets [10]. However, we must recognize that this procedure is tedious and time consuming. Recently, our research group has been proposed

* Corresponding author. Tel.: +34 96 354 3158; fax: +34 96 354 4838.

E-mail address: salvador.garrigues@uv.es (S. Garrigues).

a simple procedure for mancozeb determination in agrochemicals based on the use of photoacoustic Fourier transform infrared spectroscopy (PAS-FTIR) measurements [11], but this method requires the employ of a special detector.

Nowadays, there is an ongoing interest in the development of fast and non-destructive techniques with no sample preparation or manipulation, which can be useful for the quality control of manufactured products or raw materials. In this sense, it is clear that vibrational spectroscopy-based techniques with a chemometric treatment of the data provide valuable tools to solve this problem in other industrial areas [12,13].

Attenuated total reflectance (ATR) accessories are especially useful for obtaining IR spectra of difficult samples that cannot be readily examined by the normal transmission mode. They are suitable for studying thick or highly absorbing solid and liquid materials, including films, coatings, powders, threads, adhesives, polymers and aqueous samples. ATR requires little or no sample preparation for most samples and is one of the most versatile sampling techniques [14].

On the other hand, taking into account that most of formulated pesticides are in solid form, diffuse reflectance infrared Fourier transform spectroscopy in the near range (DR-NIR) is a technique which can be considered highly useful, since it was developed to facilitate analysis with minimal sample preparation and without physical alteration from a wide variety of samples.

In spite of the aforementioned considerations, in our knowledge, only one work related to the quality control of metronidazole based on near infrared reflectance has been previously published [15].

The aim of this paper is to develop, evaluate and compare aforementioned two vibrational sampling techniques (ATR-MIR using a diamond accessory and DR-NIR) in terms of precision, accuracy, sensitivity, sampling frequency and reagents consume for its use in the quality control of a variety of solid commercial pesticide formulations containing mancozeb.

2. Experimental

2.1. Apparatus and reagents

A Bruker model Multipurpose Analyzer (MPA) FT-NIR spectrometer controlled by OPUS[®] for Windows[®] software from Bruker GmbH (Bremen, Germany) and equipped with a single detector onto which the radiation is focused by means of an integrating sphere, used as measurement accessory, was employed for NIR spectra acquisition.

For ATR spectra acquisition it was employed a DuraSamplIR with a three-reflection diamond/KRS-5 composite DiCompTM DuraDiskTM, which was installed on a Bruker FTIR spectrometer model Tensor 27 equipped with a KBr beamsplitter and a DLaTGS detector.

For instrumental and measurement control and data acquisition it was employed the OPUS program (Version 4.1) from Bruker. Spectra treatment and data manipulation were carried out using Omnic 2.1 software from Nicolet (Madison, WI, USA). PLS calibration models were obtained by using TurboQuant Analyst 6.0 software developed by Thermo Nicolet Corp.

A Dionex P680 High Performance Liquid Chromatograph (Sunny Vale, CA, USA), with an UVD 170U variable wavelength UV–vis detector and equipped with a C-18 reversed phase (Kromasil) column (250 mm × 4.6 mm i.d. and 5 μm particle diameter), was employed for the determination of mancozeb in the reference methodology.

Mancozeb standard (88.1%, w/w) was supplied by Riedel-de-Haën (Seelze, Germany) and acetonitrile, chloroform, hexane and sodium hydroxide (all of them analytical reagent grade), and also methanol (HPLC gradient grade), were purchased from Scharlau (Barcelona, Spain). EDTA disodium salt 2-hydrate was supplied by Panreac (Barcelona, Spain) and tetrabutylammonium hydrogen sulfate, methyl iodide and 1, 2-propanediol were obtained from Fluka (Buchs, Switzerland). Kaolin was purchased from Afrasa S.A. (Valencia, Spain) and commercially available mancozeb samples were obtained directly from the Spanish market.

Samples evaluated could be classified in four groups corresponding to: (i) group 1 integrated by samples which contain mancozeb and copper oxychloride, (ii) group 2 of samples formulated with fosetyl-Al, (iii) group 3 corresponding to formulations of mancozeb and metalaxyl and (iv) group 4 of samples that contain mancozeb and cymoxanil.

2.2. Reference procedure

A high performance liquid chromatography (HPLC) method based on the work of Gustafsson and Thompson [16] was used as reference procedure for mancozeb determination based on a previous methylation process. Lo et al. [9] also used this methodology to determine and distinguish different dithiocarbamates such as propineb, thiram and mancozeb, maneb and zineb.

A 10–20 mg of sample were weighted inside a 100 ml beaker and 50 ml of 0.25 M EDTA in 0.45 M sodium hydroxide solution (pH 9.5–9.6) were added and stirred during 10 min. The EDTA extract was filtered through a Whatman 42 (Brentford, Middlesex, UK), 2.5 μm pore size cellulose filter paper. The extraction beaker and the filter were rinsed with 20 ml water. The pH of the solution was adjusted to 6.5–8.5 by addition of 8 ml of HCl 2 M and 5 ml of aqueous tetrabutylammonium hydrogen sulfate solution 0.4 M. The mixture was shaken in a separatory funnel for 5 min with 30 ml of methyl iodide 0.05 M in chloroform:hexane 3:1. The organic phase was collected and the aqueous phase was rinsed with 10 ml of methyl iodide solution. Both organic phases were combined and concentrated by rotary evaporation at 30 °C after the addition of 5 ml of 1,2-propanediol 20% (v/v) in chloroform. The residue was transferred to a 10 ml volumetric flask and diluted to the volume with methanol. After manual stirring 0.5 g of the solution were diluted to 10 g with methanol and 20 μl of this solution were directly injected in a 50:50 acetonitrile:water mobile phase of 1 ml min⁻¹ carrier flow and mancozeb determined, in the isocratic mode, by absorbance measurements at 272 nm. Area values of the chromatogram peaks obtained at 9.3 min for samples were interpolated in an external calibration line established from five standard solutions of mancozeb containing till 92.5 mg l⁻¹ treated in the same way than samples.

Additionally, samples of group 2, that contains fosetyl-Al, were previously mixed with 50 ml slightly hot water (60 °C) to solve fosetyl-Al and to avoid its interference in the determination of mancozeb. After that, the slurry was centrifuged during 3 min at 3000 rpm and the procedure continued by the aforementioned way.

Samples of group 1 cannot be analyzed by using the selected methodology due to the copper oxychloride interferences. So, values provided by the manufacturer were taken as reference for data evaluation.

2.3. Diamond attenuated total reflectance (DATR-MIR) procedure

Powdered samples or standards were placed onto the DATR accessory and an integrated torque press was used to apply a constant force of 25 lbs. Spectra were recorded between 4000 and 600 cm^{-1} , using a nominal resolution of 4 cm^{-1} , accumulating 32 scans per spectrum with a mirror velocity of 10 KHz (26 s per spectrum).

Unknown samples are firstly identified and classified from DATR spectra using an hierarchical cluster and later the analyte is quantified by using a calibration model developed for this kind of sample.

Although, it is commonly accepted that to make a useful PLS trial calibration a minimum of one hundred samples is required [17], a simplest approach, that uses external standards as calibration set in the PLS model, has been developed to determine mancozeb in different commercial samples.

PLS models were built using nine external standards covering a concentration range from 5.43 to 83.59% (w/w) as calibration set. These standards were prepared by mixing, in an agate mortar, different amounts of mancozeb and kaolin and the wavenumber range, baseline correction and number of factors, were selected as a function of the type of sample. An heterogeneous population of 11 different samples, containing different co-formulated products, has been used as validation set.

In order to minimize the cross-contamination the DATR crystal surface was cleaned between samples using soft paper slightly wetted with acetone.

2.4. Diffuse reflectance (DR-NIR) procedure

Powdered samples were placed in 2 ml standard glass chromatographic vials (12 mm \times 32 mm) of 9.5 mm internal diameter used as measurement cell. The spectra were collected in Kubelka–Munk mode with a nominal resolution of 8 cm^{-1} , accumulating 36 scans per spectrum (17 s data acquisition). The closed integrating sphere was used to collect the corresponding background at the same instrumental conditions than samples.

Sample type was identified based on the use dendrographic spectra treatment and from this information, the appropriate PLS calibration model was selected for mancozeb determination in each unknown sample.

PLS models were built using the nine aforementioned external standards and choosing, for each group of sample types, the appropriate wavelength range and number of factors.

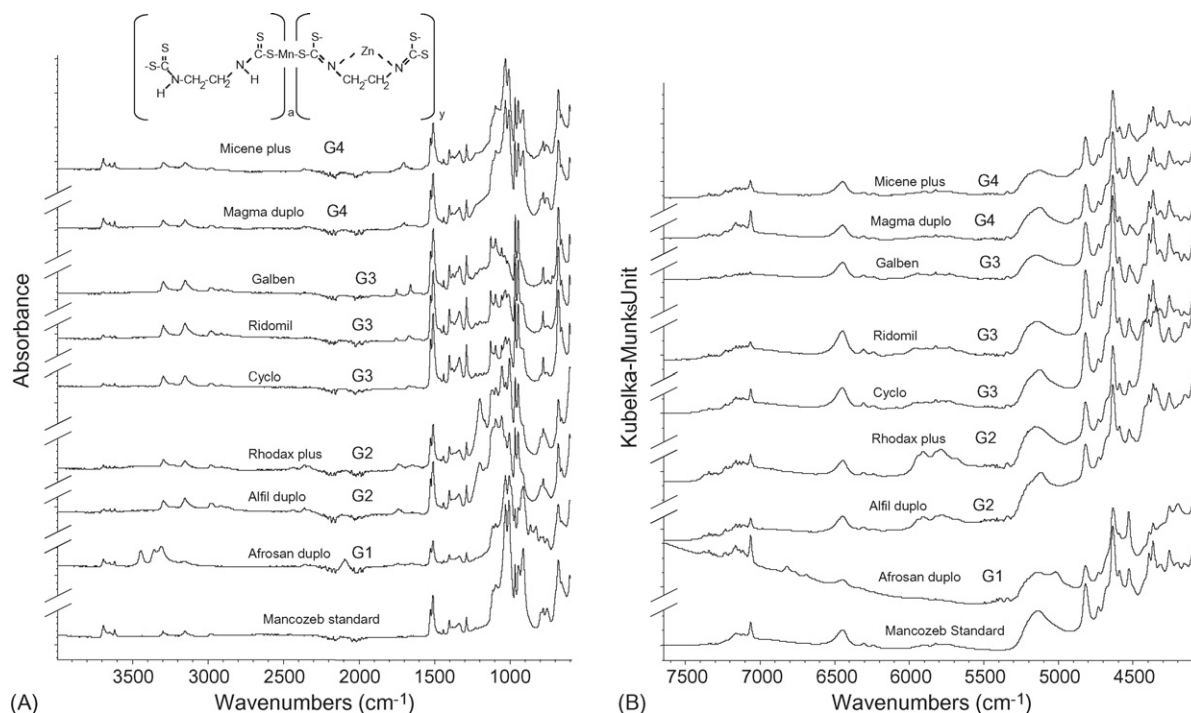


Fig. 1. Diamond attenuated total reflectance MIR (A) and diffuse reflectance NIR (B) spectra of the different formulations assayed. Instrumental conditions: 4 cm^{-1} nominal resolution and 32 cumulated scans per spectrum, and 8 cm^{-1} nominal resolution and 36 cumulated scans per spectrum were used for DATR-MIR and DR-NIR, respectively. Note: It was also included the spectrum of a mancozeb standard of 66.24% (w/w) mixed with kaolin. Spectra were shift on the y-axis to clearly show their bands.

3. Results and discussion

3.1. DATR-MIR and DR-NIR spectra of mancozeb

Fig. 1 shows DATR-MIR (A) and DR-NIR (B) spectra of a mancozeb standard in kaolin and different commercial samples of agrochemicals containing mancozeb. It can be appreciate that for both spectral regions, MIR and NIR, the main absorption bands corresponding to mancozeb are present in samples and standards, and additionally than these, characteristic bands of the other active constituents contained in formulations, such as copper oxychloride, fosetyl-AI, metalaxyl or cymoxanil are also evidenced.

For MIR spectra, bands located at 1528 and 1512 cm^{-1} are due to the amide II band in CSNH structures and seem to be free from matrix interferences and thus could be useful for mancozeb determination in pesticide formulations. Other less intense bands located at 1402, 1335, 1287, 1039 and 968 cm^{-1} can be associated to CNH stretching-bending, CNH stretch-open, C=S and CNC stretching and NCS deformation, respectively [18].

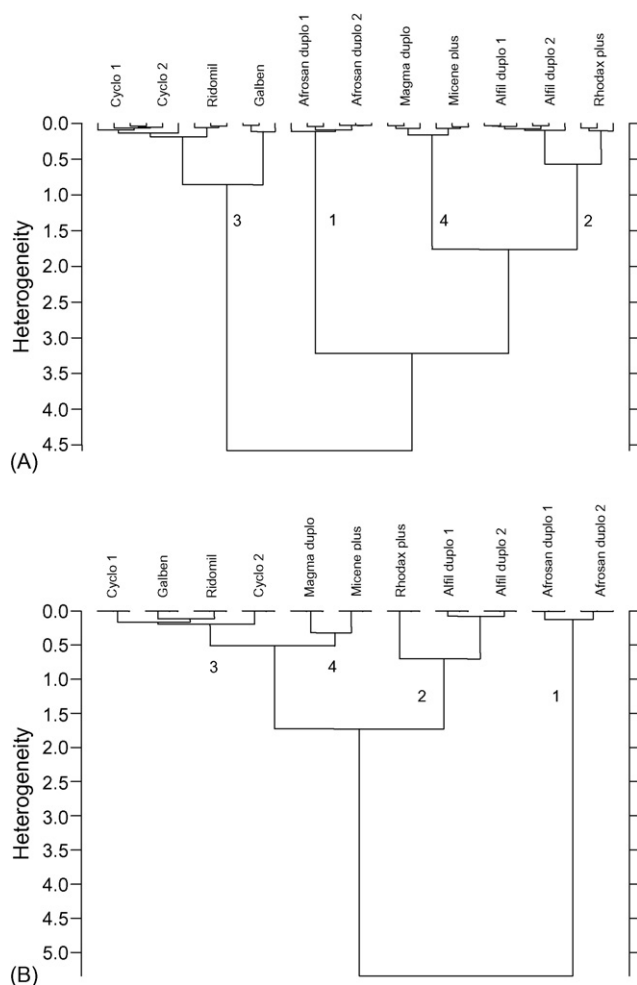


Fig. 2. Dendrographic classification of 11 agrochemical samples containing mancozeb using the Euclidian distance based on their DATR-MIR spectra (A) and their DR-NIR spectra (B) using vector normalization pre-processing for the regions compressed between 4000 and 600 cm^{-1} and the region between 7500 and 4000 cm^{-1} , respectively. To identify groups 1–4 see the text.

Table 1
Prediction capabilities of linear PLS-DATR-MIR for mancozeb determination in commercial pesticide formulations

Calibration conditions	Figures of merit		ATR corrected spectra												
	PLS factors extracted		Raw spectra		RMSEC	RMSEP	RMSEP	RMSEC	RMSEP	RMSEP	QC	d_{x-y} (%)	s_{x-y} (%)	s_{trip} (%)	QC
Spectral region (cm^{-1})	RMSEC (%)	RMSEP (%)	RMSEC (%)	RMSEP (%)	d_{x-y} (%)	s_{x-y} (%)	s_{trip} (%)	QC (%)	RMSEC (%)	RMSEP (%)	RMSEP (%)	d_{x-y} (%)	s_{x-y} (%)	s_{trip} (%)	QC (%)
Group 1 1360–1306	3	1.4	1.1	6	-0.3	1.1	0.5	8	1.3	1.0	6	-0.03	1.1	0.5	8
Group 2 1527–1508, 3192–3108	2	2.5	5	13	3	4	3	14	2.1 ^a	3 ^a	8 ^a	0.11 ^a	3 ^a	3 ^a	2 ^a
Group 3 1383–1323	1	2.9	3	4	0.4	3	3	2	2.5	3	4	1.5	3	3	3
Group 4 1753–1207	1	3.5	10	21	7	7	4	32	3.3	9	19	7	6	3	30

Note: RMSEC and RMSEP are the root mean square error of calibration and prediction, respectively. RMSEP is the RMSEP divided by the mean value of mancozeb concentration in the validation dataset. s_{trip} is the standard deviation of three replicates. d_{x-y} and s_{x-y} are the mean difference and the standard deviation of mean differences between predicted vs. actual mancozeb concentration (% w/w), respectively. QC is the quality coefficient. No baseline correction has been used in groups 1, 2 and 4. In group 3, a linear removed correction has been applied.

^a Values obtained when three PLS factors were extracted.

In the case of NIR spectra, it can be seen several bands corresponding to mancozeb. The band located at 6448 cm^{-1} related to the CSNHR first overtone, band centred at 4817, 4730 and 4632 cm^{-1} could be associated to the band combination of the structure CSNHR and the bands situated at 5137 cm^{-1} correspond to the second overtone of C=S in CSNHR. Moreover, it is possible to distinguish the band at 4392 cm^{-1} related to C–H stretch or CH_2 deformation. Finally, bands located at 4365 and 4254 cm^{-1} could be related to C–H and CH_2 second overtone, respectively [19].

3.2. Clustering of mancozeb samples from their MIR and NIR spectra

Pesticide formulations considered as samples in the present study correspond to mancozeb associated with other constituents, appropriate solvents or surfactants.

In order to evaluate possible classes among samples considered, taking into account the additional co-formulated products, a clustering discriminant study was made before PLS data treatment.

The similarity between samples was evaluated using the distance concept, calculated using a mathematical relationship (i.e., Euclidean norm) of numerical properties of the samples (i.e., absorbance at different wavelengths).

In our opinion, this previous step is an important task, which allows us to select properly the PLS model, thus improving the prediction of unknown samples. It must be indicated that the classification of samples is based on their spectra but could be interpreted through the obtained clusters considering the differences in sample composition.

Cluster analysis from MIR and NIR spectra, was carried out using vector normalization pre-processing for the regions compressed between 4000 and 600 cm^{-1} and between 7500 and 4000 cm^{-1} , respectively, and employing the standard algorithm which uses the Euclidean distance to determine the spectral distances.

In both cases, in order to calculate the spectral distances between the clusters, Ward's algorithm, which attempts to find the most homogeneous groups, was used. Thus,

instead of the spectral distance the growth in heterogeneity is monitored.

Results are presented in the two dendrograms of Fig. 2. It can be appreciated that all commercially available samples employed for this study were classified in the same four groups regardless of whether the MIR or NIR spectral region were tested, thus achieving a good classification agreement with their composition in attending to the additional co-formulated active constituents.

3.3. MIR and NIR partial least square modelization for mancozeb determination

The use of an external monoparametric calibration for the determination of mancozeb in commercial formulations by using both spectral regions, provided a very poor linearity and high relative errors for all sample groups considered and, because of that, the possibility to use a multivariate calibration technique, such as partial least squares (PLS), for the treatment of data, was evaluated for each group of samples selected from the hierarchical cluster analysis.

Although, several spectral regions were tested and different models were built and compared in terms of root mean square standard error of prediction (RMSEP) values in order to evaluate their prediction capabilities for the samples analyzed at both spectral regions, MIR and NIR, only most significant results will be summarized in this paper.

In order to validate the two vibrational methodologies assayed, different quality indicators were given. Among them, it was considered: (i) the mean difference (d_{x-y}) between vibrational-PLS predicted values and reference data; (ii) the standard deviation of mean differences (s_{x-y}); (iii) the quality coefficient (QC); (iv) the pooled standard deviation for validation samples (s_{trip}) [20]. As stated by Massart et al., the QC is to be preferred over correlation coefficient of the regression between predicted and reference data "not only because it gives a better idea of the spread of the data points around the fitted straight line but also because it gives some indication on the percentage error to be expected for the estimated concentration". QC was calculated as the mean square sum of the

Table 2
Prediction capabilities of non-linear PLS-DATR-MIR for mancozeb determination in commercial pesticide formulations

Calibration conditions			Figures of merit							
Spectral region (cm^{-1})	Baseline correction (cm^{-1})	PLS factors extracted	r	RMSEC (% w/w)	RMSEP (% w/w)	RRMSEP (%)	d_{x-y} (% w/w)	s_{x-y} (% w/w)	s_{trip} (% w/w)	QC (%)
Group 1 1382–1288	None	4	0.999	1.4	0.8	5	–0.6	0.6	0.4	6
Group 2 1533–1506, 3192–3108	None	4	0.998	1.8	2	6	–1.0	1.9	2	3
Group 3 1543–1488	None	3	0.998	2.0	3	5	–0.7	3	1.6	5
Group 4 1421–1306	Linear removed	5	0.999	1.8	2	5	0.4	2	1.9	5

Note: The meaning of each parameter as indicated in footnote of Table 1.

relative prediction error of each validation sample (predicted minus actual concentration) divided by the actual concentration. Several figures for the fitting of the model to the data, such as root mean square error of calibration (RMSEC) and multiple correlation coefficient (r), were also used [21].

3.4. Linear PLS-DATR-MIR modelling

Table 1 shows the analytical features of PLS-DATR-MIR models based on the use of both, raw and ATR corrected spectra (ATR correction multiplies the sample spectrum by a wavelength-dependent factor to adjust the relative peak intensities), using mancozeb standards prepared by mixing different amounts of the pesticide with kaolin, as calibration set, for mancozeb determination in pesticide formulations as a function of the use of different spectral regions and baseline criteria for each group of samples considered. The spectral regions studied were those for which the contribution of the concomitants and the other constituents was minimum. Mean centring spectra data pre-treatment was employed to eliminate common spectral information in both cases.

The leave one out cross-validation procedure was used to obtain the best number of latent variables for each pesticide using the predicted residual error sum of squares (PRESS).

In spite of the use of the most appropriate spectral regions for each one of the four sample groups established and on the fact that good correlation coefficients (r) were obtained using a low number of PLS factors, prediction capabilities achieved were not acceptable in all the cases, providing QC values ranging from 2 to 32%. It can be seen that the ATR correction, provides a slight improvement of results obtained without correction. However, in the case of samples corresponding to group 4, analytical characteristics obtained using linear PLS were absolutely unacceptable, obtaining a QC parameter value of the order of 30%.

3.5. Non-linear PLS-DATR-MIR modelization for mancozeb

On considering the possibility that the system being modelled exhibit a non-linear behaviour, probably due to the high concentrations employed for calibration or because possible interactions between co-formulated products, a non-linear PLS approach was applied in order to obtain satisfactory and robust calibration models.

Several spectral regions were tested, taking into consideration the DATR spectra of the other substances present in the samples to avoid spectral interferences, and different models were built but only most significant results are indicated in Table 2.

It can be seen the prediction capabilities achieved when non-linear models were built for each group.

Although the spectral regions employed for the non-linear modelization are not the same than those used for linear modelling for groups 3 and 4, all of them agree with the respective spectra for the additional co-formulated ingredients.

The numbers of PLS extracted factors used in non-linear modelization are slightly higher than the number of factors

Table 3
Prediction capabilities of PLS-DR-NIR for mancozeb determination in commercial pesticide formulations

Spectral region (cm ⁻¹)	Calibration conditions		Figures of merit													
	PLS factors extracted	Raw spectra	Raw spectra					Automatic baseline corrected spectra								
			RMSEC (% w/w)	RMSEP (% w/w)	RRMSEP (%)	d _{x-y} (% w/w)	s _{x-y} (% w/w)	s _{trip} (% w/w)	QC (%)	RMSEC (% w/w)	RMSEP (% w/w)	RRMSEP (%)	d _{x-y} (% w/w)	s _{x-y} (% w/w)	s _{trip} (% w/w)	QC (%)
Group 1 4435–4335	2		1.7	0.8	5	-0.5	0.7	0.6	5	1.7	0.7	4	-0.12	0.7	0.6	4
Group 2 4810–4663	5		1.5	3	8	0.7	3	2	6	1.5	3	7	0.7	3	2	6
Group 3 4852–4784, 4709–4663	2		3.9	3	4	-0.5	3	2	4	3.9	3	4	-0.5	3	2	4
Group 4 4887–4659	4		1.8	1.9	4	1.7	0.8	0.6	6	1.8	1.6	3	1.4	0.9	0.6	5

Note: The meaning of each parameter as indicated in footnote of Table 1. Linear removed correction has been used in groups 1, 2 and 4. In group 3, a baseline established from 4879 to 4759 cm⁻¹ in the first region and a linear removed correction has been applied for second region.

required for linear models, because the first approach includes the additional factors needed in order to explain the non-linearity of the system. However, the number of extracted factors for these models, through cross-validation, ranged between 3 and 5, and thus they can be considered enough robust and flexible in the prediction of the response, on considering the matrix of samples.

As it can be seen in Table 2, good correlation coefficients were achieved providing RMSEC values ranging between 1.4 and 2.0% (w/w). The non-linear PLS models developed provide QC values from 3 to 6%, for the different groups of samples. They were of the same order than those obtained by linear approach except in the case of group 4 where, probably due to the composition of this type of samples (the concomitant or the other active constituent interfere or interact with the analyte), a clear improvement of the results has been obtained.

3.6. PLS-DR-NIR modelling

Table 3 shows the analytical features of PLS-DR-NIR models built for each group of samples considered also based on the use of both, raw and corrected spectra, using the aforementioned mancozeb standards as calibration set. Mean centring spectra data pre-treatment was also employed in both cases.

As can be seen, for this situation, spectral regions used are different for each one of the four groups established taking into account their respective co-formulated active constituents NIR spectra.

Good correlation coefficients were obtained for a number of PLS factors between 2 and 5, showing RMSEC values from 1.5 to 3.9% (w/w), as it can be seen in Table 3.

In this case, the general automatic baseline correction applied, in which software selects some baseline points and

automatically corrects the selected spectra, slightly improves the prediction capabilities, providing QC values between 4 and 6%.

3.7. Analysis of commercially available formulations

DATR-MIR and DR-NIR methodologies provided statistically comparable results with those obtained by HPLC reference method or manufacturer values (in the case of group 1) for mancozeb analysis in 11 commercially available formulations, as can be seen in Table 4.

Occasionally, standard deviations for DATR-MIR and DR-NIR data are slightly higher than HPLC ones. In deed, we should measure spectra with high repeatability. Unfortunately, in DATR spectroscopy, spectra of solid samples can vary considerably when applying different pressures to the sample as this is directly influencing the contact of the sample with the crystal.

Moreover, it can be seen that accuracy errors obtained for the comparison of data found by both vibrational methodologies with HPLC were lower than 7% in all cases studied.

On the other hand, the regression between all the average values of results found for all commercial samples assayed by non-linear PLS-DATR-MIR and PLS-DR-NIR procedures as a function of HPLC reference method provided equations of $C_{\text{DATR}} = (0.1 \pm 1.6) + (0.99 \pm 0.03)C_{\text{HPLC}}$ and $C_{\text{DR}} = (1.1 \pm 1.6) + (0.98 \pm 0.03)C_{\text{HPLC}}$ with correlation coefficient values of $r=0.996$ and with $r=0.996$, providing root mean square error (RMSE) values of 2.1 and 2.0, respectively.

A regression between data obtained through both vibrational procedures provided an equation of $C_{\text{DR}} = (1 \pm 2) + (0.99 \pm 0.04)C_{\text{DATR}}$ with $r=0.993$, in this case with a RMSE value of 2.7.

Table 4
Determination of mancozeb in pesticide formulations by HPLC-UV and vibrational methodologies base on DATR-MIR and DR-NIR procedures

Sample	HPLC-UV (% w/w) ^a	DATR-MIR (% w/w) ^a	Er ^b (%)	DR-NIR (% w/w) ^a	Er ^c (%)
Group 1*					
Afrosan duplo 1	17.5 ± 0.6	17.3 ± 0.2	-0.9	17.8 ± 0.8	1.7
Afrosan duplo 2	17.5 ± 0.8	16.5 ± 0.5	-5.8	16.9 ± 0.3	-3.4
Group 2					
Alfil duplo 1	36.3 ± 0.8	35.2 ± 1.5	-3.0	38.4 ± 1.4	5.8
Alfil duplo 2	34.2 ± 1.1	33 ± 3	-2.9	32 ± 4	-6.4
Rhodax plus	35.0 ± 0.7	34.2 ± 1.3	-2.3	36.8 ± 1.1	5.1
Group 3					
Cyclo 1	78.1 ± 0.7	77.1 ± 1.4	-1.3	75.1 ± 1.7	-3.8
Cyclo 2	67.0 ± 0.9	70.7 ± 1.7	5.5	69 ± 3	3.0
Galben	76.9 ± 1.8	72 ± 2	-6.4	78.9 ± 0.9	2.6
Ridomil	74.0 ± 1.8	73.2 ± 1.4	-1.1	71 ± 2	-4.1
Group 4					
Magma duplo	39.7 ± 0.4	42 ± 3	5.0	41.7 ± 0.4	5.0
Micene plus	50.9 ± 1.7	49.7 ± 1.0	-2.4	51.6 ± 0.8	1.4

^a Concentration values are the average of two independent analysis measured in triplicate for HPLC procedure and three independent measurements for vibrational procedures ± the corresponding standard deviation of values found.

^b Accuracy error (%) found by comparing the DATR-MIR values with results obtained by HPLC.

^c Accuracy error (%) found by comparing the DR-NIR values with results obtained by HPLC.

* Note: For group 1, the concentration values of samples used as reference correspond to those declared by the manufacturer.

Additionally it has been checked, for all samples analyzed, the elliptic joint confidence test for the slope and the intercept of the aforementioned regressions, being observed the good comparability between the methodologies assayed. So it can conclude that the regression lines obtained present slope and intercept values statistically comparable with 1 and 0, respectively, which evidence the absence of systematic errors.

4. Conclusion

It can conclude that both vibrational procedures developed provide simple, rapid and reliable tools for mancozeb determination in the agrochemicals considered. Moreover, these methods are non-destructive and they allow collection of good-quality infrared spectra from any solid sample with almost no sample preparation.

Although both vibrational procedures can be used to collect data from a reduced amount of sample, providing quantitative results, without any sample preparation step, DR-NIR technique could be considered the most appropriate because a clean step is not required and samples and standards can be stored in the measurement cells for additional studies.

On the other hand, both, DATR-MIR and DR-NIR procedures offer main advantages versus HPLC procedure such as a strong reduction of the volume of reagents consumed and waste generated, and the increase of the measurement frequency from 2 h^{-1} in the case of HPLC to 60 or 120 h^{-1} for DATR and DR, respectively.

So, both proposed spectrometric methodologies are fast and environmentally friendly alternatives to the classic reference chromatographic procedures used for routine analysis of agrochemicals.

Acknowledgements

The authors acknowledge the financial support of Ministerio de Educación y Ciencia (*Project CTQ2005-05604/BQU, FEDER*) and Direcció General d'Investigació i Transferència Tecnològica de la Generalitat Valenciana (*Project ACOMP06-*

161). S. Armenta also acknowledges the FPU Grant of the MECED (Ref. AP2002-1874).

References

- [1] EPA: Pesticides–2000/2001 Pesticide Sales and Usage Report, Biological and Analysis Division Office of Pesticide Programs, Washington, 2002, <http://www.epa.gov/oppbead1/pestsales/01pestsales/sales2001.html>.
- [2] Pesticide Registration Program, US Environmental Protection Agency (US EPA), Washington, 2004, <http://www.epa.gov/pesticides/factsheets/registration.htm>.
- [3] EXTTOXNET. Extension Toxicology Network. Pesticide Information Profiles, 1996, <http://exttoxnet.orst.edu/pips/mancozeb.htm>.
- [4] E.D. Caldas, M.H. Conceição, M.C.C. Miranda, L.C.K.R. de Souza, J.F. Lima, *J. Agric. Food Chem.* 49 (2001) 4521.
- [5] A. Zena, P. Conte, A. Piccolo, *Fresenius Environ. Bull.* 8 (1999) 116.
- [6] M. Bekbolet, *Chim. Acta Turc.* 18 (1990) 353–357.
- [7] H. van Lishaut, W. Schwack, *J. AOAC Int.* 83 (2000) 720.
- [8] R.J. Cassella, V.A. Salim, S. Garrigues, R.E. Santelli, M. de la Guardia, *Anal. Sci.* 18 (2002) 1253.
- [9] C.C. Lo, M.H. Ho, M.D. Hung, *J. Agric. Food Chem.* 44 (1996) 2720.
- [10] S. Armenta, S. Garrigues, M. de la Guardia, *Talanta* 65 (2005) 971.
- [11] S. Armenta, J. Moros, S. Garrigues, M. de la Guardia, *Anal. Chim. Acta* 567 (2006) 255–261.
- [12] A. Salari, E. Richard, *Int. J. Pharm.* 163 (1998) 157.
- [13] G.A. Norton, J.F. McClelland, *Miner. Eng.* 10 (1997) 237.
- [14] A.J. Vreugdenhil, M.S. Donley, N.T. Grebasch, R.J. Passinault, *Prog. Org. Coat.* 41 (2001) 254.
- [15] X.J. Cui, Z.Y. Zhang, P.D. Harrington, Y.L. Ren, *Chem. J. Chin. Univ.* 25 (2004) 1251.
- [16] K.H. Gustaffson, R.A. Thompson, *J. Agric. Food Chem.* 29 (1981) 729.
- [17] A.M.C. Davies, *Spectrosc. Eur.* 18 (2004) 23–24.
- [18] D. Lin-Vien, N.B. Colthup, W.G. Fateley, J.G. Grasselli, *Infrared and Raman Characteristic Frequencies of Organic Molecules*, Academic Press, London, 1991.
- [19] J.S. Shenk, J.J. Workman, M.O. Westerhaus, Application of NIR spectroscopy to agricultural products, in: D.A. Burns, E.W. Ciurezak (Eds.), *Handbook of Near-Infrared Analysis. Practical Spectroscopy Series*, vol. 13, Marcel Dekker, Inc., New York, 1992, pp. 393–395.
- [20] D.L. Massart, B.G.M. Vandeginste, L.M.C. Buydens, S. de Jong, P.J. Lewi, J. Verbeke, *Handbook of Chemometrics and Qualimetrics (Part A and B)*, Elsevier Science B.V., Amsterdam, 1997.
- [21] J. Moros, F.A. Iñón, S. Garrigues, M. de la Guardia, *Anal. Chim. Acta* 538 (2005) 181.

A new BOD estimation method employing a double-mediator system by ferricyanide and menadione using the eukaryote *Saccharomyces cerevisiae*

Hideaki Nakamura^{a,b,*}, Kyota Suzuki^a, Hiroaki Ishikuro^a, Shintaro Kinoshita^a,
Rui Koizumi^a, Seisaku Okuma^a, Masao Gotoh^{a,b}, Isao Karube^{a,b,*}

^a School of Bionics, Tokyo University of Technology, 1404-1 Katakura, Hachioji, Tokyo 192-0982, Japan

^b Research Center of Advanced Bionics (RCAB), National Institute of Advanced Industrial Science and Technology (AIST), Tokyo University of Technology, 1404-1 Katakura, Hachioji, Tokyo 192-0982, Japan

Received 12 September 2006; received in revised form 15 October 2006; accepted 15 October 2006

Available online 13 November 2006

Abstract

A new biochemical oxygen demand (BOD) sensing method employing a double-mediator (DM) system coupled with ferricyanide and a lipophilic mediator, menadione and the eukaryote *Saccharomyces cerevisiae* has been developed. In this study, a stirred micro-batch-type microbial sensor with a 560 μL volume and a two-electrode system was used. The chronamperometric response of this sensor had a linear response between 1 μM and 10 mM hexacyanoferrate(II) ($r^2 = 0.9995$, 14 points, $n = 3$, average of relative standard deviation and R.S.D._{av} = 1.3%). Next, the optimum conditions for BOD estimation by the DM system (BOD_{DM}) were investigated and the findings revealed that the concentration of ethanol, used to dissolve menadione, influenced the sensor response and a relationship between the sensor output and glucose glutamic acid concentration was obtained over a range of 6.6–220 $\text{mg O}_2 \text{ L}^{-1}$ (five points, $n = 3$, R.S.D._{av} 6.6%) when using a reaction mixture incubated for 15 min. Subsequently, the characterization of this sensor was studied. The sensor responses to 14 pure organic substances were compared with the conventional BOD₅ method and other biosensor methods. Similar results with the BOD biosensor system using *Trichosporon cutaneum* were obtained. In addition, the influence of chloride ion, artificial seawater and heavy metal ions on the sensor response was investigated. A slight influence of 20.0 g L^{-1} chloride ion and artificial seawater (18.4 $\text{g L}^{-1} \text{ Cl}^-$) was observed. Thus, the possibility of BOD determination for seawater was suggested in this study. In addition, no influence of the heavy metal ions (1.0 $\text{mg L}^{-1} \text{ Fe}^{3+}$, Cu^{2+} , Mn^{2+} , Cr^{3+} and Zn^{2+}) was observed. Real sample measurements using both river water and seawater were performed and compared with those obtained from the BOD₅ method. Finally, stable responses were obtained for 14 days when the yeast suspension was stored at 4 °C (response reduction, 93%; R.S.D. for 6 testing days, 9.1%).

© 2006 Elsevier B.V. All rights reserved.

Keywords: Eukaryote BOD biosensor; Double-mediator system; Menadione; *Saccharomyces cerevisiae*; Salt-tolerant

1. Introduction

The biochemical oxygen demand (BOD) has been used widely for several decades as an index of organic pollution in industrial wastewater or natural waters. The conventional 5-day (BOD₅) method is time-consuming and requires 5 days to obtain

results (JIS K 0102) [1]. To solve the problem, the first microbial biosensor for rapid BOD estimation was developed by Karube et al. [2]. Since this method was proposed, many variations of this BOD sensor have been developed. The history of BOD sensor developments was well summarized in two literature by Nakamura and Karube [3,4]. After the first report, a practical sensor system was developed by Hikuma et al. [5]. It employed the eukaryote *Trichosporon cutaneum* as an omnivorous and viable microbe and was utilized as an indication of the dissolved oxygen concentration (BOD_{DO}). This BOD_{DO} method was established as a Japanese Industrial Standard (JIS K 3602) [6], and many variations followed, such as thermophilic bacteria for long-term stability [7], dead *Bacillus subtilis* cells [8],

* Corresponding authors at: Research Center of Advanced Bionics (RCAB), National Institute of Advanced Industrial Science and Technology (AIST), Tokyo University of Technology, 1404-1 Katakura, Hachioji, Tokyo 192-0982, Japan. Tel.: +81 4 26 372149; fax: +81 4 26 374058.

E-mail addresses: nakamura@bs.teu.ac.jp (H. Nakamura), karube@bs.teu.ac.jp (I. Karube).

slime mold [9], *Pseudomonas putida* SG10 for highly sensitive detection [10,11] and multi-microorganisms for seawater [12]. In addition, this principle was applied to soil diagnosis for agricultural fields [13]. However, these methods required a sensitive DO electrode due to the extremely low solubility of oxygen in water ($8.84 \text{ mg O}_2 \text{ L}^{-1}$ at 1 atm, 20°C). Hence, a practical and portable system has not yet been developed. Alternative methods have been created; these sensors indicate bacterial luminescence by *Photobacterium phosphoreum* [14] and surface photovoltage with *T. cutaneum* [15], although neither sensor has been realized for practical use as a portable device.

As a next-generation technique, the single-mediator (SM) system was applied using ferricyanide (FC) and bacteria *Pseudomonas fluorescens* biovar V as a new estimation method of the BOD (BOD_{SM}) by Yoshida et al. [16]. FC proved to be an efficient mediator for shuttle electrons from the redox center of reduced bacterial enzymes to the electrode in the presence of organic compounds [17,18]. The BOD_{SM} sensor could easily be improved as a portable device with bacterial sensor chips because of the use of highly dissolved FC [19]. However, *P. fluorescens*, which is used in the BOD_{SM} sensor developments, is a prokaryote, known as a unicellular organism; therefore, sensor stability was the greatest concern with regard to the sensor's practical applications.

In recent years, a double-mediator (DM) system combining FC and menadione, a lipophilic mediator, was studied using the eukaryote *Saccharomyces cerevisiae* by Baronian et al. [20]. The study revealed that menadione can penetrate the outer cell membrane. Eukaryotes, such as yeasts that function under both aerobic and anaerobic conditions, are easily handled, omnivorous to many kinds of organic substances, and stable in saline solutions. Therefore, the baker's yeast *S. cerevisiae* was selected as the most available and suitable microbe for the new estimation method of BOD.

2. Experimental

2.1. Materials

Menadione (Vitamin K_3 , 2-methyl-1,4-naphthoquinone) was purchased from MP Biochemicals, LLC (Germany). Potassium FC, potassium hexacyanoferrate(II), glucose, glutamic acid, and ethanol were purchased from Wako Pure Chemicals (Osaka, Japan). Triton X-100TM (TritonTM) was purchased from Sigma Chemicals (USA). The other chemicals used in this study were of reagent grade. Water was used after reverse osmosis.

Ten-fold-concentrated phosphate-buffered saline (PBS10) contained 2 g KH_2PO_4 , 29 g $\text{Na}_2\text{HPO}_4 \cdot 12\text{H}_2\text{O}$, 80 g NaCl and 2 g KCl and was adjusted to pH 7.0 with HCl; a total volume of 1 L was obtained by mixing with pure water. PBS was prepared by 10-fold dilution of PBS10. To calibrate the amperometric response of the BOD sensor, a standard was prepared by dissolving equimolar amounts of both potassium hexacyanoferrate(II) and potassium FC to a concentration of 400 mM (FF mixture).

For the BOD_{DM} measurement, 480 mM FC was prepared in PBS10. TritonTM was also dissolved in PBS10 to give a 1.5%

(w/v) solution. For experimental use, a 0.05% solution was prepared from the 1.5% solution with PBS10 before use. Menadione was dissolved in 99.5% ethanol to give an 80 mM solution and stored in a light-proof container [20]. The LB medium was prepared with 0.25 g of NaCl, 0.5 g of Bacto Triptone, and 0.25 g of yeast extract in 50 mL at pH 7.0. A BOD standard solution containing 1.5 g L^{-1} glucose and 1.5 g L^{-1} glutamic acid (GGA) was employed as a model wastewater of $2200 \text{ mg O}_2 \text{ L}^{-1}$ according to the Japan Industrial Standard committee (JIS K 0102, 1974) [1]. All of the solutions were stored at 4°C .

2.2. Microorganism and cell cultures

Baker's dry yeast was purchased from Nisshin Foods Inc. (Super Camellia, Tokyo) and grown by two steps. In pre-culture, the cells were grown under aerobic conditions at 180 rpm and 28°C for 9 h in 2 mL of a sterilized YPD medium (40 mg of glucose, 40 mg of PolypeptoneTM and 20 mg of yeast extract in 2 mL, pH 7.0) using a test tube. One microlitre of the pre-cultured medium was inoculated to the fresh YPD medium (200 mL), and the main culture was performed at 120 rpm for 15 h using a Sakaguchi flask. After growth, the yeast cells were harvested by centrifugation for 3 min at 3000 rpm and washed three times with a 0.9% NaCl solution (4°C). The yeast was re-suspended in 25 mL of a NaCl solution and starved by shaking at 120 rpm and 28°C for 2 h. Following starvation, the yeast was washed three times, re-suspended in a NaCl solution to an optical density (OD_{600}) of 45, and stored at 4°C before use.

2.3. Construction of the BOD sensor

The sensor device was built using pilling polyethylene terephthalate (PET) sheets (0.2 mm thickness) and expanded plastic boards (1 mm thickness) (Fig. 1). A screen-printed carbon electrode sheet was placed upside down and sandwiched between one expanded plastic board and three boards. The area of each electrode was determined to be 18 mm^2 ($7.5 \text{ mm} \times 2.4 \text{ mm}$). In addition, a PET sheet was glued to the bottom. The sensor device employing a two-electrode system had a cuvette volume of $562.5 \mu\text{L}$ ($10 \text{ mm} \times 12.5 \text{ mm} \times 4.5 \text{ mm}$), which enabled setting a magnetic micro-stirrer bar ($8.0 \text{ mm} \times 1.5 \text{ mm}$) in the cuvette.

2.4. Experimental procedure

The sensor device was stirred using a micro-stirrer (Cellstar CC-303, AsOne, Japan) and controlled through an electrochemical analyzer (SHV-100, Hokuto Denko or CHI-1202, BAS, USA). Prior to the electrochemical measurement, the stirrer was stopped, and chronoamperometry was performed by poisoning the carbon-working electrode $+900 \text{ mV}$ relative to the carbon reference/counter electrode for 3 s. The current output obtained at the endpoint of the chronoamperometry was taken as the sensor response. In this study, a sufficiently high potential was applied for the oxidation of hexacyanoferrate(II) to prevent

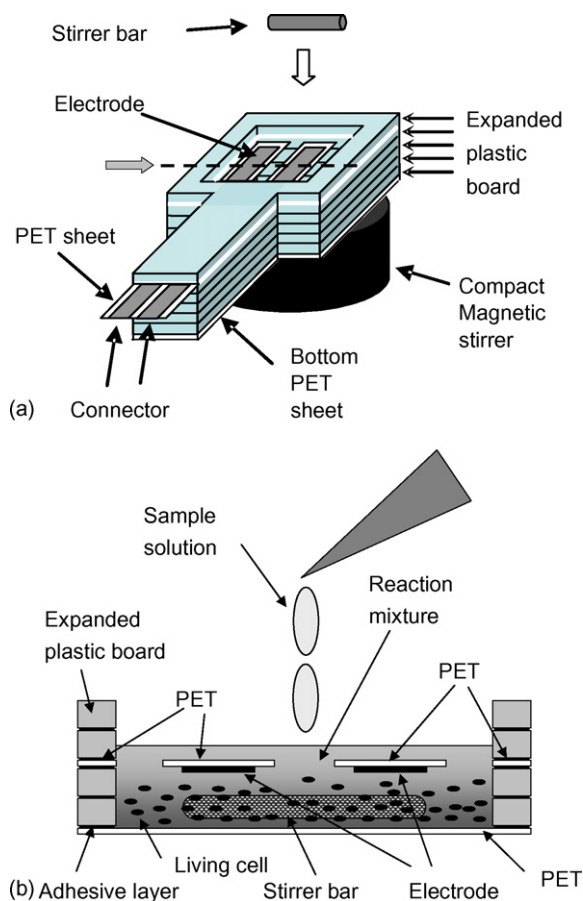


Fig. 1. Schematic diagram of the sensor device. (a) Squint view of the sensor device. (b) Cross-sectional view from a gray arrow in the diagram of the squint view.

the equilibrium potential at the working electrode from having an influence on the drift. In addition, we decided to ignore the influence of electro-active substances dissolved in real samples on the chronoamperometry. All experiments were performed three times at room temperature and with a reaction volume of 500 μL .

The sensor device was preconditioned using diluted household bleach and stirring at 100 rpm for 4 min. The sensor device's response was verified by confirming a 155 μA signal to 10 mM FF.

For the calibration curve to the hexacyanoferrate(II) concentration, the designated concentration of the FF mixture was added to the sensor cuvette for one measurement, and the measurement was performed without reaction time and stirring.

In the experiments using the microbial sensor, 41.5 μL of 480 mM FC, 5 μL of 20 mM or 80 mM menadione, 5 μL of 0.05% (w/v) TritonTM, 50 μL of a yeast suspension ($\text{OD}_{600} = 45$), or 25 μL of a yeast suspension with 25 μL of 0.9% NaCl, 350 μL of sample, and 48.5 μL of water were added to the sensor cuvette to give a final volume of 500 μL . The reaction in the sensor cuvette was started by the final addition of the yeast suspension under stirring at 100 rpm. One electrochemical measurement was performed after a 15 min incubation.

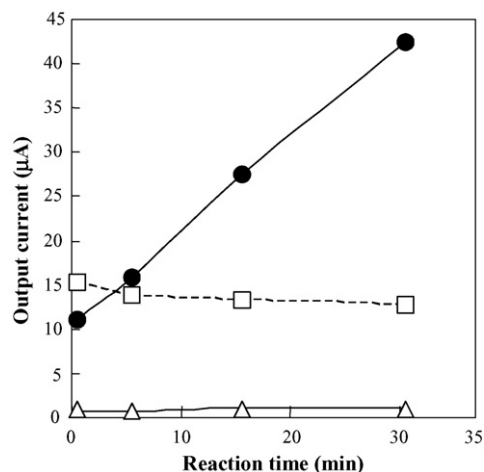


Fig. 2. Sensor responses to the double-mediating reaction. (●) With both FC and menadione, (□) with menadione only and (△) with FC only. Fifty microlitres of 240 mM FC in PBS (pH 7.0), 1.5 μL of 20 mM menadione, 30 μL of a yeast suspension ($\text{OD}_{600} = 15$), and 60 μL of an LB medium were added to the sensor cuvette, and the final volume was adjusted to 300 μL by PBS. The electrochemical measurement was performed at 0.5, 5.5, 15.5 and 30.5 min after the addition of the yeast suspension.

2. Results and discussion

2.1. Sensor responses by a DM system

As part of the preliminary investigation, we examined the possibility of obtaining a sensor response from living yeast cells containing a reaction mixture using SHV-100 without stirring. Fig. 2 shows the results obtained under three different conditions. The response from yeast suspensions increased when the reaction mixture contained both FC and menadione. These results show that menadione can penetrate the yeast outer wall and produce a menadione radical, which then transfers the electron to FC. The FC is reduced to hexacyanoferrate(II), which is finally reoxidized to FC at the working electrode.

On the other hand, in the absence of either FC or menadione, no sensor response changes were observed. The results indicate that FC without menadione could not act as an electron acceptor of *S. cerevisiae* during the catabolic process of organic substances, although the menadione response 0.5 min later was greater than the DM response, possibly due to the presence of decomposed menadione. The other side, menadione without FC produced menadione radical; however, the radical could not be detectable to the electrode. On the bases of these facts, the responses were not obtained from these measuring conditions.

2.2. Characterization of a sensor system

Our sensor system was fabricated to evaluate the microbial BOD_{DM} method, and its basic response was examined using CHI-1202 by generating a calibration curve with unstirred 500 μL aliquots of potassium hexacyanoferrate(II). As shown in Fig. 3, a calibration curve was obtained from the 0 to 50 mM FF mixture, a linear range with excellent correlation ($r^2 = 0.9995$,

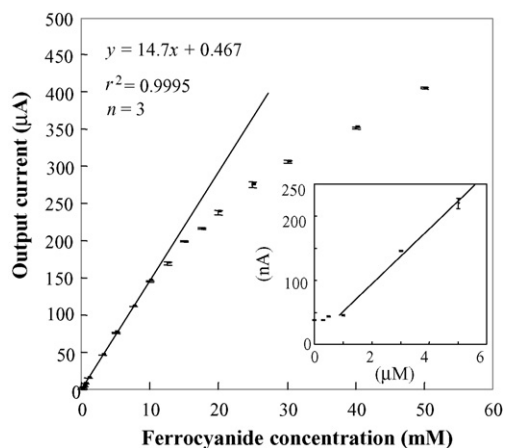


Fig. 3. Calibration curve for potassium hexacyanoferrate(II) dissolved in PBS.

$y = 14.7x + 0.467$, 14 points, $n = 3$, averaged R.S.D. = 1.26% from the $1 \mu\text{M}$ to 10 mM FF mixture, and a detection limit from the $0.5 \mu\text{M}$ FF mixture. Thus, 40 mM FC was adopted as the initial FC concentration for subsequent BOD_{DM} experiments.

2.3. Optimization of the sensor responses

For the optimization of the measuring conditions, a micro-stir system was adopted to improve both the reaction efficiency and measuring reproducibility. For this purpose, the design of the sensor device was slightly changed to create space for rotating a micro-stir bar, and the rotation speed was set to 100 rpm. In addition, the reaction time was set to 15 min for rapid estimation. By repetitive use of the sensor device, the magnitudes of the sensor responses were reduced (data not shown), probably due to adsorption of hydrophobic menadione on the electrode surface. The regeneration of the electrode surface was then examined using a diluted bleaching agent for 4 min, which enabled the repetitive use of the device. Thus, the reproducible measurements by this microbial sensor could be realized, and the relative standard deviation (R.S.D.) taken by three measurements could be less than 10%.

Subsequently, the optimization of the electric potential of the working electrode, the pH in the reaction mixture, and the concentration of TritonTM, phosphate, menadione, and ethanol was investigated.

The working electrode was held at a sufficiently high electric potential to reoxidize the hexacyanoferrate(II) ion produced by the reduction of FC in the menadione radical as a result of the existence of microorganisms. Therefore, the operating potential was held at +900 mV versus a counter electrode serving as a reference electrode in this study.

The effects of the pH on the sensor responses to $110 \text{ mg O}_2 \text{ L}^{-1}$ GGA were investigated at pH 5.0, 6.0, 7.0, 8.0 and 9.0 by the addition of $5 \mu\text{L}$ of 80 mM menadione and $50 \mu\text{L}$ of a yeast suspension ($\text{OD}_{600} = 45$) (data not shown). As a result, almost identical responses between pH 6.0 and pH 9.0 were obtained; however, the responses at pH 5.0 were slightly smaller than the other responses. This is quite likely because the solubility of menadione in an aquatic solution is lowered under acidic

conditions. In general, the pH of natural water and wastewater is nearly neutral; therefore, the potential of the BOD_{MD} sensor could be shown by this experiment. For subsequent experiments, measurements were performed at pH 7.0.

To reduce the adsorption of menadione onto the surface of the carbon electrodes, TritonTM as a surfactant was used in this study. At first, the effects of TritonTM on the responses to a 10 mM FF mixture were investigated using a pure TritonTM solution from 0.0001, 0.0001, 0.001, 0.005, 0.01, 0.1 and 1% (w/v). Then, the responses were dramatically reduced from 0.001% TritonTM due to the formation of a membrane on the electrode surface (data not shown). Next, we examined the effects of TritonTM at 0.00001, 0.00025, 0.0005, 0.001, 0.001, 0.01 and 0.1% on the response of the BOD_{DM} sensor to $110 \text{ mg O}_2 \text{ L}^{-1}$ GGA. The responses gently decreased with an increase in the concentration of TritonTM. In general, the existence of a surfactant in a cell suspension is fatal to microorganisms. However, it was insignificant when using yeast because yeast has a thick outer-cell wall. Thus, the concentration of TritonTM was set at 0.0005% as a final concentration in subsequent experiments.

Microbial sensor responses are known to decrease when the phosphate concentration drops below 10 mM [5]. Thus, the effects of phosphate on the responses to $110 \text{ mg O}_2 \text{ L}^{-1}$ GGA were examined at 2.0, 10, and 40 mM phosphate as the final concentration in the sensor cuvette. The response decreased with a decrease in the phosphate concentration from 2 mM (data not shown). Here, we adopted the phosphate concentration of 8.9 mM , which is close to 10 mM , as a final concentration, which is possibly enough to obtain a sufficient response.

Ethanol is used as a solvent of menadione and is an assimilable organic substance. Hence, the effects of ethanol on the responses to $110 \text{ mg O}_2 \text{ L}^{-1}$ GGA were investigated at 1.0, 1.5 and 2.0% (v/v) as the final concentration in the sensor cuvette. As we expected, the responses increased with a linear increase in the ethanol concentration (data not shown). These results suggested that the oxidation rate of ethanol was faster than that of some substrates, such as glucose and glutamic acid. This result indicated that the amount of ethanol used as a solvent of menadione has to be reduced as much as possible; thus, 1.0% (v/v) ethanol was adopted as a final concentration in the sensor cuvette.

Subsequently, the effects of the menadione concentration on the sensor responses to $110 \text{ mg O}_2 \text{ L}^{-1}$ GGA were examined from 0.1 to 0.8 mM at the final concentration in the sensor cuvette. As shown in Fig. 4, the responses drastically and efficiently increased with an increase in the menadione concentration up to 0.2 mM .

Hence, the optimum conditions obtained by these experiments were used for all further studies.

2.4. Calibration curve for GGA

Various concentrations of the standard BOD solution were applied to the system to obtain calibration curves under three different conditions, as shown in Fig. 5. The response increased with increasing the BOD concentration of the standard GGA solution, and the best relationship could be obtained under the conditions using $5 \mu\text{L}$ of 80 mM menadione and $50 \mu\text{L}$ of

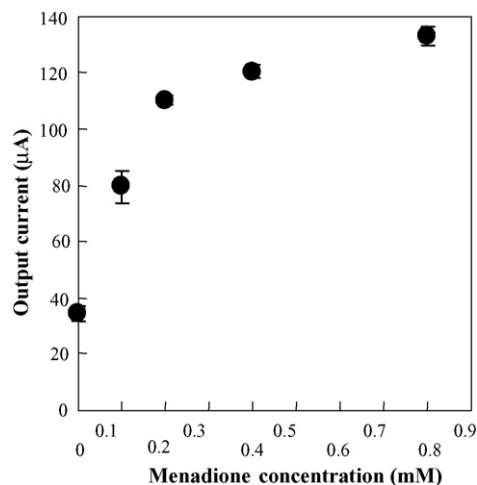


Fig. 4. Effects of menadione.

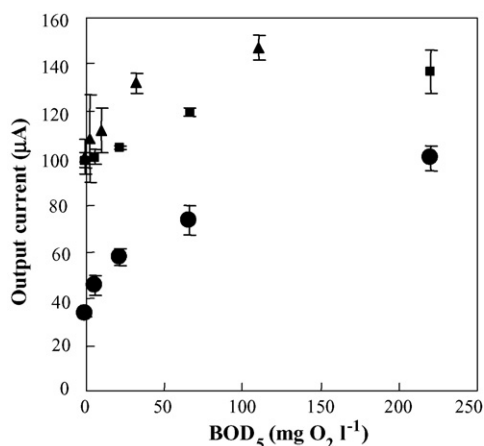


Fig. 5. Calibration curve for GGA. (▲) Five microlitres of 80 mM menadione and 50 µL of a yeast suspension (OD₆₀₀ = 45), (■) 5 µL of 20 mM menadione and 50 µL of a yeast suspension, (●) 5 µL of 20 mM menadione and 25 µL of a yeast suspension with 25 µL of a 0.9% NaCl solution.

yeast suspension (OD₆₀₀ = 45). Then, a relationship between the increase in the output current (BOD response) and the BOD concentration from 6.6 to 220 mg O₂ L⁻¹ with the GGA solution was obtained in the BOD_{DM} sensor. The reproducibility of the sensor responses in the calibration curve was 6.6% (average of R.S.D.s). Under the other two conditions, the detection limit was compromised due to the high background responses caused by the endogenous activity of the yeast. In subsequent experiments, 0.2 mM menadione was adopted as the final concentration.

2.5. Sensor responses to organic substances

The BOD sensors should have the ability to detect a wide spectrum of organic substances. Therefore, the BOD values for various kinds of pure organic substances were measured using our BOD_{DM} sensor to confirm the characteristics of this method. The BOD values obtained by the sensor were determined using the procedure described above for the GGA measurement. Each pure organic substance was prepared at 300 mg L⁻¹ so that it would be within the range of the calibration curve. Table 1 shows the substrate specificity of the BOD_{DM} sensor method relative to the reported data from BOD_{SPV} [15], BOD_{DO} [5], BOD₅ [21], BOD_{LUM} [14] and BOD_{SM} [16] for the compounds. Due to differences in the dissolved oxygen concentration, microorganism type, BOD standard solution, and incubation time for the BOD₅ method, it was not possible to obtain accurate comparisons of the six methods.

In Table 1, the values from our BOD_{DM} sensor method for the substances evaluated show that the glucose response was significantly higher than the other substances. A microbe metabolizes glucose through glycolysis. Glycolysis is generally faster than the TCA cycle; therefore, the major factor of the response might be glycolysis in a short response time. There is no consumption of oxygen in glycolysis, and the production of only two molecules of NADH requires a small amount of oxygen in the following reaction of ATP production. Compared to the TCA

Table 1
Comparison of BOD values of various organic samples^a

Substrate	BOD _{DM} ^b Eukaryote (<i>S. cerevisiae</i>) ^c	BOD _{SPV} [15] Eukaryote (<i>T. cutaneum</i>) ^c	BOD _{DO} [5] Eukaryote (<i>T. cutaneum</i>) ^c	BOD ₅ [21] Consortium ^c –	BOD _{LUM} [14] Prokaryote (<i>P. phosphoreum</i>) ^c	BOD _{SM} [16] Prokaryote (<i>P. fluorescens</i>) ^c
Glucose	1.13	0.66	0.72	0.50–0.78	0.62	1.54
Fructose	0.74	0.73	0.54	0.71	0.57	0.35
Sucrose	0.40	0.45	0.36	0.49–0.76	0.50	0.07
Lactose	0.07	0.04	0.06	0.45–0.72	0.31	0.02
Soluble starch	0.03	0.07	0.07	0.22–0.71	0.02	–
Asparagine	0.28	–	–	0.58	0.48	0.29
Alanine	0.25	–	–	0.55	–	0.73
Glycine	0.25	0.36	0.45	0.52–0.55	0.50	–
Glutamic acid	0.15	0.40	0.70	0.64	0.73	0.59
Histidine	0.63	0.34	0.35	0.55	–	0.27
Citric acid	0.18	0.18	0.72	0.63–0.88	–	–
Lactic acid	0.11	0.14	0.17	0.40	0.32	0.66
Propanol	0.31	–	0.28	0.47–1.50	0.28	0.29
Glycerol	0.23	0.44	0.51	0.62–0.83	0.53	0.05

^a Values are expressed in mg O₂ mg⁻¹ substrate.

^b Concentration of each pure organic substances were 300 mg L⁻¹ for each substance.

^c Microbe.

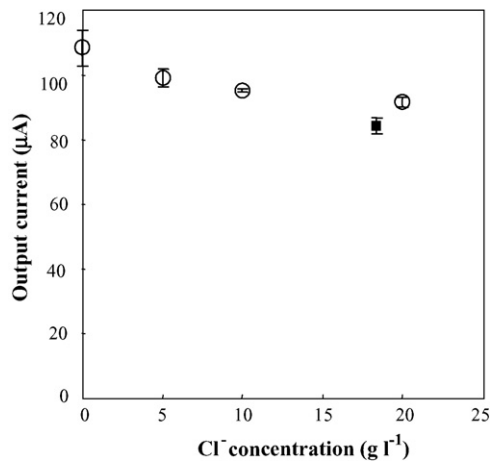


Fig. 6. Influence of the chloride ion. (○) Cl⁻ ion in a NaCl solution, (■) artificial seawater.

cycle, glycolysis makes only a small contribution to oxygen consumption in the oxygen electrode method. Thus, a relatively small response would probably be obtained for compounds that are metabolized in the TCA cycle. In addition, the sensor methods using yeast, including our method, showed quite similar profiles to various kinds of pure organic substances. While the most important requisite for the microorganisms used with the BOD sensor is to have a wide substrate spectrum for degradation, it would be extremely unlikely to have the same spectra for different microbial species. Therefore, this is sufficiently adequate to demonstrate that the BOD_{DM} method is valid for the BOD determination.

2.6. Influences of chemicals

The influence of the chloride ion on the sensor responses of 220 mg O₂ L⁻¹ GGA was investigated from 5.00 to 20.0 g L⁻¹ Cl⁻ ion. In Fig. 6, the responses were slightly influenced by the increasing concentration of the Cl⁻ ion. In addition, the influence of artificial seawater (26.5 g NaCl, 3.26 g MgCl₂, 2.07 g MgSO₄, 1.36 g CaSO₄, and 0.714 g KCl in 1 L water) on the sensor responses of 220 mg O₂ L⁻¹ GGA was also investigated, and the responses had a relative value of 77% of that of the control. However, *S. cerevisiae* is known to be a salt-tolerant microbe; therefore, these results suggest that the BOD_{DM} sensor has potential for the BOD evaluation of seawater when a standard solution prepared with artificial seawater is used.

Most real samples, such as river water, seawater, and effluent, contain various heavy metal ions, such as Fe³⁺, Cu²⁺, Mn²⁺, Cr³⁺, and Zn²⁺, and the presence of these heavy metal ions in the sample may interfere with the activity of microorganisms [22]. Thus, the influence of heavy metal ions on the response was investigated at 1 mg L⁻¹ because the highest concentration of these ions in a polluted Japanese river should be below 1 mg L⁻¹ [23]. To perform the examinations, chlorides were used as a counter ion of heavy metal ions. The BOD of 220 mg O₂ L⁻¹ GGA was used as a control. The results shown in Table 2 reveal that Fe³⁺, Cu²⁺, Mn²⁺, Cr³⁺, and Zn²⁺ (1 mg L⁻¹, each) have no effect on the response of the sensor.

Table 2

Influences of heavy metal ions on the biosensor response to 220 mg O₂ L⁻¹ BOD

Heavy metal ion (1 mg L ⁻¹)	Relative value (%)
Control	100
Fe ³⁺	98.8
Cu ²⁺	102
Mn ²⁺	103
Cr ³⁺	99.1
Zn ²⁺	99.9

2.7. Investigation of the yeast storage condition

The storage conditions for living yeast cells were examined next. For this purpose, two storage conditions of yeast suspensions (OD₆₀₀ = 45) were examined, namely, at 28 °C with a rotating speed of 120 rpm and 4 °C, respectively. In the case of storage at 28 °C, the responses after 1 day were significantly reduced relative to those obtained on the first day, although responses to the GGA sample could be obtained by the residual activity of living yeast (data not shown). On the other hand, stable results as reproducible responses to 220 mg O₂ L⁻¹ GGA were obtained under storage at 4 °C for 14 days. The responses after 14 days decreased to 93% from their original values, and the reproducibility of the responses obtained from 6 testing days was 9.1% (R.S.D.). In addition, the responses after 30 days decreased to 73% from their original values. These results demonstrate once again the high survival ability of the yeast.

2.8. Real sample application

Samples of both river water and seawater with BODs of 0, 75, and 150 mg O₂ L⁻¹ as a result of the added GGA solution were measured using our BOD_{DM} sensor and the BOD₅ method (Fig. 7). Here, a GGA solution with a 10% volume was added to the sample solution. For the seawater sample, the GGA solution was prepared using artificial seawater containing 2.65% NaCl, 0.326% MgCl₂, 0.207% MgSO₄, 0.136% CaSO₄, and 0.0714% KCl. The river water was sampled from the Yudono River in Hachioji, Tokyo (24.8 °C, pH 7.2, DO

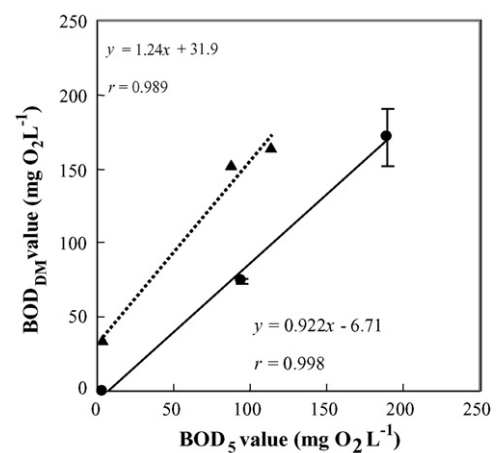


Fig. 7. Correlation of the BOD value calculated from the response of the BOD_{DM} method with the BOD₅ method for river (●) and sea (▲) samples.

8.8 mg L⁻¹, COD_{Mn} 6 mg L⁻¹, BOD₅ 4.22 mg L⁻¹; conductivity, 0.24 mS cm⁻¹; salinity, 0‰). An excellent correlation coefficient of 0.998 for these results using river water was obtained for the BOD_{DM} sensor with two sets of measurements and for the BOD₅ method with one set of measurements. The seawater was sampled from Tokyo Bay in Odaiba, Tokyo (25.4 °C, pH 8.0, DO 7.6 mg L⁻¹, COD_{Mn} 7.5 mg L⁻¹, BOD₅ 3.61 mg L⁻¹; conductivity, 29.6 mS cm⁻¹; salinity, 3.28‰). The correlation coefficient for these results using seawater was 0.989 for both the BOD_{DM} sensor and the BOD₅ method with one set of measurements. The BOD₅ values were lower than those obtained using the BOD_{DM} sensor, probably due to insufficient microbial activity in the BOD₅ samples. The seawater sample with a BOD of 150 mg O₂ L⁻¹ as a result of the added GGA solution showed relatively high values with the present sensor methods. These results might be expected as the averaged relative variances for the BOD_{DM} sensor. These results demonstrate the potential of our BOD_{DM} sensor method as a salt-tolerant BOD determination method.

3. Conclusions

In this study, we demonstrated the use of a BOD sensor mediated by the eukaryote *S. cerevisiae* by employing the DM system. First, we designed a microbial sensor device equipped with a micro-stirrer system to determine the potassium hexacyanoferrate(II), which formed as a result of the assimilation of organic substances by *S. cerevisiae* in the presence of FC and menadione. The sensor device showed excellent response characteristics to hexacyanoferrate(II), and sensor responses to organic substances were obtained only when the reaction mixture contained *S. cerevisiae* in the presence of FC and menadione. By optimizing the BOD_{DM} sensor, a calibration curve with a wide range was obtained by the GGA solution. Next, we examined the sensor responses to pure organic substances and compared them with those obtained with the conventional 5-day method and other BOD sensor methods. In this investigation, we found that the BOD_{DM} method offers a wide range of assimilability to several categories of organic substances. To investigate the effects of chemicals on the sensor responses, chloride ion, seawater, and heavy metal ions were employed, and the responses were not significantly influenced by the chloride ion and seawater. Furthermore, they were not affected by the heavy metal ions. Thus, we found that our BOD_{DM} sensor system was tolerant to naturally existing chemicals. Finally, we demonstrated the possibility of measuring real samples by comparing them with the conventional BOD₅ method using both fresh water and seawater as real samples.

In this study, we proposed a new BOD estimation method using a eukaryote microbe. This BOD_{DM} sensor can be easily applied to practical mobile system employing a disposable DM sensor chip because it takes advantage of some of yeast's specific

properties: wide availability, ease of handling, omnivorousness to a wide range of organic substances, and high survival ability with high resistance to the influences of naturally existing chemicals. In addition, many possibilities for developing different kinds of DM sensors were shown. As an example, the development of a sensitive ethanol sensor employing this DM microbial sensor principle is in progress. Consequently, this study is important for the development of microbial sensors using a eukaryote microbe as a new generation.

Acknowledgements

The authors acknowledge Mr. Mitsutoshi Yataka, Mr. Yuta Abe, Mr. Tomoki Ohmomo, Mr. Tomoyuki Sakamaki and Mr. Masaki Ito for their assistance with the experiments.

References

- [1] Japanese Industrial Standard Committee, JIS K 0102, Japanese Standard Association, Tokyo, 1974.
- [2] I. Karube, S. Mitsuda, T. Matsunaga, S. Suzuki, J. Ferment. Technol. 55 (1977) 243.
- [3] H. Nakamura, I. Karube, Anal. Bioanal. Chem. 377 (2003) 466.
- [4] H. Nakamura, I. Karube, in: C.A. Grimes (Ed.), Encyclopaedia of Sensors, vol. 10, American Scientific Publishers, USA, 2005, pp. 1–40 (Chapter 15).
- [5] M. Hikuma, H. Suzuki, T. Yasuda, I. Karube, S. Suzuki, Eur. J. Appl. Microbiol. Biotechnol. 8 (1979) 289.
- [6] Japanese Industrial Standard Committee, JIS K 3602, Japanese Standard Association, Tokyo, 1990.
- [7] I. Karube, K. Yokoyama, K. Sode, E. Tamiya, Anal. Lett. 22 (1989) 791.
- [8] T.C. Tan, Z. Qian, Sens. Actuators B 40 (1997) 65.
- [9] M. Suzuki, S. Takahashi, M. Ishibashi, K. Natsume, Sens. Mater. 7 (1995) 159.
- [10] G.J. Chee, Y. Nomura, I. Karube, Anal. Chim. Acta 379 (1999) 185.
- [11] G.J. Chee, Y. Nomura, K. Ikebukuro, I. Karube, Biosens. Bioelectron. 21 (2005) 67.
- [12] Y. Jiang, L.L. Xiao, L. Zhao, X. Chen, X. Wang, K.Y. Wong, Talanta 70 (2006) 97.
- [13] Y. Hashimoto, H. Nakamura, K. Asaga, I. Karube, submitted for publication.
- [14] C.K. Hyun, N. Inoue, E. Tamiya, T. Takeuchi, I. Karube, Biotechnol. Bioeng. 41 (1993) 1107.
- [15] Y. Murakami, T. Kikuchi, A. Yamaura, T. Sakaguchi, K. Yokoyama, Y. Ito, M. Takiue, H. Uchida, T. Katsube, E. Tamiya, Sens. Actuators B 53 (1998) 163.
- [16] N. Yoshida, K. Yano, T. Morita, S.J. McNiven, H. Nakamura, I. Karube, Analyst 125 (2000) 2280.
- [17] G. Ramsay, A.P.F. Turner, Anal. Chim. Acta 215 (1988) 61.
- [18] T. Kalab, P. Skladal, Electroanalysis 6 (1994) 1004.
- [19] N. Yoshida, J. Hoashi, T. Morita, S.J. McNiven, H. Nakamura, I. Karube, J. Biotechnol. 88 (2001) 269.
- [20] K. Baronian, A.J. Downard, R.K. Lowen, N. Pasco, Appl. Microbiol. Biotechnol. 60 (2002) 108.
- [21] R.G. Bond, C.P. Straub, in: R.G. Bond, C.P. Straub (Eds.), Handbook of Environmental Control, vol. 3, Cleveland, Ohio, USA, 1973, pp. 671–686.
- [22] Y.E. Collins, G. Stotzky, Factors Affecting the Toxicity of Heavy Metals to microbes, Metal Ions and Bacteria, NY, 1989, pp. 31–90.
- [23] River Bureau, Annual Report on River Water Quality in Japan, Ministry of Construction, Japan, 1997.

New automatized method with amperometric detection for the determination of azithromycin

Miriam E. Palomeque^{a,*}, Patricia I. Ortíz^{b,*}

^a *Departamento de Química, Universidad Nacional del Sur, Bahía Blanca, Buenos Aires, Argentina*

^b *INFIQC, Departamento de Físico Química, Facultad de Ciencias Químicas, Universidad Nacional de Córdoba, Córdoba, Argentina*

Received 22 June 2006; received in revised form 5 September 2006; accepted 1 October 2006

Available online 20 November 2006

Abstract

A FIA–amperometric method for azithromycin determination was developed. A working glassy carbon electrode and a Ag/AgCl/NaCl (3 M) reference electrode were used. The determination is based on the electrochemical oxidation of the azithromycin at 0.9 V in Britton–Robinson buffer solution (pH 8.0). Due to the adsorption of the reaction products on the electrode surface, an effective cleaner cycle was implemented. By using the optimum chemical and FIA conditions, a concentration linear range of 1.0–10.0 mg L⁻¹ and a detection limit (LOD) of 0.76 mg L⁻¹ are obtained. The method was validated and satisfactorily applied to the determination of azithromycin in pharmaceutical formulations.

© 2006 Elsevier B.V. All rights reserved.

Keywords: FIA; Amperometry; Azithromycin; Pharmaceutical preparations

1. Introduction

Azithromycin (AZ) (*N*-methyl-9a-aza-9-deoxy-9-dihydro-9a-homoerythromycin A) is a novel macrolide antibiotic and a semisynthetic acid-stable erythromycin derivative. It is used against respiratory tract and skin infections and sexually transmitted diseases.

Azithromycin has been determined in biological fluids by several methods [1–4]. However, few methods for its determination in pharmaceutical formulations were described in the literature such as: chromatography with electrochemical detection [5], fluorimetry with a previous drug derivatization [6], square-wave voltammetry [7] and cyclic voltammetry [8]. Generally, these methods are slow, tedious and in some cases require expensive equipment.

As far as we know, there is only one report of a FIA method for the determination of AZ, based on the synergistic enhancement in the chemiluminescence signal of luminol–hydrogen peroxide system [9].

The US Pharmacopeia [10] proposes a chromatographic method with amperometric detection that needs the use of a specific “Gamma-alumina” column that is expensive and difficult to obtain commercially. Thus, we develop a new FIA–amperometric method for determining this analyte. In this paper, we propose a new continuous flow system with electrochemical detection for AZ determination in pure and dosage forms. The amperometric detection was performed using a glassy carbon working electrode, Ag/AgCl/3 M NaCl reference electrode and a stainless steel auxiliary electrode. A cleaner cycle using isopropyl alcohol has been developed in order to desorb the oxidation products from the electrode surface.

2. Experimental

2.1. Materials and reagents

Solutions were prepared with analytical reagent-grade chemicals and ultra pure water (Milli-Q, Millipore System, 18.3 MΩ cm⁻¹).

Azithromycin dihydrated (Unifarma) standard solution was obtained by dissolving 0.005 g with 5.0 mL ethyl alcohol and making up to 250 mL with water. It was freshly prepared every day and further standard solutions were obtained by appropriate dilutions with water.

* Corresponding authors. Tel.: +54 351 4812695.

E-mail addresses: palomeque@criba.edu.ar, mirpalom@efn.uncor.edu (M.E. Palomeque), portiz@fcq.unc.edu.ar (P.I. Ortíz).

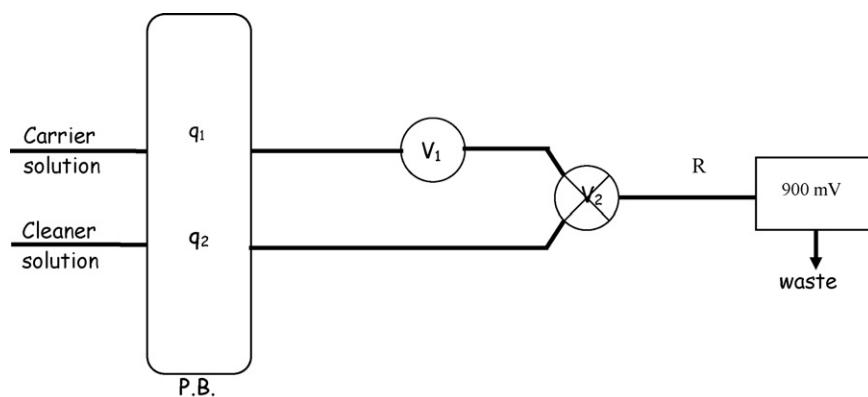


Fig. 1. P.B.: peristaltic pump; q_1 and q_2 : flow rates; V_1 : injection valve; V_2 : selection valve; carrier solution: Britton–Robinson pH 8 and KCl in ethanol/water (9.5% v/v); cleaner solution: isopropyl alcohol; R: reactor (length 10 cm).

All buffer solutions, 0.05 mol L⁻¹ acetate buffer (J.T. Baker), 0.05 mol L⁻¹ phosphate buffer (Cicarelli), 0.04 mol L⁻¹ Britton–Robinson buffer (prepared by mixing boric (Cicarelli), phosphoric (Sintorgan) and acetic (J.T. Baker) acids and adding the necessary amount of sodium hydroxide solution (J.T. Baker)) were prepared weighing appropriate amounts of the drug in pure water. Isopropyl alcohol (Merck), methanol (Sintorgan), ethanol (J.T. Baker) and acetone (Cicarelli) were used for cleaning the electrode. Ammonium acetate (J.T. Baker), sodium perchlorate (Anedra) and potassium chloride (J.T. Baker) were used for fixing the ionic strength.

2.2. Instrumentation

Cyclic voltammetry experiments were performed with an Autolab PGSTAT 30 (Ecochemie) electrochemical analyzer coupled to a personal computer. A Ag/AgCl/NaCl (3 M) and Pt were used as reference and auxiliary electrodes, respectively. A glassy carbon disk (3 mm diameter MF-2012 BAS) was used as working electrode. The glassy carbon electrode was mechanically polished with alumina (0.05 μm) before each experiment.

Amperometric experiments were performed with the Bio-analytical System (BAS) Model LC-4C amperometric detector in connection with a Linseis $x-t$ recorder. The working glassy carbon electrode (BAS MF-1000), the reference electrode, Ag/AgCl/3 M NaCl (BAS MF-2021) and an auxiliary stainless steel electrode were all housed in a thin layer flow cell cabinet (BAS CC-5). The flow assembly was provided with two Rheodyne 5041 injection valves and a Gilson Minipuls 3 peristaltic pump as propulsion system. All the reaction coils were made of PTFE tubing (0.5 mm).

All the results are the average of at least four injections, and all experiments were carried out at room temperature.

2.3. Sample preparation

Ten tablets were accurately weighed and crushed to a fine powder in an agata mortar. Accurately weighed quantities of this powder containing approximately 5 mg of AZ dihydrated were diluted in 25 mL of ethyl alcohol and making up to 250 mL with pure water. Appropriate volumes from these solutions

were taken and making up to 25 mL with water for AZ determination.

2.4. Procedure

The FIA system for AZ determination is depicted in Fig. 1. A sample volume was injected (V_1) in a buffer solution carrier stream (Britton–Robinson pH 8, KCl 0.2 mol L⁻¹ and 9.5% (v/v) ethylic alcohol) through the detector. The amperometric signal due to AZ oxidation was measured at 900 mV. When the FIA signal was obtained the selection valve V_2 was switched and the cleaner solution (isopropyl alcohol) passes through the detector during 90 s in order to clean the working electrode. After this time the valve V_2 is switched again for injecting a new sample volume. The electrode must be polished after five successive injections.

3. Results and discussion

3.1. Cyclic voltammetry study

Cyclic voltammograms were obtained in different buffer solutions in order to select the appropriate medium. Acetate, phosphate and Britton–Robinson buffer solutions of different pH values were analyzed (Fig. 2). As it can be observed, during the positive scan an anodic current peak is obtained in all the solutions analyzed, due to the oxidation of the amino groups. However, during the negative scan only a very small reduction peak is observed at ca. 0.95 V, for buffer solutions with pH values higher than 7.00. Indicating that the oxidation process is mainly irreversible. The potential peak value depends on the buffer pH and composition. For acetate buffer solutions (pH 4.5) a not very well defined peak at ca. 1.0 V is obtained, for phosphate buffer solutions (pH 11.0) the oxidation peak is obtained even at more positive potential values (ca. 1.2 V), while for Britton–Robinson buffer solutions the current peak is observed at 0.85 V. On the other hand, when phosphate and Britton–Robinson buffer solutions were used the anodic current peak was observed only at pH higher than 7. It is worthy to note that, the anodic current peak shows an important decrease with successive potential scans, suggesting an adsorption process of the reaction products on

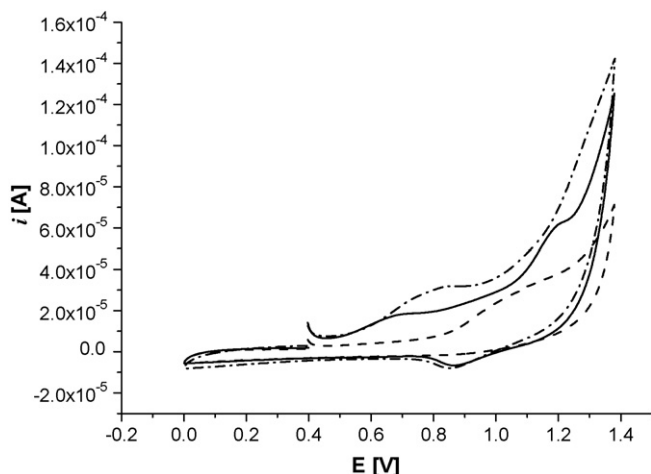


Fig. 2. Voltammograms of azithromycin (260 mg L^{-1}) in different buffer solutions, $\text{KCl } 1 \text{ mol L}^{-1}$ and 10% (v/v) of acetonitrile (straight line: phosphate; pH 11.0, dash-dot line: Britton–Robinson, pH 11.0; dash line: acetic/acetate, pH 4.5).

the electrode surface. Britton–Robinson buffer solution (pH 8.0) was selected as the appropriate medium; due to AZ oxidation process shows the best response.

3.2. Selection of the FIA system

Initially, a single FIA system was proposed. The sample was injected into a carrier solution (Buffer solution) and then flowed through the electrochemical detector. However, with this procedure a noticeable current decrease was observed (Fig. 3a), this behaviour is in agreement with that obtained by cyclic voltammetry, where after the first cycle no current peaks are observed due to fact that the oxidation process poison the electrode surface. As the current signal shows an important decrease with successive sample injections, a cleaner cycle was included in the FIA system in order to improve the analytical performance. An additional valve was used to make the selection between the carrier solution and the cleaner solution (Fig. 1).

By using a standard AZ solution of 20 mg L^{-1} and without polishing the electrode, different organic solvents (acetonitrile, acetone, methyl alcohol, ethyl alcohol and isopropyl alcohol) and different percentages of organic solvent and water (60–100%, v/v) were tested as cleaner solution. The best results

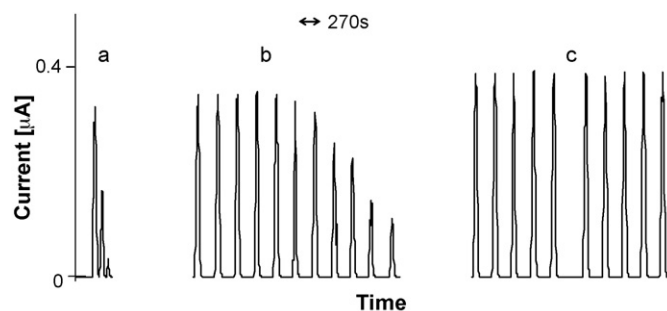


Fig. 3. Signals obtained after successive injections of AZ (applied potential 0.780 V), (a) without clean up and polishing, (b) with electrode clean up and without polishing and (c) with the recommended procedure.

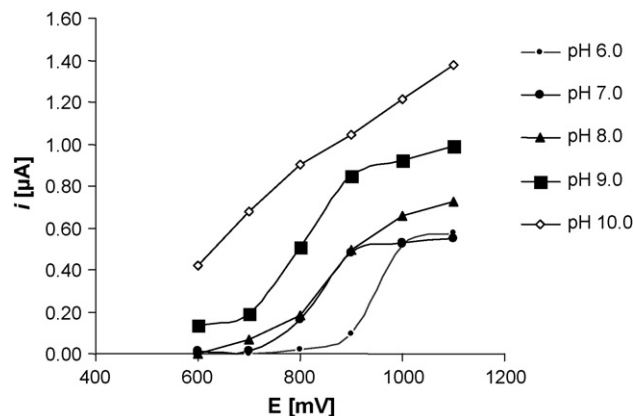


Fig. 4. Hydrodynamic voltammograms of azithromycin (19.0 mg L^{-1}) in Britton–Robinson buffer solutions at different pH. Sample injection volume: $50 \mu\text{L}$, carrier flow rate: 0.6 mL min^{-1} .

were obtained with pure isopropyl alcohol, as it allowed performing at least five sample injections with reproducible signals (Fig. 3b). Another procedure that was also analyzed was to mechanically polish the electrode surface after five consecutive injections including the cleaner cycle (Fig. 3c). As it can be observed a very good reproducibility was obtained, so this last procedure was chosen for all the experiments.

A double channel FIA system with a cleaner cycle was also tested. The sample was injected in a pure water stream and then it merges with a buffer solution stream to pass through the detector. The cleaner cycle was included by the same way described above. The selected manifold (Fig. 1) offers the best results as FIA peaks have the appropriate shape and height.

3.3. Optimization of chemical and FIA variables

Fig. 4 shows hydrodynamic voltammograms (19.0 mg L^{-1} AZ) at different pH values, the applied potential was analyzed between 0.600 and 1.200 V . As it can be observed a current plateau is reached at 0.900 V for pH values between 7.0 and 9.0 . Although for pH 8 the plateau is not very well defined, an almost constant current is obtained for potential values higher than 0.900 V . Therefore, this potential value and a pH 8.0 were selected as working conditions, as current signals show better reproducibility.

All the variables influencing the performance of the method were studied and optimized in order to obtain a good compromise between the shape of the FIA peak, current signals and reproducibility. They were tested using the univariate method. The studied range of chemical and FIA variables and their optimum values are listed in Table 1.

A Britton–Robinson buffer solution (pH 8) was used as supporting electrolyte of the carrier stream, however different organic solvents percentages and salt concentrations to fix the ionic strength were proved in order to obtain the best operational conditions. The organic solvents tested were acetonitrile, acetone, methyl alcohol, ethyl alcohol and isopropyl alcohol and the percentages (v/v) ranged between 5 and 30%. For fixing the ionic strength, ammonium acetate, sodium perchlorate and

Table 1
Studied range of the chemical and FIA variables and their optimum values

Variable	Studied range	Optimum value
Sample volume [μL]	50–200	100
Carrier flow rate [mL min^{-1}]	0.5–2.0	0.9
Cleaner solution flow rate [mL min^{-1}]	0.5–2.0	0.6
Isopropyl alcohol/water ratio [%, v/v]	50–100	100
Cleaner cycle time [s]	30–120	90
Ethyl alcohol/water ratio [%, v/v]	5–30	9.5
KCl concentration [mol L^{-1}]	0.05–2	0.2

potassium chloride were tested. Best results were obtained with ethyl alcohol at 9.5% and KCl 0.20 mol L^{-1} (Table 1).

The sample volume was varied in a wide range, and $100 \mu\text{L}$ was selected as this volume represents the best compromise between current peak height and shape, as at higher volumes a shape loose in the current peaks is observed.

Other parameters that were analyzed were the carrier and cleaner solution flow rates. For the carrier flow rate, the signal reaches a plateau between 0.7 and 1.0 mL min^{-1} , thus a flow rate of 0.90 mL min^{-1} was selected. By the other side, for the cleaner solution flow rate a value of 0.6 mL min^{-1} was chosen as it lets a relatively high speed for the cleaner cycle. Then, the cleaner cycle time was tested from 30 s and it was necessary at least 90 s to obtain good reproducibility.

3.4. Analytical parameters

Using the optimum experimental conditions, the calibration curve for standard azithromycin solutions obtained by using the least square method, was linear over the range 1.0 – 10.0 mg L^{-1} and the detection limit (LOD) for $S/N=3.3$ was 0.76 mg L^{-1} . The regression calibration equation was $i (\mu\text{A}) = [-(0.051 \pm 0.016)] + [(0.0707 \pm 0.0035) C_{AZ} (\text{mg L}^{-1})]$, with a correlation coefficient of 0.9987. The R.S.D. value (intra-day reproducibility) at 1.4 and 5.3 mg L^{-1} ($n=5$) was found to be 2.4 and 1.6%, respectively. The inter-day reproducibility (R.S.D.%) of the proposed method was calculated after obtaining nine independent calibration graphs on different days and with different conditions (standard solution, reagent solution, working electrode, etc.). The mean slope obtained was $(0.0722 \pm 0.002) (\mu\text{A mg}^{-1} \text{ L})$ with a R.S.D.% = 3.8 and a sample throughput 12 h^{-1} , including the cleaner cycle and working electrode polishing.

3.5. Applications to real samples

The potential interference of excipients that are commonly used in pharmaceutical preparations was evaluated. In this study, no interference (relative error $< \pm 5\%$ on the signal of 4.8 mg L^{-1} of AZ solution) for lactose, sucrose, glucose (>100 -fold in excess over analyte concentration), starch (saturated solution), glycerol, saccharin (>50 -fold in excess), manganese sulphate and magnesium sulphate (>25 -fold in excess) were found, when the developed flow injection procedure was applied. The presence of ascorbic acid caused an increase in the peak

Table 2
Comparison of the slopes

Samples	Slopes of standard addition method calibration	$t_{\text{calculated value}}$
Labye	0.0725 ± 0.0019	0.43
Doyle	0.0713 ± 0.0035	0.11

Slope of the proposed method: 0.0707 ± 0.0035 , $t_{\text{tabulated}}(8, \alpha=5\%) = 2.306$.

Table 3
Determination of azithromycin in two pharmaceutical formulations with the proposed method

Sample	Amount [mg/tablet]		%Error ^a
	Labelled	Found	
Labye	209.6	201.8 (9.1) ^b	3.7
Doyle	524.1	522.9 (12.4)	0.2

^a The % error are based on the labelled amount.

^b Standard deviations ($n=5$).

height on the azithromycin determination, so the determination is not possible in samples that contain this component without a previous separation step.

The matrix interference can introduce systematic errors on the analytical determination. The relative systematic errors can be detected by applying the standard addition calibration method to different real samples [11]. Thus, a comparison between the slopes of the standard addition calibration lines and a standard calibration line was carried out. If the matrix does not interfere, both lines must have the same slope.

Table 2 shows the calibration slopes lines obtained with the proposed method and with the standard addition method applied to different pharmaceutical samples. The slopes comparison was done by applying the “*t*” test. As it can be seen, the slopes were not significantly different.

The method was applied to determine azithromycin in pharmaceutical formulations and the results are shown in Table 3. As it can be observed, they are into the range recommended by Pharmacopoeias for this type of analyses.

In order to validate the proposed method the official method must have been used, however the chromatographic column that is described for that purpose was not available. So, the validation was performed using spiked real samples and determining the recovery percentages. The results are shown in Table 4 and they are satisfactory. It demonstrates that the proposed method

Table 4
Recoveries values obtained from standard additions of the analyte to real samples

Sample	Amount [mg/tablet] Added found \pm S.D. ^a		Recoveries [%]
Labye ^b	95.5	92.3 ± 1.6	96.6
	212.2	205.3 ± 3.2	96.7
Doyle ^c	265.1	269.5 ± 10.3	101.7
	589.1	602.3 ± 7.4	102.2

^a Mean values and relative standard deviation of three determinations.

^b Labyes laboratory.

^c Raffo laboratory.

is appropriated for determining azitromycin in this kind of samples.

4. Conclusion

The developed method presents good sensitivity and reproducibility. It is the first automatized FIA–amperometric method with a cycle to clean the working electrode on-line for the determination of azitromycin. It was satisfactorily demonstrated that the method is appropriated for its determination in pharmaceutical preparations.

This is an alternative method with some advantages such as: simplicity, high analytical sensitivity, inexpensive and presents an appropriated accuracy, precision and linear range to determine AZ in dosage form without previous sample preparation nor derivatization.

Acknowledgements

The authors wish to acknowledge CONICET, Agencia Córdoba Ciencia, Fundación Antorchas and SeCyT-UNC for

financial support. MP thanks Universidad Nacional del Sur, Argentina for the permission to leave.

References

- [1] C. Taninaka, H. Ohtani, E. Hanada, H. Kotaki, H. Sato, T. Iga, *J. Chromatogr. B* 738 (2000) 405.
- [2] G. Bahrami, S. Mirzaeei, A. Kiani, *J. Chromatogr. B* 820 (2005) 277–281.
- [3] R.V.S. Nirogi, V.N. Kandikere, M. Shukla, K. Mudigonda, S. Maurya, R. Boosi, A. Yerramilli, *Anal. Chim. Acta* 53 (2005) 1.
- [4] E. Wilms, H. Trumpie, W. Veenendaal, D. Tour, *J. Chromatogr. B* 814 (2005) 37.
- [5] R. Gandhi, C.L. Kaul, R. Panchagnula, *J. Pharm. Biomed. Anal.* 23 (2000) 1073.
- [6] P.Y. Kashaba, *J. Pharm. Biomed. Anal.* 27 (2002) 923.
- [7] O.A. El-Moaty Farghaly, N.A.L. Mohamed, *Talanta* 62 (2004) 531.
- [8] B. Nigovic, B. Simunic, *J. Pharm. Biomed. Anal.* 32 (2003) 197.
- [9] Z.H. Song, C.N. Wang, *Bioorg. Med. Chem.* 11 (2003) 5375.
- [10] United States Pharmacopoeia/National Formulary, USP23/NF18, USP Convention Inc., Rockville, MD, 1995, p. 152.
- [11] D.L. Massart, B.G.M. Vandeginste, L.M.C. Buydens, S. De Jong, P.J. Lewi, J. Smeyers-Verbeke, *Handbook of Chemometrics and Qualimetrics, Part A*, Elsevier, Amsterdam, 1997.

Determination of naphthalene and total methyl-naphthalenes in gasoline using direct injection-mass spectrometry

José Luis Pérez Pavón*, Miguel del Nogal Sánchez, M^a Esther Fernández Laespada, Carmelo García Pinto, Bernardo Moreno Cordero

Departamento de Química Analítica, Nutrición y Bromatología, Facultad de Ciencias Químicas, Universidad de Salamanca, 37008 Salamanca, Spain

Received 19 June 2006; received in revised form 5 October 2006; accepted 19 October 2006
Available online 28 November 2006

Abstract

A high-speed determination of naphthalene and total methyl-naphthalenes using a non-separative method based on direct injection into the mass spectrometer was performed. The results obtained for total methyl-naphthalenes were very similar to those provided with fast gas chromatography–mass spectrometry (GC–MS). However, the non-separative method afforded higher concentrations in the determination of naphthalene than those found when fast GC–MS was used. We propose a correction that removes this error very satisfactorily and allows the same results to be obtained with both methodologies. The non-separative method is rapid, simple and – in view of the results – highly suitable for the determination of naphthalene and total methyl-naphthalenes in gasoline samples.

© 2006 Elsevier B.V. All rights reserved.

Keywords: Naphthalene; Methyl-naphthalenes; Gasoline; Direct injection; Mass spectrometry

1. Introduction

Naphthalene is the simplest and most abundant of the polycyclic aromatic hydrocarbons (PAHs) present in gasoline and diesel fuels [1]. It is a natural constituent of coal tar and crude oil, and is used in the manufacture of dyes, plastics, leather tanning agents and many other products.

Naphthalene is defined as a hazardous air pollutant by the US Environmental Protection Agency (USEPA) and its fumes can irritate the eyes, skin and the respiratory tract. If inhaled over a long period of time, naphthalene may cause kidney and liver damage, skin allergy and dermatitis, cataracts and retinal damage and it may attack the central nervous system. It is also a blood toxicant: exposures to high concentration can damage or destroy red blood cells, causing hemolytic anemia [2]. Naphthalene and 2-methyl-naphthalene are considered to be tumorigenic and mutagenic compounds and 1-methyl-naphthalene is a mutagen [3].

Gas chromatography (GS) is one of the techniques most widely employed to quantify mixtures of organic compounds. In the analysis of hydrocarbons, including naphthalene and methyl-naphthalenes, which are present in gasolines [4–6], gasoline and diesel engine emissions [7,8], aircraft exhausts [9] and the water-soluble fraction of gasoline in seawater [10], gas chromatography is generally combined with mass spectrometry (MS) detection [3–10] and flame ionization detection [3,6–8].

However, the chromatographic procedures are in general slow and time-consuming. Several alternatives can be employed to speed up GC separations. These include the use of shorter capillary columns, with narrower bores and fast temperature programming [11,12].

Additionally, the development of non-separative methods for the resolution of analytical problems related to environmental pollution due to the presence of hydrocarbons from gasoline is currently of great interest, mainly owing to their fast analysis speeds. Sometimes it is not necessary to separate the individual compounds of a given sample to resolve the analytical problem in hand, it sufficing to obtain a signal profile of the sample formed by all the components integrating it. Some methods based on this type of generation of signals corresponding to the whole set of components are near infrared spectroscopy (NIR) [13], Fourier

* Corresponding author. Fax: +34 923 294483.
E-mail address: jlpp@usal.es (J.L.P. Pavón).

transform infrared spectroscopy (FT-IR) [14,15], proton nuclear magnetic resonance spectroscopy (^1H NMR) [16,17], membrane introduction mass spectrometry (MIMS) [18], electronic noses based on gas sensors [19], direct injection of samples into the mass spectrometer [12] and headspace mass spectrometry (HS-MS) [12,20–23], among others.

Here, we propose a rapid method based on direct injection of samples into the mass spectrometer (direct injection-mass spectrometry) for the determination of naphthalene and total methylnaphthalenes in different gasoline samples. Additionally, a series of analyses by fast GC–MS was performed to compare the results obtained with those provided by the non-separative method. An instrumental configuration comprising a gas chromatograph and a mass spectrometer was used. Change from the chromatographic to the non-separative mode was accomplished simply by maintaining the temperature of the oven of the chromatograph sufficiently high to prevent analyte retention, such that – under these conditions – the chromatograph column would act as a simple transfer line [12,22,24] to the mass detector.

2. Experimental

2.1. Reagents and samples

Naphthalene, 2-methylnaphthalene and 1-methylnaphthalene were supplied by Acros Organics (Geel, Belgium). The different solutions of the compounds were prepared by dilution of the commercial product in methanol (Merck, Darmstadt, Germany).

Fourteen different types of gasoline were obtained from service stations. These samples were diluted 62.5-fold in methanol for injection into the analysis system.

2.2. Procedures

2.2.1. Fast gas chromatography–mass spectrometry measurements

Gas chromatography was performed on a DB-VRX capillary column (20 m \times 0.18 mm \times 1 μm) using an Agilent 6890 gas chromatograph. The carrier gas was helium N50 (99.995% pure; Air Liquide). One microlitre of sample was introduced through an automatic liquid sample injection system (Agilent 7683). The injection port was operated in the split injection mode (1:10) and the injector temperature was 250 °C. The column was used with the following temperature program: 60 °C for 1.5 min; this was increased at a rate of 70 °C/min to 150 °C, and then further increased at 50 °C/min to 240 °C and held for 2.5 min. These temperature ramps are the maximum ones permitted by the instrumental configuration employed. The detector was a quadrupole mass spectrometer (HP 5973 N). The m/z range was 35–200 amu, and naphthalene, 2-methylnaphthalene and 1-methylnaphthalene were identified by comparison of the experimental spectra with those of the NIST'98 database (NIST/EPA/NIH Mass Spectral Library, Version 1.6).

2.2.2. Direct injection-mass spectrometry measurements

Using the same automatic injector described above, 1 μL of sample was injected into the GC–MS. The column can be

replaced by a short deactivated capillary or the oven temperature can be maintained high enough to prevent the retention of the injected volatile compounds. The second option was chosen, the column was maintained at 240 °C throughout the time of analysis. The injection port was maintained at a temperature of 250 °C. A split ratio of 1:10 was used. The same m/z range was used.

2.3. Data analysis

Data acquisition was performed with Enhanced ChemStation, G1701CA Ver. C 00.00 software [25] from Agilent Technologies.

The plotting of the information contained in the chromatograms with contour plots was accomplished using Matlab Ver. 6.5. [26]

3. Results and discussion

3.1. Preliminary study of fast GC–MS data

Fig. 1a shows the chromatogram obtained when a gasoline sample was analysed. Only 12% of the peaks have widths ($W_{1/2}$) greater than 1 s. The remaining 88% have widths of less than 1 s and 60% of these have widths corresponding to less than 500 ms. Considering that peak widths between 1 and 3 s [11] correspond to fast chromatography and widths of less than 300 ms to very

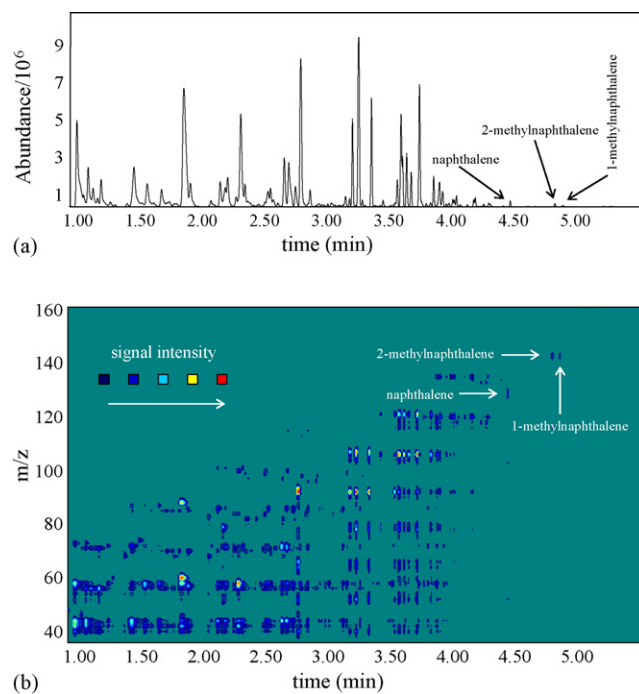


Fig. 1. (a) TIC chromatogram of a gasoline sample showing the retention times for naphthalene, 2-methylnaphthalene and 1-methylnaphthalene. (b) Contour plots with time (0.90–5.50 min) and m/z ratio axes (35–160) for the previous gasoline sample. The intensity of each m/z variable is plotted with different colours, in such way that the mass spectrum at each retention time can be observed (For interpretation of the references to colours in this figure legend, the reader is referred to the web version of the article.)

fast chromatography, this case is intermediate between the two levels.

In the chromatogram obtained, with the NIST'98 database it was possible to detect 138 peaks in approximately 5 min. With a match quality index greater than 80% 118 compounds were identified, of which 75 were identified with a match quality index greater than 90%.

Among the compounds identified were naphthalene ($t_R = 4.409$ min), 2-methylnaphthalene ($t_R = 4.763$ min) and 1-methylnaphthalene ($t_R = 4.825$ min). These compounds had a fitting index with respect to the spectra from the database of 95%.

An easy and rapid way to obtain an overall image of the mass spectrum of each compound in the sample consists of representing the different m/z variables recorded against the time of analysis. Fig. 1b is a plot of this type for the previous gasoline sample. The intensity of each m/z variable is plotted with different colours. It is thus possible to visualise in a single image all the information contained in the chromatogram (mass spectrum, signal intensity and elution time) and select or search for the zones of interest. Fig. 1b shows the plot corresponding to a data matrix where each row represents the analysis time and each column contains the intensities for the m/z ratios. Fig. 2 was obtained when only the information contained between 2.90 and 5.50 min and the m/z 125 and 145 ratios was considered. The most abundant m/z ratio of naphthalene is that of 128. In the case of 2-methylnaphthalene and 1-methylnaphthalene, the most intense ratio is $m/z = 142$.

Fig. 3 shows the extracted ion chromatogram for the two above m/z ratios. Using this strategy of the selection of m/z ratios, it is easy to detect the existence of other analytes with the same m/z ratios as the compounds of interest. In the case of naphthalene there are other compounds that contain the m/z 128 ratio. However, very few compounds contribute to the m/z 142 ratio. Accordingly, direct injection into the mass spectrometer will tend to show excessive error in quantifying naphthalene. The

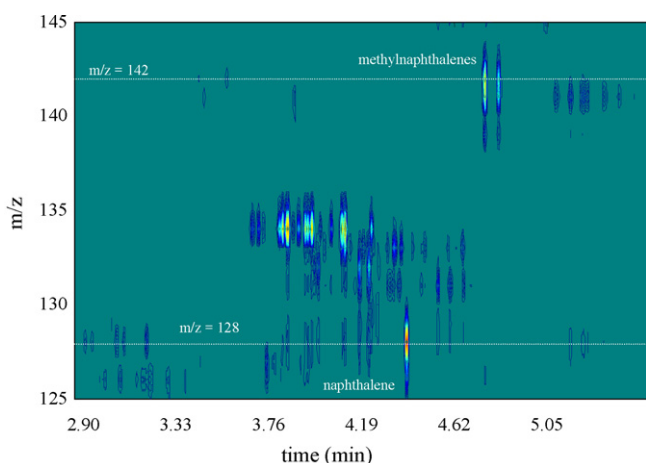


Fig. 2. Contour plots with time (2.90–5.50 min) and m/z ratio (125–145) axes for the gasoline sample in Fig. 1. The dotted lines indicate that as well as naphthalene there are other compounds with the m/z 128 ratio in their spectrum, whilst there are scarcely any interfering compounds for the m/z 142 ratio of methylnaphthalenes.

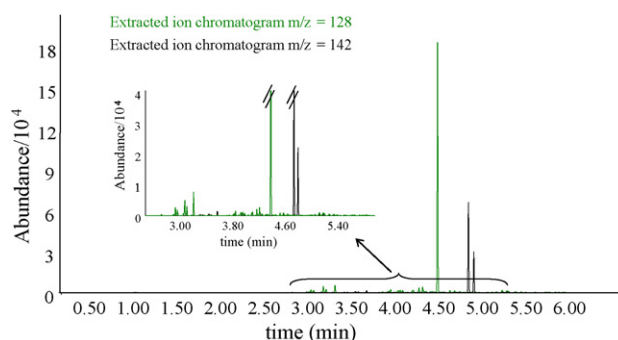


Fig. 3. Extracted ion chromatograms for the m/z 128 and 142 ratios in the gasoline sample of Fig. 1.

presence of interfering compounds if a non-separative method is used can also be predicted from Fig. 2.

3.2. Fast GC–MS method

In order to compare the results obtained upon using the direct injection method, all the gasoline samples were also analysed with the chromatographic method described previously in Section 2.

Five calibration standards containing the three analytes studied at concentrations uniformly distributed along the experimental domain were prepared. The standard concentrations were 0, 4.90, 9.80, 14.7 and 19.6 mg/L for naphthalene, 0, 2.48, 4.96, 7.45 and 9.93 mg/L for 2-methylnaphthalene and 0, 0.99, 1.98, 2.97 and 3.96 mg/L for 1-methylnaphthalene. All the standards were measured in triplicate. The variables used in the univariate calibrations were the peak areas of the three compounds in the extracted ion chromatogram for the 128 ratio in the case of naphthalene and for 142 in the case of 2-methylnaphthalene and 1-methylnaphthalene. Table 1 shows the analytical characteristics of the method. In all three cases, good correlation coefficients were obtained. The relative standard error for the second level studied ($n = 5$) was 2.2, 2.6 and 3.1% for the determination of naphthalene, 2-methylnaphthalene and 1-methylnaphthalene, respectively. Accuracy was measured by leave-one-out internal validation. The value obtained in this prediction was compared with the added value of the three compounds. The relative errors in this step for the whole set of samples were 3.4, 3.3 and 3.2% for naphthalene, 2-methylnaphthalene and 1-methylnaphthalene, respectively.

The concentration of the three compounds assayed was then determined in the 14 gasoline samples. These were measured in duplicate. The results are shown in Table 2.

3.3. Direct injection-MS method

Fig. 4 shows the characteristic profile of a gasoline sample analysed with the methodology based on direct injection of the sample into the mass spectrometer described above (Section 2). In this figure, the mass spectrum that represents the sum of the intensities of all the ions detected during the data acquisition period is shown. This mass spectrum shows the set of fragmentation patterns characteristic of linear and branched (43, 57,

Table 1

Analytical characteristics of the methods based on fast gas chromatography-mass spectrometry and direct injection-mass spectrometry for the determination of naphthalene (A), 2-methylnaphthalene (B) and 1-methylnaphthalene (C)

	Fast gas chromatography–mass spectrometry		
	A	B	C
Equation	$(9.6 \pm 0.2)10^4 \times -(0.7 \pm 2.7)10^4$	$(5.5 \pm 0.1)10^4 \times -(0.4 \pm 0.8)10^4$	$(5.6 \pm 0.1)10^4 \times +(0.2 \pm 0.3)10^4$
Correlation coefficient	0.9984	0.9982	0.9985
R.S.D. (level 2, $n=5$) (%)	2.2	2.6	3.1
Validation relative error (%)	3.4	3.3	3.2
	Direct injection-mass spectrometry		
	A	B + C	
Equation	$(6.0 \pm 0.2)10^4 \times -(1.4 \pm 2.0)10^4$	$(3.4 \pm 0.7)10^4 \times +(0.8 \pm 0.7)10^4$	
Correlation coefficient	0.9979	0.9983	
R.S.D. (level 2, $n=5$)	4.9%	2.8%	
Validation relative error	3.8%	2.2%	

Table 2

Concentration of naphthalene, 2-methylnaphthalene and 1-methylnaphthalene expressed as percent (w/v) for the 14 gasoline samples analysed with the method based on fast gas chromatography

	Naphthalene	2-methylnaphthalene	1-methylnaphthalene
Gasoline 1	0.060 ± 0.003	0.037 ± 0.002	0.016 ± 0.001
Gasoline 2	0.059 ± 0.003	0.040 ± 0.002	0.017 ± 0.001
Gasoline 3	0.064 ± 0.003	0.041 ± 0.002	0.018 ± 0.001
Gasoline 4	0.057 ± 0.003	0.040 ± 0.002	0.017 ± 0.001
Gasoline 5	0.070 ± 0.003	0.046 ± 0.002	0.019 ± 0.001
Gasoline 6	0.055 ± 0.003	0.035 ± 0.002	0.015 ± 0.001
Gasoline 7	0.056 ± 0.003	0.040 ± 0.002	0.018 ± 0.001
Gasoline 8	0.068 ± 0.003	0.044 ± 0.002	0.019 ± 0.001
Gasoline 9	0.069 ± 0.003	0.041 ± 0.002	0.018 ± 0.001
Gasoline 10	0.056 ± 0.003	0.042 ± 0.002	0.019 ± 0.001
Gasoline 11	0.084 ± 0.003	0.051 ± 0.002	0.022 ± 0.001
Gasoline 12	0.083 ± 0.003	0.043 ± 0.002	0.019 ± 0.001
Gasoline 13	0.061 ± 0.003	0.037 ± 0.002	0.016 ± 0.001
Gasoline 14	0.064 ± 0.003	0.043 ± 0.002	0.018 ± 0.001

71, 85), cyclic (41, 55, 69, 83) and aromatic (77, 78, 91, 105) hydrocarbons present in the gasolines.

The concentration range studied in the case of naphthalene was identical to that of the chromatographic method. However, this time it was not possible to determine the concentration of

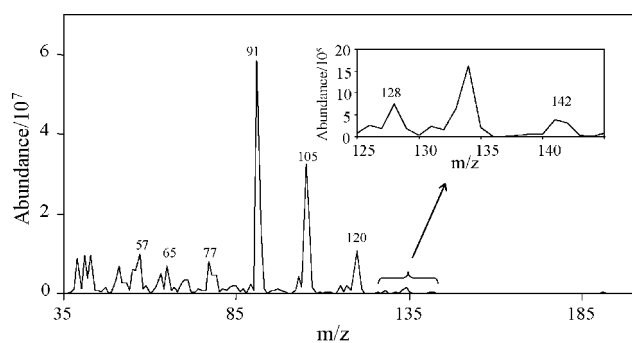


Fig. 4. Profile signal obtained upon analysing a gasoline sample with the method based on direct injection. This kind of signal is a mass spectrum that represents the sum of the intensities of all the ions detected during the data acquisition time.

2-methylnaphthalene and 1-methylnaphthalene independently because both show an almost identical mass spectrum. Nevertheless, the calibration model generated did allow quantification of the total concentration of the methylnaphthalenes. In this case, the standard concentrations were 0, 3.97, 6.95, 9.93, 12.9 and 15.9 mg/L. All the standards were measured in triplicate. The analytical variable employed in each calibration model was the total intensity of the m/z 128 ratio throughout the time of data acquisition (2 min) in the case of naphthalene and the m/z 142 ratio in the case of the methylnaphthalenes. Table 1 shows the analytical characteristics of the method. In both cases, correlation coefficients close to unity were obtained, together with a relative standard deviation of less than 5%. The models were validated with the above-described procedure. The relative errors in this step were 3.8 and 2.2% for naphthalene and the total methylnaphthalenes, respectively.

3.3.1. Determination of naphthalene

The naphthalene concentration was determined in the 14 samples of gasoline. These were measured in duplicate. The results are shown in Table 3a. The relative errors of the direct injection method with respect to the chromatographic one are also shown.

In light of these results, it is clear that the non-separative method differs with respect to the chromatographic method in the quantification of naphthalene in gasoline samples containing small amounts of other compounds that contribute to m/z 128. The concentrations found when the method based on direct injection was used were always higher than those obtained with fast gas chromatography, as would be expected since they included the whole of the m/z 128, and it is not possible to assign the abundance corresponding exclusively to naphthalene.

Table 4 shows the compounds that contribute to this m/z ratio in most of the gasoline samples employed. In the Table, it is possible to differentiate four zones with different interferences. Zone 1 (2.744–3.234 min) has mainly linear and branched hydrocarbons of nine carbon atoms whose molecular peak coincides with the m/z 128 ratio. Zone 2 (3.741–4.132 min) has C4

Table 3
Concentration of naphthalene expressed as percent (w/v) for the 14 gasoline samples analysed with the method based on direct injection before (a) and after (b) performing the proposed correction

	(a) Before applying the correction		(b) After applying the correction	
	Naphthalene (% w/v)	Relative error	Naphthalene (% w/v)	Relative error
Gasoline 1	0.079 ± 0.004	32	0.066 ± 0.003	10
Gasoline 2	0.075 ± 0.004	27	0.063 ± 0.003	6.8
Gasoline 3	0.077 ± 0.004	20	0.066 ± 0.003	3.1
Gasoline 4	0.072 ± 0.004	26	0.059 ± 0.003	3.5
Gasoline 5	0.091 ± 0.004	30	0.075 ± 0.003	7.1
Gasoline 6	0.070 ± 0.004	27	0.056 ± 0.003	1.8
Gasoline 7	0.073 ± 0.004	30	0.056 ± 0.003	0.1
Gasoline 8	0.086 ± 0.004	26	0.070 ± 0.003	2.9
Gasoline 9	0.088 ± 0.004	28	0.067 ± 0.003	−2.9
Gasoline 10	0.075 ± 0.004	34	0.063 ± 0.003	12
Gasoline 11	0.098 ± 0.004	17	0.083 ± 0.003	−1.2
Gasoline 12	0.094 ± 0.004	13	0.084 ± 0.003	1.2
Gasoline 13	0.075 ± 0.004	23	0.063 ± 0.003	3.3
Gasoline 14	0.078 ± 0.004	22	0.054 ± 0.003	−16

The relative errors of this method with respect to the chromatography procedure are also shown.

benzene derivatives. Zone 3 (4.198–4.239 min) has compounds derived from indene and zone 4 (4.765–5.211 min) has C1 and C2 naphthalene derivatives.

A possible strategy for avoiding the contribution of other compounds to the m/z 128 ratio could be the selection of another variable. The 129 m/z ratio is also present in the mass spectrum of naphthalene and the intensity of the interferences was lower in the four zones described above.

The calibration model corresponding to the m/z 129 variable ($(65.1 \pm 0.7)10^2 \times -(6 \pm 9)10^2$, $r^2 = 0.9982$) was validated

Table 4
Set of compounds identified in a gasoline sample whose mass spectrum contains the m/z 128 ratio

t_R (min)	Compound	Match quality
Zone 1		
2.744	Toluene	94
2.932	C2-Heptane	93
2.987	C2-Heptane	90
3.101	C1-Octane	91
3.132	C1-Octane	91
3.234	Nonane	92
Zone 2		
3.741	C4-Benzene	91
3.837	C4-Benzene	93
3.921	C4-Benzene	93
3.953	C4-Benzene	94
3.966	C4-Benzene	92
3.982	C4-Benzene	95
4.069	C4-Benzene	92
4.119	C4-Benzene	95
4.132	C4-Benzene	95
Zone 3		
4.198	Dihydro-C1-indene	91
4.239	Dihydro-C1-indene	90
Zone 4		
4.765	C1-Naphthalene	91
5.150	C2-Naphthalene	91
5.211	C2-Naphthalene	91

in the same way as above. The relative error of this step was 3.2%. The relative standard deviation (level 2, $n = 5$) was 6.2%. The values are considered to be sufficiently good. However, when the naphthalene concentration was determined in the 14 gasoline samples, there was also a positive systematic error.

3.3.1.1. *Mathematical correction of signals.* In order to eliminate the positive error obtained with the method based on direct injection in the determination of naphthalene, we propose a mathematical correction which somehow separates the contribution to intensity of m/z 129 characteristic of naphthalene from that arising from other compounds present in small amounts in most gasolines.

Fig. 5 shows the intensity of the m/z 129 and 131 ions when analysing a gasoline sample with the chromatographic method. The m/z 131 is not present in the mass spectrum of naphthalene, but is in most of the hydrocarbons that interfere with the m/z 129 signal of naphthalene. The contribution of these compounds to the m/z 129 intensity could then be corrected with their m/z 131 signals. No similar correcting variable could be found for m/z 128, the most abundant m/z for naphthalene. The proposed

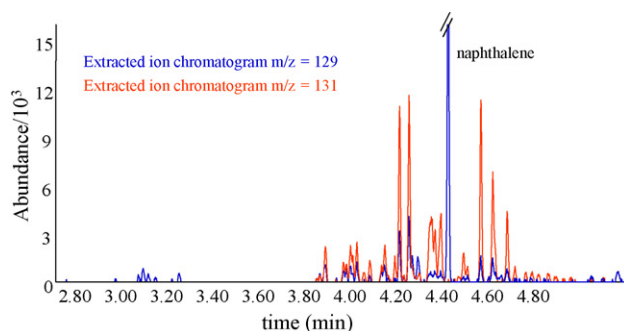


Fig. 5. Extracted ion chromatograms in a gasoline sample for the m/z ratios used in the mathematical correction: 129 and 131.

mathematical correction is:

$$I_{m/z\ 129}^{\text{corrected}} = I_{m/z\ 129}^{\text{total}} - K I_{m/z\ 131}^{\text{total}} \quad (1)$$

where $I_{m/z\ 129}^{\text{corrected}}$ is the value of the abundance of the m/z ratio of interest after removing the contribution of the interferences; $I_{m/z\ 129}^{\text{total}}$ and $I_{m/z\ 131}^{\text{total}}$ are the total abundance values for the 129 and 131 m/z ratios, respectively, along the analysis time and K is a constant value, obtained from the expression:

$$K = \frac{I_{m/z\ 129}^{\text{interferences}}}{I_{m/z\ 131}} \quad (2)$$

where $I_{m/z\ 129}^{\text{interferences}}$ is the intensity of m/z 129 that does not correspond to naphthalene and $I_{m/z\ 131}$ is the abundance of m/z 131, taking into account the whole run time.

The value of K was obtained by means of the chromatographic method since it is necessary to separate the value associated with $I_{m/z\ 129}^{\text{interferences}}$ from $I_{(m/z)\ 129}^{\text{total}}$. The intensity ratio K ranged between 0.38 and 0.44 for all the gasoline samples. With a view to proposing a single correction system that would be valid for different types of gasoline, we chose the mean value ($K=0.427$) for all the samples as a compromise.

Once the value of K has been established, the value of $I_{m/z\ 129}^{\text{corrected}}$ (Eq. (1)) for the different gasoline samples can be obtained from the results afforded by the non-separative method since the variables involved correspond to the intensity of m/z 129 and 131 along the signal recording time.

Now, the method based on direct injection afforded results (Table 3b) that were very similar to those obtained with the chromatography method.

3.3.2. Determination of total methyl-naphthalenes

The total concentration of methyl-naphthalenes was determined in the 14 gasoline samples. These were measured in duplicate. The results are shown in Table 5. The relative errors of the direct injection method with respect to the chromatographic one are also shown.

Table 5
Concentration of total methyl-naphthalenes expressed as percent (w/v) for the 14 gasoline samples analysed with the method based on direct injection

	Total methyl-naphthalenes (% w/v)	Relative error
Gasoline 1	0.053 ± 0.002	0.1
Gasoline 2	0.056 ± 0.002	-1.8
Gasoline 3	0.053 ± 0.002	-10
Gasoline 4	0.056 ± 0.002	-3.4
Gasoline 5	0.068 ± 0.002	4.6
Gasoline 6	0.047 ± 0.002	-6.0
Gasoline 7	0.055 ± 0.002	-5.2
Gasoline 8	0.064 ± 0.002	1.6
Gasoline 9	0.062 ± 0.002	6.9
Gasoline 10	0.059 ± 0.002	-1.7
Gasoline 11	0.071 ± 0.002	-2.7
Gasoline 12	0.057 ± 0.002	-8.1
Gasoline 13	0.051 ± 0.002	-1.9
Gasoline 14	0.057 ± 0.002	-6.6

The relative errors of this method with respect to the chromatography procedure are also shown.

In this case, the presence of compounds other than the methyl-naphthalenes contributing to the m/z 142 variable was very reduced (Figs. 2 and 3), and the determination could be carried out directly without using mathematical signal corrections.

3.4. Time of analysis

The two methods required different times of analysis. The methodology based on fast gas chromatography required 7.09 min for the temperature program to be completed and to ensure complete elution of the compounds present in the sample injected. Additionally, about 6 min were necessary to measure the next sample since the column had to be cooled down from the final temperature attained (240 °C) to the initial conditions of 60 °C. Considering the time invested in re-establishing the initial conditions, the analysis time per sample was therefore in the region of 13 min.

When direct injection was used, the signal recording time was 2 min. Immediately after analysing a sample, the injection system is ready for the next sample and its introduction into the device because the column temperature (240 °C) remains constant throughout the period of sample analysis. Taking into account the time necessary for washing the injection syringe, sample capture and actual injection, the interval between samples was 2.5 min.

Whereas with fast gas chromatography it is only possible to analyse four samples per hour, direct injection allows the measurement of 24 samples. This implies an important increase in sample throughput.

4. Conclusions

The proposed method has been successfully applied to the rapid detection and quantification of naphthalene and total methyl-naphthalenes in 14 different types of gasolines.

In view of the results obtained, fast GC-MS and direct injection-MS can be said to afford similar results. However, when the non-separative method is used, a certain error may arise due to the presence of other compounds that contribute to the intensity at the m/z characteristic of the compound studied. This positive systematic error in the determination of the concentration of naphthalene was satisfactorily corrected using the algorithm proposed here.

The great advantage of the direct injection method is that it is possible to determine naphthalene and total methyl-naphthalenes without the need to perform chromatographic separation, such that the time of analysis per sample is reduced from 13 to only 2.5 min.

Acknowledgments

We acknowledge the financial support of the DGI (Project CTQ2004-01379/BQU) and the Consejería de Educación y Cultura of the Junta de Castilla y León (Project SA057A05) for this research.

References

- [1] L.C. Marr, T.W. Kirchstetter, R.A. Harley, A.H. Miguel, S.V. Hering, S.K. Hammond, *Environ. Sci. Technol.* 33 (1999) 3091.
- [2] R. Lu, J. Wu, R.P. Turco, A.M. Winer, R. Atkinson, J. Arey, S.E. Paulson, F.W. Lurmann, A.H. Miguel, A. Eiguren-Fernández, *Atmos. Environ.* 39 (2005) 489.
- [3] M.H. Topal, J. Wang, Y.A. Levendis, J.B. Carlson, J. Jordan, *Fuel* 83 (2004) 2357.
- [4] P.M.L. Sandercock, E. Du Pasquier, *Forensic Sci. Int.* 134 (2003) 1.
- [5] P.M.L. Sandercock, E. Du Pasquier, *Forensic Sci. Int.* 140 (2004) 43.
- [6] J.W. Diehl, F.P. Di Sanzo, *J. Chromatogr. A* 1080 (2005) 157.
- [7] N.R. Khalili, P.A. Scheff, T. Holsen, *Atmos. Environ.* 29 (1995) 533.
- [8] H. Wingfors, A. Sjödin, P. Haglund, E. Brorström-Lundén, *Atmos. Environ.* 35 (2001) 6361.
- [9] I. Iavicoli, M. Chiarotti, A. Bergamaschi, R. Marsili, G. Carelli, *J. Chromatogr. A* (2006), doi:10.1016/j.chroma.2006.08.010.
- [10] T. Saeed, M. Al-Mutairi, *Environ. Int.* 25 (1999) 117.
- [11] E. Matisova, M. Dömötövá, *J. Chromatogr. A* 1000 (2003) 199.
- [12] J.L. Pérez Pavón, M. del Nogal Sánchez, C. García Pinto, M.E. Fernández Laespada, B. Moreno Cordero, *J. Chromatogr. A* 1048 (2004) 133.
- [13] C.C. Felício, L.P. Brás, J.A. Lopes, L. Cabrita, J.C. Menezes, *Chemom. Intell. Lab. Syst.* 78 (2005) 74.
- [14] E. López-Anreus, S. Garrigues, M. de la Guardia, *Anal. Chim. Acta* 333 (1996) 157.
- [15] E. Ródenas-Torralba, J. Ventura-Gayete, A. Morales-Rubio, S. Garrigues, M. de la Guardia, *Anal. Chim. Acta* 512 (2004) 215.
- [16] A.P. Singh, S. Mukherji, A.K. Tewari, W.R. Kalsi, A.S. Sarpal, *Fuel* 82 (2003) 23.
- [17] J. Burri, R. Crockett, R. Hany, D. Rentsch, *Fuel* 83 (2004) 187.
- [18] R.M. Alberici, C.G. Zampronio, R.J. Poppi, M.N. Eberlin, *Analyst* 127 (2002) 230.
- [19] K. Brudzewski, S. Osowski, T. Markiewicz, J. Ulaczyk, *Sens. Actuators B* 113 (2006) 135.
- [20] J.L. Pérez Pavón, M. del Nogal Sánchez, C. García Pinto, M.E. Fernández Laespada, B. Moreno Cordero, A. Guerrero Peña, *Anal. Chem.* 75 (2003) 2034.
- [21] J.L. Pérez Pavón, M. del Nogal Sánchez, C. García Pinto, M.E. Fernández Laespada, B. Moreno Cordero, *Anal. Chem.* 75 (2003) 6361.
- [22] J.L. Pérez Pavón, A. Guerrero Peña, C. García Pinto, B. Moreno Cordero, *J. Chromatogr. A* 1047 (2004) 101.
- [23] M. del Nogal Sánchez, J.L. Pérez Pavón, M.E. Fernández Laespada, C. García Pinto, B. Moreno Cordero, *Anal. Bional. Chem.* 382 (2005) 372.
- [24] J.L. Pérez Pavón, M. del Nogal Sánchez, C. García Pinto, M.E. Fernández Laespada, B. Moreno Cordero, A. Guerrero Peña, *Trends Anal. Chem.* 25 (2006) 257.
- [25] Enhanced ChemStation, G1701CA, Version C 00.00, Agilent Technologies, 1999.
- [26] Matlab, Version 6.5, The Mathworks Inc., Natick, MA, 2000.

Review

Non-linear regression methods in NIRS quantitative analysis

D. Pérez-Marín*, A. Garrido-Varo, J.E. Guerrero

Department of Animal Production, E.T.S.I.A.M. Universidad de Córdoba, Spain

Received 17 May 2006; received in revised form 17 October 2006; accepted 19 October 2006

Available online 21 November 2006

Abstract

Due to its speed and precision, near-infrared reflectance spectroscopy (NIRS) has become a widely used analytical technique in many industries. It offers, moreover, a number of other advantages which make it ideal for meeting current demands in terms of control and traceability: low cost per sample analysed; little or no need for sample preparation; ability to analyse a wide range of products and parameters; a high degree of reproducibility and repeatability. NIRS can be built into in-line processes, and – since no reagents are required – produces no waste. However, the major drawback to the use of NIRS for its most traditional application (the generation of prediction equations) is that it is a secondary method, and as such needs to be calibrated using a conventional reference method. For quantitative applications, calibration involves ascertaining the optimum mathematical relationship between spectral data and data provided by the reference method. The model may be fairly complex, since the NIRS spectrum is highly variable and contains physical/chemical information for the sample which may be redundant. As a result, multivariate calibration is required, based on a set of absorption values from several wavelengths. Since the relationship to be modelled is often non-linear, classical regression methods are unsuitable, and more complex strategies and algorithms must be sought in order to model this non-linearity. This overview addresses the most widely used non-linear algorithms in the management of NIRS data.

© 2006 Elsevier B.V. All rights reserved.

Keywords: NIRS; Calibration; Non-linear; ANN; Local regressions

Contents

1. Introduction	28
2. Classical calibration strategy	29
3. Non-linear approaches to calibration	29
3.1. Artificial neural networks: basic principles	30
3.1.1. ANN architecture	30
3.1.2. Functioning of the neural network	32
3.1.3. ANN models	32
3.2. Local calibrations	36
3.2.1. CARNAC	36
3.2.2. Locally-weighted regression	37
3.2.3. LOCAL algorithm	37
4. Applications of non-linear methods to NIRS data	38
References	40

1. Introduction

The most traditional application of NIRS, i.e. the quantitative analysis, requires the development of calibrations or prediction models. Calibration may be defined as the development of a chemometric model that relates spectral data for the samples

* Corresponding author at: Ctra Madrid-Cádiz km 396, Campus Rabanales, Ed. Producción Animal, Spain. Tel.: +34 957 218555; fax: +34 957 218436.

E-mail addresses: pa2pemad@uco.es, pa1gavaa@uco.es (D. Pérez-Marín).

comprising the training set to the values provided by the reference method for the parameter in question. The calibration equation thus obtained enables prediction of the content in other samples similar to those included in the calibration set. The model may be fairly complex, since the spectrum obtained in the normal working region of NIRS equipment (1100–2500 nm) is highly variable, and contains physical/chemical information on the sample [1,2]. Because it is therefore difficult to find specific wavelengths in the near-infrared region, there is a need for multivariate calibration, based on a set of absorption values from several wavelengths [3].

A good calibration method for this type of data should meet two essential requirements: the mathematical models applied should provide an efficient estimation, and they should overcome the problem of colinearity, which is quite marked when working with NIR spectroscopic information and gives rise to unstable predictions [4].

The accuracy of the NIRS predictions obtained from such models is governed by three major factors: the accuracy of the reference datum, the size and distribution of the calibration set used, and the method of adjustment selected [5–7].

2. Classical calibration strategy

Classical calibration strategy for developing quantitative NIRS applications is based on obtaining what are termed “global” or “universal” calibrations using multivariate methods for the linear fitting of the information available. According to Shenk et al. [6], a global calibration is one which can be used to predict 90–95% of samples of a given product. Therefore, the first step in the calibration process is to define the sample domain to be covered by the calibration [5,8].

Specific calibrations, based on a small range of samples, generally perform better than those based on a broader and more varied sample set, provided that the samples to be predicted are well represented in the calibration set. Thus, given that specific calibrations are only applicable to a small sample set, the aim is to obtain global calibrations that can be applied to the largest possible number of samples [9]. When handling NIR spectroscopic data, it is traditionally assumed that Lambert–Beer’s Law can be applied [10]; this law states that absorption values are linearly related to the concentration concerned in each sample. As a result, most mathematical techniques applied for the development of calibrations are based on linear fitting methods, mainly multiple linear regression (MLR), principal component regression (PCR) and, especially, partial least squares regression (PLSR).

Different variants of MLR (“step-up” and “step-wise”) provide model fitting using a small number of spectral variables selected from the whole NIR spectrum. The selected wavelengths are those which display the strongest correlation between the absorption value and the corresponding reference datum [11,12].

PCR and PLSR are calibration methods that work with the whole spectrum, although synthesising it into a series of linearly-independent variables in order to avoid data colinearity [1]. Their chief advantage is that they obviate the need to select

wavelengths for model development; at the same time, however, their use may hinder chemical interpretation [12,13]. PCR uses only spectral data to calculate new mutually-orthogonal variables termed principal components, which are then used for multiple regression fitting. PLSR is a similar procedure, which assumes that spectral information is a function of a small number of linearly-independent variables; however, calculation of those variables is based not only on spectral data but also on reference values for the parameter measured in each sample [14]. PLS regression is the most widely used method in NIRS agrofood applications.

When working with regression methods like these, it is essential to set an optimum number of factors or terms for the adjusted model. For this purpose, regression methods are generally used in conjunction with the standard error of cross validation (SECV), which additionally enables estimation of the predictive ability of the calibration obtained. Cross validation consists in dividing the calibration set into a series of groups (4, 5, 6, etc., depending on the number of calibration samples), each of which is used to validate the equation developed with the others. Cross validation enables all the samples to be used for both calibration and validation, and prevents overfitting of the model [1].

Shenk and Westerhaus [2] argue that SECV is the best estimator of the predictive capacity of an equation, and is equivalent to the mean standard error of prediction (SEP) of 10 randomly-selected groups.

3. Non-linear approaches to calibration

In many current and potential applications of NIR spectroscopic measurement, the relationship to be modelled is not always linear. The source of non-linearity may vary widely, and is difficult to identify. In NIRS, as in other spectroscopic techniques, some deviations from linearity are of known origin (breakdown of the Lambert–Beer law at high analyte concentrations, non-linear detector response, light-source scatter), whilst others are intrinsic to the parameter to be measured [15].

This means that classical regression methods are not always the most suitable option. Extrinsic deviations from linearity may be corrected by mathematical pretreatment of the signal prior to using linear calibration techniques. Intrinsic deviations, by contrast, require the use of special non-linearity adjustment tools [15,16]. Barton et al. [17] report that when dealing with highly-varied sample sets, in which the parameters measured may vary considerably, the precision of the predictions generated by universal calibrations tends to decrease due to the non-linear nature of the data; they suggest three possible solutions for handling the calibration of large sample populations. The most conservative option would be to accept less precision in prediction errors and/or to develop wherever possible specific calibrations for different types of product. The second option is the use of artificial neural networks for regression purposes, in order to take into account the non-linear relations inherent in the use of large spectral libraries. The third suggested option is to use local approaches based on the development of specific calibrations for each sample to be predicted, enabling existing non-

linearity to be addressed through the production of “local” linear models.

3.1. Artificial neural networks: basic principles

Artificial neural networks (ANN) imitate the structure and functioning of the human nervous system, to build parallel, distributed and adaptive information-processing systems, able to display a degree of intelligent behaviour [18]. From a mathematical viewpoint, ANN may be defined as non-parametric non-linear regression estimators [19], which have been seen as suitable for the carrying out of tasks not readily addressed using classical techniques [20]. The wide range of applications of ANN is due largely to their ability to deal with complex functions, enabling the modelling of non-linear relationships [21].

The basic elements of the biological neural system are neurons, which are grouped in clusters, each containing millions of neurons, arranged in layers and constituting a system with its own functionality. A similar hierarchical structure is used to build an artificial neural system. The essential element is the artificial neuron; neurons are arranged in layers, several of which together form a neural network.

The term processor or neuron is used to describe a simple calculating device which provides a single response or output to an input vector coming from outside or from another neuron. The standard artificial neuron model comprises the following elements [22,23]:

- A set of inputs, $x_j(t)$.
- Synaptic weights of neuron i , w_{ij} representing the intensity of the interaction between each synaptic neuron j and the postsynaptic neuron i .
- Propagation rule $\sigma(w_{ij}, x_j(t))$, which gives the value of the postsynaptic potential $h_i(t) = \sigma(w_{ij}, x_j(t))$ of neuron i as a function of weights and inputs.
- Activation function $f_i(a_i(t-1), h_i(t))$, which gives current activation status $a_i(t) = f_i(a_i(t-1), h_i(t))$ of neuron i , as a function of its previous status $a_i(t-1)$ and its current postsynaptic potential. For some training algorithms the activation function needs to be derivable. Sigmoid functions are the most commonly used for this purpose.
- Output function $F_i(a_i(t))$, which gives current output $y_i(t) = F_i(a_i(t))$ of neuron i as a function of its activation status.

Thus, the operation of neuron i may be expressed as:

$$y_i(t) = F_i(f_i[a_i(t-1), \sigma_i(w_{ij}, x_j(t))])$$

One of the most striking features of the artificial neuron, and one of particular interest for ANN, is its formulation as a non-linear device, since highly non-linear problems are not readily addressed using conventional techniques.

3.1.1. ANN architecture

The topology, structure or connection pattern of a neural network is termed “architecture”. The main parameters of the network are: number of layers, number of neurons per layer and

type of connection between neurons. Various types of neural architecture are thus possible, including single-layer and multi-layer networks.

Layers, in turn, may be classed as input layers, output layers or hidden layers. An input layer consists of neurons that receive data or signals from outside; the neurons in the output layer provide the neural network response, whilst the hidden layer, which is not directly connected to the outside, gives the neural network additional degrees of freedom, thus providing greater computational richness [18].

Similarly, depending on the flow of data, we can speak of “feedforward” networks, in which information flows only from input neurons to output neurons, and there is no propagation signal within a given layer or between one layer and a previous layer, as against “recurrent” or “feedback” networks, in which information can flow in any direction, including from output to input [20].

Connections between neurons may be excitatory or inhibitory, depending on whether the synaptic weight is positive or negative. A distinction is also drawn between intralayer connections (between neurons in the same layer) and interlayer connections (between neurons in different layers).

Optimisation of network topology is probably the most tedious step in developing a model. Network architecture is the characteristic most influencing the flexibility of the model generated [24,25]. The basic operation of a neuron is always the same: it picks up network inputs and returns output signals, transforming them by means of a transfer function. But it is essential to select network parameters: inputs and outputs, number of layers and number of neurons per layer, as well as the transfer function to be used in each layer.

3.1.1.1. Network inputs and outputs. When working with NIRS data, the number of network inputs refers to absorption data, expressed in any of the forms routinely used in classical regression methods (log(1/R) possibly pretreated with derivatives and scatter correction, principal components, PLS factors), whilst network outputs are the results predicted for the parameter measured.

The number of samples in the training set is often a limiting factor when using ANN. As in other regression methods, a minimum number of samples is required to develop a model using neural networks. The number of parameters to be fitted tends to be high, leading to overfitting of data if the training set comprises only a small number of samples.

To estimate the minimum number of training samples allowing theoretical generalisation, a parameter called the Vapnik-Chervonenkis dimension (VCDim) can be used. For a multilayer perceptron with one hidden layer, the lower limit of the VCDim to achieve good generalisation of the ANN is approximated as twice the total number of weights in the network [19]. Martín and Sanz [18] are more demanding in this respect, suggesting that the number of training patterns required p will be of the order $p = 10\omega$, where ω is the number of weights in the network. Definitely, the ratio of the number of samples to the number of adjustable parameters should be kept as high as possible to ensure adequate determination of the problem.

One way of achieving this is to compress input data, especially when they consist (as in NIRS data) of absorbances recorded at several hundred wavelengths [3,19,20,21]. If all absorbance data are used as inputs for training the neural network, the number of weights to be estimated will be too high. Network training will take a long time (hours, depending on the complexity of the network architecture). But the main disadvantage of using all wavelengths as inputs is one of dimensionality, since there will be too many parameters in the model and too few samples in the training set to enable fitting. This could pose problems, particularly where there is excess noise in the calibration set. Data compression tools, in addition to reducing the size of input data, enable the elimination of irrelevant information such as noise or redundancies present in a data matrix. Borggaard [32] reports that reducing input size has a number of advantages: briefly, correct data compression increases network training speed, reduces storage memory, enhances the generalising capacity of the model obtained, makes models more robust with respect to measurement noise, avoids overfitting, and overall provides a simpler model.

Nevertheless, orthogonality of input variables is less critical for ANN that can handle colinear input data than for linear regression methods [19], since the network can extract the relevant information [20].

Of the various methods for reducing data colinearity, the most widely used and successful is the principal-components method, recommended by Despagne and Massart [19] over the PLS method. Principal component analysis is extensively used for data synthesis, since the principal components successively represent the sources of maximum variance in the data. To determine the optimum number of principal components to be used as inputs, the same procedures used in principal component regression can be applied; this choice, however, is not critical, since models developed using ANN are constructed iteratively for successive optimisation of network topology. One drawback of the method is that principal components lose stability as the ratio of number of samples/number of wavelengths declines [31].

Most applications of ANN to the processing of spectroscopic data for quantitative analysis use principal components as input variables [15,21,26–31]; although PLS factors and Fourier transforms are also used [21,30].

Moreover, additional signal preprocessing methods are available to improve the efficiency of ANN models when applied to NIRS data, the same used together with classical regression techniques. Naes et al. [29] report that application of scatter correction to input variables produces better results. This suggests that ANN, though highly flexible, cannot always work with the marked non-linearity derived from the scatter effect in NIR spectra. Westerhaus and Reeves [33] obtained better results using the first derivative for the preprocessing of spectroscopic data than using the original variables or only a small number of variables.

Regarding the net outputs, for quantitative applications of this type, it is recommended that a single neuron be used in the output layer [19,26].

3.1.1.2. Number of layers and neurons in the network. Network design should match the complexity of the problem to be

addressed, limiting size as much as possible [34] to avoid over-training the model [18,35].

As more hidden units are added to the network, bias is reduced and the number of functions that can be fitted increases exponentially. Svozil et al. [36] suggest that optimal network topology depends not on the number of inputs and outputs but on the number of samples in the training set, the amount of noise and the complexity of the function to be trained. The usual procedure is to test numerous networks with varying numbers of hidden units, estimate generalisation error for each and select the network with the lowest generalisation error.

Methods to determine the optimum number of hidden layers tend to be based on trial and error. One can start from very simple networks, gradually increasing complexity until an optimum architecture is achieved; alternatively, one can start with complex networks and gradually reduce the number of layers and nodes [21,24]. In either case, the search for an optimum model requires considerable effort and computation time. For many applications, this computational effort is pointless; Cirovic [21] suggests that in such cases an empirical rule can be applied, which states that the number of parameters to be fitted should be roughly half the number of samples available.

Svozil et al. [36] argue that there is no theoretical reason for using more than two hidden layers, whilst Despagne and Massart [19] report that better results are never obtained on calibration problems using two hidden layers instead of one, even if learning is sometimes faster. Moreover, since use of two hidden layers accentuates the problem of convergence on local minima, it is important to use several repetitions of the same network. The additional layer makes the gradient more unstable and slows down considerably the training process. It is generally recommended that only one hidden layer be used in multivariate calibration, unless the relationship to the model seems to be discontinuous, in which case an additional hidden layer is necessary [19,36].

Another parameter to be optimised in network design is the number of nodes in the hidden layer. In principle, the number of hidden nodes determines the complexity of the network and should be optimised for each application [37].

The predictive ability of the network is governed by the number of units or nodes in the hidden layer(s) and by the values of the weights obtained. If the number of hidden units is insufficient, prediction errors tend to be elevated due to poor model fitting. However, too many hidden units can cause overfitting, with a proportional increase in prediction errors [38,39].

It is possible to determine a minimum number of hidden nodes below which the network is not complex enough to model the problem addressed. Similarly, above a certain maximum number, the network becomes too complex, and might incorporate data noise in training [26]. The way to determine the optimum number of hidden nodes is to start with a minimum number and keep adding one new unit [31].

Generally, a network with n sigmoidal hidden nodes could approximate the response of $2n - 1$ samples. It is considered advisable to reduce the number of hidden nodes as much as possible in order to achieve a simpler, more robust model, producing

results that are more stable and independent of the set of initial random weights [19].

3.1.1.3. Transfer function. The sum of input weights is transformed by means of a transfer function which may be linear or non-linear. The transfer functions most widely used in hidden layers are the sigmoid or hyperbolic tangent functions, which enable a large number of non-linearities to be fitted [19,26,40]. Long et al. [26] report that ANN provide greater stability than non-linear techniques against slight input signal perturbations and noise. This is due, amongst other things, to use of the sigmoid function.

The transfer function in the output layer may be linear or non-linear. The linear function is more widely used for developing quantitative models, due to its wider and more dynamic range [19,20,26].

3.1.2. Functioning of the neural network

One of the chief characteristics of the ANN is that they are trainable systems, able to undertake a given type of processing, learning from a set of training patterns or examples. Training ends when the neural network is able to generalise a given solution to a given problem [26]. ANN training is usually slow, although once the network is trained, predictions are virtually instantaneous [41].

ANN training consists in modifying synaptic weights following a certain training rule, usually constructed by optimisation of an error or cost function. The learning process is iterative, in that weights are successively updated until the network achieves the desired performance. Error estimation as a function of weights tends to be quite irregular, and consequently for the same architecture different initial weights may lead to different end results [19,31]. For that reason, Tetko et al. [42] suggest that the same network design should be repeated several times with different batches of initial weights.

ANN learning may be supervised or unsupervised. In both cases, the aim is to estimate multivariate input/output functions or probability densities. For the development of calibrations, supervised learning is used; in this case, certain information is provided on these functions, whereas the unsupervised or self-organising network requires no external information. Supervised learning rules tend to be computationally more complex but results are also more accurate [18].

In supervised learning, the network is presented with a training set of samples (with reference data), and iteratively adjusts weights until its output approaches the desired output for all possible inputs. Weight correction, the most important step in the training process, is generally performed after each new input (immediate correction), i.e. as soon as the error is detected, but can also be performed once all inputs have been processed (deferred correction), in which case individual errors for all data pairs are accumulated and the cumulative error is used for correction [24].

It is important to distinguish between the level of error achieved by the end of the training stage, usually calculated as the mean squares error of the results provided by the network for the training data set, and the error made by the trained network

when predicting samples from outside the training set, which is a measure of its “generalising ability”, i.e. its ability to provide a correct response to patterns not used in training.

The performance of a neural network should not be judged on the results obtained with the training set, which will usually be perfectly fitted since ANN are powerful non-linear estimators, able to model very complex situations. Given a sufficiently large network, training errors can be reduced as much as required simply by carrying out more iterations. The efficacy of the model must thus be judged on the basis of its performance with a validation set different from the calibration set [4,19], measured in terms of the generalisation error. Good generalisation is more valuable than a very low training error [18]. Moreover, it is important that the training set contain a sufficient number of samples, and that sample distribution reflect the variability of the total population, in order to achieve strong generalising ability and thus avoid extrapolation in the prediction phase [19,39].

After an initial phase in which oscillations may appear, the training error tends to fall steadily, whilst beyond a certain point the generalisation error starts to increase, suggesting a progressive decline in learning. This is because the network progressively adapts to the training set, adjusting to the problem and improving generalisation. However, at a given moment the system overadapts to the peculiarities of the training set, learning even data noise, leading to an increase in prediction error on unknown sets. By this time, the network is simply memorising training-set patterns; this situation is termed “overfitting” or “overtraining”. It is therefore essential to match network size and topology to the complexity of the problem being addressed; size should be limited as much as possible to avoid overtraining [18,34,35].

Some authors recommend the use of cross-validation during development of a supervised neural network, as a control measure to stop training at the optimal point of minimal error, thus avoiding overfitting [18]. However, Gemperline [30], and Despaigne and Massart [19] argue that this approach is unsuited to the concept and functioning of ANN, although it is suitable for parametric linear models, in which perturbation caused by the removal of one or a few samples from the training set has little influence on the model parameters, and therefore the cumulative cross-validation error obtained is a reliable validation-error estimate for the model constructed with all samples. The situation changes for networks applied to non-linear problems characterised by complex error surfaces, since the solutions obtained when two different samples are removed from the training set can differ significantly from each other. For that reason, a critical aspect in the development of any calibration model is the division of data into two subsets: a training set (used to estimate model parameters) and a validation set (used to evaluate the model’s generalising ability on new samples).

3.1.3. ANN models

Several different types of ANN have been developed. All are composed of small, interconnected units (“neurons”), whose individual behaviour determines the overall behaviour of the network. The most common is the multilayer perceptron, although

other types such as radial basis function (RBF) networks have more recently come into use in analytical chemistry.

3.1.3.1. The multilayer perceptron. The multilayer perceptron is a feedforward supervised network comprising several layers: an input layer, an output layer and one or more hidden layers. Its architecture was designed to overcome the limitations of the single, or single-layer, perceptron which can only represent separate linear functions.

Information is received through the input layer and passed through the hidden layer(s); the response is generated in the output layer. An example of the architecture of a multilayer perceptron is shown in Fig. 1.

In comparison to the single perceptron, the multilayer perceptron incorporates not only additional hidden layers but also a sigmoid transfer function enabling the modelling of non-linear responses [20,32]. The multilayer perceptron is thus able to act as a universal approximator of functions [43,44], i.e. a network of this type can learn any function or continuous relation between a group of input and output variables. This makes it a highly flexible non-linear tool, whose performance outclasses that of classical statistical models in many areas. Moreover, this type of neural network can be used for the development of quantitative prediction models requiring a high degree of accuracy and precision, as well as for classification purposes [32].

A number of algorithms exist for fitting weights within a network designed for a specific application. The choice depends on training speed, as well as the degree of accuracy and precision of the final model obtained.

(a) *Error back-propagation learning algorithm (BP):* The multilayer perceptron can be trained using a learning algorithm known as “back-propagation” (BP) or one of its variants. This combination is the most widely used; indeed, over 90% of studies use a multilayer perceptron with back-propagation for chemical applications [21,24]. It is also one of the best suited to spectroscopic applications, in which the accuracy achieved at regression is of major importance [32].

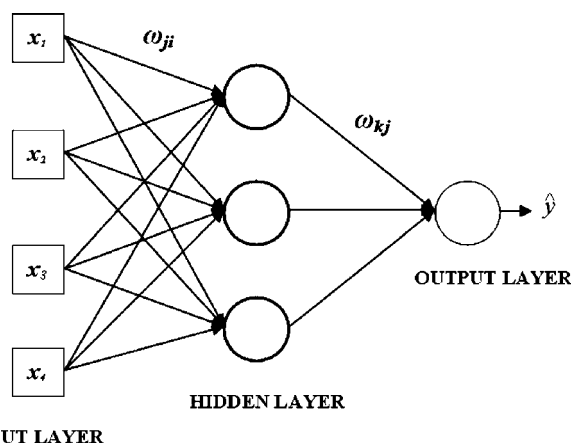


Fig. 1. Topology of a multilayer perceptron with 4 neurons in the input layer, 3 neurons in the hidden layer and 1 neuron in the output layer.

The back-propagation learning algorithm was first introduced by Werbos [45] and its application to neural network training was later made popular by Rumelhart et al. [46]. This algorithm is also termed the generalised delta rule or gradient descent method, since it is an extension of the delta rule proposed by Widrow and Hoff [47] to networks with intermediate layers.

BP is one of the so-called “error-correction learning algorithms”, which adjust weights in proportion to the differences between actual output and desired output, in order to minimise actual network error [24,41]. Its attraction lies in the good definition of the correction equations on which it is based. These equations are applied through the layers forming the network; weight correction starts in the last (output) layer, and works back through the immediately preceding layer and ultimately to the input layer; hence its name (Fig. 2).

The aim of the training process is to identify a group of weights that, introduced into Eq. (1), minimise the model fitting error.

$$y = \sum_{i=1}^N a_i u_i + \sum_{j=1}^n \sigma \left(\sum_{i=1}^N w_{ij} a_i + b_j \right) v_j + B \quad (1)$$

where

- σ is the sigmoid function defined as $\sigma(x) = 1/(1 + \exp(-x))$.
- u_i is the weight of the direct connection from input neuron i to the output layer.
- w_{ij} is the weight of the connection from the input layer to the hidden layer.
- v_i is the weight of the connection from the hidden layer to the output layer.
- b_i is the weight of the connection from the bias neuron (output always equal to 1) and to the neuron i in the input layer.
- B is the size of the bias to the output layer.

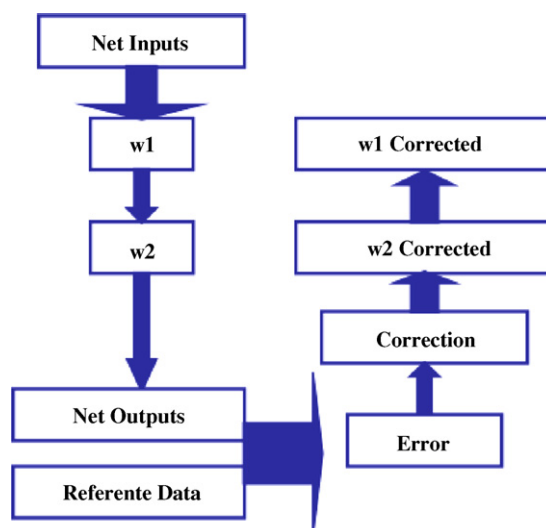


Fig. 2. Flowchart of an error-backpropagation algorithm for weight correction.

In the BP algorithm, the cost function for weight fitting is calculated from the expression (2):

$$\text{COST} = \text{SEC}^2_{xN} = \sum_{i=1}^N (\hat{y}_i - y_i)^2 \quad (2)$$

Through an iterative process, the aim is to change the value of all the weights in Eq. (1) so that the cost function is reduced. The predicted value \hat{y} can be expressed as a function of all the weights. This enables us to calculate the partial derivatives of \hat{y} with respect to each of the individual weights w_{ij} , u_i , v_i , b_i and B that form the gradient of the cost function. If the total weights vector is defined as $W = (w_{ij}, u_i, v_i, b_i, B)$, the gradient of the function can be expressed as (3):

$$\frac{d\text{COST}}{dW} = \left(\frac{\delta\text{COST}}{\delta w_{11}}, \dots, \frac{\delta\text{COST}}{\delta u_1}, \dots, \frac{\delta\text{COST}}{\delta v_1}, \dots, \frac{\delta\text{COST}}{\delta b_1}, \frac{\delta\text{COST}}{\delta B} \right) \quad (3)$$

The procedure for training a given multilayer-perceptron architecture using the error-backpropagation algorithm is as follows [32]:

1. Initialise all weights to some random number and introduce a new variable called the sum gradient vector. Initial weights should always be low-value positive and negative natural numbers; if null initial weights are used, training cannot progress.
2. Set the sum gradient vector to zero.
3. Present n samples to the neural network, obtaining a predicted value for each by applying Eq. (1). Calculate the new sum gradient vector for each of the n samples using the expression (4),

$$\text{Sum gradient} = \text{Sum gradient} + \frac{d\text{COST}}{dW} \quad (4)$$

4. Modify the weights vector according to the expression (5)

$$W = W - \text{lambda} \times \text{sum gradient} \quad (5)$$

where lambda is the learning rate.

Repeat steps 2–4 for a preselected number of epochs or until the SEC has reached a satisfactorily low value. Network training time increases exponentially with the number of iterations preselected [41], although convergence usually requires at least 10,000 epochs [26,29].

Prior to the start of training, the learning rate should be fixed; this is an important parameter for obtaining the model when backpropagation is used as the learning rule. The learning rate determines the rate at which information is encoded into the network [26] and the magnitude of changes in output [41]. If it is set too low, the convergence of the weights to an optimum may be very slow, with the added risk of getting stuck at a local minimum, even though greater output accuracy is ensured. If the rate is set too high, the system may oscillate. The appropriate value for the learning rate depends on the transfer function in the

output layer. For a linear function, normally used for developing quantitative models, values should be in the range 0.001–0.1, whilst for a sigmoid transfer function the learning rate should be between 0.5 and 1 [20].

BP is a highly-generalised method, and as such has advantages and drawbacks. The main advantage is that it can be applied to a large number of different problems, frequently providing good solutions in a not-overlong time. The two major disadvantages are the slowness of the convergence process and the danger of overtraining, arising directly from the network's generalising ability. The BP algorithm uses the gradient descent technique for weight correction, i.e. it scans the error surface seeking the minimum of the error function; it is not guaranteed to reach the global minimum of the error function, for the training process may become locked in a local minimum.

Several modifications of the back-propagation algorithm have been put forward, and research continues to focus on overcoming these two disadvantages. Most modifications have addressed the slowness of convergence, whilst a few have sought to enhance generalisation.

The designers of the BP model [46] suggested that greater efficiency might be achieved by including in the algorithm an additional term known as momentum. This term, which is proportional to the increase of the previous iteration (inertia), ranges in value between 0 and 1, and is generally set close to 1. Thus, if increments in a given weight are always in the same direction, the updates at each iteration will be greater; however, if the increments oscillate, the effective increment will be cancelled out. Thus, in narrow, deep areas of the error hypersurface, low-dimension weights, which might oscillate from one side of the dip to the other, undergo small increments, whilst weights in directly-downhill directions will be enhanced [48]. This is a way of accelerating the effective learning rate in certain directions, whilst also ensuring the averaging-out of noisy data as well as giving a smoother search for optimal weights by eliminating oscillations in the descent [32].

The choice of the BP algorithm as a learning rule is a good option when working with large sample sets, which also contain a large amount of redundant information [49].

(b) *The Levenberg–Marquardt learning algorithm (LM)*: Since the development of the back-propagation method, there has been growing interest in the search for new and better learning algorithms, the choice of an appropriate training method being a critical aspect of building a neural network [50].

Second-order optimisation methods, based on determination of the Jacobian matrix of partial derivatives of the cost function, descend through the error surface using information provided by the rate of change of the gradient [18]. These techniques are more robust, and typically have a convergence time one or two orders of magnitude smaller than the gradient method [19], although they are far more complex to implement and require more calculation resources [18].

One of the most popular and rapid second-order methods for training multilayer feedforward networks is the Levenberg–Marquardt (LM) algorithm, which has been successfully used in a number of applications, and has proved both stable and efficient [18,19,39].

The LM algorithm is essentially an effective modification of the Newton–Gauss method [51,52], whose excellent local convergence properties it combines with a constant error decrease provided by gradient descent [53,54]. The LM algorithm is specifically designed for minimising a sum-of-squares error, typical when working with one-way networks such as the multilayer perceptron. For this error function, the Hessian matrix (H) can be written as:

$$H = J^T J$$

and the error surface gradient as

$$g = J^T e$$

where e is the mean-squared network error and J is the Jacobian matrix of first derivatives of network errors to network weights, developed as follows:

$$J(\omega) = \begin{bmatrix} \frac{\partial e_1(\omega)}{\partial \omega_1} & \frac{\partial e_1(\omega)}{\partial \omega_2} & \cdots & \frac{\partial e_1(\omega)}{\partial \omega_N} \\ \frac{\partial e_2(\omega)}{\partial \omega_1} & \frac{\partial e_2(\omega)}{\partial \omega_2} & \cdots & \frac{\partial e_2(\omega)}{\partial \omega_N} \\ \vdots & \vdots & \ddots & \vdots \\ \frac{\partial e_N(\omega)}{\partial \omega_1} & \frac{\partial e_N(\omega)}{\partial \omega_2} & \cdots & \frac{\partial e_N(\omega)}{\partial \omega_N} \end{bmatrix}$$

For weight updating, the LM algorithm uses that approximation to the Hessian matrix in the following Newton-type adaptation

$$\Delta\omega = (J^T J + \mu I)^{-1} J^T e$$

The control parameter μ is a scalar whose value is adjusted at each training step, according to the evolution of the error: its value decreases after every iteration in which the error decreases, and increases only when the error increases. Thus, the value taken by μ in training will govern the approximation either to the Newton–Gauss method or to the steepest-gradient method. When the value is very high, it approximates to a gradient descent, whilst if the value is low the result approximates to that obtained using the Newton–Gauss method. Since the Newton–Gauss is faster and more accurate close to the minimum error than the gradient descent, the aim of training with the LM algorithm is to switch as rapidly as possible to the Newton–Gauss method. Thus, the error function will always be reduced at each iteration.

The LM algorithm has excellent convergence properties; it is capable of finding a minimum much faster than the BP algorithm, with a smaller number of hidden units, yielding a more precise estimation of the prediction error. Theoretically, the BP algorithm should be capable of achieving the same results as the LM method; the higher prediction errors must be assigned to slow and incomplete convergence [39].

However, the LM algorithm has certain limitations. One is that it can only be used in networks with a single output neuron, which uses sum-of-squares as the error function to be minimised [49]. Another drawback is that training requires considerable computational capacity, arising from the need to calculate the

Jacobian matrix of the error function and to invert matrices with dimensions equal to the number of the weights of the network [54]. Thus, if m is the number of weights, it becomes necessary to calculate and store m^2 elements of the Jacobian matrix at each iteration, and calculate its inverse, which requires around m^3 operations to be performed [55,56].

In very large neural networks, in which numerous parameters need to be estimated, the increased memory requirements of this algorithm render it impractical. However, the LM method can be extremely effective in medium- to large-scale problems, with up to several hundred weights, since it can train the same network from 10 to 100 times faster than the BP algorithm [50,54,56].

A further disadvantage is that the LM algorithm is a local optimisation method, and thus affords no guarantee of convergence to the global minimum of the cost function. In first-order methods, this drawback can be overcome by the introduction of a momentum term. Using LM, if iterations converge towards a local minimum, there is no way of escaping and the optimal solution will not be obtained, in which case the whole training process will have to be restarted. This drawback, however, is to an extent offset by the increased rate of convergence of this algorithm, which becomes quadratic as the iterations converge towards a solution [54].

3.1.3.2. Radial basis function. Radial basis functions were introduced in the field of artificial neural networks by Broomhead and Lowe [57] and Moody and Darkin [58], and their use has subsequently been reported in various specific books on artificial neural networks [35,53].

The radial basis function model may be considered a hybrid neural network, in that it incorporates both supervised and unsupervised learning [18]. RBF, like multilayer perceptrons, enable arbitrary non-linear systems to be modelled, with the advantage that the training time required tends to be much shorter. The two models are closely related: both use one-way layers, both are universal approximators, and both are applied to the same sort of task. The architecture of an RBF network consists of three neuron layers – one input, one hidden and one output – and is therefore similar to that of a multilayer perceptron with a single hidden layer. However, the main difference between the two is related to the transfer function in the hidden layer, which in RBF networks tends to be Gaussian [20].

In RBF networks the hidden-layer neurons, instead of calculating a weighted sum of inputs and applying a sigmoid, calculate the Euclidean distance between the synaptic-weights vector (which in this type of network is termed the centre or centroid) and the input, and apply a Gaussian radial transfer function to that distance. Thus, neurons in RBF networks are of the local-response type, in that they only respond with appreciable intensity when the input vector and the centroid occupy nearby positions in the input space; in contrast, the hidden neurons in a multilayer perceptron have an infinite response range, since any input vector – regardless of its whereabouts in the input space – can prompt activation of the neuron [18].

RBF networks divide the input space into hyperspheres, and each hidden neuron produces a non-linear local approximation in the hidden layer, which combines linearly in the output layer;

this enables complex relations to be approximated in a different way from that of the multilayer perceptron, which divides the input space into hyperplanes [20].

For a RBF network with n neurons in the input layer, m neurons in the hidden layer and 1 neuron in the output layer, the network output is expressed by the following formula:

$$\bar{y}(x) = \omega_0 + \sum_{i=1}^m \omega_i \phi_i(x)$$

where ω_i represents the weights of the connections between the hidden layer i and the output neuron; ω_0 the value of the threshold on the output neuron, $x(x_1, x_2, \dots, x_n)$ the inputs and $\phi(x)$ is the radial basis function or hidden-neuron activation function.

The Gaussian radial basis functions are defined by the expression:

$$\phi_i(x) = e^{-(|x-c_j|/b_j)^2}$$

where $|x - c_j|$ is the Euclidean distance between the input vector (x) and the centre of the radial function (c_j), whilst the parameter b represents the width of the Gaussian function.

RBF networks are faster to train than their back-propagation counterparts, although the execution phase is slower due to the large number of hidden layers required. This is precisely because – as commented earlier – the intermediate neurons in RBF networks act locally, whilst those of the multilayer perceptron act globally; since a single perceptron node covers a larger input space, fewer nodes are required [18].

Although introduced only recently, radial basis functions have numerous practical applications, thanks to their simplicity, generality and speed of learning.

3.2. Local calibrations

Naes et al. [3] suggest that most regression surfaces can be fitted locally using linear models. Local regression approximations apply this general concept to each new sample to be predicted. Shenk et al. [59] maintain that, in theory, the best prediction model should compute a specific calibration equation for each sample analysed, using a small calibration data set tailored to the unknown sample from a large library of samples. They suggest that this method, termed local regression, combines the advantages of global calibration in using one database to cover a large product domain, with the accuracy obtainable with specific calibrations.

The essential idea behind local regression methods is thus to search for and select, within a large spectral library, a set of samples spectrally similar to the unknown sample to be predicted, and then develop a specific calibration for that sample using the selected samples as a calibration set (Fig. 3). This process is repeated for each sample to be predicted. This may at first appear to be a long and tedious process; in practice, however, each local calibration is usually developed with a small number of samples and, therefore, the number of principal components or PLS factors in the regression is lower than for global calibrations, thus also reducing computational requirements.

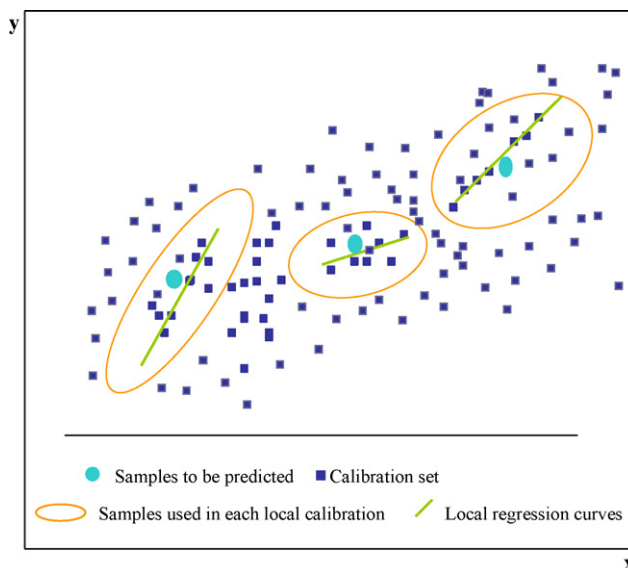


Fig. 3. Diagram showing the basic functioning of a local calibration (adapted from Naes and Isaksson [60]).

Local calibration approximations can improve the results obtained by global calibration in two different ways [61]. First, as indicated earlier, they can model the non-linearity present in the data by selecting sample subsets that display a more restricted range for the parameter analysed, to which the application of linear regression techniques is suitable. Second, they can exploit the non-homogeneity of the samples in the initial sample library, using spectral information to select local calibration sets which have, for example, similar particle sizes or similar moisture content to the unknown sample.

Within the general framework defining the basic principles of local calibration, the methods put forward vary considerably in terms of both the selection of the calibration set to be used and the way of performing subsequent regression [62,63].

The literature focuses mainly on three types of local approximations: *Comparison Analysis Using Restructured Near Infrared and Constituent Data* (CARNAC), *Locally-Weighted Regression* (LWR) and the LOCAL algorithm patented by Shenk and Westerhaus. More recently, Fearn and Davies [63] have proposed a fourth local calibration method termed *Locally-Biased Regression* (LBR). In order to be useful for a specific application, each method requires the optimisation of several parameters.

Since the first three local regression methods indicated above are the most widely used for NIRS applications, a more detailed theoretical description is given below.

3.2.1. CARNAC

The CARNAC method put forward by Davies et al. [64] is a rapid, simple local regression approximation. It is based on the idea that quantitative predictions can be obtained from databases containing spectral information and reference data, rather than through some form of regression analysis derived from that database.

The major effort in this method is invested in the first stage of any local approximation, i.e. the selection of calibration samples similar to the sample to be predicted. For that reason, Davies [65] prefers to refer to CARNAC as a method of database analysis rather than of local regression.

The procedure is based on three essential concepts: database compression, database modification and similarity analysis [66].

In the original version of CARNAC, the spectral database is compressed using Fourier transformation (FT). Then, for each analyte in the database, a modified database is computed by selecting a subset of the FT data. This is achieved by the use of step-wise multiple linear regression between the FT spectral data and the reference analyte values for each sample from the database. For each analyte, the spectrum of the unknown sample is modified and compared with each of the samples in the modified database, by calculating a similarity index (SI). The SI for each sample is calculated from the correlation coefficient (r) between the unknown sample and a member of the database, using the following expression: $SI = 1/(1 - r^2)$.

Samples with a high similarity index are then selected, and samples identified as outliers are eliminated. In the CARNAC method, sample selection takes into account both spectral data and the value of the parameter studied for each sample [62]. Finally, the predicted value for the unknown sample is calculated from a weighted average of the analyte values in the subset [65].

Shenk et al. [59] report that, because of the simplified method of sample selection and calculation of the predicted values, CARNAC is a very fast local method. However, it is not widely used in routine analysis, since it is not included in the commercial software provided with NIRS instruments.

More recently, a new version of CARNAC has been developed, which does not require data compression by Fourier transformation, but instead directly uses principal components or wavelengths [63,66].

3.2.2. Locally-weighted regression

The LWR algorithm developed by Naes and Isaksson [60] is a modification of the method put forward by Cleveland and Devlin [67]. Fearn and Davies [63] define it as a local version of principal component regression.

The LWR method performs a principal component analysis, usually after mathematical pretreatment of the signal, in order to compress the spectral library into a number of principal components (PC), which should be predetermined. A subset of samples similar to the unknown sample, expressed in the same PC scores, is then selected on the basis of the smallest Mahalanobis distances (H). In calculating these distances, a larger or smaller weight can be assigned to each component, depending on its correlation with analytical values from the calibration database [68]. In order to predict the unknown sample, a calibration equation is then derived using the selected samples, by linear principal component regression, assigning a different weight to each calibration sample depending on its spectral distance from the unknown [4]. Traditionally, a tri-cube weight function is used:

$$W(d) = (1 - d^3)^3, \quad 0 \leq d \leq 1$$

where d is the distance between the unknown and the calibration samples. The parameter d should be normalised so that the distance from the unknown sample to the furthest calibration sample is equal to 1 [3].

One disadvantage of LWR is the colinearity problem, which in this case affects not only the stability of predictions but also the measurement of the distances determining proximity in the multivariate spectral space. Naes [4] suggests that the directions of the vectors with the lowest values are usually irrelevant for prediction purposes and should not be included in distance measurements. Naes et al. [69] proposed that only the first PC (or PLS factors) should be used both in distance measurements and for fitting the regression equation.

Experience has shown that the LWR algorithm can be performed with a smaller number of PC (2 or 3) than that required for global approximations using PCR or PLS regression, simply because the most relevant information is found close to the first PC, but non-linearly. This suggests that the remaining PC used for linear regression are required only to correct any non-linear relationships between the unknown and the first PC. Since the first components are more stable and less sensitive to slight changes in the spectrum than later ones, it is fair to expect the LWR approximation to be more readily transferred between instruments and less sensitive to outliers [4]. However, Aastveit and Marum [70] argue that the number of PC needed to define the model is strongly dependent on the heterogeneity of the product analysed.

Development of the LWR algorithm requires optimisation of the number of PC to use and the number of samples to include in the training set for local calibration. The optimum value for both parameters should be determined for each particular application. Similarly, the distances and weight functions to be applied should be preset [3].

Fearn and Davies [63] indicate that in the original LWR procedure, only the regression calculation stage is a local approximation, since the principal component analysis performed is global. Perhaps for this reason, Aastveit and Marum [70] suggested a modification of the LWR method, in which PC analysis is performed locally, i.e. for each estimation PC are recalculated with the selected sample subset. As a result, the calculated PC are more explanatory and determinant, although they may also be more unstable.

Wang et al. [71] later put forward a new version, called LWR2, in which the selection of samples similar to the unknown is made with reference not only to spectral distance in the defined principal component space, but also to reference analytical values.

3.2.3. LOCAL algorithm

The LOCAL algorithm patented by Shenk and Westerhaus [72] is another local approximation designed for the management of large spectral libraries [6,73]. Shenk et al. [6] report that using the LOCAL algorithm can improve the predictive capacity of a model obtained with a global calibration strategy between 10 and 30%, depending on the spectral diversity of the samples in the sample library.

This algorithm works by searching through a wide sample collection to select samples spectrally similar to the analyte. The selected samples are then used to develop a specific calibration equation for predicting the unknown sample. The stability of predictions is achieved by building up spectral libraries containing a sufficiently large number of samples to cover the maximum possible variability of the product and the parameter in question [74].

The selection of calibration samples is controlled by the value of the correlation coefficient between the spectrum of the unknown sample and those of the available database. Those samples displaying the greatest correlation with the sample are selected to form part of the training set. The maximum number of samples used for calibration can be set manually by the operator by a correlation cut-off value [59,75]. This is a key parameter to be determined when using the LOCAL algorithm, since setting the number of samples too low or too high may affect the accuracy of predictions. The most suitable number is between 60 and 120 samples [76], although it will depend on the type of product, the parameter to be predicted and the distribution of the spectral library as a whole [70]. Moreover, a minimum correlation value can be established in order to ensure that the selected samples closely match the sample to be predicted.

It is also important to set the minimum number of calibration samples required to develop the prediction equation, thus ensuring a sufficient sample size [17].

After defining the calibration data set, the procedure computes the specific calibration equation, using partial least square (PLS) regression. As in any regression of this type, it is essential to determine the optimum number of terms or factors to be used. Usually, as indicated earlier, cross-validation is used in global calibrations. However, Shenk et al. [59] suggest that this approach is not the most suitable for the LOCAL algorithm, for two main reasons. First, cross-validation identifies the optimum number of PLS terms within a given data set, but does not consider the information from the unknown sample. Second, cross-validation is time-consuming and would slow down the prediction speed of the LOCAL algorithm.

The authors developed two alternative methods for setting the optimum number of terms. In the first, the operator sets the number of PLS factors, from 1 to 50. The second method calculates a weighted average of the predicted values generated by regression models using various numbers of factors. The weights are determined by two factors: the size of the regression coefficients for each PLS factor and the residuals for the analysed sample spectrum. The formula to calculate weights (W) is as follows:

$$W_{1\dots k} = \frac{1}{\text{DT-residual}_{1\dots k} \times \text{DT-beta}_{1\dots k}}$$

where k is the number of PLS terms, $\text{DT-residual}_{1\dots k}$ the standard deviation of spectral data residuals and $\text{DT-beta}_{1\dots k}$ the standard deviation of regression coefficients of spectral data.

PLS models with large regression coefficients are given low weight to avoid overfitting, whilst PLS models providing a poor

fit to the unknown sample spectrum are given low weight to avoid underfitting [17].

An additional option to this second method is to exclude from the calculation of the final predictions the values obtained with the first PLS factors; it is generally recommended that the first 3–5 terms be discarded, since – according to Shenk et al. [59] – these tend to play little part in the generation of predictions.

Finally, to check the accuracy of predictions, the Mahalanobis-distance statistics H_{global} and $H_{\text{neighbour}}$, are calculated using the principal components of the selected calibration samples. H_{global} expresses the distance to the centre of the population of an unknown sample, whilst $H_{\text{neighbour}}$ refers to the distance from that sample to the nearest or “neighbouring” sample [8,59].

Again, optimisation of all the factors involved in defining this type of local regression should be performed for each analytical parameter and product; there are no specific recommendations that can be generalised to all applications [6,74].

Compared with the other local regression techniques addressed here, the LOCAL algorithm developed by Shenk and Westerhaus has a greater speed of prediction (1–2 s per sample), that allows this procedure to be implemented in routine analysis in any laboratory [75].

These local regression approximations have been successfully used in numerous NIRS applications for the analysis and characterisation of a range of products. The most widely used are LWR and the LOCAL algorithm, probably due in part to their greater availability: LWR can be implemented in commercial chemometric packages such as Unscrambler (Camo A/S Oslo, Norway), whilst the LOCAL algorithm has been included in the WINISI software package (Infrasoft International, Port Matilda, PA, USA).

4. Applications of non-linear methods to NIRS data

As has been previously commented, in many applications of NIR spectroscopy, the relationship to be modelled is non-linear. Over the past 15 years, there have been an increasing amount of scientific papers which demonstrate the application of non-linear regression tools for modelling NIRS data in different science fields and products.

Tables 1–3 summarise most of the works done till now, grouping it by three large areas: “Agriculture”, “Foods” and “Chemistry, Pharmaceutical and Others”.

It can be stressed that the majority of the reviewed applications use non-linear methods for developing quantitative regression models, although a more limited number of papers refers to its use in qualitative applications. Moreover, it can be observed that in NIRS applications, ANN trained using the back-propagation algorithm is one of the most widely studied non-linear methods. Nevertheless, more recently, the applications of others methods are growing, as ANN trained with fast algorithms such as Levenberg–Marquardt, or local regression methods, and more specially the LOCAL algorithm of Shenk and Westerhaus [59].

Table 1
Applications of non-linear methods to NIRS data management in agriculture

Product	Parameter	Regression method	Reference
Wheat	Crude protein	ANN-MLP BP	[26]
Wheat and Barley	Moisture, protein	ANN	[77]
Wheat	Protein	ANN-MLP BP LOCAL algorithm	[78]
Wheat	Protein	LOCAL algorithm	[17]
Corn	Crude fibre	ANN-MLP BP LOCAL algorithm	[78]
Corn	Moisture, protein, Oil	ANN	[79]
Ground Corn Grain and Haylage	Dry matter, protein, ADF	LOCAL algorithm	[59]
Grain	Dry matter, protein, ADF	LOCAL algorithm	[74]
Tobacco	Nicotine level	ANN-MLP BP	[80,81]
Tobacco	Type and origin	ANN-MLP BP	[82]
Tobacco	Classification and Composition	ANN-MLP BP	[83]
Animal feeds	Crude protein, ADF	ANN-MLP BP ANN-MLP EDBD ANN-MLP DBD	[33]
Feeds	Dry matter, protein, fat	LOCAL algorithm	[74]
Compound feeds	Moisture, protein, fat, fiber	ANN	[84]
Compound feeds	Moisture, protein, fat	ANN	[85]
Compound feeds	Ingredient percentage	ANN-MLP BP ANN-MLP LM ANN-RBF	[86]
Compound feeds	Ingredient percentage	LOCAL algorithm	[87]
Forages	Protein, in vitro dry matter digestibility, NDF, ADF, crude fiber	LWR	[70]
Forages	Protein, cellulose, organic matter digestibility	LR	[61]
Forages	Dry matter, protein, ADF	LOCAL algorithm	[74]
Forages	Dry matter, protein, NDF	ANN LOCAL algorithm	[88]
Silage	Protein	ANN-MLP BP LOCAL algorithm	[78]
Undried grass silage	Dry matter, ammonia N	LBR	[63]
Molasses	Purity	ANN	[85]
Soils	Organic matter	ANN-MLP LM	[90]

Table 1 (Continued)

Product	Parameter	Regression method	Reference
Soils	Organic matter	ANN-MLP BP ANN-RBF	[91]
Iberian pig fat	Classification of Iberian pig carcasses according with feeding system	ANN- MLP EDBD ANN-DRS ANN-LVQ ANN-CL	[89]

ANN: artificial neural network; MLP: multilayer perceptron; BP: back-propagation; LM: Levenberg–Marquardt; EDBD: extended delta-bar-delta; DBD: delta-bar-delta; RBF: radial basis function; DRS: direct random search; LVQ: learning vector quantisation; CL: competitive linear network; LR: local regression; LWR: local weighted regression; LBR: locally-biased regression.

Table 2
Applications of non-linear methods to NIRS data management in foods

Product	Parameter	Regression Method	Reference
Meat products	Protein	ANN-MLP BP	[92]
Pork meat	Protein, fat, moisture	ANN-MLP BP	[28]
Cooked meat	Heat treatment	LWR	[93]
Meat	Max. cooking temperature	ANN-MLP BP	[38]
Meat	Moisture, protein, fat	LWR	[94]
Meat		LWR	[68]
Meat	Moisture	ANN-MLP BP	[29]
Meat	Water, fat, temperature	LWR1 LWR2	[95]
Meat	Fat	ANN-MLP BP LOCAL algorithm	[78]
Meat	Dry matter, protein, fat	LOCAL algorithm	[74]
Meat	Moisture, protein, fat, collagen	ANN	[79]
Meat	Fat	LOCAL ANN	[96]
Apple	Brix	ANN-MLP BP LOCAL algorithm	[78]
Apple	Sucrose, pH, acidity, firmness	ANN	[79]
Kiwifruit	Classification	ANN-MLP BP	[97]
Olive oils	Authentication	ANN-MLP BP	[98]
Beer	Real extract, original extract, ethanol	ANN-MLP BP	[99]
Yogurt	Classification	ANN-MLP BP	[100]
Tea	Identification categories	ANN-MLP BP	[101]
Tea	Varieties discrimination	ANN-MLP BP	[102]
Red grape	Anthocyanin, total soluble solids, pH	LOCAL algorithm	[103]

ANN: artificial neural network; MLP: multilayer perceptron; BP: back-propagation; LWR: local weighted regression.

Table 3
Applications of non-linear methods to NIRS data management in chemistry, pharmaceutical and others

Product	Parameter	Regression method	Reference
Amino acids	Identification	ANN-MLP BP	[104]
Chemical mixtures	Moisture	ANN-MLP BP ANN-RBF	[105]
Pure compounds	Classification	ANN-KNN	[106]
Post-consumer packages	Identification of package material	ANN-MLP ANN-FAM	[107]
Plastic	Classification according resin type	ANN-MLP BP	[40]
Carbon tetrachloride solutions	Methanol, ethanol	ANN-MLP BP	[108]
Fermentation process	Ethanol, glucose	ANN-MLP BP	[109]
Distillation process	Water content	ANN LWR	[110]
Pharmaceutical production	Main reactant, impurity	LWR	[16]
Tablets and powder	Paracetamol, amantadine hydrochloride	ANN-MLP BP	[111]
Powder	Paracetamol, diphenhydramine hydrochloride	ANN-MLP BP	[112]
Tablets	Aspirin, phenacetin	ANN-RBF	[113]
Tablets	Aminopyrine, phenacetin	ANN-MLP BP	[114]
Powder	Metronidazole	ANN-MLP BP	[115]
Chinese medicines	Genuineness	ANN-MLP BP	[116]
Acrylic fibres	Moisture	ANN-MLP BP	[117]
Acrylic fibres	Finishing oil content	ANN-MLP BP	[118]
Polymer	Stiffness	ANN-MLP BP	[29]
Polyester resins	Hydroxyl, acid number	ANN-MLP BP	[119]
Biological matrices	Glucose	ANN-MLP LM	[120]
Latex and ethanol plastic spheres mixed in water	Ethanol content	ANN-MLP BP	[28]
Fluid bed granulation	Moisture	ANN-MLP BP	[121]
Sediments	Chemical composition	ANN-MLP BP	[31]

ANN: artificial neural network; MLP: multilayer perceptron; BP: back-propagation; LM: Levenberg–Marquardt; LWR: local weighted regression; RBF: radial basis function; FAM: fuzzy-art map; KNN: kohonen neural networks.

References

- [1] J.S. Shenk, M.O. Westerhaus, *Analysis of Agriculture and Food Products by Near Infrared Reflectance Spectroscopy*, NIRSystems, Monograph, 1995.
- [2] J.S. Shenk, M.O. Westerhaus, in: A.M.C. Davies, P. Williams (Eds.), *Near Infrared Spectroscopy: The Future Waves*, NIR Publications, Chichester, West Sussex, UK, 1996, pp. 198–202.
- [3] T. Naes, T. Isaksson, T. Fearn, A. Davies, *A User-friendly Guide to Multivariate Calibration and Classification*, NIR Publications, Chichester, UK, 2002.
- [4] T. Naes, in: K.I. Hildrum, T. Isaksson, T. Naes, A. Tandberg (Eds.), *Near Infrared Spectroscopy. Bridging the Gap Between Data Analysis and NIR Applications*, Ellis Horwood Limited, Chichester, West Sussex, UK, 1992, pp. 51–60.
- [5] J.S. Shenk, M.O. Westerhaus, *Crop Sci.* 31 (1991) 469.
- [6] J.S. Shenk, J.J. Workman, M.O. Westerhaus, in: D.A. Burns, E.W. Ciurczak (Eds.), *Handbook of Near Infrared Analysis, Practical Spectroscopy Series*, vol. 27, second ed., Marcel Dekker, USA, 2001, p. 419.
- [7] P.C. Williams, in: P.K. Williams, K. Norris (Eds.), *Near-Infrared Technology in the Agricultural and Food Industries*, second ed., American Association of Cereal Chemists, Inc., St. Paul, Minnesota, USA, 2001, pp. 145–169.
- [8] J.S. Shenk, M.O. Westerhaus, *Crop Sci.* 31 (1991) 1548.
- [9] S.M. Abrams, J.S. Shenk, M.O. Westerhaus, F.E. Barton II, *J. Dairy Sci.* 70 (1987) 806.
- [10] W.R. Hruschka, in: P. Williams, K. Norris (Eds.), *Near-infrared Technology in the Agricultural and Food Industries*, second ed., American Association of Cereal Chemists, Inc., St. Paul, Minnesota, USA, 2001, pp. 39–58.
- [11] H. Martens, T. Naes, *Multivariate Calibration*, John Wiley & Sons, Chichester, 1989.
- [12] J.J. Workman, in: D.A. Burns, E.W. Ciurczak (Eds.), *Handbook of Near Infrared Analysis, Practical Spectroscopy Series*, vol. 13, Marcel Dekker, Inc., New York, USA, 1992, pp. 247–280.
- [13] H. Mark, J. Workman, *Statistics in Spectroscopy*, Academic Press, Inc., USA, 1991.
- [14] M.O. Westerhaus, J. Workman, J.B. Reeves III, H. Mark, in: C.A. Roberts, J. Workman, J.B. Reeves III (Eds.), *Near-infrared Spectroscopy in Agriculture, ASA, CSSA y SSSA, Inc., Madison, Wisconsin, USA, 2004*, pp. 133–174.
- [15] E. Bertran, M. Blanco, S. MasPOCH, M.C. Ortiz, M.S. Sánchez, L.A. Sarabia, *Chemometr. Intell. Lab. Syst.* 49 (1999) 215.
- [16] L. Stordrange, O.M. Kvalheim, P.A. Hazle, D. Malthe-Sørensen, F.O. Libnau, *J. Near Infrared Spectrosc.* 11 (2003) 55.
- [17] F.E. Barton II, J.S. Shenk, M.O. Westerhaus, D.B. Funk, *J. Near Infrared Spectrosc.* 8 (2000) 201.
- [18] B. Martín, A. Sanz, *Redes Neuronales y Sistemas Borrosos*, second ed., RA-MA, Madrid, España, 2001.
- [19] F. Despagne, L. Massart, *Analyst* 123 (1998) 157.
- [20] B.G.M. Vandeginste, D.L. Massart, L.M.C. Buydens, S. De Jong, P.J. Lewi, J. Smeyers-Verbeke, *Handbook of Chemometrics and Qualimetrics: Part B*, Elsevier Science B.V., Amsterdam, The Netherlands, 1998, pp. 649–699.
- [21] D.A. Cirovic, *Trends Anal. Chem.* 16 (1997) 148.
- [22] D.E. Rumelhart, J.L. McClelland, *Parallel Distributed Processing*, Vol. 1, Foundations, The MIT Press, Cambridge, USA, 1986.
- [23] J.L. McClelland, D.E. Rumelhart, *Parallel Distributed Processing*, vol. 2, Psychological and Biological Models, The MIT Press, Cambridge, USA, 1986.

- [24] J. Zupan, J. Gasteiger, *Neural Networks for Chemist. An Introduction*, VCH, Germany, 1993.
- [25] J. Zupan, J. Gasteiger, *Neural Networks for Chemist. An Introduction*, second ed., VCH, Germany, 1999.
- [26] J.R. Long, V.G. Gregoriou, P.J. Gemperline, *Anal. Chem.* 62 (1990) 1791.
- [27] P.J. Gemperline, J.R. Long, V.G. Gregoriou, *Anal. Chem.* 63 (1991) 2313.
- [28] C. Borggaard, H.H. Thodberg, *Anal. Chem.* 64 (1992) 545.
- [29] T. Naes, K. Kvaal, T. Isaksson, C. Miller, *J. Near Infrared Spectrosc.* 1 (1993) 1.
- [30] P.J. Gemperline, *Chemometr. Intell. Lab. Syst.* 39 (1997) 29.
- [31] T. Udelhoven, B. Schütt, *Chemometr. Intell. Lab. Syst.* 51 (2000) 9.
- [32] C. Borggaard, in: P. Williams, K. Norris (Eds.), *Near-Infrared Technology in the Agricultural and Food Industries*, AACCC, Inc., St. Paul, Minnesota, USA, 2001, pp. 101–107.
- [33] M.O. Westerhaus, J.B. Reeves III, in: K.I. Hildrum, T. Isaksson, T. Naes, A. Tandberg (Eds.), *Near Infrared Spectroscopy. Bridging the Gap Between Data Analysis and NIR Applications*, Ellis Horwood Limited, Chichester, West Sussex, UK, 1992, pp. 79–84.
- [34] R. Yu, J. Jiang, *Chemometr. Intell. Lab. Syst.* 45 (1999) 191.
- [35] S. Haykin, *Neural Networks. A Comprehensive Foundation*, second ed., Prentice-Hall, USA, 1999.
- [36] D. Svozil, V. Kvasnicka, J. Pospíchal, *Chemometr. Intell. Lab. Syst.* 39 (1997) 43.
- [37] P. Geladi, *J. Near Infrared Spectrosc.* 4 (1996) 243.
- [38] K. Kvaal, T. Naes, T. Isaksson, M.R. Ellekjaes, in: K.I. Hildrum, T. Isaksson, T. Naes, A. Tandberg (Eds.), *Near Infrared Spectroscopy. Bridging the Gap Between Data Analysis and NIR Applications*, Ellis Horwood Limited, Chichester, West Sussex, UK, 1992, pp. 97–102.
- [39] E.P.P.A. Derks, L.M.C. Buydens, *Chemometr. Intell. Lab. Syst.* 41 (1998) 171.
- [40] M.K. Alam, S. Stanton, G.A. Hebner, in: D.A. Burns, E.W. Ciurczak (Eds.), *Handbook of Near-Infrared Analysis*, second ed., Marcel Dekker, Inc., New York, USA, 2001, p. 703.
- [41] M.C. Hemmer, in: J.M. Chalmers, P.R. Griffiths (Eds.), *Handbook of Vibrational Spectroscopy*, vol. 3, John Wiley & Sons Ltd., Australia, 2001, pp. 1962–1982.
- [42] I.V. Tetko, D.J. Livingstone, A.I. Luik, *J. Chem. Inf. Comput. Sci.* 35 (1995) 826.
- [43] K. Funahashi, *Neural Networks* 2 (1989) 183.
- [44] K. Hornik, M. Stinchcombe, H. White, *Neural Networks* 2 (1989) 359.
- [45] P.J. Werbos, *Beyond regression: new tools for prediction and analysis in the behavioural sciences*, Ph.D. Thesis, Harvard University, Boston, MA, 1974.
- [46] D.E. Rumelhart, G.E. Hinton, R.J. Williams, *Nature* 323 (1986) 533.
- [47] B. Widrow, M.E. Hoff, *Adaptive switching circuits*, IRE WESCON, Convention Record, New York, 1960, pp. 96–104.
- [48] C.M. Bishop, *Rev. Sci. Instrum.* 65 (1994) 1803.
- [49] Statsoft 1984–2003, *Neural Networks, Manual*, Copyright StatSoft, Inc. <http://www.statsoftinc.com/textbook/stneunet.html#multilayera> (31th March 2006).
- [50] M.T. Hagan, M.B. Menhaj, *IEEE Trans. Neural Networks* 5 (1994) 989.
- [51] K. Levenberg, *Q. J. Appl. Math.* II-2 (1944) 164.
- [52] D.W. Marquardt, *J. Soc. Industrial Appl. Math.* 11 (1963) 431.
- [53] C.M. Bishop, *Neural Networks for Pattern Recognition*, OXFORD University Press Inc., New York, USA, 1995.
- [54] N. Ampazis, S.J. Perantonis, *IEEE Trans. Neural Networks* 13 (2002) 1064.
- [55] G. Zhou, J. Si, *IEEE Trans. Neural Networks* 9 (1998) 448.
- [56] G. Lera, M. Pinzotas, *IEEE Trans. Neural Networks* 13 (2002) 1200.
- [57] D.S. Broomhead, D. Lowe, *Complex Syst.* 2 (1988) 321.
- [58] J. Moody, C.J. Darken, *Neural Computation* 1 (1989) 281.
- [59] J.S. Shenk, M.O. Westerhaus, P. Berzaghi, *J. Near Infrared Spectrosc.* 5 (1997) 223.
- [60] T. Naes, T. Isaksson, in: R. Biston, N. Bartiaux-Thill (Eds.), *Third International Conference on Near Infrared Spectroscopy*, Proceedings, vol. 1, Agricultural Research Centre Publishing, Gembloux, Belgium, 1990.
- [61] G. Sinnaeve, P. Dardenne, R. Agneessens, *J. Near Infrared Spectrosc.* 2 (1994) 163.
- [62] R.S. Anderssen, B.G. Osborne, I.J. Wesley, *J. Near Infrared Spectrosc.* 11 (2003) 39.
- [63] T. Fearn, A.M.C. Davies, *J. Near Infrared Spectrosc.* 11 (2003) 467.
- [64] A.M.C. Davies, H.V. Britcher, J.G. Franklin, S.M. Ring, A. Grant, W.F. McClure, *Mikrochim. Acta (Wien) I* (1988) 61.
- [65] A.M.C. Davies, *Spectrosc. Europe* 11-4 (1999) 22.
- [66] A.M.C. Davies, in: A.M.C. Davies, R.K. Cho (Eds.), *Near Infrared Spectroscopy: Proceedings of the 10th International Conference*, NIR Publications, Chichester, West Sussex, UK, 2002, pp. 29–32.
- [67] W.S. Cleveland, S.J. Devlin, *J. Am. Stat. Assoc.* 83 (1988) 596.
- [68] T. Naes, T. Isaksson, *Appl. Spectrosc.* 46 (1992) 34.
- [69] T. Naes, T. Isaksson, B.R. Kowalski, *Anal. Chem.* 62 (1990) 664.
- [70] A.H. Aastveit, P. Marum, *Appl. Spectrosc.* 47 (1993) 463.
- [71] Z. Wang, T. Isaksson, B.R. Kowalski, *Anal. Chem.* 66 (1994) 249.
- [72] J.S. Shenk, M.O. Westerhaus, U.S. Patent 5798526 (1998).
- [73] J.S. Shenk, M.O. Westerhaus, S.M. Abrams, in: G.C. Marten, F.E. Barton (Eds.), *Near Infrared Spectroscopy (NIRS): Analysis of Forage Quality*, USDA, ARS, Agriculture Handbook no. 643, 1989, pp. 104–110.
- [74] P. Berzaghi, J.S. Shenk, M.O. Westerhaus, *J. Near Infrared Spectrosc.* 8 (2000) 1.
- [75] J.S. Shenk, P. Berzaghi, M.O. Westerhaus, in: A.M.C. Davies, R. Giangiacomo (Eds.), *Near Infrared Spectroscopy. Proceedings of the 9th International Conference on Near Infrared Spectroscopy*, NIR Publications, Chichester, West Sussex, UK, 1999, pp. 211–214.
- [76] ISI, *The complete software solution using a single screen for routine analysis, robust calibrations, and networking*, Manual, FOSS NIRSystems/TECATOR, Infrasoft International, LLC, Sylver Spring MD, USA, 2000.
- [77] N.B. Büchmann, in: A.M.C. Davies, P. Williams (Eds.), *Near Infrared Spectroscopy: The future Waves*, NIR Publications, Chichester, West Sussex, UK, 1996, pp. 479–483.
- [78] P. Dardenne, G. Sinnaeve, V. Baeten, *J. Near Infrared Spectrosc.* 8 (2000) 229.
- [79] R.P. Cogdill, P. Dardenne, *J. Near Infrared Spectrosc.* 12 (2004) 93.
- [80] W.F. McClure, M. Hana, J. Sugiyama, in: I. Murray, I.A. Cowe (Eds.), *Near Infrared Spectroscopy. Making Light Work: Advances in Near Infrared Spectroscopy*, Ian Michael Publications, Chichester, West Sussex, UK, 1992, pp. 200–209.
- [81] M. Hana, W.F. McClure, T.B. Whitaker, *J. Near Infrared Spectrosc.* 3 (1995) 133.
- [82] M. Hana, W.F. McClure, *J. Near Infrared Spectrosc.* 5 (1997) 19.
- [83] S. Lo, in: A.M.C. Davies, P. Williams (Eds.), *Near Infrared Spectroscopy: The Future Waves*, NIR Publications, Chichester, UK, 1996, pp. 441–447.
- [84] N.B. Büchmann, in: G.D. Batten, P. Flinn, L.A. Welsh, A.B. Blakeney (Eds.), *Leaping Ahead with Near Infrared Spectroscopy*, NIR Spectroscopy Group, Royal Australian Chemical Institute, Victoria, Australia, 1995, pp. 248–251.
- [85] N.B. Büchmann, I.A. Cowe, in: A.M.C. Davies, R.K. Cho (Eds.), *Near Infrared Spectroscopy: Proceedings of the 10th International Conference*, NIR Publications, Chichester, West Sussex, UK, 2002, pp. 71–75.
- [86] D. Pérez-Marín, A. Garrido-Varo, J.E. Guerrero, J.C. Gutiérrez-Estrada, *Appl. Spectrosc.* 60 (2006) 1062.
- [87] D. Pérez-Marín, A. Garrido-Varo, J.E. Guerrero, *Appl. Spectrosc.* 59 (2005) 69.
- [88] P. Berzaghi, P.C. Flinn, P. Dardenne, M. Lagerholm, J.S. Shenk, M.O. Westerhaus, I.A. Cowe, in: A.M.C. Davies, R.K. Cho (Eds.), *Near Infrared Spectroscopy: Proceedings of the 10th International Conference*, NIR Publications, Chichester, West Sussex, UK, 2002, pp. 107–112.
- [89] C. Hervás, A. Garrido, B. Lucena, N. García, E. De Pedro, *J. Near Infrared Spectrosc.* 2 (1994) 177.
- [90] H.R. Ingleby, T.G. Crowe, *Canadian Biosyst. Eng.* 43 (2001) 7.1.
- [91] P.H. Fidêncio, R.J. Poppi, J.C. Andrade, *Anal. Chim. Acta* 453 (2002) 125.
- [92] C. Borggaard, A.J. Rasmussen, in: K.I. Hildrum, T. Isaksson, T. Naes, A. Tandberg (Eds.), *Near Infrared Spectroscopy. Bridging the Gap Between Data Analysis and NIR Applications*, Ellis Horwood Limited, Chichester, West Sussex, UK, 1992, pp. 73–78.

- [93] M.R. Ellekjaer, K.I. Hildrum, in: I. Murray, I.A. Cowe (Eds.), *Making Light Work: Advances in Near Infrared Spectroscopy*, VCH, New York, USA, 1992, pp. 408–414.
- [94] T. Isaksson, T. Naes, in: I. Murray, I.A. Cowe (Eds.), *Making Light Work: Advances in Near Infrared Spectroscopy*, VCH, New York, USA, 1992, pp. 140–146.
- [95] Z. Wang, T. Isaksson, B.R. Kowalski, *Anal. Chem.* 66 (1994) 249.
- [96] P. Dardenne, J.A. Fernández, *Chemometr. Intell. Lab. Syst.* 80 (2006) 236.
- [97] J. Kim, A. Mowat, P. Poole, N. Kasabov, *Chemometr. Intell. Lab. Syst.* 51 (2000) 201.
- [98] E. Bertran, M. Blanco, J. Coello, H. Iturriaga, S. MasPOCH, I. Montoliu, *J. Near Infrared Spectrosc.* 8 (2000) 45.
- [99] F.A. Iñón, S. Garrigues, M. De la Guardia, *Anal. Chim. Acta* 571 (2006) 167.
- [100] Y. He, S. Feng, X. Deng, X. Li, *Food Res. Int.* 39 (2006) 645.
- [101] J. Zhao, Q. Chen, X. Huang, C.H. Fang, *J. Pharm. Biomed. Anal.* 41 (2006) 1198.
- [102] Y. He, X. Li, X. Deng, *J. Food Eng.* (2006).
- [103] R.G. Damberg, D. Cozzolino, W.U. Cynkar, L. Janik, M. Gishen, *J. Near Infrared Spectrosc.* 14 (2006) 71.
- [104] T. Sato, *J. Near Infrared Spectrosc.* 1 (1993) 199.
- [105] M. Carlin, T. Kavli, B. Lillekjendlie, *Chemometr. Intell. Lab. Syst.* 23 (1994) 163.
- [106] P. Cáceres-Alonso, A. García-Tejedor, J. Near Infrared Spectrosc. 3 (1995) 97.
- [107] R. Feldhoff, T. Huth-Fehre, T. Kantimm, L. Quick, K. Cammann, *J. Near Infrared Spectrosc.* 3 (1995) 3.
- [108] Y. Li, C.W. Brown, *J. Near Infrared Spectrosc.* 7 (1999) 55.
- [109] Y. Li, C.W. Brown, *J. Near Infrared Spectrosc.* 7 (1999) 101.
- [110] F. Despagne, L. Massart, P. Chabot, *Anal. Chem.* 72 (2000) 1657.
- [111] Y. Dou, Y. Sun, Y. Ren, P. Ju, Y. Ren, *J. Pharm. Biomed. Anal.* 37 (2005) 543.
- [112] Y. Dou, Y. Sun, Y. Ren, *Anal. Chim. Acta* 528 (2005) 55.
- [113] Y. Dou, H. Mi, L. Zhao, Y. Ren, *Spectrochim. Acta Part A* 65 (2006) 79.
- [114] Y. Dou, H. Mi, L. Zhao, Y. Ren, *Anal. Biochem.* 351 (2006) 174.
- [115] L. Zhao, Y. Dou, H. Mi, M. Ren, *Spectrochim. Acta Part A* (2006).
- [116] Y. Ke, C. Yiyu, *Chin. J. Anal. Chem.* 34 (2006) 561.
- [117] M. Blanco, J. Coello, H. Iturriaga, S. MasPOCH, J. Pagès, *Chemometr. Intell. Lab. Syst.* 50 (2000) 75.
- [118] M. Blanco, J. Pagès, *Anal. Chim. Acta* 463 (2002) 295.
- [119] E. Marengo, M. Bobba, E. Robotti, M. Lenti, *Anal. Chim. Acta* 511 (2004) 313.
- [120] Q. Ding, G.W. Small, M.A. Arnold, *Anal. Chim. Acta* 384 (1999) 333.
- [121] J. Rantanen, E. Räsänen, O. Antikainen, J. Mannermaa, J. Yliruusi, *Chemometr. Intell. Lab. Syst.* 56 (2001) 51.

Short communication

Solute-induced dissolution of hydrophobic ionic liquids in water[☆]

Paul G. Rickert^a, Dominique C. Stepinski^a, David J. Rausch^a, Ruth M. Bergeron^b,
Sandrine Jakab^{a,c}, Mark L. Dietz^{a,*}

^a Chemistry Division, Argonne National Laboratory, Argonne, IL 60439, United States

^b North America-Analytical Sciences, BP, Naperville, IL 60563, United States

^c Ecole Nationale Supérieure de Chimie de Paris, Paris, France

Received 11 August 2006; received in revised form 16 October 2006; accepted 19 October 2006

Available online 20 November 2006

Abstract

Significant solubilization of ostensibly water-immiscible ionic liquids (ILs) in acidic aqueous phases is induced by the presence of any of a variety of neutral extractants, the apparent result of the formation of the protonated form of the extractant and its subsequent exchange for the cationic component of the IL. The extent of this solubilization is shown to diminish with increasing hydrophobicity of the IL cation and decreasing extractant basicity. These observations raise concerns as to the viability of ILs as “drop in replacements” for traditional organic solvents in the solvent extraction of metal ions.

© 2006 Elsevier B.V. All rights reserved.

Keywords: Ionic liquids; Crown ether; Neutral organophosphorus extractant; Solubility

1. Introduction

In recent years, there has been increasing interest in the development of environmentally benign separation processes, both as an end in itself and in conjunction with the design of “green” methods for manufacturing, synthesis, and analysis. An important aspect of efforts to devise greener separations is the identification, evaluation, and application of novel solvent systems that exhibit few or none of the drawbacks associated with their conventional organic counterparts [1]. Of particular recent interest among alternative solvents have been ionic liquids (ILs), low-melting (≤ 100 – 150 °C) ionic salts generally consisting of a bulky, asymmetric organic cation together with any of a wide variety of anions. These compounds exhibit a number of characteristics that make them attractive as the potential basis

for improved analytical- and process-scale separation methods, among them a near-absence of vapor pressure (and thus, negligible fugative emissions), the ability to solubilize a variety of compounds, high thermal stability, a wide liquid range, and an extraordinary degree of tunability [2].

Among separation methods, few could more clearly benefit from increased attention to environmental “friendliness” than liquid–liquid (l–l) extraction. Despite numerous advantages over competing techniques (*e.g.*, flexibility, simplicity, the possibility of continuous operation), as traditionally practiced, l–l extraction suffers from a significant drawback: the need for water-immiscible organic solvents that are often toxic, flammable, or volatile [3]. As a result, considerable attention has been devoted to the assessment of the utility of ILs as replacements for these conventional molecular solvents, and IL-based systems for the extraction of simple organic compounds [4–7], biomolecules (*e.g.*, amino acids) [8,9], and metal ions [10–40] have been proposed. Among the many issues that will ultimately govern the viability of ILs as replacements for traditional organic solvents in these applications is their aqueous solubility. Although certain results indicate that the water solubility of the hydrophobic ionic liquids most often employed as extraction solvents (*i.e.*, hexafluorophosphate (PF_6^-) and bis[(trifluoromethyl)sulfonyl]imide (TF_2N^-) salts of *N,N'*-dialkylimidazolium cations) is not appreciable [13,26], other studies employing more “process relevant”

[☆] The submitted manuscript has been created by the University of Chicago as Operator of Argonne National Laboratory (“Argonne”) under Contract No. W-31-109-ENG-38 with the U.S. Department of Energy. The U.S. Government retains for itself, and others acting on its behalf, a paid-up, non-exclusive, irrevocable worldwide license in said article to reproduce, prepare derivative works, distribute copies to the public, and perform publicly and display publicly, by or on behalf of the Government.

* Corresponding author. Tel.: +1 630 252 3647; fax: +1 630 252 7501.
E-mail address: mdietz@anl.gov (M.L. Dietz).

(i.e., real world) aqueous phases (e.g., mineral acid solutions, in the case of metal ion extraction) suggest that under certain conditions, their solubility may be significant [13,31]. Repeated contact of certain ostensibly water-immiscible ILs with aqueous phases containing high nitric acid concentrations, for example, has been reported to lead to degradation of the biphasic system [31]. In this report, we demonstrate that in contrast to the behavior of conventional organic solvents, the presence in a hydrophobic IL of certain solutes (in particular, neutral extractants/ligands) can significantly increase the solubility of the ionic liquid in acidic aqueous media. This observation has negative implications for the utility of ionic liquids as environmentally benign replacements for traditional organic solvents in certain separations applications.

2. Experimental

2.1. Materials

The 1-alkyl-3-methylimidazolium ionic liquids were prepared and purified according to published methods [41]. The dicyclohexano-18-crown-6 (DCH18C6; Aldrich, Milwaukee, WI) was a mixture of the *cis-syn-cis* (A) and *cis-anti-cis* (B) isomers, consistent with prior work [11,13,31,38–40]. Tri-*n*-butyl phosphate (TBP; Aldrich) was distilled ($T = 143\text{ }^{\circ}\text{C}$) at reduced (20 mm) pressure prior to use, while bis-2-ethylhexylphosphoric acid (HDEHP) was purified by copper salt precipitation. Dibutyl butylphosphonate (DBBP; Aldrich), butyl dibutylphosphinate (BDBP; Organometallics Inc., Hampstead, NH), and tributylphosphine oxide (TBPO; Aldrich) were used as received. Aqueous acid solutions were prepared from Milli-Q2 water and Ultrex II nitric acid (J. T. Baker Chemical Co.). All other reagents were analytical grade and were used without further purification.

2.2. Methods

2.2.1. 1-Octanol solubilization

The solubility of 1-octanol in water and in various nitric acid solutions was determined by gas chromatography. Briefly, a measured volume of 1-octanol (or a solution of DCH18C6 therein) was combined with an equal volume of the aqueous phase of interest in a constant temperature bath ($T = 25\text{ }^{\circ}\text{C}$) and gently stirred for at least 24 h. Following centrifugation, a measured portion of the aqueous phase (0.50 mL) was contacted three times with $6\times$ its volume (3.00 mL) of methylene chloride, and the combined extracts diluted to a known volume with eicosane-spiked (100 ppm) CH_2Cl_2 . Triplicate injections of each sample (typically 2–3 μL) were then made into an HP-5890 gas chromatograph (initial temperature, $120\text{ }^{\circ}\text{C}$; initial time, 3.00 min; ramp, $40\text{ }^{\circ}\text{C}/\text{min}$; final temperature, $260\text{ }^{\circ}\text{C}$; final time, 3.00 min; detector temperature, $300\text{ }^{\circ}\text{C}$; injector temperature, $300\text{ }^{\circ}\text{C}$) equipped with a flame ionization detector, along with injections of a series of standards comprising known masses of 1-octanol in eicosane-spiked (100 ppm) CH_2Cl_2 . The octanol content of each sample was determined by comparison of the 1-octanol/eicosane peak area ratio to that of the standards. Multiple

determinations of the solubility of 1-octanol in water indicate that the reported values are reproducible to within $\pm 10\text{--}15\%$.

2.2.2. Ionic liquid solubilization

The solubility of the ionic liquids, 1-pentyl-3-methylimidazolium bis[(trifluoromethyl)sulfonyl]imide ($\text{C}_5\text{mim}^+\text{TF}_2\text{N}^-$) and its *n*-octyl- ($\text{C}_8\text{mim}^+\text{TF}_2\text{N}^-$) and *n*-decyl- ($\text{C}_{10}\text{mim}^+\text{TF}_2\text{N}^-$) analogs, in water and in various nitric acid solutions was determined by ^1H NMR. Briefly, a measured volume of the ionic liquid (or a solution of an extractant therein) was contacted with an equal volume of the aqueous phase of interest in a constant temperature bath ($25\text{ }^{\circ}\text{C}$) and gently stirred for at least 24 h. Following centrifugation, a known aliquot of the aqueous phase was taken to dryness on a rotary evaporator and the residue taken up in deuterated toluene for NMR analysis. The C_nmim^+ content of each sample was determined by comparison of the area of the C_n -side chain methylene ($(\text{CH}_2)_2$) or methyl (CH_3) proton peak to that of a series of standards prepared by dissolution of the same IL in *d*-toluene.

3. Results and discussion

3.1. Crown ether in 1-octanol

Prior work in this laboratory has shown that important insights into the behavior of IL-based solvent systems can often be obtained by direct comparison to analogous systems employing conventional organic solvents such as 1-octanol [31]. For this reason, our initial studies sought to determine the influence of changing aqueous acidity and organic phase solute (i.e., extractant) concentration on the extent of dissolution of 1-octanol in water. Fig. 1 depicts the effect of increasing concentrations of dicyclohexano-18-crown-6 (DCH18C6) (chosen for this investigation because it is among the most widely studied metal ion extractants in ionic liquid systems [11,13,14,31,32,36,38–40]) on this dissolution. As can be seen, the presence of increasing amounts of DCH18C6 is accompanied by a slight decrease in the solubility of the alcohol in water. Such a decrease is not unexpected, as for mixtures of sparingly soluble solutes in contact with water, the equilibrium aqueous solubility of each constituent is expected to be proportional to its respective mole fraction in the mixture [42]. It is worth noting that the water solubility of 1-octanol observed here in the absence of any crown ether, $4.82 \times 10^{-3}\text{ M}$, is in excellent agreement with the previously reported value of $4.5 \times 10^{-3}\text{ M}$ [43].

Fig. 2 depicts the effect of increasing aqueous acidity (i.e., HNO_3) on the solubility of 1-octanol in water. As shown, increasing acidity is accompanied by a slight increase in solubilization of the alcohol up to ca. 1 M HNO_3 , above which further increases have no measurable effect. As is well known, the solubility of an organic solute (e.g., benzene) in aqueous solution can be altered by addition of inorganic salts (e.g., NaCl) [44]. Frequently, a decrease in the solubility of the organic solute is observed, which has been attributed to the binding of a portion of the water by the ions of the added salt and its consequent unavailability as a solvent [44]. In this system, however, an additional factor, interaction of 1-octanol and nitric acid, must be consid-

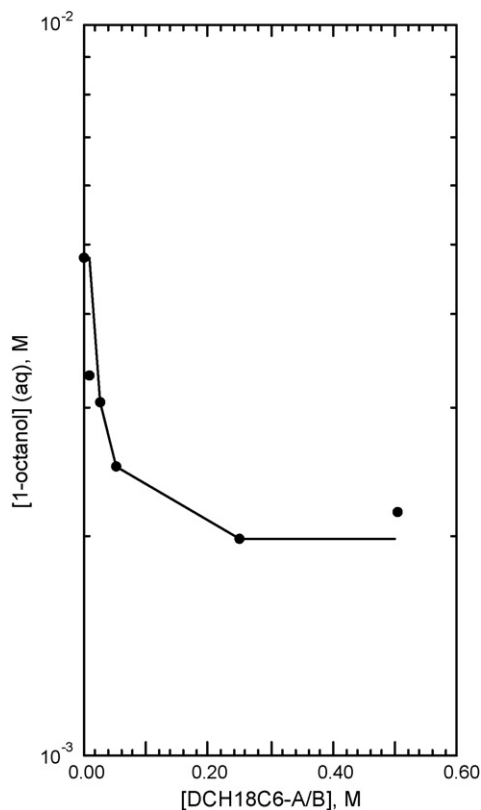


Fig. 1. The effect of dicyclohexano-18-crown-6 concentration on the solubility of 1-octanol in water ($T=25\text{ }^{\circ}\text{C}$).

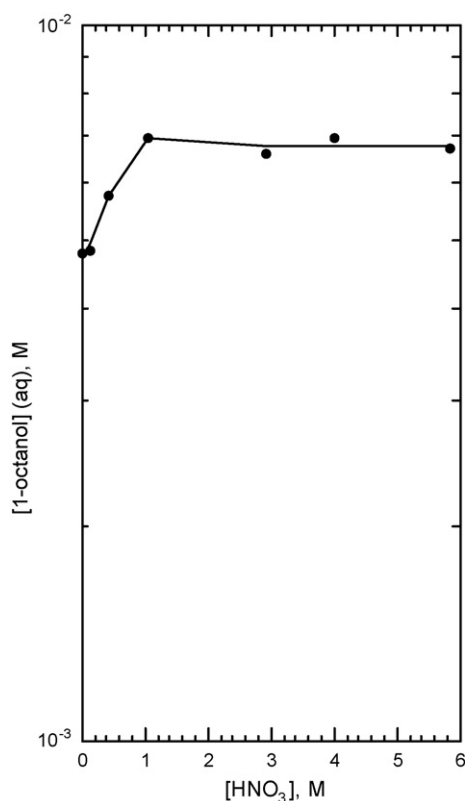


Fig. 2. The effect of aqueous nitric acid concentration on the solubility of 1-octanol in water ($T=25\text{ }^{\circ}\text{C}$).

Table 1

Effect of DCH18C6 concentration on the solubility of 1-octanol in aqueous (4 M) nitric acid

[DCH18C6] _{org} (M)	[1-octanol] _{aq} (M)
0	0.00694
0.010	0.00628
0.025	0.00561
0.050	0.00561
0.100	0.00656
0.250	0.00672
0.500	0.00594

ered. Previous work has demonstrated that 1-octanol can extract significant quantities of nitric acid (as much as 0.6 mol of acid for each mole of 1-octanol at sufficiently high acidities) [45]. Other work concerning the effect of mineral acids on the aqueous solubility of various aliphatic alcohols has shown that increasing acidity leads to protonation of the alcohol [46], which is accompanied by an increase in its water solubility [47]. Taken together, this suggests that the observed effect of aqueous acidity in this system (Fig. 2) represents a balance between the tendency of added nitric acid to decrease the solubility of the alcohol *via* “salting out” and to increase its solubility by protonation.

Table 1 summarizes the results of measurements of the solubility of 1-octanol in 4 M HNO_3 (*i.e.*, on the plateau region of Fig. 2) in the presence of increasing quantities of DCH18C6. In this system, three effects might reasonably be anticipated as the extractant concentration is raised: a decrease in 1-octanol solubility in the aqueous phase arising from its lower mole fraction in the organic phase [42]; a decrease in its solubility in the aqueous phase arising from preferential interaction of the crown ether with nitric acid and the accompanying decrease in 1-octanol protonation [47,48]; and lastly, a diminution of the salting out effect of HNO_3 (and thus, an increase in the solubility of 1-octanol in the aqueous phase) caused by extraction of HNO_3 by the crown ether [49]. The net effect of these three factors is apparently such that no appreciable difference between the aqueous solubility of 1-octanol in the presence of 0.01 M and 0.50 M crown ether is observed.

3.2. Crown ether in ionic liquids

In contrast, analogous experiments employing three ionic liquids, 1-pentyl-3-methylimidazolium bis[(trifluoromethyl) sulfonyl]imide ($\text{C}_5\text{mim}^+\text{Tf}_2\text{N}^-$) and its *n*-octyl- ($\text{C}_8\text{mim}^+\text{Tf}_2\text{N}^-$) and *n*-decyl- ($\text{C}_{10}\text{mim}^+\text{Tf}_2\text{N}^-$) analogs, containing increasing concentrations of the same extractant (DCH18C6), each contacted with an acidic (1 M HNO_3) aqueous phase, yield markedly different results. That is, in each case, an increase in the initial IL phase concentration of the crown ether is accompanied by a corresponding increase in the solubility of the ionic liquid (as reflected in the concentration of the IL cation) in the aqueous phase. In fact, as shown in Fig. 3, a log–log plot of IL solubility versus DCH18C6 concentration yields a line of near-unit slope (0.85, 1.10, and 1.00 for the $\text{C}_5\text{mim}^+\text{Tf}_2\text{N}^-$, $\text{C}_8\text{mim}^+\text{Tf}_2\text{N}^-$, and $\text{C}_{10}\text{mim}^+\text{Tf}_2\text{N}^-$, respectively) for each of the three systems. All of these solubilities, it must be noted, have

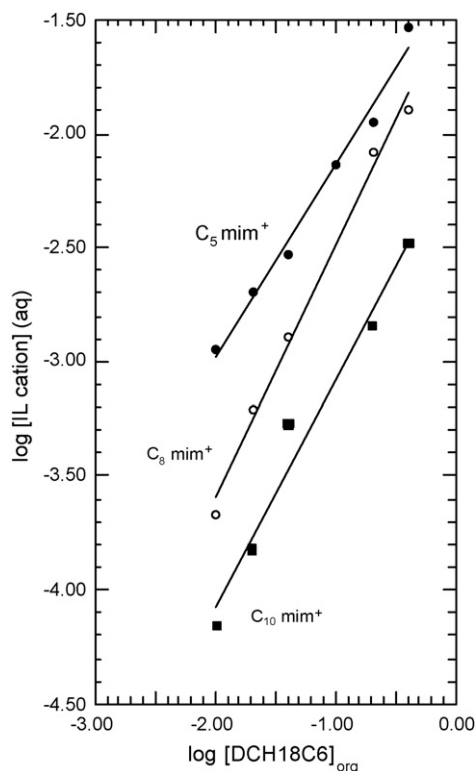
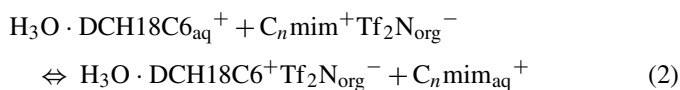
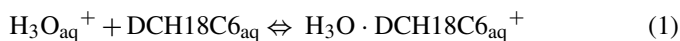


Fig. 3. The effect of dicyclohexano-18-crown-6 concentration on the solubility of $C_n\text{mim}^+\text{Tf}_2\text{N}^-$ ILs in 1 M HNO_3 ($T=25^\circ\text{C}$).

been corrected for that of the ILs in 1 M HNO_3 in the absence of any crown ether (Fig. 4) (1.9×10^{-2} M, 1.4×10^{-3} M, and 2.6×10^{-4} M for the $C_5\text{mim}^+\text{Tf}_2\text{N}^-$, C_8 -, and C_{10} -compounds, respectively) and thus, represent only the additional solubility induced by the presence of the extractant. Such results are consistent with a mechanism for IL solubilization in which nitric acid forms a cationic 1:1 hydronium ion:DCH18C6 adduct in the aqueous phase, which is subsequently exchanged for the cationic constituent of the ionic liquid, resulting in loss of the IL (*i.e.*, dissolution) to the aqueous phase:



This scheme is supported by examination of the infrared spectrum of the IL ($C_5\text{mim}^+\text{Tf}_2\text{N}^-$) phase before and after its equilibration with nitric acid (1 M), the latter of which exhibits absorbance bands characteristic of oxonium salts [50] (most importantly, a prominent band centered at *ca.* 2184 cm^{-1}).

It would be anticipated from Eq. (2) that as the hydrophobicity of the IL is increased (*i.e.*, as n rises), this exchange process would become progressively more difficult, and the solubilizing effect of the extractant diminished. As can be seen from Fig. 3, this is indeed the case. That is, the effect of a given concentration of DCH18C6 in the IL phase is smaller for $C_{10}\text{mim}^+\text{Tf}_2\text{N}^-$ than for $C_8\text{mim}^+\text{Tf}_2\text{N}^-$, which in turn, is smaller than for $C_5\text{mim}^+\text{Tf}_2\text{N}^-$. It would also be expected that for an aqueous phase containing no acid, the addition of the

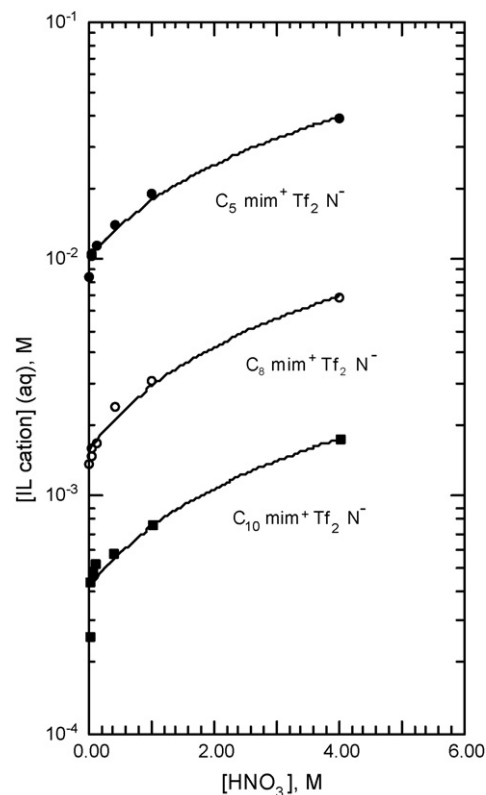


Fig. 4. The effect of aqueous nitric acid concentration on the solubility of $C_n\text{mim}^+\text{Tf}_2\text{N}^-$ ILs in water ($T=25^\circ\text{C}$).

crown ether would yield no systematic increase in the solubility of the ILs. This too is the case.

3.3. Organophosphorus extractants in ionic liquids

To determine if the increased solubility of ionic liquids in acidic aqueous solution that accompanies addition of DCH18C6 is a peculiarity of this extractant or represents a general phenomenon whereby the protonated form of a neutral extractant will exchange with the cationic constituent of an ionic liquid, thus increasing the aqueous solubility of the IL, the effect of the addition of four neutral organophosphorus reagents (tri-*n*-butylphosphate (TBP), dibutyl butylphosphonate (DBBP), butyl dibutylphosphinate (BDBP), and tributyl phosphine oxide (TBPO)) upon the solubility of $C_5\text{mim}^+\text{Tf}_2\text{N}^-$ in an acidic aqueous phase was determined. For purposes of comparison, the effect of the addition of bis-(2-ethylhexyl)phosphoric acid (HDEHP), an acidic organophosphorus extractant, on the solubilization of $C_{10}\text{mim}^+\text{Tf}_2\text{N}^-$ was also examined. (The limited solubility of HDEHP in $C_5\text{mim}^+\text{Tf}_2\text{N}^-$ precluded the use of this IL for the comparison.) As shown in Fig. 5, as was the case for the crown ether, increasing neutral organophosphorus reagent concentrations are accompanied by a proportionate increase in the solubilization of the IL cation in the aqueous phase (here, 1 M HNO_3). This observation is consistent with the work of Yakshin et al. [51], whose studies of three of these extractants indicated that they are readily protonated by strong inorganic acids. In addition, as would be expected, the variation in the sol-

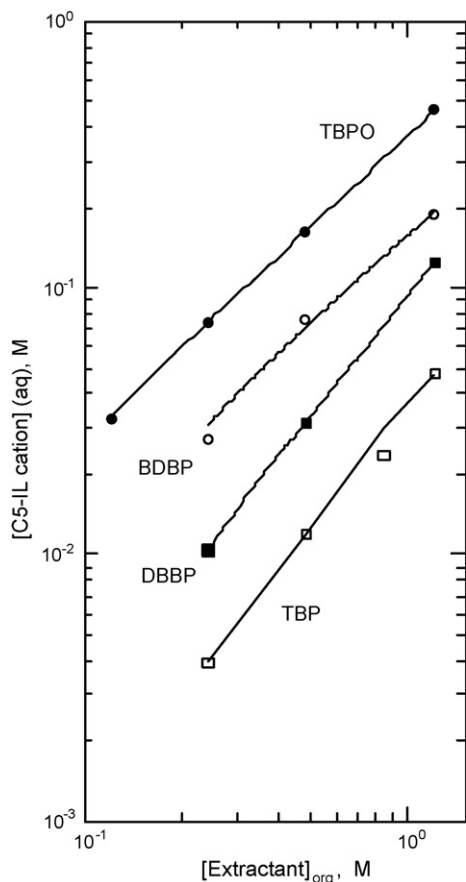


Fig. 5. The effect of neutral organophosphorus extractant concentration on the solubility of $C_5mim^+Tf_2N^-$ in 1 M HNO_3 ($T = 25^\circ C$).

ubilizing effect with extractant ($TBP < DBBP < BDBP < TBPO$) follows the same order as the extractant basicity (as reflected in the value of the protonation constant [51]). In contrast to the behavior of the neutral extractants, no systematic increase in the solubility of the C_{10} -IL in the aqueous phase (ca. 8×10^{-4} M) is observed as the concentration of the acidic reagent (HDEHP) is varied over the same range. Taken together with the results observed for DCH18C6, these data suggest that the increased solubilization of ostensibly hydrophobic ILs in acidic aqueous phases observed upon addition of a neutral extractant represents a general property of IL-neutral extractant combinations.

4. Conclusions

The results presented here raise significant concerns regarding the viability of ionic liquids as replacements for conventional organic solvents in the extraction of metal ions from acidic media by neutral ligands/extractants. As we have demonstrated previously, high metal ion loading of a neutral extractant in an IL can lead to significant aqueous phase dissolution of the IL [31]. Unfortunately, the present results indicate that even in the absence of any metal ion extraction, appreciable loss of IL can occur as a result of the interaction of the extractant with matrix acid. Given that the aqueous solutions resulting from the digestion or leaching of many “real-world” (e.g., environmental,

biological, or geological) samples for subsequent analysis are often highly acidic [52], this clearly poses a problem. Although our results for neutral organophosphorus extractants suggest that IL solubilization can be reduced by employing a weakly basic extractant, the solubilization is not entirely eliminated. These results suggest the need for both caution in attempts to employ ILs as “drop-in replacements” for conventional organic solvents in extraction systems involving neutral extractants and additional research to either identify ILs less prone to solubilization losses or to devise alternative configurations employing ILs in extractive separations (e.g., “task-specific” [53,54] or solid-supported [55,56] ILs). Work addressing these opportunities is now underway in this laboratory.

Acknowledgement

This work was performed under the auspices of the Office of Basic Energy Sciences, Division of Chemical Sciences, United States Department of Energy under contract number W-31-109-ENG-38.

References

- [1] J.G. Huddleston, H.D. Willauer, R.P. Swatloski, A.E. Visser, R.D. Rogers, *Chem. Commun.* (1998) 1765.
- [2] J.F. Brennecke, E.J. Maginn, *AIChE J.* 47 (2001) 2384.
- [3] W.M. Nelson, *Green Solvents for Chemistry: Perspectives and Practice*, Oxford University Press, New York, 2003.
- [4] M.H. Abraham, A.M. Zissimos, J.G. Huddleston, H.D. Willauer, R.D. Rogers, W.E. Acree Jr., *Ind. Eng. Chem. Res.* 42 (2003) 413.
- [5] J. Liu, Y. Chi, J. Peng, G. Jiang, A. Jonsson, *J. Chem. Eng. Data* 49 (2004) 1422.
- [6] M. Matsumoto, K. Mochiduki, K. Fukunishi, K. Kondo, *Sep. Purif. Technol.* 40 (2004) 97.
- [7] J. Liu, Y. Chi, G. Jiang, C. Tai, J. Peng, J.-T. Hu, *J. Chromatogr. A* 1026 (2004) 143.
- [8] S. Smirnova, I.I. Torocheshnikova, A.A. Formanovsky, I.V. Pletnev, *Anal. Chem. Biochem.* 378 (2004) 1369.
- [9] J. Wang, Y. Pei, Y. Zhao, Z. Hu, *Green Chem.* 7 (2005) 196.
- [10] R.D. Rogers, A.E. Visser, R.P. Swatloski, D.H. Hartman, in: K.C. Liddell, D.J. Chaiko (Eds.), *Metal Separation Technologies Beyond 2000*, The Minerals, Metals & Materials Society, Warrendale, PA, 1999, pp. 139–147.
- [11] S. Dai, Y.H. Ju, C.E. Barnes, *J. Chem. Soc., Dalton Trans.* (1999) 1201.
- [12] A.E. Visser, R.P. Swatloski, D.H. Hartman, J.G. Huddleston, R.D. Rogers, in: G.J. Lumetta, R.D. Rogers, A.S. Gopalan (Eds.), *Calixarenes for Separations*, American Chemical Society, Washington, DC, 2000, pp. 223–236.
- [13] A.E. Visser, R.P. Swatloski, W.M. Reichert, S.T. Griffin, R.D. Rogers, *Ind. Eng. Chem. Res.* 39 (2000) 3596.
- [14] S. Chun, S.V. Dzyuba, R.A. Bartsch, *Anal. Chem.* 73 (2001) 3737.
- [15] A.E. Visser, R.P. Swatloski, S.T. Griffin, D.H. Hartman, R.D. Rogers, *Sep. Sci. Technol.* 36 (2001) 785.
- [16] R.A. Bartsch, S. Chun, S.V. Dzyuba, in: R.D. Rogers, K.R. Seddon (Eds.), *Ionic Liquids: Industrial Applications for Green Chemistry*, American Chemical Society, Washington, DC, 2002, pp. 58–68.
- [17] A.E. Visser, J.D. Holbrey, R.D. Rogers, in: K.C. Sole, P.M. Cole, J.S. Preston, D.J. Robison (Eds.), *Proceedings of the International Solvent Extraction Conference, ISEC 2002*, South African Institute of Mining and Metallurgy, Marshalltown, South Africa, 2002, pp. 474–480.
- [18] K. Nakashima, F. Kubota, T. Maruyama, M. Goto, *Anal. Sci.* 19 (2003) 1097.
- [19] A.E. Visser, R.D. Rogers, *J. Solid State Chem.* 171 (2003) 109.
- [20] A.E. Visser, M.P. Jensen, I. Laszak, K.L. Nash, G.R. Choppin, R.D. Rogers, *Inorg. Chem.* 42 (2003) 2197.

- [21] G.-T. Wei, J.-C. Chen, Z. Yang, *J. Chin. Chem. Soc.* 50 (2003) 1123.
- [22] G.-T. Wei, Z. Yang, J.-C. Chen, *Anal. Chim. Acta* 488 (2003) 183.
- [23] K. Shimojo, M. Goto, *Chem. Lett.* 33 (2004) 320.
- [24] K. Shimojo, M. Goto, *Anal. Chem.* 76 (2004) 5039.
- [25] H. Luo, S. Dai, P.V. Bonnesen, *Anal. Chem.* 76 (2004) 2773.
- [26] H. Luo, S. Dai, P.V. Bonnesen, A.C. Buchanan III, J.D. Holbrey, N.J. Bridges, R.D. Rogers, *Anal. Chem.* 76 (2004) 3078.
- [27] P. Giridhar, K.A. Venkatesan, T.G. Srinivasan, P.R.V. Rao, *J. Nucl. Radioanal. Sci.* 5 (2004) 21.
- [28] K. Nakashima, F. Kubota, T. Maruyama, M. Goto, *Ind. Eng. Chem. Res.* 44 (2005) 4368.
- [29] P. Giridhar, K.A. Venkatesan, T.G. Srinivasan, P.R.V. Rao, *J. Radioanal. Nucl. Chem.* 265 (2005) 31.
- [30] N. Hirayama, M. Deguchi, H. Kawasumi, T. Honjo, *Talanta* 65 (2005) 255.
- [31] M.L. Dietz, J.A. Dzielawa, *Chem. Commun.* (2001) 2124.
- [32] M.P. Jensen, J.A. Dzielawa, P. Rickert, M.L. Dietz, *J. Am. Chem. Soc.* 124 (2002) 10664.
- [33] M.L. Dietz, J.A. Dzielawa, M.P. Jensen, M.A. Firestone, in: R.D. Rogers, K.R. Seddon (Eds.), *Ionic Liquids as Green Solvents: Progress and Prospects*, American Chemical Society, Washington, DC, 2003, pp. 526–543.
- [34] M.P. Jensen, J. Neufeind, J.V. Beitz, S. Skanthakumar, L. Soderholm, *J. Am. Chem. Soc.* 125 (2003) 15466.
- [35] M.L. Dietz, M.P. Jensen, J.V. Beitz, J.A. Dzielawa, in: C.A. Young, A.M. Alfantazi, C.G. Anderson, D.B. Dreisinger, B. Harris, A. James (Eds.), *Hydrometallurgy 2003—Proceedings of the Fifth International Conference in Honor of Prof. Ian Ritchie. Vol. 1: Leaching and Solution Purification*, The Minerals, Metals, and Materials Society, Warrendale, PA, 2003, pp. 929–939.
- [36] M.L. Dietz, J.A. Dzielawa, I. Laszak, B.A. Young, M.P. Jensen, *Green Chem.* 5 (2003) 682.
- [37] M.L. Dietz, J.A. Dzielawa, M.P. Jensen, J.V. Beitz, M. Borkowski, in: R.D. Rogers, K.R. Seddon (Eds.), *Ionic Liquids IIIB: Fundamentals, Progress, Challenges and Opportunities*, American Chemical Society, Washington, DC, 2005, pp. 2–18.
- [38] D.C. Stepinski, M.P. Jensen, J.A. Dzielawa, M.L. Dietz, *Green Chem.* 7 (2005) 151.
- [39] M.L. Dietz, D.C. Stepinski, *Green Chem.* 7 (2005) 747.
- [40] H. Heitzman, B.A. Young, D.J. Rausch, P. Rickert, D.C. Stepinski, M.L. Dietz, *Talanta* 69 (2006) 527.
- [41] P. Bonhôte, A.-P. Dias, N. Papageorgiou, K. Kalyanasundaram, M. Grätzel, *Inorg. Chem.* 35 (1996) 1168.
- [42] I. Sanemasa, Y. Miyazaki, S. Arakawa, M. Kumamaru, T. Deguchi, *Bull. Chem. Soc. Jpn.* 60 (1987) 517.
- [43] A.J. Dallas, P.W. Carr, *J. Chem. Soc., Perkin Trans. 2* (1992) 2155.
- [44] V. Boddu, A. Krishnaiah, D.S. Viswanath, *J. Chem. Eng. Data* 46 (2001) 1172.
- [45] E. Högfeldt, B. Bolander, *Acta Chem. Scand.* 18 (1964) 548.
- [46] E.M. Arnett, J.N. Anderson, *J. Am. Chem. Soc.* 85 (1963) 1542.
- [47] N.C. Deno, J.O. Turner, *J. Org. Chem.* 31 (1966) 1969.
- [48] E.M. Arnett, C.Y. Wu, *J. Am. Chem. Soc.* 84 (1962) 1684.
- [49] M.L. Dietz, A.H. Bond, M. Clapper, J.W. Finch, *Radiochim. Acta* 85 (1999) 119.
- [50] R.M. Izatt, B.L. Haymore, J.S. Bradshaw, J.J. Christensen, *Inorg. Chem.* 14 (1975) 3132.
- [51] V.V. Yakshin, N.M. Meshcheryakov, E.G. Il'in, E.M. Ignatov, B.N. Laskorin, *Dokl. Akad. Nauk SSSR* 278 (1984) 162.
- [52] E.P. Horwitz, M.L. Dietz, D.E. Fisher, *Anal. Chem.* 63 (1991) 522.
- [53] J.H. Davis Jr., *Chem. Lett.* 33 (2004) 1072.
- [54] S. Lee, *Chem. Commun.* (2006) 1049.
- [55] C.S.J. Cazin, M. Veith, P. Braunstein, R.B. Bedford, *Synthesis* (2005) 622.
- [56] S.-J. Liu, F. Zhou, L. Zhao, X.-H. Xiao, X. Liu, S.-X. Jiang, *Chem. Lett.* 33 (2004) 496.

Validation of a method for the analysis of quinolones residues in bovine muscle by liquid chromatography with electrospray ionisation tandem mass spectrometry detection

A. Rubies^a, R. Vaquerizo^b, F. Centrich^a, R. Compañó^{b,*}, M. Granados^b, M.D. Prat^b

^a *Laboratori Agència Salut Pública de Barcelona, Avda. de les Drassanes 13-15, E-08001 Barcelona, Spain*

^b *Departament de Química Analítica, Universitat de Barcelona, Martí i Franquès 1-11, E-08028 Barcelona, Spain*

Received 17 July 2006; received in revised form 11 October 2006; accepted 19 October 2006

Available online 28 November 2006

Abstract

A liquid chromatography–tandem mass spectrometry method for the determination and confirmation of nine quinolones was optimised and validated according to Commission Decision 2002/657/EC. Analytes were extracted from veal muscle with water and extracts purified with 96-well plates Oasis HLB cartridges. Separation was carried out in a silica-based C₁₈ column (50 mm × 2.1 mm) with mobile phases consisting of water/acetonitrile mixtures containing acetic acid. Linear calibration curves in the ranges 4–400 and 50–800 ng g⁻¹, with correlation coefficients at least 0.995, were obtained for all the analytes. At concentration levels above 10 ng g⁻¹, quantification errors were lower than 10% and repeatability and within-laboratory reproducibility standard deviations below 6% and 10%, respectively. Decision limits and detection capabilities are reported. © 2006 Elsevier B.V. All rights reserved.

Keywords: Quinolones; Residue analysis; Bovine muscle; Liquid chromatography; Tandem mass spectrometry

1. Introduction

The presence of residues of veterinary drugs in food of animal origin is a matter of concern for the authorities responsible for public health. Within the European legislation devoted to food safety, there are three legislative acts which are especially relevant for analytical laboratories. The Council Regulation 2377/90/EC [1] which deals with the establishment of maximum residue limits (MRLs), the Council Directive 96/23/EC [2] which establishes national monitoring plans and a network of analytical residue laboratories (routine, National Reference and Community Reference) and the Commission Decision 2002/657/EC [3] that provides performance criteria and validation procedures for the analytical methods used in testing official samples.

Quinolones are antibacterial agents widely used in veterinary and human medicine, subjected to regulation. The European Union [4] and the Joint FAO/WHO Expert Committee on Food Additives [5] have established MRLs for some quinolones in tissues of several animal species, milk and eggs.

Numerous analytical methods for quinolones at residual levels, for either screening or confirmatory purposes, have been developed in the last twenty years. In 2002 we published a review article [6] covering the papers published in the period 1969–2000. A more general review [7] on methods for veterinary drugs and growth-promoting agents in products of animal origin and feeds was published in 2005. In recent years, and especially since the publication of Decision 2002/657/EC, liquid chromatography (LC) coupled to mass spectrometry (MS) has become the preferred technique for confirmation and quantification of drug residues in food samples. Methods based on LC–MS [8] and LC–tandem MS [9–11] have been the object of specific reviews.

Since the publication of the aforementioned review articles, LC methods with UV spectrophotometric detection [12–15], fluorimetric detection [13,15–17] and MS or MSⁿ [17–22] detection have been proposed. Almost all of them are multiresidue methods aiming to increase the rapidity and simplicity of the existing ones. Most of these methods apply a solid-phase extraction, in the conventional off-line mode, for the clean-up of the extracts. C₈, C₁₈, cationic-exchange, polymeric or mixed (C₈ and cationic-exchange) cartridges are the solid phases used. Huang et al. [15] apply an on-line solid-phase microextraction,

* Corresponding author. Tel.: +34 93 4039119; fax: +34 93 4021233.
E-mail address: compano@ub.edu (R. Compañó).

Table 1
MRL values established by the EU and the JECFA of FAO/WHO for quinolones in bovine muscle [4,5]

Quinolone	MRL (EU) ($\mu\text{g kg}^{-1}$)	MRL (JECFA) ($\mu\text{g kg}^{-1}$)
MAR	150	–
ENR + CIP	100	–
DAN	200	200
NOR	–	–
SAR	–	–
DIF	400	–
OXO	100	–
FLU	200	500

based on a monolithic phase, for the extraction and purification of fluoroquinolones from eggs. Liquid–liquid extraction has been proposed for clean-up purposes in only one case [17]. LC separations are usually carried out with C8 or C18 pure silica base columns of 150 mm length, leading to chromatographic runs usually lasting between 15 and 30 min. Detection limits of methods based on fluorescence or MS detection range between tenth of ng/g to a few ng/g. Those of methods based on UV detection tend to be one order of magnitude higher. However, all the methods are sensitive enough to detect quinolones far below the MRL. Only a few methods [16,20] have been validated in accordance with the requirements of the Commission Decision 2002/657/EC.

All the methods mentioned afford interesting issues that can be useful for specific applications. However, we can conclude that any one of them implies a dramatic improvement compared to the remaining ones. Suitable sample preparation is still the key to obtaining good sample throughput in residue analysis. This paper reports the development and intralaboratory validation of an LC–MS/MS method to quantify and confirm the presence of enrofloxacin (ENR), ciprofloxacin (CIP), danofloxacin (DAN), difloxacin (DIF), marbofloxacin (MAR), sarafloxacin (SAR), norfloxacin (NOR), oxolinic acid (OXO) and flumequine (FLU) in veal muscle. Structures of the compounds are shown in Fig. 1 and their MRLs in bovine muscle are listed in Table 1. A previously reported extraction method [20] has been adapted. The use of Oasis HLB 96-well plates and multichannel pipettes, as well as a short (50 mm) LC column, allows speeding-up of the sample treatment and LC separation.

2. Experimental

2.1. Reagents and solutions

Standards of DAN, ENR, CIP, NOR, SAR, DIF and FLU, of Vetranal or Pestanal grade, were obtained from Fluka (Buchs, Switzerland). OXO, BioChemika quality was also purchased from Sigma (St. Louis, MO, USA). MAR was kindly supplied by Vétoquinol (Lure, France). Deuterated Norfloxacin (D5), used as internal standard, was obtained from Witega (Berlin, Germany). Chemicals for sample extraction were of analytical grade. Solvents for preparing the LC mobile phase were of HPLC grade. All of them were obtained from Merck (Darmstadt, Ger-

many) and Carlo Erba (Rodano, Italy). SPE cartridges Oasis HLB (60 mg), in 96-well plates, were obtained from Waters (Milford, USA). Ultrapure water was obtained with a Millipore Milli-Q A10 system (Billerica, MA, USA).

Stock standard solutions (200 mg L^{-1}) of MAR, DAN, ENR, CIP, NOR, SAR, DIF were prepared by dissolving the compounds in 0.02 M phosphoric acid. 0.01 M NaOH was used for OXO and FLU. When necessary, sonication was applied to ensure the complete dissolution of the substances. Solutions were stored in dark glass bottles at 4°C and were stable over three months. An intermediate standard solution containing 20 mg L^{-1} of each quinolone was prepared by dilution of the stock solutions with acetonitrile. The 0.4 mg L^{-1} working solution was daily prepared by dilution of the former standard with aqueous 0.1% acetic acid. It is stable for at least one working day.

The stock solution of norfloxacin D5 (200 mg L^{-1}) was prepared dissolving the substance in 2 ml of chloroform and diluting up to 25 ml with methanol.

A binary mobile phase with a gradient elution was used. Mobile phase A was an aqueous 0.1% acetic acid solution and mobile phase B was a mixture acetonitrile:water:acetic acid (90:10:0.1).

2.2. Instrumentation

LC–ESI–MS/MS measurements were carried out with a Waters 2695 HPLC system (Milford, USA) coupled to a Quattro-micro triple quadrupole mass spectrometer from Micromass (Waters) using an electrospray source. The column used was an X-Terra MS C₁₈ (50 mm \times 2.1 mm; 2.5 μm particle diameter) from Waters with a guard column MAX-RP 4 mm \times 2 mm from Phenomenex (CA, USA).

Instrument control and data processing were carried out by means of Masslynx 4.0 software.

A Hettich refrigerated centrifuge (Tuttlingen, Germany) was used in the extraction process. A concentrator workstation Turbovap LV, Zymark (MA, USA) was used to evaporate the extracts.

2.3. Samples

Veal muscle samples of several animals were obtained from the veterinary inspection. They were microbiologically tested to ensure they are blank tissues. After fat was removed they were pooled, minced and stored at -20°C . Samples were thawed before analysis.

Spiked samples were prepared by adding a microvolume of a standard solution containing the nine quinolones to each portion of the weighed samples. Spiked samples were left to stand at 4°C for 24 h in the dark before analysis.

2.4. Procedures

2.4.1. Extraction and clean-up

To 1 g of minced sample, placed in a 20 ml glass tube, 50 μL of a 0.4 mg L^{-1} internal standard solution were added and left to stand for 30 min at room temperature. Then, the sample was

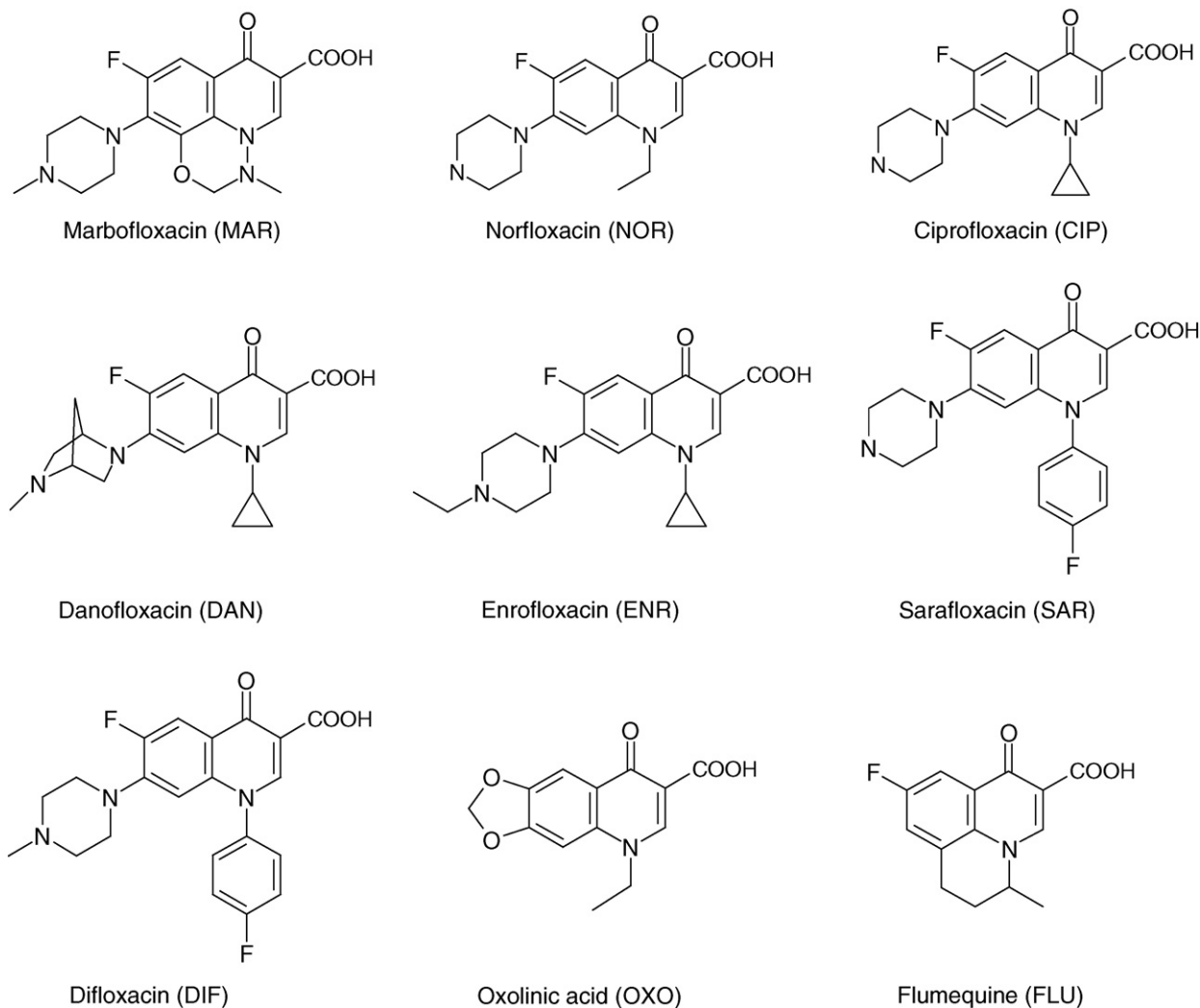


Fig. 1. Structures of the quinolones studied.

extracted for 5 min in an ultrasonic bath with 3 mL of ultrapure water and centrifuged for 10 min (10 °C, 3000 g). Extracts were kept for further clean-up.

Using a multichannel pipette, Oasis HLB 60 mg cartridges of a 96-wells plate were conditioned with 1.5 ml methanol and 1.5 ml water. 1.5 ml of the supernatant extracts were loaded in the cartridges. Cartridges were rinsed with 1.5 ml of water and 1.5 ml of hexane and dried by maintaining in vacuum for 2 min. Analytes were eluted with 2 ml of methanol, eluates transferred to the Turbovap glass tubs and evaporated to dryness under a nitrogen stream (25 min, 40 °C, 15 psi). The purified extracts were reconstituted with 250 μ L of mobile phase, placed in an ultrasonic bath for 5 min, filtered (Durapore of 0.45 μ m from Millipore) and injected (25 μ l) into the LC system.

Calibration was carried out with tissue samples spiked with the analytes in the range 4–800 μ g Kg⁻¹ and with the internal standard.

2.4.2. Liquid chromatography/mass spectrometry

The separation was performed at 40 °C with the following gradient elution program: (time in min, % mobile phase A):

(0, 99), (6, 85), (8, 45), (10, 45), (10.1, 99). Column was re-equilibrated for 7 min before each run. The mobile phase flow was 0.3 ml min⁻¹. Samples were kept in the auto sampler at 15 °C.

The electrospray ionisation source was operated in the positive mode with the following working conditions: capillary voltage +3.0 kV, source block and desolvation temperatures at 120 and 400 °C, respectively, desolvation and nebuliser gas (N₂) flows at 650 and 50 L h⁻¹, respectively, argon pressure in the collision cell at 3 \times 10⁻³ mbar. The values of cone voltage and collision energy are given in Table 2. Full scan spectra were obtained over the range of *m/z* from 50 to 400 at a cycle time of 500 ms and an interscan time of 100 ms. Data acquisition for quantification and confirmation was performed in the multiple reaction monitoring (MRM) mode with a dwell time of 50 ms for each transition. Two transitions were followed for identification but only one was used for quantification (in bold in Table 2).

Identification was carried out by retention time and confirmation was performed using ion ratio criteria (2002/657/EC) [3].

Table 2
Optimal ESI–MS/MS conditions (fragment ions in bold are used for quantification)

Quinolone	t_R (min)	Precursor ion (m/z)	Cone voltage (V)	Collision energy (eV)	Product ion (m/z)
MAR	5.82	363.3	35	15 20	320.1 345.3
NOR	6.41	320.2	35	18 20	276.4 302.4
NOR-D5 (IS)	6.41	325.3	30	20	307.3
CIP	6.68	332.2	35	18 22	288.3 314.3
DAN	7.28	358.2	35	18 25	314.3 340.3
ENR	7.46	360.3	30	20 25	316.3 245.3
SAR	7.77	386.3	35	20 25	342.3 299.3
DIF	7.98	400.3	35	20 28	356.4 299.3
OXO	10.36	262.3	35	20 30	244.3 216.1
FLU	11.03	262.2	35	20 30	244.3 202.3

3. Results and discussion

3.1. Sample treatment

The sample treatment procedure was kept as simple as possible and consists of an extraction of analytes from matrix with pure water and a further SPE clean-up on 96-well-extraction plates. The use of water as extracting solvent has been adapted from a recently published method [20]. The centrifuged aqueous extracts can be directly loaded in the cartridges with no additional treatments. The use of 96-well extraction plates, which are designed for applications where a large number of samples are processed, and a multichannel pipette allows the analysis of 24 samples in a working day.

Recovery rates were evaluated from the analysis of four blank samples spiked with the nine analytes at four concentration levels. To determine absolute recovery rates, the analytical responses obtained from samples spiked with the analytes at the beginning of the sample preparation were compared with those obtained from extracts spiked after the reconstitution of the SPE eluates, just before LC injection. Data from the analysed samples led to recovery rates ranging from 40 to 55%, except for NOR, CIP and DAN, which showed recovery rates of 36, 37 and 30%, respectively. Although the method has low absolute recoveries for some analytes, they can be considered acceptable since they are reproducible (R.S.D. < 9%) and recovery rates are corrected by performing calibration using spiked blank tissues.

3.2. Optimisation of LS/MS/MS parameters

In order to shorten the separation time as much as possible, LC separation of the nine quinolones was carried out in a 50 mm × 2.1 mm column. The chromatogram obtained using the gradient program described under procedures resulted in a good resolution for all the quinolones. Although, in general, complete

separation of analytes is not required in MS/MS detection, a good resolution avoids the possibility of ionisation suppression.

To achieve maximum sensitivity, the mass spectrometry parameters were optimised by infusion of standard solutions of each quinolone in 0.1% acetic acid/acetonitrile (99:1). The optimal conditions are given in the experimental section.

The protonated molecular ion $[MH]^+$ was selected as precursor ion for all compounds. The product ion spectra obtained depended on the collision energy. In general, the most intense fragment ion observed is $[MH-H_2O]^+$. The loss of CO_2 , as well as the further loss of piperazinic ring fragments (C_2H_5N for SAR, C_3H_7N for DIF and C_4H_9N for ENR) are other detected product ions for quinolones with a piperazinyl ring. The mass spectra and fragment ions observed in the MS/MS experiments agree with the fragmentation given by other authors [23].

OXO and FLU, which have no substituent at C7, showed less fragmentation. Moreover, they do not even show the fragment $[MH-CO_2]^+$. Besides the $[MH-H_2O]^+$, ions at m/z 216 and 202 are the most intense fragments observed for OXO and FLU, respectively. The ion at m/z 216 corresponds to the loss of C_2H_4 and that at 202 is probably due to the loss of $CH_3-CH=CH_2$ from the ring structure between N-1 and C-8 [23]. The product ion spectra obtained for all analytes at the optimal conditions are shown in Fig. 2. Because the molecular weights of OXO and FLU are identical and the most intense transition for both compounds lead to product ions at m/z 244, separation on the basis of retention in the LC column is required for these analytes. The described LC separation provides a complete separation, as can be seen in the MRM chromatograms shown in Fig. 3.

3.3. Method validation

The method was validated according to the criteria specified in the Commission Decision 2002/675/EC for a quantitative confirmation method. For analytes with an established MRL,

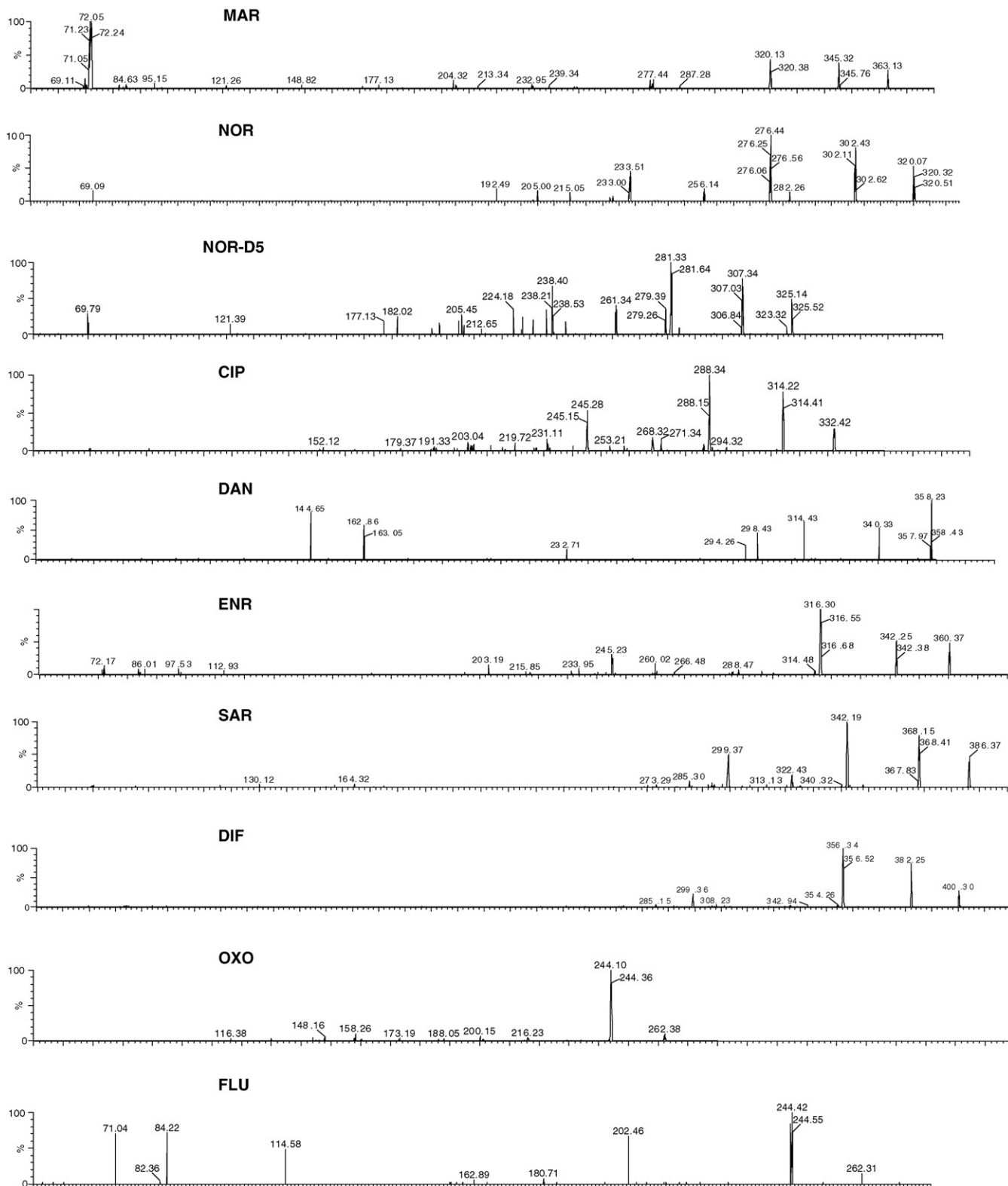


Fig. 2. LC-MS/MS product ion spectra of $[MH]^+$ for all the quinolones studied.

validation parameters were determined at concentration levels of 0.5 MRL, 1 MRL, 1.5 MRL and 2 MRL. For SAR and NOR, for which neither MRL nor MRPL have been established, the selected levels were 4, 50, 100 and 150 ng g^{-1} . The lowest level selected was 4 ng g^{-1} because preliminary data

indicated that the detection limits for SAR and NOR are about this value. The validation parameters measured to evaluate the method were specificity, linear range, precision (repeatability and within-laboratory reproducibility), trueness, decision limit and detection capability.

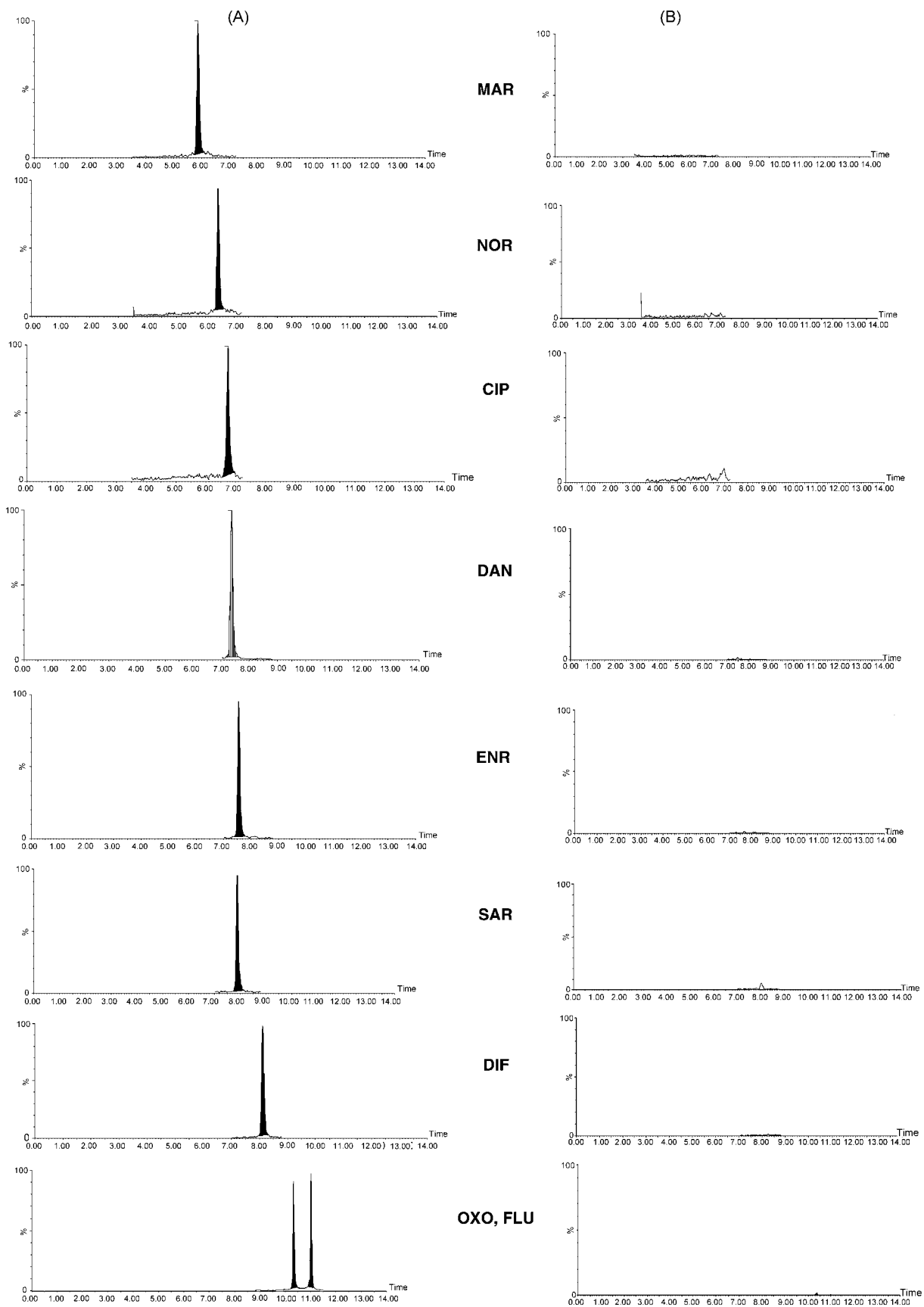


Fig. 3. MRM chromatograms of extracts of bovine muscle spiked at 4 ng g^{-1} (A) and of a blank muscle (B).

Table 3
Calibration parameters

Quinolone	Range	Slope	Intercept	Correlation coefficient	Residuals % ^a	Residuals % ^b
MAR	50–800	0.0632	0.318	0.997	1.9	1.2–6.1
NOR	5–400	0.0528	0.003	0.999	14	0.5–3.0
CIP	5–400	0.0642	0.198	0.999	6.6	0.5–5.6
DAN	50–800	0.0905	-0.045	0.998	6.2	0.9–7.2
ENR	4–400	0.1306	0.258	0.997	1.5	0.1–5.7
SAR	4–400	0.0826	0.087	0.999	6.2	0.1–4.0
DIF	50–800	0.1227	2.608	0.998	12.1	1.1–8.0
OXO	50–800	0.1635	3.789	0.995	19.6	1.8–9.7
FLU	50–800	0.1274	2.715	0.996	14	0.8–8.3

Deviation of the measurement from its predicted value: ^aAt the lower concentration level. ^bAt the remaining levels.

Table 4
Trueness and precision

Quinolone	Nominal conc. (ng g ⁻¹)	Mean conc. ng g ⁻¹	Error (%)	Repeatability (%) (n = 6)	Reproducibility (%) ^a	R.S.D. max (%) ^b
MAR	75	79.4	5.8	5.1	6.5	23.6
	150	147	-2.0	4.3	6.2	21.3
	225	247	9.8	5.9	6.0	20.0
	300	317	5.6	3.5	3.6	19.2
NOR	4	3.69	-7.7	5.2	11.1	36.7
	50	49.4	-1.1	4.8	7.4	25.1
	100	105	5.0	5.2	5.6	22.6
	150	155	3.3	4.9	5.0	21.3
CIP	50	51.9	3.9	5.7	6.6	25.1
	100	106	6.0	6.6	8.7	22.6
	150	164	9.4	4.9	5.9	21.3
	200	213	6.8	6.8	6.2	20.4
DAN	100	104	3.8	4.2	4.8	22.6
	200	203	1.4	5.1	5.2	20.4
	300	314	4.5	5.9	6.5	19.2
	400	391	-2.2	6.1	6.2	18.4
ENR	50	54.7	9.4	5.8	10.9	25.1
	100	106	6.3	6.7	7.4	22.6
	150	163	8.7	5.5	10.1	21.3
	200	214	7.2	6.7	6.8	20.4
SAR	4	4.56	14.0	6.2	16.0	36.7
	50	54.7	9.4	4.3	9.1	25.1
	100	109	9.0	8.8	7.2	22.6
	150	164	9.4	5.6	4.7	21.3
DIF	200	218	9.2	5.8	5.9	20.4
	400	390	-2.5	4.3	6.6	18.4
	600	653	8.8	8.2	9.1	17.3
	800	782	-2.3	5.6	6.3	16.5
OXO	50	48.5	-3.0	7.8	8.4	25.1
	100	106	6.0	5.6	7.2	22.6
	150	155	3.2	9.5	10.1	21.3
	200	196	-2.0	6.2	7.6	20.4
FLU	100	108	8.0	6.5	7.1	22.6
	200	218	8.9	4.8	6.6	20.4
	300	294	-2.0	5.8	7.5	19.2
	400	407	1.8	5.2	4.7	18.4

^a n = 18, in six-fold on three different days.

^b Values calculated with the Horwith equation.

Table 5
Decision limit and detection capability (ng g^{-1})

Quinolone	CC α	CC β
MAR	164	183
NOR	2.0 ^a	2.4
CIP	108	117
DAN	217	232
ENR	112	124
SAR	5.1 ^a	6.0
DIF	443	485
OXO	109	118
FLU	219	239

^a Calibration curve method.

The specificity was assessed by analysing blank tissue samples. The absence of background peaks, above a signal-to-noise ratio of 3, at the retention times of the target compounds, showed that the method is free of endogeneous interferences. The chromatogram of a blank sample tissue is shown in Fig. 3.

The calibration curves for each compound were built using blank muscle samples ($n=7$) spiked in the 4–400 or in the 50–800 ng g^{-1} range, depending on the analyte. The linear regression analysis was carried out by plotting the peak area ratio of the analyte and I.S. versus the analyte concentrations. The calibration parameters are summarised in Table 3. As can be seen, good linearity was observed: correlation coefficients were at least 0.995 for all the analytes, while residuals were below 20% in the low level and below 10% in high concentration range. Trueness and precision (repeatability and within-laboratory reproducibility) of the method were determined using independently spiked blank muscle samples at four different levels (18 spiked samples for each level). Samples were analysed in six-fold on three different days, using daily prepared standard solutions. The results, summarised in Table 4 show the good accuracy of the method. Errors, expressed as the difference between the mean found and the nominal concentration (%), are below 10% for concentration levels higher than 10 ng g^{-1} and below 20% for levels lower than 10 ng g^{-1} . Values of the within-laboratory coefficient of variation are lower than half of the values calculated by the Horwitz equation.

The decision limits (CC α) were calculated as the mean values of the found concentrations plus 1.64 times the corresponding standard deviations, when analysing blank tissue samples spiked at the MRL (for MRLs substances) or from the curve calibration method (for NOR and SAR, for which neither MRL nor MRPL have been established). For quinolones with established MRL, this parameter was calculated with values already obtained for the determination of the trueness and precision. For SAR and NOR, CC α was first calculated as the concentration corresponding to the y-intercept plus 2.33 times its standard deviation.

The detection capability (CC β) was calculated as the decision limit plus 1.64 times the corresponding standard deviations when analysing 20 blank tissue samples spiked at the CC α level. Table 5 summarises the obtained CC α and CC β values.

The method also fulfills the criteria for residue identification. It scores four identification points through the measurement of two product ions plus the precursor ion. The ion ratio for each

analyte in samples matches the ion ratio for the standards within the run, since differences between calculated ratios were lower than 20%.

4. Conclusions

The liquid chromatography–tandem mass spectrometry method proposed fulfils the requirements of the Commission Decision 2002/657/EC. Thus, it can be applied in laboratories involved in official residue controls, for the determination and confirmation of nine quinolones in veal muscle and similar matrices. The use of Oasis HLB 96-well plates and multichannel pipettes reduces the time devoted to sample treatment. Likewise, the LC separation has been sped-up with the use of a short (50 mm) LC column. The method is now routinely used in the laboratory of the *Agència de Salut Pública de Barcelona* to confirm non-compliant samples from a microbiological screening test. It has been shown that up to 24 suspicious samples can be analysed per working day.

Acknowledgements

Financial support from the Spanish Ministerio de Educación y Ciencia (Projects AGL2002-04448-C02-01 and AGL2005-07700-C06-04) is gratefully acknowledged.

References

- [1] Official Journal of the European Union L224 of the 18 August 1990.
- [2] Official Journal of the European Union L125 of the 23 May 1996.
- [3] Official Journal of the European Union L221 of the 17 August 2002.
- [4] Consolidated version of the Annexes I to IV of the Council Regulation 2377/90/EC. Updated up to 12.10.2005. Obtained from http://www.ec.europa.eu/enterprise/pharmaceuticals/pharmacos/index_en.htm.
- [5] <http://www.codexalimentarius.net/web/jecfa.jsp>.
- [6] J.A. Hernández-Artaseros, J. Barbosa, R. Compañó, M.D. Prat, J. Chromatogr. A 945 (2002) 1.
- [7] A.A.M. Stolker, U.A.Th. Brinkman, J. Chromatogr. A 1067 (2005) 15.
- [8] D. Corcia, M. Nazzari, J. Chromatogr. A 974 (2002) 53.
- [9] G. Balizs, A. Hewitt, Anal. Chim. Acta 492 (2003) 105.
- [10] S.I. Kotretsou, Crit. Rev. Food Sci. Nutr. 44 (2004) 173.
- [11] A. Gentili, D. Perret, S. Marchese, Trends Anal. Chem. 24 (2005) 704.
- [12] S. Bailac, O. Ballesteros, E. Jiménez-Lozano, D. Barrón, V. Sanz-Nebot, A. Navalón, J.L. Vilchez, J. Barbosa, J. Chromatogr. A 1029 (2004) 145.
- [13] M.D. Marazuela, M.C. Moreno-Bondi, J. Chromatogr. A 1034 (2004) 25.
- [14] V.F. Samanidou, E.A. Christodoulou, I.N. Papadoyannis, J. Sep. Sci. 28 (2005) 555.
- [15] J.F. Huang, B. Lin, Q.W. Yu, Y.Q. Feng, Anal. Bioanal. Chem. 384 (2006) 1228.
- [16] E. Verdon, P. Couedor, B. Roudaut, P. Sanders, J. AOAC Int. 88 (2005) 1179.
- [17] M.J. Schneider, L. Vázquez-Moreno, M.C. Bermúdez-Almada, R. Barraza, M. Ortega-Nieblas, J. AOAC Int. 88 (2005) 1160.
- [18] B. Toussaint, M. Chedin, G. Bordin, A.R. Rodríguez, J. Chromatogr. A 1088 (2005) 32.
- [19] B. Toussaint, M. Chedin, U. Vincent, G. Bordin, A.R. Rodríguez, J. Chromatogr. A 1088 (2005) 40.
- [20] N. Van Hoof, K. De Wasch, L. Okerman, W. Reybroek, S. Poelmans, H. Noppe, H. De Brabander, Anal. Chim. Acta 529 (2005) 265.
- [21] M.P. Hermo, D. Barrón, J. Barbosa, J. Chromatogr. A 1104 (2006) 132.
- [22] S. Bailac, D. Barrón, V. Sanz-Nebot, J. Barbosa, J. Sep. Sci. 29 (2006) 131.
- [23] D. Volmer, B. Mansoori, S.J. Locke, Anal. Chem. 69 (1997) 4143.

Long-wavelength fluorescence polarization immunoassay for surfactant determination

M.L. Sánchez-Martínez^a, M.P. Aguilar-Caballos^a,
S.A. Eremin^b, A. Gómez-Hens^{a,*}

^a Department of Analytical Chemistry, University of Córdoba, Campus of Rabanales, Marie-Curie Annex building, 14071 Córdoba, Spain

^b Department of Chemical Enzymology, M.V. Lomonosov Moscow State University, Moscow 119992, Russia

Received 13 March 2006; received in revised form 5 October 2006; accepted 19 October 2006

Available online 27 November 2006

Abstract

A new homogeneous fluoroimmunoassay method based on the use of dynamic long-wavelength fluorescence polarization is presented here for the first time. This methodology, which is applied to the determination of linear alkylbenzenesulfonates (LASs) in water samples, involves the use of a new long-wavelength tracer synthesized from the oxazine dye Nile Blue (NB) via a carbodiimide method. This tracer exhibits fluorescent properties at λ_{ex} 626 and λ_{em} 674 nm. The variation of fluorescence polarization with time is followed using the T-format configuration of the spectrofluorimeter and the analytical parameter used is the initial rate, which is measured in only 0.7 s. The dynamic range of the calibration graph is 0.05–4.7 mg/L, with a detection limit of 0.03 mg/L. The precision, expressed as relative standard deviation was assayed at 0.05 and 1 mg/L, giving values in the range 7.6–9.1%. Other anionic, cationic and non-ionic surfactants were tolerated at much higher concentration levels than that of the analyte. The method has proven its practical usefulness for the analysis of water samples, in which only a solid phase extraction step is necessary. Recoveries ranged from 80.8 to 119.8%, with a mean value of 100.8%.

© 2006 Elsevier B.V. All rights reserved.

Keywords: Long-wavelength; Stopped-flow; Fluorescence polarization immunoassay; Nile Blue; Linear alkyl benzene sulfonates

1. Introduction

Fluorescence polarization immunoassay (FPIA) is a powerful tool for the immunochemical determination of haptens owing to the dependence of polarization measurements on molecular size of immunoreagents. Tracers often used in FPIA systems are synthesized from fluorescein derivatives, which provide adequate fluorescent signals. However, these signals can be influenced by some light scattering phenomena owing to the relatively short Stokes' shift (ca. 30 nm) of the fluorescein-derived tracer, increasing the dispersion when the tracer is bound to the antibody. Also, the measurements can be affected by the background fluorescent emission signal from sample matrix. A potential option to minimize or to avoid this shortcoming is the performance of luminescence measurements using long-wavelength fluorophores (LWFs) [1]. This approach only has been applied

up to date using ruthenium complexes [1,2], although its practical usefulness to the analysis of real samples has not been described yet. In addition to the relatively long excitation and emission wavelengths of LWFs, they have other features, such as: (1) low probability of photobleaching owing to their long excitation wavelength, (2) relatively high quantum yields and (3) relaxation times in the nanosecond scale. This last characteristic can be very suitable for the use of LWFs as labels for haptens in FPIA, since the depolarization time of the fluorophore has to be of the same order as those of haptens. This fact allows the observation of the increase in the fluorescence polarization because of the decrease in the diffusional rotation of the molecule by the formation of the antibody–antigen complex. The performance of kinetic measurements is another approach that can improve the detection limits in FPIA, as they are not influenced by static background signals. The automation of dynamic measurements in FPIA can be achieved using the stopped-flow (SF) mixing technique, giving rise to SF-FPIA [3], in which measurements are performed shortly after mixing, the manipulation of reagents is simplified, and their consumption is reduced.

* Corresponding author. Tel.: +34 957218645; fax: +34 957218644.

E-mail address: qaigohea@uco.es (A. Gómez-Hens).

Linear alkylbenzene sulfonates (LASs) are the main group of anionic surfactants coming from very different sources, such as household and industrial products, among others [4]. Although these surfactants can be aerobically degraded, this treatment is not efficient enough, so that LASs can persist in water in relatively high concentrations. The control of total LASs in water samples is still an important issue although some countries have tried to reduce their consumption to avoid this problem. Their isomer and/or homologue identification and determination are mainly carried out by LC/MS methods [5–10]. Photometric detection has been proposed for the determination of the total content of anionic surfactants in water by using several dyes [11–13]. Regarding total LASs, there are some immunochemical methods described for their determination based on FPIA [14], ELISA [15,16], flow injection enzyme immunoassay [17] and immunoaffinity chromatography [18]. These are simpler approaches than LC/MS methods when only total LAS estimation is needed to indicate the contamination level of samples. The FPIA method [14] was performed using a fluorescein derivative as a tracer and static fluorescence polarization measurements. As LASs do not have any carboxylic acid group in their structure, the use of hapten mimics was necessary for the development of the fluorescent tracer. Several antibody-tracer combinations were assayed due to the fact that FPIA measurements can be influenced by the length of the spacer arm between hapten and fluorophore. The most sensitive assay was achieved using 3-(sulfophenyl-butyric acid) (3-p-SPh-but), featuring the method a detection limit of 0.5 mg/L. However, the practical usefulness was not described, unlike other immunoassay methods based on ELISA [15,16] and immunoaffinity chromatography [18], which have been applied to the analysis of sea [16], ground [15,16,18] and waste-water [18] samples.

The aim of the work presented here has been to improve the features of conventional FPIA using dynamic long-wavelength measurements. The usefulness of this approach has been shown by its application to the determination of LASs in water samples. A new tracer has been synthesized for this purpose by means of a covalent linking between Nile Blue (NB) and the LAS mimic 3-p-SPh-but. NB is an oxazine dye that exhibits a wide fluorescent emission band with a maximum at 670–680 nm. Recently, it has been described that the rotational diffusion of the 9-aminoacridine and NB labeled polymer solutions changed depending the polymer conformation [19]. This fact has allowed the use of time-resolved fluorescence anisotropy for monitoring the polymer structure in different solvents. However, to the best of our knowledge, NB has not been used before to develop FPIA methods. The analytical parameter used is the initial rate obtained by monitoring the changes in fluorescence polarization with time throughout the formation of the antibody–antigen complex, using SF mixing technique.

2. Experimental

2.1. Instrumental

An SLM Aminco (Urbana, IL) Model 8100 photon counting spectrofluorometer, equipped with a 450 W xenon arc lamp,

three polarizers (Glan-Thompson calcite prism type) and two R928 photomultiplier tubes was used. Polarization data were obtained by placing one of the polarizers in the excitation channel and the other two in each emission channel of the T-optic spectrofluorimeter. The excitation wavelength was set at 626 nm, using the excitation monochromator. The emission wavelength was selected using Schott RG-665 filters in both emission channels. Excitation slits were set to provide 2-nm band passes. The instrument was fitted with a stopped-flow module [20] furnished with an observation cell of 1-cm path length. The solutions in the cell compartment were kept at a constant temperature of 30 °C by circulating water from a thermostated tank. A 24-port Visi-Prep vacuum device from Supelco (Bellefonte, PA, USA) and C₈ cartridges (500 mg of sorbent) (Análisis Vínicos, Tomelloso, Spain) were used to perform a SPE step.

2.2. Reagents

All reagents used were of analytical grade. Lyophilized antibodies were polyclonal antibodies raised in rabbits against a LAS mimic, 3-(p-sulfophenyl-butyric) acid (3-p-SPh-but), which were obtained according to an immunization procedure before described for LAS determination [17]. A 0.01 M phosphate buffer solution in distilled water (0.45 mL) at pH 7.7 was used to reconstitute the antibodies, obtaining a 2.2×10^{-4} M stock solution. The standard used for LAS was the linear 4-dodecylbenzenesulfonic acid sodium salt (LDS, technical mixture, 80%) (Sigma, MO, USA) and a 4 mg/mL stock solution was prepared in methanol and stored at 4 °C. The same LAS mimic (3-p-SPh-but) was used together with NB and *N*-hydroxysuccinimide (NHS), (Sigma), and 1,3-dicyclohexylcarbodiimide (DCC) (Aldrich, Steinheim, Germany), to synthesize the long-wavelength fluorescent tracer according to a carbodiimide procedure [14], which involves the formation of a *N*-hydroxysuccinimidyl ester. An amount (0.4 mmol) of 3-p-SPh-but was dissolved in 0.5 mL of dimethylformamide (DMF) and added to a solution containing NHS (0.8 mmol) and DCC (1.6 mmol) in 0.5 mL of DMF. This mixture was kept in the dark for 24 h at room temperature. A precipitate from dicyclohexylurea appeared, but it was decanted and 250 μ L of the supernatant were added to NB (0.01 mmol) and the suspension was kept in the dark for 2 days at room temperature. TLC with silica gel plates and chloroform/methanol (2:1) as mobile phase was used to obtain the blue band of the tracer ($R_f=0.72$), which was scrapped from the plate and eluted using methanol. The tracer concentration was calculated using $\epsilon_{624} = 8.12 \times 10^4 \text{ M}^{-1} \text{ cm}^{-1}$. Appropriate working solutions were prepared in phosphate buffer (0.01 M, pH 7.7).

2.3. Procedures

2.3.1. Determination of LASs by long-wavelength FPIA

A solution (2 mL) containing anti-LAS antibodies (220 nM) prepared in phosphate buffer (0.01 M, pH 7.7) was used to fill in one of the two 2-mL drive syringes of the stopped-flow module. The other syringe contained a premixed aqueous solution (2 mL) of tracer (71 nM) and LDS standard or sample at a final

concentration between 0.05 and 4.7 mg/L in phosphate buffer. In each run, 0.15 mL of each solution was mixed in the mixing chamber, which is at the same time the observation cell, and the variation of the fluorescence polarization with time throughout the immunochemical reaction was monitored for 5 s. All measurements were carried out at 30 °C. Data were processed by the computer, furnished with a linear regression program for application of the initial rate method. The reaction rate was determined in ca. 0.7 s, and each standard or sample was assayed in triplicate.

2.3.2. Determination of LASs in water samples

Acidified water sample (pH 2) was microfiltered through a 0.45 μm nylon disk. Then, 100-mL water aliquots were subjected onto a reversed-phase extraction step using 500 mg C₈ cartridges, previously conditioned with 10 mL of methanol and 10 mL of distilled water. After sample application, cartridges were eluted with 1 mL of methanol and 200 μL of this solution were treated as described above for LAS determination.

3. Results and discussion

3.1. Long-wavelength SF-FPIA measurements

Immunochemical methods previously reported for LAS determination are based on systems in which the reaction has reached the equilibrium, and are performed in a homogeneous, such as FPIA [14], or heterogeneous format, such as ELISA [15,16], flow enzyme immunoassay [17] or immunoaffinity chromatography [18]. The present method can be considered innovative because it combines two different aspects: (1) measurements of fluorescence polarization are carried out at long wavelength and (2) dynamic methodology is used to obtain more selective luminescence measurements without the separation of free and bound tracer. The joint use of both approaches allows the minimization or elimination of potential interferences owing to background static signals and scattering light phenomena from sample matrix. The initial reaction rate of the immunochemical reaction can be obtained by measuring the variation of the polarization degree: $P = (A - B)/(A + B)$ with time, in which A and B are the fluorescence intensities measured with emission polarizers placed in parallel and perpendicular form, respectively, to the excitation polarizer fixed in the vertical position. This parameter decreased when the analyte concentration increased, and therefore, it is a function of the analyte concentration. Fig. 1 shows a scheme of the instrumentation used: the variation of A and B intensities with the time is measured using the T-format configuration of the spectrofluorimeter and the value of the initial rate is obtained by the microcomputer, which automatically processes the kinetic curves. The initial rate obtained is inversely proportional to the analyte concentration.

The distribution of the reactants in the syringes of the stopped-flow module was checked out in order to obtain adequate initial rate values. Several reagent distributions were assayed with this purpose, such as the placement of antibodies and tracer together in one syringe and the analyte in the second one, or the antibodies in one syringe and the tracer and analyte together in the

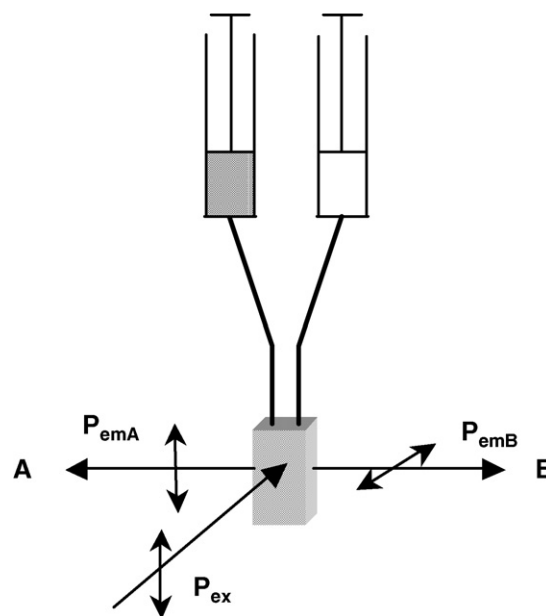


Fig. 1. Scheme of the instrumentation used to perform SF-FPIA methodology. P_{ex} : excitation polarizer; P_{emA} , P_{emB} : emission polarizers perpendicularly arranged one to each other measuring the fluorescence intensities A and B , respectively.

second syringe. The kinetic curves obtained using the second approach were faster than those using the first one, which is a logical behavior since the displacement reaction follows a more complicated mechanism than the direct competition of tracer and analyte for the active sites of antibodies. Fig. 2 shows the kinetic curves obtained in the absence and in the presence of different LDS concentrations using the competitive distribution.

The long-wavelength tracer used in this work has been synthesized by covalent linking formation using a carbodiimide method. 1,3-Dicyclohexylcarbodiimide (DCC) was used

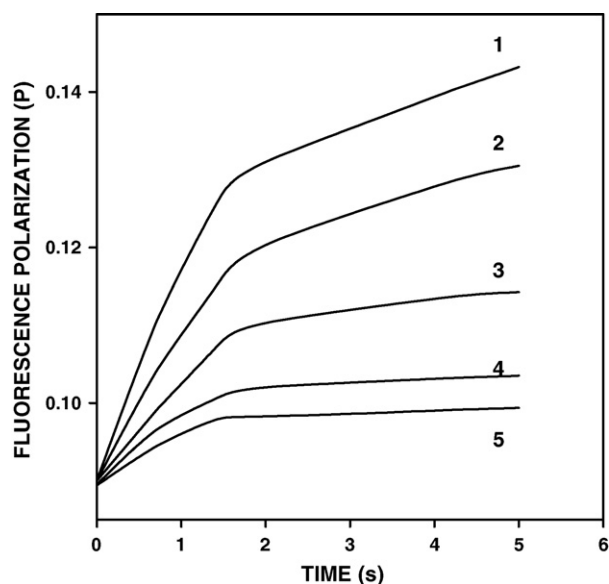


Fig. 2. Kinetic curves obtained for (1) 0, (2) 0.1, (3) 0.5, (4) 1 and (5) 2 mg/L LDS. [antibodies]=220 nM; [tracer]=71 nM; pH 7.7; [phosphate buffer]=0.01 M; 30 °C.

to activate the carboxylic acid group together with *N*-hydroxysuccinimide (NHS) to form the *N*-hydroxysuccinimidyl ester of LAS mimic, which is coupled to the amino group of NB. The reaction mixture was purified by TLC to obtain the tracer band. It was possible to observe a new blue band from the tracer during the purification step, which was not present for the same reaction mixture in absence of the surfactant. The synthesized tracer features fluorescent properties with λ_{ex} 626 and λ_{em} 674 nm as excitation and emission wavelengths, respectively. The Stokes' shift of this tracer (~ 48 nm) is longer than that provided by fluorescein derivatives (~ 30 nm), which can help to reduce the scattering light phenomena mentioned above.

3.2. Optimization of the SF-FPIA system

Tracer and antibody concentrations are interrelated parameters, from which the sensitivity of the assay depends on. Tracer concentration was assayed in the range 7.1–2.5 μM , finding that concentrations between 71 and 140 nM gave a suitable fluorescence intensity, which allows the achievement of adequate initial rate values. Then, the influence of antibody concentration was checked by assaying antibody dilution curves (Fig. 3) at two tracer concentrations, which were 71 (curve 1) and 140 nM (curve 2), respectively. As it can be seen from this figure, the initial rate obtained for the first tracer concentration was higher than that for the second one. An 1/1000 antibody dilution was chosen.

The immunochemical system was optimized by applying the univariate method to initial rate measurements. All concentrations given here are initial concentrations in the syringes (twice the actual concentrations in the reaction mixture at time zero after mixing). Each kinetic result was the average of three measurements. The analytical parameter used for the optimization of chemical variables, calibration and application to real sam-

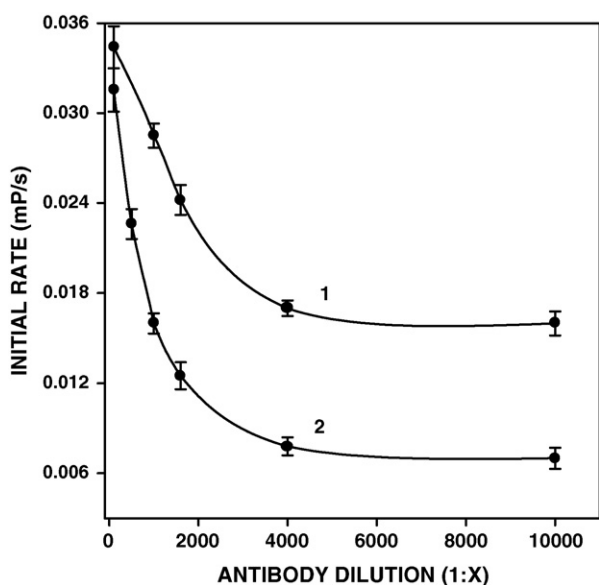


Fig. 3. Antibody dilution curves obtained at (1) 71 nM and (2) 140 nM tracer concentrations. pH 7.7; [phosphate buffer] = 0.01 M; 30 °C.

ples was the normalized signal (B/B_0), in which B is the initial rate obtained in the presence of the analyte and B_0 the initial rate for the blank signal obtained in the absence of the analyte.

The optimization of the pH was carried out in the range 6.5–8.3, finding that the optimum pH was 7.6–7.8 (Fig. 4A). It can be seen that the maximum variation is obtained at this pH range, since the normalized signal decreases when the analyte causes a higher inhibition. Owing to that the stock solution of the tracer was dissolved in methanol, and also that this solvent is chosen to perform the SPE sample pretreatment, its influence on the initial rate of the system was investigated in the range 0.02–40%. As Fig. 4B shows, there is an increase in the normalized initial rate in the presence of the analyte, which means a decrease in the sensitivity of the assay. However, at 10% of methanol, this change in the normalized signal was relatively slight (ca. 5%), being chosen this methanol concentration to perform the method. The temperature of the system was adjusted to 30 °C for the optimum development of the immunochemical reaction, as it has been previously described [18].

3.3. Analytical figures of merit

The dynamic range of the calibration graph (Fig. 5), which was obtained by using the initial rate method and the normalized signal (B/B_0) as analytical parameter was 0.05–4.7 mg/L. The calibration data were processed by non linear regression using the 2001 Sigma Plot software and fitted to a 3-parameter sigmoidal curve, given by the equation $\{a/[1 + e^{-(x-x_0)/b}]\}$, in which y is the normalized signal for the initial rate, and x is the log[LDS] expressed in milligram per liter. The values of a , b and x_0 were 1.23 ± 0.03 , -0.78 ± 0.02 and -0.74 ± 0.05 , being the correlation coefficient 0.998. This value is indicative of a good fitness of the experimental values to the calibration curve. The detection limit, calculated according IUPAC recommendations [21], was 0.03 mg/L, which is about 16-times lower than that afforded by the conventional FPIA method [14]. The precision was evaluated at two LDS concentrations, 0.05 and 1 mg/L, and expressed as relative standard deviation, giving 7.6 and 9.1%, respectively.

The influence of cationic, anionic and non-ionic surfactants, such as cetyltrimethylammonium bromide (CTAB), sodium dodecylsulfate (SDS) and Triton X-100 on the determination of 2.8 μM LDS, was checked out at concentrations below and above their critical micellar concentration (c.m.c.). It was found that the system was independent on CTAB and Triton X-100 concentrations up to 1.3 mM and 0.03%, respectively. SDS did not affect the system up to a 0.49 mM concentration, from which an increase in the initial rate was observed.

3.4. Applications

The method was applied to the analysis of waste and ground water samples. After sample microfiltration, an SPE step was used to both pre-concentrate and clean-up them. This SPE step cannot be considered a time-consuming procedure as up to 24

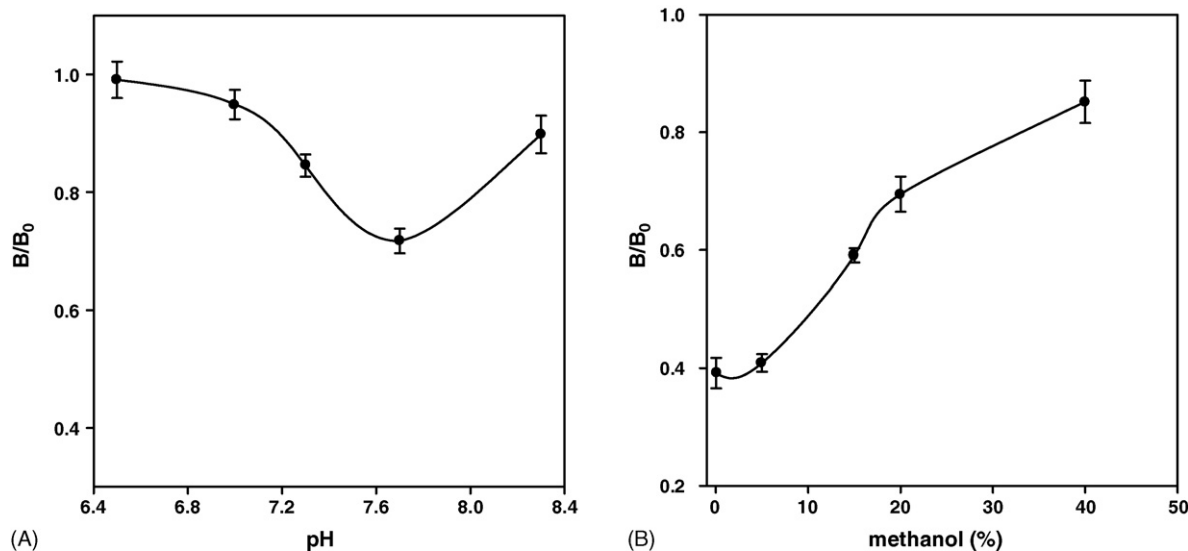


Fig. 4. Influence of (A) pH and (B) methanol on the system. B/B_0 : normalized signal (B : initial rate in the presence of LDS; B_0 : initial rate in the absence of analyte. [antibodies] = 220 nM; [tracer] = 71 nM; [phosphate buffer] = 0.01 M, 30 °C. In (A) [LDS] = 0.1 mg/L; [methanol] = 0.02%. In (B) [LDS] = 0.5 mg/L; pH = 7.7.

samples can be simultaneously processed with an automatic sample loading device [18]. The calibration curve was obtained using 10% methanol, which afforded adequate initial rate values, and also a final preconcentration factor for the samples of 10. This factor allows the achievement of a detection limit for LASs in water samples of 3 $\mu\text{g/L}$, which is comparable to that afforded by an ELISA method [16]. The analysis of the two water samples (Table 1) showed that only the waste-water sample contained a low LAS concentration (70 $\mu\text{g/L}$). Table 1 also summarizes the analytical recoveries, which were obtained by adding three different amounts of LDS to each sample and subtracting the results from similarly prepared unspiked samples. The values obtained ranged from 80.8 to 119.8%, with a mean recovery value of 100.8%.

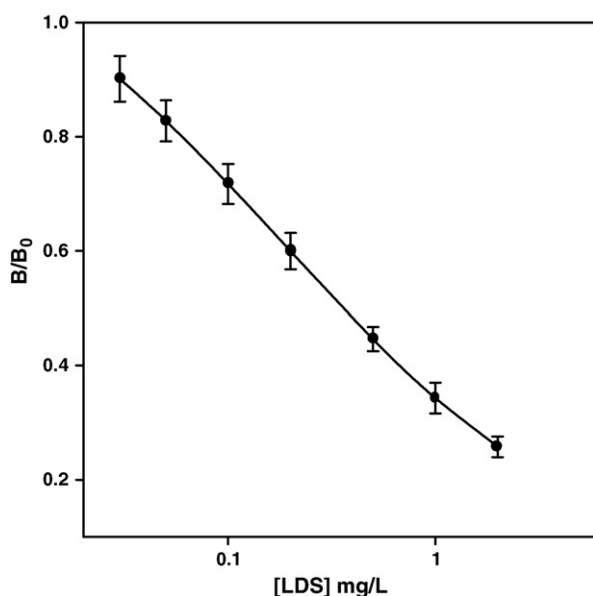


Fig. 5. Calibration curve obtained for LDS. [antibodies] = 220 nM; [tracer] = 71 nM; [phosphate buffer] = 0.01 M; [methanol] = 10%; 30 °C.

Table 1
Analysis of water samples

Sample	Content ^a (ng/mL)	Added (ng/mL)	Found ^a (ng/mL)	Recovery (%)
Waste-water	70 ± 4	10	9 ± 1	94.5
		20	22 ± 2	110.0
		50	49 ± 4	98.0
Ground water	–	10	12 ± 1	119.8
		20	20 ± 2	101.5
		50	40 ± 3	80.8

^a Mean of three determinations ± S.D.

4. Conclusions

From these results, it can be concluded that long-wavelength SF-FPIA is a useful alternative to improve the features of conventional FPIA, which has been shown by its application to the determination of total LASs in water samples. This study shows that the use of long-wavelength dynamic measurements improves the detection limits obtained by this homogeneous immunoassay, reaching similar values to those obtained using the heterogeneous format [15–17]. Also, the use of initial rate measurements, which are obtained in less than 1 s, allows the achievement of a high sample throughput and the application of FPIA to the analysis of water samples.

Acknowledgement

Authors are grateful to the Spanish Ministerio de Ciencia y Tecnología (MCyT) for the financial support (Grant No. BQU2003-03027).

References

- [1] A. Gómez-Hens, M.P. Aguilar-Caballeros, Trends Anal. Chem. 23 (2004) 127.

- [2] A. Durkop, F. Lehmann, O.S. Wolfbeis, *Anal. Bioanal. Chem.* 372 (2002) 688.
- [3] A. Gómez-Hens, M.P. Aguilar-Caballo, *Comb. Chem. High Throughput Screen.* 6 (2003) 177.
- [4] I.C. Consultants Ltd., Final Report on Pollutants in Urban Waste Water and Sewage Sludge, European Communities 2001 p. 6 (<http://europa.eu.int>).
- [5] U. Ceglarek, J. Efer, A. Schreiber, E. Zwanziger, W. Engewald, *Fresenius J. Anal. Chem.* 365 (1999) 674.
- [6] A. Nishigaki, C. Kuroiwa, M. Shibukawa, *Anal. Sci.* 20 (2004) 143.
- [7] L. Lunar, S. Rubio, D. Pérez-Bendito, *J. Chromatogr. A* 1031 (2004) 17.
- [8] J. Riu, E. Martínez, D. Barceló, A. Ginebreda, L.L. Tirapu, *Fresenius J. Anal. Chem.* 371 (2001) 448.
- [9] S. González, M. Petrovic, D. Barceló, *J. Chromatogr. A* 1052 (2004) 111.
- [10] K. Bester, N. Theobald, H.F. Schröder, *Chemosphere* 45 (2001) 817.
- [11] Y. Yamini, S. Borhany, M. Yazdan, *Microchim. Acta* 147 (2004) 45.
- [12] A.F. Lavorante, A. Morales-Rubio, M. De la Guardia, B.F. Reis, *Anal. Bioanal. Chem.* 381 (2005) 1305.
- [13] J.X. Yang, H.W. Gao, Z.J. Hu, M.H. Jiang, *J. AOAC Int.* 88 (2005) 866.
- [14] J. Yakovleva, A. Lobanova, I. Michura, A. Formanovsky, M. Fránek, J. Zeravik, S. Eremin, *Anal. Lett.* 35 (2002) 2279.
- [15] M. Fujita, M. Ike, Y. Goda, S. Fujimoto, Y. Toyoda, K.I. Miyagawa, *Environ. Sci. Technol.* 32 (1998) 1143.
- [16] J. Ramón-Azcón, R. Galve, F. Sánchez-Baeza, M.P. Marco, *Anal. Chem.* 78 (2006) 71.
- [17] M. Fránek, J. Zeravik, S.A. Eremin, J. Yakovleva, M. Badea, A. Danet, C. Nistor, N. Ocio, J. Emnéus, *Fresenius J. Anal. Chem.* 371 (2001) 456.
- [18] M.L. Sánchez-Martínez, M.P. Aguilar-Caballo, S.A. Eremin, A. Gómez-Hens, *Anal. Chim. Acta* 553 (2005) 93.
- [19] H.P.M. de Oliveira, M.H. Gehlen, *J. Braz. Chem. Soc.* 14 (2003) 738.
- [20] A. Loriguillo, M. Silva, D. Pérez-Bendito, *Anal. Chim. Acta* 199 (1987) 29.
- [21] G.L. Long, J.D. Winefordner, *Anal. Chem.* 55 (1983) 712A.

Development and application of a capillary electrophoresis based method for the assessment of monosaccharide in soil using acid hydrolysis

Sérgio M. Santos, Armando C. Duarte, Valdemar I. Esteves*

CESAM & Department of Chemistry, University of Aveiro, Aveiro, Portugal

Received 16 June 2006; received in revised form 27 September 2006; accepted 5 October 2006

Available online 15 November 2006

Abstract

An efficient methodology for the determination of carbohydrate content in soils, employing acid hydrolysis and subsequent capillary electrophoresis analysis (CE), is here described. Polysaccharides present in soil samples were hydrolyzed, at 100 °C during 4 h, to their monosaccharide form, by addition of 2 mol dm⁻³ trifluoroacetic acid (TFA) directly to soil. The resulting monosaccharides were then quantitatively derivatized with 4-aminobenzoic acid ethyl ester, via reductive amination with sodium cyanoborohydride, and separated by CE, coupled to an UV–vis diode array set at 300 nm. Separation electrolyte consisted of 5.0 × 10⁻² mol dm⁻³ sodium tetraborate buffer (pH 10.2) and 6 × 10⁻³ mol dm⁻³ sodium dodecylsulphate. A 78 cm long capillary with an internal and external diameter of 75 and 375 μm, respectively, was used and separation performed at 16 °C, with an applied voltage of 30 kV. Quantification was undertaken using ribose as the internal standard. As an application example, carbohydrate composition (w/w) of a farmyard manure fertilized soil was found to vary between 0.0045 ± 0.0003% (glucose) and 0.0267 ± 0.0002% (arabinose) of the total soil content. Xylose, rhamnose, mannose, fucose and galactose content were also studied in the present work.

© 2006 Elsevier B.V. All rights reserved.

Keywords: CE; MECK; Monosaccharides; Soil

1. Introduction

Soil organic matter (SOM) is a heterogeneous mixture of biogenic materials at various stages of decomposition [1]. Among these, free and bound lipids, carbohydrates and amino acids play an important role, and form the major fraction of analytically recognizable compounds [2]. Carbohydrates account for almost 50% of the plant litter entering the soil system. They are labile compounds, which are usually rapidly metabolized by the soil microbial biomass. Their degradation may be retarded by the presence of the mineral matrix and several studies reported a stabilization of carbohydrates by interaction with soil minerals, as well as their incorporation into stable aggregates [3].

The wide diversity of carbohydrates in nature has led to development of many analytical techniques, though many are not quantitative and prone to interferences. A crucial point in the analysis of soil carbohydrates is hydrolysis. Amelung et al. [4] suggested a procedure employing trifluoroacetic acid (TFA),

instead of the widely used sulphuric acid, because it is volatile and can be easily removed by evaporation. Analytical methods based on gas chromatography (GC), reversed-phase high-performance liquid chromatography (HPLC) or anion-exchange HPLC have been used for the separation and determination of hydrolyzed monosaccharides [5,6]. A methodology employing capillary zone electrophoresis (CZE) has also been efficiently applied to wood-derived neutral and acidic monosaccharide analysis [7]. In comparison to GC and HPLC based techniques, CZE generally offers superior separation efficiency and faster analytical run times. However, CZE has less commercially available detectors and, therefore, UV–vis absorption is by far the most widely used detection method. In order to overcome the high detection limit of carbohydrates at wavelengths above 200 nm, derivatization, with a suitable chromophore has been suggested by Rydlund and Dahlman [7] and Dahlman et al. [8]. These authors described the separation and simultaneous determination of several monosaccharides, using a concentrated borate buffer, but encountered difficulties in the separation of glucose, mannose and arabinose.

The use of surfactants has been extensively used in the separation of neutral substances by CZE [9]. This technique is

* Corresponding author. Tel.: +351 234401408
E-mail address: valdemar@dq.ua.pt (V.I. Esteves).

named micellar electrokinetic chromatography (MECK), and is a hybrid of capillary electrophoresis and partition chromatography. In order to perform MECK, a surfactant solution at concentration higher than its critical micelle concentration must be used as separation electrolyte.

The aim of this study has been the development of a rapid and simple analytical methodology, employing MECK, for the efficient separation and determination of monosaccharides obtained upon hydrolysis of soil carbohydrates. The accomplishment of an efficient separation was based on the use of sodium dodecylsulphate (a surfactant).

2. Experimental procedure

2.1. Reagents

Rhamnose, xylose, ribose, glucose, mannose, arabinose, fucose, galactose, sodium cyanoborohydride and mesityl oxide were from analytical grade and were purchased from Sigma–Aldrich. Organic solvents were of HPLC grade and were purchased, as well as sodium dodecylsulphate (SDS, a surfactant) and 4-aminobenzoic acid ethyl ester (ABEE), from Riedel-de-Haën. All other reagents, either analytical-reagent grade or better, were obtained from Sigma–Aldrich and Panreac. Ultra-pure water for preparation of sample and buffer solution was obtained from a Milli-Q Millipore (Milli-Q plus 185) system.

2.2. Apparatus

The CE system consisted of a Beckman P/ACE MDQ unit, equipped with a photodiode array UV/vis detection system set at 300 nm. A fused-silica capillary with a total length of 78 cm (69.5 cm from sample inlet to detector) and an internal diameter of 75 μm (external diameter of 375 μm) was used. Hydrostatic injections (3 s, 0.5 psi) were used. Separation was performed with an applied voltage of 30 kV, at a controlled temperature of 16 $^{\circ}\text{C}$. Separation electrolyte consisted of a $5.0 \times 10^{-2} \text{ mol dm}^{-3}$ sodium tetraborate (Borax) and

$6 \times 10^{-3} \text{ mol dm}^{-3}$ SDS solution, pH adjusted to 10.2 with concentrated NaOH.

2.3. Acid hydrolysis

Soil sample was collected at 30 cm depth, on a farmyard manure fertilized terrain, and was, prior to use, air-dried and sieved through a 2 mm mesh size sieve. Quantitative aliquots of about 4 g were placed in glass tubes, with a plastic screw cap, and added 4.0 mL of trifluoroacetic acid. The tubes were closed and placed in a heating block set at 100 $^{\circ}\text{C}$, for 4 h [7]. These were then allowed to cool to room temperature, centrifuged for 3 min at 6000 rpm, and the supernatant separated and used within a week. Prior to derivatization, 1 mL of the collected supernatant was supplemented with 0.04 mL of an aqueous solution of ribose $1.0 \times 10^{-2} \text{ mol dm}^{-3}$ (internal standard).

The effects of TFA concentration and agitation in the efficiency of hydrolysis were assessed by using TFA concentrations of 2 and 3 mol dm^{-3} , along with presence and absence of agitation.

2.4. Standard calibration solutions

Six mixed standard calibration solutions were prepared, with concentrations ranging from 5.0×10^{-5} to $1.0 \times 10^{-3} \text{ mol dm}^{-3}$ on all monosaccharides, except ribose. The concentration of ribose was held constant at $4.0 \times 10^{-4} \text{ mol dm}^{-3}$, thus acting as internal standard

2.5. Derivatization of monosaccharides

As schematically shown in Fig. 1, and following the procedure suggested by Dahlman et al. [8], derivatization of monosaccharides with ABEE was performed through a reductive amination, using sodium cyanoborohydride, under slightly acidic conditions. A stock derivatizing solution was prepared by dissolving ABEE (10 mg/mL) and acetic acid (100 mg/mL) in methanol. Prior to derivatization procedure, 10 mg of sodium cyanoborohydride were added to 1 mL of stock solution, thus

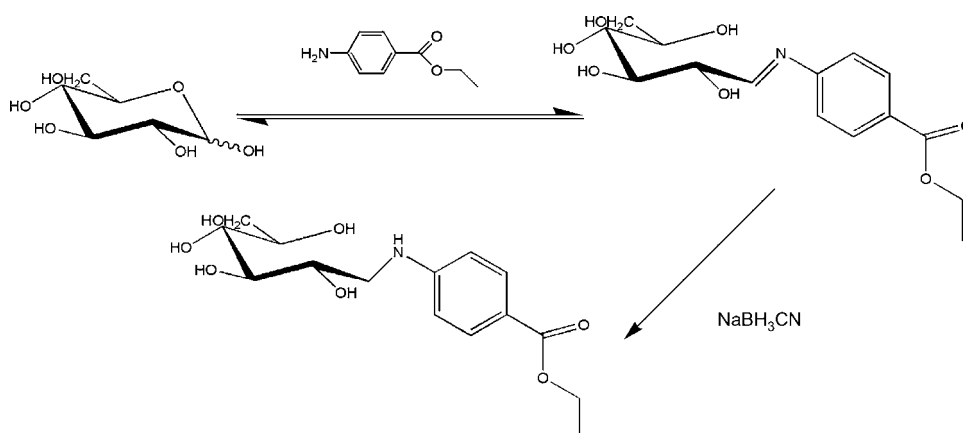


Fig. 1. Schematics of the derivatization reaction of glucose with 4-aminobenzoic acid ethyl ester (ABEE).

obtaining derivatization reagent (DR). A 500 μL DR solution aliquot was added to 500 μL of the supplemented acidic-hydrolysate/standard-calibration-solution, in a glass tube with a plastic screw cap. The cap was screwed on and the tube placed in a heating block set at 80 $^{\circ}\text{C}$, for 1 h. After heating, the tube was removed. Five hundred microliter of $5.0 \times 10^{-2} \text{ mol dm}^{-3}$ borax solution (pH adjusted to 10.2 with concentrated NaOH) was immediately added, and the content was vigorously shaken, in order to precipitate part of the excess of ABEE. The resulting suspension was allowed to cool to room temperature and the precipitate was removed using a 0.22 μm membrane filter (Millipore). The resulting clear solution was then analyzed by CZE within 48 h, thus minimizing degradation of the derivatized monosaccharides.

3. Results and discussion

3.1. Capillary zone electrophoresis—electrophoretic mobilities

During experimental development of the present CZE based method (employing $5.0 \times 10^{-2} \text{ mol dm}^{-3}$ borax electrolyte), peak resolution was found to be very sensitive upon small variations on instrumental conditions. Small variations (about 2 kV) in the applied voltage, as well as in the separation temperature (1 $^{\circ}\text{C}$), produced sudden peak overlap, which is highly undesirable in an analytical methodology. The addition of the surfactant SDS, to the separation electrolyte, revealed to be an appropriate way to overcome peak overlapping and, consequently, allowed the increase of the applied voltage (from 20 to 30 kV) causing a reduction in migration times. A decrease of the separation temperature (from 25 to 16 $^{\circ}\text{C}$) was necessary to conveniently resolve mannose's and arabinose's peaks. The influence of SDS concentration, in the separation efficiency was then evaluated. SDS concentrations ranging from 4×10^{-3} to $20 \times 10^{-3} \text{ mol dm}^{-3}$ (4, 5, 6, 7, 8, 10 and $20 \times 10^{-3} \text{ mol dm}^{-3}$) were tested. The electrophoretic mobilities of monosaccharide derivates, ABEE and electroosmotic flow (EOF) were calculated

at each of the studied SDS concentrations. The determination of EOF mobility was performed using mesityl oxide as neutral marker. The following expressions [10] were used to calculate effective electrophoretic mobilities of electroosmotic flow (1) and of derivatized monosaccharides (2):

$$\mu_{\text{eof}} = L_d \times L_t \times (V \times t_{\text{eo}})^{-1} \quad (1)$$

$$\mu_{\text{ep},i} = \mu_{\text{obs},i} - \mu_{\text{eof}} = L_d \times L_t \times V^{-1} \times (t_{\text{m},i}^{-1} - t_{\text{eo}}^{-1}) \quad (2)$$

where μ_{eof} is the EOF mobility; $\mu_{\text{ep},i}$ and $\mu_{\text{obs},i}$ the effective electrophoretic mobility and observed mobility of analyte i , respectively; L_t and L_d the total length and length from sample inlet to detector, respectively; V the applied voltage; $t_{\text{m},i}$ and t_{eo} are the migration time of analyte i and of EOF, respectively.

The obtained results are depicted in Fig. 2. Identical mobility dependence on SDS concentration was observed for all derivatized monosaccharides: low dependence was observed on concentrations up to $6 \times 10^{-3} \text{ mol dm}^{-3}$; however, with higher concentrations, mobilities increased and, at $20 \times 10^{-3} \text{ mol dm}^{-3}$, became almost 1.5 times higher than at $4 \times 10^{-3} \text{ mol dm}^{-3}$. Ideal surfactant concentration was found to be $6 \times 10^{-3} \text{ mol dm}^{-3}$ because mobilities associated to mannose and arabinose derivates differed more than at any other concentrations (Fig. 2), and, consequently, differences in migration times were bigger. On the other hand, for SDS concentrations above $6 \times 10^{-3} \text{ mol dm}^{-3}$, EOF mobility was strongly and inversely correlated to the surfactant concentration, as shown in Fig. 2. One of the main advantages for the use of SDS was its capacity to highly influence ABEE mobility and, consequently, its migration time, thus avoiding any ABEE peak overlap due to excess of derivatizing reagent. The comparison of Fig. 3 with Fig. 4 shows how the absence of SDS can produce a high degree of peak overlapping and how the increasing concentration of the surfactant can cause an important change of ABEE peak position. A typical electropherogram, for a mixture standard solution of concentration $8.0 \times 10^{-4} \text{ mol dm}^{-3}$, obtained with optimal instrumental conditions (30 kV, 16 $^{\circ}\text{C}$, $6 \times 10^{-3} \text{ mol dm}^{-3}$ SDS), is shown in Fig. 5 where it can be

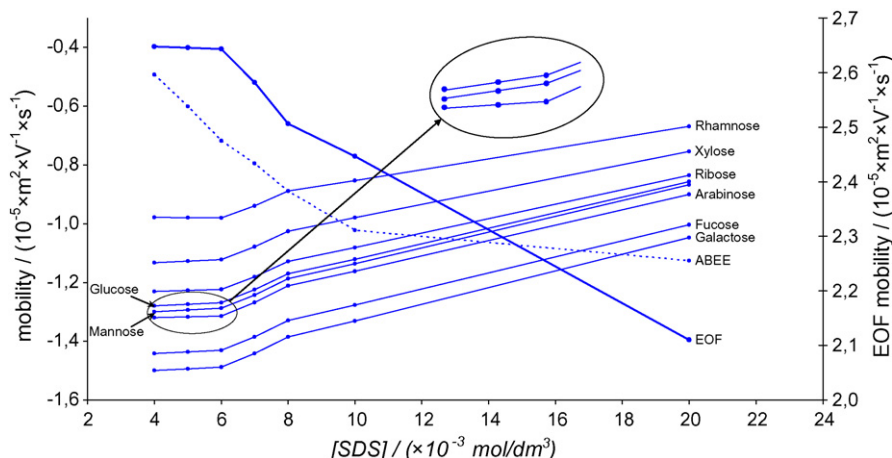


Fig. 2. Electrophoretic mobilities for derivatizing reagent (ABEE, dotted line), monosaccharide derivates (thin lines) and electroosmotic flow (thick line) at different SDS concentrations. Separation was performed with an applied voltage of 30 kV, at 16 $^{\circ}\text{C}$.

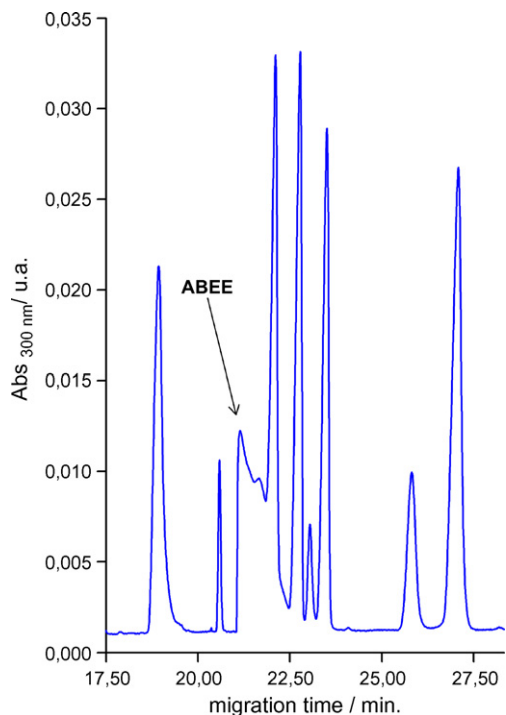


Fig. 3. General aspect of electropherograms obtained without SDS showing overlap of ABEE peak. Separation conditions as indicated in Fig. 2.

seen that all monosaccharide derivatives were appropriately resolved.

3.1.1. Critical micellar concentration for SDS

According to Nakamura et al. [9], below the critical micellar concentration (CMC), a neutral electroosmosis marker (mesityl oxide) is thought theoretically to migrate on the EOF generated

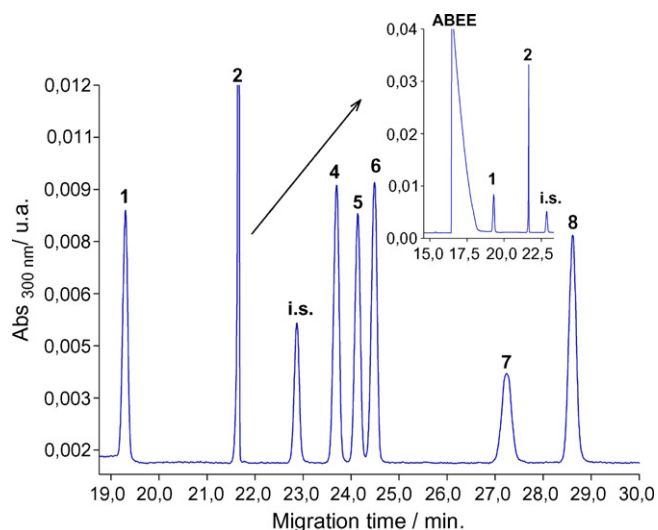


Fig. 5. Typical electropherogram obtained with optimized separation conditions: 30 kV, 16 °C, 6×10^{-3} mol dm $^{-3}$ SDS. Peak identification: (1) rhamnose, (2) xylose, (i.s.) ribose (internal standard), (4) glucose, (5) mannose, (6) arabinose, (7) fucose and (8) galactose. All monosaccharides with concentration 8.0×10^{-4} mol dm $^{-3}$ except ribose (4.0×10^{-4} mol dm $^{-3}$).

by the ξ -potential due to the ionized silanol groups at the inner capillary wall. Above CMC, the EOF mobility should decrease with increasing surfactant concentration because neutral compounds begin to be incorporated into the surfactant micelles. The plot of electroosmotic mobility as function of SDS concentration will produce two straight lines whose interception corresponds to the CMC value [9]. Thus, based on the obtained results, the CMC for SDS, under the described conditions, is set at 6×10^{-3} mol dm $^{-3}$, because of the most abrupt change in the electroosmotic mobility found at that concentration. The

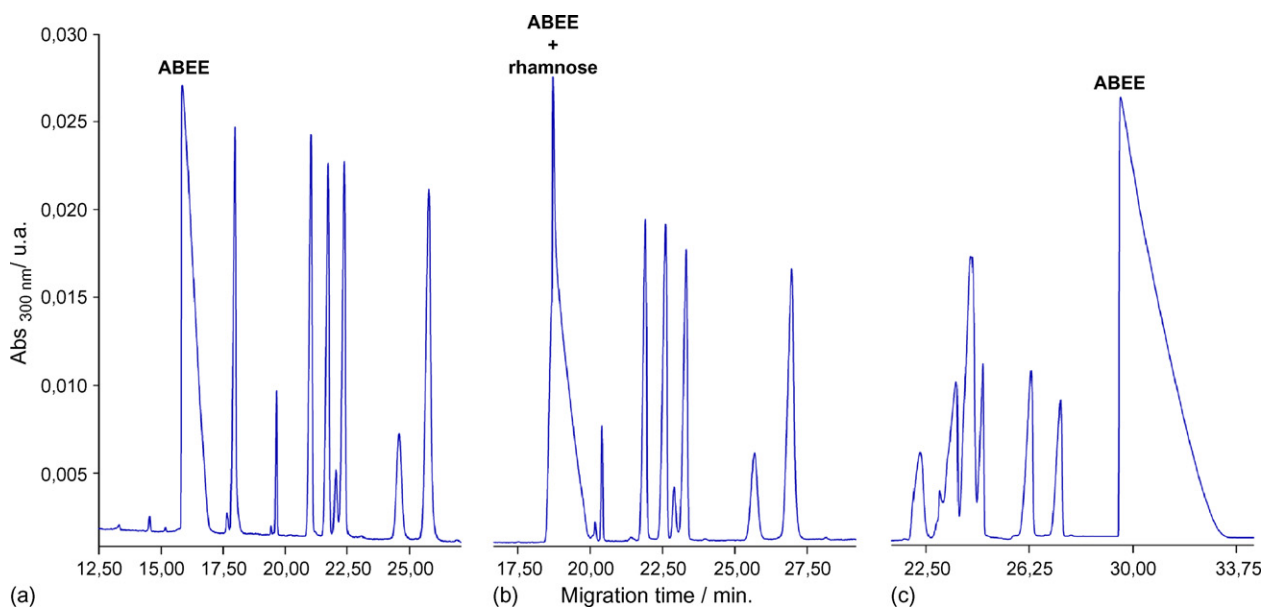


Fig. 4. General aspect of electropherograms obtained with different concentration of SDS: (a) 4×10^{-3} mol dm $^{-3}$, (b) 8×10^{-3} mol dm $^{-3}$ and (c) 20×10^{-3} mol dm $^{-3}$. A clear change in overall peak positioning is observed for ABEE, with increasing SDS concentration. Separation conditions as indicated in Fig. 2.

Table 1
Linear regression coefficients and LOD for the eight monosaccharides used in the calibration of the CZE analysis

Monosaccharide	Quantification	Linear regression ($y = (a \pm \sigma_a) + (b \pm \sigma_b)x$)		
	Limit of detection (mol dm^{-3})	Equation parameters		Correlation coefficient (r)
		$(a \pm \sigma_a)$	$(b \pm \sigma_b)$	
Rhamnose	8.09×10^{-5}	$-0.09_0 \pm 0.04_4$	$0.89_6 \pm 0.02_8$	0.9980
Xylose	5.95×10^{-5}	$-0.09_1 \pm 0.04_2$	$1.18_3 \pm 0.02_8$	0.9988
Glucose	8.28×10^{-5}	$-0.14_8 \pm 0.05_6$	$1.13_1 \pm 0.03_7$	0.9979
Mannose	6.89×10^{-5}	$-0.09_9 \pm 0.04_4$	$1.06_9 \pm 0.03_2$	0.9982
Arabinose	9.17×10^{-5}	$-0.14_1 \pm 0.06_5$	$1.18_0 \pm 0.04_4$	0.9973
Fucose	5.14×10^{-5}	$-0.06_7 \pm 0.03_3$	$1.05_6 \pm 0.03_4$	0.9979
Galactose	8.25×10^{-5}	$-0.11_8 \pm 0.06_5$	$1.32_2 \pm 0.04_6$	0.9976

(Separation conditions: 30 kV, 16 °C, 6×10^{-3} mol dm⁻³ SDS).

obtained value is in agreement with that in ref. [11]. However, a second change, though less abrupt, in electroosmotic mobility is found at SDS concentration of 8×10^{-3} mol dm⁻³. This may be due to a change in micelle shape, size and conformation [12]. A similar behaviour in mobilities is observed for monosaccharide derivatives.

3.2. Calibration curves

Calibration curves for all derivatized monosaccharides, except ribose, were established based upon five injection replicates of each standard solution. The internal standard method was applied, using ribose as the internal standard. Linear calibration curves, and respective parameters, were obtained for all derivatives by means of a least-squares linear regression [13]. In Table 1, regression equation parameters (of form $y = a + bx$) and regression coefficients (r) for each monosaccharide derivative are presented, together with the limit of detection (LOD), which was calculated according to

$$\text{LOD} = [\text{IS}] \times 3\sigma_{x/y} \times b^{-1} \quad (3)$$

where b and $\sigma_{x/y}$ stand for the slope and the standard deviation associated to the regression, respectively [13]. Fucose was found to be the monosaccharide derivative with the lowest detection limit (5.14×10^{-5} mol dm⁻³), while arabinose had the highest (9.17×10^{-5} mol dm⁻³). Correlation coefficients (r) for all derivatives were above 0.9970. All calibration curves were found to be linear over the concentration range of the standard solutions (5.0×10^{-5} – 1.0×10^{-3} mol dm⁻³). As shown in Table 2, the

Table 2
Monosaccharide derivatives characteristic migration times

Monosaccharide	t_m mean (min)	Repeatability R.S.D. (%)
Rhamnose	19.25	0.86
Xylose	21.73	0.57
Ribose	22.94	0.57
Glucose	23.62	0.49
Mannose	23.90	0.45
Arabinose	24.34	0.52
Fucose	27.26	0.46
Galactose	28.93	0.45

t_m , migration time; R.S.D., relative standard deviation ($n = 12$).

relative standard deviation of monosaccharide-derivates characteristic migration times were adequately low (always below 1%) which, in a CE analysis, is highly desirable. For this results could be contributing the use of a fresh buffer for each run of analysis.

3.3. MECK analysis

3.3.1. Study of hydrolysis conditions

The effects of TFA concentration and agitation in the efficiency of the hydrolysis were studied. TFA concentrations of 2 and 3 mol dm⁻³, along with presence and absence of agitation, were employed. The obtained results are summarized in Fig. 6. The influence of agitation, while using 2 mol dm⁻³ TFA, was found to produce no significant differences in the percentage of obtained monosaccharides. The obtained composition, for all referred analytes, under the described conditions, varied between $0.0047 \pm 0.0002\%$ (glucose) and $0.026 \pm 0.002\%$ (arabinose). Identical results were obtained when absence of agitation, coupled to the use of 3 mol dm⁻³ TFA, was applied. In such case, hydrolysis yielded values that ranged from $0.0045 \pm 0.0003\%$ (glucose) to $0.0267 \pm 0.0002\%$ (arabinose). However, the application of agitation, coupled to 3 mol dm⁻³ TFA, produced different results: for monosaccharides present in small amounts, the accomplished results were similar to those previously obtained ($\approx 0.0055\%$ (rhamnose), $\approx 0.0050\%$ (glucose) and $\approx 0.0090\%$ (mannose)); for monosaccharides present in higher amounts (xylose, arabinose and galactose), hydrolysis yielded lower results than those obtained without agitation, or when 2 mol dm⁻³ TFA was employed. In such case, the excess of TFA appears to be participating in degradation reactions of the hydrolyzed monosaccharides; agitation probably accelerates these reactions because it provides higher dispersion of monosaccharides within the acidic medium. Facing the obtained results, the use of agitation, or of high concentrations of TFA, does not produce better results than those obtained by simple use of 2 mol dm⁻³ TFA, with no agitation. The use of 3 mol dm⁻³ TFA and agitation can degrade some of the monosaccharides.

3.3.2. MECK analysis of hydrolyzed soil monosaccharides

A typical MECK analysis of a soil hydrolysate obtained with 2 mol dm⁻³ TFA and no agitation is shown in Fig. 7. The

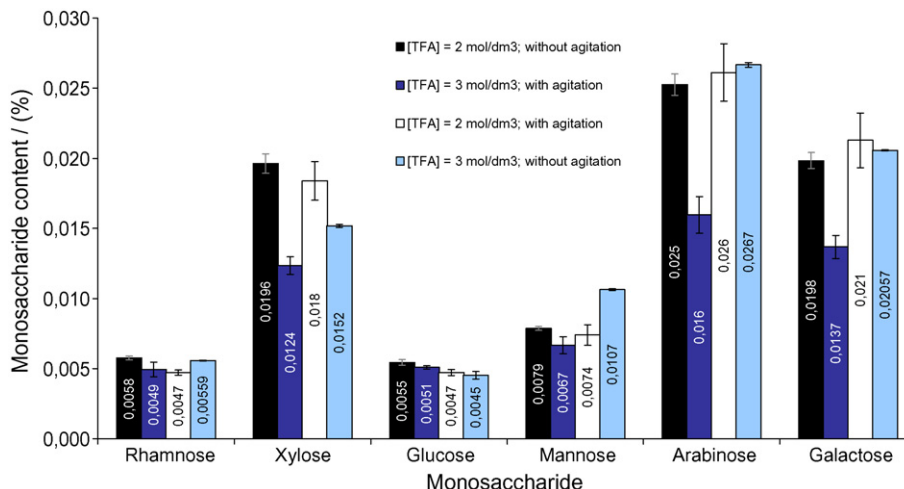


Fig. 6. Monosaccharide content in soil samples, subjected to different hydrolysis conditions. Results are the mean of three replicates and error bars correspond to the associated standard deviation.

monosaccharides present in the electropherograms were identified by both migration times and comparison of absorption spectra with that of derivatized reference compounds. The electropherograms (as shown in Fig. 7) contained a large peak, corresponding to the excess of derivatizing reagent (ABEE), and seven others, corresponding to seven of the eight studied monosaccharide derivatives; fucose was undetected, for it was probably below LOD ($5.14 \times 10^{-5} \text{ mol dm}^{-3}$), or even absent, in all soil hydrolysates.

MECK analysis of sample hydrolysates revealed a high content of xylose, arabinose and galactose, which probably originate from the presence of hemicelluloses, such as arabinoxylans and galactomannans in soil samples [14]. On the other hand, rhamnose, glucose and mannose were found to be in low contents, and probably originate from pectins, celluloses and hemicelluloses [14].

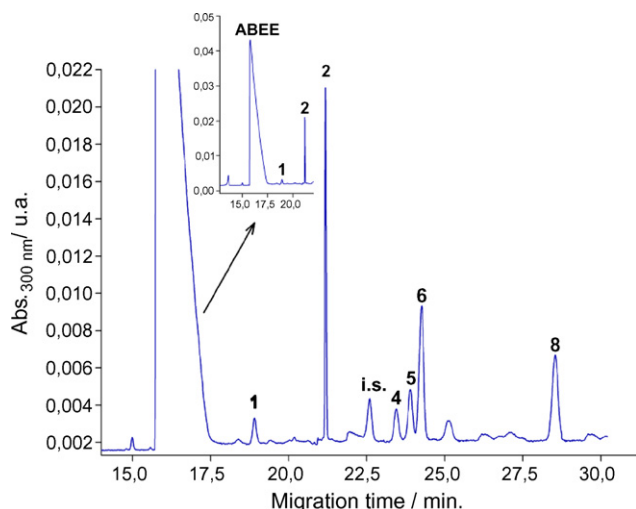


Fig. 7. Typical electropherogram obtained from a soil hydrolysate analysis. Separation conditions and peak identification as indicated in Fig. 5.

4. Conclusions

A simple and rapid analytical procedure based on capillary electrophoresis, for the hydrolysis, identification and quantification of eight monosaccharides derived from a farmyard manure fertilized soil sample has been here described. This procedure employed a 2 mol dm^{-3} TFA acid hydrolysis of carbohydrates, present in samples, in order to obtain the correspondent monosaccharides. The effect of TFA concentration on hydrolysis yield was found to be degradative when both agitation and high acid concentration were simultaneously applied. Monosaccharides were then tagged with 4-aminobenzoic acid ethyl ester, via reductive amination to enhance UV-vis detection, and separated by CZE using a $5.0 \times 10^{-2} \text{ mol dm}^{-3}$ sodium tetraborate and $6 \times 10^{-3} \text{ mol dm}^{-3}$ SDS electrolyte (pH 10.2). All monosaccharides were efficiently separated, with minimal detectable concentrations above $5.14 \times 10^{-5} \text{ mol dm}^{-3}$. The use of SDS allowed efficient separation, as well as avoided peak overlay due to excess of derivatizing reagent, overrunning the separation problems encountered by Rydlund and Dahlman [7] and Dahlman et al. [8]. Soil hydrolysates were found to contain quantifiable amounts of rhamnose, xylose, glucose, mannose, arabinose and galactose. The described procedure can be used as a useful tool for the characterization of soil monosaccharides.

Acknowledgement

The authors wish to acknowledge the financial support from FCT (Fundação para a Ciência e Tecnologia) research project POCTI/CTA/48059/2002.

References

- [1] D.A.N. Ussiri, C.E. Johnson, *Geoderma* 111 (2003) 123–149.
- [2] B. Allard, *Geoderma* 130 (1–2) (2006) 77–96.
- [3] I. Kögel-Knabner, *Soil Biol. Biochem.* 34 (2002) 139–162.

- [4] W. Amelung, M.V. Cheshire, G. Guggenberger, *Soil Biol. Biochem.* 28 (12) (1996) 1631–1639.
- [5] D.A. Martens, K.L. Loeffelmann, *Soil Biol. Biochem.* 34 (2002) 1393–1399.
- [6] C. Rumpel, M. Dignac, *Soil Biol. Biochem.* 38 (6) (2006) 1478–1481.
- [7] A. Rydlund, O. Dahlman, *J. Chromatogr. A* 738 (1996) 129–140.
- [8] O. Dahlman, A. Jacobs, A. Liljenberg, A.I. Olsson, *J. Chromatogr. A* 891 (2000) 157–174.
- [9] H. Nakamura, A. Sano, K. Matsuura, *Analytical Sciences* 14 (1998) 379–382.
- [10] M. Wang, F. Qu, X. Shan, J. Lin, *J. Chromatogr. A* 989 (2003) 285–292.
- [11] C. Lin, I. Fang, Y. Deng, W. Liao, H. Cheng, W. Huang, *J. Chromatogr. A* 1051 (2004) 85–94.
- [12] R. Kuhn, S. Hoffstetter-Kuhn, *Capillary Electrophoresis: Principles and Practice*, Springer-Verlag, Berlin, Germany, 1993, pp. 191–198.
- [13] J.N. Miller, J.C. Miller, *Statistics and Chemometrics for Analytical Chemistry*, fourth ed., Prentice Hall, Dorset, England, 2000, pp. 107–123.
- [14] H.-D. Belitz, W. Grosch, P. Schieberle, *Food Chemistry*, third ed., Springer-Verlag, Berlin, Germany, 2004, pp. 245–339.

Voltammetric determination of food colorants using a polyallylamine modified tubular electrode in a multicommutated flow system

M. Luísa S. Silva^a, M. Beatriz Q. Garcia^{a,*}, José L.F.C. Lima^a, E. Barrado^b

^a *Requimte, Departamento de Química-Física, Faculdade de Farmácia da Universidade do Porto, Rua Aníbal Cunha, 164, 4099-030 Porto, Portugal*

^b *Departamento de Química Analítica, Facultad de Ciencias de la Universidad de Valladolid, Prado de la Magdalena s/n, 47005 Valladolid, Spain*

Received 31 July 2006; received in revised form 17 October 2006; accepted 19 October 2006

Available online 28 November 2006

Abstract

This work describes the construction of a polyallylamine modified tubular glassy carbon electrode and its application in the electroreduction of food azo colorants (tartrazine, sunset yellow and allura red) by square wave voltammetry. The electrode modification prevented the surface fouling and, simultaneously, enhanced the analytical signal intensity. The developed unit was coupled to a multicommutated flow system which, given the complexity of samples, was designed to allow the implementation of the standard additions method in an automatic way, using only one standard solution.

The described method presented a linear range up to about $2.0 \times 10^{-4} \text{ mol l}^{-1}$ for the referred colorants, with a detection limit of $1.8 \times 10^{-6} \text{ mol l}^{-1}$ for tartrazine, $3.5 \times 10^{-6} \text{ mol l}^{-1}$ for sunset yellow and $1.4 \times 10^{-6} \text{ mol l}^{-1}$ for allura red. The method was applied in the analysis of these colorants in several food samples, and no statistically significant difference between the results obtained by the proposed and the comparative method (HPLC) was found, at a 95% confidence level. Repeatability in the analysis of samples (expressed in R.S.D.) was about 3% ($n = 10$).

© 2006 Elsevier B.V. All rights reserved.

Keywords: Modified tubular electrode; Voltammetry; Multicommutation; Polyallylamine; Tartrazine; Sunset yellow; Allura red; Food colorants

1. Introduction

The use of colorants as food additives has been exploited by food industry with the aim of enhancing the aesthetic appeal of foodstuffs to the consumer. Azo colorants, such as tartrazine (E102), sunset yellow (E110) and allura red (E129), constitute one of the major synthetic colorant groups, used commercially in food, drinks, medicines and cosmetics. Its vast application is due to an inexpensive production and to a large colour spectrum that can be obtained, when compared with natural colorants [1].

Some colorants can trigger adverse effects, namely tartrazine, which can cause the appearance of allergies and asthma [2] and childhood hyperactivity [3]. The colorants allowed to be used in food products and the authorized maximum levels are regulated by the Portuguese [4] and European [5] legislation.

Quantification of colorants in food products prompted the need for the development of analytical methodologies, namely

spectrophotometric [6–12] and chromatographic methods [13]. Voltammetric methods were also reported [1,2,14–19], presenting high sensitivity, simplicity and low cost. However, all of them use mercury electrodes, whose toxicity justifies the search for alternative electrode materials. Besides, the majority of the referred methodologies use the standard additions method for sample analysis, which is carried out in a non-automatic way, increasing the slowness of measurements and demanding specialized operators.

In this work, the construction, evaluation and application of a polyallylamine modified tubular glassy carbon electrode is proposed, as an alternative to the use of mercury electrode, for the determination of food colorants, which is based on the electroreduction of the azo dyes. For the first time, the modification of a tubular glassy carbon electrode with a polyelectrolyte coating is described, taking advantage of the ion-exchange and permselectivity characteristics of the polyallylamine film in relation to negatively charged species.

The developed unit was coupled to a multicommutated flow system [20], which was designed to enable the implementation, in an automatic way, of the standard additions method, considering the complexity of samples.

* Corresponding author. Tel.: +351 222078966; fax: +351 222004427.
E-mail address: bquinaz@ff.up.pt (M.B.Q. Garcia).

2. Experimental

2.1. Reagents and solutions

Reagents of p.a. quality were used, without having been subjected to any additional purification. In the preparation of solutions, water purified by the Millipore Milli Q system (conductivity $<0.1 \mu\text{S cm}^{-1}$) was used.

As supporting electrolyte and, simultaneously, carrier solution in the flow system, a hydrochloric acid solution 0.5 mol l^{-1} , prepared by dilution of concentrated HCl (Merck), was used.

Stock solutions of tartrazine (Sigma), sunset yellow (Aldrich) and allura red (Aldrich) $1.0 \times 10^{-3} \text{ mol l}^{-1}$ were prepared by weighing and dissolution of the solid colorants in HCl 0.5 mol l^{-1} . Working solutions were prepared by dilution of the respective stock solutions in HCl 0.5 mol l^{-1} .

For the working electrode surface coating, a polyallylamine hydrochloride solution 15.0 g l^{-1} , prepared by weighing and dissolution of the correspondent quantity of the polyelectrolyte (Aldrich), was used.

Solid samples were dissolved in HCl 0.5 mol l^{-1} warmed to about 70°C , centrifuged for 10 min at 3000 rpm and filtered. Liquid samples were diluted in HCl 0.5 mol l^{-1} and filtered.

2.2. Equipment

In the developed multicommutated flow system (Fig. 1A) solutions and samples were aspirated by an automatic burette (Crison model Micro BU 2031) equipped with a 10 ml syringe. To control the selection and direction of solutions and samples inside the manifold four 3-way solenoid valves (161 T031, NRResearch) were used. A homemade power driver, based on an

integrated ULN 2003 circuit, was used to operate solenoid valves [21]. Control of the analytical system was made through an interface card (PC-LABCard model PCL-711B, Advantech) and a microcomputer. The software was developed in QuickBasic Version 4.5 (Microsoft) and allowed to control the functioning of the burette and the solenoid valves. Connection between the components of the flow system was made with Teflon tubes (Omnifit), of 0.8 mm inner diameter. Voltammetric measurements were carried out in an Autolab electrochemical system (Eco Chemie model PGSTAT 10) and data acquisition was accomplished through GPES software (Version 4.6).

Scanning electron microscopy (SEM) micrographs were obtained using an electron microscope JEOL, model JSM-35C.

To perform sample analysis by the comparative method, a chromatograph Varian, model 9012, with UV-Vis detector, model 9050, was used. The HPLC system was equipped with a column C18 ($150 \text{ mm} \times 4.6 \text{ mm i.d.}$ and particle size $5 \mu\text{m}$) Waters Spherisorb ODS2.

2.3. Voltammetric detector with a polyallylamine modified tubular electrode

Usually, in multicommutated flow systems, solutions are aspirated instead of being propelled, which simplifies the flow manifolds since, in this case, only one propulsion device is needed for the driving of all solutions. As a consequence, flow systems present an inner pressure lower than the atmospheric pressure, demanding that all manifold components, including the detector, are tightly fixed, in order to avoid air entrance. The construction of the voltammetric detector was based in a tubular detector with modified electrodes recently described [22], which demonstrated to have the required robustness to be used in flow systems in which solutions are aspirated.

The detector, of tubular configuration (Fig. 1B), was constituted by a central Perspex support, which encased the working and auxiliary electrodes, both of glassy carbon, with 2.0 mm thickness and a central orifice of 0.8 mm diameter (this value was diminished after the surface coating with polyallylamine solution), being firmly fixed to the central support by two rubber disks, also perforated in the centre. A Metrohm (Ag/AgCl-KCl 3.0 mol l^{-1} , model 6.0727.000) electrode was used as the reference electrode, fixed by a threaded screw to the Perspex support. Electric contact with working and auxiliary electrodes was established through two metallic contacts threaded into the Perspex support. The tubular detector had an inner volume of $15.0 \mu\text{l}$ (volume between working and auxiliary electrodes).

For cleaning and modification (coating of the active surface) of the working electrode, this was withdrawn from the tubular detector and was firstly polished, using a cotton thread soaked in alumina aqueous slurry of $0.075 \mu\text{m}$ and washed with deionised water. The surface coating, by droplet evaporation method, consisted in the deposition of $20 \mu\text{l}$ of polyallylamine hydrochloride solution 15.0 g l^{-1} directly into the central orifice of the electrode. It was kept at 70°C , and was overturned several times until the complete evaporation of the solvent (about 15 min), as a way to assure uniformity of the deposit on the cylindrical wall of the electrode.

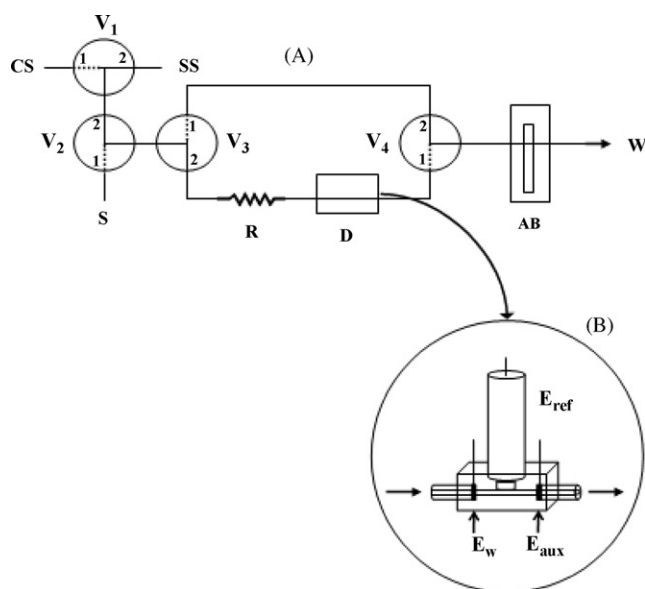


Fig. 1. (A) Multicommutated flow system for food colorants determination: V_1 , V_2 , V_3 and V_4 , three-way solenoid valves; CS, carrier solution ($\text{HCl } 0.5 \text{ mol l}^{-1}$); SS, standard solution $1 \times 10^{-4} \text{ mol l}^{-1}$; S, sample; R, reactor; D, tubular voltammetric detector; AB, automatic burette equipped with a 10 ml syringe; W, waste. (B) Schematic representation of the tubular detector: E_{ref} , reference electrode; E_w , polyallylamine modified working electrode; E_{aux} , auxiliary electrode.

The evaluation of the modified electrode behaviour showed that it was necessary to repeat the cleaning and coating process after 60 determinations carried out with the same polyallylamine film.

3. Results and discussion

3.1. Characterization and behaviour of the polyallylamine modified tubular electrode

The electrochemical behaviour of synthetic azo dyes has been widely studied [23–26] and their reduction mechanism postulates a step-wise breakage of the molecule, in acidic media, involving four electrons and four protons.

The behaviour of the polyallylamine modified tubular electrode was studied relatively to the reduction of tartrazine, sunset yellow and allura red, and the optimization of the parameters concerning the modification procedure was performed with the purpose of obtaining the maximum sensitivity and reproducibility of the measurements. All experiments were carried out with solutions of each colorant with a concentration of $1.0 \times 10^{-4} \text{ mol l}^{-1}$, aspirating a volume of $150 \mu\text{l}$, which was transported towards the detector by the carrier solution, with a flow rate of 0.96 ml min^{-1} . Voltammetric measurements were made in stopped flow, when the sample plug reached the detector and the analytical signal (cathodic peak current intensity— I_p) was the highest.

The effect of the supporting electrolyte composition, used in the preparation of solutions and as carrier solution in the flow system, was studied, being tested hydrochloric acid solution 0.5 mol l^{-1} , phosphoric acid and sodium di-hydrogen phosphate buffer solution 0.5 mol l^{-1} (pH 1.8), acetic acid and sodium acetate buffer solution 0.5 mol l^{-1} (pH 4.5) and sodium carbonate and sodium hydrogen carbonate buffer solution 0.5 mol l^{-1} (pH 9.9). Solutions of each colorant were prepared in the referred supporting electrolytes and analyzed. The results indicated that the I_p value increased with the decrease of the pH, so the hydrochloric acid solution was chosen for the following experiments.

To evaluate the effect of the electrode modification on the I_p of the colorants, the electrode surface was coated with a polyallylamine solution with concentrations between 0.1 and 1.0 g l^{-1} and the obtained I_p values were compared. It was shown that the I_p value was higher for the coated electrode, when compared to the bare electrode, and the increase in I_p was in direct proportion to the polyallylamine concentration in the film. The enhancement in the I_p value was due to a selective preconcentration of the colorants by the polyallylamine film. In acidic conditions, this cationic polyelectrolyte becomes highly positively charged [27] binding easily to the anionic dyes via an ion-exchange process.

The concentration of the polyallylamine solution used on the electrode coating, which influenced the film thickness, was optimized by coating the electrode surface with polyelectrolyte solution concentrations between 1.0 and 35.0 g l^{-1} , depositing on the electrode cavity a volume of $20 \mu\text{l}$. For all colorants, I_p increased with increasing polyallylamine concentrations, up to

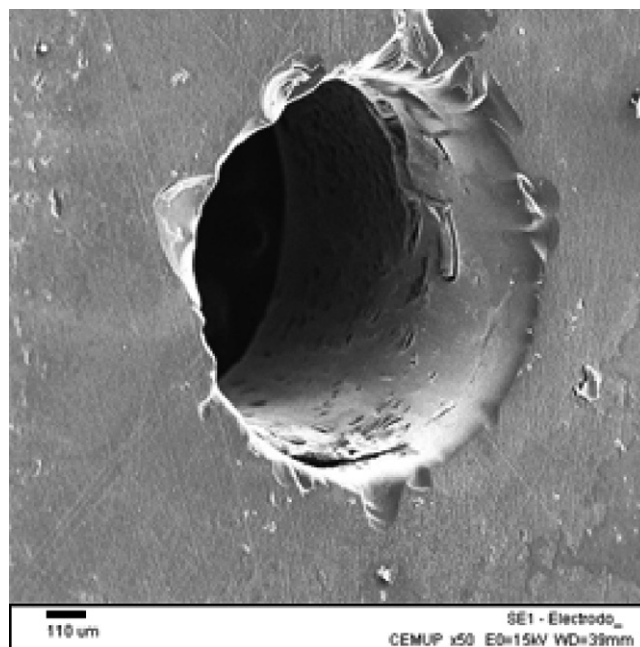


Fig. 2. SEM micrograph of the polyallylamine film on the tubular working electrode (polyallylamine solution 15 g l^{-1} , $20 \mu\text{l}$), magnification $50\times$.

15.0 g l^{-1} , and diminished for higher concentrations. The initial increase of the analytical signal was due to an increase in the ion-exchange sites between the polyelectrolyte and the colorants. However, for more concentrated polyallylamine solutions, the obtained films were thicker, which hindered the diffusion of the colorants towards the glassy carbon surface, decreasing I_p .

The morphology of the film was examined in detail in SEM micrographs (Fig. 2), and it enabled to observe the uniformity and adherence of the film to the glassy carbon support. It was also possible to verify that the film thickness was about $6 \mu\text{m}$.

To evaluate the reproducibility of the modification procedure, which is reflected in the reproducibility of I_p , three electrodes were modified in 2 different days and used to analyse colorant solutions. It was shown that, for each modified electrode, I_p values obtained in different days presented a R.S.D. of about 3%, evidencing the reproducibility of the modification procedure.

The stability of the modified electrode was studied by carrying out consecutive measurements of each colorant solution and monitoring the repeatability of I_p values, whose R.S.D. was used to check the film conditions. I_p values presented good repeatability up to 60 determinations, with a R.S.D. of about 2%, and with a clean baseline. Beyond that number of measurements, the analytical signal became less repetitive; therefore the electrode was withdrawn from the detector and submitted to a polishing to remove the film, followed by a new coating.

The square wave voltammetry parameters were optimized, keeping constant the step potential and amplitude (2.5 and 50 mV, respectively) and shifting the frequency value between 10 and 80 Hz. I_p increased for all colorants with the increase of frequency, throughout the tested interval. It was chosen the value of 50 Hz, for which the best relation between I_p and peak width was obtained. Afterwards, step potential value was changed between 2 and 6 mV, and I_p increased with the increase

in step potential, stabilizing for values higher than 4 mV, being this value selected for the following experiments. Finally, amplitude values were varied between 20 and 100 mV. It was shown that I_p increased almost linearly with the increase in amplitude up to 80 mV, becoming constant beyond that value, which was chosen for the next trials.

3.2. Optimization of the multicommutated flow system parameters

Considering the highly complex matrix of the samples intended to be analysed, the multicommutated flow system was designed to enable the implementation of standard additions method, in an automatic way and with continuous flow.

In the automatic system based on the multicommutation concept (Fig. 1A), valves V_1 and V_2 allowed insertion of carrier solution (CS), standard solution (SS) or sample (S) depending on each valve status. Valves V_3 and V_4 were used to define two parallel analytical pathways, one of them including the reactor (R) and the detector (D) and the other one, meant to be used for sample exchange. The existence of the parallel pathway allowed to minimize the contact time between samples and working electrode, reducing its surface fouling and, additionally, it enabled a faster sample exchange, increasing the sampling rate. The automatic burette (AB) with the syringe was placed at the end of the analytical manifold, after the detector, and was used to aspirate all the solutions.

The strategy used to insert sample and standard additions was based on binary sampling, which consisted in the alternate insertion of sample (V_2 in position 1), carrier solution (V_1 in position 1 and V_2 in position 2) and/or standard solution (V_1 in position 2 and V_2 in position 2) plugs (Fig. 3). The sample volume aspirated to the system was controlled by flow rate and by sampling time, defined as the time interval during which valve V_2 remained in position 1. By using binary sampling to insert the sample, the sampling time was defined as the sum of all time intervals during which valve V_2 remained in position 1. Insertion by binary sampling allowed a better homogenization between sample, carrier and standard solution plugs.

The developed automatic system required only one colorant standard solution to carry out standard additions, which was an advantage considering the time needed to prepare the solutions. The standard additions were performed by increasing the aspiration time of standard for each addition, keeping constant the sample aspiration time. The increase in the standard aspiration time did not change the sample dilution factor because, simultaneously, the carrier solution aspiration time decreased in the same proportion. With the developed system it was possible to perform a variable number of standard additions for each sample, simply requiring an adjustment in the aspiration times of standard and carrier solutions.

Three flow system parameters were chosen for optimization, namely sample volume (V), reactor length (L) and flow rate (F), and all trials were carried out with a sunset yellow solution $1.0 \times 10^{-4} \text{ mol l}^{-1}$, keeping constant all the parameters previously optimized. It was used only one colorant for the system

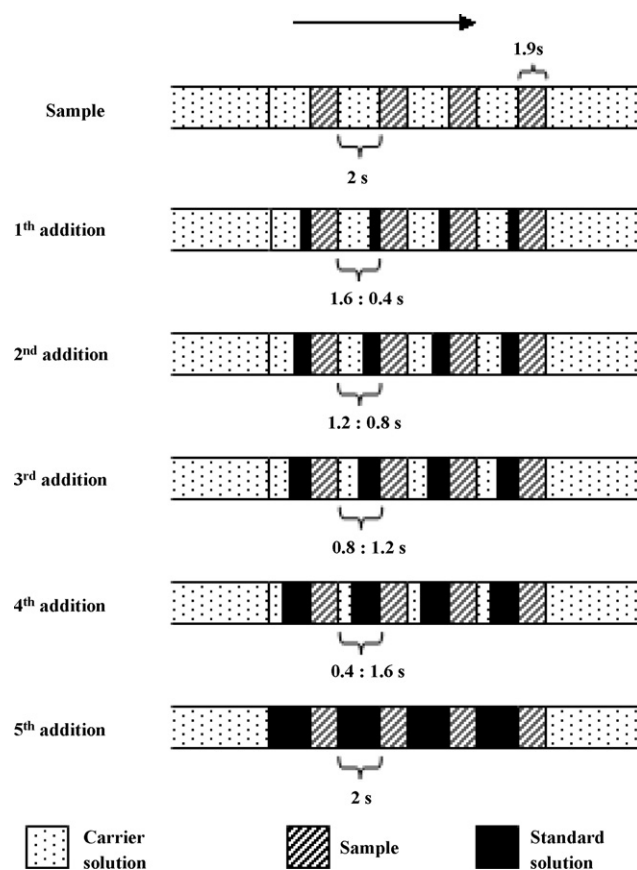


Fig. 3. Schematic representation of binary sampling for several standard additions.

optimization since the influence of physical parameters in the analytical signal was similar to the three colorants.

The parameters were optimized by using a complete factorial design (3 factors and 2 levels). The output variable to optimize was the maximum I_p value, bearing in mind the concentration level predicted in food samples (lower than $1.0 \times 10^{-4} \text{ mol l}^{-1}$). Trials were performed in duplicate and in a random way to minimize the effect of uncontrollable factors. The factors levels were selected according to previous studies, which enabled to observe their effect in the analytical signal. Regarding the sample volume, the values of 50 and 150 μl were chosen for low (–) and high (+) levels, respectively. Volumes lower than 50 μl excessively diminished I_p and values higher than 150 μl would make the analytical cycle longer, affecting negatively the sampling rate. As for reactor length, the values of 30 and 75 cm were selected for (–) and (+) levels. The use of longer reactors would unnecessarily decrease I_p and sampling rate, without bringing benefits in the analytical signal repeatability, since binary sampling guaranteed a good homogenization of the plugs. Concerning flow rate, the values of 0.96 and 1.92 ml min^{-1} were chosen for (–) and (+) levels. It was shown that higher flow rates caused a decrease in I_p for successive determinations, which could be a consequence of film erosion, and flow rates lower than 0.96 ml min^{-1} diminished sampling rate.

The factors levels, as well as the factorial design matrix and the obtained results, are shown in a resumed way in Table 1.

Table 1
Levels of the factors to be optimized, design matrix and ANOVA of the experimental results

Factors	Levels							Response
	Low (–)						High (+)	
Injection volume, V (μl)	50						150	
Reactor length, L (cm)	30.0						75.0	
Flow rate, F (ml min^{-1})	0.96						1.92	
Trial no.	Design matrix							Response
	V	L	F	$V \times L$	$V \times F$	$L \times F$	$V \times L \times F$	
1	–	–	–	+	+	+	–	4.868
2	+	–	–	–	–	–	+	14.930
3	–	+	–	–	+	–	+	3.446
4	–	–	+	+	–	–	+	4.266
5	–	+	+	–	–	+	–	3.078
6	+	–	+	–	+	–	–	14.225
7	+	+	–	+	–	–	–	13.425
8	+	+	+	+	+	+	+	11.790
Effect	9.678	–1.638	–0.828	–0.332	–0.342	–0.174	–0.291	
F_{exp}	8122.2	232.55	59.396	9.580	10.165	2.629	7.337	
F_{crit}	7.571							

Analysis of the results (using Yates algorithm) led to the conclusion that V was the factor that most significantly influenced I_p , given that the experimental F value (F_{exp}) was much higher than the critical F value (F_{crit}). I_p was maximum for V in the (+) level, independently of the other factors levels. Despite the influence shown by L and F on I_p , it was not possible to deduce clearly, from the Table, which were the levels that generated the higher I_p . Thus, V was kept on (+) level (150 μl) and a supermodified simplex [28] was carried out to optimize L and F . As the flow rates allowed by the automatic burette are discrete values, whenever the trial flow rate was not one of the allowed flow rates, it was used the nearest flow rate possible, never with a difference higher than 0.11 ml min^{-1} between them. According to the obtained results with the supermodified simplex, the levels combination that enabled the highest analytical signal to be obtained was $L=32$ cm and $F=1.2$ ml min^{-1} .

The analytical cycle was constituted by three major steps, namely sample exchange and manifold cleaning, insertion of sample, carrier and/or standard solutions, by binary sampling, and transport to the detector (Table 2).

After optimization of all parameters, solutions of tartrazine, sunset yellow and allura red with concentrations between 1.0×10^{-5} and 3.0×10^{-4} mol l^{-1} were analyzed, and a linear correlation between colorant concentration and I_p up to 1.5×10^{-4} mol l^{-1} , for sunset yellow and allura red, and up to 2.0×10^{-4} mol l^{-1} for tartrazine, was obtained, occurring

Table 2
Analytical cycle designed for colorants determination in foodstuffs

Step	Valve Status				t / s	Description
	V_1	V_2	V_3	V_4		
1	–	1	1	2	20	Sample exchange
2	1	2	1	2	30	Manifold cleaning
4x	–	1	2	1	1.9	Binary sampling (e.g. 1^{st} standard addition)
	2	2	2	1	0.4	
	1	2	2	1	1.6	
6	1	2	2	1	20	Transport to detector

electrode saturation for higher concentrations. The detection limits, calculated from the regression equation (with $y_B = a$ and $S_B = S_{y/x}$) [29] were 1.8×10^{-6} mol l^{-1} for tartrazine, 3.5×10^{-6} mol l^{-1} for sunset yellow and 1.4×10^{-6} mol l^{-1} for allura red.

The repeatability of measurements, expressed as R.S.D. of I_p , was evaluated through successive determinations of each colorant solution with a concentration of 1.0×10^{-4} mol l^{-1} , and the obtained R.S.D. was about 3% ($n=10$).

3.3. Interference studies

Considering the application of the developed method in the analysis of foodstuffs, the effect of several compounds normally present in these kinds of samples (gelatin, magnesium chloride, sodium benzoate, sodium citrate, ascorbic acid, citric acid, glucose and sucrose) on I_p was evaluated. Solutions containing tartrazine, sunset yellow or allura red, with a concentration of 1.0×10^{-4} mol l^{-1} , and the foreign compound in a higher concentration (maximum 100:1) were analyzed. The interfering concentration of each compound was considered as being that which caused a variation in I_p greater than or equal to $\pm 5\%$ in relation to the analytical signal obtained in its absence. In accordance with the obtained results, it was possible to conclude that none of the studied compounds interfered in the colorants determination, even when they were present in a 100-fold higher concentration. Gelatin, in contrast, caused a decrease in I_p when was present in a concentration higher than 1.0 g l^{-1} , which could be due to a blocking effect to the access of colorants to the electrode surface [30].

3.4. Sample analysis

To evaluate the applicability of the proposed method, several food samples containing tartrazine, sunset yellow or allura

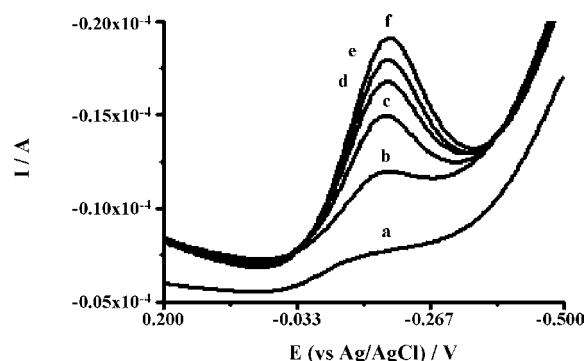


Fig. 4. Voltammograms obtained in the analysis of an energetic drink, with the polyallylamine modified electrode. The several voltammograms correspond to the signal obtained for the blank (a), the sample (b) and 4 successive additions of a sunset yellow standard solution (c–f). Electrode modified with 20 μl of a 15 g l^{-1} polyallylamine solution, sample volume 150 μl , reactor length 32 cm, flow rate 1.2 ml min^{-1} , standard additions of sunset yellow $1 \times 10^{-4} \text{ mol l}^{-1}$.

red were analyzed. For standard additions a $1.0 \times 10^{-4} \text{ mol l}^{-1}$ solution of the respective colorant was used.

In the determinations performed by the comparative method (HPLC) [8,11], samples were dissolved or diluted in water, centrifuged and filtered. Fig. 4 shows the voltammograms obtained in the determination of sunset yellow in an energetic drink for dehydration. The several voltammograms correspond to the signal obtained for the blank, the sample and four successive additions of a sunset yellow standard solution.

Table 3 shows the results obtained in the analysis of samples by the proposed and the comparative methods. Analysis of results enabled to conclude that all samples presented a colorant content within the authorized limits.

The agreement between the results provided by the proposed and the comparative methods was evaluated through the Student t -test for paired samples, in which the t value (-1.70) was lower than the critical t value (2.31, two tail), for a 95% confidence level ($n = 9$). The regression line between the results obtained by the proposed and the comparative methods showed a correlation coefficient of 0.9996, with $a = 1.35 \pm 1.68$ and $b = 0.95 \pm 0.02$, for a 95% confidence level.

The high precision with which binary sampling was performed, conferred by the use of solenoid valves, allowed to carry out a single standard addition for each sample, providing the same result in colorant concentration that was obtained with more standard additions.

Repeatability of results obtained by the proposed method was evaluated by carrying out 10 successive determinations of all samples, and the R.S.D. value was never higher than 3%.

4. Conclusions

The developed method showed to be an advantageous alternative to the described methods for food colorants determination, providing similar results to those obtained with the chromatographic method, being comparatively faster, cheaper and less laborious. However, mixtures of colorants cannot be quantified by this approach due to peaks overlapping, since the three colorants have similar peak potentials (within the range from 0.15 to 0.30 V).

The polyallylamine modified glassy carbon tubular electrode, here described for the first time, showed to be a valuable option as a substitute to the use of the dropping mercury electrode, for food colorants quantification. The polyelectrolyte film enabled, simultaneously, the protection of the electrode surface from contamination by sample matrix constituents and an enhancement in the analytical signal intensity, improving the measurements sensitivity. Although glassy carbon electrodes are not, commonly, employed in reduction reactions, the modified electrode presented good stability in the negative potential range in which the colorants reduction occurred.

The tubular configuration of the electrode and the film stability allowed to combine it with a multicommutated flow system, facilitating the analysis of complex samples such as food samples, overcoming the frequent problems of electrode fouling and the necessary sample pretreatment before measurement. The use of the multicommutated flow system enabled automation of standard additions, performed in an easier and faster way, compared to the same procedure when it is carried out in batch conditions. The number of standard additions that could be performed was

Table 3

Results obtained in the determination of the colorants tartrazine, sunset yellow and allura red in foodstuffs, by the proposed and the comparative methods

Food sample	Colorant	Reduction peak potential, E_p (V)	Colorant concentration ^a		Relative deviation (%)
			Proposed method	Comparative method (HPLC)	
Gelatin powder (pineapple)	Tartrazine	−0.28	56 ± 3^b	55 ± 8^b	+1.8
Gelatin powder (peach)			79 ± 3^b	82 ± 7^b	−3.7
Juice powder (pineapple)			39 ± 1^b	37.9 ± 0.9^b	+2.9
Gelatin powder (tutti-frutti)			136 ± 6^b	143 ± 1^b	−4.9
Gelatin powder (banana)			87 ± 1^b	90 ± 2^b	−3.3
Energetic drink for dehydration I	Sunset yellow	−0.20	8.9 ± 0.6^c	9.3 ± 0.1^c	−4.3
Energetic drink for dehydration II			8.5 ± 0.1^c	8.5 ± 0.1^c	0
Gelatin powder (strawberry)	Allura red	−0.18	68 ± 3^b	70 ± 4^b	−2.9
Alcoholic drink			11.9 ± 0.2^c	11.7 ± 0.4^c	+1.7

^a Average \pm standard deviation of 3 determinations.

^b Values in mg/kg.

^c Values in mg/l.

changeable, requiring only an adjustment in the aspiration times of standard solution. Nevertheless, it was possible to carry out a single standard addition per sample, providing the same accuracy that was obtained when two or more standard additions were performed.

Acknowledgements

The authors thank to CRUP the financial support provided for the Portuguese–Spanish researcher exchange (Acção Integrada E-41/03, HP2002-0039), to CEMUP—Centro de Materiais da Univ. Porto for providing the equipment in which the SEM analysis was performed and the Technology Department of Faculty of Pharmacy Univ. Porto for providing the HPLC equipment. M.L.S. Silva thanks FCT and FSE (III Quadro Comunitário de Apoio) for a Ph.D. grant (BD/10385/02).

References

- [1] P.L. López-de Alba, L. López-Martínez, L.M. De-León-Rodríguez, *Electroanalysis* 14 (2002) 197.
- [2] J.J.B. Nevado, J.R. Flores, M.J.V. Llerena, *Fresenius J. Anal. Chem.* 357 (1997) 989.
- [3] K.S. Rowe, K.J. Rowe, *J. Pediatr.* 125 (1994) 691.
- [4] Portaria no. 759/96 de 26-12-1996, *Diário da República I Série B*, 298, pp. 4647–4670.
- [5] European Parliament and Council Directive 94/36/EC of 30-06-1994, *Official Journal of the European Communities No. L 237*, pp. 13–29.
- [6] P.L. López-de Alba, K. Wróbel-Kaczmarczyk, K. Wróbel, L. López-Martínez, J.A. Hernández, *Anal. Chim. Acta* 330 (1996) 19.
- [7] P.L. López-de Alba, L. López-Martínez, L.I. Michelini-Rodríguez, K. Wróbel, K. Wróbel, J.A. Hernández, *Analyst* 122 (1997) 1575.
- [8] J.J.B. Nevado, J.R. Flores, C.G. Cabanillas, M.J.V. Llerena, A.C. Salcedo, *Talanta* 46 (1998) 933.
- [9] J.J. Berzas, J.R. Flores, M.J.V. Llerena, N.R. Fariñas, *Anal. Chim. Acta* 391 (1999) 353.
- [10] E. Dinç, E. Baydan, M. Kanbur, F. Onur, *Talanta* 58 (2002) 579.
- [11] E.C. Vidotti, J.C. Cancino, C.C. Oliveira, M.C.E. Rollemberg, *Anal. Sci.* 21 (2005) 149.
- [12] E.C. Vidotti, M.C.E. Rollemberg, *Quim. Nova* 29 (2006) 230.
- [13] M.A. Prado, H.T. Godoy, *Quim. Nova* 27 (2004) 22.
- [14] A.G. Fogg, K.S. Yoo, *Analyst* 104 (1979) 723.
- [15] F.B. Dominguez, F.G. Diego, J.H. Mendez, *Talanta* 37 (1990) 655.
- [16] Y. Ni, J. Bai, L. Jin, *Anal. Chim. Acta* 329 (1996) 65.
- [17] Y. Ni, J. Bai, *Talanta* 44 (1997) 105.
- [18] J.J.B. Nevado, J.R. Flores, M.J.V. Llerena, *Talanta* 44 (1997) 467.
- [19] M.A. Kapor, H. Yamanaka, P.A. Carneiro, M.V.B. Zanoni, *Eclét. Quím.* 26 (2001) 53.
- [20] B.F. Reis, M.F. Giné, E.A.G. Zagatto, J.L.F.C. Lima, R.A. Lapa, *Anal. Chim. Acta* 293 (1994) 129.
- [21] R.A.S. Lapa, J.L.F.C. Lima, B.F. Reis, J.L.M. Santos, E.A.G. Zagatto, *Anal. Chim. Acta* 351 (1997) 223.
- [22] M.L.S. Silva, M.B.Q. Garcia, J.L.F.C. Lima, E. Barrado, *Anal. Chim. Acta* 573–574 (2006) 383.
- [23] J.P. Hart, W.F. Smyth, *Analyst* 105 (1980) 929.
- [24] A.G. Fogg, D. Bhanot, *Analyst* 105 (1980) 868.
- [25] A.G. Fogg, D. Bhanot, *Analyst* 106 (1981) 883.
- [26] R.N. Goyal, M.S. Verma, N.K. Singhal, *Croat. Chem. Acta* 71 (1998) 715.
- [27] S.E. Burke, C.J. Barrett, *Biomacromolecules* 6 (2005) 1419.
- [28] M.W. Routh, P.A. Swartz, M.B. Denton, *Anal. Chem.* 49 (1977) 1422.
- [29] J.N. Miller, J.C. Miller, *Statistics and Chemometrics for Analytical Chemistry*, fourth ed., Pearson Education Limited, Harlow, 2000, pp. 120–123.
- [30] A.A. Barros, J.O. Cabral, *Analyst* 113 (1988) 853.

Measurement and characterization of singlet oxygen production in copper ion-catalyzed aerobic oxidation of ascorbic acid

Bo Song^a, Guilan Wang^b, Jingli Yuan^{a,b,*}

^a Department of Analytical Chemistry, Dalian Institute of Chemical Physics, Chinese Academy of Sciences, Dalian, PR China

^b State Key Laboratory of Fine Chemicals, Department of Chemistry, Dalian University of Technology, Dalian 116012, PR China

Received 26 June 2006; received in revised form 9 October 2006; accepted 17 October 2006

Available online 20 November 2006

Abstract

Production of singlet molecular oxygen ($^1\text{O}_2$) in the aerobic oxidation of ascorbic acid catalyzed by copper ion was measured and characterized using [4'-(9-anthryl)-2,2':6',2''-terpyridine-6,6''-diyl]bis(methylenenitrilo)tetrakis(acetate)- Eu^{3+} (ATTA- Eu^{3+}) as a highly sensitive and selective time-resolved luminescence probe for $^1\text{O}_2$. The $^1\text{O}_2$ produced in the reaction was further characterized and confirmed by (i) chemical trapping of $^1\text{O}_2$ with 9,10-diphenylanthracene (DPA), the corresponding endoperoxide was detected by HPLC and (ii) spin trapping of $^1\text{O}_2$ with 2,2,6,6-tetramethyl-4-piperidinol (TMP-OH), the corresponding free radical of TMP-OH oxide (TMPO $^{\bullet}$) was detected by electron spin resonance (ESR) spectroscopy. The effects of deuterium oxide, sodium azide and histidine on the $^1\text{O}_2$ signal were investigated. The mechanism investigation of $^1\text{O}_2$ production implied that the ascorbic acid–Cu(I) complex formed in the reaction could be an important intermediate for the $^1\text{O}_2$ production. The reaction of ascorbic acid with copper ion monitored by ^1H NMR and absorption spectroscopy demonstrated the formation of a copper ion–ascorbic acid complex. Except for Cu^{2+} and Cu^+ –ascorbic acid systems, no detectable $^1\text{O}_2$ was produced in other transition metal cation–ascorbic acid systems in the studied range.

© 2006 Elsevier B.V. All rights reserved.

Keywords: Ascorbic acid; Aerobic oxidation; Europium; Singlet oxygen production; Time-resolved luminescence

1. Introduction

Ascorbic acid (or Vitamin C) is ubiquitous to living systems, and a wide variety of its biological functions have been proposed. Experimental and epidemiological studies have demonstrated that ascorbic acid has anticarcinogenic and chemopreventive actions [1,2] by scavenging physiologically relevant reactive oxygen species and reactive nitrogen species. As an effective water-soluble antioxidant in plasma, ascorbic acid can prevent lipid peroxidation induced by peroxy radicals or the gas-phase of cigarette smoke, and possibly protect against cardiovascular disease [3,4]. This has led to the proposal that dietary supplementation with ascorbic acid may be useful in disease prevention. Paradoxically, ascorbic acid is also known to act as a pro-oxidant in vitro, the mechanisms underlying these actions are

still unclear. Ascorbic acid can assist metal ion-induced oxidative modifications of lipid, protein and DNA [5–7]. Rosenthal and Benhur have shown that the photohaemolysis rate of human red blood cells sensitized by chloroaluminium phthalocyanine sulphate can be increased by ascorbic acid [8]. A mechanism that ascorbic acid induces the decomposition of lipid hydroperoxides to genotoxic bifunctional electrophiles in vitro has been provided [9]. In the presence of the redox active metal ion, ascorbic acid may contribute to oxidative damage of biomolecules by ascorbic acid-induced Fenton reaction [10], or by H_2O_2 and $\text{O}_2^{\bullet-}$ produced in the oxidation of ascorbic acid by molecular oxygen [11]. However, until now there is still no unequivocal evidence to demonstrate the $^1\text{O}_2$ production in the metal ion-mediated aerobic oxidation of ascorbic acid.

In some biological systems, $^1\text{O}_2$ is thought to be an important toxic species in vivo since it can oxidize various kinds of biological molecules such as proteins, DNA and lipids [12–15]. Singlet oxygen has been proposed to be involved in the cell signaling cascade and in the induction of gene expression [16,17]. Furthermore, it was suggested that $^1\text{O}_2$ should be involved in changes in the mitochondrial membrane pore transition [18]

* Corresponding author at: Department of Analytical Chemistry, Dalian Institute of Chemical Physics, 457 Zhongshan Road, Dalian, Liaoning Province 116023, PR China. Tel.: +86 411 84379660; fax: +86 411 84379660.

E-mail address: jingliyuan@yahoo.com.cn (J. Yuan).

and be a key to the bactericidal response of certain antibiotics [19,20]. Regarding photoinduced processes, $^1\text{O}_2$ is believed to be involved in the photosensitivity of patients with erythropoietic protoporphyria and drug phototoxicity [21,22], and its formation has been extensively employed therapeutically [23]. In addition, there is overwhelming evidence that excited state species produced by biochemical reactions in cells and tissues exposed to oxidative stress may subsequently react with ground-state oxygen to yield $^1\text{O}_2$ as in photosensitization [24].

Time-resolved fluorometry combined with the use of lanthanide complex-based luminescence probes has provided an excellent way for developing highly sensitive bioaffinity assays [25,26]. The most important advantage of this technique is that the method can effectively eliminate the short-lived background noise from the biological samples and optical components. We have recently demonstrated that an europium(III) complex, [4'-(9-anthryl)-2,2':6',2''-terpyridine-6,6''-diyl]bis(methylenenitrilo)tetrakis (acetate)- Eu^{3+} (ATTA- Eu^{3+}), can be used as a highly sensitive and selective time-resolved luminescence probe for $^1\text{O}_2$ [27]. In the present work, the $^1\text{O}_2$ production in the aerobic oxidation of ascorbic acid catalyzed by copper ion was investigated by using ATTA- Eu^{3+} as a probe. To confirm the $^1\text{O}_2$ production in the system, the reaction was further characterized by using 9,10-diphenylanthracene (DPA) and 2,2,6,6-tetramethyl-4-piperidinol (TMP-OH) as chemical trapping and electron spin resonance (ESR) probes for $^1\text{O}_2$, the corresponding products of $^1\text{O}_2$ reacted with DPA and TMP-OH were detected by HPLC [28] and ESR spectroscopy [29], respectively. Effects of various reaction conditions on the yield of $^1\text{O}_2$ and the $^1\text{O}_2$ production mechanism in the system were also investigated.

2. Experimental

2.1. Chemicals and materials

Ascorbic acid, 2,2,6,6-tetramethyl-4-piperidinol and 9,10-diphenylanthracene were purchased from Acros Organics. Deuterium oxide (99.9%) was obtained from Cambridge Isotope Laboratories, Inc., dehydroascorbic acid (DHA) was obtained from Aldrich. Superoxide dismutase (SOD) from bovine erythrocytes (specific activity, 4520 units/mg), and catalase from bovine liver (specific activity, 2860 units/mg) were obtained from Sigma. Prior to use, hydrogen peroxide was diluted immediately from a stabilized 30% solution, and was assayed by using its molar absorption coefficient of $43.6\text{ M}^{-1}\text{ cm}^{-1}$ at 240 nm [30]. The ATTA- Eu^{3+} complex was synthesized by using a previous method [27]. The ATTA- Eu^{3+} endoperoxide (EP-ATTA- Eu^{3+}) and 9,10-diphenylanthracene endoperoxide (DPAO₂) were synthesized according to the literature methods [27,31], respectively. Unless otherwise stated, all chemical materials were purchased from commercial sources and used without further purification.

2.2. Time-resolved luminescence assay

All reactions were carried out in 0.05 M Tris-HCl buffer of pH 7.4 with 100 nM ATTA- Eu^{3+} , 1.0 mM ascorbic acid

and 10 μM CuSO_4 at room temperature under air for 1 h. The time-resolved luminescence measurement was carried out on a Perkin-Elmer Victor 1420 Multilabel Counter with the measurement conditions of excitation wavelength, 340 nm; emission wavelength, 615 nm; delay time, 0.2 ms; window time (counting time), 0.4 ms; cycling time, 1.0 ms.

2.3. ESR assay

The H_2O -based or D_2O -based solution (10 ml) containing 1.0 mM ascorbic acid, 20 μM CuSO_4 and 50 mM TMP-OH were stirred for 5 h at room temperature under oxygen. To the solution were added ascorbic acid (2 mg) and 20 μl CuSO_4 (10 mM) at intervals of 1 h during the reaction. After the reaction, the solution was injected into the quartz capillary for ESR analysis. The ESR spectra were recorded at room temperature on a JES-FE1XG X-band spectrometer (JEOL, Japan) with 100-kHz field modulation and the settings of central field, 3360 G; sweep width, 250 G; microwave power, 5 mW; response 0.1 s.

2.4. HPLC assay

A mixture of 5 ml H_2O (or D_2O), 5 ml tetrahydrofuran, 1.8 mg ascorbic acid, 10 μl CuSO_4 (50 mM) and 13.2 mg DPA was stirred for 6 h at 37 °C under oxygen. To the solution were added ascorbic acid (2 mg) and 10 μl CuSO_4 (50 mM) at intervals of 1 h during the reaction. The solution was extracted with CHCl_3 (2×20 ml). The organic phase was dried with Na_2SO_4 and evaporated. The residue was dissolved in acetone, and then used for HPLC analysis. The HPLC analysis was carried out on an HPLC instrument (Micro-Tech Scientific Inc.) equipped with a 150 mm \times 0.32 mm C_{18} reverse-phase column and a linear UV-200 detector, using the increasing linear gradient of acetonitrile/ H_2O from 60 to 95% with flow-rate of 3.0 ml/min. The elution was monitored at 210 nm.

2.5. ^1H NMR assay

Reaction of 50 mM CuSO_4 with 50 mM ascorbic acid (or DHA) was carried out in D_2O at room temperature. The ^1H NMR spectra were measured on a Bruker DRX 400 spectrometer (400 MHz).

2.6. Absorption spectrum assay

Reaction of 0.1 mM ascorbic acid with 0.1 mM CuSO_4 (or CuCl) was carried out in 0.05 M NH_4Cl buffer of pH 6.5 at room temperature. The absorption spectra were recorded on a Perkin-Elmer Lambda 35 UV-vis spectrometer.

3. Results and discussion

3.1. Singlet oxygen production in copper ion-catalyzed aerobic oxidation of ascorbic acid

Europium(III) complex, ATTA- Eu^{3+} , is a highly sensitive and selective time-resolved luminescence probe for $^1\text{O}_2$ [27].

Table 1

Effects of sodium azide, histidine, SOD, catalase, EDTA, H₂O₂ and mannitol on luminescence intensity of Cu²⁺-ascorbic acid-ATTA-Eu³⁺ reaction system

Reaction system	Relative luminescence intensity ^a , $(I - I_0)/I_0$
Control ^b	0.00
Control + 10 μM Cu ²⁺ + 1 mM ascorbic acid	1.19
Control + 10 μM Cu ²⁺	-0.09
Control + 1 mM ascorbic acid	0.18
Control + 10 μM Cu ²⁺ + 1 mM ascorbic acid + 20 mM NaN ₃	0.20
Control + 10 μM Cu ²⁺ + 1 mM ascorbic acid + 1 mM histidine	0.08
Control + 10 μM Cu ²⁺ + 1 mM ascorbic acid + 1 μM SOD	1.16
Control + 10 μM Cu ²⁺ + 1 mM ascorbic acid + 0.5 μM catalase	-0.01
Control + 10 μM Cu ²⁺ + 1 mM ascorbic acid + 1 mM EDTA ^c	0.02
Control + 10 μM Cu ²⁺ + 1 mM ascorbic acid + 1 mM H ₂ O ₂	2.01
Control + 10 μM Cu ²⁺ + 1 mM ascorbic acid + 5 mM mannitol	1.26
Control + 1 mM H ₂ O ₂	0.20

All reactions were carried out in 0.05 M Tris-HCl buffer of pH 7.4 under air at room temperature for 1 h.

^a I_0 and I are the luminescence intensities before and after the reaction, respectively.

^b 100 nM ATTA-Eu³⁺ in 0.05 M Tris-HCl buffer of pH 7.4.

^c It was confirmed that the luminescence intensity of 100 nM EP-ATTA-Eu³⁺ in the presence of 1 mM EDTA is almost unchanged (~1% decreased), which indicates that EDTA does not quench the luminescence of the Eu³⁺ probe under this condition.

This probe can specifically and rapidly react with ¹O₂ to form its endoperoxide (EP-ATTA-Eu³⁺), accompanied by a remarkable increase of its luminescence intensity. The incubation of ascorbic acid (1.0 mM) and CuSO₄ (10 μM) in the 0.05 M Tris-HCl buffer of pH 7.4 containing 100 nM ATTA-Eu³⁺ under air at room temperature for 1 h resulted in a 1.2-fold increase [$(I - I_0)/I_0$] of luminescence intensity of the Eu³⁺ probe (Table 1). Based on the time-resolved luminescence dilution curve of EP-ATTA-Eu³⁺ (Fig. 1), the amount of EP-ATTA-Eu³⁺ formed in this reaction was estimated to be 7.9 nM. Because ascorbic acid itself is also a quencher of ¹O₂ [32], the yield of ¹O₂ in the reaction is considered being higher than 7.9 nM. The results of Table 1 also show that sodium azide and histidine, the quenchers of ¹O₂ [33,34], can effectively inhibit the augmentation of luminescence intensity of the Eu³⁺ probe, which clearly indicates that the increase of luminescence intensity of the Eu³⁺ probe is caused by ¹O₂ produced in the reaction process of copper ion-catalyzed aerobic oxidation of ascorbic acid.

A chemical trapping probe, DPA, was further used to detect ¹O₂ produced in the system. This probe can specifically react

with ¹O₂ to form a thermostable endoperoxide (DPAO₂), therefore the confirmation of DPAO₂ formed in the system can provide an unambiguous evidence for the ¹O₂ production [28]. As shown in Fig. 2, the incubation of ascorbic acid and CuSO₄ in the presence of DPA resulted in the formation of DPAO₂. Upon replacement of H₂O by D₂O, the quantity of DPAO₂ was increased, which is consistent with the fact that the lifetime of ¹O₂ in D₂O is longer than that in H₂O.

Some sterically hindered amines can react with ¹O₂ to produce nitroxide radicals [29], so TMP-OH, a molecule that can specifically react with ¹O₂ to form a stable free radical TMPO•, was also used as an ESR probe of ¹O₂ to further confirm the ¹O₂ production in the ascorbic acid-Cu²⁺ reaction system. As shown in Fig. 3, after incubating ascorbic acid with CuSO₄ in the presence of TMP-OH, a typical three-line ESR spectrum of TMPO• with equal intensities ($a^N = 16.9$ G, $g = 2.0054$) was recorded. Upon replacement of H₂O by D₂O, the signal intensity is obviously increased. These results again demonstrated that ¹O₂ was produced in the system.

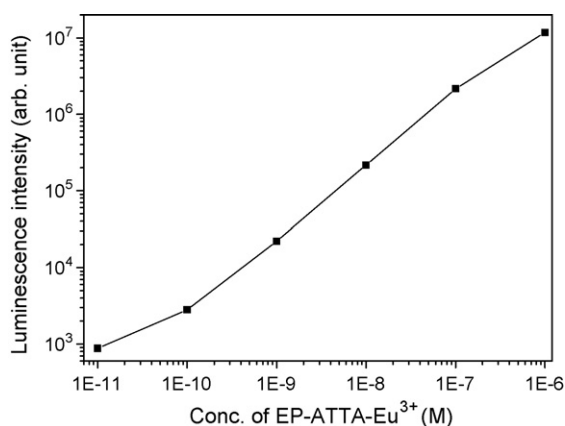


Fig. 1. Time-resolved luminescence dilution curve of EP-ATTA-Eu³⁺ in 0.05 M Tris-HCl buffer of pH 7.4.

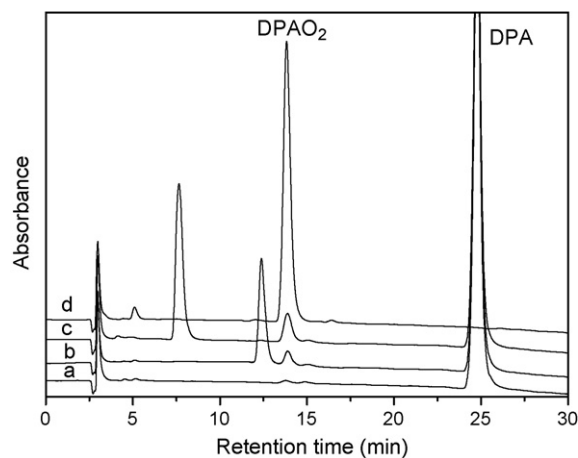


Fig. 2. Detection of ¹O₂ in Cu²⁺-ascorbic acid system by HPLC using DPA as a probe. (a) DPA, (b) ascorbic acid + CuSO₄ + DPA in H₂O, (c) ascorbic acid + CuSO₄ + DPA in D₂O and (d) DPAO₂.



Fig. 3. ESR spectra of TMP-OH-ascorbic acid-CuSO₄ reaction system in: (A) D₂O and (B) H₂O.

It has been reported that several reactive oxygen species (O₂^{•-}, H₂O₂ and •OH) can be produced in metal ion-ascorbic acid reaction systems [10,11]. However, these studies did not show the ¹O₂ production in the systems. In this work, three chemical probes specific for ¹O₂, ATTA-Eu³⁺, DPA and TMP-OH, and corresponding detection methods, time-resolved luminescence, HPLC and ESR, were used to detect and confirm the ¹O₂ production in copper ion-ascorbic acid reaction system. It was found that the ¹O₂ production in the system could be stimulated by D₂O and inhibited by histidine and azide in the above detections. These findings strongly demonstrated the ¹O₂ production in the reaction of copper ion-catalyzed aerobic oxidation of ascorbic acid.

3.2. Influence factors of ¹O₂ production in ascorbic acid-copper ion system

Fig. 4 shows that molecular oxygen is required for ¹O₂ production since the amount of ¹O₂ formed is strongly affected by the concentration of molecular oxygen in the system. As shown in Fig. 4, the increase of luminescence intensity of the Eu³⁺ probe was hardly detected in the ascorbic acid-Cu²⁺-ATTA-Eu³⁺ system under argon. In contrast to this, the increase rate of luminescence intensity in the system under molecular oxygen was distinctly faster than that under air.

The effect of pH on the ¹O₂ production was measured by using the reaction of 1.0 mM ascorbic acid with 10 μM CuSO₄ in

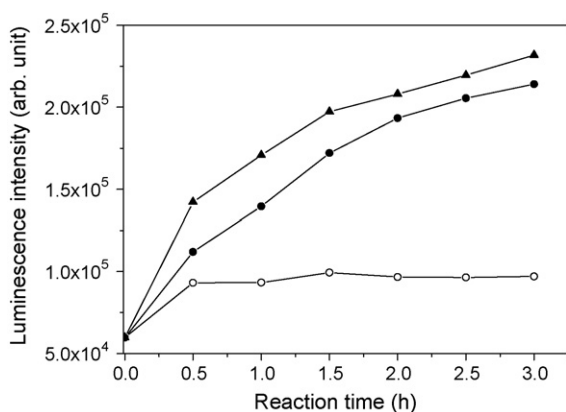


Fig. 4. Reaction kinetic curves of Cu²⁺-ascorbic acid-ATTA-Eu³⁺ system in Ar (○), air (●) and O₂ (▲) concentrated 0.05 M Tris-HCl buffer of pH 7.4.

the presence of 100 nM ATTA-Eu³⁺ in 0.05 M Tris-HCl buffers with different pHs (from 3 to 10) at room temperature for 1 h. The results show that luminescence intensities of the Eu³⁺ probe are maximal between pH 3 and 7, and remarkably reduced at higher pH, which indicates the ¹O₂ production in the system can be strongly inhibited at higher pH due to the formation of Cu(II) hydroxide (because the Eu³⁺ complex itself is not stable in a buffer of pH <3 [27], the effect of lower pH was not investigated).

An oxidation process of ascorbic acid catalyzed by Cu²⁺ was recorded by monitoring the decrease of absorbance at 265 nm, meantime ¹O₂ production process was also recorded by monitoring the increase of luminescence intensity of the Eu³⁺ probe. As shown in Fig. 5, the luminescence intensity of the Eu³⁺ probe was increased with the consumption of ascorbic acid, and tended to a stable value till ascorbic acid was exhausted. At this moment, the addition of another ascorbic acid can cause the sequential increase in the luminescence intensity of the Eu³⁺ probe (data not shown). These results indicate that ¹O₂ is produced during the oxidation of ascorbic acid.

Reaction products of the copper ion-catalyzed aerobic oxidation of ascorbic acid were measured by ¹H NMR spectroscopy. The reactions for ¹H NMR measurement were carried out in D₂O at higher concentrations in order to increase the NMR signals of the products. Compared with the spectrum of free ascorbic acid (50 mM), the spectrum of the reaction product of 50 mM ascorbic acid with 50 mM Cu²⁺ showed obvious changes. After the reaction, the signals of ascorbic acid at 3.72, 4.05 and 4.94 ppm, corresponding to the C6, C5 and C4 protons, were broadened and shifted to 3.73, 4.13 and 4.71 ppm, respectively. This result implied that ascorbic acid-copper complex could be formed in the reaction system, and the ascorbic acid coordination most likely occurred through the ring hydroxyl groups on C2 and C3 because the extent of chemical shift between free and reacted ascorbic acid was increased in the order of C6 < C5 < C4 [6]. It is known that DHA is a main oxidation product of ascorbic acid [11]. The ¹H NMR spectra show that DHA can also react with copper ion to form DHA-copper complex. The signals of C5 and C6 protons of DHA were shifted and broadened after DHA was incubated with Cu²⁺. As expected, the signals of C5 and C6 pro-

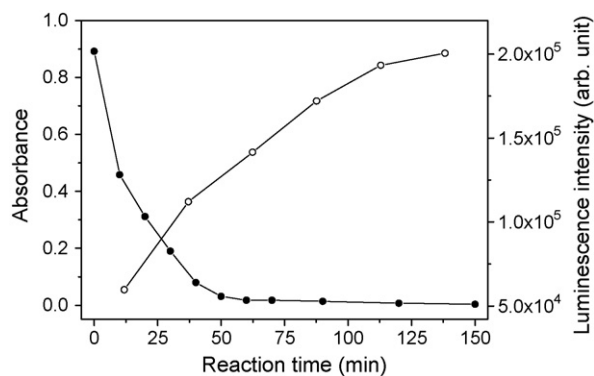


Fig. 5. Oxidation process of Cu²⁺ catalyzed ascorbic acid recorded by monitoring the decrease of absorbance at 265 nm (●), and the ¹O₂ production process of Cu²⁺-ascorbic acid-ATTA-Eu³⁺ system recorded by monitoring the increase of luminescence intensity of the Eu³⁺ probe (○).

tons of DHA–copper complex at 4.56 and 4.12–4.25 ppm were observed in the ascorbic acid–Cu²⁺ system, and the quantity of DHA formed was increased with the increase of reaction time.

To determine roles of Cu²⁺ and Cu⁺ ions and confirm the formation of copper ion–ascorbic acid complex in the reaction system, the absorption spectra of Cu²⁺ and Cu⁺–ascorbic acid systems were measured. When ascorbic acid was incubated with Cu²⁺ ion, the absorption peak of ascorbic acid at 265 nm almost disappeared (Fig. 6c). The incubation of ascorbic acid with Cu⁺ ion caused the shift of the absorption peak from 265 to 243 nm, and the new peak is not the absorption peak of DHA–Cu(I) complex (Fig. 6e versus d). These results implied that the Cu(I)–ascorbic acid complex could be a intermediate in the copper ion–ascorbic acid reaction system.

The effects of superoxide dismutase, catalase, ethylenediamine tetraacetic acid (EDTA), H₂O₂ and mannitol on the luminescence intensity of the Cu²⁺–ascorbic acid–ATTA–Eu³⁺ system are shown in Table 1. When a chelating agent EDTA was added to the ascorbic acid–Cu²⁺–ATTA–Eu³⁺ system, the increase of luminescence intensity of the Eu³⁺ probe was inhibited, whereas the luminescence intensity of EP–ATTA–Eu³⁺ is almost uninfluenced by EDTA (~1% decreased). These results indicate that the inhibition of luminescence intensity of the Eu³⁺ probe is caused by the formation of EDTA–Cu²⁺ complex, which inhibits the formation of ascorbic acid–copper ion complex, and thus the ¹O₂ production is inhibited. This result is also consistent with the interpretation that the ¹O₂ production in the system can be strongly inhibited at higher pH due to the formation of Cu(II) hydroxide.

3.3. Reaction mechanism consideration

It has been reported that some reactive oxygen species, superoxide anion, hydroxyl radical and hydrogen peroxide, can be formed in the aerobic oxidation process of ascorbic acid catalyzed by copper ion [35]. In this work, we demonstrated that ¹O₂ can also be produced in the system, and its production can not be inhibited by adding SOD, a quencher of superox-

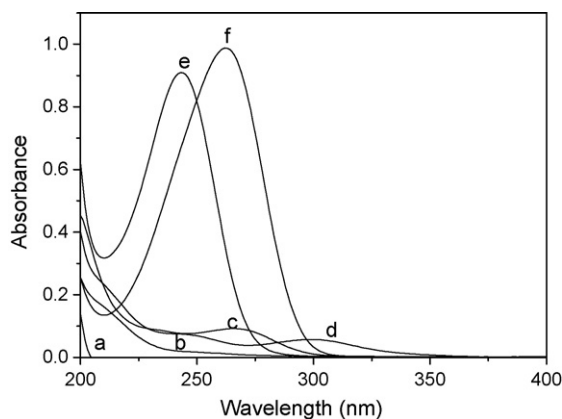


Fig. 6. Absorption spectroscopic analysis of the copper ion (Cu²⁺ or Cu⁺)–ascorbic acid reaction. (a) 0.1 mM CuCl only, (b) 0.1 mM CuSO₄ only, (c) 0.1 mM CuSO₄ + 0.1 mM ascorbic acid, (d) 0.1 mM CuCl + 0.1 mM DHA, (e) 0.1 mM CuCl + 0.1 mM ascorbic acid and (f) 0.1 mM ascorbic acid only.

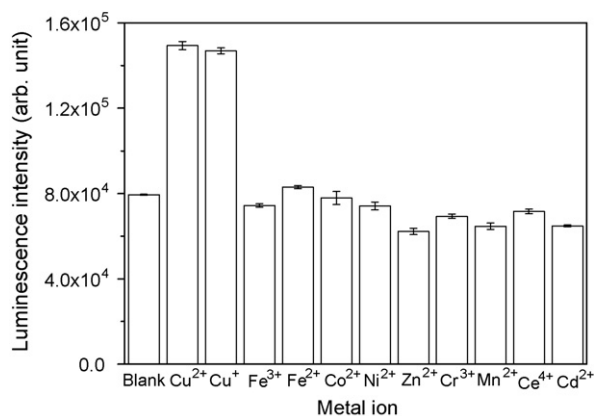


Fig. 7. Effects of different metal ions on luminescence intensities of the metal ion–ATTA–Eu³⁺–ascorbic acid reaction systems.

ide anion [11], and mannitol, a quencher of hydroxyl radical [36]. These facts indicate that superoxide anion and hydroxyl radical are not the major intermediates for the ¹O₂ production in the reaction. However, the ¹O₂ production can be strongly inhibited by adding catalase, a quencher of hydrogen peroxide [36], and stimulated by adding hydrogen peroxide, which shows that hydrogen peroxide is a major intermediate for the ¹O₂ production. According to our results, we can conclude that the ¹O₂ production in copper ion–catalyzed aerobic oxidation of ascorbic acid is not based on the Haber–Weiss mechanism [37], and a ascorbic acid–Cu(I)–hydrogen peroxide complex should be a key intermediate for the ¹O₂ production.

The selectivity in the process of the ¹O₂ production on its metal ion catalyst was also investigated. After a series of metal cations (10 μM) were incubated with 1.0 mM ascorbic acid–100 nM ATTA–Eu³⁺ in 0.05 M Tris–HCl buffer of pH 7.4 under air at room temperature for 1 h, luminescence intensities of the Eu³⁺ probe were measured with time-resolved mode. As shown in Fig. 7, except for the Cu²⁺ and Cu⁺ systems, the ¹O₂ production cannot be observed in other transition metal cation systems. These results show that the ¹O₂ production in the aerobic oxidation of ascorbic acid has a high selectivity on its catalyst. Although some metal ions, such as ferric ion, can also catalyze the aerobic oxidation of ascorbic acid [35], except for copper ion, no ¹O₂ was detected in other transition metal ion–catalyzed oxidation systems of ascorbic acid in the studied range. This fact means that the aerobic oxidations of ascorbic acid catalyzed by different metal ions could have different reaction mechanisms. Maybe the ¹O₂ production in copper ion–catalyzed aerobic oxidation of ascorbic acid can explain the oxidative damages that perhaps are caused by ascorbic acid in some biological processes.

4. Conclusion

In the present work, ¹O₂ production in copper ion–catalyzed aerobic oxidation of ascorbic acid has been measured and characterized. The yield, influence factors and mechanism of ¹O₂ formed were studied. Although ascorbic acid is thought to be an excellent reducing agent in biological systems, it is able to

serve as a donor antioxidant in free radical-mediated oxidative processes, and can also stimulate the oxidative damages in some biological processes. Maybe the $^1\text{O}_2$ production in copper ion-catalyzed aerobic oxidation of ascorbic acid can explain the pro-oxidant mechanism of ascorbic acid in certain biological processes. It is well known that reactive oxygen species can act as the subcellular messenger in several gene regulatory and signal transduction pathways, so ascorbic acid, both donor and acceptor of reactive oxygen species, is able to activate certain genes and signaling pathways by modulating the redox state of the cell. Our findings may contribute to a better understanding not only about the complicated functions of ascorbic acid in biological systems, but also the role of metal ion catalysis in free radical-associated pathologies.

Acknowledgement

The present work was supported by the National Natural Science Foundation of China (No. 20575069).

References

- [1] G. Block, *Am. J. Clin. Nutr.* 53 (1991) 270S.
- [2] I.M. Drake, M.J. Davies, N.P. Mapstone, M.F. Dixon, C.J. Schorah, K.L. White, D.M. Chalmers, A.T. Axon, *Carcinogenesis* 17 (1996) 559.
- [3] B. Frei, L. England, B.N. Ames, *Proc. Natl. Acad. Sci. U.S.A.* 86 (1989) 6377.
- [4] B. Frei, T.M. Forte, B.N. Ames, C.E. Cross, *Biochem. J.* 277 (1991) 133.
- [5] G. Quievryn, E. Peterson, J. Messer, A. Zhitkovich, *Biochemistry* 42 (2003) 1062.
- [6] M. Yazzie, S.L. Gamble, E.R. Civitello, D.M. Stearns, *Chem. Res. Toxicol.* 16 (2003) 524.
- [7] B. Macías, M.V. Villa, F. Sanz, J. Borrás, M. González-Álvarez, G. Alzuet, *J. Inorg. Biochem.* 99 (2005) 1441.
- [8] I. Rosenthal, E. Benhur, *Int. J. Radiat. Biol.* 62 (1992) 481.
- [9] S.H. Lee, T. Oe, I.A. Blair, *Science* 292 (2001) 2083.
- [10] T.L. Duarte, J. Lunec, *Free Radic. Res.* 39 (2005) 671.
- [11] M. Scarpa, R. Stevanato, P. Viglino, A. Rigo, *J. Biol. Chem.* 258 (1983) 6695.
- [12] P. Kang, C.S. Foote, *J. Am. Chem. Soc.* 124 (2002) 4865.
- [13] M.J. Davies, *Biochem. Biophys. Res. Commun.* 305 (2003) 761.
- [14] G.R. Martinez, D. Gasparutto, J.L. Ravanat, J. Cadet, M.H.G. Medeiros, P.D. Mascio, *Free Radic. Biol. Med.* 38 (2005) 1491.
- [15] B. Epe, M. Pflaum, S. Boitoux, *Mutat. Res.* 299 (1993) 135.
- [16] L.O. Klotz, K. Briviba, H. Sies, *Methods Enzymol.* 319 (2000) 130.
- [17] S.W. Ryter, R.M. Tyrrell, *Free Radic. Biol. Med.* 24 (1998) 1520.
- [18] C. Beghetto, C. Renken, O. Eriksson, G. Jori, P. Bernardi, F. Ricchelli, *Eur. J. Biochem.* 267 (2000) 5585.
- [19] P. Wentworth, L.H. Jones, A.D. Wentworth, X.Y. Zhu, N.A. Larsen, I. Wilson, X. Xu, W.A. Goddard, K.D. Janda, A. Eschenmoser, R.A. Lerner, *Science* 293 (2001) 1806.
- [20] P. Wentworth, J.E. McDunn, A.D. Wentworth, C. Takeuchi, J. Nieva, T. Jones, C. Bautista, J.M. Ruedi, A. Gutierrez, K.D. Janda, B.M. Babior, A. Eschenmoser, R.A. Lerner, *Science* 298 (2002) 2195.
- [21] D.E. Moore, V.J. Hemmens, H. Yip, *Photochem. Photobiol.* 39 (1984) 57.
- [22] C. Thomas, R.S. MacGill, G.C. Miller, R.S. Pardini, *Photochem. Photobiol.* 55 (1992) 47.
- [23] J.M. O'Brien, R.J. Singh, J.B. Feix, B. Kalyanaraman, F. Seiber, *Photochem. Photobiol.* 54 (1991) 851.
- [24] M.E. Murphy, H. Sies, *Methods Enzymol.* 186 (1990) 595.
- [25] Z. Ye, M. Tan, G. Wang, J. Yuan, *Talanta* 65 (2005) 206.
- [26] G. Wang, J. Yuan, X. Hai, K. Matsumoto, *Talanta* 70 (2006) 133.
- [27] B. Song, G. Wang, J. Yuan, *Chem. Commun.* (2005) 3553.
- [28] S. Miyamoto, G.R. Martinez, A.P.B. Martins, M.H.G. Medeiros, P.D. Mascio, *J. Am. Chem. Soc.* 125 (2003) 4510.
- [29] Y. Lion, M. Delmelle, A.V. De Vorst, *Nature* 263 (1976) 442.
- [30] B. Lei, N. Adachi, T. Arai, *Brain Res. Protoc.* 3 (1998) 33.
- [31] N.J. Turro, M.F. Chow, J. Rigaudy, *J. Am. Chem. Soc.* 103 (1981) 7218.
- [32] R.S. Bodannes, P.C. Chan, *FEBS Lett.* 105 (1979) 195.
- [33] J.R. Harbour, S.L. Issler, *J. Am. Chem. Soc.* 104 (1982) 903.
- [34] A. Michaeli, J. Feitelson, *Photochem. Photobiol.* 59 (1994) 284.
- [35] M.M. Taqui-Khan, A.E. Martell, *J. Am. Chem. Soc.* 89 (1967) 4176.
- [36] J. Bakker, F.J. Gommers, I. Nieuwenhuis, H. Wynberg, *J. Biol. Chem.* 254 (1979) 1841.
- [37] L.A. MacManus-Spencer, K. McNeill, *J. Am. Chem. Soc.* 127 (2005) 8954.

Dealing with missing values and outliers in principal component analysis

I. Stanimirova, M. Daszykowski, B. Walczak*

Department of Chemometrics, Institute of Chemistry, The University of Silesia, 9 Szkolna Street, 40-006 Katowice, Poland

Received 19 June 2006; received in revised form 3 October 2006; accepted 5 October 2006

Available online 7 November 2006

Abstract

An efficient methodology for dealing with missing values and outlying observations simultaneously in principal component analysis (PCA) is proposed. The concept described in the paper consists of using a robust technique to obtain robust principal components combined with the expectation maximization approach to process data with missing elements. It is shown that the proposed strategy works well for highly contaminated data containing different amounts of missing elements. The authors come to this conclusion on the basis of the results obtained from a simulation study and from analysis of a real environmental data set.

© 2006 Elsevier B.V. All rights reserved.

Keywords: Expectation maximization approach; Robust PCA; Missing elements

1. Introduction

Principal component analysis (PCA) is one of the most used tools in chemometrics thanks to its very attractive properties. It allows relatively easy projecting of data from a higher to a lower dimensional space and then reconstructing them without any preliminary assumptions about the data distribution. As a least squares method, PCA is optimal in terms of mean squared error and its parameters are obtained from the data directly. However, despite these features, PCA is known to possess some shortcomings. One is that it is strongly affected by the presence of outliers, i.e. objects exhibiting far different values for some of the measured variables in comparison with the majority of objects. Therefore, the obtained principal components will not describe the majority of the data well and one cannot get a proper insight into the data structure. A way to deal with this problem is to remove the outlying objects observed on the score plots and to repeat the PCA analysis again. Another, more efficient way is to apply a robust, i.e. not sensitive to outliers, variant of PCA. Several robust PCA approaches have been proposed and their robust properties have been extensively tested over the last years. They are either based on projec-

tion pursuit approach [1–6] or on obtaining robust estimates of the covariance matrix [7–10] or on a combination of both [11].

Another shortcoming of the classical approach to PCA is that it fails to process missing elements, which frequently occur in the experimental data. What is often done in this situation is to delete the experimental variable (data column) or object (data row) containing the missing elements or to replace the missing element with the corresponding column's or row's mean. However, the deleting process leads to loss of supposedly important information and is undesired when the amount of missing elements is large. From statistical point of view, any replacement action provides a wrong estimation of the mean, standard deviation, sample covariance and moreover destroys the correlation structure of the data. From practical point of view, this can lead to improper conclusions and can set incorrect hypothesis still in the beginning of the analysis. For instance, in environmental data analysis a possible pollution can go unnoticed or a costly remediation procedure can take place when this is unnecessary. There are better ways for dealing with missing data. Different methods treating the problem of missing information in principal component analysis have been discussed in the literature [12–16]. Among them is the self-consistent iterative procedure called expectation maximization (EM). It is a flexible method, which allows computing model's parameters while filling in the missing information directly.

* Corresponding author. Tel.: +48 32 359 2115; fax: +48 32 259 9978.
E-mail address: beata@us.edu.pl (B. Walczak).

Dealing with missing data and outlying observations simultaneously is an ongoing problem. The presence of outlying observations in the data disturbs a correct replacement of missing elements as well as the presence of missing elements does not allow adequate outliers' identification.

In this paper, we propose a computationally efficient and relatively simple method for exploring data containing missing elements and outliers in terms of PCA. The proposed approach, denoted later in the text as EM-SPCA, consists of implementing a robust version of PCA, such as spherical PCA, in the expectation maximization algorithm. For convenience, the results obtained from EM-SPCA are compared to expectation maximization classical PCA (EM-PCA) by the use of simulated and real data sets.

2. Theory

2.1. Classical principal component analysis (PCA)

Principal component analysis, is mostly used for data compression and visualization [17]. The main goal of this method is to explain the information contained in the data by a set of the so-called principal components, PCs. The PCs are mutually orthogonal and are a linear combination of the original data variables. Since the orthogonal PCs are constructed to maximize the description of the data variance, the first PC describes the largest portion of the data variability, whereas the following ones, the information not explained by the previous PCs. Moreover, each PC carries different information about the data variability. In most applications, PCA allows compression of the data to a few PCs that can be later used to visualize the data structure and they contain almost the same information as the original data. Therefore, PCA is usually the first step in almost any data analysis, and PCs serve as an input to most of the chemometric techniques, e.g. clustering methods, neural networks, etc. Despite of the compression issue that PCA offers, it is vulnerable to outliers in the data due to its least squares nature. Outliers strongly affect the data variance and the true correlation structure of the data. This implies a crucial impact upon overall picture of the data structure since the outliers are responsible for rotating the PCs axes towards them. The robust versions of PCA are considered as a remedy to the problem with outliers.

2.2. Robust PCA by means of spherical PCA

The spherical PCA, SPCA, aims to construct a robust PCA model [18], i.e. a PCA model not influenced by outlying objects. In spherical PCA, this goal is fulfilled by projecting the data objects onto a hyper-sphere of unit radius with center in the robust center of data. In order to define a robust center of the data, the L1-median estimator is used. The L1-median center is a point in the multivariate space that minimizes the sum of all the Euclidian distances between this point and data objects [19].

The authors of SPCA proposed another approach to robust PCA called elliptical PCA. In this method, data are firstly scaled, i.e. each element of data variable is divided by its corresponding robust scale measure (for example the Q_n estimator [20]) and

SPCA is then performed. In elliptical PCA, EPCA, the objects are projected onto a hyper-ellipse instead of on a hyper-sphere. The radii of a hyper-ellipse are proportional to the robust scales of the data variables. However, it is pointed out by Boente and Fraiman [21] that elliptical PCA has problems with consistency. Therefore, only spherical PCA is considered in this paper.

In the first step of the SPCA approach, the data are centered about L1-median. The projection of objects onto a hyper-sphere with a robust center at L1-median and with a unit radius, \mathbf{x}_i^p , can be presented as:

$$\mathbf{x}_i^p = \frac{\mathbf{x}_i - \mu_{L1}(\mathbf{X})}{\|\mathbf{x}_i - \mu_{L1}(\mathbf{X})\|} + \mu_{L1}(\mathbf{X}) \quad (1)$$

where \mathbf{x}_i is the i th data object, $1/\|\mathbf{x}_i - \mu_{L1}(\mathbf{X})\|^2$ is its weight, $\mu_{L1}(\mathbf{X})$ is the L1-median center and $\|\cdot\|$ denotes the Euclidean norm.

At this point, it is important to notice that the denominator of the above formula informs about the Euclidean distance of each object from the robust data center. Therefore, objects being far from the robust data center are far from data majority as well, and thus, they receive small weights. By using such a weighing scheme, the influence of outliers upon the PCA model is diminished.

Later on, classical PCA is performed on the data projected onto a sphere what essentially corresponds to PCA applied to weighted data. After the PCA decomposition, robust scores and robust loadings are obtained.

Once the robust PCA model is constructed, it is possible to perform outlier identification on the basis of two types of distances, namely robust and orthogonal distances, describing every data object [22]. In fact, the robust distance is the Mahalanobis distance of an object, which informs about its location with respect to the robust data center within the space of the robust scores. Robust distance (RD_i) of the i th object is expressed as:

$$RD_i = \sqrt{\sum_{a=1}^f \frac{t_{ia}^2}{v_a}} \quad (2)$$

where $a = 1, 2, \dots, f$ denotes the number of robust principal components, t_a the a th principal component and the v_a is its eigenvalue.

The orthogonal distance of an object describes how far the object from the space of the robust model is. Orthogonal distances for all objects are computed as follows:

$$OD = \|\mathbf{X} - \mu_{L1}(\mathbf{X}) - \mathbf{T}\mathbf{P}^T\| \quad (3)$$

where the robust scores matrix, \mathbf{T} , and robust loadings matrix, \mathbf{P} , contain f factors.

Taking both distances into account, the data objects can be classified into four categories. The regular objects are characterized by small robust and orthogonal distances. Good leverage objects have large robust distances and small orthogonal distances. High residuals objects have small robust distances, but large orthogonal distances, whereas bad leverage observations have large both robust and orthogonal distances. In order to identify objects with large distances compared to the majority of

objects, one can use robust z -scores. The robust z -scores are obtained by centering each type of distance, d , about its median, $\mu(d)$ and dividing the elements by their corresponding robust scale, $\sigma(d)$ (e.g. the Q_n robust scale) as follows:

$$z = \frac{|d - \mu(d)|}{\sigma(d)}. \quad (4)$$

To identify objects with large distances, one can use a default cut-off value equal to three.

The Q_n estimator is a robust measure of scale and for a single variable, s , it corresponds to the first quartile of the sorted pair-wise differences between all variable elements. It can be expressed as follows:

$$Q_n = 2.2219c\{|s_i - s_j|; i < j\}_{(k)} \quad (5)$$

where

$$k = \binom{h}{2} \approx \binom{m}{2} / 4,$$

$h = [m/2] + 1$ and c is a correction factor, which depends on the number of objects, m . When the number of objects increases c tends to 1.

For comparison purpose, the same type of plots can be constructed in classical PCA. The classical distance is then calculated using the classical PCA score vectors. The classical z -scores are obtained by the use of classical measures of location and scale, i.e. mean and standard deviation.

Although there are many robust PCA approaches available (e.g. [1–11]), the main advantage of the spherical PCA approach is its conceptual simplicity and computational efficiency since the most time demanding step is PCA. By the use of the so-called kernel approaches to PCA for wide data matrices, the algorithm can be considerably speeded up [23], and thus, the construction of the SPCA model is fast. Since the EM method is computationally time-consuming, a fast robust PCA procedure should be applied. Therefore, SPCA will be considered here.

Despite its attractive properties, SPCA has a shortcoming: it fails to perform appropriate outlier's identification when data contain clusters. An outlier is an object, which is far from data majority. When data contain groups, the objects belonging to a whole group might be undesirably considered outliers [22].

2.3. EM-PCA and EM-SPCA

Classical PCA and spherical PCA, described above, can be implemented relatively easy in the expectation maximization framework. The EM procedure starts with initialization of the missing elements using for instance, the corresponding row's and column's means. In the follow-up iterations, the missing elements are re-filled in with their predicted values according to the currently constructed PCA or SPCA model. In general, the PCA model can be presented as a product of two matrices:

$$X = TP^T, \quad (6)$$

where X is the original data matrix of m objects and n variables, T of dimension $m \times f$ holds the first f score vectors and P ($n \times f$) is the matrix containing the PCA loadings.

The EM algorithm iterates while the convergence criterion is not satisfied, which means while small changes in the model's residuals in two consecutive iterations are not observed. Once the convergence of the algorithm is reached, the elements replacing the missing values have residuals equal to zero. This means that the filled in values perfectly fit the PCA model of definite complexity and therefore, the differences between the original X (with filled in missing values according to PCA model) and predicted X are equal to zero. For the remaining elements (observed elements) these differences are not zeros. The missing elements are not taken into account in the model construction. The model is determined only based on the observed elements.

The steps of EM-PCA can be schematically described in the following way:

1. Initialize the missing elements by column's and row's means.
2. Preprocess the data.
3. Perform singular value decomposition (SVD) of the complete data set or other method of data decomposition.
4. Predict X according to the PCA model described by Eq. (6) using the predefined number of factors.
5. Re-fill in the missing elements with their predicted values according to the currently constructed model and go to step 2 while the convergence criterion is not fulfilled.

The algorithm of EM-SPCA follows almost the same scheme, but steps 2, and 3 are combined together as one, which performs spherical PCA and missing elements are initialized using the column's and row's medians in step 1. Like classical PCA, the prediction of X is also done according to the model described by Eq. (6), but using the robust scores and loadings.

In the above-described algorithms, the complexity of the final EM-PCA or EM-SPCA is assumed to be known beforehand. When this is not the case, a variant of a cross validation procedure should be involved. However, for a large data set, this can be a very time-consuming step. In EM-PCA, the selection of an optimal number of factors can be performed based on the minimum observed on the curve displaying eigenvalues versus number of factors. A similar way of a factor selection procedure can be adopted in EM-SPCA using robust eigenvalues. Another possibility can be to use the number of factors, which explain about 80% of data information [22]. This is also the rule used in our study.

Another important issue is how to preprocess data with missing values. Usually in classical PCA, the data are first centered, which involves the subtraction of the column's means from each corresponding data element. Centering or any other transformation of the data has to be performed within the iterative steps of the EM algorithm. This implies a proper estimation of the column's means or/and standard deviations together with the process of re-filling in the missing information in the data. Concerning the EM robust PCA approach, when there are large

differences in the variables' range and units, a standardization procedure in spherical PCA is considered.

3. Results and discussion

3.1. A simulation study

The goal of the simulation study is to show the performance of the proposed method, EM-SPCA, in exploring data containing missing elements and outliers simultaneously. For this purpose, a data set of a definite complexity was generated from the normal distribution, $N(0,1)$. This means that each element of X ($m \times n$) comes from the population with zero mean and unit standard deviation. In order to obtain data of definite complexity, after data decomposition by means of PCA, X is reconstructed according to the PCA model defined by Eq. (6), using score and loading matrices (T of dimension $m \times f$ and P of dimension $n \times f$) with selected number of latent factors, f . The choice of latent factors depends entirely on the user and does not follow any special requirements. Furthermore, a normally distributed noise is additionally added to the data. The final simulation model is $X = TP^T + E$, where E is a $m \times n$ matrix, the elements of which are generated from multivariate normal distribution, $N(0,1)$. To keep the level of noise low, the generated values are multiplied by 0.2. In this way, a data set without missing elements and outliers, but with known complexity is created. In our study, X is of dimension 98×20 with complexity four, i.e. the original data matrix, X , was reconstructed using four PCs.

In the next step of the study, different percentages (5, 10, 15, 20, 25, 30, 35, 40, 45 and 50, respectively) of elements were deleted from the data. The deleting mechanism is done completely at random, which means that the missingness is not related to variables of the data in terms defined by Rubin [24]. In order to simulate different patterns of a particular amount of missing elements, the deleting procedure was repeated 50 times. Moreover, to obtain information about the variability in the data depending on the different percentages of missing elements, the changes in the model's residuals evaluated only for observed elements can be traced. As it was already mentioned above, the residuals for the values replacing the missing elements are equal to zero. The root mean squared (RMS) error is evaluated as an average of 50 repetitions.

Fig. 1 presents the results from a comparative study of two algorithms, i.e. EM-PCA and EM-Spherical PCA, applied to normally distributed data with missing elements. Such a comparative study aims to show that the robust estimator performs similarly to the classical estimator at normal models. The models are indeed of complexity equal to four explaining above 90% of data information.

In general, the averaged RMS values decrease with the increasing percentage of missing elements (see Fig. 1a). This trend is expected since RMS is evaluated only for the observed elements, the number of which decreases with the increasing number of missing elements. Another important observation is that all the averaged RMS values obtained from the EM-SPCA algorithm are slightly higher than the RMS values obtained from EM-PCA. This is not also a surprising observation, because the

robust estimators by definition show higher variance at normal models. There are no objects exceeding the cut-off values in the classical and robust distance–distance plots drawn for data with missing elements. Such plots are presented, for example, for data containing 10% of missing elements in Fig. 1b and c.

A more interesting case is to compare the performances of the methods when data contain both outliers and missing elements. Therefore, 10% of outliers were included in the original data. For this purpose, the error term E added to X is chosen such that 90% of objects have the normal distribution $N(0,1)$ multiplied by factor 0.1 to keep the level of noise low, and 10% of objects, being outliers, have multivariate distribution $N(10,1)$. Higher percentages of outliers were not considered in our study, because the breakdown point of SPCA is the highest possible one. In other words, the method will provide correct estimates even for highly contaminated data.

Fig. 1d shows clearly that the robust technique outperforms the classical EM-PCA method. The mean trimmed RMS values are much smaller for EM-SPCA than for the EM-PCA approach. The trimming operation has a sense only for the robust approach in order to honestly represent the model fit in the data. The outliers have high residuals, i.e. high orthogonal distances, when using a robust approach and their influence on RMS has to be discarded. In our study, the trimming procedure is done by weighting the objects exceeding the cut-off value of orthogonal distance. The orthogonal outliers and bad leverage observations receive weights proportional to the inverses of their distances to the cut-off line. The object, which is farther from the cut-off line, receives the smaller weight and consequently, it has the smaller impact on the RMS value estimated. In the simulated data set, the outliers are objects with nos. 1–10. Furthermore, the classical distance–distance plot (see Fig. 1e) fails to identify the ten outliers (nos. 1–10), whereas they are correctly found in the robust distance–distance plot (see Fig. 1f).

3.2. Convergence properties of the proposed method

Concerning the issues of the algorithm's convergence, one can monitor the stability of the replaced missing values in consecutive iterations or the changes in the objective function defined for the k th iteration as:

$$SS_k = \sum_p \sum_q (x_{pq})^2, \quad p, q \in \text{missing elements} \quad (7)$$

The model obtained will be the same in both situations. In our study, the differences in replaced values were traced. The calculations were considered converged when the sum of squared differences estimated for the re-filled values of the missing elements in two consecutive iterations were smaller than 10^{-8} . In general, the algorithm's convergence depends upon the complexity of the PCA model, percentage of missing elements and their distribution and most importantly upon the correlation structure of the data. If the data correlation structure is well defined, the convergence is achieved very rapidly. Otherwise, the convergence is slow and eventually not reached. For illustration, the number of iterations necessary to satisfy the convergence crite-

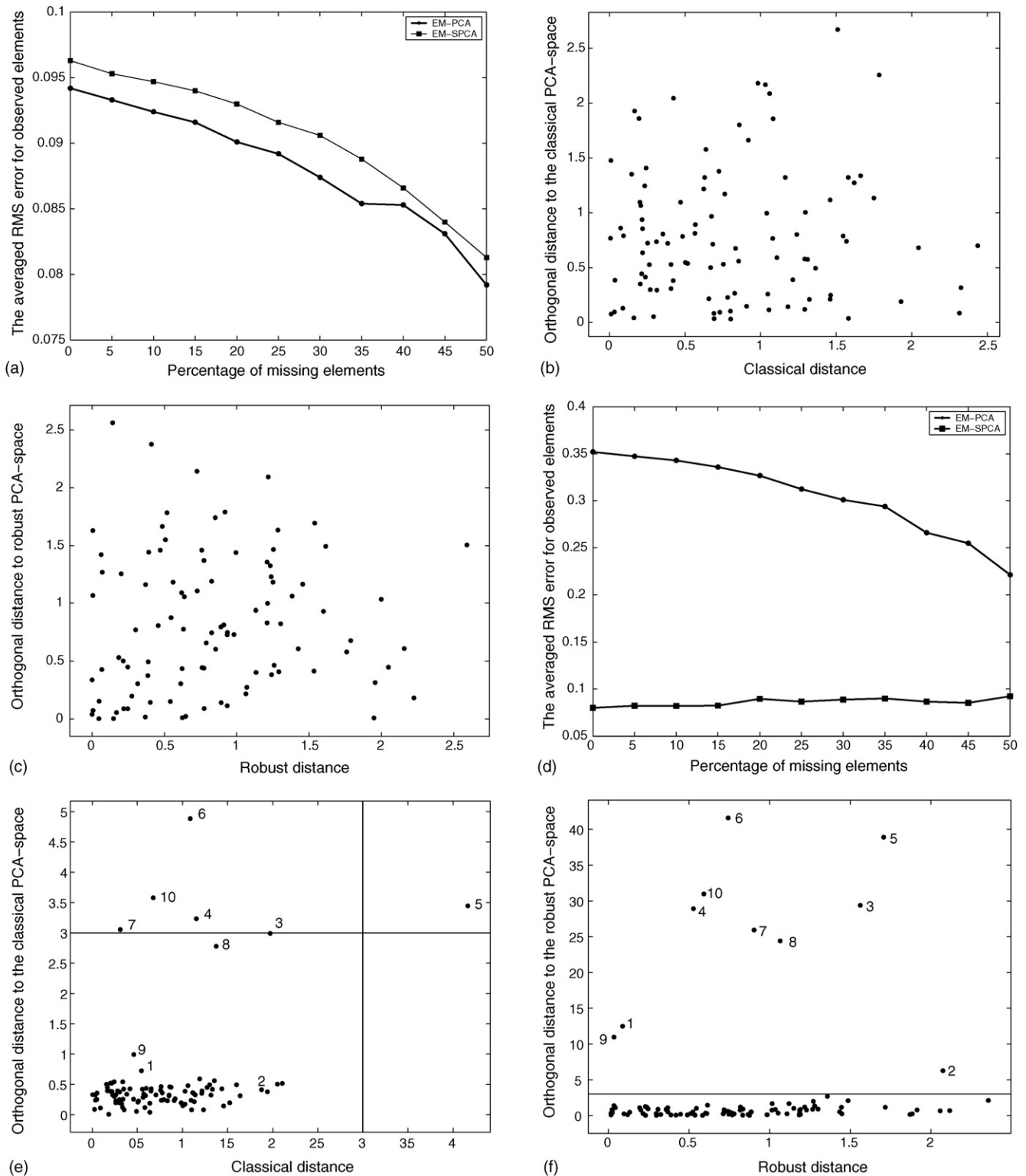


Fig. 1. Results of a simulation study: (a) the averaged RMS error calculated for observed elements as a function of percentage of missing elements for EM-PCA and EM-SPCA applied to normally distributed data, (b) the classical distance–distance plot constructed via EM-PCA applied to normally distributed data with 10% of missing elements, (c) the robust distance–distance plot constructed via EM-SPCA applied to normally distributed data with 10% of missing elements, (d) the averaged RMS error calculated for observed elements as a function of percentage of missing elements for EM-PCA and EM-SPCA applied to contaminated data, (e) the classical distance–distance plot constructed via EM-PCA applied to contaminated data with 10% of missing elements and (f) the robust distance–distance plot constructed via EM-SPCA applied to contaminated data with 10% of missing elements.

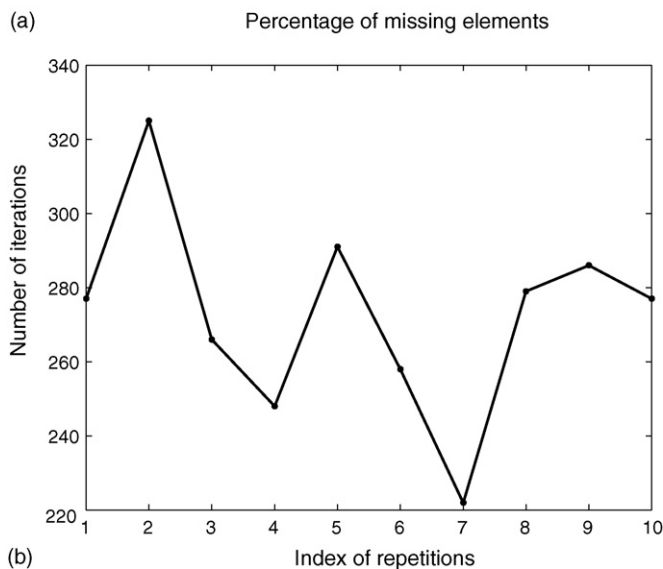
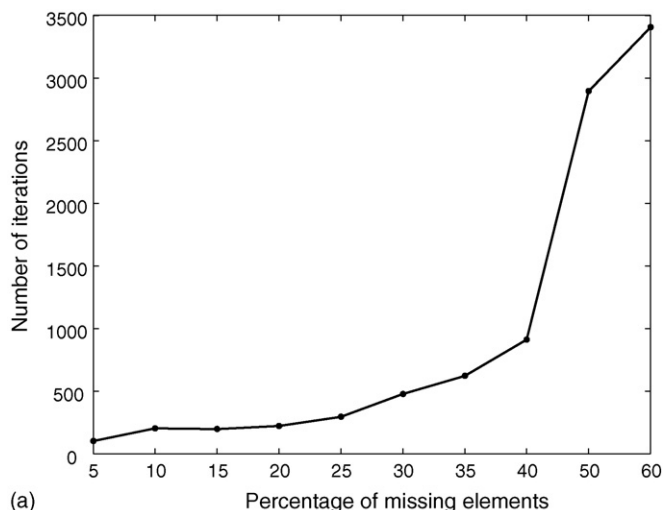


Fig. 2. Convergence properties of EM-SPCA: (a) number of iterations as a function of percentage of missing elements (number of iterations is an average of 50 runs of the algorithm applied to data with different random patterns of missing elements) and (b) number of iterations needed to achieve convergence in 10 consecutive runs of the algorithm.

tion is shown as a function of percentage of missing elements in the data in Fig. 2. The number of iterations is a mean value of 50 repetitions.

The number of iterations increases with the increasing number of missing elements (see Fig. 2a). Moreover, different number of iterations is needed depending upon the distribution of missing elements. This is shown for data containing outliers and 20% of missing elements in Fig. 2b. It is important to stress that the EM algorithm converges to the optimal solution no matter the number of iterations or the pattern of missing elements.

3.3. Application of EM-PCA and EM-SPCA to a real data set

The environmental data set contains the annual mean levels of nine major ions (H^+ , NH_4^+ , Na^+ , K^+ , Ca^{2+} , Mg^{2+} , Cl^- , NO_3^- and SO_4^{2-}) measured in various sampling sites (Haunsberg, Innervillgraten, Kufstein, Reutte, Litschau, Luntz, Nassfeld,

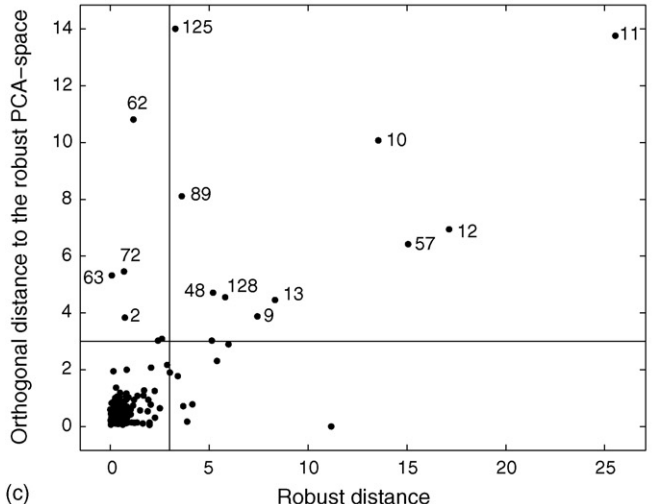
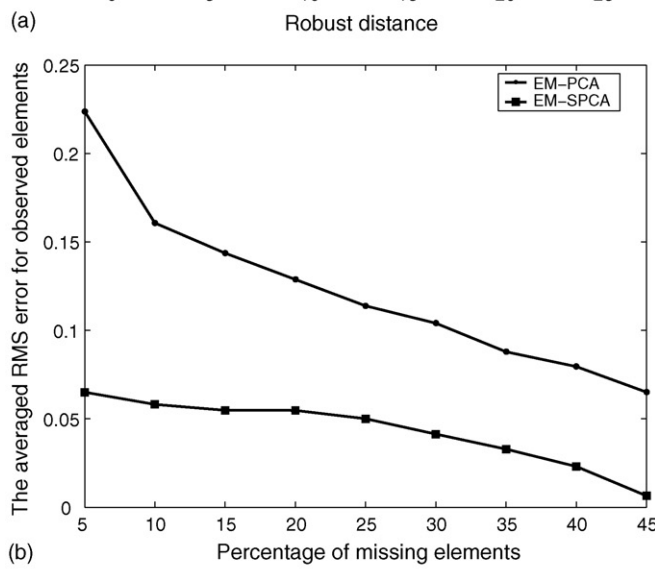
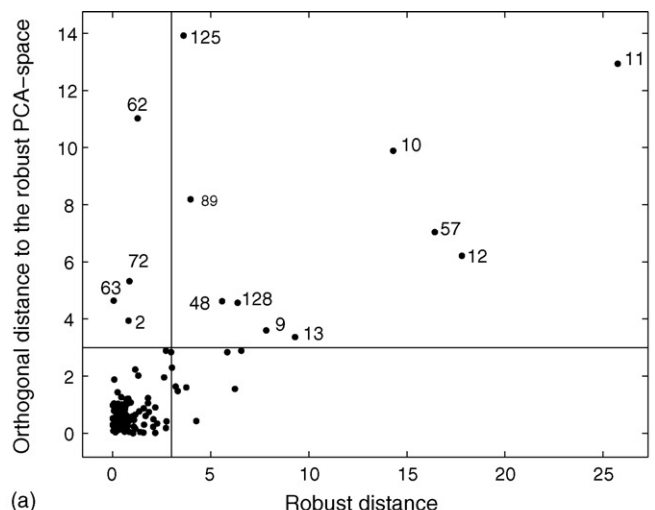


Fig. 3. Results of the study on a real data set: (a) the robust distance–distance plot constructed via SPCA (with standardization) applied to data without missing elements, (b) the averaged RMS error calculated for observed elements as a function of percentage of missing elements for EM-PCA and EM-SPCA applied to the studied environmental data and (c) the robust distance–distance plot constructed via EM-SPCA applied to the environmental data set containing 5% of missing elements.

Nasswald, Lobau, Sonnblick and Werfenweng) in Austria, over different periods of time (1988–1999). The data set is known to have several outlying observations [22], but there are no missing elements. The distance–distance plot obtained from SPCA (with standardization) applied to data without missing elements is shown in Fig. 3a. The diagnostic plot is constructed using four robust PCs explaining around 84% of data information. All objects exceeding the cut-off line of orthogonal distance are considered outliers. The largest orthogonal distances are observed for objects nos. 10, 11, 62 and 125 (see Fig. 3a). Unlike objects 62 and 125, objects 10 and 11 exhibit large robust distances as well.

The measured variables are in different ranges and units and the autoscaling procedure lends them the same importance in the data analysis. In EM-PCA, autoscaling is performed using column's means and standard deviations, whereas in EM-Spherical PCA this is done using column's medians and robust scales, Q_n . As already mentioned, the data transformation should be performed within the steps of the EM approach. In this way, the mean, median, standard deviation and robust scale are updated together with the missing information in the data.

The results from the comparison study of the EM-PCA and EM-SPCA approaches are presented in Fig. 3b for environmental data where different percentages of elements were deleted. The complexity of all the models is four. It can be seen that the EM-SPCA method clearly outperforms the EM-PCA in terms of lower trimmed RMS values. Every RMS value is a mean of 50 repetitions in Fig. 3b. Similarly to the results obtained from the simulation study, RMS decreases with the increasing percentage of missing elements. Looking at the distance–distance plot obtained for data with 5% nondetects, one can observe (see Fig. 3c) the same outliers identified like in the case without missing elements in the data.

4. Conclusions

The presented study proposes a combined approach for dealing successfully with missing elements and outliers present simultaneously in the data. It basically consists of robust version of PCA embedded within the expectation maximization framework. The robust version of PCA used in our study has been shown to have good robust properties. Only slightly worse performance at normal data models has been observed. Another attractive property is its computational efficiency.

The simulation study showed that EM-Spherical PCA is an efficient tool for processing data containing missing elements and outliers. When the experimental parameters measured has to be scaled in a robust way then a standardization step within the EM-SPCA algorithm should be concerned. This situation is demonstrated on a real environmental data set known to contain outlying observations. The EM-SPCA method (with standardization) was applied to these data after deleting different amounts of elements. The results lead to the same general conclusion as

the one of the simulation study and namely that expectation maximization robust PCA is the preferred method over the classical approach when exploring data sets with nondetects and outliers. In particular, it is shown that EM-SPCA with implemented robust scaling outperforms EM-PCA with non-robust standardization.

Acknowledgements

I. Stanimirova and B. Walczak are grateful for financial support concerning scientific activities within the Sixth Framework Programme of the European Union, project TRACE—“TRACING food Commodities in Europe” (project no. FOOD-CT-2005-006942). The publication reflects only the author's views and the community is not liable for any use that may be made of the information contained therein.

M. Daszykowski is grateful to Foundation for Polish Science for the financial support.

References

- [1] G. Li, Z. Chen, *J. Am. Stat. Assoc.* 80 (1985) 759–766.
- [2] L. Ammann, *J. Am. Stat. Assoc.* 88 (1993) 505–514.
- [3] C. Croux, A. Ruiz-Gazen, *COMPSTAT: Proceedings in Computational Statistics 1996*, Physica-Verlag, Heidelberg, Germany, 1996, pp. 211–217.
- [4] C. Croux, A. Ruiz-Gazen, High breakdown estimators for principal components: The Projection Pursuit approach revisited, vol. 29, *The IMS Bulletin*, 2000, p. 270.
- [5] M. Hubert, P. Rousseeuw, S. Verboven, *Chemometr. Intell. Lab. Syst.* 60 (2002) 101–111.
- [6] R.A. Maronna, *Ann. Stat.* 4 (1976) 51–67.
- [7] C. Croux, G. Haesbroeck, *Biometrika* 87 (2000) 603–618.
- [8] M. Hubert, S. Engelen, *Bioinformatics* 20 (2004) 1728–1736.
- [9] M. Hubert, P.J. Rousseeuw, K. Vanden Branden, *Technometrics* 47 (2005) 64–79.
- [10] H. Hove, Y.-Z. Liang, O.M. Kvalheim, *Chemometr. Intell. Lab. Syst.* 27 (1995) 33–40.
- [11] R.A. Maronna, *Technometrics* 47 (2005) 264–273.
- [12] B. Grung, R. Manne, *Chemometr. Intell. Lab. Syst.* 42 (1998) 125–139.
- [13] S. Roweis, *IEEE 2001 Int. Conf. on Computer Vision (ICCV 2001)*, Vancouver, Canada, July 2001.
- [14] B. Walczak, D.L. Massart, Part I, *Chemometr. Intell. Lab. Syst.* 58 (2001) 15–27.
- [15] A. Smoliński, B. Walczak, J.W. Einax, *Chemosphere* 49 (2002) 233–245.
- [16] P.R.C. Nelson, P.A. Taylor, J.F. McGregor, *Chemometr. Intell. Lab. Syst.* 35 (1996) 45–65.
- [17] S. Wold, K. Esbensen, P. Geladi, *Chemometr. Intell. Lab. Syst.* 2 (1987) 37–52.
- [18] N. Locantore, J.S. Marron, D.G. Simpson, N. Tripoli, J.T. Zhang, K.L. Cohen, *Sociedad de Estadística e Investigación Operativa Test* 8 (1999) 1–74.
- [19] P.J. Huber, *Robust Statistics*, Wiley, New York, The USA, 1981.
- [20] P.J. Rousseeuw, C. Croux, *J. Am. Stat. Assoc.* 88 (1993) 1273–1283.
- [21] G. Boente, R. Fraiman, *Test* 8 (1999) 28–35.
- [22] I. Stanimirova, B. Walczak, D.L. Massart, V. Simeonov, *Chemometr. Intell. Lab. Syst.* 71 (2004) 83–95.
- [23] W. Wu, D.L. Massart, S. de Jong, *Chemometr. Intell. Lab. Syst.* 36 (1997) 165–172.
- [24] D.B. Rubin, *Biometrika* 63 (1976) 581–592.

Spectrophotometric determination of Fenitrothion in formulations and environmental samples

P. Subrahmanyam^{a,b}, B. Krishnapriya^{a,b}, L. Ravindra Reddy^{a,b},
B. Jayaraj^{a,b}, P. Chiranjeevi^{a,b,*}

^a Department of Mathematics, S.V. University, Tirupati 517502, Andhra Pradesh, India

^b Environmental Monitoring Laboratories, Department of Chemistry, S.V. University, Tirupati 517502, Andhra Pradesh, India

Received 5 September 2006; received in revised form 1 October 2006; accepted 1 October 2006

Available online 13 November 2006

Abstract

A facile, rapid and sensitive spectrophotometric method was developed for the determination of Fenitrothion in its formulations, water, food grain and agriculture soil samples with newly synthesised reagent. The method was based on the alkaline hydrolysis of Fenitrothion pesticide and resultant hydrolysed product of Fenitrothion was coupled with diazotised 4,4'-methylene bis-(*p*-amino-2'-carboxybenzanilide) in basic medium to give yellow coloured product having λ_{\max} 482 nm. The formation of coloured derivatives with the coupling agent is instantaneous and stable for 30 h. Beer's law was obeyed in the concentration range 0.2–13.0 $\mu\text{g mL}^{-1}$. The proposed method is sensitive, easy to operate and permitted the determination of Fenitrothion with a detection limits 0.075 $\mu\text{g mL}^{-1}$. The experimental results indicate that the procedure can eliminate the fundamental interferences caused by other pesticides and non-target ions, which made these methods more sensitive and selective. The method was applicable to the determination of Fenitrothion residue in water, food grain and soil samples up to ng level.

© 2006 Elsevier B.V. All rights reserved.

Keywords: Fenitrothion; 4,4'-Methylene-bis-(*p*-amino-2'-carboxybenzanilide); Diazotization method (DM); Spectrophotometry; Water; Food grain and agriculture soil samples

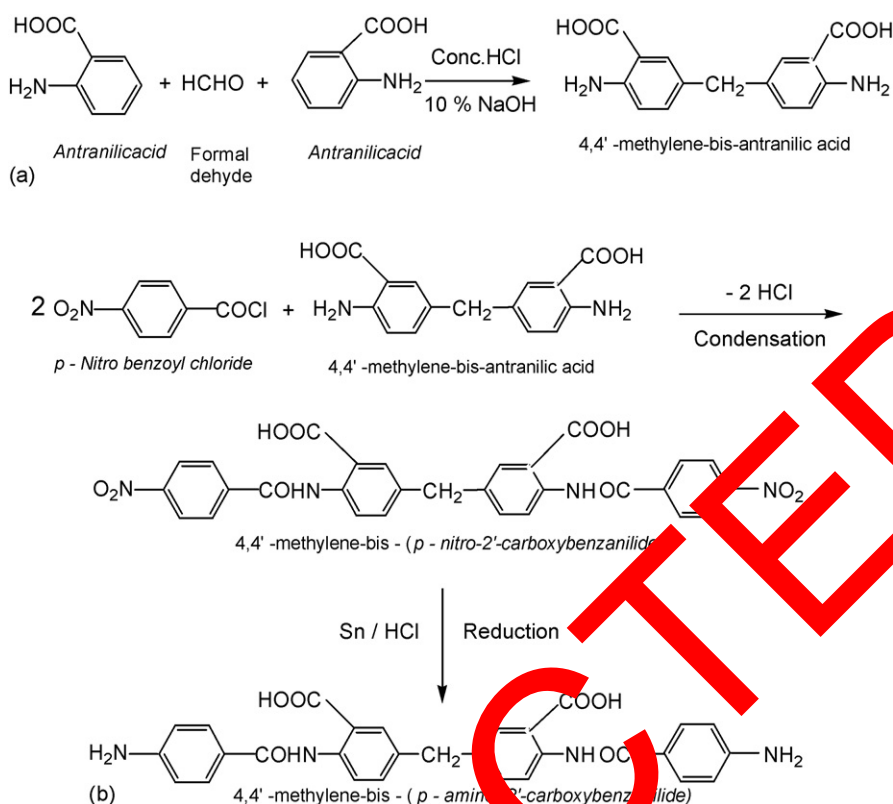
1. Introduction

Fenitrothion (*o,o*-dimethyl-*o*, *p*-nitro-3-methylphenyl phosphorothionate) belongs to an organophosphorus pesticide, extensively applied on crops. Due to indiscriminate application, it finds a way to surface water bodies, through agriculture runoff and municipal waste water systems by ingestion and inhalation. Finally, it reaches the human system. Many methods have been developed for the determination of Fenitrothion [1–11]. The spectrophotometric methods based on the using diazotization in the presence of oxidising agents and its metabolites by various alkaline hydrolysis of the pesticides have been determined [12–17].

In view of its wide applicability still there is a need for the development of sensitive and reliable methods for the assessment of quality of insecticide formulations and the quantitative residual analysis of Fenitrothion in water and agriculture soil samples. The present paper deals with a simple, sensitive and economical spectrophotometric method for the determination of Fenitrothion in its formulations, water and agriculture soil samples. Here, authors successfully synthesised a new reagent, 4,4'-methylene-bis-(*p*-amino-2'-carboxybenzanilide) for the sensitive, selective spectrophotometric determination of Fenitrothion based on the hydrolysed product followed by diazotization. These methods offers better advantages of sensitivity, selectivity and reproducibility than the reported methods [18]. The quantitative and qualitative estimation of these pesticides in their formulations, water (spiked), food grains (wheat and rice) and agriculture soil samples were determined using their spectral data. This forms additional advantageous spectrophotometric methods to analyse Fenitrothion pesticide in water, food grain and agriculture soil samples.

* Corresponding author at: Environmental Monitoring Laboratories, Department of Chemistry, S.V. University, Tirupati 517502, Andhra Pradesh, India. Tel.: +91 877 2250556; fax: +91 877 2261274.

E-mail address: chiranjeevipattium@gmail.com (P. Chiranjeevi).



Scheme 1. (a) Synthesis of 4,4'-methylene-bis-antranilic acid. (b) Synthesis of 4,4'-methylene-bis-(*p*-nitro-2'-carboxybenzanilide).

2. Experimental

2.1. Synthesis of 4,4'-methylene-bis-(*p*-amino-2'-carboxybenzanilide)

Antranilic acid of 13.3 g was dissolved in 125 mL acetone and 25 mL of 36.5% hydrochloric acid at 50 °C. The reaction mixture was then treated with 35 mL of 2% aqueous formaldehyde solution at 60 °C with stirring for 1 h and neutralised with 5 M sodium hydroxide. The solid obtained was filtered, washed with hot water, dried and recrystallized from acetic acid (mp 135 °C; yield, 87%) as shown in Scheme 1a.

A 4.25 g of *p*-nitro benzoyl chloride was dissolved in 50 mL of ethanol and added 10 g of 4,4'-methylene-bis-antranilic acid to perform condensation by heating on water bath at 50–65 °C for 3 h. The reaction mechanism is shown in Scheme 1b. The crude product was collected and reduction with 0.5 g of Sn and 5 mL of concentrated HCl were added and the mixture is left for 30 min to reduce from nitro group to amino group. The product was filtered and purified with acetone and recrystallized by aqueous ethanol (mp 242 °C, yield, 72%) as shown in Scheme 2.

2.2. Apparatus and reagents

A HITACHI U 2001 spectrophotometric with 1.0 cm matched quartz cells were used for all absorbance measurement. An Elico Li-29 model pH metre with combined glass electrode was used for pH measurements.

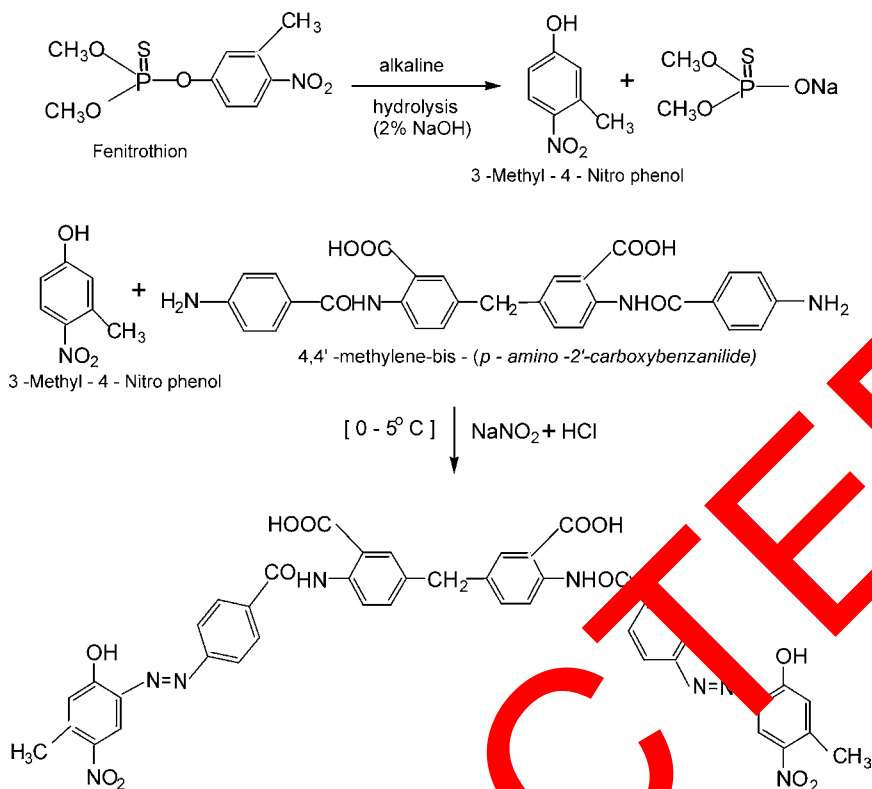
All the chemicals and reagents used were of analytical reagent grade and double-distilled water was used through out experiments. The reagents like sodium hydroxide, sodium nitrate, potassium carbonate, anhydrous sodium sulphate and HCl were purchased from S.D. Fine Chemicals, Mumbai, India. Anthranilic acid, acetone, formaldehyde, *p*-nitrobenzylchloride, methanol, chloroform and tin were purchased from Merck Chemicals, Mumbai, India. The technical grade samples of Fenitrothion pesticide in the form of 50% wettable powder and 75% EC were obtained from Bayer India Ltd., Mumbai, India. The reagents like sodium hydroxide (2%), sodium nitrate (0.3%), 1N HCl were prepared. The solvents like methanol, chloroform, acetone were purified and employed for the present investigation.

2.2.1. Stock Fenitrothion solution (1 mg mL⁻¹)

A stock solution (1 mg mL⁻¹) of Fenitrothion (Rallis India Limited, Bangalore, India) was dissolved in methanol and working standard solution (10 μg mL⁻¹) was prepared by appropriate dilution with distilled water.

2.2.2. 4,4'-Methylene-bis-(*p*-amino-2'-carboxybenzanilide) (2%)

4,4'-Methylene-bis-(*p*-amino-2'-hydroxybenzanilide) (2%) was prepared by dissolving 2 g of 4,4'-methylene-bis-(*p*-amino-2'-carboxybenzanilide) in 20 mL of 5 M HCl and then made up to 100 mL with distilled water.



Scheme 2. Reaction mechanism of the 4,4'-methylene-bis-(*p*-amino-2'-carboxybenzanilide) with Fenitrothion.

2.2.3. Potassium carbonate solution (0.1 M)

Potassium carbonate solution (0.1 M) was prepared by dissolving 1.3821 g of potassium carbonate in distilled water and diluted to 100 mL.

2.2.4. Sodium hydroxide solution (2%)

Sodium hydroxide solution (2%) was prepared by dissolving 2 g of sodium hydroxide in distilled water and diluted to 100 mL.

2.2.5. Sodium nitrate solution (0.3%)

Sodium nitrate solution (0.3%) was prepared by dissolving 0.3 g of sodium nitrate in distilled water and diluted to 100 mL.

2.2.6. 1N HCl solution

HCl solution of 1N was prepared by diluting concentrated HCl with distilled water.

2.2.7. Buffer (pH 8.0–10.0)

An amount of 5 mL concentrated sulphuric acid is added to 250 mL distilled water in a 500 mL flask. A 25 g of mono potassium dihydrogen phosphate is added to this, shaken until dissolution is complete and diluted to 500 mL for pH 8.0–10.0.

2.3. Procedure for the determination of Fenitrothion residues

The coloured derivatives of Fenitrothion were prepared by azo coupling reaction, 20 mL of Fenitrothion standard solution was taken in a clean dry 100 mL beaker, 5 mL of 2%

NaOH solution was added and kept for 20 min for complete hydrolysis to yield 3-methyl-4-nitro phenol. Diazonium salt 4,4'-methylene-bis-(*p*-amino-2'-carboxybenzanilide) was prepared using 4 mL of 0.3% NaNO₂ and 4 mL of 1N HCl for coupling reaction at 0–5 °C. The reaction mechanism of the colour compounds was shown in Scheme 2. The pH of the reaction was maintained between 8.0 and 10.0 as shown in Fig. 2. The spectra for the above reactions were recorded in the UV–vis region as shown in Fig. 1 and optical, precision and accuracy data were shown in Table 1. Beer's law was obeyed over the range from of 0.2–13.0 μg mL⁻¹. This data were used for the analysis for water, food grain and agriculture soil samples.

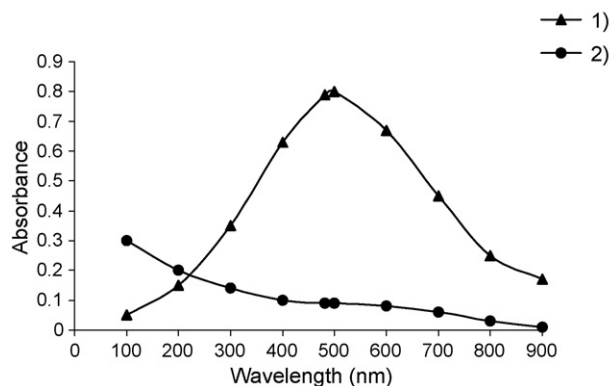


Fig. 1. Absorption spectra of the Fenitrothion. (1) Fenitrothion + 4,4'-methylene-bis-(*p*-nitro-2'-carboxybenzanilide), (2) reagent blank.

Table 1
Optical characteristics, precision and accuracy of the method with coupling reagent 4,4'-methylene-bis-(*p*-amino-2'-carboxybenzanilide)

Optical characteristics	Diazotisation method (DM)
Concentration range ($\mu\text{g mL}^{-1}$)	0.2–13.0
λ_{max} (nm)	482
Colour	Orange
Limit of detection ($\mu\text{g mL}^{-1}$)	0.077
Limit of quantification ($\mu\text{g mL}^{-1}$)	4.147
Stability of the colour (h)	30 h
Molar absorptivity ($\text{L mol}^{-1} \text{cm}^{-1}$)	1.859×10^4
Sandell's sensitivity ($\mu\text{g cm}^{-2}$)	0.0147
Regression equation ($Y = bx + a$)	
Slope (b)	0.0299
Intercept (a)	0.0197
Standard error (%)	0.0015
Standard deviation (S.D.) ^a	0.267
Correlation coefficient	1.002
Relative error (%)	1.10

^a Calculation for five samples containing same amount of Fenitrothion where x is the concentration in $\mu\text{g mL}^{-1}$.

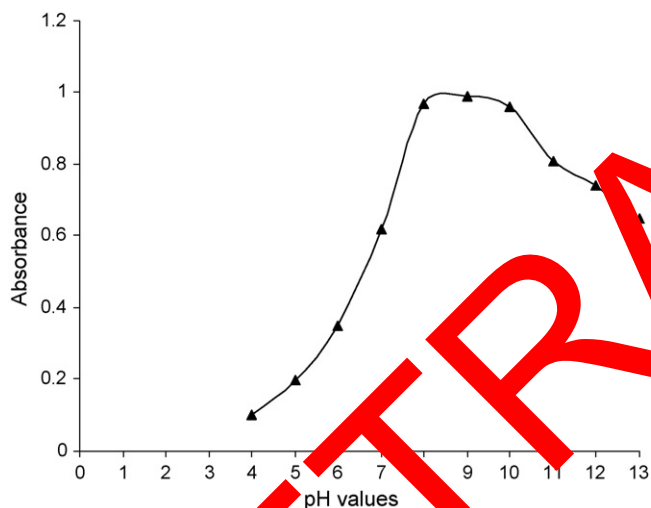


Fig. 2. Effect of pH on diazotisation method for determination of Fenitrothion.

2.4. Procedure for the determination of Fenitrothion in its formulation

Fenitrothion 25% wettable powder, 75% EC and 98.7% technical grade were analysed using the aforesaid procedure by

Table 3
Recovery of Fenitrothion residue from spiked water samples

Sample number	Diazotisation method (DM)			<i>F</i> -test	<i>t</i> -Test	Reported method [18] recovery \pm S.D. ^a (%)
	Taken ($\mu\text{g mL}^{-1}$)	Found ($\mu\text{g mL}^{-1}$)	Recovery \pm S.D. ^a (%)			
1.	30.70	30.58	99.60 \pm 0.129	0.673	0.434	99.40 \pm 0.030
2.	60.50	60.00	99.00 \pm 0.170	0.673	1.454	97.60 \pm 0.031
3.	90.60	90.36	99.70 \pm 0.309	0.453	0.229	99.60 \pm 0.275
4.	120.30	120.10	99.80 \pm 0.275	0.490	0.221	99.70 \pm 0.310
5.	135.40	135.20	99.80 \pm 0.221	0.677	0.169	99.67 \pm 0.036
6.	150.50	150.40	99.90 \pm 0.310	0.284	0.294	99.80 \pm 0.036

^a $n = 5$.

Table 2
Determination of Fenitrothion in its insecticidal formulation using coupling agent 4,4'-methylene-bis-(*p*-amino-2'-carboxybenzanilide)

Formulation	4,4'-Methylene-bis-(<i>p</i> -amino-2'-carboxy benzanilide)
25% Wettable powder	24.94 \pm 0.07
75% EC	74.95 \pm 0.04

coupling with diazotised compound 4,4'-methylene-bis-(*p*-amino-2'-carboxybenzanilide). The method was compared with already reported methods in literature [18]. Percentage recovery of the Fenitrothion in the above formulations was shown in Table 2.

2.5. Procedure for the determination of Fenitrothion in water samples

The water samples were spiked with concentrations in the ranges from 30.70–150.50 $\mu\text{g mL}^{-1}$ in methanol in this method under study are given in Table 3. The spiked water samples were extracted with chloroform. The combined extracts were washed with 0.1 M potassium carbonate solution to break any emulsion formed during the extraction and dried over anhydrous sodium sulphate. Finally, chloroform was evaporated to dryness on a steam bath and the residue was dissolved in methanol and the amount was determined using the procedures described earlier.

2.6. Procedure for the determination of Fenitrothion in grain samples (wheat and rice)

The grain samples (rice and wheat) of 50 g each were taken in warming blender and blended for 5 min with 100 mL of chloroform. The samples were spiked with different concentrations of insecticides ranging from 45.94 to 304.20 $\mu\text{g mL}^{-1}$ in methanol and blended for 3 min chloroform was filtered and the residue was retained. The residue was washed twice with 10 mL of chloroform and blended for 3 min. The chloroform extracts were evaporated on a steam bath and the residue was dissolved in methanol and the amount was determined by the procedure outlined earlier. The results are summarised in Table 4.

Table 4
Recovery of Fenitrothion residue from grain samples (rice and wheat)

Sample number	Diazotisation method (μM)						Reported Method [18]						
	Rice			Wheat			Rice			Wheat			
	Taken (μg mL ⁻¹)	Found (μg mL ⁻¹)	Recovery ± S.D. ^a (%)	F-test	t-Test	t-Test	Taken (μg mL ⁻¹)	Found (μg mL ⁻¹)	Recovery ± S.D. ^a (%)	F-test	t-Test	Rice	Wheat
1.	45.94	44.90	97.70 ± 0.182	1.006	3.516	2.494	48.95	48.86	99.80 ± 0.091	0.284	2.494	94.00 ± 0.182	97.50 ± 0.182
2.	85.58	84.92	99.23 ± 0.182	0.583	1.170	2.214	88.12	86.94	98.79 ± 0.560	0.013	2.214	98.00 ± 0.258	98.10 ± 0.091
3.	135.50	134.80	99.56 ± 0.150	0.754	0.322	0.474	137.42	136.84	99.60 ± 0.182	0.284	0.474	99.00 ± 0.182	99.32 ± 0.091
4.	165.30	164.80	99.70 ± 0.182	0.284	0.004	0.290	184.81	184.17	99.67 ± 0.070	0.677	0.290	99.05 ± 0.091	99.45 ± 0.091
5.	235.70	232.15	98.50 ± 0.567	0.004	0.952	0.394	302.14	300.30	99.40 ± 0.182	0.284	0.394	97.50 ± 0.182	99.20 ± 0.091
6.	304.20	302.04	99.30 ± 0.182	0.000	0.216	0.241	303.14	301.30	99.40 ± 0.091	1.000	0.241	98.90 ± 0.182	99.25 ± 0.091

^a n = 5.

2.7. Procedure for the determination of Fenitrothion in agriculture wastewater and soil samples

Agriculture wastewater samples (10 mL) were collected from S.V. Agricultural Research Station, Tirupati, India and the water samples were extracted with chloroform (2 × 10 mL). The chloroform extracts was then evaporated to dryness under reduced pressure and the residue was dissolved in 25 mL of 50% methanol and amount of the Fenitrothion was determined by the described procedure earlier. A 10 g of agricultural soil samples was extracted according to the reported method [18] and the amount of the Fenitrothion was analysed by the aforesaid procedure.

3. Results and discussions

Table 1 shows that the reaction of coloured products to the coupling reaction of the pesticide samples with the reagents under study are instantaneous and stable over a reasonable period of time indicates its advantage over reported methods [18]. Beer's law was observed in the concentration range from 0.2 to 13 μg mL⁻¹ indicating low Sandell's sensitive values. The results obtained for Fenitrothion (Table 1) was reproducible with low relative standard deviation ranges from 0.257. Limit of quantification (LOQ) is determined by taking the ratio of standard deviation (σ) of the blank with respect to water and the slope of calibration curve(s) multiplied by a factor of 3. This means that LOQ is approximately three times limit of detection (LOD). Naturally, the LOQ slightly crosses the lower limit of Beer's law range. However, LOD is well below the lower limit of Beer's law range. The upper limit of the Beer–Lambert's range is determined by a plot of absorbance against concentration at the value of λ_{max}. Beyond this limit the correlation results were strongly affected. The correlation coefficient values obtained for this reaction was very close to unity suggesting that the absorbance depends upon the concentration of the Fenitrothion. The values obtained for the relative standard deviation and percentage error suggest that these new procedures offer a good precision and accuracy.

The data included in Table 2 show that the active ingredient present in the formulations of Fenitrothion can be successfully determined spectrophotometrically using the new reagent. The results of these recoveries reveal that the amounts close to the manufacturer's specifications and these are favourably compared with the method reported in literature [18] was shown in Table 5. These observations suggested that the other ingredients present in these formulations do not interfere. Hence, the methods can be adopted as an additional method for a routine control of the purity of the commercial insecticide formulations. The data presented in Tables 3 and 4 suggested that the percentage of pesticide recovery from fortified water and grain samples range from 97.70 to 99.90%. Tables 3 and 4 indicate that the percentage recovery of the Fenitrothion from water and grain samples is as follows:

- water samples > wheat samples;
- wheat samples > rice samples;
- water samples > rice samples.

Table 5
Comparison of Fenitrothion in its formulations and environmental samples

Samples	Fenitrothion added ($\mu\text{g mL}^{-1}$)	Proposed method				Reported method [18] recovery \pm S.D. ^a (%)
		Found ($\mu\text{g mL}^{-1}$)	Recovery \pm S.D. ^a (%)	F-test	t-Test	
Formulation						
5% Dust	–	4.91	98.90 \pm 0.14	0.286	4.29	94.50 \pm 0.08
25% Wettable powder	–	24.25	99.28 \pm 0.13	0.321	4.71	95.50 \pm 0.08
75% EC	–	74.21	98.77 \pm 0.08	0.929	4.22	97.62 \pm 0.07
Water samples^b						
Spiked water	9.0	8.86	98.77 \pm 0.08	0.929	4.22	97.50 \pm 0.07
Natural water	9.0	8.92	99.44 \pm 0.11	0.754	0.32	97.50 \pm 0.07
Food grains						
Rice	15.0	14.81	98.00 \pm 0.14	0.013	2.214	97.70 \pm 0.18
Wheat	15.0	14.75	98.73 \pm 0.09	0.094	0.952	97.50 \pm 0.56
Agriculture soil samples^c						
Sample 1	25.0	24.38	98.40 \pm 0.09	0.57	0.35	96.73 \pm 0.13
Sample 2	25.0	24.31	98.10 \pm 0.07	0.091	0.50	97.70 \pm 0.182

Recovery in (%), amounts of insecticide in μg .

^a Average values for $n=6$.

^b Agricultural samples collected from S.V. Agricultural Research Institute, Tirupati, Andhra Pradesh, India.

^c Agricultural samples collected from Mallam, Chittamuru Mandal, Nellore District, Andhra Pradesh, India.

These methods reveal that the percentage recovery of the Fenitrothion in food grains was observed as: rice > wheat.

It is evident from tables that the proposed methods are simple, convenient, rapid and sensitive. Moreover, these methods do not involve elaborate cleanup procedures as is required by the other methods. Hence, our proposed methods describe here would serve as additional techniques for the estimation of the Fenitrothion in spiked water, food grain and agriculture soil samples.

3.1. Analytical application

The proposed methods were applied to the determination of Fenitrothion in spiked water, food grains (rice and wheat) and agriculture soil samples. The results obtained were in good agreement with the reported method [18] were given in Table 5.

4. Conclusion

The present study describes simple analytical procedure for the determination of Fenitrothion in its formulations, fortified water and food grains. The comparison of the proposed method with the other methods or the determination of Fenitrothion by spectrophotometry was given in Table 5. The preparation of the coupling reagent 4,4'-methylene-bis-(*p*-amino-2'-carboxybenzanilide) is simple and convenient to synthesis in any ordinary laboratory. The colour derivatives of the Fenitrothion are more stable than the other reported methods [18].

The proposed method has the following distinct advantages:

- (i) Need not to purchase the reagents for the determination of Fenitrothion.

- (ii) The results of the Fenitrothion recovery from spiked water and food grain samples with the reagents have good agreement results than the reported methods in literature [18].
- (iii) The proposed methods can be applied routine control for the determination of Fenitrothion in its commercial formulations and environmental samples.
- (iv) All the non-target species do not interfere with the present method.
- (v) The statistical analysis of the results indicate that the present method has good precision and accuracy and the present method does not involve elaborated cleanup procedure as required by the other methods.

Acknowledgements

The authors are grateful to Bayer (India) Ltd., Bombay, for the supply of technical grade Fenitrothion and the Head of the Department, Department of Biotechnology, S.V. University, Tirupati for providing instrumental facility to carry out this work.

References

- [1] M. Lurini, A. Lagan, N.M. Petronion, M.V. Russo, *Talanta* 27 (1980) 45.
- [2] E. Morlthoff, *Phanzenschutz-Nachr* (Am. Ed), 21, 1968, p. 331.
- [3] V.L. Kurunshkin, Y.N. Bogoslowvskil, Y.N. Aif Saint, *J. Chromatorgr.* 58 (1982) 10.
- [4] Y. Aoki, M. Takeda, M. Vchiyama, *J. Assoc. Offic. Anal. Chem.* 58 (1976) 1286.
- [5] D.C. Abbott, J.O.C. Bunidge, J. Thomas, K.S. Webb, *Analyst* 93 (1967) 170.
- [6] G.W. Ivic, J.E. Casida, *J. Agric. Food Chem.* 19 (1971) 405.
- [7] H. Stan, H.J. Goebel, *J. Chromatogr.* 268 (1983) 55.
- [8] B.S. Attri, *J. Ent. Abstr. Ent. News Lett. (India)* 6 (1976) 37.
- [9] M. Umeda, *J. Pharm. Soc. Jpn.* 83 (1963) 951.
- [10] C.S.P. Sastry, D. Vijaya, *Talanta* 34 (1986) 372.
- [11] D.K. Das, T.V. Mathew, A.K. Mukherjee, S.N. Mitra, *J. Food Sci. Technol.* 7 (1970) 62.

[12] S.N. Deshmuckh, T.S. Sidhu, *J. Food Sci. Technol.* 11 (1974) 81.
[13] N. Ramakrishna, B.V. Ramachandra, *Analyst* 101 (1976) 528.
[14] C.S.P. Sastry, D. Vijaya, *J. Food Sci. Technol.* 23 (1986) 336.
[15] P. Murthy, N. Krishna, *Bull. Environ. Contam. Toxicol.* 32 (1984) 59.

[16] Y. Nishizawa, *Bull. Agric. Chem. Soc. Jpn.* 24 (1960) 744.
[17] Y. Nishizawa, *J. Agric. Biol. Chem.* 25 (1961) 605.
[18] M.V. Norris, E.W. Easter, L. Fuller, E.J. Kuchar, *J. Agric. Food. Chem.* 6 (1958) 111.

RETRACTED

Highly selective flow injection spectrophotometric determination of gold based on its catalytic effect on the oxidation of variamine blue by potassium iodate in aqueous *N,N*-dimethylformamide medium

Demetrius G. Themelis^{a,*}, Anastasios V. Trellopoulos^a,
Paraskevas D. Tzanavaras^b, Michael Sofoniou^a

^a Laboratory of Analytical Chemistry, Department of Chemistry, Aristotle University of Thessaloniki, GR-54124 Thessaloniki, Greece

^b Quality Control Department, Cosmopharm Ltd., P.O. Box 42, 20100 Korinthos, Greece

Received 27 July 2006; received in revised form 6 October 2006; accepted 19 October 2006

Available online 21 November 2006

Abstract

A highly selective and simple flow injection method is reported for the determination of Au(III) in jewel samples. The method is based on the catalytic effect of Au(III) on the oxidation of 4-amino-4'-methoxydiphenylamine hydrochloride (Variamine Blue B base, VB) by KIO₃. The colored reaction product was monitored spectrophotometrically at 546 nm. A volume fraction of 40% *N,N*-dimethylformamide (DMF) greatly enhances the selectivity of the method. The chemical (pH and concentrations of reagents) and instrumental variables (sample injection volume, reagents flow rates, reaction coil length) affecting the determination were studied and optimized. Under the selected values, the analyte could be determined in the range of 0.1–12.0 mg L⁻¹ ($r = 0.9997$), at a sampling rate of 120 h⁻¹. The proposed assay was precise ($s_r = 0.8\%$ at 5.0 mg L⁻¹ Au(III), $n = 12$) and adequately sensitive with a 3σ limit of detection of 0.03 mg L⁻¹. The method was successfully applied to the analysis of jewel samples. The obtained results were favorably compared to flame atomic absorption spectrometry (FAAS) used as a reference method.

© 2006 Elsevier B.V. All rights reserved.

Keywords: Flow-injection analysis; Gold; Spectrophotometry; Variamine Blue B base; Jewel samples

1. Introduction

The rapid, sensitive, highly selective, and routine automatic determination of Au(III) traces in environmental, geological, metallurgical, and technological samples has received increasing attention in recent years. An ideal automatic analytical method for routine analysis should be simple to operate, cost-effective, robust, precise, and accurate and have a high sample analysis frequency. Flow injection (FI) analysis is a well-established analytical technique that fulfilled the above-mentioned demands.

The majority of the FI methods developed for the determination of Au(III) are using on-line sorption preconcentration procedures with various detection systems, such as flame atomic absorption spectrometry (FAAS) [1–11], inductively couple plasma mass spectrometry (ICP-MS) [12–14], induc-

tively couple plasma atomic emission spectrometry (ICP-AES) [15], chemical vapor-generation atomic absorption spectrometry (CVG-AAS) [16,17], chemical vapor-generation graphite furnace atomic absorption spectrometry (CVG-ETAAS) [18], and spectrofluorimetry [19].

Although these methods are generally sensitive, the procedures involved can prove to be complex and were implemented using hardly available and expensive sophisticated instruments that require skilled and well-qualified personnel for operation and maintenance. Besides, they are subject to a number of interferences, which frequently require the use of masking agents, extraction with toxic organic solvents or prior separation. Furthermore, most of them are using unique chemicals and there are difficulties in selecting the most suitable sorbent which must meet specific requirements, i.e., rapid sorption and desorption of the analytes, in order to be used in FI on-line preconcentration and separation systems.

FI-spectrophotometry is an advantageous alternative to the previously mentioned systems for the analysis of gold, in terms

* Corresponding author. Tel.: +30 2310 997804; fax: +30 2310 997719.
E-mail address: themelis@chem.auth.gr (D.G. Themelis).

of simplicity and low operational cost. So far, one rather selective FI-spectrophotometric method has been reported for the determination of gold in ores and anode slimes [20]. The method is based on the reaction of gold(III) and 5-(4-sulphophenylazo)-8-aminoquinoline (SPA) in the presence of cetyltrimethylammonium bromide (CTAB). However, this method shows some drawbacks, such as high detection limit (1.1 mg L^{-1}), limited throughput rate (45 h^{-1}), a rather complicated five-channel manifold, and the usage of unique chemicals, such as SPA, which is not commercially available and must be synthesized.

The present FI-spectrophotometric work shows better analytical figures of merits and without the limitations of the above FI-spectrophotometric method. The developed assay is based on the catalytic effect of Au(III) on the oxidation of 4-amino-4'-methoxydiphenylamine hydrochloride (Variamine Blue B base, VB) by KIO_3 in aqueous *N,N*-dimethylformamide (DMF) medium [21]. The usage of DMF highly enhanced the selectivity of the method. Low detection limit (0.03 mg L^{-1}) and broad linear dynamic range ($0.1\text{--}12 \text{ mg L}^{-1}$) were achieved without any preconcentration step, while simple and cost-effective instrumentation is used throughout the work. The applicability of the developed procedure was assessed by successfully analyzing jewel samples and the method was favorably compared to flame atomic absorption spectrometry used as a reference method.

2. Experimental

2.1. Reagents

All chemicals were of analytical-reagent grade and were provided by Merck (Darmstadt, Germany) unless stated otherwise and all solutions were made up with ultra-pure quality water, which was produced by a Milli-Q system (Millipore Bedford, USA).

Working Au(III) solutions ($\text{pH} \approx 0.8$ with HCl) were made daily by appropriate dilutions of the stock Au(III) solution ($\gamma = 1000 \text{ mg L}^{-1}$, in $w(\text{HCl}) = 8\%$, Merck). The mentioned acidity of the Au(III) solutions prevents the ions from hydrolysis.

The 4-amino-4'-methoxydiphenylamine hydrochloride was provided by Sigma (St. Louis, USA). The stock solution of VB ($c(\text{VB}) = 1 \times 10^{-3} \text{ mol L}^{-1}$) was prepared daily by dissolving the appropriate amount in 100 mL of water. Working solutions of VB were prepared by dilution immediately before use and they contained a volume fraction of 40% *N,N*-dimethylformamide.

Constant ionic strength ($I = 0.2 \text{ mol L}^{-1}$) buffer solution ($\text{pH} \approx 0.8$) was prepared from CH_3COONa and HCl solutions (1.0 mol L^{-1} each), adjusting the ionic strength by the addition of appropriate amounts of KCl.

All solutions were de-gassed with purified nitrogen prior to use. All stock solutions were stored in polyethylene containers. All the polyethylene containers and glassware used for aqueous solutions containing metal ions were cleaned in (1 + 1) nitric acid, while the rest were cleaned in Decon 90 ($w = 3\%$) and then all were rinsed with ultra-pure quality Milli-Q water before use.

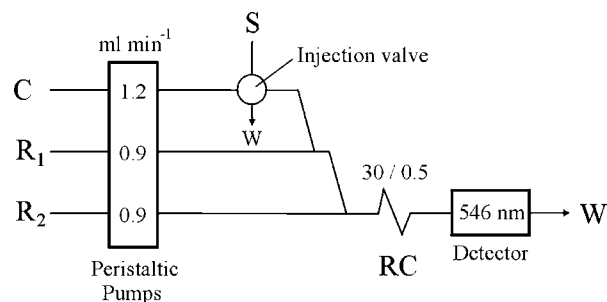


Fig. 1. Preferred FI manifold for the determination of Au(III). S: sample ($V = 100 \mu\text{L}$), C: carrier stream of buffer solution ($\text{pH} 0.75$), R_1 : $5 \times 10^{-5} \text{ mol L}^{-1}$ KIO_3 reagent stream, R_2 : $5 \times 10^{-5} \text{ mol L}^{-1}$ VB in $\phi = 40\%$ DMF reagent stream, W: waste, RC: reaction coil. Numbers above coil denote coil length (cm)/i.d. (mm).

2.2. Instrumentation

The FI system used was a Tecator 5010 analyzer (Tecator, Hoganas, Sweden) with a Tecator chemifold Type III SR that is shown schematically in Fig. 1. The detector used was a Tecator 5023 FI star double-beam spectrophotometer, consisting of a 5032-detector controller and a 5023-011 spectrophotometer optical unit. A printer was included with the detection system and allowed modification of the readout from the 5032-detector controller by means of direct digital communication with the 5010 analyzer. The absorbance of the colored oxidation product was monitored at 546 nm through a 1 cm path length flow cell with an internal volume of $18 \mu\text{L}$. The flow system comprised 0.5 mm i.d. Teflon tubing throughout. Tygon pump tubes were used for delivering aqueous solutions while solvent flexible pump tubes were used for DMF solutions.

A Perkin-Elmer Model 5100 PC atomic absorption spectrometer (Norwalk, CT, USA) was used to determine Au(III) by using FAAS as the reference method. The impact bead data for FAAS measurements were: wavelength = 242.8 nm; slit = 0.7 nm.

A Haake E12 thermocirculating water bath was used in order to study the effect of temperature during the preliminary studies.

An Orion EA940 pH-meter (Cambridge, MA, USA) was employed for the pH measurements with absolute accuracy limits at the pH measurements being defined by NIST buffers.

2.3. Procedure for aqueous solutions

Using the preferred FI set up in Fig. 1, $100 \mu\text{L}$ of a solution containing between 0.1 and 12.0 mg L^{-1} Au(III) were injected directly into the carrier pH adjusting stream (C), which merged successively with the KIO_3 (R_1) and the VB (R_2) reagent streams. The colored oxidation product was formed on passage of the mixture through a 30 cm long reaction coil (RC) and its absorbance was measured in the flow-through cell at 546 nm. The transient signal from the detector was recorded as a peak, the height of which was proportional to the Au(III) concentration in the sample, and was used for all measurements. The recorded peaks were sharp and the baseline was stable. The cycle time was set at 30 s with a 15 s cycle injection time. Using the cycle time of 30 s, 120 injections per hour were made. Five replicate injections per sample were made in all instances.

2.4. Pretreatment and determination of gold in jewel samples

The jewel samples were first washed with ethanol to remove fat and dirt. When dry, an accurately weighed amount of ca. 0.5 g sample turnings were transferred to a beaker and 20 mL of aqua regia were added. The beaker was covered and heated gently by a thermostated hot-plate until the dissolution of the sample. When the dissolution of the sample was completed, the resulting solution was carefully evaporated to a small volume (5–7 mL) to remove NO_3^- ions. After cooling at room temperature, the resulting solution was diluted to 100 mL in a volumetric flask with Milli-Q water, adjusting its acidity to $\text{pH} \approx 0.8$ with HCl. Furthermore, 0.25 mL of the resulting solution was diluted to 250 mL in a volumetric flask with Milli-Q water to bring the sample within the dynamic range of the calibration graph, adjusting its final acidity to $\text{pH} \approx 0.8$ by HCl. Finally, the sample was analyzed using both the above-described FI procedure for aqueous solutions and the reference FAAS method, after filtration through a 45 μm filter.

3. Results and discussion

3.1. Preliminary studies

It is well established that VB can be oxidized by KIO_3 in organic/aqueous medium to form iminoquinone derivatives [22]. Using the FI system shown in Fig. 1, preliminary experiments confirmed the catalytic action of Au(III) to the oxidation of VB by KIO_3 under flow conditions. The reaction product showed maximum absorption at 546 nm. A buffer solution ($\text{pH} \approx 1.1$, $I = 0.2 \text{ mol L}^{-1}$) was prepared from CH_3COONa and HCl solutions (1.0 mol L^{-1} each), adjusting the ionic strength by the addition of appropriate amount of KCl. The amount concentrations of VB, KIO_3 were fixed at 5.0×10^{-5} and $1.0 \times 10^{-4} \text{ mol L}^{-1}$, respectively. A 5.0 mg L^{-1} Au(III) standard solution was used throughout the preliminary experiments.

It is known that the use of organic solvents increases both the sensitivity and the selectivity of the catalytic activity of metal ions. So, in the preliminary studies a volume fraction of 30% DMF was added in the VB reagent solution rather than being a separate stream, in order to simplify the manifold.

Also, experiments showed that there is no dependence of the reaction rate on temperature within the range 15–35 °C, confirming the findings of the batch method [21]. Therefore, further experiments were performed without preliminary thermostatic control of the solutions. The injection volume was 60 μL , while all flow rates were fixed at 0.9 mL min^{-1} and the length of the reaction coil was 60 cm.

3.2. Investigation of chemical variables

The chemical variables that affect the determination were studied using the set up shown in Fig. 1 at an Au(III) mass concentration of 5 mg L^{-1} . The univariate approach was adopted throughout. The starting values of the FI variables were: $V = 60 \mu\text{L}$, $l(\text{RC}) = 60 \text{ cm}$ and $q(\text{C}) = q(\text{KIO}_3) =$

$q(\text{VB}) = 0.9 \text{ mL min}^{-1}$. Five replicate injections were made in all instances.

The influence of the pH of the carrier stream on the reaction development was studied in the range 0.8–5.2. The amount concentrations of VB and KIO_3 were fixed at 5.0×10^{-5} and $1.0 \times 10^{-4} \text{ mol L}^{-1}$, respectively, and the volume fraction of DMF in VB was 30%. The results showed that the sensitivity was decreased by ca. 25%, increasing the pH from 0.8 to 2.0, and then it continues decreasing slightly until the pH reaches the value of 5.2. A pH of 0.8 was selected for further studies both to ensure that hydrolysis of the analyte is prevented and to get the highest possible sensitivity.

Keeping the pH at ca. 0.8, the effect of the amount concentration of the VB reagent solution was studied in a range 1.0×10^{-5} to $2.5 \times 10^{-4} \text{ mol L}^{-1}$. The amount concentration of KIO_3 was fixed at $1.0 \times 10^{-4} \text{ mol L}^{-1}$, while the volume fraction of DMF in VB was kept constant at 30% in all cases. The experiments showed that the signals increased for VB amount concentrations in the range 1.0×10^{-5} to $2.0 \times 10^{-5} \text{ mol L}^{-1}$, leveled-off in the range 2.0×10^{-5} to $7.5 \times 10^{-5} \text{ mol L}^{-1}$, and decreased thereafter. A VB amount concentration of $5.0 \times 10^{-5} \text{ mol L}^{-1}$ was used for further experiments.

The effect of the KIO_3 amount concentration was studied in a range 5.0×10^{-6} to $2.0 \times 10^{-4} \text{ mol L}^{-1}$, keeping the other chemical variables at the selected values mentioned above. The experiments showed a maximum absorbance for a KIO_3 amount concentration of $5 \times 10^{-5} \text{ mol L}^{-1}$. This concentration was, therefore, chosen in all subsequent experiments.

The effect of DMF volume fraction in the VB reagent solution was studied in the range of 0–60%. The pH and the amount concentration of VB and KIO_3 reagents solutions were kept at their selected values stated above. An increase of the absorbance was observed, reaching a maximum at a DMF volume fraction of 40%. This value was selected for further experiments. Additionally, selectivity experiments using Fe(III), Cu(II), Ru(IV), Os(VIII), as model ions, confirmed the findings of the batch procedure [21], since a ca. 50-fold increase of the tolerance of the method against Fe(III), 40-fold increase against Cu(II), 4-fold increase against Os(VIII), and 2-fold increase against Ru(IV) was observed in the presence of DMF. After these findings, the usage of DMF was adopted for the rest of selectivity studies described in Section 3.5.

3.3. Investigation of the FI variables

In order to proceed with the final system design, the effect of the FI variables was studied by using the univariate approach. The effects of sample injection volume, reaction coil length, and the flow rate of each stream were studied under the above-preferred chemical variables. The cycle time was set within the range of 30–45 s with a 15–25 s cycle injection time depending on the variable examined. Au(III) standard was prepared at 5.0 mg L^{-1} and this standard was investigated as a function of the FI operating variables.

In FI, the sensitivity of a method may be varied as a function of sample injection volume. To increase the sensitivity, a larger volume of sample is injected and, thus, a higher product

concentration is observed. This is especially important when using a fixed path length spectrophotometric detector. Keeping all flow rates fixed at 0.9 mL min^{-1} and the reaction coil length at 60 cm, the injection loop volume was varied from 30 to 200 μL by changing the length of sample loop in the injection valve. The peak heights increased nonlinearly with increasing sample size. This property of FI is a result of limited sample zone dispersion. A sample volume of 100 μL was selected as a compromise between sensitivity and sample injection rate.

The influence of the reaction coil length was investigated in the range 12–200 cm using 0.5 mm i.d. Teflon tubing throughout. In this reaction coil, the colored oxidation product of VB by KIO_3 catalyzed by Au(III) was formed. The length of the reaction coil determined the time the reaction was allowed to proceed prior to detector. At the same time, the colored oxidation product was subject to dispersion as it traveled through the tubing. There was an optimal coil length that maximized the reaction rate before the dispersion effects began to predominate. The signal intensity goes through a maximum at a reaction coil length of 30 cm, thus this value was chosen for subsequent studies. At a length greater than 30 cm, any further production of the colored oxidation product was negated by the dispersion effects.

The flow rate of the carrier stream was varied in the range $0.5\text{--}2.4 \text{ mL min}^{-1}$. The peak heights increased nonlinearly with increasing carrier flow rate, but leveled off at a flow rate of above 1.6 mL min^{-1} . However, flow rates higher than 1.2 mL min^{-1} resulted in unstable baseline and decreased precision of the assay. Therefore, a carrier flow rate of 1.2 mL min^{-1} was adopted for further experiments.

Under the selected flow rate of the carrier stream, the effect of the KIO_3 and the VB flow rates were studied in a range $0.5\text{--}2.4 \text{ mL min}^{-1}$. In both cases, the maximum sensitivity was obtained at the flow rate of 0.9 mL min^{-1} . This value was selected for both the reagent and the oxidant streams. At flow rates greater than 0.9 mL min^{-1} , any further production of the colored oxidation product was negated by dispersion effects.

3.4. Features of the proposed method

Under the preferred chemical and instrumental conditions described above and using the FI set up shown in Fig. 1 and a cycle time of 30 s (120 injections per hour), a calibration graph in the range of $0.1\text{--}12.0 \text{ mg L}^{-1}$ Au(III) is described by the least-squares equation,

$$A = (1.8 \pm 5.4) \times 10^{-3} + (79.9 \pm 0.7) \times 10^{-3} \gamma(\text{Au(III)})$$

Table 3
Analysis of real samples

Sample	Au(III) found by FI ^a (mg g^{-1})	Au(III) found by FAAS (mg g^{-1})	e_r (%) ^b	t^c
S ₁	749	767	−2.3	1.88
S ₂	882	903	−2.3	1.92

^a Mean of five results.

^b Relative error.

^c The critical value of t for 8 degrees of freedom is 2.31 ($P=0.05$).

Table 1
Selectivity against various ions on the determination of 5.0 mg L^{-1} Au(III) using the selected conditions given under the procedure for aqueous solutions

Ion added ^a	Tolerated mass concentration ratio
SO_4^{2-}	1500
PO_4^{3-}	1000
F^-	800
Cu(II)	400
Os(VIII)	200
Mn(II), Ru(IV)	100
Cr(III), Fe(III)	50

^a These ions in the stated level caused a relative error of $\leq \pm 3\%$.

Table 2
Accuracy studies of the proposed method

Au(III) added (mg L^{-1})	Au(III) found ^a (mg L^{-1})	R^b (%)
1.00	0.97	97
2.00	2.06	103
3.00	2.94	98

^a Mean of five results.

^b Percent recovery.

where A is the peak height absorbance as measured by the detector, and $\gamma(\text{Au(III)})$ is the mass concentration of the analyte, in mg L^{-1} , with a relative standard deviation of $s_r = 0.8\%$ (at 5.0 mg L^{-1} , $n = 12$), a correlation coefficient of $r = 0.9997$, and a 3σ detection limit of 0.03 mg L^{-1} . All the standards were run in five replicate injections ($n = 5$), while for the detection limit calculation, the blank was run in 10 replicate injections ($n = 10$).

3.5. Selectivity studies

Using the FI setup shown in Fig. 1 and under the preferred conditions described above, the possible interfering effects of many diverse ions upon the determination were examined, at $\gamma(\text{Au(III)}) = 5 \text{ mg L}^{-1}$. The criterion for no interference was a change of less than $\pm 3\%$ of the average absorbance signal. The results are summarized in Table 1. The following ions were studied in addition to those included in Table 1: Al(III), Ag(I), Bi(III), Ca(II), Cd(II), Co(II), Hg(II), Mg(II), Mo(VI), Ni(II), Pb(III), Pd(II), Pt(IV), Rh(III), Sn(II), Ti(IV), W(VI), and Zn(II). These ions do not interfere even at a maximum tolerable mass concentration ratio of 2000:1. The main advantage of the use of aqueous DMF medium allows the possibility of determining Au(III) in the presence of adequate excess of Cu(II), which is especially important in the analysis of ores, minerals, indus-

trial samples, and jewelry objects containing Au(III) and Cu(II) [21].

3.6. Determination of gold in real samples

The proposed FI method was successfully applied to the analysis of two jewel samples. The accuracy of the assay was validated by recovery experiments after spiking the samples with known amounts of Au(III) standard to final mass concentrations of 1.0, 2.0, and 3.0 mg L⁻¹. The results are shown in Table 2. In all cases, the recoveries were satisfactory and varied between 97 and 103%. Five replicate injections ($n=5$) for each sample were made in all instances. The accuracy was further validated by comparison of the results obtained by the FI analysis of the samples with those obtained by the FAAS as a reference method. These findings are summarized in Table 3. The calculated relative errors were $e_r = -2.3$ for both analyzed samples and verified statistically by the t -test.

4. Conclusions

The proposed FI spectrophotometric method for the determination of Au(III) in jewel samples fulfils the major demands of routine analysis. It is simple with no complicated procedures before the determination of the analyte, easy to handle, it has low operational cost compared to the FI complex on-line sorption preconcentration procedures with hard available and expensive sophisticated instruments, and offers high sampling rate, minimum sample pretreatment and good dynamic range for the direct

determination of the analyte. Additionally, it shows high selectivity, adequate detection limit, no dangerous reagents or unique chemicals used and good precision and accuracy in all cases.

References

- [1] S. Xu, L. Sun, Z. Fang, *Anal. Chim. Acta* 245 (1991) 7.
- [2] M.J.C. Taylor, D.E. Barnes, G.D. Marsall, *Anal. Chim. Acta* 265 (1992) 71.
- [3] W. Qi, X. Wu, C. Zhou, H. Wu, Y. Gao, *Anal. Chim. Acta* 270 (1992) 205.
- [4] S. Lin, H. Hwang, *Talanta* 40 (1993) 1077.
- [5] K. Pyrzynska, *J. Anal. At. Spectrom.* 9 (1994) 801.
- [6] P. Di, D.E. Davey, *Talanta* 42 (1995) 1081.
- [7] P. Liu, Q. Pu, Z. Su, *Analyst* 125 (2000) 147.
- [8] P. Liu, Q.S. Pu, Q.Y. Sun, Z.X. Su, *Fresenius J. Anal. Chem.* 366 (2000) 816.
- [9] P. Liu, X. Wu, Q. Sun, Z. Su, Q. Pu, *At. Spectrosc.* 22 (2001) 392.
- [10] S. Zhang, Q. Pu, P. Liu, Q. Sun, Z. Su, *Anal. Chim. Acta* 452 (2002) 223.
- [11] P. Liu, Z. Su, X. Wu, Q. Pu, *J. Anal. At. Spectrom.* 17 (2002) 125.
- [12] K.K. Falkner, J.M. Edmond, *Anal. Chem.* 62 (1990) 1477.
- [13] M.M. Gomez, C.W. McLeod, *J. Anal. At. Spectrom.* 10 (1995) 89.
- [14] D. Pozebon, V.L. Dressler, A.J. Curtius, *Anal. Chim. Acta* 438 (2001) 215.
- [15] M.M. Gomez, C.W. McLeod, *J. Anal. At. Spectrom.* 8 (1993) 461.
- [16] X. Du, S. Xu, *Fresenius J. Anal. Chem.* 370 (2001) 1065.
- [17] S. Xu, R.E. Sturgeon, *Spectrochim. Acta Part B* 60 (2005) 101.
- [18] H. Ma, X. Fan, H. Zhou, S. Xu, *Spectrochim. Acta Part B* 58 (2003) 33.
- [19] B. Tang, H. Zhang, Y. Wang, *Anal. Chim. Acta* 525 (2004) 305.
- [20] Z. Zuotao, T. McCreedy, A. Townshend, *Anal. Chim. Acta* 401 (1999) 237.
- [21] O.A. Bilenko, S.P. Mushtakova, *Zh. Anal. Khim* 41 (1986) 65, *J. Anal. Chem. USSR (Engl. Transl.)* 41 (1986) 50.
- [22] A.N. Pankratov, O.A. Bilenko, S.P. Mushtakova, *Zh. Anal. Khim* 44 (1989) 2180, *J. Anal. Chem. USSR (Engl. Transl.)* 44 (1989) 1718.

An automated FTIR method for the routine quantitative determination of moisture in lubricants: An alternative to Karl Fischer titration

Frederik R. van de Voort^{a,*}, Jacqueline Sedman^a, Robert Cocciardi^b, Steve Juneau^c

^a McGill IR Group, Department of Food Science and Agricultural Chemistry, Macdonald Campus of McGill University, 21,111 Lakeshore Road, Sainte-Anne-de-Bellevue, Quebec, Canada H9X 3V9

^b Thermal-Lube Inc., 255 Avenue Labrosse, Pointe-Claire, Quebec, Canada H9R 1A3

^c Naval Engineering Test Establishment, 9401 Wanklyn Street, LaSalle, Quebec, Canada H8R 1Z2

Received 16 August 2006; received in revised form 16 October 2006; accepted 19 October 2006

Available online 29 November 2006

Abstract

An accurate primary Fourier transform infrared (FTIR) method for the determination of moisture in mineral and ester based lubricants has been developed based on the extraction of moisture into dry acetonitrile. FTIR evaluation of acetonitrile extracts from new and used lubricants as well as common lubricant additives and contaminants which might co-extract indicated that phenolic constituents interfered significantly with moisture measurements. By measuring moisture at 3676 cm^{-1} on the shoulder of the asymmetric OH stretching band, spectral interferences from extracted phenolic constituents were minimized. The spectra of calibration standards (0–2100 ppm), prepared by gravimetric addition of water to dry acetonitrile, were recorded in a $1000\text{-}\mu\text{m}$ CaF_2 transmission flow cell and produced linear standard curves having an S.D. of $\sim\pm 20$ ppm. Lubricant sample preparation involved the vigorous shaking (20 min) of a 1:1.5 (w/v) mixture of lubricant and dry acetonitrile, centrifugation to separate the phases, acquisition of the FTIR spectrum of the upper acetonitrile layer, and subtraction of the spectrum of the dry acetonitrile used for extraction. A Continuous Oil Analyzer and Treatment (COAT[®]) FTIR system was programmed to allow the automated analysis of acetonitrile extracts, and the methodology was validated by analyzing 58 new and used oils, independently analyzed by the Karl Fischer (KF) method. Linear regression of FTIR versus KF results for these oils produced a linear plot with a between-method S.D. of ± 80 ppm. As implemented on the COAT[®] system, this FTIR method is capable of analyzing 72 acetonitrile extracts/h and provides a high-speed alternative to the KF titrimetric procedures for the determination of water in lubricants.

© 2006 Elsevier B.V. All rights reserved.

Keywords: Acetonitrile; FTIR spectroscopy; Lubricants; Moisture content; Karl Fischer

1. Introduction

The level of moisture in lubricants is an essential parameter, as water is one of the most widespread and destructive lubricant contaminants. Water contamination can lead to corrosion and excessive wear of machinery, and the presence of emulsified water in a lubricant can impair its effectiveness. Among the variety of American Society for Testing and Materials (ASTM) methods available for the determination of moisture in lubricants and related products, the ASTM D6304 coulometric Karl Fischer (KF) method [1], performed with a water evaporator accessory (WAP), is considered the gold standard. The WAP is used to

rapidly heat the oil sample under vacuum to vaporize water in the sample, which is flushed with dry nitrogen into the KF reagent solution. This procedure minimizes matrix effects commonly associated with lubricant additives, which can undergo aldol condensation and redox side reactions that can affect KF results if oil is directly added to the KF reagent. Thus, ASTM D6304 with a WAP is considered the most comprehensive and accurate procedure available for the analysis of moisture in lubricants and petroleum products, including lubricant additives, base oils, fully formulated lubricants and automatic transmission fluids, amongst others. Most oil analysis laboratories invest in a Karl Fischer apparatus for the quantitative determination of moisture along with other equipment for conducting other pertinent analyses such as particulate contamination, acid number, viscosity, ferrography, elemental analysis, oxidation and more, all at substantial cost in terms of equipment and consumables.

* Corresponding author. Tel.: +1 514 398 8618; fax: +1 514 398 7977.
E-mail address: frederik.vandervoort@mcgill.ca (F.R. van de Voort).

Among the instruments often found in commercial oil analysis laboratories is a Fourier transform infrared (FTIR) spectrometer. This instrumentation is used for lubricant condition monitoring, which involves the trending of a wide range of parameters, including oxidation, nitration, sulfate by-products, soot, glycol contamination, diesel fuel dilution, antiwear depletion and water contamination (see Ref. [2] and references cited therein). FTIR condition monitoring by direct trending [3] is a semi-quantitative procedure, in that no calibration against a primary reference method is performed. Instead, results are reported in terms of peak areas or heights (or baseline tilt in the case of soot) and interpreted in relation to empirically established criteria. Whereas this methodology provides a means of detecting water contamination in in-service lubricants over time, it does not allow for quantitative determination of the amount of water present owing to overlap of the IR absorption bands used to monitor water contamination with those of other OH-containing constituents (often present in lubricating oils). On the other hand, in the differential version of this methodology, the spectral contributions of these constituents are, in principle, eliminated by subtracting out the spectrum of a new oil of the same formulation as the samples being analyzed, and the water content may be estimated from a calibration equation obtained using gravimetrically prepared standards. However, the use of this methodology as the basis for the development of a generally applicable quantitative method is highly problematic not only because of the limitations associated with the need to have the appropriate reference oil at hand but also because the absorption bands of water are subject to matrix effects such as hydrogen bonding, which differential spectroscopy cannot compensate for. These complications have stymied the development of a quantitative FTIR procedure that would be competitive with the KF method.

An alternative approach developed in our laboratory to overcome these limitations made use of the stoichiometric reaction of water with dimethoxypropane (DMP) to produce acetone, coupled with differential spectroscopy to eliminate the spectral contributions of the oil [4]. The moisture content of the sample was determined by measuring the intensity of the $\nu(\text{C}=\text{O})$ absorption of acetone, calibrations being derived by standard addition of water to a dry oil. This method accurately detects moisture levels as low as 50 ppm and is workable for compressor, hydraulic, and gear oils. However, it gives erroneously high values for gasoline and diesel engine oils that are over-based with calcium carbonate, because the acid catalyst required for the reaction is neutralized by the base, thereby producing CO_2 and more H_2O . This method is also problematic for mineral-based lubricants containing substantial levels of ester-based additives as well as ester-based lubricants, as the $\nu(\text{C}=\text{O})$ absorption of the acetone produced by the reaction is masked by the ester carbonyl absorption. This problem also prevents the FTIR-DMP approach from being used for the analysis of moisture in edible oils, as they are predominantly triacylglycerols. This limitation led to the development of an alternative FTIR method based on the extraction of moisture from edible oils using dry acetonitrile followed by measurement of the water absorption bands in the spectrum and quantification based on a calibration devel-

oped using acetonitrile-water standards [5]. This paper describes the adaptation of this spectroscopic approach to the analysis of new and used lubricants and its implementation as an automated method as well as its validation against the KF method.

2. Experimental

2.1. Materials

Additive-free (unformulated) mineral and ester base oils and commercial additive packages were obtained from Thermal-Lube Inc. (Pointe-Claire, PQ, Canada). Ester and mineral base oils were blended with additive packages and/or constituents commonly found in new or used oils, including esters, polyalkylglycols, fatty acid rust inhibitors, phosphate-based antiwear additives, sulfurized olefin extreme pressure additives, and phenolic and amine antioxidants. Reagent-grade acetonitrile (Fisher Scientific, Nepean, ON, Canada) was dried and kept dry over 4–8 mesh 3 Å molecular sieves and dispensed using a re-pipette, with its air inlet protected by desiccant to prevent moisture ingress. Formulated commercial lubricants, including diesel engine, compressor, hydraulic, gear and other oils (Table 1), were obtained from a variety of industrial suppliers. Samples of used oils were provided by the Naval Engineering Test Establishment (NETE; Montreal, PQ, Canada), Insight Services Inc. (Cleveland, OH), and the U.S. Armed Forces Technical Support Center (TSC) of the tri-service Joint Oil Analysis Program (JOAP). From among these new and used oils, a subset of samples was selected to represent a variety of oil types and different moisture contents and submitted to NETE for KF analysis.

2.2. Instrumentation

Details of the COAT[®] FTIR Oil Analyzer (shown in Fig. 1) and its software have been described elsewhere [6]. Briefly, an ABB Bomem (Quebec City, PQ, Canada) WorkIR FTIR spectrometer equipped with a DTGS detector and controlled by an IBM-compatible Pentium 150-MHz PC running proprietary Windows-based UMPIRE PRO[™] (Universal Method Platform for InfraRed Evaluation) software (Thermal-Lube, Pointe-Claire, PQ, Canada) is connected to a Gilson autosampler (Gilson Inc., Middleton, WI). The software controls the spectrometer, autosampler, and pump and handles spectral data processing automatically.

For the moisture analysis procedure, acetonitrile extracts were placed in septum-capped vials and loaded into autosampler trays. They were then sequentially aspirated under computer control into a 1000- μm CaF_2 transmission flow cell (International Crystal Laboratories, Garfield, NJ), using a sharpened stainless steel needle to penetrate the sealed vials. Pump time was set at 30 s/sample. The spectra of the samples were collected by co-addition of eight scans at a resolution of 8 cm^{-1} with a gain of 1.0. Weak Beer-Norton apodization was employed.

2.3. Analytical protocol

For sample preparation, 10 g of sample ($\pm 0.0001\text{ g}$) was weighed on an analytical balance into a tared 50-mL clinical cen-

Table 1
Partial listing of commercial lubricants and the functional categories assigned to them by the manufacturer

Lubricant	Category	Lubricant	Category
Rimula X SAE 40	Diesel engine oil	Mobil Vacuoline 133	Bearing oil
Mil-L-9000	Diesel engine oil	Mobil Vacuoline 525	Bearing oil
OMD 113	Diesel engine oil	Mobil Gear 632	Gear oil
Mobil Delvac 1240	Diesel engine oil	Mobil Rarus 424J	Compressor oil
Mobil DTE BB	Bearing oil	Tellus T15	Hydraulic oil
RP ThermalGlyde 220	Gear oil	Tellus 68	Hydraulic oil
Mobil DTE 832	Compressor oil	Omala 220(P)	Gear oil
Hydrex AW 32	Bearing oil	Turbo T46	Turbine oil
Mobil Rarus 1024	Compressor oil	Turbo P100	Turbine oil
Terrestic 220	Anti-friction bearing oil	Tonna T220	Slide-way oil
Terrestic 68	Turbine oil	Rimula X 15w/40	Diesel engine oil
Mobil Gear SHC 460	Gear oil	Morlina 10	Bearing oil
Mobil Gear SHC 460	Gear oil	Rando HD-46(P)	Hydraulic oil
Mobil Delo 400	Diesel engine oil	Meropa 320P	Gear oil
Mobil DTE 26	Hydraulic oil	Cosmolubric HF-130	Polyol ester oil
Mobil DTE Heavy Medium	Turbine oil	Hydro FE-56	Polyol ester oil

trifuge tube, and 15 mL of dry acetonitrile was dispensed into the tube using a re-pipette. The samples were mixed vigorously for 20 min using a multi-sample, reciprocal action shaker (Eberbach Corporation, Ann Arbor, MI), and then the oil and acetonitrile phases were separated by centrifugation (Eppendorf Canada Ltd., Mississauga, ON) for 10 min at $\sim 10,000$ rcf (relative centrifugal force). The upper acetonitrile layer was transferred into a 20-mL autosampler vial, which was then capped with a septum cap having a Mylar liner. The vials were loaded into the autosampler tray from position #3 onward, with the first two

vials in the tray being reserved for the dry acetonitrile used to extract the samples, the first serving as a rinse solvent and the second to collect the spectrum of the solvent. The single-beam spectra of the solvent and samples were ratioed against an open-beam background spectrum collected at the beginning of each run to give their respective absorbance spectra, and the absorbance spectrum of the dry acetonitrile solvent was subtracted from the absorbance spectrum of each sample to give its differential spectrum. To compensate for the partial miscibility of ester-based oils with acetonitrile, the spectra of their acetonitrile extracts were multiplied (prior to spectral subtraction) by the ratio of the height of the acetonitrile $\nu(\text{C}\equiv\text{N})$ band at 2068 cm^{-1} (measured relative to a two-point baseline between 2125 and 2033 cm^{-1}) in the spectrum of the dry acetonitrile solvent to the height of this band in the spectrum of the acetonitrile sample extract.

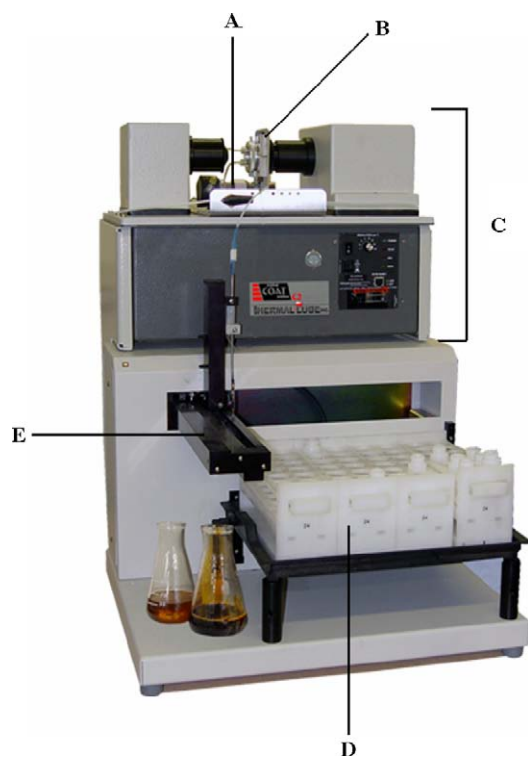


Fig. 1. COAT FTIR Oil Analyzer used for the analysis of moisture. The system consists of a micro gear pump (A), cell holder (B), FTIR spectrometer (C), autosampler tray (D) and robotic arm (E).

2.4. KF analysis

The KF apparatus used by the NETE laboratory for oil analysis was a Mettler Toledo DL32 (Columbus, OH) equipped with a WAP and used Hydranal (Sigma–Aldrich Inc., St. Louis, MO) KF reagents for moisture quantification. The system was validated using KF moisture standards (Sigma–Aldrich Inc., Milwaukee, WI) by loading 0.1 g of each standard and heating it to $220\text{ }^{\circ}\text{C}$, flushing with dry nitrogen for 60 s and titrating until the end point was reached, corresponding to a drift of less than $5\text{ }\mu\text{g}/\text{min}$. Lubricant analysis used 1.0 g of sample heated to $160\text{ }^{\circ}\text{C}$ with a nitrogen flush time of 210 s and then titrated to the same endpoint as the moisture standards. Data obtained from the KF analyses were used to evaluate the efficacy of the FTIR moisture method.

2.5. Calibration and validation

Seven water/acetonitrile calibration standards were prepared by gravimetrically adding distilled water to dry acetonitrile to cover a range of 300–2100 ppm moisture. The FTIR spectrum

of dry acetonitrile was subtracted from the spectra of the standards in a 1:1 ratio to remove the spectral contributions of acetonitrile. A linear regression calibration equation relating the amount of moisture added (in ppm) to the absorbance value at 3676 cm^{-1} (relative to a baseline point at 3738 cm^{-1}) in the differential spectra of the calibration standards was used to predict the moisture content of oil samples in order to assess the extraction recovery, repeatability, reproducibility, and accuracy of the method. Percent recovery was evaluated by spiking 10 different types of oil samples with increasing amounts of water (200–1000 ppm in ~ 200 ppm increments) and assessed by dividing the FTIR-predicted values by their respective theoretical gravimetric values and multiplying by 100. Repeatability and reproducibility were evaluated by running three replicates of 12 new and used oil samples having high and low water contents consecutively and on 3 different days and were assessed by calculating the average standard deviation of the replicates. Accuracy was evaluated using 58 validation samples, 23 of which came from JOAP with the balance being commercial samples and samples prepared in our laboratory. All these validation samples were analyzed by KF titration in the NETE laboratory. The accuracy of the FTIR method was assessed by linear regression of the FTIR-predicted values against the reference KF values and calculation of the standard error of prediction (SEP).

3. Results and discussion

3.1. General considerations

Acetonitrile is a highly suitable solvent for the extraction of water from lubricants and its subsequent quantitation by FTIR spectroscopy for several reasons. First, it is sufficiently polar to be largely immiscible with both mineral- and ester-based lubricants and is capable of efficiently extracting water from them. Moreover, because acetonitrile does not absorb strongly in the portions of the mid-IR spectrum where water absorbs, pathlengths of up to $1000\ \mu\text{m}$ may be employed for the analysis of low levels of moisture, thereby providing high sensitivity. Fig. 2 presents the OH stretching region in the spectra of a series of calibration standards prepared by addition of water to acetonitrile from which the spectrum of acetonitrile has been subtracted out. Owing to the binding of water molecules exclusively to acetonitrile rather than to each other at these high dilutions [7], these spectra of water exhibit distinct symmetric and asymmetric OH stretching bands (3630 and 3540 cm^{-1}), rather than the single broad band normally observed. Both bands respond linearly to added water and maintain consistent ratios relative to each other over the concentration range examined (300–2100 ppm).

In addition to extracting water from oils, acetonitrile is also capable of extracting some other polar constituents, such as alcohols, phenolic compounds, hydroperoxides, and organic acids, but not ionic constituents. Since formulated lubricants contain a wide variety of added constituents and can accumulate various undefined contaminants during the lubricant's in-service life, a number of species may be co-extracted with water into ace-

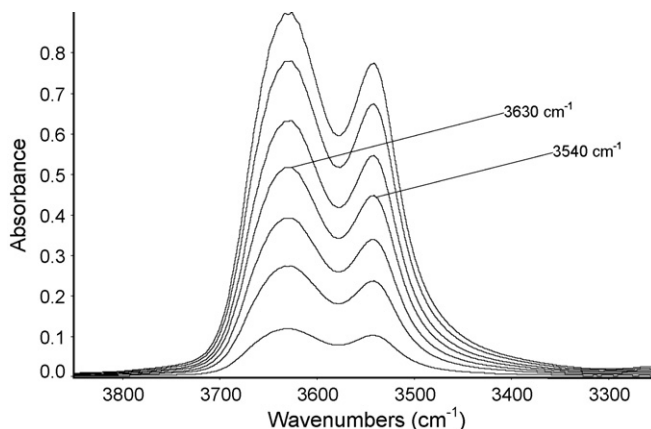


Fig. 2. Differential spectra of water in acetonitrile over a concentration range of 300–2100 ppm, illustrating the two main water absorption bands, the symmetric and asymmetric OH stretching bands at 3630 and 3540 cm^{-1} , respectively.

tonitrile. Such potential sources of spectral interferences were examined by recording the spectra of acetonitrile extracts from a wide variety of commercial new and used lubricants. Fig. 3 presents the 3850 – 3200 cm^{-1} region of the differential spectra obtained after subtraction of the spectrum of dry acetonitrile from the spectra of the standards and indicates that a variety of constituents other than moisture were extracted into acetonitrile.

Although Fig. 3 shows that measurements at either of the peak maxima of the water absorption bands would be subject to substantial interference from various co-extracted components, interference on the high-frequency side of the 3630-cm^{-1} band was judged to be minimal. This is illustrated in Fig. 4, in which the spectrum of the acetonitrile extract of a mineral-based oil spiked with 286 ppm of water is superimposed on the spectra obtained after extraction of the same oil spiked with 0.2 and 0.5% (w/w) 2,6-di-*tert*-butyl-4-methylphenol, corresponding to the levels at which phenolic antioxidants are commonly present in lubricant formulations. In the case of ester-based oils, the bands of OH-containing constituents are broadened and shifted toward lower wavenumbers as a result of hydrogen bonding with the ester carbonyl group, thus generally being clear of the

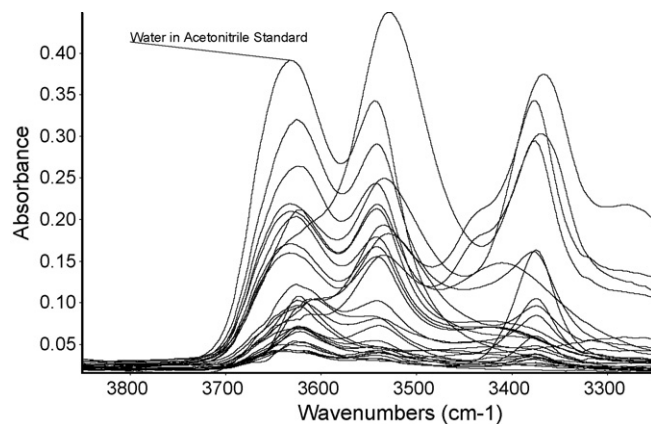


Fig. 3. Differential spectra of acetonitrile extracts from a wide variety of commercial new and used lubricants in relation to a differential spectrum of moisture in acetonitrile, illustrating the spectral variability produced in the OH region.

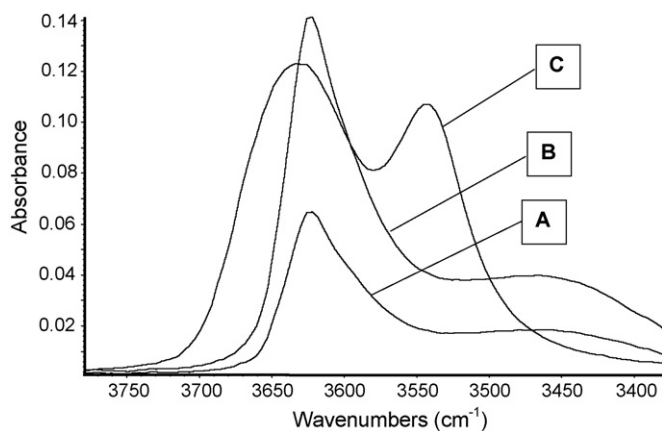


Fig. 4. Differential spectrum of a mineral-based oil spiked with 0.2% (A) and 0.5% (B) 2,6-di-*tert*-butyl-4-methylphenol and extracted with acetonitrile and a differential spectrum of 286 ppm water (C) spiked into the same base oil and extracted into acetonitrile.

3630 cm^{-1} water band. Accordingly, the possibility of employing a location on the high-frequency tail of the 3630- cm^{-1} band for the quantitation of water was investigated.

In principle, absorption measurements on the tail of a peak are less reliable than measurements at the peak maximum since they are more likely to be affected by changes in spectral band shapes resulting from intermolecular interactions such as hydrogen bonding. However, in the present case, such matrix effects are expected to be minimal, as the samples are very dilute acetonitrile solutions in which water has been shown to be well dispersed without extensive hydrogen bonding (see Fig. 2). To select the optimal measurement frequency, calibration equations were derived by measuring the absorbance of water/acetonitrile standards at 15 frequencies between 3700 and 3590 cm^{-1} at 8- cm^{-1} intervals. These calibration equations were then used to predict the amount of water in a mineral oil sample spiked with a high level of phenol antioxidant (0.5%, w/w) and 286 ppm water. The results showed that the absorption of the phenol antioxidant contributed to the predicted water content at wavenumbers lower than 3676 cm^{-1} , with the magnitude of this contribution ranging from ~ 40 ppm at 3660 cm^{-1} to ~ 300 ppm at the peak of the 3630- cm^{-1} water absorption band. At 3676 cm^{-1} , the presence of the phenol antioxidant contributed < 20 ppm to the predicted water content, and therefore 3676 cm^{-1} was chosen as the optimal frequency for measuring water in acetonitrile extracts of lubricating oils.

A second important consideration in developing this methodology was to compensate for the partial miscibility of certain types of lubricating oils with acetonitrile, which would result in underestimation of the moisture content of the oil owing to dilution of the acetonitrile extract by oil. The most common base oil types are mineral oils, synthetic hydrocarbon oils, various synthetic ester-based oils, and polyalkylglycols. Mineral and synthetic hydrocarbon base oils are effectively immiscible with acetonitrile and separate completely with centrifugation, while at the other extreme, polyalkylglycols are completely miscible. Synthetic esters were found to have varying degrees of miscibility with acetonitrile, as evidenced by the observation of the

ester $\nu(\text{C}=\text{O})$ absorption at $\sim 1730 \text{cm}^{-1}$ in the spectra of their acetonitrile extracts. To compensate for the partial miscibility with acetonitrile of ester-based oils and hydrocarbon oils containing substantial amounts of ester additives, the spectra were multiplied by a dilution correction factor prior to the subtraction of the acetonitrile spectrum. The spectral multiplier was calculated as the ratio of the height of the acetonitrile $\nu(\text{C}\equiv\text{N})$ band at 2068 cm^{-1} (measured relative to a two-point baseline between 2125 and 2033 cm^{-1}) in the spectrum of the dry acetonitrile solvent to the height of this band in the spectrum of the acetonitrile sample extract. Based on the magnitude of this dilution correction factor, the miscibility of the ester-based oils with acetonitrile was estimated to fall within the range of 2–20% depending on the type of ester base stock and hydrocarbon chain length.

Given that various constituents and additive packages commonly found in mineral and hydrocarbon based oils could affect the oil's miscibility with acetonitrile, a variety of such constituents were examined, including detergents, dispersants, demulsifiers, antioxidants, antiwear and extreme pressure additives, rust inhibitors, pour point depressants and viscosity modifiers, and these were not found to significantly affect the miscibility of the base oils with acetonitrile. Used mineral based and synthetic hydrocarbon based engine oils, hydraulic, compressor and gear fluids also were not found to extract significantly into acetonitrile (not more than 2%). As indicated above, certain amounts of degradation by-products and additives were spectrally found to be extracted, but the resulting dilution effect (assessed spectroscopically as described above for the ester-based oils) was not significant.

3.2. Calibration

A calibration was developed using standards prepared simply by adding water to acetonitrile at levels from 300 to 2100 ppm. Owing to the low absorptivity of acetonitrile in the spectral region of interest, a cell pathlength of $\sim 1000 \mu\text{m}$ could be employed. After subtraction of the spectrum of the dry acetonitrile from the spectra of the standards, the following calibration equation was obtained using absorbance measurements made at 3676 cm^{-1} relative to a baseline at 3738 cm^{-1} :

$$\text{H}_2\text{O (ppm)} = 5427.3A_{3676/3738 \text{cm}^{-1}} - 15.0,$$

$$R^2 = 0.999, \quad \text{S.D.} = 10.9 \quad (1)$$

As indicated by the regression S.D. of ~ 11 ppm, the long pathlength allowed very high sensitivity to be attained. This equation was programmed into the COAT[®] system to analyze the moisture content of the acetonitrile extracts of lubricant samples automatically, providing results directly in ppm moisture.

3.3. Validation and comparison to Karl Fischer titration

The analytical performance of the acetonitrile extraction/FTIR method was first evaluated in terms of extraction recovery, repeatability and reproducibility. Recovery was assessed by spiking various amounts of water (200–1000 ppm)

Table 2
Average percent recovery and S.D. for 10 different oil samples

Oil type	Spiked additive	Average recovery ^a (%)	S.D. (%)
Mineral base oil	–	97.9	0.80
Mineral base oil	Heavy-duty diesel engine oil additive (13.5%)	95.9	5.25
Mineral base oil	Antiwear hydraulic oil additive (3%)	97.7	1.46
Mineral base oil	Industrial gear oil additive (3%)	100.2	4.29
Ester base oil	–	101.1	0.52
Synthetic air compressor lubricant	–	101.9	5.65
Engine oil	–	92.9	2.78
Hydraulic fluid	–	104.9	5.27
Turbine fluid	–	96.5	4.54
Gear fluid	–	94.4	6.41

^a Average recovery: average of % recovery values for same sample spiked with 200, 400, 600, 800 and 1000 ppm water.

into 10 samples of different types of oil, mixing vigorously on a reciprocal shaker to ensure that the water was well dispersed in the oil, and then analyzing the samples by the acetonitrile extraction/FTIR method. For certain types of oil samples, recovery increased as the time of mixing increased, as exemplified by the following recovery data obtained for a fully formulated hydraulic oil spiked with ~600 ppm water: 2 min, 62%; 5 min, 80%; 10 min, 84%; 20 min, 92%. Average recoveries for the 10 different oil samples spiked with 200–1000 ppm water in ~200 ppm increments and mixed for 20 min were >90%, with 4 out of the 10 samples having 100% recovery (Table 2). Thus, recovery was deemed satisfactory with a 20-min mixing time, confirming the capability of acetonitrile to extract most of the water present in lubricating oils.

For the assessment of repeatability and reproducibility, 12 oil samples were analyzed in triplicate within the same run and on 3 different days, respectively. The data obtained are summarized in Table 3. The average S.D. for repeatability was ~8 ppm and the average S.D. for reproducibility was ~80 ppm. The much higher S.D. of the data for reproducibility suggests that atmospheric moisture level variations on different days may have affected the results, indicating a certain level of moisture ingress during sample preparation.

Generally, FTIR spectroscopy is considered a secondary method requiring calibration against a recognized primary method, such as KF titration; however, the FTIR method in this

case is in fact a primary method, traceable to gravimetrically prepared water/acetonitrile standards, and, as such, the FTIR moisture values predicted for lubricant samples should be accurate. A performance comparison against the KF procedure was undertaken to determine the validity of this assumption. Thus, a set of used military vehicle oils ($n=23$) and a further 35 carefully selected samples were analyzed in the NETE laboratory by the KF method and were also analyzed by the acetonitrile FTIR method. Fig. 5 presents a plot of the FTIR moisture predictions versus the KF results which yielded the following conventional and zero-regression equations, respectively:

$$\text{FTIR H}_2\text{O} = 36.6 + 0.987 \text{ KF H}_2\text{O},$$

$$R = 0.950, \quad \text{S.D.} = 80 \text{ ppm} \quad (2)$$

$$\text{FTIR H}_2\text{O} = 1.063 \text{ KF H}_2\text{O},$$

$$R = 0.950, \quad \text{S.D.} = 83 \text{ ppm} \quad (3)$$

The intercept in Eq. (2) is well within the regression S.D., and the change in the S.D. when the regression was forced through the origin (Eq. (3)) was minimal, confirming that the FTIR results are not biased with respect to the KF data. Thus, the FTIR method tracks the moisture content of the oils in the same manner as the KF method, with an overall SEP of ~80 ppm relative to the KF reference values. The SEP is comparable to the S.D.

Table 3
Repeatability and reproducibility data for quantitation of water in 12 oil samples (mean and S.D. of three replicates)

Sample no.	Type of oil	Repeatability		Reproducibility	
		Mean (ppm)	S.D. (ppm)	Mean (ppm)	S.D. (ppm)
1	New motor oil	361.7	1.53	324.2	50.34
2	Used motor oil	755.7	10.12	666.6	108.31
3	Used motor oil	552.3	2.52	511.4	84.75
4	New bearing oil	–5.0	8.54	39.3	50.95
5	New turbine oil	31.0	10.54	67.3	52.08
6	New engine oil	473.3	4.04	504.4	102.60
7	Polyol ester oil	342.7	10.69	467.6	207.43
8	New hydraulic oil	77.3	8.08	83.4	64.72
9	New gear oil	96.7	10.12	104.2	62.34
10	New turbine oil	86.3	8.39	92.1	53.24
11	Used motor oil	547.0	11.79	554.0	74.75
12	Used motor oil	590.7	9.29	584.2	65.24

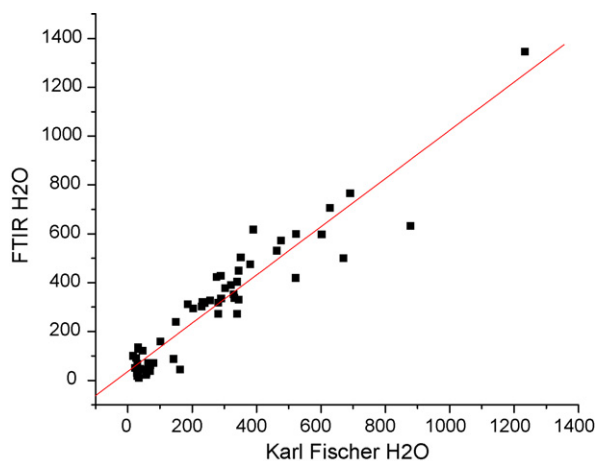


Fig. 5. Regression of FTIR moisture predictions vs. the KF results for 58 used and new oil samples.

for reproducibility of the FTIR method and indicates excellent agreement between the FTIR and KF results.

Overall, the results of the validation study indicate that the FTIR analysis of lubricant acetonitrile extracts is a viable and accurate means of determining moisture content in a wide range of lubricants. The rate of automated analysis on the COAT[®] system employed in this work is 72 acetonitrile extracts/h; in addition, the sample preparation steps, apart from weighing out the oil, can be performed in batch mode while the previous set of samples is being processed. Accordingly, this FTIR method provides a practical instrumental alternative to KF analyses, allowing for the rapid, automated determination of moisture with a high degree of accuracy. This methodology may be implemented together with other FTIR methods developed in our laboratory for the automated analysis of lubricants, including acid number and base number [8] as well as lubricant condition monitoring [2], thereby replacing several conventional, tedious

physical and chemical methods by FTIR methodology. As such, FTIR analysis offers substantial benefits to commercial oil analysis laboratories in terms of both sample turnaround and cost savings.

Acknowledgements

F.R. van de Voort would like to thank Thermal-Lube Inc. for supporting his sabbatical sojourn at their research facilities in Pointe-Claire, Quebec, Canada. Thanks also go to Dr. E. Urbanski of the Joint Oil Analysis Program run out of the U.S. Navy Technical Support Center in Pensacola, Florida, for providing lubricant samples. The very helpful collaboration of the Naval Engineering Test Establishment, facilitated by its Director, Mr. Mike Davies, is much appreciated. The authors acknowledge the Natural Sciences and Engineering Research Council (NSERC) of Canada for partial financial support of this research.

References

- [1] ASTM D6304: Standard Test Method for Determination of Water in Petroleum Products, Lubricating Oils, and Additives by Coulometric Karl Fischer Titration, ASTM International Standards.
- [2] F.R. van de Voort, J. Sedman, R.A. Cocciardi, D. Pinchuk, *Tribol. Trans.* 49 (3) (2006) 410.
- [3] ASTM E2412: Standard Practice for Condition Monitoring of Used Lubricants by Trend Analysis Using Fourier Transform Infrared (FT-IR) Spectrometry, ASTM International Standards.
- [4] F.R. van de Voort, J. Sedman, V. Yaylayan, C. Saint Laurent, C. Mucciardi, *Appl. Spectrosc.* 58 (2) (2004) 193.
- [5] A. Al-Alawi, F.R. van de Voort, J. Sedman, *Appl. Spectrosc.* 59 (10) (2005) 1295.
- [6] A. Al-Alawi, F.R. van de Voort, J. Sedman, A. Ghetler, *JALA* 11 (1) (2006) 23.
- [7] A. Le Narvor, E. Gentric, P. Saumagne, *Can. J. Chem.* 49 (1971) 1933.
- [8] F.R. van de Voort, J. Sedman, V. Yaylayan, C. Saint Laurent, *Appl. Spectrosc.* 57 (11) (2003) 1425.

Rapid and sensitive liquid chromatography–tandem mass spectrometry for the quantitation of epirubicin and identification of metabolites in biological samples

Rachel Wall^{a,*}, Gillian McMahon^b, John Crown^c, Martin Clynes^a, Robert O'Connor^a

^a National Institute for Cellular Biotechnology (NICB), Dublin City University (DCU), Dublin 9, Ireland

^b School of Chemical Sciences, DCU, Dublin 9, Ireland

^c Dept. of Medical Oncology, St Vincent's University Hospital, Dublin 4, Ireland

Received 13 March 2006; received in revised form 28 September 2006; accepted 5 October 2006

Available online 20 November 2006

Abstract

A highly sensitive and selective liquid chromatography–mass spectrometry (LC–MS) method has been developed for the determination of epirubicin in serum and cell specimens using daunorubicin as an internal standard. Using atmospheric pressure chemical ionisation (APCI), the epirubicin metabolites were readily distinguishable by their fragmentation pattern in the mass spectrometer. Selected reaction monitoring (SRM) mode was employed for quantitation of epirubicin and the metabolites. Following extraction, chromatography was performed on a C18 column with a mobile phase consisting of water–acetonitrile–formic acid, pH 3.2, with a flow rate of 200 μ l/min. The limit of detection (LOD) and the limit of quantitation (LOQ) of this method in serum were determined to be 1.0 and 2.5 ng/ml, respectively. Linearity of the method was verified over the concentration range of 2.5–2000 ng/ml, with a high correlation coefficient ($R^2 \geq 0.998$). For the extraction procedure, an aliquot of 500 μ l serum, spiked with internal standard, was extracted using a chloroform–2-isopropanol (2:1, v/v) mixture. The method has been applied to the analysis of epirubicin in cancer cell samples and the identification of known and unknown metabolites in clinical trial patient serum samples.

© 2006 Elsevier B.V. All rights reserved.

Keywords: Liquid chromatography–mass spectrometry (LC–MS); Anthracyclines; Epirubicin; Atmospheric pressure chemical ionisation (APCI); Serum; Cell culture

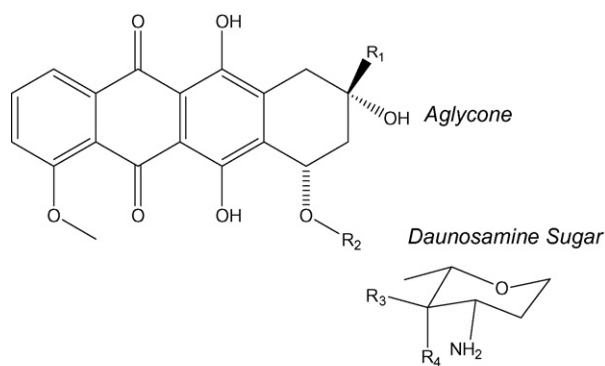
1. Introduction

Cancer is the second largest cause of mortality in Western society. Typical treatments involve surgery, chemotherapy and radiotherapy. Chemotherapeutic drug administration is the most common form of treatment, especially for advanced or metastatic disease. The anthracycline anti-tumour antibiotics are a class of chemotherapy drugs with broad activity against a wide range of tumours, including breast and lung. Various anthracyclines such as epirubicin and doxorubicin, are used as monotherapy or as part of a multi-chemotherapeutic drug regimen and they work by intercalating with the cancer cell DNA. The clinical application of anthracyclines is limited by their toxicity, including cumulative dose-related cardiotoxicity and myelosuppression [1]. The activity of these agents is also

affected by a number of drug resistance mechanisms including tumour over-expression of drug efflux pumps [2]. Therapeutic drug monitoring of anti-cancer agents during treatment has been found to be beneficial to the outcome of patients as attenuating the administered dose may reduce toxicity and side effects while potentially improving the efficacy of the chemotherapeutic agents [3].

The structures of doxorubicin and epirubicin along with their active metabolites (relevant to this study) are shown in Fig. 1. Anthracyclines consist of a planar, hydrophobic tetracycline ring linked to a daunosamine sugar through a glycosidic linkage. Both agents are used in the treatment of many solid malignancies. Epirubicin is the 4'-epimer of doxorubicin i.e. the structures are identical except for the differing spatial orientation of the hydroxyl group at the C-4' daunosamine ring. This spatial orientation does not alter the therapeutic efficacy of the drug but renders epirubicin less cardiotoxic than doxorubicin [4]. Epirubicin also has an increased lipophilicity, which increases cell penetration [5]. Epirubicin and doxorubicin are conjugated with

* Corresponding author. Tel.: +353 1 700 5700; fax: +353 1 700 5484.
E-mail address: Rachel.wall@dcu.ie (R. Wall).



Anthracycline	R ₁	R ₂	R ₃	R ₄	Ret Time (min)
Epirubicin	-C(=O)CH ₂ OH	Daunosamine Sugar	OH	H	5.3
Daunorubicin	-C(=O)CH ₃	Daunosamine Sugar	H	OH	8.5
Doxorubicin	-C(=O)CH ₂ OH	Daunosamine Sugar	H	OH	4.8
13-dihydroepirubicin	-CH ₂ (OH)CH ₂ OH	Daunosamine Sugar	OH	H	3.2
13-dihydroadriamycinone	-CH ₂ (OH)CH ₂ OH	H	-	-	7.0
Adriamycinone	-C(=O)CH ₂ OH	H	-	-	13.9

Fig. 1. Chemical structures and retention times of the anthracyclines and their metabolites.

glucuronide on the 4' equatorial hydroxyl and excreted in the bile [6,7] and their metabolites are relatively non-cytotoxic.

Determination of the anthracyclines and their respective metabolites in plasma and serum, in particular epirubicin, has been achieved using high performance liquid chromatography, employing various detectors, as summarised in Table 1 [4,8–13]. Lachatre et al. reported a liquid chromatography–mass spectrometry (LC–MS) method for a number of the anthracyclines and their metabolites but with long runtimes [9]. Arnold et al. developed an assay using a smaller sample volume and a much shorter runtime of 5 min largely based on resolution of the MS detector itself [8].

Electrochemical and fluorescence detection have been employed and have yielded good sensitivity for the anthracyclines [13]. However, the best sensitivities to date for the anthracyclines have been obtained with MS detection with, for example, Sottani and colleagues reporting limits of quantification of 0.1 ng/ml and 0.03 ng/ml, respectively when extracting 5 ml urine samples [13]. The increase physicochemical complexity of plasma, serum and cells/tissue makes quantitation more difficult and hence generally reduces sensitivity. Sample extraction methods for the anthracyclines range from liquid–liquid extraction (LLE) and protein precipitation to solid phase extraction (SPE). Our desire to develop a method which could extract and measure anthracyclines even in cell samples where the drug is very highly bound to DNA led us to employ a LLE method in this analysis.

The aim of this work was to develop a rapid, routine and sensitive analytical method for the separation and quantita-

tion of epirubicin and identification of its metabolites from different and complex biological matrices where high drug binding and the presence of significant endogenous contaminants can reduce sensitivity and applicability. This was achieved and the validated assay presented here permits sensitive quantitation of epirubicin levels in serum samples and in cancer cells at physiologically and pharmacologically relevant concentrations.

2. Experimental

2.1. Chemicals and reagents

Epirubicin, daunorubicin and doxorubicin were obtained as a clinical formulation while the metabolites of epirubicin – 13-dihydroepirubicin (DHE), 13-dihydroadriamycinone (DHA) and adriamycinone (AME) – were obtained as a gift from Farmitalia Nerviano (Italy) in powdered form. Fetal calf serum was purchased from Sigma–Aldrich (Ireland). The extraction reagents and solvents were analytical grade. HPLC-grade chloroform and isopropanol were obtained from Labscan Ltd., Ireland. Ultra pure water was obtained in-house by using a Millipore RO System connected to an Ultra high pure water unit supplied by Elga. Polypropylene extraction tubes were obtained from Sarstedt Ltd. Spectral grade acetonitrile (ACN) and LC–MS Chromasolv water, for use with the LC–MS, were supplied by Riedel-de-Haen. Formic acid (ACS reagent) was purchased from Sigma–Aldrich and was used for preparing mobile phase for the LC–MS system.

Table 1
Examples of some literature procedures for the extraction and separation of anthracyclines

Analytes determined	Sample preparation	Sample vol. (μl)	Analytical method	Sensitivity (ng/ml)	Recovery (%)	Total runtime (min)	Ref.
Epirubicin	SPE	500	HPLC–ESI–MS/MS	LODs	71	30	Lachatre et al. [8]
Doxorubicin				1.0			
Daunorubicin				0.5			
Idarubicin				1.0			
Doxorubicinol				2.5			
Daunorubicinol				2.0			
Idarubicinol				0.5			
Aclarubicin (IS)	–						
				LOD			
Doxorubicin	LLE-protein denaturation	100	HPLC–ESI–MS/MS	0.14	84	5	Arnold et al. [9]
Doxorubicinol					–112		
Doxorubicinone							
Daunorubicin							
				LOQ			
Epirubicin	SPE	200	HPLC–electro-chemical detection	1.0	89	25	Ricciarello et al. [10]
Doxorubicin					–93		
Epirubicinol							
Doxorubicinol							
				LOQ			
Epirubicin	Protein precipitation	200	HPLC–fluorescence detection	5.0	94	26	Barker et al. [4]
Epirubicinol					–104		
7-Deoxydoxo-rubicinone							
7-Deoxydoxo-rubicinolone							
				LOD			
Doxorubicin	Protein precipitation	150	HPLC–fluorescence detection	1.0	93	~5	Alvarez-Cedron et al. [11]
					–110		
				LODs			
Doxorubicin	SPE	100	HPLC–ESI–MS/MS	0.04	79	25	Sottani et al. [13]
Epirubicin				0.04			
Daunorubicin				0.01			
Idarubicin				0.01			

Key: LLE = liquid–liquid extraction, SPE = solid-phase extraction, ESI = electrospray ionisation.

2.2. Standards and solutions

Stock solutions of epirubicin and doxorubicin were supplied at 2 mg/ml (3.45 mM) while daunorubicin was supplied in a 10 mg/ml (17.525 mM) solution, all in saline. Working standards of the anthracyclines, typically 10-fold greater than the required concentration, were prepared as aqueous solutions (in water), aliquoted into small 1.7-ml microcentrifuge tubes (Costar) and stored frozen at -20°C . The metabolites DHE, DHA and AME were prepared in water to 1 $\mu\text{g}/\text{ml}$.

2.3. Patient samples

Serum from patients who were administered epirubicin as part of a clinical trial carried out jointly between National Institute of Cellular Biotechnology (NICB) and St. Vincent's University Hospital were obtained and analysed. The LC–MS/MS method was used to identify known metabolites of epirubicin as well as identifying unknown metabolites that might be present. Epirubicin and its metabolites were extracted from serum as described in Section 2.5 below.

2.4. Cell samples

The A549, a lung carcinoma cell line was grown in DMEM (Dulbecco's Modified Eagle's Medium): Hams F12 50:50 medium supplemented with 5% FCS (Sigma) and 2 mM L-glutamine (Gibco). Caco2, a colon adenocarcinoma, H1299, a large cell lung carcinoma, H460, a large cell lung carcinoma and MiaPaCa-2/Gemzar, a Gemzar-selected pancreatic carcinoma were kindly provided by colleagues at the NICB. The drug accumulation study for the various cell lines were carried out in the same cell culture medium containing 5% FCS.

The various cell lines were seeded in T25 cm^2 flasks and given one day to attach to the flask surface. The cells were exposed to epirubicin in the culture medium, after which the drug media were removed, the cells were washed with cold PBS, trypsinised and transferred to extraction tubes. They were then centrifuged, a cell count performed and the cell pellet was frozen at -20°C . All results are reported as mean and standard deviation (SD) of triplicate flasks. Prior to extraction, the cell pellet was resuspended in 200 μl of water to which 20 μl of 30% silver nitrate

were added. The function of the silver nitrate is to denature the DNA strands thus enabling the release of intercalated drug. After this addition, the sample was prepared as described in Section 2.5 below.

2.5. Biological sample preparation and extraction

The samples were prepared as follows: 500 μl of serum (fetal calf serum for standards and human serum for patient samples) or 200 μl of cell suspension in water and silver nitrate (from Section 2.4) were added to 200 μl ultrapure water, 100 μl of daunorubicin made up in ultra pure water (internal standard), 100 μl of the epirubicin standard (or just ultrapure water for the patient samples), 700 μl of ice cold isopropanol and 100 μl of a 1 M ammonium formate buffer (pH 8.5) to control the pH. The contents of the tube were gently inverted and 1400 μl of chloroform added using a glass pipette. The contents of the tube were mixed on a blood tube mixer for 5 min and centrifuged at 4000 rpm for 5 min. The liquid clarified into two separate layers, the bottom organic layer containing the drugs of interest. Using a glass Pasteur pipette, 1.1 ml was carefully transferred to the appropriate autosampler vial. The solvents were evaporated under nitrogen and frozen at -20°C until analysis. Prior to LC–MS, samples were reconstituted in 50 μl of mobile phase [14,15].

2.6. Equipment and conditions

The LC–MS instrument used was a GE Healthcare (Amersham Biosciences) EttanTM Multi Dimensional Liquid Chromatographic system (MDLC) interfaced to ThermoFinniganTM PDA detector and a LTQTM Mass Spectrometer. It was integrated into and operated from Thermo Electron's XcaliburTM software. The chromatographic separation was performed on a Phenomenex[®] Prodigy ODS(3) 100 Å, 5 μm , 150 mm \times 2.1 mm column with a mobile phase of 72:28:0.1 (v/v/v) water–acetonitrile–formic acid delivered isocratically at a flow-rate of 200 $\mu\text{l}/\text{min}$. The monitoring wavelength was 254 nm and an injection volume of 20 μl was used.

The sheath gas, auxiliary gas and sweep gas flow rate (arbitrary units) for the APCI unit were set to 25, 5, and 0 units. The discharge current was 6 kV. The capillary temperature was 175°C and the vaporiser temperature was 450°C . The capillary voltage was 31 V while the tube lens was set to 100 V. Mass spectral data were collected in the scan range 200–700 m/z . Selected reaction monitoring (SRM) mode was used for quantitation using the transition ion: m/z 544 \rightarrow 397, the $[\text{M} + \text{H}^+]$ epirubicin adduct and 528 \rightarrow 363, the $[\text{M} + \text{H}^+]$ daunorubicin adduct. Collision energy values used were 15, 20 and 35% of 5 V which correlates to 0.75, 1, 1.75 V.

3. Results and discussion

3.1. Liquid chromatography optimisation

Two reversed-phase C18 columns were tested during the method development part of this work—a Phenomenex[®] Prodigy, 5 μm , 150 mm \times 2.1 mm and a Zorbax SB-C18 Rapid

Resolution 3.5 μm 50 mm \times 2.1 mm. Both columns gave rapid separations but the Phenomenex[®] Prodigy column was chosen due to the fact that there was better retention and resolution of the compounds of interest on this column, allowing for elution of metabolites that would be more polar than doxorubicin or epirubicin.

In terms of mobile phase, various mixtures of water–acetonitrile–formic acid were examined, the final and optimal combination being 72:28:0.1 (v/v/v) with a pH of 3.2. This resulted in a total runtime of 14 min for all compounds and individual retention times as follows: doxorubicin—4.8 min, epirubicin—5.3 min, daunorubicin—8.5 min, DHE—3.2 min, DHA—7.0 min and AME—13.9 min.

As anthracyclines are weak bases with $\text{p}K_{\text{a}}$ values of ~ 7.5 , to maximise stability, ensure protonation and ionisation, it was important to keep the pH low. This had the additional advantage of improving resolution and controlling peak tailing by reducing surface silanol effects. Mobile phases of differing pH (3.0, 3.5 and 4.5) were tested to study the effect on the MS signal intensity of the molecular and fragment ions. Increasing pH led to a 3–5 times loss in signal intensity and hence sensitivity. The optimal pH for the LC–MS analysis was 3.2 and this also provided appropriate chromatographic resolution of the peaks of interest in a reasonable run time.

Daunorubicin is commonly used as an internal standard (IS) in the majority of literature publications in this field. It is extremely similar in structure to many of the anthracyclines and has similar (though not identical) stability and ionisation properties. Anthracyclines are extremely “sticky” to most surfaces especially at lower concentrations and it is therefore important that some form of anthracycline be used as an IS to reduce the potential for analytical error (see Section 3 of uncertainty).

While our method precludes the simultaneous quantitation of all three anthracyclines, clinically and experimentally only one anthracycline drug (and its metabolites) is typically encountered in the sample matrix. Daunorubicin has a much more limited clinical application profile (typically leukaemia) when compared to the broad applicability of doxorubicin or epirubicin. Our method might also be used to quantitate daunorubicin by the use of epirubicin or doxorubicin as the IS anthracycline.

3.2. Mass spectrometry optimisation

During method development, both epirubicin and doxorubicin and their known metabolites were identified by directly infusing a known concentration of each into the MS with mobile phase at a flow rate of 200 $\mu\text{l}/\text{min}$ and obtaining the molecular ion, as a protonated or sodiated adduct. It was possible to detect the parent drugs and their metabolites at concentrations as low as 5 ng/ml by direct infusion. Both atmospheric pressure chemical ionisation (APCI) and electrospray ionisation (ESI) in the positive mode were investigated in this project. It was calculated, from the peak areas of epirubicin and daunorubicin, that the APCI ionisation mode was approximately 7 and 4 times more sensitive for the two analytes, respectively. Other reports have described APCI to be generally more robust and less sensitive

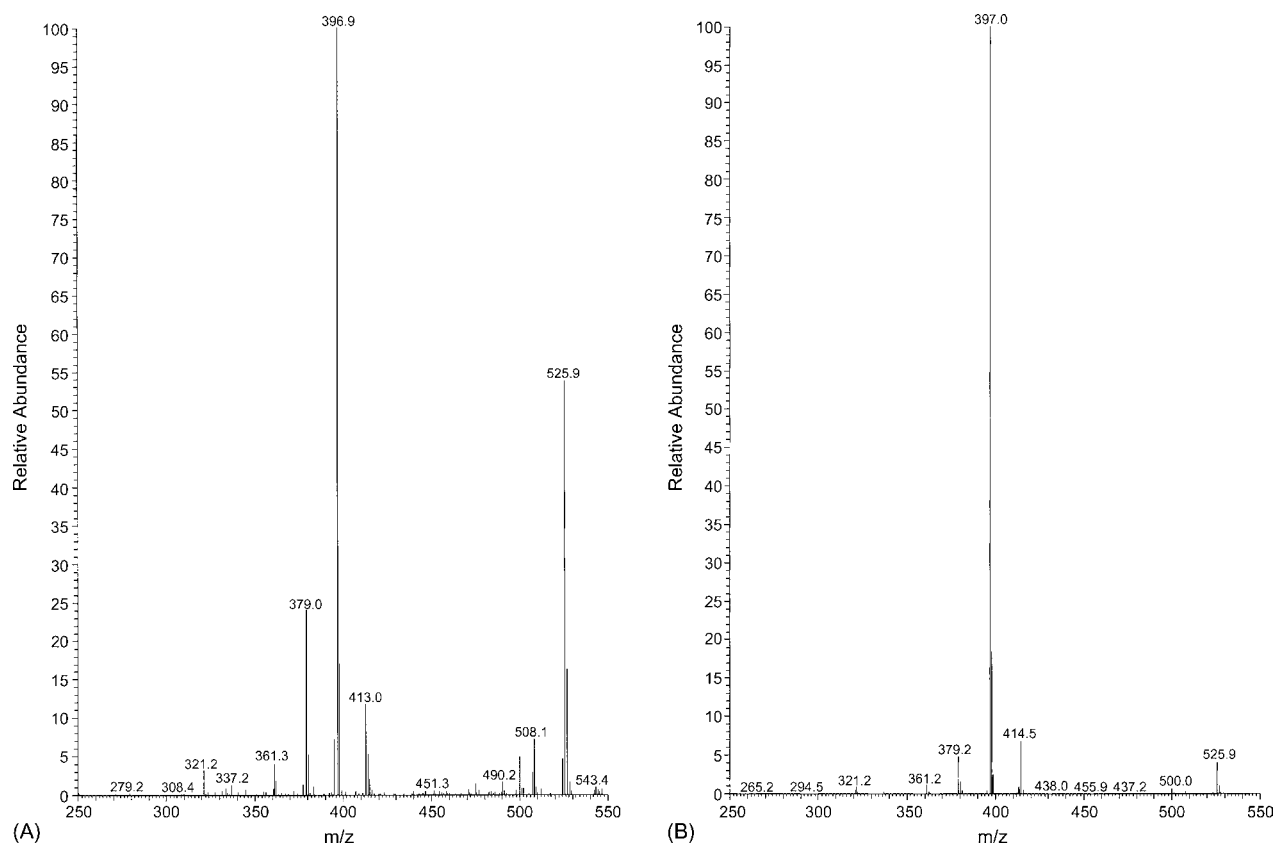


Fig. 2. Fragmentation patterns (MS/MS) of epirubicin (A) and doxorubicin (B). Both have an identical molecular ion $[M + H^+]$ of 544 but exhibit different fragmentation (product) ions. Epirubicin fragments to m/z 397 and 526 while doxorubicin predominantly fragments to m/z 397.

to matrix effects when compared to ESI [16]. APCI is also less prone to ion suppression than ESI.

The molecular ion of each analyte was isolated and subjected to a collision energy resulting in fragmentation ions. Fig. 2 displays the molecular ion of the protonated species and the fragmentation patterns observed for both doxorubicin and epirubicin. It is interesting to note that although they are epimers with identical molecular weight and similar structure, they exhibit a different fragmentation pattern—epirubicin fragments to m/z 397 and 526 while doxorubicin predominantly fragments to m/z 397. This differing fragmentation pattern was repeatable and independent of concentration. Following this, a mixture of the parent drugs and their metabolites were analysed by LC–MS, using the selected reaction monitoring mode (SRM). SRM involves the selection of a precursor ion, fragmentation of it and measurement of the unique product (daughter) ions.

3.3. LC–MS method validation

The overall LC–MS method was validated using the following performance parameters—*intra-day* precision (repeatability) and *inter-day* precision (intermediate precision), accuracy, linearity and range, sensitivity (LOD and LOQ), recovery and sample stability. Many of these were determined according to the guidelines described by Shah and Ermer [17,18]. The major findings of the validation study are shown in Tables 2 and 3.

3.3.1. Precision

Intra-day precision and accuracy were assessed over a concentration range of 2.5–2000 ng/ml (4.3–3450 nM) by extraction and analysis, on the same day, of three drug-free serum samples spiked with epirubicin. *Inter-day* precision and accuracy were determined by extracting and analysing a set of spiked standards

Table 2

Intra- and inter-day accuracy and precision data for the LC–MS determination of epirubicin in serum

Spiked concentration (ng/ml)	Mean concentration observed	% Accuracy	%R.S.D.
<i>Intra-assay</i> accuracy and precision study ($n = 3$)			
2.5	2.3	92.0	7.2
5	5.5	110.0	10.9
10	10.1	101.0	18.0
50	54.2	108.4	12.1
100	100.7	100.7	0.9
500	469.1	93.8	19.3
1000	1193.4	119.3	10.2
2000	1828.5	91.4	14.7
<i>Inter-assay</i> accuracy and precision study ($n = 4$)			
2.5	2.5	100.0	5.1
10	9.8	98.0	8.0
50	50.3	100.6	12.9
500	469.6	93.9	4.8
2000	1935.1	96.8	15.0

Table 3
% Recovery from serum and freeze thaw stability of standards for spiked epirubicin samples

Concentration (ng/ml)	Mean % Recovery		%R.S.D.		
Intra-assay recovery $n = 3$					
2.5	97.0		11.9		
50	121.5		3.4		
500	111.7		5.8		
Conc.	Day1	Day2	Day3	Day4	Day5
Stability determination (values expressed as a percentage average of the assayed amount on day 1) ($n = 3$)					
2.5	100	113.5	107.5	78.7	66.5
50	100	85.7	81.6	45.2	42.7
500	100	79.9	113.2	89.7	80.2

over the same range as above each day for 4 days. The percent relative standard deviation (%R.S.D.) was used as the indicator of precision. Accuracy was calculated by dividing the average calculated drug concentration by the spiked concentration. The drug concentration in extracted samples was calculated from peak area ratios of analyte/internal standard (IS). Data shown in Table 2.

3.3.2. Linearity and range

Regression analysis was used to assess the linearity between the areas ratios (analyte/IS) and the concentration of epirubicin. A standard concentration curve over the range 2.5–2000 ng/ml (4.3–3450 nM) was prepared in serum. Standard plots of peak area versus concentrations typically become non-linear if a broad concentration range is employed and the bias of the regression line tends to make estimates of lower concentration values on the curve much less accurate. We therefore employed a log–log plot of the peak area ratio versus concentration in all calculations. The log–log plot revealed a linear relationship between peak area and drug concentration for this assay, with a correlation coefficient (R^2) of >0.998, and accuracies within 20% of their theoretical values. Thus, utilising a log–log plot, the assay was linear over the concentration range relevant for *in vivo* therapeutic quantitation [17,19]. At higher concentrations the response became non-linear, due to instrumental limitations. The wide dynamic concentration range observed for this LC–MS method has a further advantage in the clinical oncology setting as it means that the entire pharmacokinetic profile of epirubicin in patient blood can be followed without dilution of samples from initial administration where concentrations are as high as 800 ng/ml to more than 24 h after administration when the concentrations fall to <50 ng/ml [4,15].

3.3.3. Sensitivity

The limit of detection (LOD) was defined as that concentration which had a signal-to-noise ratio of 3:1. The limit of quantification (LOQ) was defined as that concentration which had a signal-to-noise ratio of at least 5:1 with an acceptable R.S.D. value [17]. The measured LOD for epirubicin in serum was found to be 1.0 ng/ml while the LOQ was found to be 2.5 ng/ml. The LOD and LOQ reported are low enough for phar-

macokinetic studies in either cell models or patient samples. The extra sensitivity afforded by this LC–MS method may ultimately enable the use of ‘fingerstick’ blood samples (μ l versus ml quantities of blood) which are significantly less invasive for the patient.

3.3.4. Recovery

Pre-spiked serum samples were used for the recovery study. Recovery was determined in triplicate at concentrations of 2.5, 50 and 500 ng/ml by extraction of blank serum samples fortified with epirubicin and IS. Fortified extracts were reconstituted with 50 μ l pure mobile phase, whereas blank extracts were reconstituted with a solution of epirubicin and IS in the mobile phase at concentrations representing 100% recovery. Extraction recovery studies were not carried out on the internal standard alone as both the concentration of daunorubicin and the extraction method remained constant, the peak area of daunorubicin remaining reproducible throughout the validation study. The extraction recovery for epirubicin ranged between 97 and 121.5% at the concentrations prepared (see Table 3).

3.3.5. Stability

Epirubicin stability was determined over four freeze–thaw cycles at 2.5, 50 and 500 ng/ml. On Day 1 triplicate fresh standards were analysed and the remaining sample frozen at -20°C in the dark. The standards were then thawed, extracted and analysed and refrozen each day for a further 4 days.

Stability studies (Table 3) showed that epirubicin was quite stable (in the dark) for two freeze–thaw cycles but after the third cycle (day 4), there was a drop of 21, 44 and 11% for the peak area ratios of the 2.5, 50 and 500 ng/ml concentrations. Further instability following the fourth cycle was apparent with a decrease in the peak area ratios for the same concentrations of 33.5, 57.3 and 19.8%. As has been reported elsewhere for the anthracyclines, drug instability was greater for lower drug concentration standards.

3.3.6. Sources of error

An analysis of factors contributing to uncertainty in the estimation of serum epirubicin concentrations was conducted using three concentrations typical of clinical values, 2.5, 50 and 500 ng/ml. Deduplication of a cause and effect analysis of the flowpath for drug determination was conducted. Sources of error in the drug mass and original concentration were ignored since the same standard vials of material were used as the master for all dilutions of the anthracyclines tested. Other determined potential sources of error were grouped and included; recovery errors associated with adsorption of the analytes to the various surfaces used in the analysis and variation in solvent extraction efficiency; repeatability errors in volume estimation of drug, serum and extraction solvent mixtures; and calibration and instrumentation errors including autosampler injection volume, spray delivery efficiency and ion quantitation. Based on EURCHEM guidelines [20] and because of the wide analytical range employed, the relevant %R.S.D. was employed as the uncertainty measurement. The combined uncertainty is therefore defined as the root of the sum of the squares of the

Table 4
Relative uncertainty values for epirubicin analysis in serum obtained at 3 concentrations

	2.5 ng/ml	50 ng/ml	500 ng/ml
Combined uncertainty (u_{comb})	14.8	18.0	20.7
Repeatability uncertainty (u_{rep})	5.1	12.9	4.8
Calibration uncertainty (u_{cal})	7.2	12.1	19.3
Recovery uncertainty (u_{rec})	11.9	3.4	5.8

repeatability, calibration and recovery errors. The data outlined in Table 4 indicate that different factors contribute to uncertainty at differing concentrations. At low concentration, the dominant contribution is from recovery uncertainty. This is consistent with literature reports for anthracyclines and many other drugs. At higher concentrations calibration uncertainty becomes the dominant contributor, suggesting that instrumentation issues have become the major cause of uncertainty. The use of an internal standard (daunorubicin) helps keep the repeatability uncertainty low.

3.4. Sample analysis

3.4.1. Cell samples

To gain an insight into how much epirubicin is taken up by a tumour cell and the optimal conditions for this take-up, a number of cell culture experiments were carried out. Fig. 3 illustrates the results from these exploratory studies. The effects of some fundamental controlling parameters in the non-small cell lung carcinoma cell line A549 were studied initially. It was concluded from these investigations that drug accumulation was

greatest after 2 h of exposure to the epirubicin (Fig. 3A). The A549 cells were also exposed to varying drug concentrations, ranging from 0.05 to 2 μM . Cellular epirubicin accumulation peaked when cells were exposed to 0.75 μM drug in medium (Fig. 3B). Increasing the concentration beyond 0.75 μM drug did not result in increased levels within the cell. Using our sensitive LC–MS method, drug concentrations in cell samples could be measured following exposure to levels of epirubicin as low as 50 nM in the medium. A549 cells were exposed to media containing varying serum concentrations, i.e. 0, 2.5, 5 and 10%. Fig. 3C illustrates that 5% serum concentration was the optimum concentration for maximum cell mass drug in this setting. Serum concentration appeared to significantly affect drug accumulation. Fig. 3D highlights the significant variation of drug accumulation between cell lines, including A549, ranging from lung, colon adenocarcinoma to pancreatic carcinoma, possibly due to different cell characteristics (cell morphology and volume) and the fundamental uptake/efflux kinetics of the lines chosen.

3.4.2. Patient samples

A number of patient serum samples were analysed and an example of the type of data obtained is shown in Fig. 4. Each patient showed different levels of the parent drug (epirubicin) and its metabolites. The three metabolites – 13-dihydroepirubicin, 13-dihydroadriamycinone and adriamycinone – were observed by selected reaction monitoring. Epirubicin and its primary metabolite, dihydroepirubicin, are shown in Fig. 4 for illustration. Small additional anthracycline peaks are evident in spectra due to similarities in the fragmentation coupled with isotope ratios. It had been anticipated that

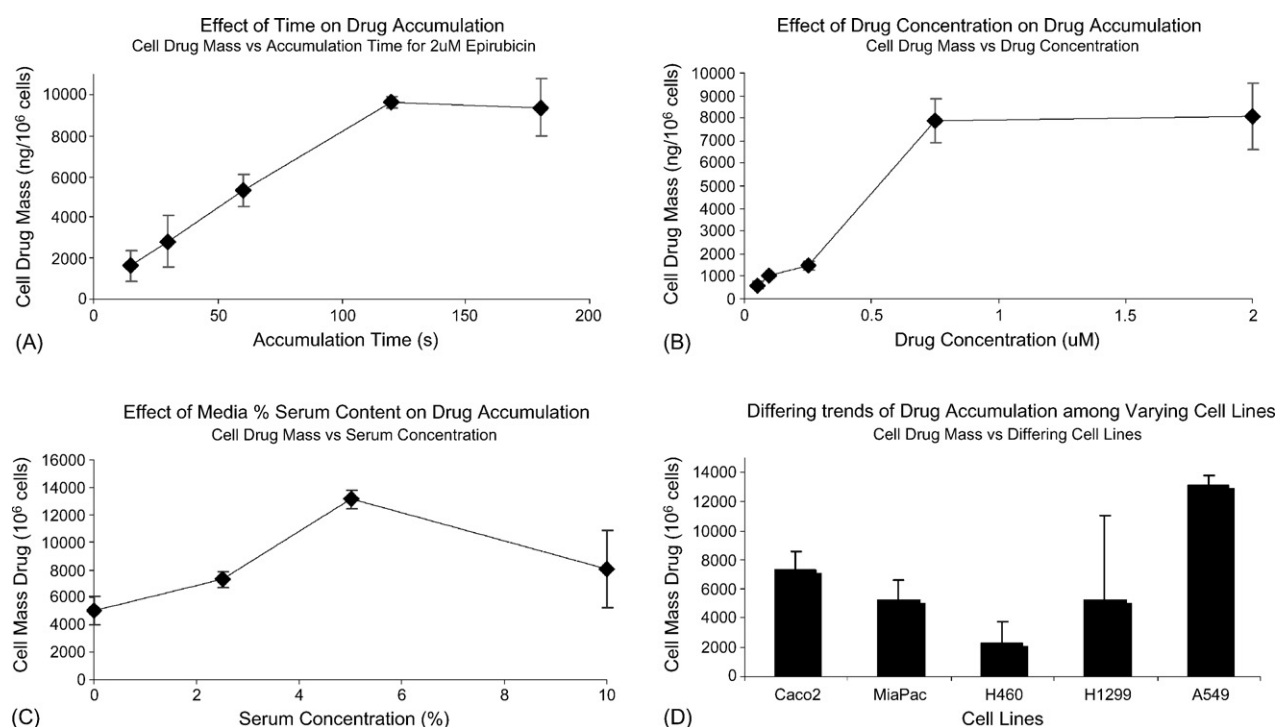


Fig. 3. Data from some of the cell sample studies investigating the effects of various parameters on epirubicin uptake in the A549 cell model (A, B, C) and between various cell lines (D).

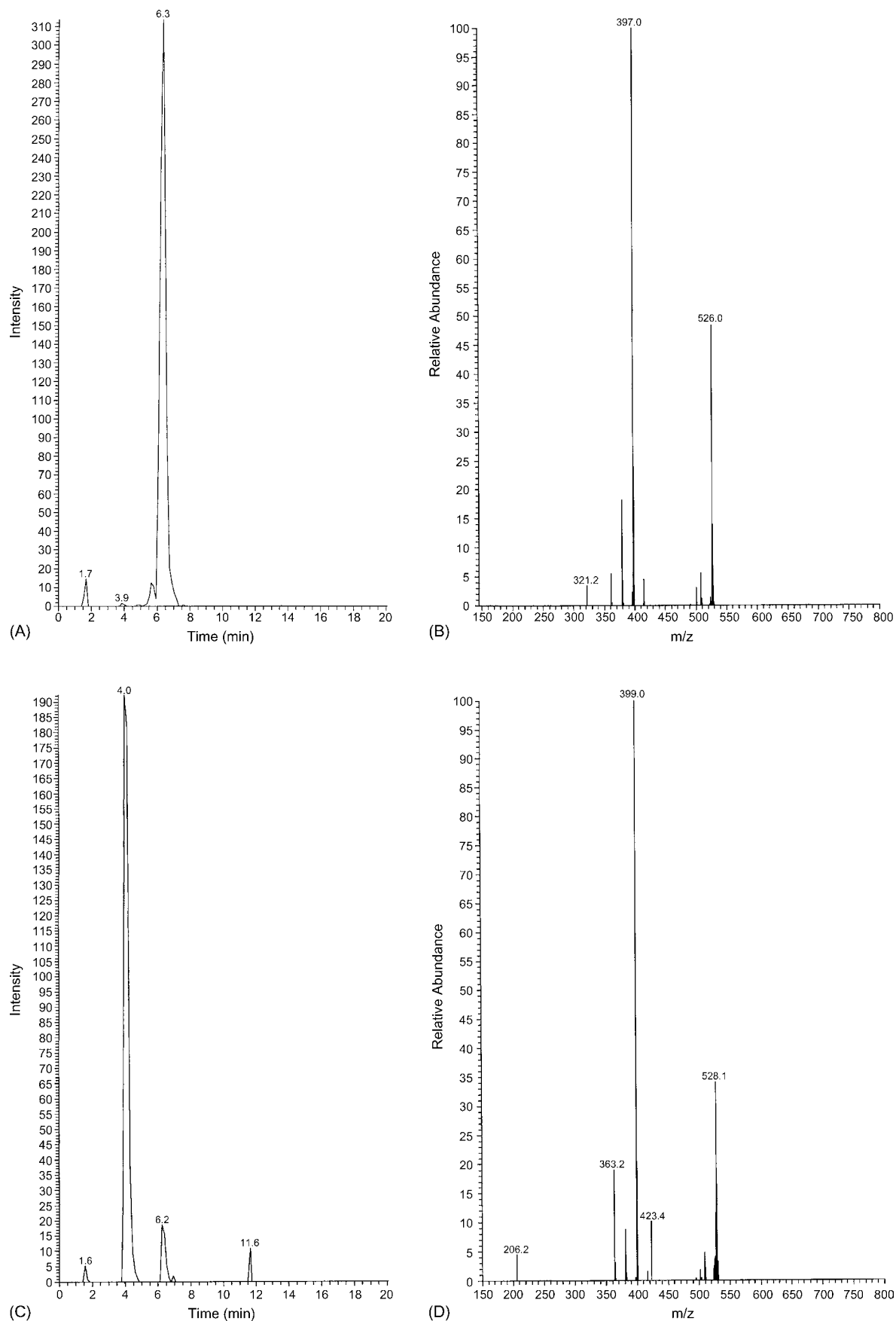


Fig. 4. Chromatographic extracted ion currents for epirubicin (A) and 13-dihydroepirubicin (C) from a patient sample. The respective MS fragmentation spectra are shown in B and D.

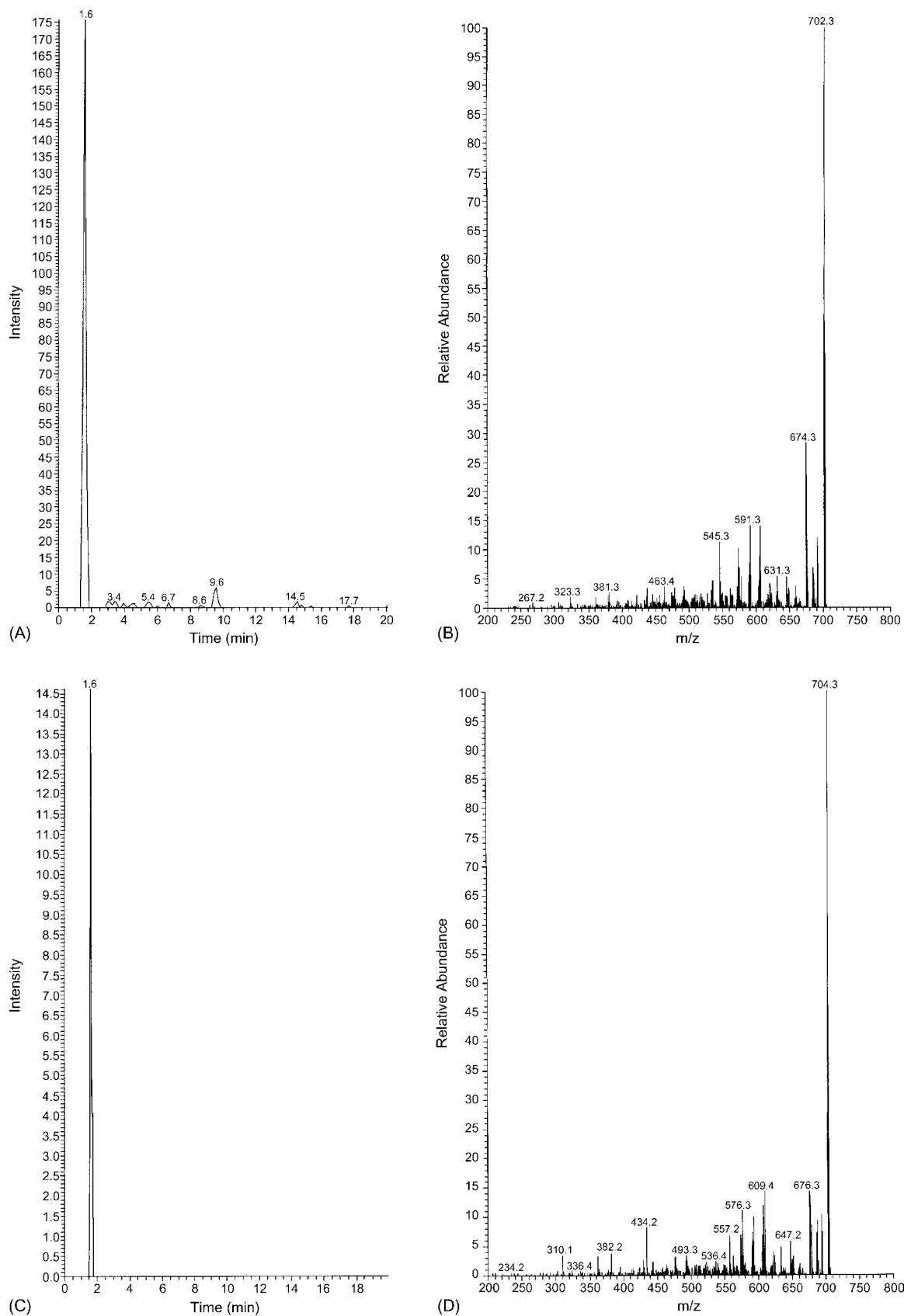


Fig. 5. Chromatographic extracted ion currents for epirubicin glucuronide (A) and epirubicinol glucuronide (C) from a patient sample. The respective MS spectra are shown in B and D.

glucuronide metabolites could also be present in patient samples and two new metabolites were indeed observed in two of the three patient samples with identical retention times of 1.60 min. The mass spectral profiles of these peaks indicated that these compounds were epirubicin glucuronide and epirubicinol glucuronide, respectively (see Fig. 5). Along with characteristic water losses, there was also a loss of 46 amu indicative of a loss of HCOOH for both metabolites, yielding m/z peaks of 674 and 676, respectively. Consistent with our observations, it has been reported in the literature that the glucuronide metabolites elute earlier than the parent drug on reversed phase LC due to their increased polarity [4].

4. Conclusions

A rapid and sensitive LC–MS method has been developed for the separation and detection of epirubicin and its metabolites (known and unknown) in biological samples. Even though these analytes are labile by nature, this paper highlights the importance of choosing the appropriate ionisation mode for enhanced sensitivity. APCI was chosen due to its greater sensitivity in comparison to ESI. Although validated for epirubicin, the method could alternatively be used to detect doxorubicin or daunorubicin and their metabolites. The optimised LC–MS/MS method permits quantitation of epirubicin in both patient serum samples and in cancer cell samples at physiologically relevant concentrations. In both cases, only small sample volumes are required. For patients, this analytical method means that we can carry out important therapeutic drug monitoring on their blood while they are undergoing chemotherapy treatment. It is envisaged that in a clinical setting, such information could be used to aid the clinical decision process in terms of attenuation of dose or even change of regimen. For the cell samples, this new method is allowing us to probe more fundamental oncology questions such the cellular uptake of epirubicin in various types of cancer cells under different conditions.

Overall, our results have shown that LC–MS² is an excellent tool for the identification and quantitation of epirubicin and its metabolites at very low levels in complex biological matrices.

Acknowledgements

We would like to thank the Irish Cancer Society for their funding and support of this project (CRI03OCO). We gratefully

appreciate the help of our colleagues in the National Institute of Cellular Biotechnology (NICB) who provided cancer cell samples and also to Jo Ballot and Joan Healy of St. Vincent's University Hospital, Dublin. The infrastructural funding which facilitated this work was provided by the Higher Education Authority (HEA) PRTL I Cycles I and III. We would like to express much appreciation to R.M. Straubinger and colleagues in the School of Pharmacy and Pharmaceutical Sciences, University at Buffalo for assistance in initiating this work.

References

- [1] P.M. Loadman, C.R. Calabrese, *J. Chromatogr. B* 764 (2001) 193.
- [2] D. Nielsen, C. Maare, T. Skovsgaard, *Gen. Pharmacol.* 27 (1996) 251.
- [3] Y.Y. Hon, W.E. Evans, *Clin. Chem.* 44 (1998) 388.
- [4] I.K. Barker, S.M. Crawford, A.F. Fell, *J. Chromatogr. B—Biomed. Applic.* 681 (1996) 323.
- [5] B.S. Andersson, S. Eksborg, R.F. Vidal, M. Sundberg, M. Carlberg, *Toxicology* 135 (1999) 11.
- [6] C. Dollery, *Therapeutic Drugs*, Churchill Livingstone, 1991.
- [7] J.H. Beijnen, W.J.M. Underberg, *J. Pharmaceut. Biomed. Anal.* 6 (1988) 677.
- [8] R.D. Arnold, J.E. Slack, R.M. Straubinger, *J. Chromatogr. B—Anal. Technol. Biomed. Life Sci.* 808 (2004) 141.
- [9] F. Lachatre, P. Marquet, S. Ragot, J.M. Gaulier, P. Cardot, J.L. Dupuy, *J. Chromatogr. B* 738 (2000) 281.
- [10] R. Ricciarello, S. Pichini, R. Pacifici, I. Altieri, M. Pellegrini, A. Fattorossi, P. Zuccaro, *J. Chromatogr. B* 707 (1998) 219.
- [11] L. Alvarez-Cedron, M.L. Sayalero, J.M. Lanao, *J. Chromatogr. B* 721 (1999) 271.
- [12] S. Fogli, R. Danesi, F. Innocenti, A. Di Paolo, G. Bocci, C. Barbara, M. Del Tacca, *Ther. Drug Monit.* 21 (1999) 367.
- [13] C. Sottani, G. Tranfo, M. Bettinelli, P. Faranda, M. Spagnoli, C. Minoia, *Rapid Commun. Mass Spectrom.* 18 (2004) 2426.
- [14] C.P. Duffy, C.J. Elliott, R.A. O'Connor, M.M. Heenan, S. Coyle, I.M. Cleary, K. Kavanagh, S. Verhaegen, C.M. O'Loughlin, R. NicAmhlaoibh, M. Clynes, *Eur. J. Cancer* 34 (1998) 1250.
- [15] R. O'Connor, M. O'Leary, J. Ballot, C. D. Collins, P. Kinsella, D.E. Mager, R.D. Arnold, L. O'Driscoll, A. Larkin, S. Kennedy, D. Fennelly, M. Clynes, J. Crown, *Cancer Chemother. Pharmacol.* (2006) (in press).
- [16] T. Pfeifer, J. Tuerk, K. Bester, M. Spiteller, *Rapid Commun. Mass Spectrom.* 16 (2002) 663.
- [17] V.P. Shah, K.K. Midha, S. Dighe, I.J. Mcgilveray, J.P. Skelly, A. Yacobi, T. Layloff, C.T. Viswanathan, C.E. Cook, R.D. McDowall, K.A. Pittman, S. Spector, *J. Pharmaceut. Sci.* 81 (1992) 309.
- [18] J. Ermer, *J. Pharmaceut. Biomed. Anal.* 24 (2001) 755.
- [19] R. O'Connor, M. O'Leary, J. Ballot, C.D. Collins, P. Kinsella, D.E. Mager, R.D. Arnold, L. O'Driscoll, A. Larkin, S. Kennedy, D. Fennelly, M. Clynes, J. Crown, *Cancer Chemother. Pharmacol.* (2006).
- [20] Eurachem/Citac, *Eurachem/Citac Guide* 4 (2000).

Short communication

Ion chromatographic determination of organic acids in food samples using a permanent coating graphite carbon column

Kenji Yoshikawa*, Miho Okamura, Miki Inokuchi, Akio Sakuragawa

*Department of Materials and Applied Chemistry, College of Science and Technology, Nihon University,
1-8-14 Kanda-Surugadai, Chiyoda-ku, Tokyo 101-8308, Japan*

Received 1 September 2006; received in revised form 14 October 2006; accepted 14 October 2006
Available online 22 November 2006

Abstract

From the viewpoint of a graphite carbon column with excellent durability, it was applied to the ion chromatography (IC) of several organic acids. The carbon column was permanently coated with the cetyltrimethylammonium (CTMA) ion, and the elution behaviors of several organic acids (acetic acid, lactic acid, succinic acid, malic acid, tartaric acid, citric acid) and inorganic anions (Cl^- , NO_2^- , NO_3^- , SO_4^{2-}) were examined according to a non-suppressed IC coupled with conductivity detector, when an ion-exchange ability was given to the graphite carbon column. When salicylic acid and sodium salicylate were used as a mobile phase, each organic acid are analyzed approximately 10 min. But the separation of malic acid, chloride and nitrite was difficult. When benzoic acid and 2-amino-2-hydroxymethyl-1,3-purpanediol (tris aminomethane) were used as a mobile phase, tartaric acid and citric acid, etc. with large valency showed tendency to which the width of each peaks extended and retention time increased. However, it was possible to separate excellently for the analytes detected within 10 min. The developed method was then applied to the determination of organic acids in several food samples.

© 2006 Elsevier B.V. All rights reserved.

Keywords: Graphite carbon column; Organic acid; Cetyltrimethylammonium; Benzoic acid; Ion chromatography

1. Introduction

Among the wide variety of methods available for determination of ions, ion chromatography (IC) based on ion-exchangers and conductivity detection has been extensively studied [1–9].

In general, organic polymer and silica-based porous ion-exchangers have been used as column packing for liquid chromatography [10–12]. Organic polymer-based ion-exchangers can be used a mobile phase of wide-ranging pH. But organic solvent and pressure resistance present any problems. On the other hand, silica-based ion-exchangers such as an ODS (C_{18}) column are generally used with an ion-interaction reagent to achieve separation of ions [13,14]. However, because the silica base is dissolved under the alkaline conditions, it may be affected ion-interaction reagent, i.e. alkaline surfactant. Moreover, It is difficult to use an ODS column for a long time.

A graphite carbon column is an alternative non-polar and inactive as stationary phase for liquid chromatography, and it has excellent chemical and physical resistance [15]. Therefore, the buffer solution in a wide-ranging pH (1–14) can be used as a mobile phase. Graphite carbon is used not only an absorbent of gas and organic matter but also a packing material for liquid chromatography, and used to analyze aromatic compounds [16–18], enantiomer of amino acids [19], element of food [20] and drug [21,22]. Though a graphite carbon column has some superior characteristics other than general-purpose column such as a ODS column, etc., it is not so widespread [23–25].

In recent years, applications of the IC that used the ion interaction chemical reagent for the graphite carbon column that doesn't have ion exchange ability are reported. These techniques are mainly based on two different methods. One is dynamic coating method [17,26] that added ion interaction reagent such as tetrabutylammonium hydroxide (TBA-OH), polyethylene imine (PEI), etc. in a mobile phase. In this method, it is not necessary to coat an ion interaction reagent on the column surface. However, in the case of non-suppressed IC that we applied this time, because a conductivity of the ion interaction reagent

* Corresponding author. Tel.: +81 3 3259 0801; fax: +81 3 3293 7572.
E-mail address: yoshikawa@chem.cst.nihon-u.ac.jp (K. Yoshikawa).

Table 1
Operating conditions for some organic acids

Column	Carbon IC BI-01 (100 mm × 4.6 mm i.d.)
Mobile phase	(1) 0.35 mM salicylic acid–0.1 mM sodium salicylate (pH 3.5) (2) 2.0 mM benzoic acid–1.2 mM tris aminomethane (pH 4.4)
Flow rate	(1) 0.8 ml/min (2) 1.0 ml/min
Column temperature	40 °C
Injection volume	100 µl
Detection	Conductivity

above-mentioned included in a mobile phase is high, more sensitive analysis is difficult, and a baseline is unstable. The other is permanent coating method [27] that coated the quaternary ammonium salt as an ion exchange site on the graphite carbon surface. In this method, it takes the time to coat an ion interaction reagent on the column surface. However, because it is not necessary to add an ion interaction reagent in the mobile phase, it is possible to apply the suppressed and non-suppressed IC. Nagashima et al. [27] have also reported a similar method for inorganic anions by suppressed IC. But, there were only a few reports on simultaneous determination of organic acids by using a permanent coating graphite carbon column.

In this work, cetyltrimethylammonium (CTMA)-coated graphite carbon column was used to separate six common organic acids (acetic acid, lactic acid, succinic acid, malic acid, tartaric acid, citric acid). These organic acids were directly detected by non-suppressed IC coupled with conductivity detector. Moreover, the separation behaviors of four inorganic anions (Cl^- , NO_2^- , NO_3^- , SO_4^{2-}) that included in food sample were examined.

The objective of this work was to establish optimal conditions of simultaneous determination of organic acids and apply to the determination of organic acids in several food samples.

2. Experimental

2.1. Apparatus

The ion chromatographic equipment consisted of a Model ICA-5120 pump, a Model ICA-5220 conductivity detector, a Model ICA-5410 column oven (Toa DKK, Tokyo, Japan), and a Model 21 chromatocorder (System Instruments, Tokyo, Japan). The separation column was a Carbon IC BI-01 (100 mm × 4.6 mm i.d., average particle size 3.0 µm, carbon content larger than 99.5%, Bio-Tech Research, Saitama, Japan).

2.2. Reagents

Salicylic acid and sodium salicylate (Wako Pure Chemical, Osaka, Japan) were used as a mobile phase with salicylate. Benzoic acid and 2-amino-2-hydroxymethyl-1,3-purpanediol (tris aminomethane: Wako Pure Chemical, Osaka, Japan) were used as a mobile phase with benzoate.

Acetic acid, lactic acid, succinic acid, malic acid, tartaric acid and citric acid (Wako Pure Chemical, Osaka, Japan) were

used as a standard solution of organic acids. Sodium chloride, sodium nitrite, sodium nitrate and sodium sulfide (Wako Pure Chemical, Osaka, Japan) were used as a standard solution of inorganic anions.

To coat the graphite carbon column, acetonitrile (Kanto Chemical, Tokyo, Japan) and cetyltrimethylammonium chloride (CTMA-Cl: Wako Pure Chemical, Osaka, Japan) was used. Deionized water, further purified with a Millipore Milli-Q system (Bedford, MA, USA) with a specific resistance of 18.2 MΩ.

2.3. Coating method

The column was at first washed with 50 and 100% (v/v) acetonitrile each for 1 h at 0.8 ml/min, and then washed with deionized water for 1 h at 0.8 ml/min. To coat the column, 2.0 mM CTMA-Cl was passed through the column at 0.8 ml/min for 2 h. After dynamically coating, the column was washed with deionized water for 2 h, and used as a permanent coating graphite carbon column. The coating carbon column is stable and available for 3 months.

In the permanent coating method, normal chain alkyl group that has hydrophobic part of the quaternary ammonium salt has been adsorbed by the surface of carbon that is hydrophobic particle. Moreover, because the polarity part of quaternary ammonium salt faces the mobile phase, ion exchange and separates ions were performed. Although main separation mechanism is ion exchange, hydrophobic interaction and distribution interaction of the stationary phase also take part.

2.4. Operating conditions

The operating conditions for ion chromatography are shown in Table 1. 0.35 mM salicylic acid–0.1 mM sodium salicylate (flow rate, 0.8 ml/min) was used as a mobile phase with salicylate. 2.0 mM benzoic acid–1.2 mM tris aminomethane (flow rate, 1.0 ml/min) was used as a mobile phase with benzoate.

3. Results and discussion

3.1. Mobile phase with salicylate

When analyzed organic acids and inorganic anions by non-suppressed IC, aromatic compounds are usually used as a mobile phase. At first, salicylic acid and sodium salicylate were used. A typical chromatogram of six organic acids and four inorganic

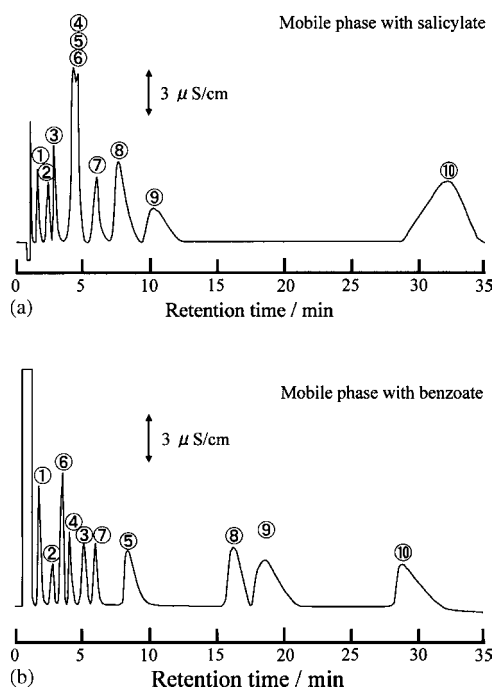


Fig. 1. Chromatogram of standard mixture. Ions (mg l^{-1}): ① acetic (50); ② lactic (20); ③ succinic (50); ④ NO_2^- (5); ⑤ malic (50); ⑥ Cl^- (5); ⑦ NO_3^- (5); ⑧ tartaric (50); ⑨ citric (50); ⑩ SO_4^{2-} (20); column: Carbon IC BI-01; mobile phase: (a) 0.35 mM salicylic acid–0.1 mM sodium salicylate (pH 3.5, flow rate 0.8 ml/min); (b) 2.0 mM benzoic acid–1.2 mM tris aminomethane (pH 4.4, flow rate 1.0 ml/min); column temperature: 40 °C.

anions is shown in Fig. 1(a). Each organic acid and inorganic anion except a sulfite is detected nearly 10 min. But the separation of malic acid, chloride and nitrite was difficult. Although the mobile phase concentration changed, simultaneous analysis of the organic acids and inorganic anions were difficult in a mobile phase with salicylate.

3.2. Mobile phase with benzoate

3.2.1. Effect of benzoic acid and tris aminomethane concentration

In order to achieve a separation of three kinds of ions (malic acid, chloride, nitrite), benzoic acid and tris aminomethane were used as a mobile phase with benzoate. Effect of tris aminomethane concentration on the retention behavior was examined with the concentration of benzoic acid fixed at 2.0 mM. The relationship between the retention time of analyte and the concentration of tris aminomethane is shown in Fig. 2. Although the retention time of most analytes steady or decrease with increasing tris aminomethane concentration, citric acid showed opposite tendency. As the tris aminomethane concentration increases (pH of a mobile phase increased), dissociation of citric acid advances. As a result, the optimum tris aminomethane concentration was determined to be 1.2 mM, based on the resolution and retention time for each analytes.

Furthermore, effect of benzoic acid concentration on the retention behavior was examined with the concentration of tris aminomethane fixed at 1.2 mM. As the concentration of benzoic acid increased, retention time decreases so that dissociation of

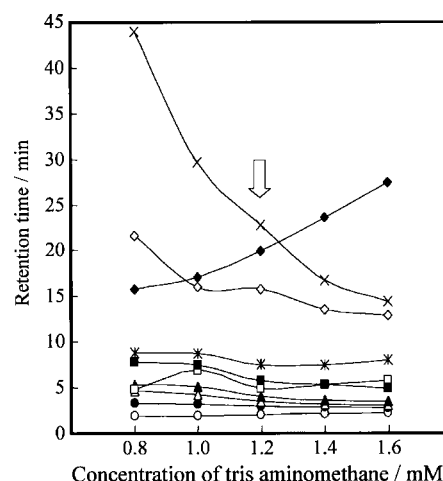


Fig. 2. Effect of tris aminomethane concentration on retention time (benzoic acid concentration fixed 2.0 mM). Ions (mg l^{-1}): ○ acetic (50); ● lactic (20); △ Cl^- (5); ▲ NO_2^- (5); □ succinic (50); ■ NO_3^- (5); ✕ malic (50); ◇ tartaric (50); ◆ citric (50); × SO_4^{2-} (20); column: Carbon IC BI-01; mobile phase: 2.0 mM benzoic acid–tris aminomethane; column temperature: 40 °C.

each organic acid retrogresses. As a result, the optimum benzoic acid concentration was determined to be 2.0 mM for the same reasons as for tris aminomethane.

Moreover, mobile phase concentration rate fixed (benzoic acid:tris aminomethane = 2.0:1.2), the relationships between the logarithm of the total concentration of mobile phase $[E]$ and the capacity factor $[k']$ are shown in Fig. 3. In the ion-exchange mode, the following relational formula (1) is obtained between the concentration of mobile phase $[E]$ and capacity factor $[k']$:

$$\text{Log } k' = -\left(\frac{y}{x}\right) \log [E] + \text{const.} \quad (1)$$

In this formula, x shows the valency of mobile phase ion, y shows the valency of analyte ion and $-(y/x)$ shows the slope of the straight line [28]. As shown in Fig. 3, in this condition (pH 4.4), the slope of the straight line is negative. The slope of monova-

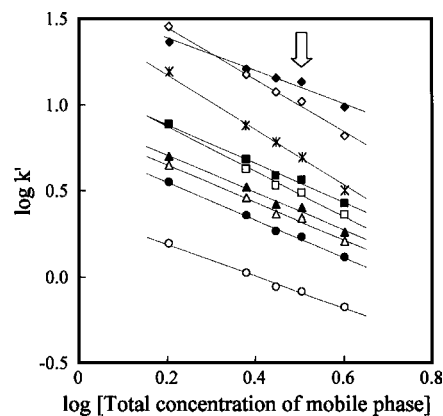


Fig. 3. Relationship between capacity factor (k') and total concentration of mobile phase. Ions (mg l^{-1}): ○ acetic (50); ● lactic (20); △ Cl^- (5); ▲ NO_2^- (5); □ succinic (50); ■ NO_3^- (5); ✕ malic (50); ◇ tartaric (50); ◆ citric (50); column: Carbon IC BI-01; mobile phase concentration rate: benzoic acid:tris aminomethane = 2.0:1.2 (pH 4.4); $\log k' = (-y/x)\log [E] + \text{const.}$, where k' is the capacity factor, x the valency of mobile phase ion, y the valency of analyte ion and E is the total concentration of mobile phase.

Table 2
Analytical precision of organic acids

Organic acid	Linearity		Reproducibility		Detection limit (mg l ⁻¹) (S/N = 3)
	Range (mg l ⁻¹)	r ² (n = 6)	mg l ⁻¹	%R.S.D. (n = 6)	
Acetic	10–200	0.9992	50	0.46	1.2
Lactic	10–100	0.9997	50	0.40	2.3
Succinic	10–200	0.9999	50	0.40	2.9
Malic	20–120	0.9990	50	0.73	4.5
Tartaric	30–200	0.9991	50	0.84	2.8
Citric	40–200	0.9998	50	0.75	3.8

R.S.D.: relative standard deviation.

lent inorganic anions (Cl⁻, NO₂⁻ and NO₃⁻) is approximately -1. However, because the slope of organic acids (especially malic acid and tartaric acid) is between -2 and -1, the separation mode could not be decided that the ion-exchange mode was predominant indiscriminately. As a result, the separation mechanism of the organic acid by the permanent coating carbon column is considered that other modes like the ion exclusion, polarity interaction etc. also take part besides the ion exchange mode. So that the dissociation constant of each organic acid may greatly influence the separation, it is important to control the separation behavior of the analysis, and know the separation mode of the column to understand the dissociation of the organic acid.

3.2.2. Effect of column temperature and flow rate

Under the composition of the mobile phase, effect of column temperature on the retention behavior was examined from 30 to 50 °C. Although the retention time of monovalent ions decreased with increasing temperature, divalent ions showed opposite tendency. The optimum column temperature was determined to be

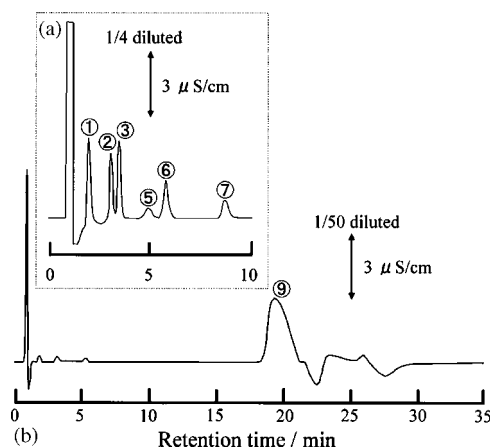


Fig. 4. Chromatogram of organic acids and inorganic anions in nutrition drink sample. Ions (mg l⁻¹): ① acetic; ② lactic; ③ Cl⁻; ⑤ succinic; ⑥ NO₃⁻; ⑦ malic; ⑨ citric; column: Carbon IC BI-01; mobile phase: 2.0 mM benzoic acid–1.2 mM tris aminomethane (pH 4.4); column temperature: 40 °C.

Table 3
Analytical results for organic acids in food sample

Sample	Organic acid	Dil. found (mg l ⁻¹)	Added (mg l ⁻¹)	Found (mg l ⁻¹)	Recovery (%)	Concentration (mg l ⁻¹)
Nutrition drink (1)	Acetic ^a	27.5	50.0	70.8	91.4	110.0
	Lactic ^a	23.2	30.0	50.6	91.2	92.8
	Succinic ^a	–	–	–	–	<DL
	Malic ^a	18.8	50.0	68.9	100.2	75.2
	Citric ^b	158.9	30.0	188.4	99.7	7945.0
Nutrition drink (2)	Acetic ^c	6.2	50.0	49.4	88.8	12.5
	Lactic ^c	73.8	30.0	95.8	92.3	147.7
	Succinic ^d	104.2	30.0	134.3	100.1	2083.8
	Citric ^c	82.0	50.0	139.8	105.9	163.9
Moromi vinegar	Acetic ^e	64.5	50.0	111.2	97.1	2065.4
	Succinic ^e	42.4	50.0	91.8	99.3	1358.4
	Malic ^e	27.7	50.0	72.1	92.8	886.2
	Citric ^e	170.6	30.0	189.6	94.5	5460.0
Yogurt	Lactic ^b	42.7	50.0	79.6	85.9	2134.5
	Succinic ^a	–	–	–	–	<DL
	Citric ^a	90.8	50.0	145.0	103.0	363.1

DL: determination limit.

^a 1/4 dil.

^b 1/50 dil.

^c 1/2 dil.

^d 1/20 dil.

^e 1/32 dil.

40 °C, based on the resolution and retention time for each analytes.

Moreover, the optimum flow rate of mobile phase was determined to be 1.0 ml/min for the same reasons as for column temperature.

3.2.3. Chromatogram of organic acids and inorganic anions

A typical chromatogram of six organic acids and four inorganic anions is shown in Fig. 1(b). Because eluting power is weaker to a mobile phase with benzoate than a mobile phase with salicylate, tartaric acid and citric acid, etc. with large valency showed tendency to which the width of each peaks extended and retention time increased. But it was possible to separate excellently for the analytes detected within 10 min. Especially, the separation of the Cl^- , NO_2^- and malic acid became possible.

3.2.4. Analytical precision

The linearity of calibration curves, reproducibility and detection limit are shown in Table 2. The calibration curves obtained from the peak areas for the organic acids were linear, with good correlation coefficients of 0.999. The relative standard deviations (R.S.D.) of peak areas were between 0.40 and 0.84% for six repeated measurements. The detection limits, summarized in Table 2, were calculated at the S/N ratio of 3. The detection limits of organic acids were between 1.2 and 4.5 mg/l.

3.2.5. Application to food samples

The proposed method was applied to analyze organic acids in food samples. Yogurt sample was prepared by adding 5 g of it in 20 ml of deionized water and then mixing in 20 min. After the sample solution had been centrifuged in 2000 rpm, 100 μl was injected into IC. Chromatogram of nutrition drink sample is shown in Fig. 4. Analytical results of organic acids in the other food sample were shown in Table 3. In addition, to confirm the reliability of the method, organic acids of each concentration is added to the food sample, and recovery test was demonstrated (shown in Table 3). Because the recovery showed nearly 100%, this method can be applied to the determination of organic acids without the matrix effect.

4. Conclusion

In this work, simultaneous determination of six common organic acids and four inorganic anions using a stationary phase of the CTMA-coated graphite carbon column and a mobile phase with benzoate was demonstrated. This method showed excel-

lent linearity, reproducibility, lower detection limits. Therefore, it was applied to the determination of organic acids in food samples such as nutritious, vinegar and yogurt without the matrix effect. The graphite carbon column has been used for six years, and the excellent durability of the column was confirmed in all our experiments.

Acknowledgements

We appreciate for the support of Kenji Nakamura and Kazue Ochi (Department of Materials and Applied Chemistry, College of Science and Technology, Nihon University) in this work.

References

- [1] M.C. Bruzzoniti, E. Mentasti, C. Sarzanini, *Anal. Chim. Acta* 382 (1999) 291.
- [2] C.L. Guan, J. Ouyang, Q.L. Li, B.H. Liu, W.R.G. Baeyens, *Talanta* 50 (2000) 1197.
- [3] S.D. Kumar, B. Maiti, P.K. Mathur, *Talanta* 53 (2001) 701.
- [4] A. Alcazar, P.L. Fernandez-Caceres, M.J. Martin, F. Pablos, A.G. Gonzalez, *Talanta* 61 (2003) 95.
- [5] R. García-Fernández, J.I. García-Alonso, A. Sanz-Medel, *J. Chromatogr. A* 1033 (2004) 127.
- [6] M.M. McDowell, M.M. Ivey, M.E. Lee, V.V.V.D. Firpo, T.M. Salmassi, C.S. Khachikian, K.L. Foster, *J. Chromatogr. A* 1039 (2004) 105.
- [7] A.A. Krokidis, N.C. Megoulas, M.A. Koupparis, *Anal. Chim. Acta* 535 (2005) 57.
- [8] R. Lin, B. De Borja, K. Srinivasan, A. Woodruff, C. Pohl, *Anal. Chim. Acta* 567 (2006) 135.
- [9] B. Zhu, Z. Zhong, J. Yao, *J. Chromatogr. A* 1118 (2006) 106.
- [10] J. Qiu, X. Jin, *J. Chromatogr. A* 950 (2002) 81.
- [11] J.J. Kirkland, *J. Chromatogr. A* 1060 (2004) 9.
- [12] K. Horvath, P. Hajos, *J. Chromatogr. A* 1104 (2006) 75.
- [13] J.S. Fritz, Z. Yan, P.R. Haddad, *J. Chromatogr. A* 997 (2003) 21.
- [14] S. Pelletier, C.A. Lucy, *J. Chromatogr. A* 1125 (2006) 189.
- [15] T. Hanai, *J. Chromatogr. A* 989 (2003) 183.
- [16] J.H. Knox, B. Kaur, *High-Performance Liquid Chromatography*, J. Wiley & Sons, New York, 1989, p. 189.
- [17] J.H. Knox, Q.H. Wan, *Chromatographia* 42 (1996) 83.
- [18] J.L. Gundersen, *J. Chromatogr. A* 914 (2001) 161.
- [19] Q.H. Wan, P.N. Shaw, M.C. Davies, D.A. Barrett, *J. Chromatogr. A* 765 (1997) 187.
- [20] J. Rosen, K.E. Hellenas, *The Analyst* 127 (2002) 880.
- [21] E. Forgacs, T. Cserhati, *J. Chromatogr. B* 681 (1996) 197.
- [22] I.D. Wilson, *Chromatographia* 52 (1996) S28.
- [23] Y. Inamoto, S. Inamoto, T. Hanai, M. Tokuda, O. Hatase, K. Yoshi, N. Sugiyama, T. Kinoshita, *Biomed. Chromatogr.* 12 (1998) 239.
- [24] A. Karlsson, M. Berglin, C. Charron, *J. Chromatogr. A* 797 (1998) 75.
- [25] P. Chaimbault, C. Elfakir, M. Lafosse, *J. Chromatogr. A* 797 (1998) 83.
- [26] T. Okamoto, A. Isozaki, H. Nagashima, *J. Chromatogr. A* 800 (1998) 239.
- [27] H. Nagashima, T. Okamoto, *J. Chromatogr. A* 855 (1999) 261.
- [28] P. Hajos, O. Horvath, V. Denke, *Anal. Chem.* 67 (1995) 434.

Study on the inclusion interactions of β -cyclodextrin and its derivative with dyes by spectrofluorimetry and its analytical application

Xiashi Zhu*, Jing Sun, Jun Wu

College of Chemistry and Chemical Engineering, Yangzhou University, Yangzhou 225002, China

Received 25 August 2006; received in revised form 28 September 2006; accepted 17 October 2006

Available online 15 November 2006

Abstract

The inclusion interactions of β -cyclodextrin (β -CD) and hydroxypropyl- β -cyclodextrin (HP- β -CD) with dyes were developed by spectrofluorimetry, and the inclusion constants of inclusion complexes were determined by direct fluorescence technique. The main factors (the host molecule, the guest molecule, and the pH) for the inclusion interaction were discussed in detail. At the same time, the inclusion interaction of HP- β -CD and vitamin B₆ (VB₆) was investigated with the competitive fluorescence inclusion method and the inclusion constant of HP- β -CD and vitamin B₆ (VB₆) was obtained by indirect fluorescence technique. On the basis of the linear relationship between the change of fluorescence intensity (ΔF) and the concentration of VB₆, a competitive fluorescence inclusion method was used to the determination of VB₆. The method has been successfully applied to the analysis of VB₆ in synthetic samples, tablets and injections with satisfactory results.

© 2006 Elsevier B.V. All rights reserved.

Keywords: Cyclodextrin; Dye; Spectrofluorimetry; Competitive inclusion; VB₆

1. Introduction

β -Cyclodextrin and its various derivatives (β -CDs) are well known, which structure is that of a truncated cone with the hydrophilic outer surface and a hydrophobic internal cavity [1] (Fig. 1). This peculiar molecular structure could include guest molecules to form inclusion complexes. The photochemical and photophysical properties of the guest molecules would be altered due to the formation of a super-molecular complex (guest- β -CDs). Thus, the physical, chemical and biochemical characters of guest molecules are modified, and the application capability of those guest molecules could be improved. So, β -CDs with inclusion properties had been widely used in various fields such as medicine [2–5], chemistry [6,7], agriculture [8], and so on.

Investigation of the inclusion mechanism of inclusion complexes plays an important part in supramolecular chemistry. So far, the method, which included spectrum (UV–vis and fluorescence), HPLC, surface tension, electrochemistry, calorimetry, dynamics and competition method [8], were used for determining inclusion constants [2,3,5,9]. Fluorescence quantum yield

[10], thermodynamic parameters of inclusion process [11], fluorescence probes [12,13], competitive inclusion method [14,15] and ¹H NMR spectroscopy [16] were applied to investigate the inclusion mechanism of inclusion complexes.

Vitamins are necessary for normal growth and activity of the body, and obtained naturally from plant, animal foods or medicines. The medicines contained vitamins are generally labile for light, heat and oxygen. While through the formation of inclusion complexes with β -CDs the stability, solubility and bioavailability of those medicines could be enhanced. At present, the method of investigation inclusion interactions of vitamin- β -CDs mainly includes: (1) direct methods which are established based upon the remarkable changes of the observed signals (such as photochemistry, electrochemistry signals) when the vitamin molecules were included into the β -CDs; (2) indirect method of determination inclusion constant could be established, namely competitive inclusion method [17] for other vitamins which signals were not changed with β -CDs-included.

In this paper, six dyes (salicylfluorone (SAF), butyl rhodamine B (BRB), methylene blue (MB), erythrosine sodium (ES), tetrachlorotetraiodo-fluorescein disodium (TCTIF) and tetrachlorofluorescein (TCF)) were chosen to study the inclusion interactions of them with β -CD and hydroxypropyl- β -cyclodextrin (HP- β -CD) by fluorescence spectroscopy and ¹H

* Corresponding author. Tel.: +86 514 7975244; fax: +86 514 7975244.
E-mail addresses: xszhu@yzu.edu.cn, zhuxiashi@sina.com (X. Zhu).

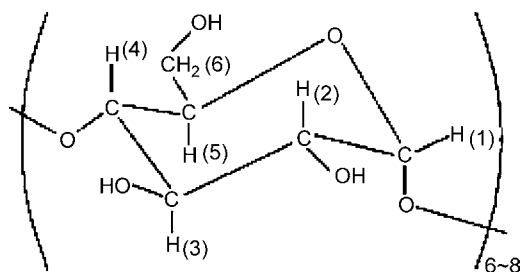


Fig. 1. Structure of CD oligosaccharide.

NMR spectroscopy technique. The influence factors of inclusion interactions (the host molecule, the guest molecule, and the pH) were discussed in detail. In addition, the inclusion interaction of VB₆-HP-β-CD was investigated with the competitive fluorescence inclusion method and the inclusion constant of the inclusion complex (VB₆-HP-β-CD) was obtained by indirect fluorescence technique. On the basis of the linear relationship between the change fluorescence intensity (ΔF) and the concentration of VB₆, a new method for the analysis of VB₆ was developed. The method has been successfully used to determine VB₆ in synthetic samples, tablets and injections with satisfactory results.

2. Experimental

2.1. Apparatus

The fluorescence measurements were performed with a F-4500 spectrofluorimeter (Hitachi, Japan). The pH measurements were made with a model pHS-25 pH meter (Shanghai, China). ¹H NMR experiments were performed on Bruker AV 600 instrument.

2.2. Reagents

All chemicals were of analytical-reagent grade. β-CD (China Medicine Group Chemical Reagent Corporation), HP-β-CD (average MW = 1425, D.S. = 5.0, Yi Ming Fine Chemical Corporation, China) were used without prior purification. The stock solutions of all dyes were prepared by directly dissolving the crystal into distilled water or ethanol. A standard stock solution of Vitamin B₆ (Nanjing Pharmacy Factory, China) was prepared. HAc-NaAc and NH₃-NH₄Cl buffer solutions were used to control the pH value. D₂O was used as the solvent in the ¹H NMR experiments.

2.3. Determination of inclusion constants by direct fluorescence method

A quantitative solution of dyes was transferred into a 25 mL volumetric flask, whereas added different amount of 0.01 mol/L β-CD or HP-β-CD. Then buffer solution was used to control the pH value of the solutions. The mixed solutions were diluted to final volume with distilled water and shaken thoroughly, then it was thermostated at 20.0 ± 1 °C and the fluorescence intensities were measured at the optimal excitation wavelength. The inclu-

sion complexes were estimated assuming a 1:1 inclusion model, and the inclusion constants could be obtained from fluorescence data by the modified Benesi-Hildebrand equation (double reciprocal plot) [18,19].

2.4. Determination of inclusion constants by indirect fluorescence method

The concentration of ES and TCTIF were 1.0 × 10⁻⁵ mol/L, and HP-β-CD concentration was 3.2 × 10⁻³ mol/L, whereas changed the concentration of VB₆. Buffer solution was used to control the pH value of the solutions (ES: pH 5.0; TCTIF: pH 7.6). The fluorescence intensities of these solutions were measured at the optimal excitation wavelength as to evaluate the inclusion constant of VB₆-HP-β-CD.

2.5. Sample preparation

Took 30 pieces of VB₆ tablets (10 mg/piece), crushed them into powder. Then took 0.2 g powder and dissolved it into water, then filtrated it. The filtrate was transferred into a 50 mL volumetric flask, and diluted to final volume with distilled water.

Took five tubes of VB₆ injections (0.1 g/2 mL) and mixed them. 0.8 mL the mixed solution was transferred into a 25 mL volumetric flask.

3. Results and discussion

3.1. Fluorescence spectra of CDs-dye inclusion complex

The fluorescence emission spectra of dyes were scanned. Fig. 2 was shown the fluorescence emission spectra of SAF in different media. The effects of the concentration of β-CDs on the fluorescence intensity of dyes were determined. The results showed that with an increase of β-CD concentration (1) the fluorescence intensities of the SAF and MB were increased; (2) the fluorescence intensity of the BRB was decreased; (3) the fluorescence intensity of the TCF, ES and TCTIF was not obvi-

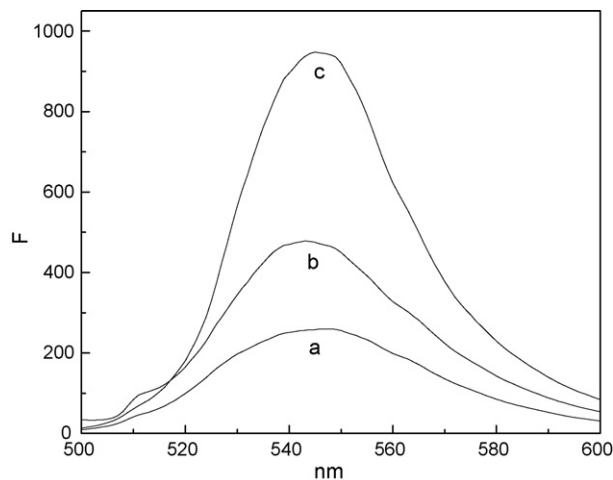


Fig. 2. Fluorescence emission spectra of SAF (1.0 × 10⁻⁵ mol/L) in different media: (a) H₂O, (b) β-CD, (c) HP-β-CD.

Table 1
Fluorescence spectrum characteristics of SAF, BRB, MB, ES, TCTIF and TCF

System	pH	λ_{ex} (nm)	λ_{em} (nm)	f^a
SAF- β -CD	3.2	486	511	0.32
SAF-HP- β -CD			510	0.51
BRB- β -CD			584	-0.30
BRB-HP- β -CD	5.0	664	688	-0.18
MB- β -CD			688	0.27
MB-HP- β -CD			688	0.30
ES- β -CD	7.6	546	550	0.02
ES-HP- β -CD			549	0.18
TCTIF- β -CD			563	0.01
TCTIF-HP- β -CD	7.6	538	564	0.17
TCF- β -CD			562	-0.03
TCF-HP- β -CD			562	0.01

β -CD: 8.0×10^{-4} mol/L, HP- β -CD: 8.0×10^{-4} mol/L.

^a Fluorescence sensitive factor $f = (F - F_0)/F_0$, where F and F_0 represent the fluorescence intensity of the dyes in the presence and absence of CDs.

ous change. While with an increase of HP- β -CD concentration (1) the fluorescence intensities of the SAF, MB, ES and TCTIF were increased; (2) the fluorescence intensity of the BRB was decreased; (3) the fluorescence intensity of the TCF was not obvious change. In this paper, fluorescence sensitive factor (f) was used to show the influence degree of CDs on the fluorescence intensity of the dyes (Table 1). The uncertainty budget for f was less than 0.01%.

3.2. The inclusion interactions of dyes and β -CDs

The photochemical and photophysical properties of the guest molecules could be altered due to the formation of a host-guest complex (dyes- β -CDs). The changes of fluorescence intensities of the dyes in the presence of β -CDs might be due to the dye molecules entered the hydrophobic cavity of CDs and the hydrophobic cavity of CDs provided the different microenvironment for the guest (dye molecules). But, the changes of fluorescence intensities might be also due to a solvent effect caused by a higher concentration of β -CDs. So the fluorescence intensities changes could only show the possibility of inclusion interactions.

To demonstrate the formation of a host-guest complex (dyes- β -CDs), several experimental techniques were used: (1) β -CDs are the cyclic oligosaccharides consisting of six or more D-(+)-glucopyranose units (Fig. 1), the effect of glucose on the fluorescence spectra of the dyes was tested, which could prove whether fluorescence spectra changes were a solvent effect caused by a higher concentration of β -CD or HP- β -CD [16]; (2) The polarity of the hydrophobic cavity of β -CD and HP- β -CD was similar to that of alcohols (R-OH), the effect of different alcohols on the fluorescence spectra of dyes were investigated, which could reflect the inclusion interactions between dyes and β -CDs; (3) The chemical shifts of CDs protons in different system was measured by ^1H NMR spectroscopy, which could be observed the deep of guest molecule entered the cavity of CDs.

To prove that these spectral changes were not a solvent effect caused by a high concentration of CDs, the effect of glucose on the spectra of dyes was tested. When the addition of glucose (in

Table 2
Chemical shifts δ of protons in β -CD, BRB- β -CD and MB- β -CD

	β -CD					
	H ₁	H ₂	H ₃	H ₄	H ₅	H ₆
$\delta_{\beta\text{-CD}}$	4.92	3.43	3.73	3.51	3.82	3.73
$\delta_{\text{BRB-}\beta\text{-CD}}$	4.89	3.41	3.57	3.47	3.65	3.50
$\delta_{\text{MB-}\beta\text{-CD}}$	4.91	3.42	3.69	3.50	3.77	3.69
$\Delta\delta_1^a$	-0.03	-0.02	-0.16	-0.04	-0.17	-0.23
$\Delta\delta_2^b$	-0.01	-0.01	-0.04	-0.01	-0.05	-0.04

^a $\Delta\delta_1 = \delta_{\text{BRB-}\beta\text{-CD}} - \delta_{\beta\text{-CD}}$.

^b $\Delta\delta_2 = \delta_{\text{MB-}\beta\text{-CD}} - \delta_{\beta\text{-CD}}$.

an equivalent mass of 2.00×10^{-3} mol/L β -CD or HP- β -CD) to a 1.00×10^{-5} mol/L of dye solution, the fluorescence spectra of the dyes were neither spectral shifts nor intensity changed, which contrasted with those found when β -CD or HP- β -CD was added. It confirmed that the β -CDs-induced changes observed in the fluorescence spectra of dyes indicated the formation of supramolecular complexes between the two molecules, namely there were the conclusion interactions between the β -CDs and dyes.

Ethanol/water, 2-propanol/water and glycerol/water were used as media to obtain the fluorescence spectra of MB at different alcohol/water ratios. It was found that the emission wavelength of MB was red-shifted, and its fluorescence intensity was gradually enhanced as the percentage of the alcohols in the mixed solvents increased. The facts suggested that the microenvironment around dye molecules in the presence of β -CD and HP- β -CD was similar to that in alcohols, thus it indicated the formation of inclusion complexes between β -CDs and MB.

According to the ^1H NMR spectra of β -CD, BRB- β -CD, and MB- β -CD, apparent changes in chemical shifts of different protons could be observed (Table 2): (1) unlike the dramatic upfield shifts of β -CD's interior H-3, H-5, and H-6 protons, which resulted from the shielding effect exerted by the inclusion of the guest molecule (BRB, MB) into β -CD's cavity, the shifts of β -CD's outside H-2 and H-4 protons could be neglected; the apparent shift changes of β -CD's H-3 indicated that the guest molecule entered the cavity along its wide rim; (2) the chemical shifts' degree of the protons ($\Delta\delta$) was BRB- β -CD > MB- β -CD, which indicated that BRB entered the cavity more deeply than MB, and the inclusion interaction of BRB with β -CD was more strong than MB with β -CD. All the facts showed obviously that the guest molecules were included in β -CD's cavity.

The inclusion interaction of β -CDs and dyes (host-guest) could be influenced by many factors. The inclusion constant K is an important parameter for characterizing the inclusion interactions of β -CDs with guest molecules. K value reflects the intensity of binding force of β -CDs with guest molecules.

The inclusion constants of the dyes with β -CDs were determined by directly fluorescence technique [18,19] and shown in Table 3. From the data, the influence factors of inclusion interactions (the host molecule, the guest molecule, and the pH) were discussed.

Table 3
Inclusion constants of the dyes with β -CD and HP- β -CD

Dyes	pH	K (L/mol)	
		β -CD ^a	HP- β -CD ^a
SAF	3.2	1069 \pm 63	11984 \pm 589
	6.0	1720 \pm 60	21032 \pm 1156
	9.0	710 \pm 21	13045 \pm 578
	3.2	8886 \pm 266	5785 \pm 135
BRB	6.0	4528 \pm 96	2090 \pm 100
	11.3	3642 \pm 42	1424 \pm 34
	3.2	353 \pm 14	285 \pm 19
MB	6.0	410 \pm 21	326 \pm 15
	9.0	358 \pm 16	178 \pm 17
	3.2	–	141 \pm 10
ES	5.0	–	340 \pm 22
	11.3	–	189 \pm 13
	5.0	–	70 \pm 5
TCTIF	7.6	–	241 \pm 15
	11.3	–	146 \pm 12
TCF	–	–	–

^a The confidence level was 95%.

3.2.1. Effect of the host molecule on inclusion interaction

β -Cyclodextrins have the hydrophilic outer surface and a hydrophobic internal cavity. The inclusion interaction of β -CDs and the guest molecules were affected by the size of the internal cavity and the hydrophilic, hydrophobic characters of the host. It is generally believed that dipole-dipole, electrostatic, van der Waals forces, hydrogen bonding, hydrophobic interaction, and the release of distortion energy of CD ring upon guest binding cooperatively govern the stability of an inclusion complex. The neutral β -CDs are not charged ($2.0 < \text{pH} < 11.0$) and the major inclusion interactions are hydrophobic interactions between the guest and CD cavity, and hydrogen bonding of the guest to $-\text{OH}$ groups or other introduced groups on CD ring [7]. As a result of additional groups of HP- β -CD comparative parent β -CD, the hydrophilic property of HP- β -CD was better than that β -CD. Meanwhile, the chemical modification enlarged the cavity of the host molecule, thus as a rule its inclusion capability was enhanced. Table 3 showed that the K value of SAF-HP- β -CD was larger than that SAF- β -CD. Moreover, compared with HP- β -CD, the inclusion interactions of ES and TCTIF with β -CD were not observed in these experiments. But the inclusion interactions of β -CDs with dyes were complicated, besides the size of the internal cavity and the hydrophilic, hydrophobic characters of the host, the other effect factors (charge of host and guest, speciation of guest molecule) were contributing and could result from the difference of K value.

3.2.2. Effect of the guest molecule on inclusion interaction

The structure of guest is very important for host-guest inclusion interaction. The shape and size of the guest must match with the cavity of β -CDs, and its polarity should be smaller than water. For SAF and BRB, their hydrophobic properties were relatively stronger; they were easy to enter the hydrophobic cavity of CDs and to form the relatively stable inclusion com-

plexes. For MB, its hydrophobic was weaker than that of BRB, so the host-guest inclusion interaction of β -CDs-MB was weaker ($K_{\text{BRB-CDs}} < K_{\text{MB-CDs}}$), which could be proved by the chemical shifts' degree of the protons ($\Delta\delta$), the chemical shifts' degree of the protons ($\Delta\delta$) was BRB- β -CD $>$ MB- β -CD, which indicated that BRB entered the cavity more deeply than MB, and the inclusion interaction of BRB with β -CD was more strong than MB with β -CD. ES and TCTIF were easy to dissolve in water for their good hydrophilic property. So their inclusion complexes with β -CDs were relatively labile, and the K values were smaller.

3.2.3. Effect of pH on inclusion interaction

The effect of pH on host-guest inclusion interaction mostly behaved that the conformation of guest were dissimilar at different pH values, namely the polarity of the guest changed. For example, SAF was a neutral molecule in neutral medium, but in acidic and basic media, it was a charged molecule. So SAF as molecule was easily included into HP- β -CD in neutral medium. Similarly, the inclusion complexes of ES and TCTIF with HP- β -CD were more stable in subacid medium than in acidic and basic media. The reason was probably that ES and TCTIF were neutral molecules in subacid medium and the hydrophobic interactions between them and the β -CDs cavity were strong; while in acidic and basic media, the guest molecules were charged, so their hydrophilic properties were better than the neutral molecules. Table 3 was shown that the inclusion constants of dyes with β -CD were more sensitive to the changes of pH values.

In a word, the factors which influence inclusion interaction were complex, and the K value reflected the general outcome about all the factors.

3.3. The inclusion interaction between VB₆ and HP- β -CD

The VB₆ itself could emit fluorescence. The wavelengths of excitation and emission were at 292 and 394 nm, respectively [17]. When VB₆ was into the cavity of CDs, its fluorescence intensity did not changed obviously. So, the direct fluorescence method to determine the inclusion constants of VB₆-HP- β -CD could not be used, the competitive inclusion method should be chosen.

Competitive inclusion method was a technique that based on two different guests completing the same CD's cavity which caused a remarkable change of the observed signal. When VB₆ was added into the solution which containing the CDs-probe, the fluorescence intensity of the fluorescence probe was reduced. That was because some VB₆ molecules replaced portion of the fluorescence probe molecules from the CD's cavity. The competitive inclusion process is as follows:



where the symbols G, V, CD-G and CD-V represent fluorescence probe molecule, VB₆, and the inclusion complexes, respectively. With $K_{\text{CD-G}}$, $K_{\text{CD-V}}$ to represent the inclusion constant of CD-G and CD-V, respectively, then $K_{\text{CD-V}}$ could be obtained from the

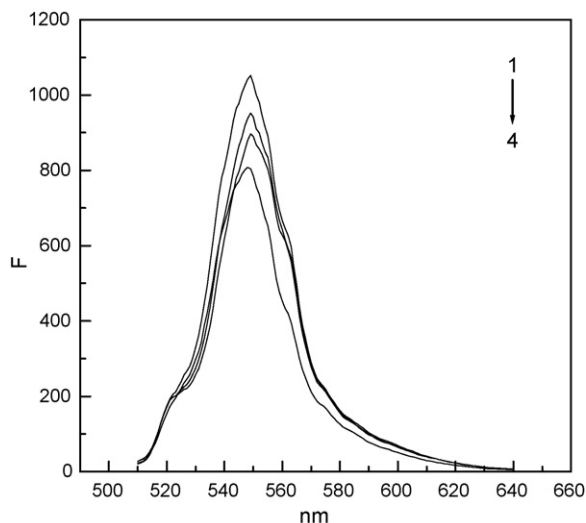


Fig. 3. Effect of VB₆ on the fluorescence spectra of ES-HP-β-CD (pH 5.0). (1) 1.0×10^{-5} mol/L ES + 2.0×10^{-3} mol/L HP-β-CD; (2–3) 1 + VB₆ (4.0×10^{-3} , 8.0×10^{-3} mol/L); (4) 1.0×10^{-5} mol/L ES.

following formula:

$$K_{\text{CD-V}} = \frac{([\text{CD}]_0 - [\text{CD}])}{[\text{CD}]([\text{V}]_0 - [\text{CD}]_0 + [\text{CD}])} \quad (2)$$

where $[\text{CD}]_0$ and $[\text{V}]_0$ represent the initial concentration of CD and VB₆ respectively, $[\text{CD}]$ was the concentration of the dissociative CD in the solution. $[\text{CD}]$ is the only unknown in this formula. It can be obtained from the following formula:

$$[\text{CD}] = \frac{F - F_G}{K_{\text{CD-G}}(F_{\text{CD-G}} - F)} \quad (3)$$

where F_G , $F_{\text{CD-G}}$ and F represent the fluorescence intensity of the dissociative G, the fluorescence intensity of the G after it included with the CD, and the fluorescence intensity of the G when G, VB₆ and CD was coexisting in the solution, respectively.

In this paper, ES and TCTIF were chosen as the fluorescence probes to observe the inclusion interaction between VB₆ and HP-β-CD. It was found that the fluorescence intensities of ES and TCTIF were gradually decreased with an increase of VB₆ concentration, respectively (Figs. 3 and 4). The inclusion interaction was taken in 5 min, and VB₆-ES(TCTIF)-CDs was stable in 30 min. It indicated that the same cavity of HP-β-CD was competed by the two guests (ES and VB₆, TCTIF and VB₆, respectively) and portion of the probe molecules were replaced out of the cavity by VB₆. According to the formulas (2) and (3),

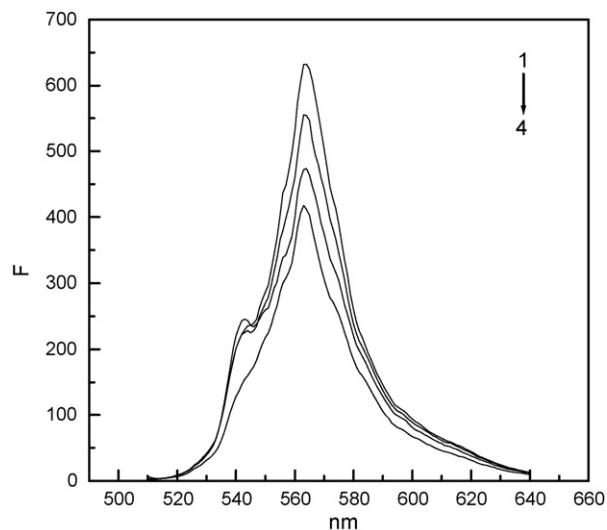


Fig. 4. Effect of VB₆ on the fluorescence spectra of TCTIF-HP-β-CD (pH 7.6). (1) 1.0×10^{-5} mol/L TCTIF + 2.0×10^{-3} mol/L HP-β-CD; (2–3) 1 + VB₆ (4.0×10^{-3} , 1.2×10^{-2} mol/L); (4) 1.0×10^{-5} mol/L TCTIF.

the inclusion constant of VB₆-HP-β-CD was determined to be $71(\pm 4)$ L/mol.

The inclusion constant of Dye-HP-β-CD (Table 3) was larger than that of VB₆-HP-β-CD, namely the dyes probes included more tightly with HP-β-CD. So enough VB₆ would be added into the system as to make the VB₆ molecules replace the probe molecules from the cavity of HP-β-CD.

3.3.1. Applications

It was observed from the above experiment that in these systems of ES-HP-β-CD or TCTIF-HP-β-CD, the VB₆ concentration had a linear relationship with the change fluorescence intensity of the systems (ΔF). The experimental conditions were optimized as follows: the concentration of ES and TCTIF was 1.0×10^{-5} mol/L, HP-β-CD concentration was 3.2×10^{-3} mol/L, and the pH value of the systems was 5.0 and 7.6, respectively.

3.3.2. Analytical parameters

The analytical characteristics for the determination of VB₆ were shown in Table 4.

3.3.3. Interferences

A study was carried out on the effects of foreign interferences on the determination of 20 mg/25 mL of VB₆ (in ES system). With a relative error of less than $\pm 1\%$, the tolerance limits for the

Table 4
Analytical parameters for the determination of VB₆

Analytical characteristic	ES-VB ₆	TCTIF-VB ₆
Linear regression equation	$\Delta F = -3.75 + 104651.98c$ (g/mL)	$\Delta F = 4.79 + 32390.79c$ (g/mL)
Linear range (g/mL)	$4.0 \times 10^{-4} - 4.0 \times 10^{-3}$	$6.4 \times 10^{-4} - 4.8 \times 10^{-3}$
Correlation coefficient	0.9987	0.9992
Limit of detection (g/mL)	1.0×10^{-4}	1.5×10^{-4}
RSD (%) ($n=5$, $c=8.0 \times 10^{-4}$ g/mL)	0.11	0.27

Table 5
Determination of VB₆ in synthetic samples

Synthetic sample	Sample ingredients (mg/mL)	Addition (mg/mL)	Amount found (mg/mL) ^a	RSD (%)	Recovery (%)
A (ES)	VB ₆ (1.6) + VC (0.6) + VB ₂ (4.0 × 10 ⁻³) + VB ₁₂ (1.6 × 10 ⁻⁴)	1.60	1.63 ± 0.02	1.1	100.6–103.1
A (TCTIF)			1.57 ± 0.02	1.3	96.7–99.4
B (ES)	VB ₆ (1.6) + VC (0.4) + VB ₂ (8.0 × 10 ⁻³) + VB ₁₂ (3.2 × 10 ⁻⁴)	1.60	1.56 ± 0.02	1.5	96.3–98.8
B (TCTIF)			1.54 ± 0.02	1.2	95.0–97.5

^a Average value of three determination, the confidence level was 95%.

Table 6
The results of determination of the sample

Sample	Marked content	Proposed method ^a	RSD (%) <i>n</i> = 3	HPLC method
Tablet mg/piece (ES)	10.0	10.6 ± 0.1	0.6	10.9 ± 0.1
Tablet mg/piece (TCTIF)		10.7 ± 0.1	1.0	
Injection g/2 mL (ES)	0.10	0.096 ± 0.001	0.6	0.11 ± 0.01
Injection g/2 mL (TCTIF)		0.095 ± 0.001	0.6	

^a The confidence level was 95%.

foreign substance were as follows (mg/25 mL): Serine, leucine, L-cysteine chloride (>300); Vitamin C (25); D-L-tryptophan (20); 3,5-iodogorgoic acid (15); Vitamin B₂ (0.3); Vitamin B₁₂ (0.02). It was shown that most of the amino acids did not influence the determination of VB₆. But VB₁₂ could absorb the fluorescence of those systems [20], it would influence the analysis, and should be separated before determination.

3.3.4. Sample analysis

The calibration graphs for VB₆ were constructed from the results obtained under the optimal conditions, and VB₆ in synthetic samples, tablets and injections were determined with standard curve method. The results were compared with the method of pharmacopoeia (HPLC) [21] (Tables 5 and 6). The *t*-test method was used to do a significant difference test for these data, and it was found that the data of both methods did not have significant difference.

4. Conclusion

In this paper, the inclusion interactions of dyes with β-CD and HP-β-CD were investigated, and the inclusion constants of dyes-β-CDs were determined by fluorescence technique. The related inclusion mechanism was discussed. The inclusion interaction of VB₆ with HP-β-CD was studied by the competitive fluorescence inclusion method. A new method for the analysis of VB₆ was developed on the basis of the linear relationship between the change fluorescence intensity of the systems (ΔF) and the concentration of VB₆. The method had been successfully applied to the determination of VB₆ in synthetic samples, tablets and injections with satisfactory results.

Acknowledgement

This work was supported by Cultivation and Construction Fund of the State Key Subject of Physical Chemistry.

References

- [1] L. Tong, Cyclodextrin Chemistry, Science Press, Beijing, 2001, p. 10.
- [2] C. Yanez, R. Salazar, L.J. Nunez, J. Pharm. Biomed. Anal. 35 (2004) 51.
- [3] S. Rawat, S.K. Jain, Eur. J. Pharm. Biopharm. 57 (2004) 263.
- [4] J.J. Berzas, A. Alanon, J.A. Lazaro, Talanta 58 (2002) 301.
- [5] S.O. Fakayode, I.M. Swamidoss, M.A. Busch, Talanta 65 (2005) 838.
- [6] O. Csernak, A. Buvári-Barcza, L. Barcza, Talanta 69 (2006) 425.
- [7] G. Zhang, S. Shuang, C. Dong, Spectrochim. Acta, Part A 59 (2003) 2935.
- [8] N.L. Pacioni, A.V. Veglia, Anal. Chim. Acta 488 (2003) 193.
- [9] H. Xu, L. Chen, L. Ma, Anal. Test. Technol. Instrum. (Chinese) 8 (2002) 72.
- [10] X. Zhu, J. Sun, L. Bao, Chin. J. Appl. Chem. 23 (2006) 323.
- [11] G. Carmen, S. Mignel, Z. Arantza, Talanta 60 (2003) 477.
- [12] G. Li, J. Li, Y. Wei, Chin. J. Spectrosc. Lab. 22 (2005) 416.
- [13] T. Wang, H. Feng, S. Li, J. Chromatogr. A 987 (2003) 485.
- [14] Y. Matsui, Y. Futjie, H. Bull, Chem. Soc. Jpn. 61 (1988) 3409.
- [15] C. You, Y. Zhao, Y. Liu, Chem. J. Chin. Univ. 22 (2001) 218.
- [16] B. Tang, X. Wang, H. Liang, J. Agric. Food Chem. 53 (2005) 8452.
- [17] X. Liu, Y. Yang, G. Zhang, Chin. J. Anal. Chem. 31 (2003) 996.
- [18] F.V. Bright, T.L. Keimig, L.B. McGown, Anal. Chim. Acta 175 (1985) 189.
- [19] G.C. Ctana, F.V. Bright, Anal. Chim. 61 (1989) 905.
- [20] B. Liu, J. Gao, G. Yang, Spectrosc. Spectral. Anal. (Chinese) 25 (2005) 1080.
- [21] Chinese Pharmacopoeia (second part), Chemical Industry Press, Beijing, 2005, p. 667.